

---

# Surface Science for Advanced Propulsion

Dr. Kevin P. Chaffee  
Dr. John J. Rusek

August 1996

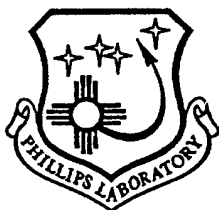
19961029 073

Final Report

---

APPROVED FOR PUBLIC RELEASE; DISTRIBUTION UNLIMITED

---

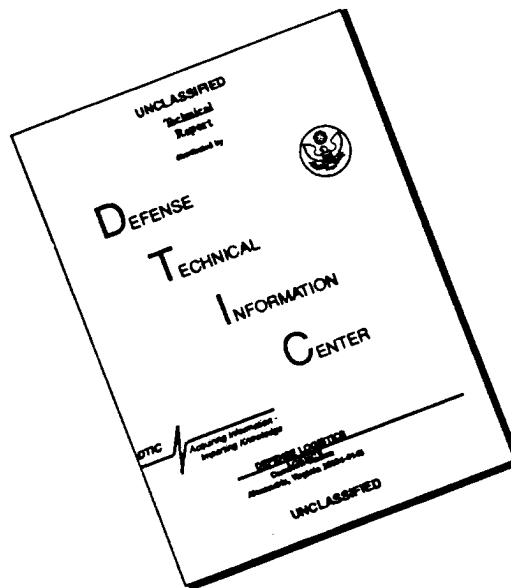


**PHILLIPS LABORATORY**  
**Propulsion Directorate**  
**AIR FORCE MATERIEL COMMAND**  
**EDWARDS AIR FORCE BASE CA 93524-7048**

DTIC QUALITY INSPECTED 1

---

# DISCLAIMER NOTICE



THIS DOCUMENT IS BEST QUALITY AVAILABLE. THE COPY FURNISHED TO DTIC CONTAINED A SIGNIFICANT NUMBER OF PAGES WHICH DO NOT REPRODUCE LEGIBLY.

## NOTICE

When U.S. Government drawings, specifications, or other data are used for any purpose other than a definitely related Government procurement operation, the fact that the Government may have formulated, furnished, or in any way supplied the said drawings, specifications, or other data, is not to be regarded by implication or otherwise, or in any way licensing the holder or any other person or corporation, or conveying any rights or permission to manufacture, use or sell any patented invention that may be related thereto.

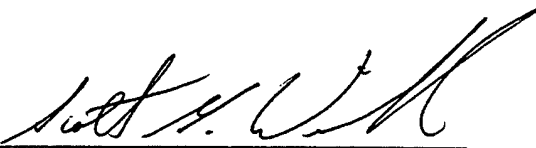
## FOREWORD

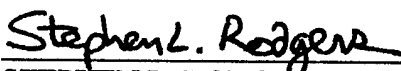
This final report was submitted on completion of JONs 573000S3, IR2NRD61, IR2RRD60 by the OL-AC PL/RKS Division at the Phillips Laboratory (AFMC), Edwards AFB CA 93524-7680. OL-AC PL project manager for the final two years of the program was Dr. Kevin P. Chaffee.

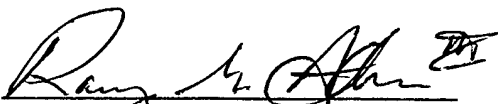
The authors wish to express appreciation to the participating research teams of beamlines X-19A and X11A at the National Synchrotron Light Source of Brookhaven National Laboratory, Dr. Guy A. DeRose of CalTech, and Dr. Charlotte Lowe-Ma, formerly of Naval Air Weapons Center (NAWC), China Lake for their assistance during data collection and analysis.

This report has been reviewed and is approved for release and distribution in accordance with the distribution statement on the cover and on the SF Form 298.

  
KEVIN P. CHAFFEE  
Project Manager

  
SCOTT G. WIERSCHKE, Capt, USAF  
Deputy Director  
Propulsion Sciences Division

  
STEPHEN L. RODGERS  
Director  
Propulsion Sciences Division

  
RANNEY E. ADAMS, III  
Public Affairs Director  
OLAC PL PAS  
96-148

<b>REPORT DOCUMENTATION PAGE</b>			<b>Form Approved</b> <b>OMB No 0704-0188</b>	
Public reporting burden for this collection of information is estimated to average 1 hour per response, including the time for reviewing instructions searching existing data sources gathering and maintaining the data needed, and completing and reviewing the collection of information. Send comments regarding this burden estimate or any other aspect of this collection of information, including suggestions for reducing this burden to Washington Headquarters Services, Directorate for Information Operations and Reports, 1215 Jefferson Davis Highway, Suite 1204, Arlington, VA 22202-4302, and to the Office of Management and Budget, Paperwork Reduction Project (0740-0188), Washington DC 20503.				
1. AGENCY USE ONLY (LEAVE BLANK)		2. REPORT DATE August 1996		3. REPORT TYPE AND DATES COVERED Final Report
4. TITLE AND SUBTITLE Surface Science for Advanced Propulsion			5. FUNDING NUMBERS C: In-House PE: 62601F PR: 5730 TA: 00S3	
6. AUTHOR(S) Kevin P. Chaffee and John J. Rusek				
7. PERFORMING ORGANIZATION NAME(S) AND ADDRESS(ES) Phillips Laboratory OL-AC PL/RKS 10 East Saturn Drive Edwards AFB CA 93524-7680			8. PERFORMING ORGANIZATION REPORT NUMBER PL-TR-96-3015	
9. SPONSORING/MONITORING AGENCY NAME(S) AND ADDRESS(ES)			10. SPONSORING/MONITORING AGENCY REPORT NUMBER	
11. SUPPLEMENTARY NOTES: Other JONs reported in this document are: IR2NRD61; IR2RRD60.  COSATI CODE(S): 07/06; 20/05				
12a. DISTRIBUTION/AVAILABILITY STATEMENT  Public Release; Distribution Unlimited			12b. DISTRIBUTION CODE  A	
13. ABSTRACT (MAXIMUM 200 WORDS) Complex composite structures are prevalent throughout the propulsion industry. Unavoidable are the many interfaces between materials of differing physical and chemical properties. In applications where nut-and-bolt fasteners are not appropriate, the "adhesive" quality of the interface becomes a serious consideration with regard to overall system integrity and reliability. Indeed, it is the ability of the structure to transfer or distribute stress when subjected to, for example, thermal and mechanical loading, that will help determine performance and failure criteria. If the materials on each side of the interface are also chemically complex (as is the case with solid propellants), then other issues such as surface segregation, diffusion, solubility, and reactivity of chemical constituents also affect the interfacial region and overall system aging. The project objective was to examine the structure, function and dynamics of the interfacial regions of advanced propulsion materials. Before the principal author joined the project, the primary focus of the program was on the ammonium perchlorate (AP)/bonding agent interaction. As the propellant community sought to lower hydrochloric acid (HCl) emissions in rocket plumes and therefore eliminate AP as an oxidizer in new propellant systems, the focus of the program shifted entirely toward the annealing phenomenon exhibited by thermotropic liquid crystal polymers (LCP): an exciting candidate material for structural applications and the subject of current research. Ammonium perchlorate presents a challenge because of its delicate, reactive nature as revealed by its low heat of formation of approximately -70.7 kcal/mole. Ion and electron beam techniques were found to be too damaging to either the ammonium perchlorate substrate and/or the organic bonding agent overlayer. For these reasons, Raman Spectroscopy, Fourier Transform Infrared Spectroscopy (FTIR) and X-ray absorption and scattering techniques were used and it is the results from these techniques that are presented within.				
14. SUBJECT TERMS Liquid crystal polymers; propellant interface; ammonium perchlorate; Raman spectroscopy; FTIR			15. NUMBER OF PAGES 312	
			16. PRICE CODE	
17. SECURITY CLASSIFICATION OF THIS PAGE Unclassified	18. SECURITY CLASSIFICATION OF THIS PAGE Unclassified	19. SECURITY CLASSIFICATION OF ABSTRACT Unclassified	20. LIMITATION OF ABSTRACT SAR	



## TABLE OF CONTENTS

<b><u>Section</u></b>	<b><u>Page</u></b>
1.0 Introduction	1
2.0 Overview	2
2.1 X-ray and Electron Scattering Results	2
2.2 Raman and FTIR Results	6
2.3 X-ray Absorption Results	9
3.0 Conclusions	13
4.0 Recommendations	14
5.0 References	15
Appendices	17
A. Additional FTIR and Raman Data	17
B. Dr. Hoffman/CWRU Reports	41
C. Dr. Lieb's Reports	266

## LIST OF FIGURES

<u>Figure</u>	<u>Page</u>
1. Scattering Vector Definition	2
2. $\theta$ -2 $\theta$ Diffractometer Setup	3
3. (001)AP Surface with and without DER-332	4
4. (210)AP Surface with and without HX-879	5
5. E-beam Etch Pit in AP Single Crystal	6
6. Raman Spectrum of AP	7
7. Raman Spectrum of AP Coated with DEA	7
8. FTIR Spectrum of AP Coated with HX-752	8
9. Schematic of EXAFS Experiment	10
10. Fluorescent EXAFS of AP	11
11. Fluorescent EXAFS of AP Coated with HX-878	12
12. $\chi(k)$ overlay for AP and HX-878/AP	12

## 1.0 INTRODUCTION

Complex composite structures are prevalent throughout the propulsion industry. Unavoidable are the many interfaces between materials of differing physical and chemical properties. An example is the problematic propellant-liner "bondline" region that has received great attention through the multi-organizational and multi-disciplinary Solid Propellant Integrity Program.<sup>1</sup> In applications where nut-and-bolt fasteners are not appropriate, the "adhesive" quality of the interface becomes a serious consideration with regard to overall system integrity and reliability. Indeed, it is the ability of the structure to transfer or distribute stress when subjected to, for example, thermal and mechanical loading, that will help determine performance and failure criteria. If the materials on each side of the interface are also chemically complex (as is the case with solid propellants), then other issues such as surface segregation, diffusion, solubility, and reactivity of chemical constituents also affect the interfacial region and overall system aging.<sup>2</sup> As with grain boundaries in metals, in some aspect an interface can be considered as a type of defect and will therefore have a significant impact on the ability of the composite to perform its intended function. For this reason, the nature of the interface becomes of critical fundamental importance.

The project objective was to examine the structure, function and dynamics of the interfacial regions of advanced propulsion materials. Before the principal author joined the project, the primary focus of the program was on the ammonium perchlorate (AP)/bonding agent interaction. As the propellant community sought to lower hydrochloric acid (HCl) emissions in rocket plumes and therefore eliminate AP as an oxidizer in new propellant systems, the focus of the program shifted entirely toward the annealing phenomenon exhibited by thermotropic liquid crystal polymers (LCP): an exciting candidate material for structural applications and the subject of current research. The LCP results relevant to these studies are presented in other reports submitted by Dr. John Rusek (this effort's first program manager - currently at Naval Weapons Center (NWC) China Lake).<sup>3,4</sup> This report will present the preliminary research on ammonium perchlorate.

Gathering information about a buried interface can be difficult, depending on the nature of the individual layers. The probe employed needs to be site specific without destroying what is to be studied. In most surface and interfacial analytical techniques, the trade-off exists between site selectivity (depth resolution and volume averaging) and sensitivity (signal-to-noise). Ammonium perchlorate presents a challenge because of its delicate, reactive nature as revealed by its low heat of formation of approximately -70.7 kcal/mole.<sup>5</sup> Ion and electron beam techniques were found to be too damaging to either the ammonium perchlorate substrate and/or the organic bonding agent overlayer. For these reasons, Raman Spectroscopy, Fourier Transform Infrared Spectroscopy (FTIR) and X-ray absorption and scattering techniques were used and it is the results from these techniques that are presented within. The data and discussion of the applicability of the X-ray and Raman techniques were obtained from research contracted with Dr. R.W. Hoffman of Case Western Reserve University (CWRU) and the FTIR results from Dr. Shannon Lieb of Butler University. The reports for these two efforts are presented in their entirety in the appendices.

## 2.0 OVERVIEW

The overview of the results reported in the appendices will be divided into three sections. First, the X-ray and electron scattering feasibility work performed by Dr. R.W. Hoffman and Dr. Charlotte Lowe-Ma will be summarized. The second section will describe the FTIR and Raman experiments performed at OL-AC PL/RKFE, Case Western Reserve University (CWRU), and Butler University. The final section will present the Extended X-ray Absorption Fine Structure (EXAFS) results of CWRU. The discussion will approximately follow chronologically the efforts made to characterize the AP/bonding agent interaction.

### 2.1 X-ray and Electron Scattering Results

Of interest was the structure of the adsorbed bonding agent layer. In principle, if the adsorbed molecule (adsorbate) reacts chemically with the substrate (so-called chemisorption), then the adsorbate would be found only where these reaction sites are present. If the reaction sites are located in a two-dimensional periodic array, then a surface diffraction technique would determine the periodicity of the adsorbate. Two techniques for finding this periodicity are Surface X-ray Diffraction (SXRD) and Low Energy Electron Diffraction (LEED).

The diffraction of electrons and X-rays are fairly well understood. As a simple introduction, in either case, the scattering vector which is defined as the difference between the vectors describing the outgoing (scattered) beam and that for incident beam

$$\mathbf{q} = \mathbf{k}_{\text{out}} - \mathbf{k}_{\text{in}} \quad (1)$$

is used to probe for periodic variations of electron density in the sample<sup>6</sup> (see Fig. 1).

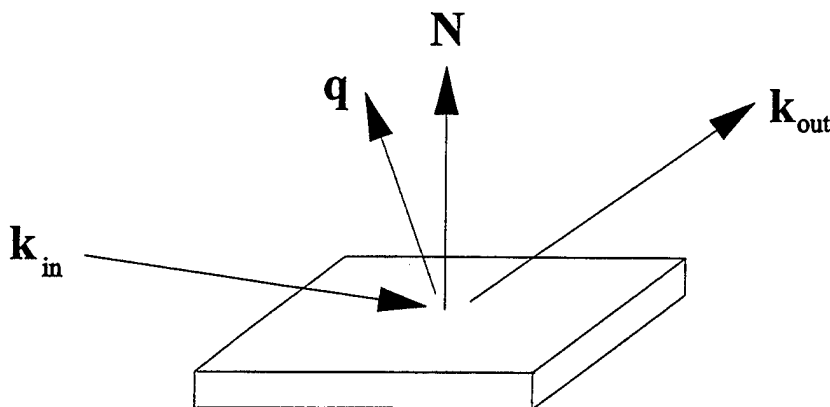


**Figure 1**  
**Scattering Vector Definition**

Here,  $k$  is the wavevector of the radiation employed and is inversely proportional to its wavelength. Considered here, of course, are X-rays that are elastically scattered, i.e., the scattered photons have the same energy as the incident ones. If the periodicity of the sample can be described by the reciprocal lattice vector  $a$ , then diffraction maxima will be observed when the Laue conditions are met. Namely, when

$$a \cdot q = 2\pi n \quad (2)$$

where  $n$  is an integer. The description for two-dimensional periodic arrays yields the same diffraction conditions given by Equation 2.

The X-ray Diffraction (XRD) experiments were conducted at Naval Air Weapons Center (NAWC) by Dr. Charlotte Lowe-Ma. A typical XRD setup is shown in Figure 2.

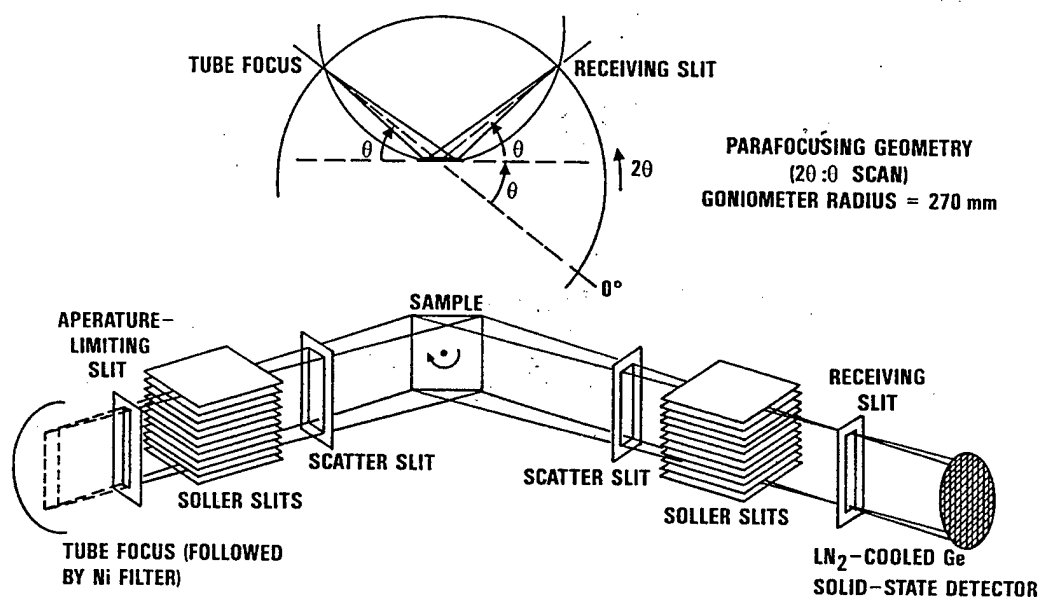


**Figure 2**  
 **$\theta$ -2 $\theta$  Diffractometer Setup**

For scattered X-ray diffraction (SXRD), the incident X-ray angle is usually kept fixed below the substrate critical angle if possible, thereby maximizing the fraction of the scattered intensity due to the adsorbed layer (this technique is applicable for X-ray absorption measurements and infrared (IR) absorption as well). The detector is then swept through an angle such that  $q$  lies either in the plane defined by  $k_{in}$  and the sample normal  $N$  (scan type 1), or nearly perpendicular to  $N$  (nearly in the plane of the sample; scan type 2). Another possibility is to use an X-ray beam incident normally onto the sample surface and

detect the back-reflected diffraction maxima. This is the standard arrangement for LEED.<sup>7</sup> LEED maintains surface sensitivity by using low energy incident electrons, thereby minimizing the inelastic scattering mean free path. For a truly two-dimensional periodic structure where there is no crystallinity in the direction of N, scan type 2 would be more appropriate. However, due to instrumental limitations and alignment difficulties, neither scan type was performed. Scattering data were taken for the  $\theta$ - $2\theta$  experiment shown in Figure 2 for a variety of scan ranges for "neat" AP crystals and for AP with a dilute solution of a bonding agent applied to the surface of the same crystal. The bonding agent solution concentration was chosen such that after evaporation of the solvent, roughly one monolayer of bonding agent would be left on the surface (1 monolayer  $\approx 1 \times 10^{15}$  atoms/cm<sup>2</sup>). In Figures 3 and 4, typical scattering curves for an epoxy resin (DER-332) and "tepan" (HX-879) are presented.

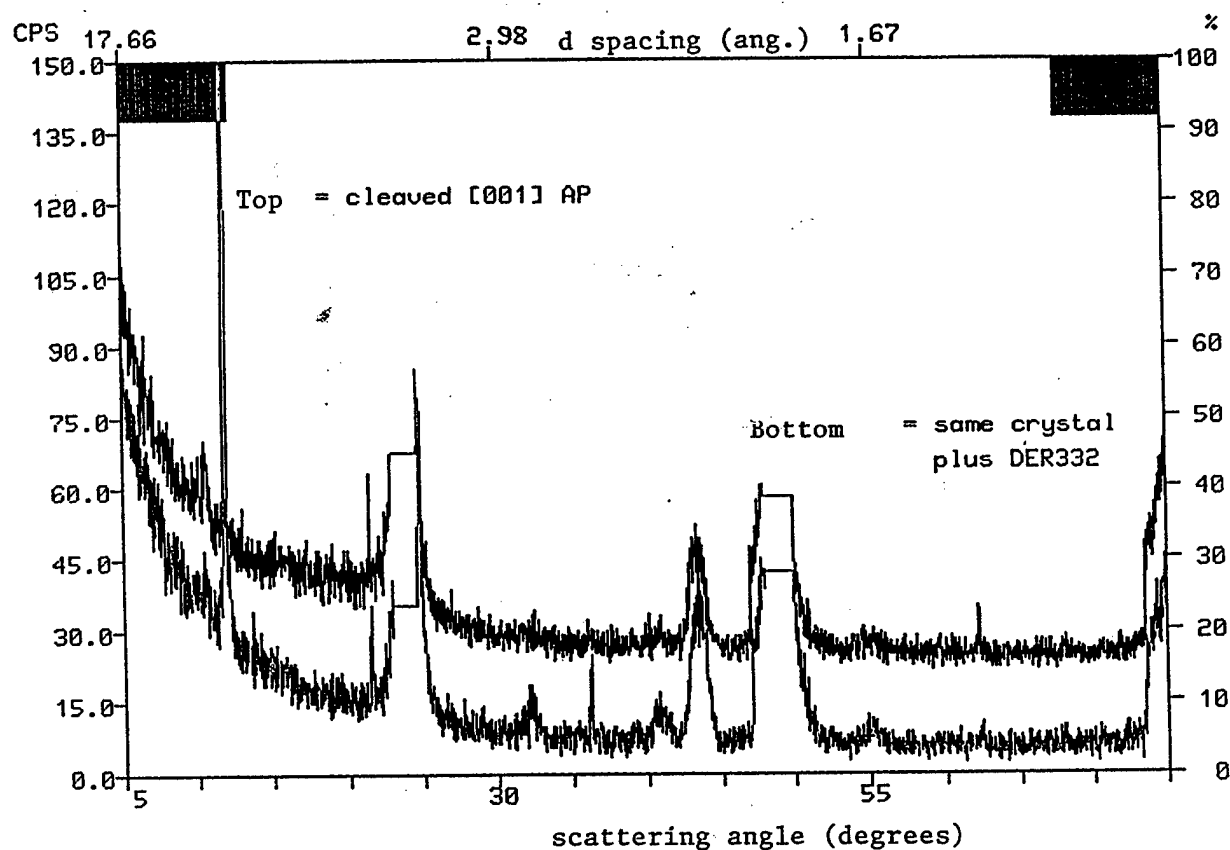


**Figure 3**  
**(001)AP Surface with and without DER- 332**

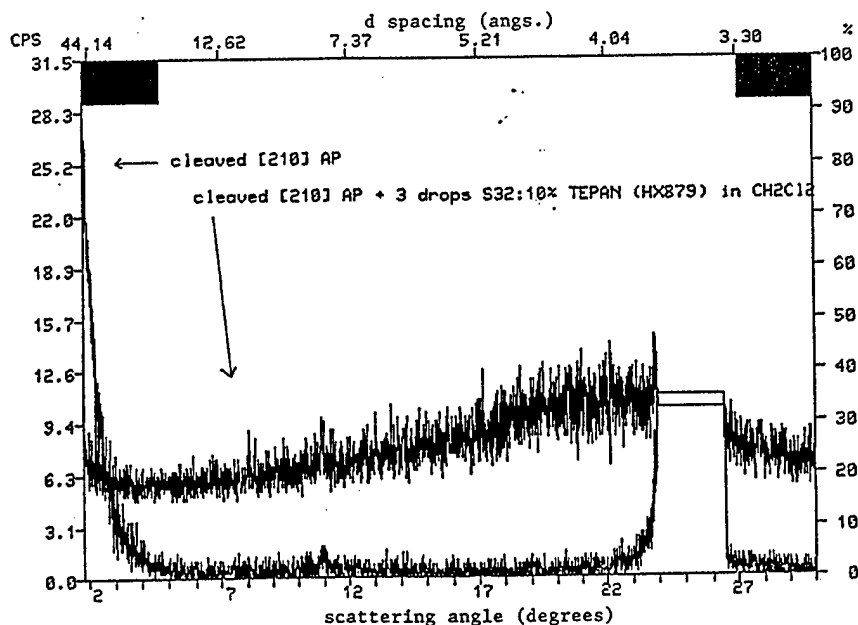


**Figure 4**  
**(210)AP Surface with and without HX-879**

For both figures, it is apparent that the differences between the neat AP crystal and those with a bonding agent applied are subtle. First, due to the loss in intensity of some of the weaker reflections in Figure 3 and the presence of the amorphous scattering hump near  $22^\circ 2\theta$  in Figure 4, the coverage was apparently significantly thicker than desired. The chemisorption of the bonding agent would affect only the near surface region of the crystal (perhaps the top two or three crystal planes). The changes in the diffraction maxima for the AP would be virtually impossible to detect. Second, the diffraction geometry was not appropriate to locate a two-dimensional adsorbate structure. It appears that most of the data taken were in the low  $2\theta$  range where the scattering comes from long crystalline repeat lengths (or large correlation distances). It was not anticipated that the adsorbate would yield scattering at these large length scales.

The LEED experiments were conducted at Case Western Reserve University by Dr. R.W. Hoffman and research associates (see App. B). It was anticipated that the electron beam (e-beam) would damage the AP crystals under at least some conditions. Preliminary experiments were conducted to ascertain the e-beam current density limits below which LEED or possibly Auger Electron Spectroscopy (AES), Reflection High Energy Electron Diffraction (RHEED), and Electron Energy Loss Spectroscopy (EELS – a vibrational spectroscopy) could be performed.<sup>8</sup> It was found that at high currents at a beam energy of 4.5 keV, the AP crystal, not surprisingly, decomposed rapidly. Figure 5 shows an e-beam etch pit into an AP crystal (App. B also discusses RHEED, EELS, and Temperature Programmed Desorption).

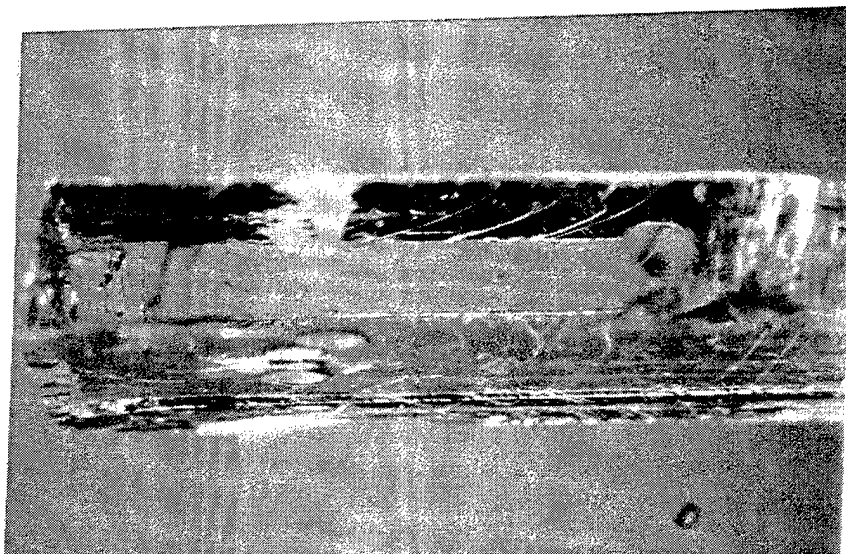


**Figure 5**  
**E-beam Etch Pit in AP Single Crystal**

It was also noted that for typical LEED e-beam characteristics (1  $\mu\text{A}$  current, 20-500 eV energy), degradation of the AP still occurred as evidenced by decomposition products detected by residual gas analysis, but at a greatly reduced rate. Long term Cl contamination of the ultrahigh vacuum apparatus was also noted. Concern remained over the viability of an organic adsorbate under the influence of an e-beam in the UHV environment. Attempts to detect LEED maxima from AP failed, presumably because of charging effects. At this point, CWRU abandoned LEED for X-ray Absorption techniques. RHEED and EELS were also attempted with little success.

## **2.2 Raman and FTIR Results**

Raman and FTIR spectroscopy experiments were performed at Case Western Reserve University and by Dr. Lieb at Butler University respectively. In Raman spectroscopy, the fraction of the incident light, usually from a laser source, scattered inelastically from the sample is analyzed. The shifts in wavenumber (proportional to the energy) from the incident radiation are characteristic of a molecule's shape and chemical composition (i.e., a measure of the polarizability of the molecules). Raman spectroscopy of adsorbates suffers typically from sensitivity issues and has not been proven to be a reliable surface technique for the study of adsorbates. That is, the surface/adsorbate Raman scattering can easily be hidden in the noise (background scattering etc.) due to the low signal strengths. However, in certain cases, the technique has proven to be quite effective. Fig. 6 shows the Raman spectrum for single crystal AP as measured from a 647.1 nm wavelength excitation source.



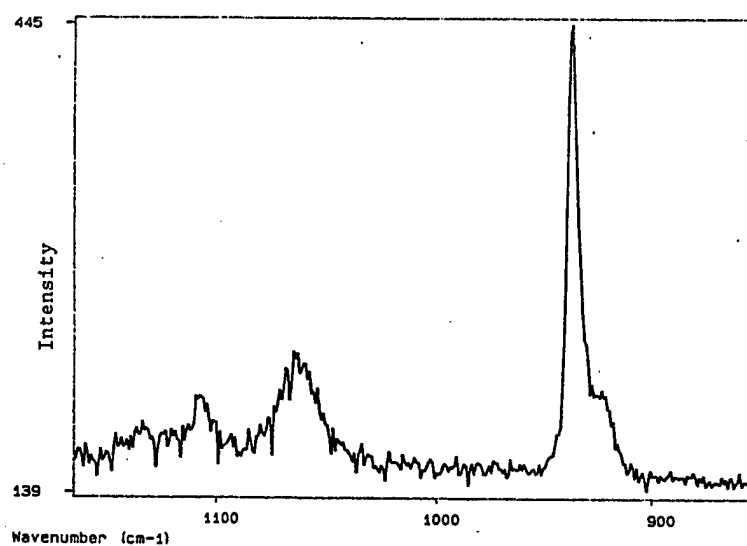


**Figure 6**  
**Raman Spectrum of AP**

This data set is consistent with the Raman scattering for AP as found by other researchers.<sup>9,10,11</sup> In Figure 7, data is for the same sample, coated with diethylamine.

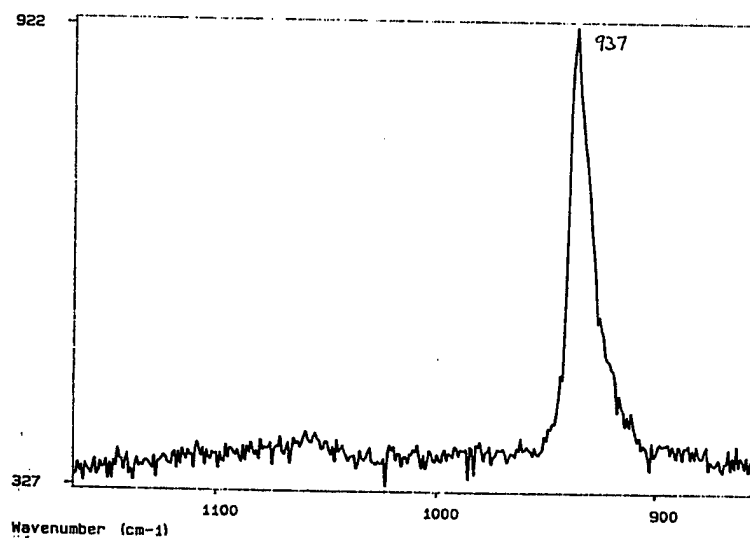


**Figure 7**  
**Raman Spectrum for AP Coated with DEA**

The wavenumber range shows the main  $\text{ClO}_4^-$  symmetric stretch modes (additional data appear in App. A). AP is a heavily hydrogen bonded solid with each  $\text{ClO}_4^-$  surrounded by seven  $\text{NH}_4^+$  and likewise for the  $\text{NH}_4^+$  ions.<sup>12</sup> It is therefore reasonable to assume a coupling, although perhaps weak, between the perchlorate and ammonium sublattices through the vibrational modes. This may be evidenced by the loss of the  $\nu_3$  free ion vibrational mode near  $1100\text{ cm}^{-1}$ .

FTIR spectroscopy differs from the Raman technique mentioned above in that the interaction is between the incident photons and permanent dipole moments (dipole-active) in the sample. This technique measures in some fashion the amount of attenuation of the incident signal as a function of wavelength: either through direct measurement of the transmitted intensity, or for greater surface sensitivity reflected intensity (Infrared Reflected Absorption Spectroscopy) or through a secondary process such as photoacoustic emission. FTIR is more sensitive to hydrocarbons but usually does not have as sharply defined peaks as Raman. In some sense, FTIR is a complementary technique to Raman scattering. FTIR was explored at the Phillips Laboratory early on in the program to assess the utility of this technique. Figure 8 shows the FTIR photoacoustic spectrum for an aziridine of unknown coverage adsorbed on AP (other data appear in App. A).<sup>13</sup>

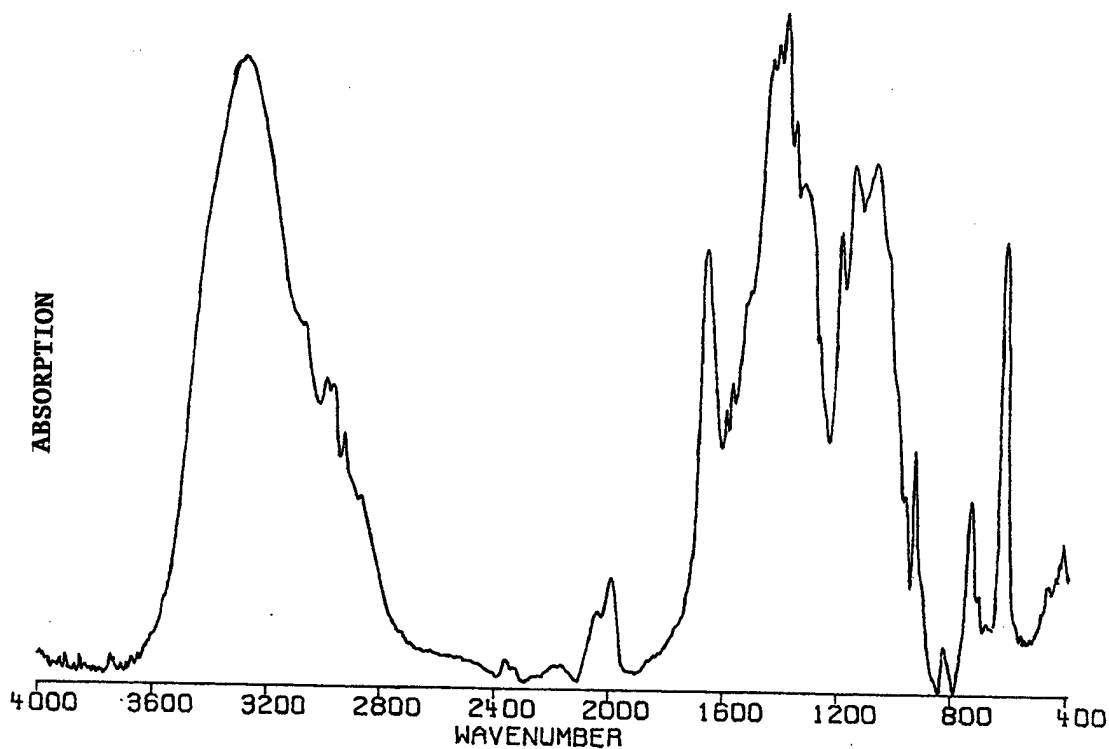


**Figure 8**  
**FTIR Spectrum of AP Coated with HX-752**

The complexity of the spectrum is obvious: this was determined to be a seriously limiting factor. The effect, which was thought to be subtle, was believed to be hidden amongst broad resonances associated with the AP and the bonding agents themselves. Note the broad ammonium bands at approximately  $1400\text{ cm}^{-1}$  and  $3000\text{ cm}^{-1}$  and the amine band near  $1300\text{ cm}^{-1}$  and  $1600\text{ cm}^{-1}$ . Certain features of Figure 8 are also readily

identifiable with the perchlorate ion: the doublet near 2000  $\text{cm}^{-1}$  and the sharp peak near 630  $\text{cm}^{-1}$ . To identify the hydrogen bonded species in an hydroxy terminated polybutadiene (HTPB)/AP system, Dr. Lieb used a model chemical system that in principle would be free from the spectral complexities mentioned above. Specifically, the hydrogen bonding of monomer, dimer and trimer allyl alcohol hydrogen bonding was investigated. Dr. Lieb's reports, presented in the appendices, do not show FTIR spectra, thereby making conclusions difficult to reach.

## 2.3 X-ray Absorption Results

The final experimental technique employed, EXAFS, received the most attention (see App. B). Photons interact with matter through three basic processes: scattering (inelastic and elastic), absorption (photoelectric effect), and pair production. For photons in the X-ray wavelength range of approximately 0.05 to 100 Å, the photoelectric effect is dominant for most elements (and pair production forbidden). The outgoing photoelectron wave will interact with the wave scattered off neighboring atoms, leading to a modulation in the absorption coefficient  $\mu$  (quantum mechanically a final state interference effect). It should be stressed that EXAFS, unlike the diffraction techniques discussed above, is a short range order technique. Mathematically, sufficiently far from the absorption edge where the single scattering approximation is valid, the EXAFS oscillations for the K-edge are given by:

$$\chi(k) = (\mu - \mu_0)/\mu_0 = \sum_j -(N_j/kR_j^2) |f_j(k, \pi)| \exp(-2\sigma^2 k^2 - 2R_j/\lambda) \sin(2kR_j + \delta_j(k)) \quad (3)$$

where

$\mu_0$  = the monotonically varying part of the absorption coefficient

$k$  = photoelectron wavenumber

$N_j$  = number of nearest neighbors of atom type  $j$

$R_j$  = distance from absorber to atoms of type  $j$

$f_j(k, \pi)$  = energy dependent backscattering function for atom of type  $j$

$\exp(-2\sigma^2 k^2 - 2R_j/\lambda)$  = Debye Waller and inelastic scattering term of mean free path  $\lambda$

$\sin(2kR_j + \delta_j(k))$  = interference term

$\delta_j(k)$  = energy dependent phase term.

The features seen near the absorption edge, the X-ray Absorption Near Edge Structure (XANES) region, contain information about unoccupied bound states, low energy continuum states, and, because of the importance of multiple scattering at these low photoelectron energies, multi-atom correlations.<sup>14</sup>

The Cl K-edge was chosen for study. The reaction of the bonding agent with the ammonium ion should affect the Cl EXAFS in the first three coordination shells. The N K-edge would require the sample to be placed in a vacuum (because of the strong absorption of  $\text{N}_2$  in the atmosphere) where the volatility of the adsorbed bonding agent would be a concern, as determined in the e-beam investigations. Experimentally, the incident X-ray energy is increased from just before the absorption edge (approximately 2823 eV for Cl) to 1000-1500 eV beyond it while measuring the incident X-ray flux and either the intensity

of the transmitted beam or the decay of the excited Cl atom. A synchrotron radiation source is preferred not only because of the superior X-ray flux and tunability of the "source," but also because the flux is a smoothly varying function of the energy. The final absorption data is scaled by the incident X-ray flux to remove any beam intensity variations. (These measurements were made at the National Synchrotron Light Source of Brookhaven National Laboratories.) The oscillations are then isolated from the monotonically varying background and Fourier analyzed.

The excited atom will decay either through the Auger process or fluorescent radiation production. For elements of low atomic number like Cl, the Auger process will dominate. However, the detection of the Auger electron was not feasible. For transmission measurements, the sample should be no thinner than  $1/\mu$  to maximize the signal to noise but not thicker than  $2-3/\mu$  to avoid signal attenuation. An AP sample meeting this requirement would be approximately  $23\text{ }\mu\text{m}$  ( $10^{-6}\text{ m}$ ) thick: far too thin to manipulate by hand with any reasonable viability.<sup>15</sup> For these reasons, fluorescent measurements were chosen. The AP was finely ground ( $10\text{ }\mu\text{m}$  diameter) and loosely pressed into a pellet approximately 0.375 in. in diameter and 1 mm thick. Samples were mounted in the fluorescent detector housing on a carousel designed at the Phillips Laboratory. Figure 9 shows a schematic of the EXAFS experiment.

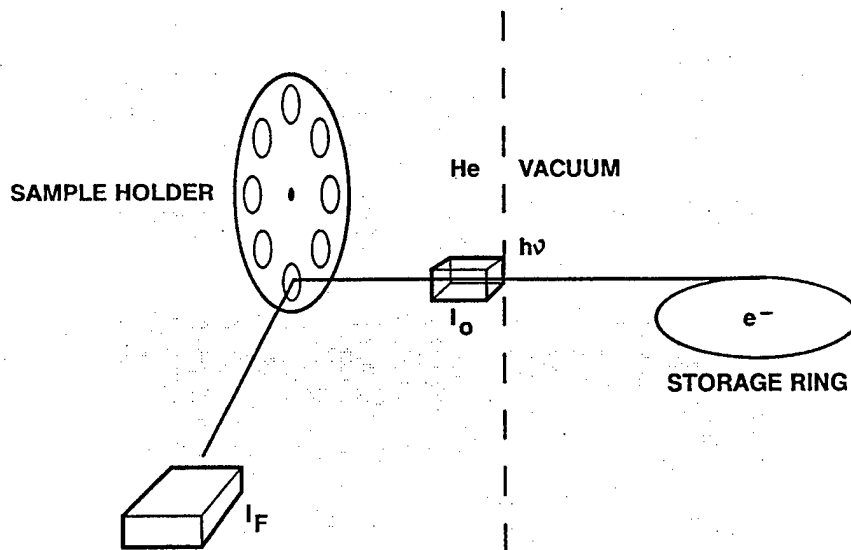


**Figure 9**  
**Schematic of EXAFS Experiment**

The absorption experiments were conducted by placing one to two dilute drops of a bonding agent onto the AP pellet. The concentrations were prepared such that assuming 100% adsorption, the assumed spherical AP particles would be coated with one or two monolayers of bonding agent. The application of the bonding agent was followed by the odor of ammonia. Figure 10 shows adsorption data for AP. Figure 11 shows EXAFS data for AP coated with HX-878 (Tepanol). Note the second adsorption edge near 3200 eV. This is due to Ar in the fluorescent chamber. CWRU attempted to use this second

absorption edge as an "internal" energy calibration but this benefit was far outweighed by the complication of removing a second edge from the middle of the EXAFS region.

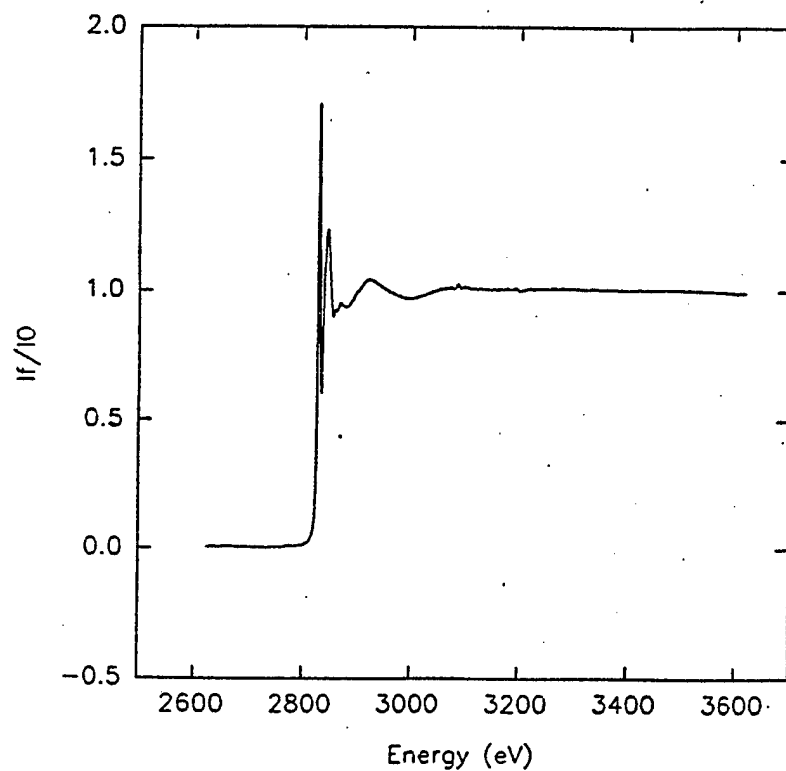


**Figure 10**  
**Fluorescent EXAFS of AP**

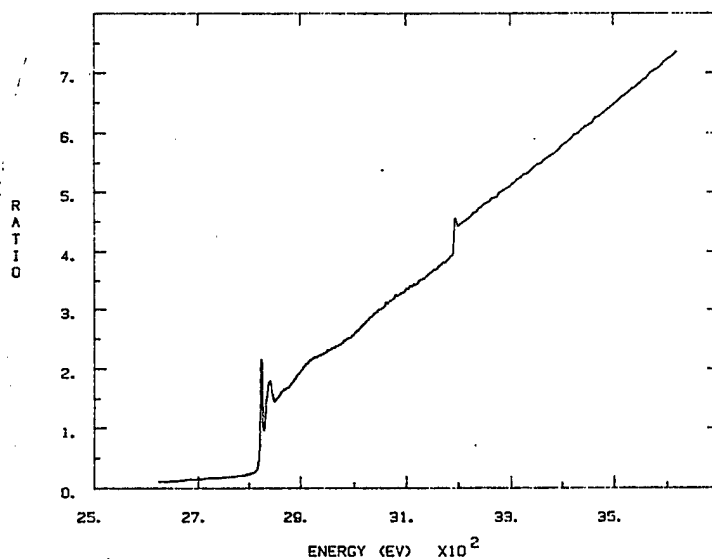


**Figure 11**  
**Fluorescent EXAFS of AP Coated with HX-878**

Although the spectra are qualitatively very similar, Fourier analysis showed subtle changes in the Cl-O coordination shell. Simulations of the expected EXAFS data, computed with the FEFF family of programs, were consistent with the observed data.<sup>16,17,18</sup> Figure 12 shows the  $\chi(k)$  plot derived from Figures 10 and 11. Note the subtle changes in amplitude and in phase of the EXAFS oscillations.

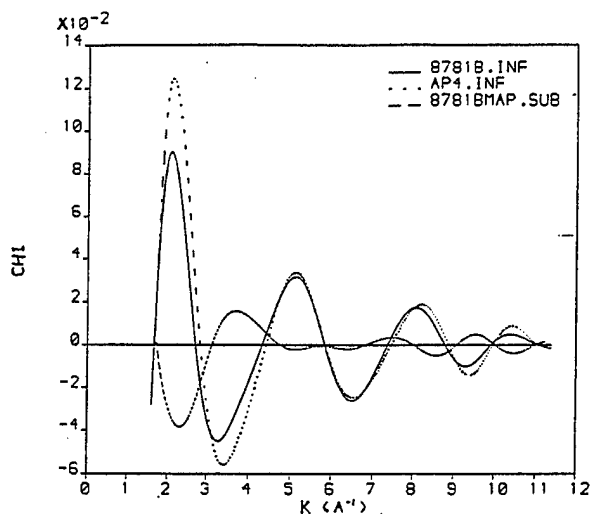


**Figure 12**  
 **$\chi(k)$  Overlay for AP and HX-878/AP**

### 3.0 CONCLUSIONS

The preceding sections have outlined what can only be called a preliminary investigation of the chemisorption of various bonding agents on ammonium perchlorate. Although the political atmosphere necessitated the premature termination of most of the experiments (the EXAFS work proceeded longer because of the interest in EXAFS of the LCP materials), several conclusions can be drawn.

Regardless of the analytical technique used, more care was needed in the creation of the adsorbate layer. It was evident in the X-ray diffraction and FTIR data that there was, in some instances, too thick (and undoubtedly nonuniform) a coating of the bonding agent, thereby effectively swamping the desired signal with information from the unreacted bonding agent. To maximize the efficiency of the EXAFS experiments, the coverage of the AP in the near surface region of the pellet (approximately 30-40  $\mu\text{m}$ . deep) needed to be complete. This is true because the self-absorption of the Cl K-edge EXAFS would prevent a detectable signal from deeper within the pellet. The EXAFS data show different results depending on whether the top side (the side to which the solution was applied) or the bottom side were analyzed, with both sides being different from unreacted AP. This makes the assumed coverage suspect.

Trivially, surface sensitivity is essential to the study of adsorbates. The XRD and FTIR techniques employed did not have the degree of surface sensitivity required to provide meaningful data because of the inappropriate scattering geometries employed. The glancing angle SXRD and IRAS would be better suited for reasons discussed earlier. Surface enhanced Raman has in recent years received increasing attention in the study of adhesives and adsorbates in general. The difficulty here lies in achieving "surface enhancement" in a wide variety of samples. For the EXAFS experiments, the bulk Cl K-edge signal was minimized by grinding to small AP particle diameter. Indeed, there were some differences noted between the uncoated and coated AP samples as well as differences from one adsorbate to the next (although the data analysis is incomplete). However, the glancing angle discussion applies equally well here. Also, electron yielded detection would also enhance the surface sensitivity. At the time of the National Synchrotron Light Source (NSLS) experiments, this apparatus was not available for use by the CWRU researchers.

To summarize, the techniques that showed the most promise for the study of the AP/binding agent interaction were the Cl K-edge EXAFS and Raman scattering. The adsorption process created noticeable differences from the neat AP. It is believed that XRD and IRAS would have been equally as useful if the proper geometries would have been available.

#### 4.0 RECOMMENDATIONS

Although the ultimate goal of this phase of the project was not met, valuable experience was gained in the application of several spectroscopic techniques to the study of intrapropellant interactions and adhesion. As the propulsion community enters different propulsion areas, the nature and identity of the two components studied here will change. The fundamental importance of the interface between different components of a composite structure however will remain. For materials of similar physical characteristics to AP and the various bonding agents, the techniques of SXRD, IRAS, Raman, and EXAFS are recommended for use.



## 5.0 REFERENCES

1. "Solid Propulsion Integrity Program (SPIP) Bondline Work Package 4.0 Annual Report 1990," NAS8-37802, NASA Marshall Space Flight Center, Huntsville AL, May 1991.
2. I. Davis, M. Hawkins, K. Jensen, R. Kunz, J. Sinclair, *Propellant/Case Interface Technology*, PL-TR-94-3006, Vols. 1 and 2, Thiokol Corporation, Brigham City UT, December 1994.
3. J.J. Rusek, *Proceedings of the Second Annual Advanced Polymer Components Symposium*, PL-TR-92-3018, Vols. 1 and 2, Air Force Astronautics Laboratory, Edwards AFB, CA, July 1992.
4. J. J. Rusek, *Advanced Polymer Components*, PL-TR-95-3034, Vols. 1 and 2, October 1995.
5. "Solid Propellant Ingredients Manual," CPIA/M3, Unit #1, pp. 3
6. H.P. Klug, L.E. Alexander, X-ray Diffraction Procedures for Amorphous and Polycrystalline Materials, John Wiley and Sons, 1954, pp. 111-160.
7. G. Ertl, J. Küppers, "Low Energy Electrons and Surface Chemistry," *Verlag Chemie*, 1974, Chapter 9.
8. D.P. Woodruff, T.A. Delchar, Modern Techniques of Surface Science, Cambridge University Press, 1986, various chapters.
9. J. Weier, H. Strauss, " $\text{NH}_3\text{D}^+$  Ions in Ammonium Perchlorate: The N-D Stretching Bands of Different Sites," *J. Chem. Phys.* **98** (6), 15 March 1993, pp. 4437-4445.
10. H. Prask, C. Choi, N. Chesser, "Ammonium Perchlorate Structure and Dynamics at Low Temperatures," *J. Chem. Phys.* **88** (8), 15 April 1988, pp. 5106-5122.
11. T. Chakraborty, S. Khatri, A. Verma, "Temperature Dependent Raman Study of Ammonium Perchlorate Single Crystals: The Orientational Dynamics of the  $\text{NH}_4^+$  Ions and Phase Transitions," *J. Chem. Phys.* **84** (12), 15 June 1986, pp. 7018-7023.
12. C. Choi, H. Prask, "Crystal Structure of Ammonium Perchlorate at 298, 78, and 10°K By Neutron Diffraction," *J. Chem. Phys.* **61** (9), 1 November 1974, pp. 3523-3529.
13. J. McClelland, "Photoacoustic Spectroscopy," *Analytical Chemistry* **55** (1), January 1983, pp. 89a-96a.

14. the reader is directed toward the excellent review:

D. Koningsberger, R. Prins, eds., "X-ray Absorption: Principles, applications, techniques, of EXAFS, SEXAFS and XANES," John Wiley and Sons, 1988.

15. Value calculated using computer program written by P. Bandyopadhyay in 1985 and modified by K. Chaffee. The program uses data from:

W. McMaster, N. Grande, J. Mallet, J. Hubbel, "Compilation of X-ray cross sections," University of California, Livermore, Report UCRL 50174.

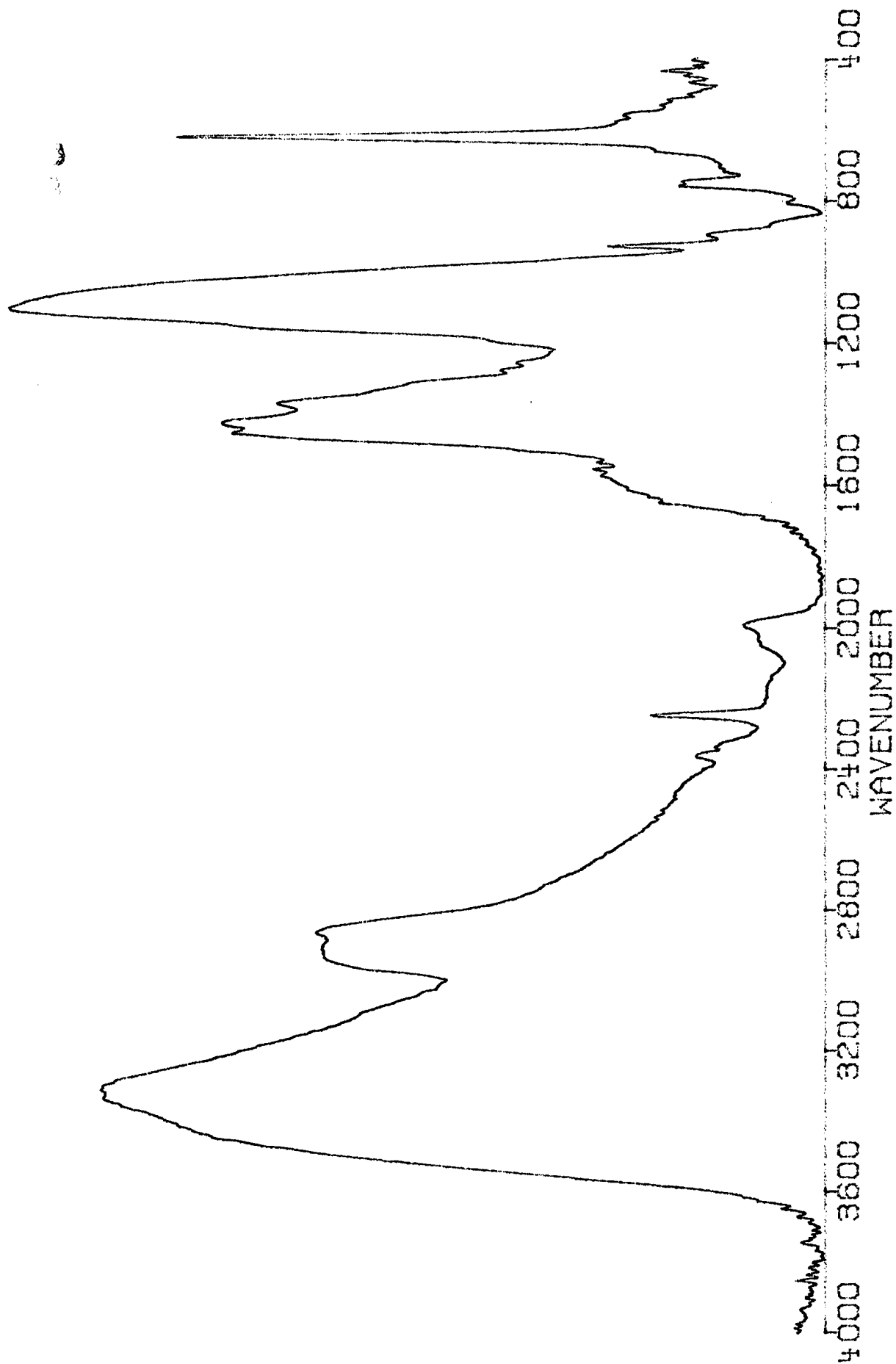
16. J Rehr, R Albers, S Zabinsky, "Higher order multiple scattering calculations of x-ray absorption fine structure," *Phys. Rev. Letters* **69** (23), 7 December 1992, pp. 3397-3400.

18. J. Deleon, J. Rehr, S. Zabinsky, R. Albers, "Ab initio curved wave x-ray absorption fine structure," *Phys. Rev. B-Condensed Matter* **44** (9), 1 September 1991, pp. 4146-4156.

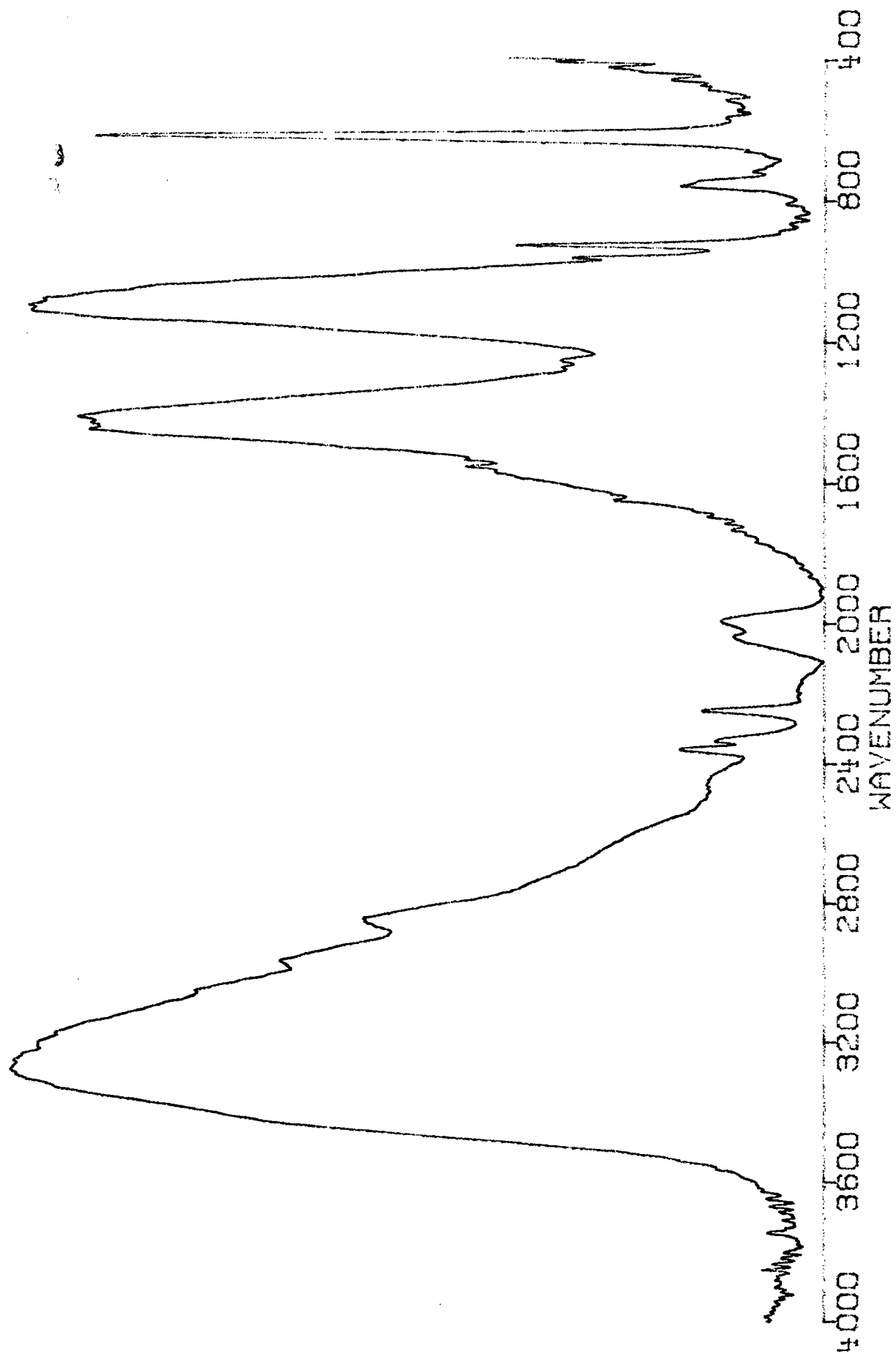
16. J. Rehr, J. Deleon, S. Zabinsky, R. Albers, "Theoretical x-ray absorption fine structure standards," *J. of the Am. Chem. Soc.* **113** (14), 3 July 1991, pp. 5135-5140.

**APPENDIX A**  
**Additional FTIR and Raman Data**

TEPANOL ON AP - PAS



TEPAN ON AP --PAS



Mode : 1 accu. | CCD

Laser : 647.1 (nm) | 150 (mw)

Time (s) : 0050.00

Remark : AP (single crystal) with DEA on about 30 min.

DILOR

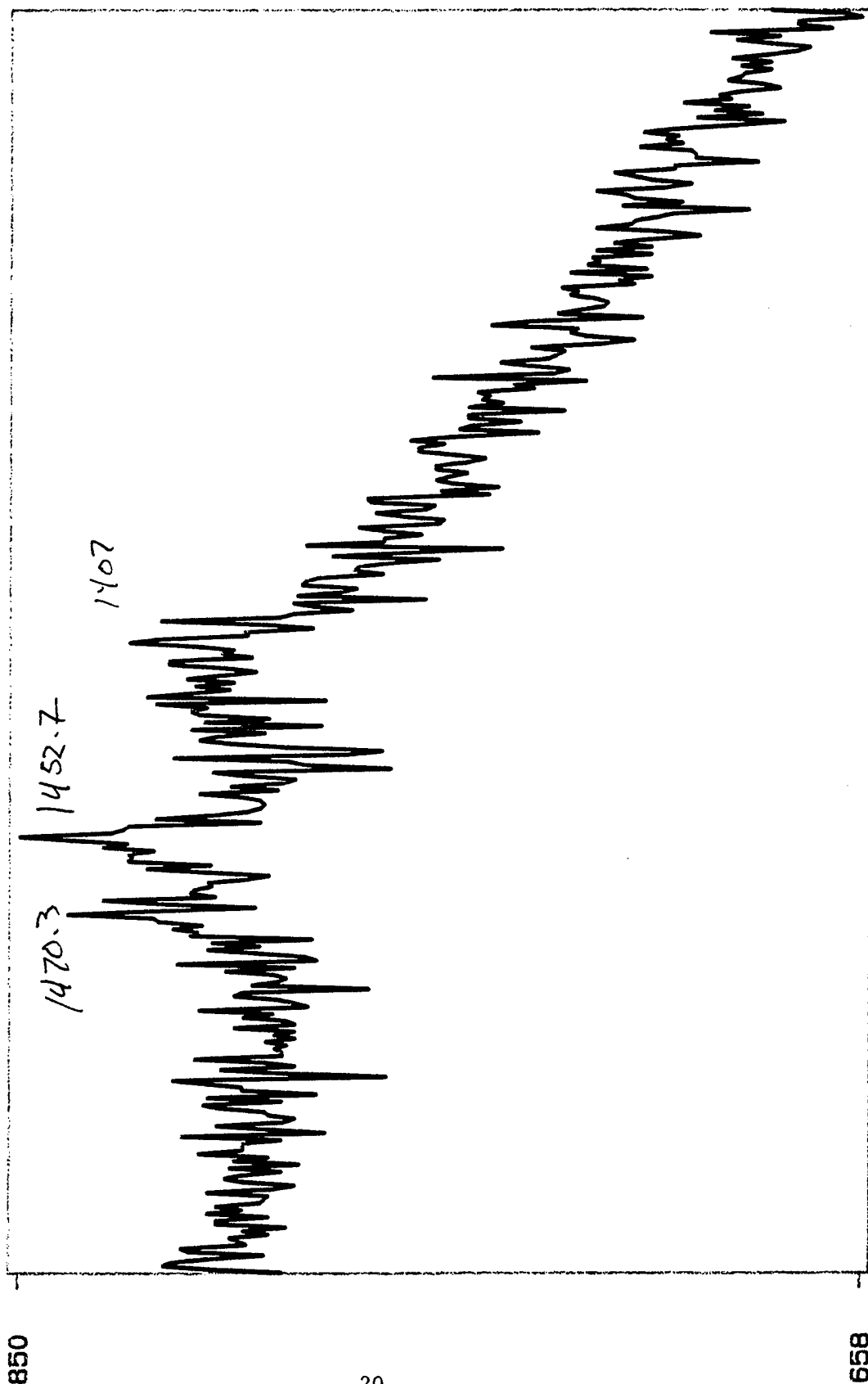
XY

Sample :

AP w/DEA

Filename :

c: \yx\JR\KC1191.804



850

658

1500

1400

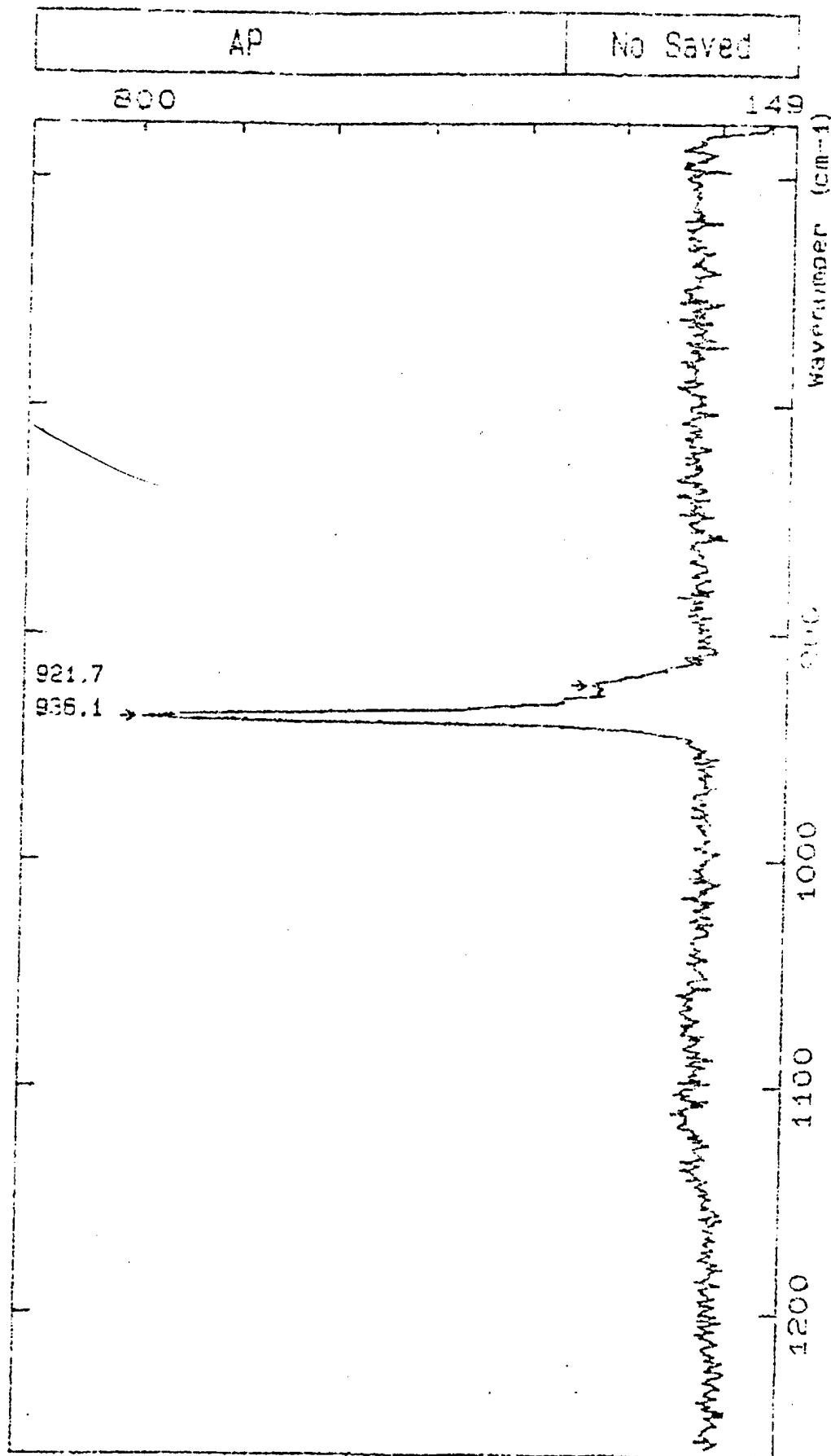
1300

Wavenumber. (cm-1)

APPLICATIONS LAB D.I.L.O.R. Version 2.00 IBM
DILOR XY

OPERATOR YW  
 DATE 29/ 12/ 1999  
 SAMPLE AP  
 GRATING 1800  
 MODE MULTICHANNEL  
 REMARK: t=10sec.

EXCITATION (nm) 647.1  
 LASER POW. (mW) 20  
 FOREMONO. (cm-1) 1100.0 FILTER  
 SPECTRO. (cm-1) 1100.0 INTEGRATION TIME (s) 0010.00  
 SLIT WIDTH (um) 300 NUMBER OF ACCUMULATIONS 1

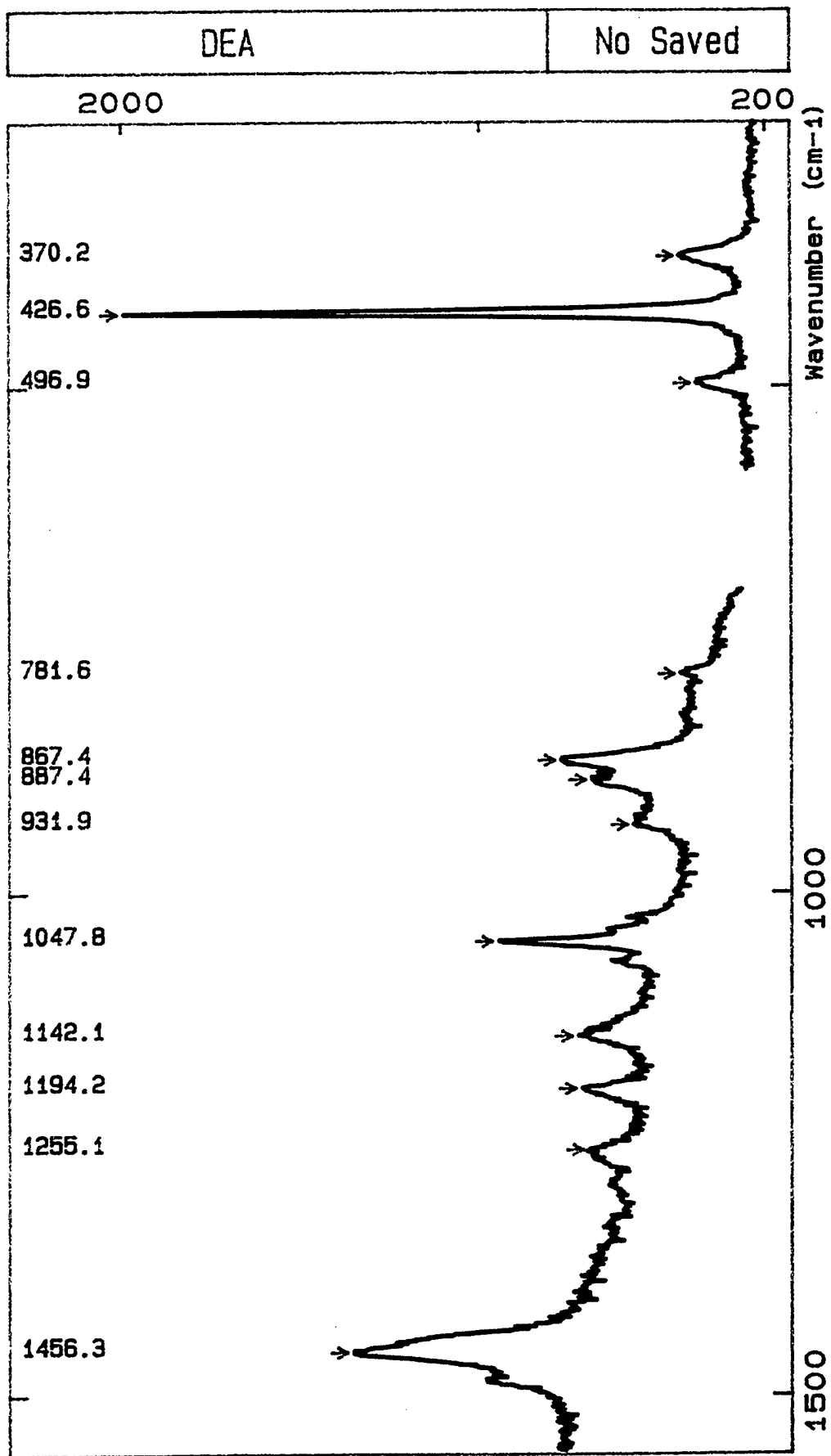


APPLICATIONS LAB D.I.L.O.R. Version 2.00 IBM
DILOR XY

OPERATOR Yaxin  
 DATE 21| 11| 1991  
 SAMPLE DEA  
 GRATING 1800  
 MODE MULTICHANNEL  
 REMARK: Neat

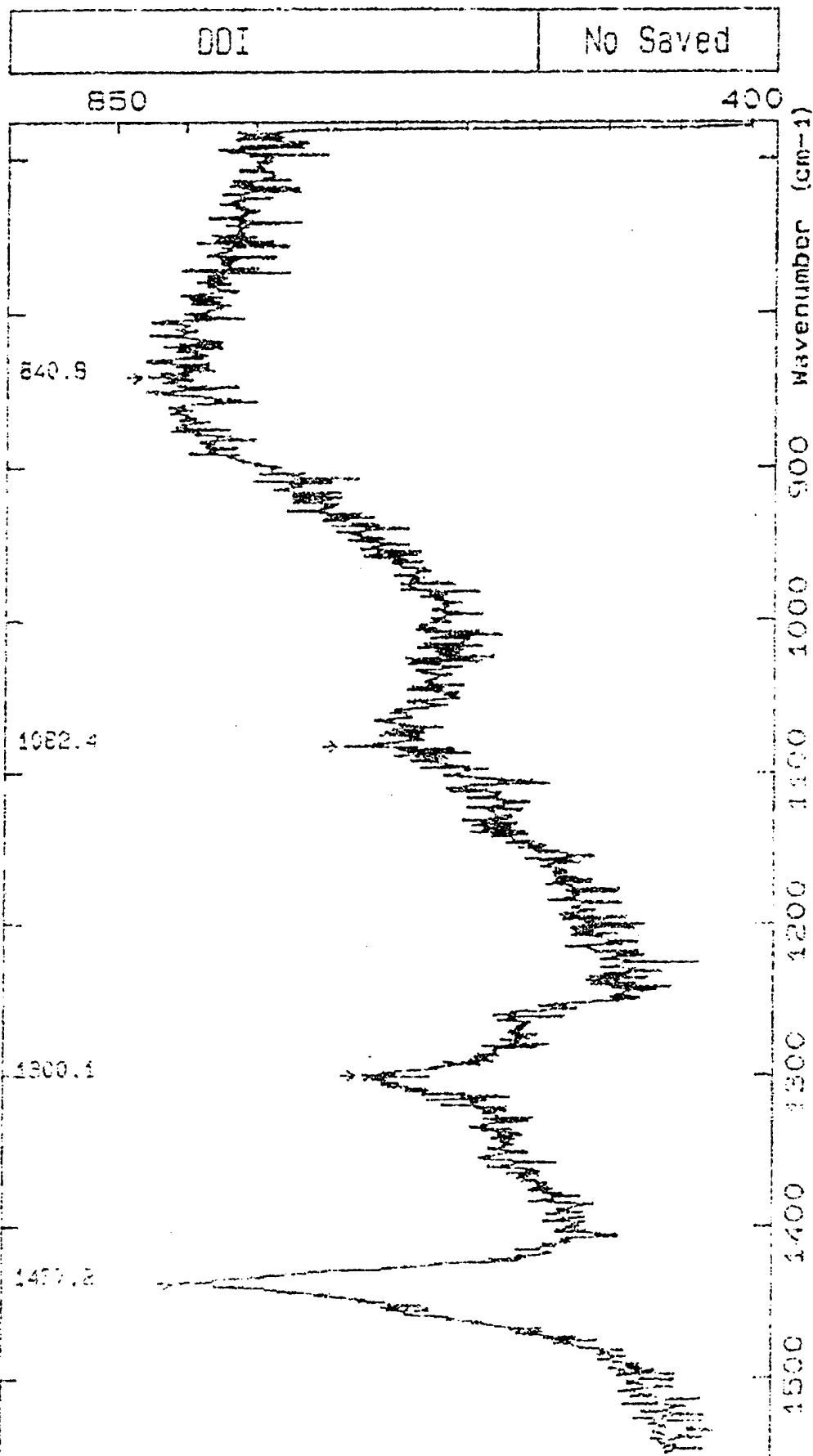
EXCITATION (nm) 647.1  
 LASER POW. (mW) 100  
 FOREMONO. (cm-1) 1400.0  
 SPECTRO. (cm-1) 1400.0  
 SLIT WIDTH (um) 100

SPECT.SLIT WIDTH (cm-1) 2.924  
 DETECTOR (nbr of diodes) 512  
 INTEGRATION TIME (s) 0010.00  
 NUMBER OF ACCUMULATIONS 1

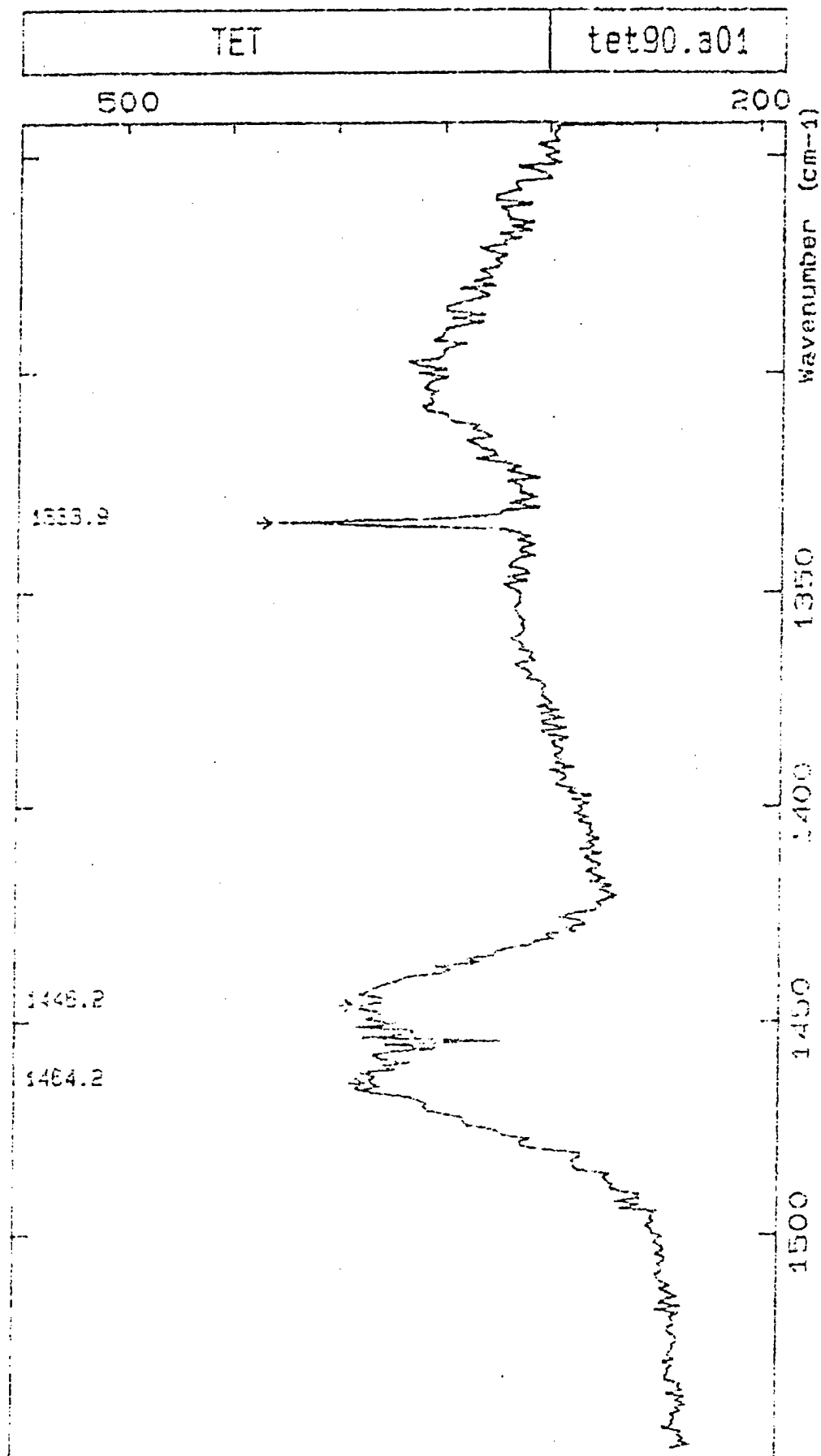


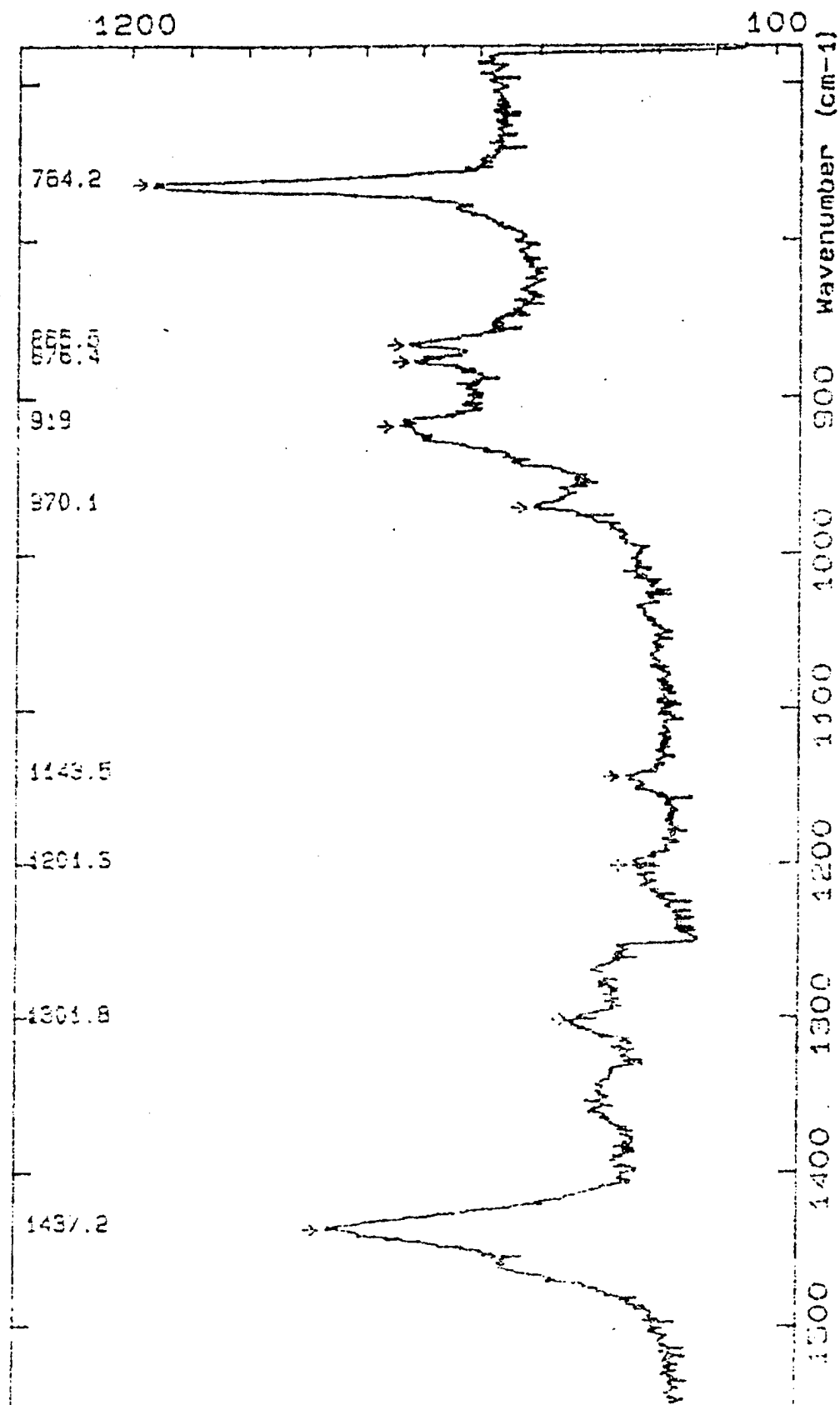


Discontinue



Tetraglycyl Tetra...





DILOR

XY

Sample :

AP w/EDA

Filename :

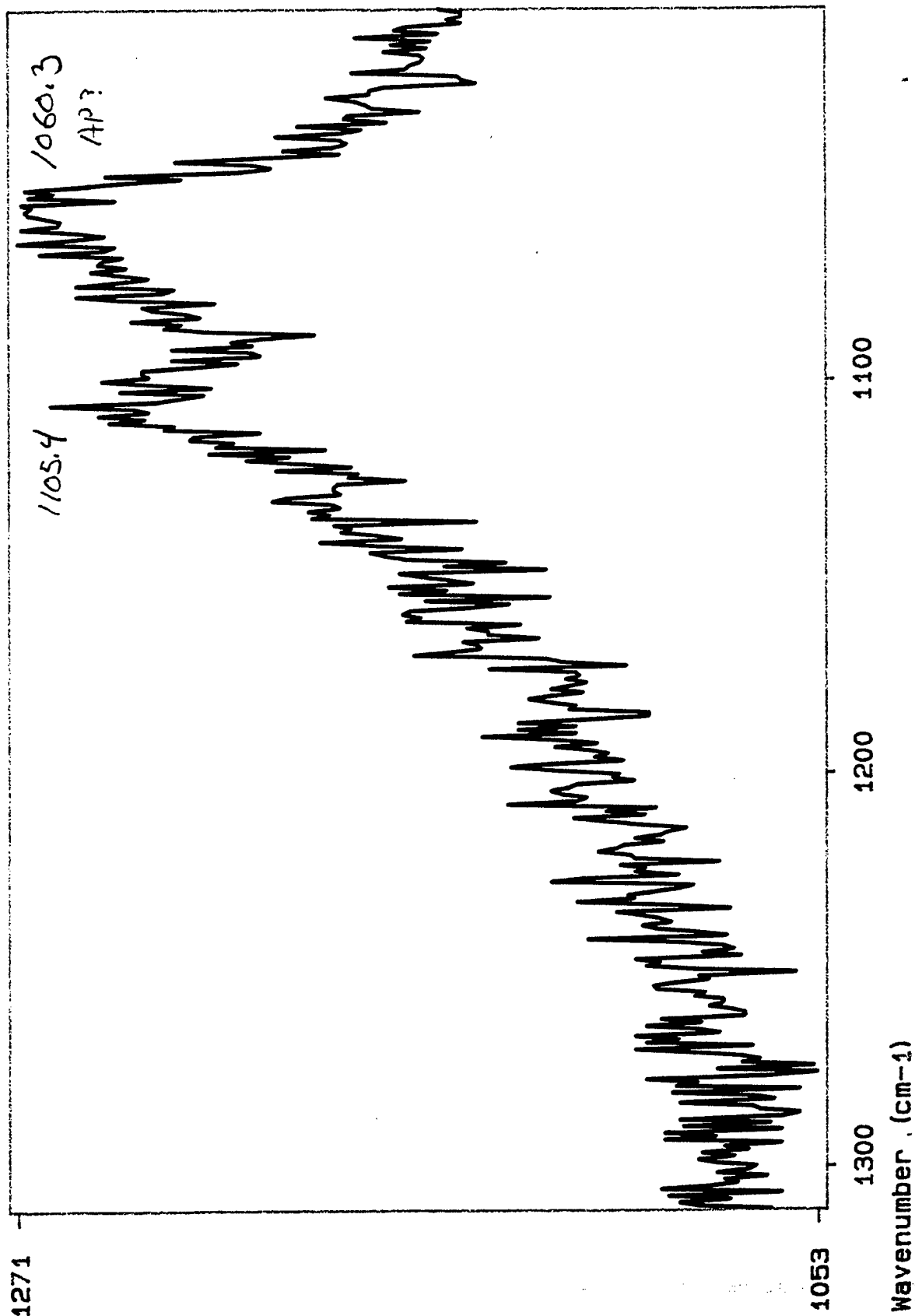
c: \yx\jr\KC1191.603

Laser : 647.1 (nm) | 130 (mw)

Mode : 1 accu. | CCD

Time (s) : 0060.00

Remark : AP with EDA on overnight



DILOR

XY

Sample :

AP w/EDA

Filename :

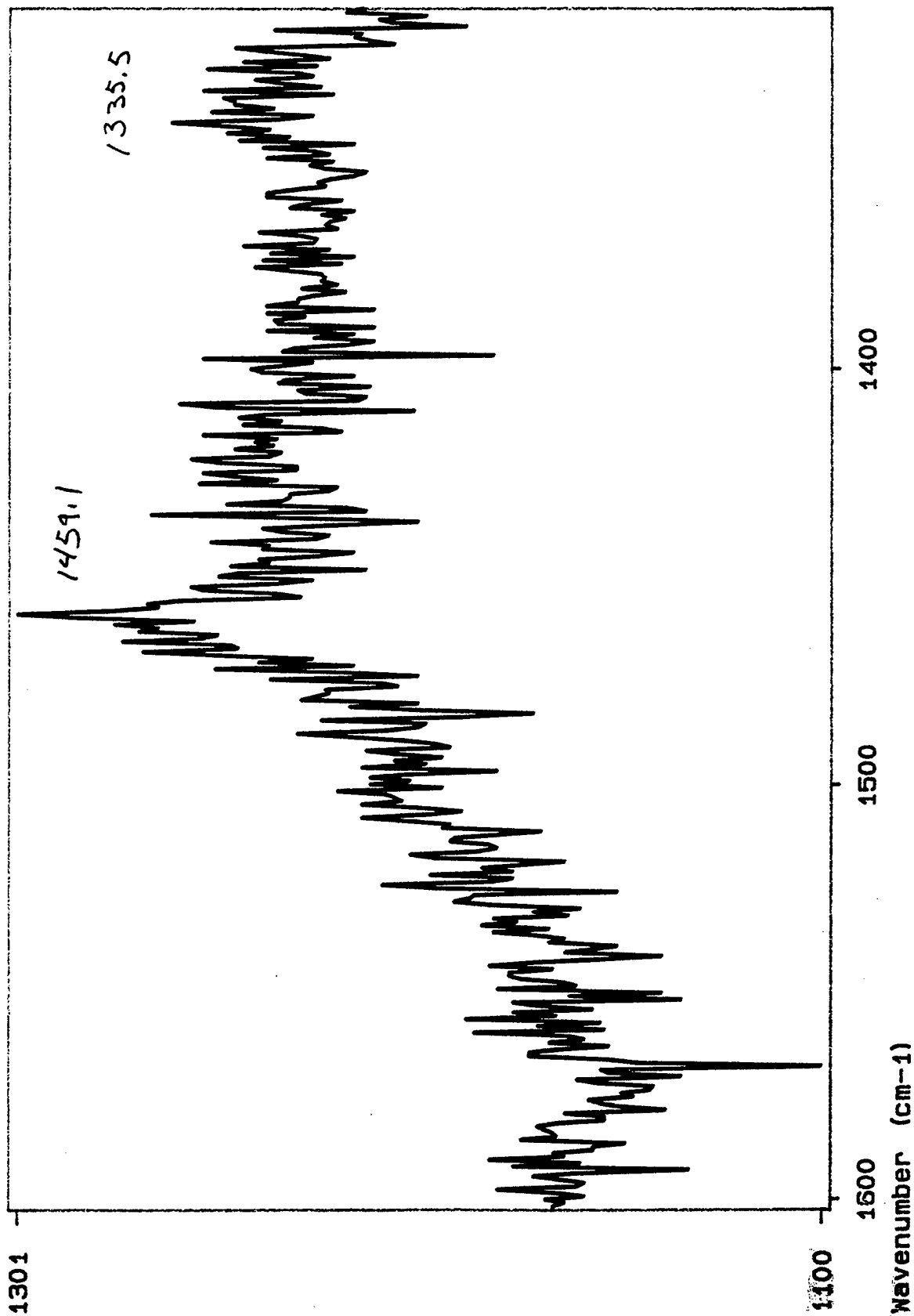
c:\yx\jr\KC1191.602

Laser : 647.1 (nm) | 130 (mw)

Mode : 1 accu. | CCD

Time (s) : 0060.00

Remark : AP with EDA on overnight



DILOR

XY

Sample :

AP w/TET

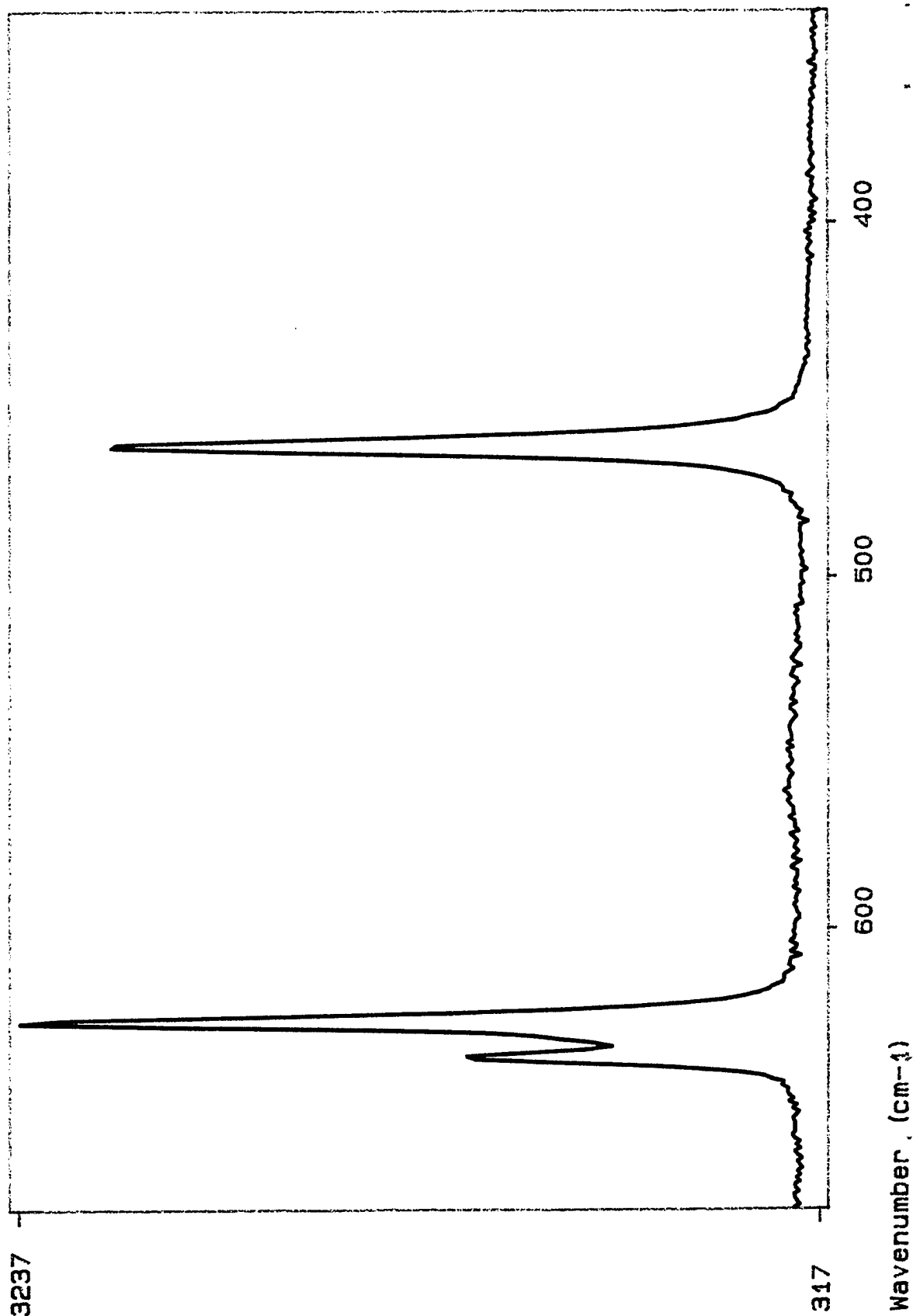
Filename :

c: \yx\JP\KC1191.706

Mode : 1 accu. | CCD Laser : 647.1 (nm) | 150 (mw)

Time (s) : 0030.00

Remark : AP (single crystal) with TET on about 90 min.



DILOR

XY

Sample :

AP w/TET

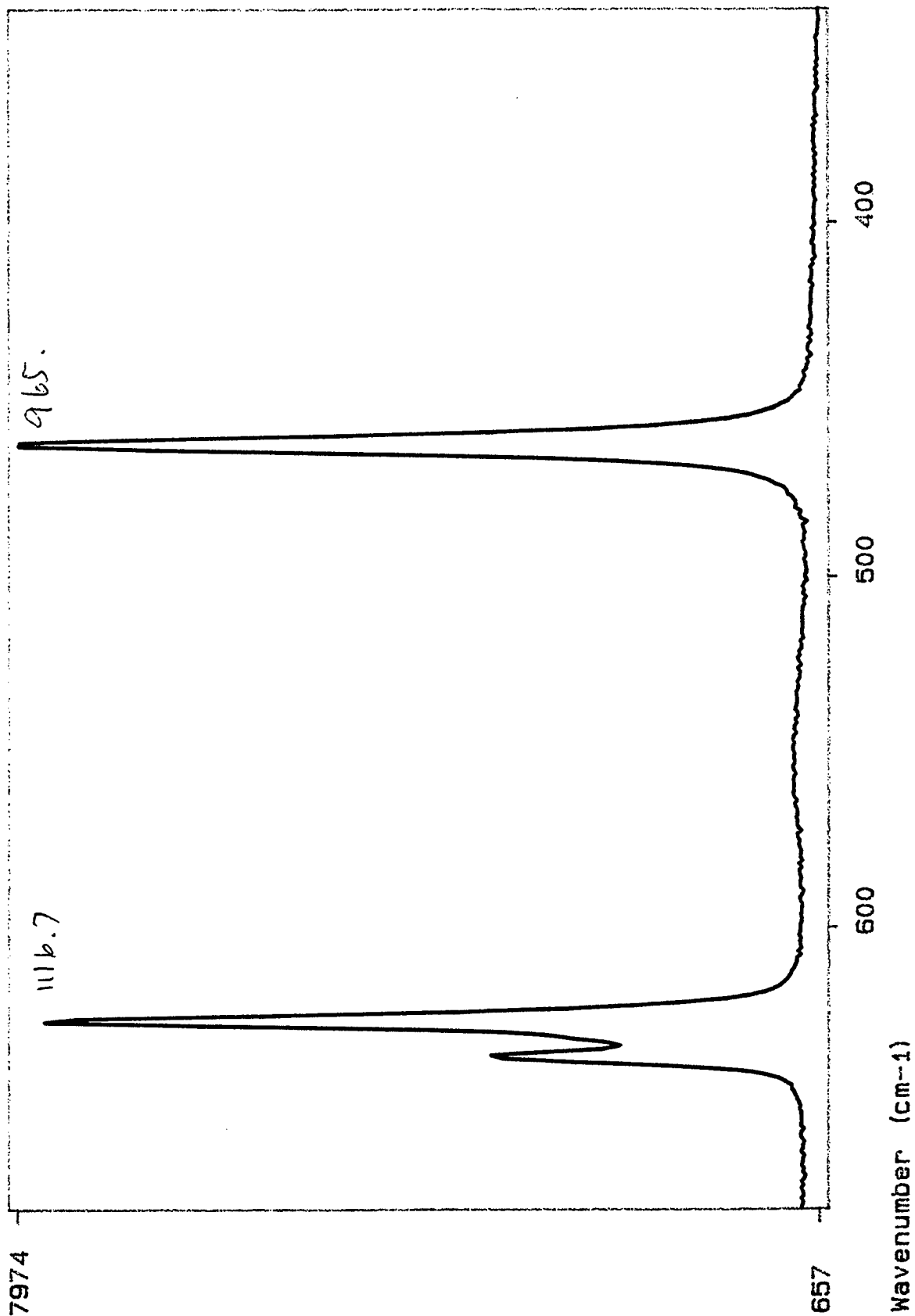
Filename :

c:\yx\JR\KC1191.702

Mode : 1 accu. | CCD Laser : 647.1 (nm) | 150 (mw)

Time (s) : 0060.00

Remark : AP (single crystal) with TET on, 40 minutes



DILOR

XY

Sample :

AP w/DEA

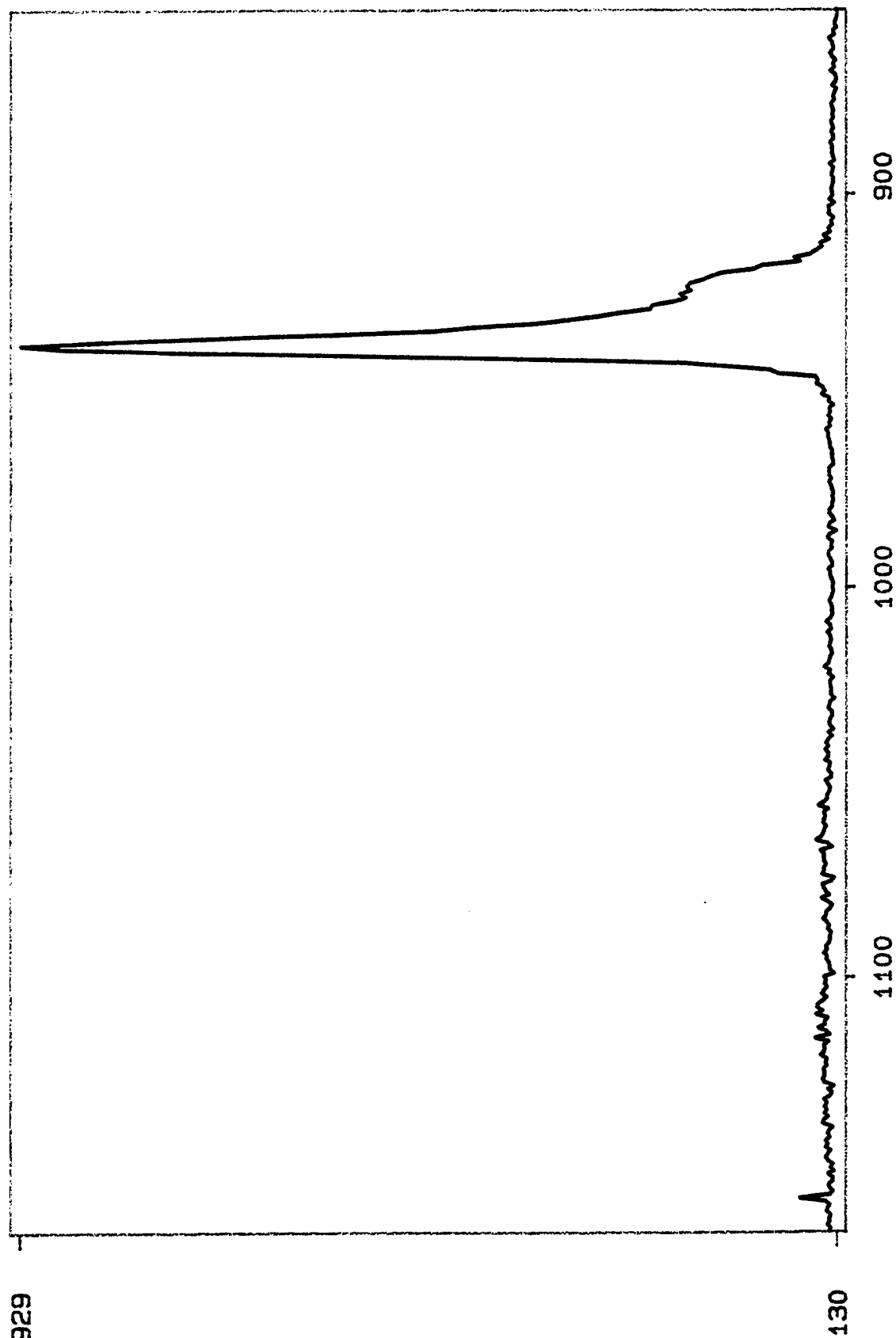
Filename :

c: \yx\JR\KC1191.801

Mode : 1 accu. | CCD Laser : 647.1 (nm) | 150 (mw)

Time (s) : 0010.00

Remark : AP (single crystal) with DEA on about 30 min.



Wavenumber (cm-1)

↑ Phase 3 peaks decreased in Pol. ampl.  
shown with data will be in this spectrum



DILOR

XY

Sample :

AP w/DEA

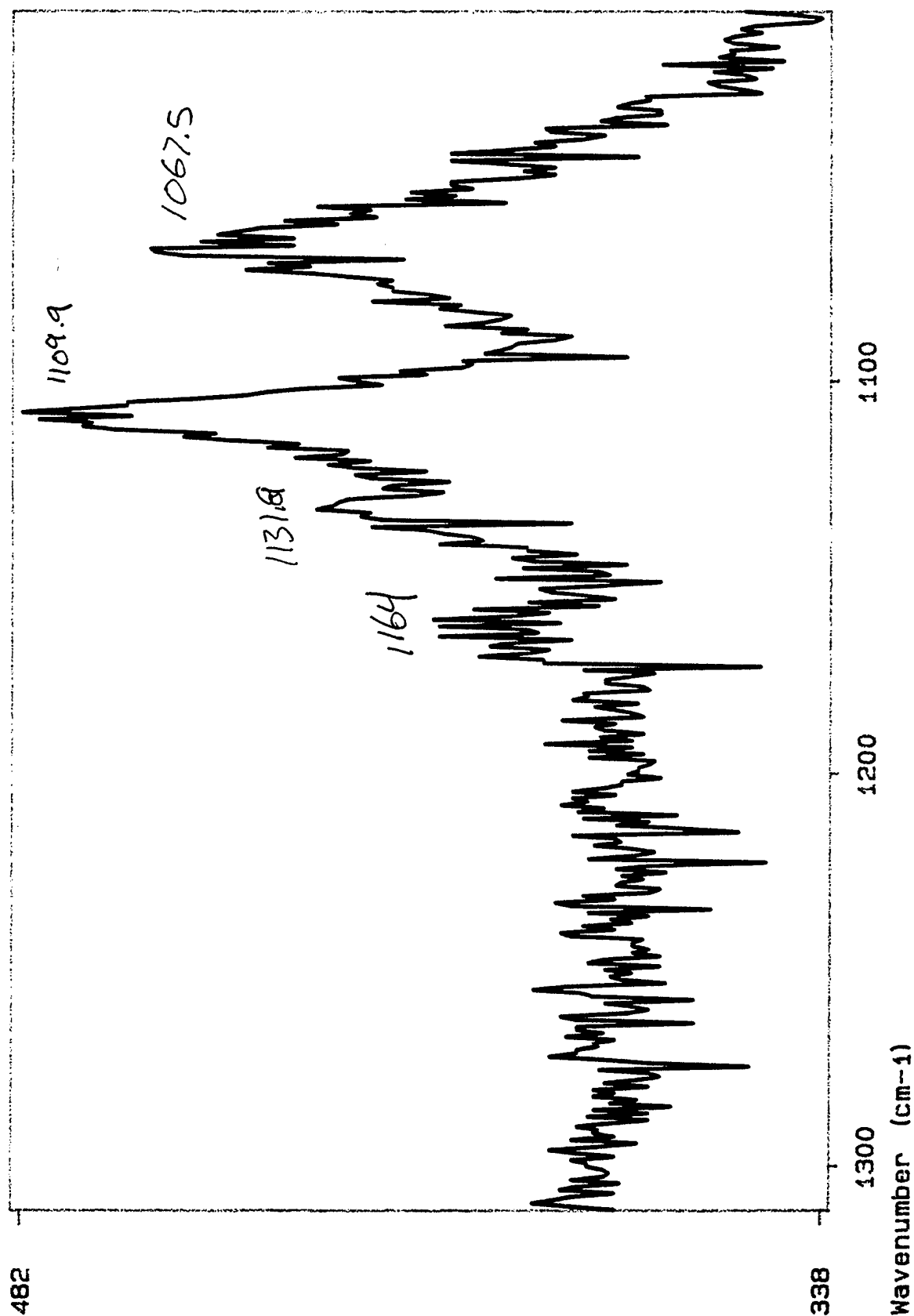
Filename :

c:\yx\JR\KC1191.803

Mode : 1 accu. | CCD Laser : 647.1 (nm) | 150 (mw)

Time (s) : 0030.00

Remark : AP (single crystal) with DEA on about 30 min.



DILOR

XY

Sample :

AP w/DEA

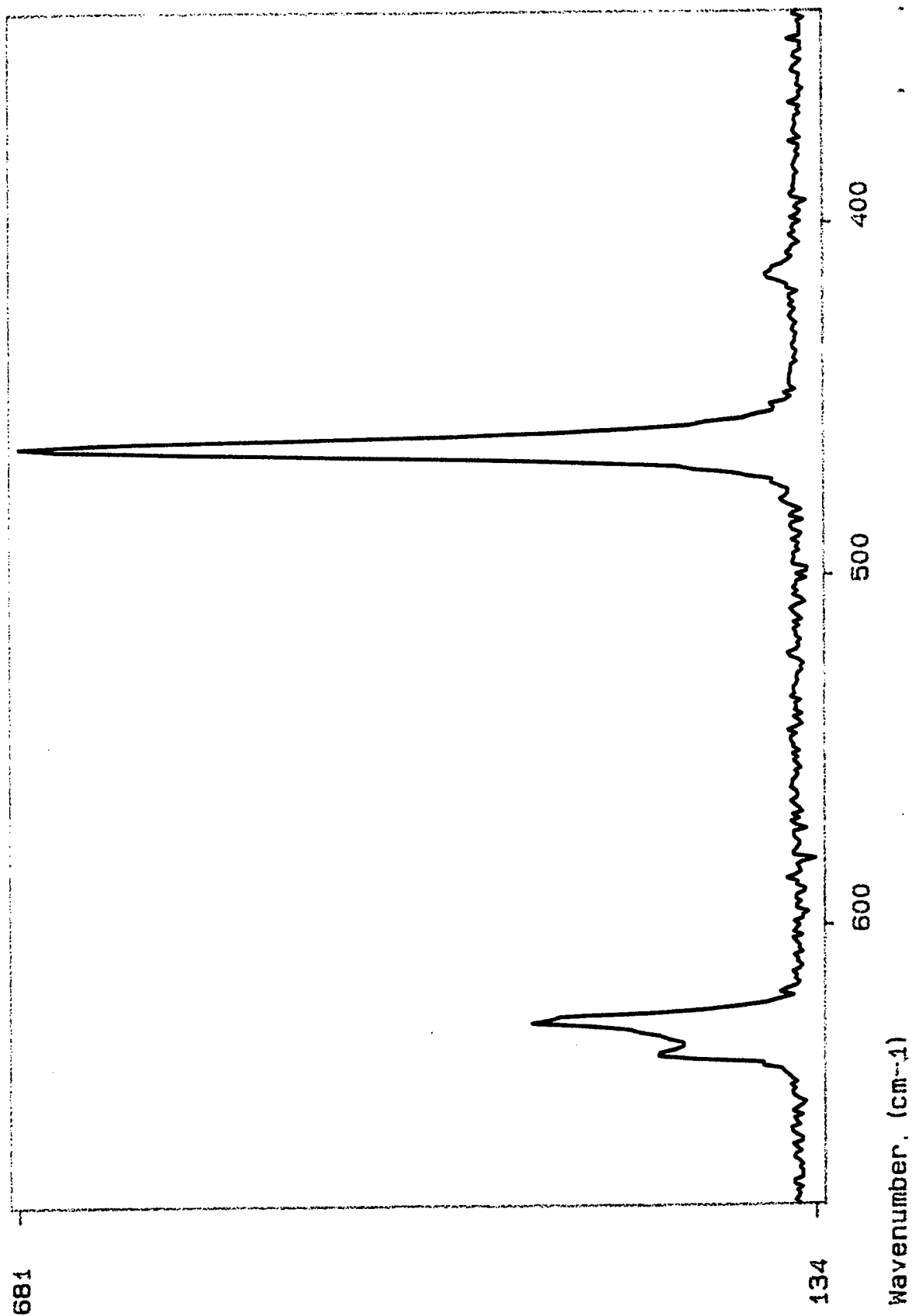
Filename :

c:\yx\JA\KC1191.802

Mode : 1 accu. | CCD Laser : 647.1 (nm) | 150 (mw)

Time (s) : 0010.00

Remark : AP (single crystal) with DEA on about 30 min.



DILOR

XY

Sample :

AP w/TET

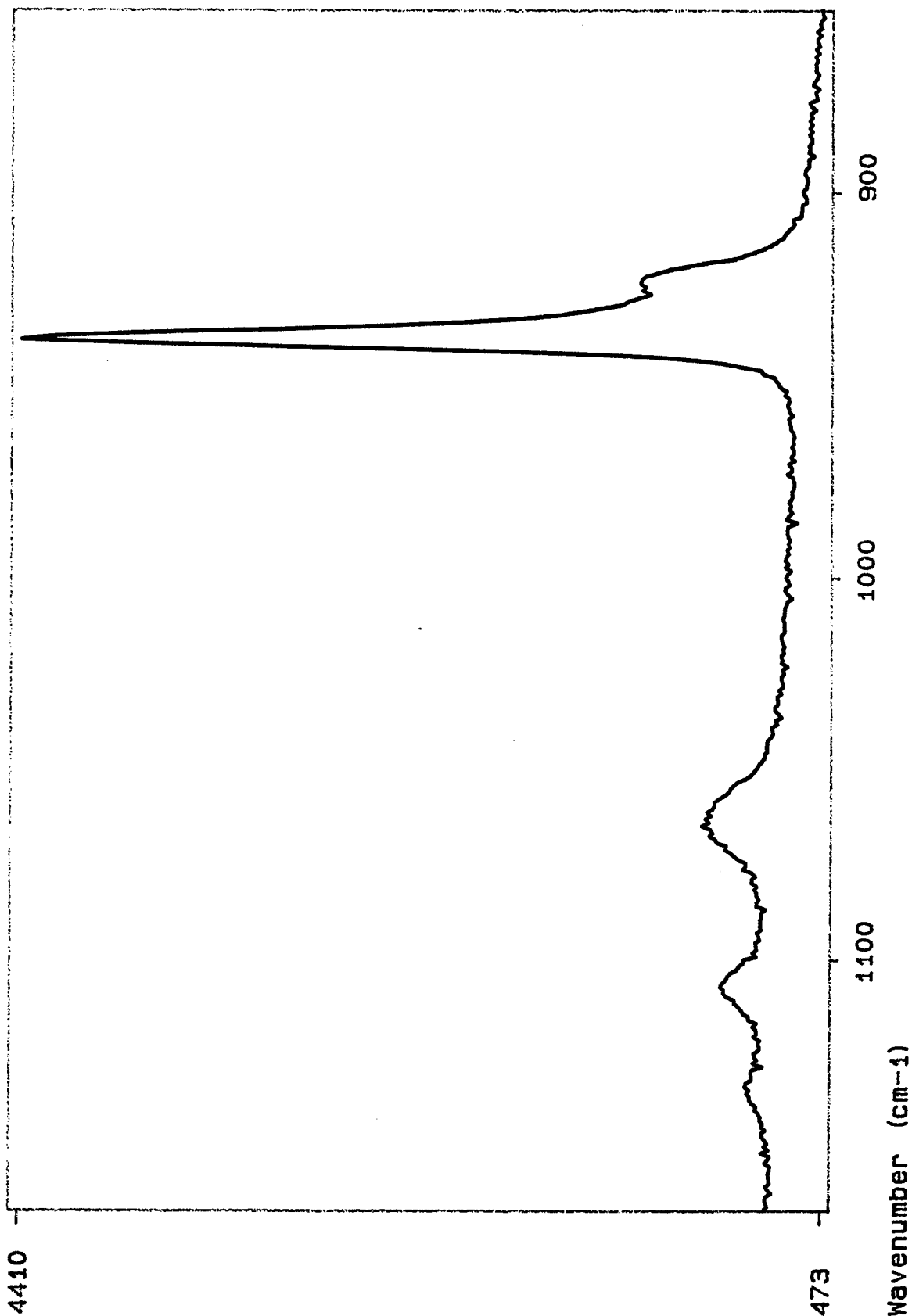
Filename :

c:\yx\JR\KC1191.705

Mode : 1 accu. | CCD Laser : 647.1 (nm) | 150 (mw)

Time (s) : 0030.00

Remark : AP (single crystal) with TET on about 90 min.



DILOR

XY

Sample :

AP w/TET

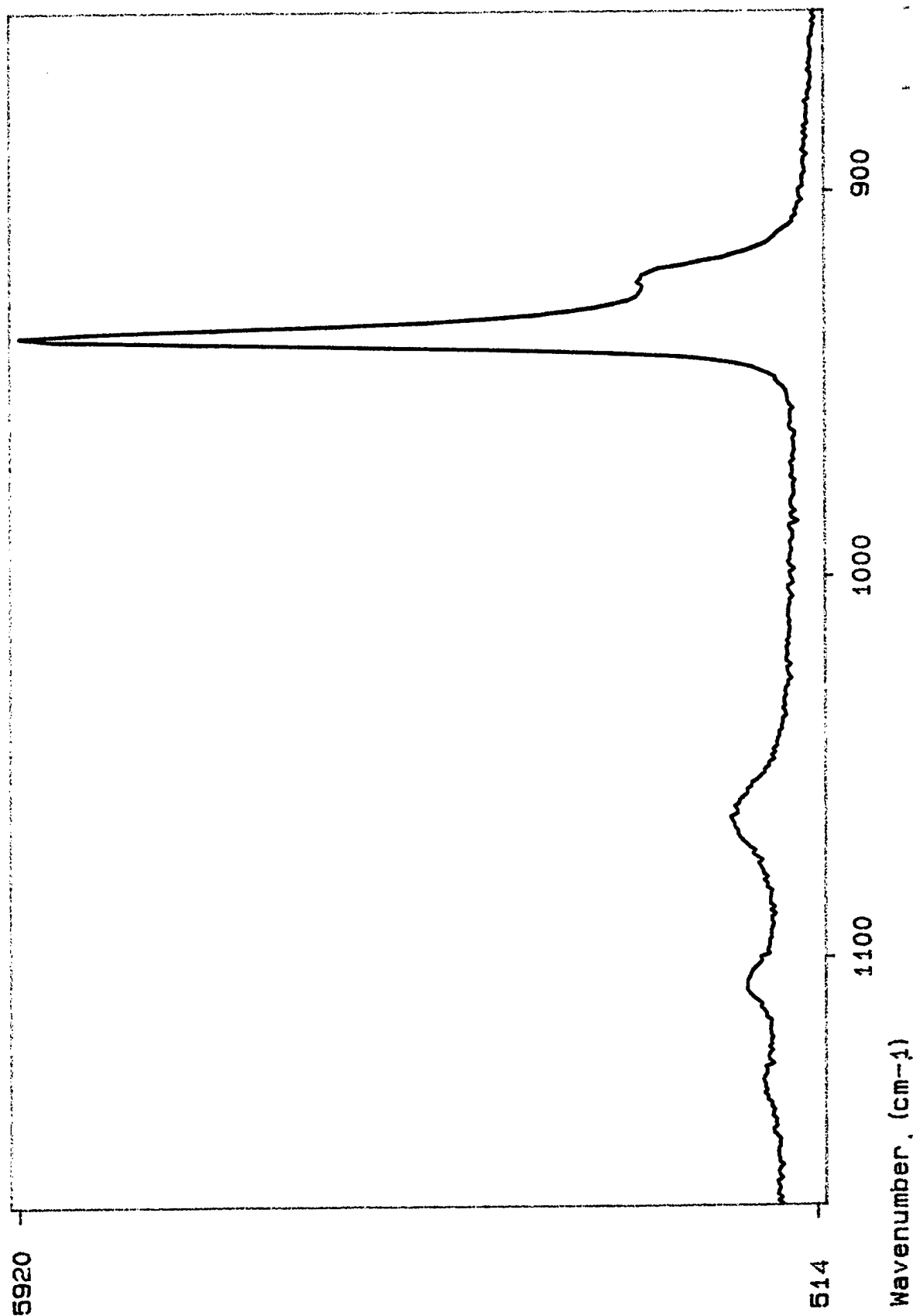
Filename :

c:\yx\JR\KC1191.703

Mode : 1 accu. | CCD Laser : 647.1 (nm) | 150 (mw)

Time (s) : 0030.00

Remark : AP (single crystal) with TET on, 60 minutes



DILOR

XY

Sample :

AP w/TET

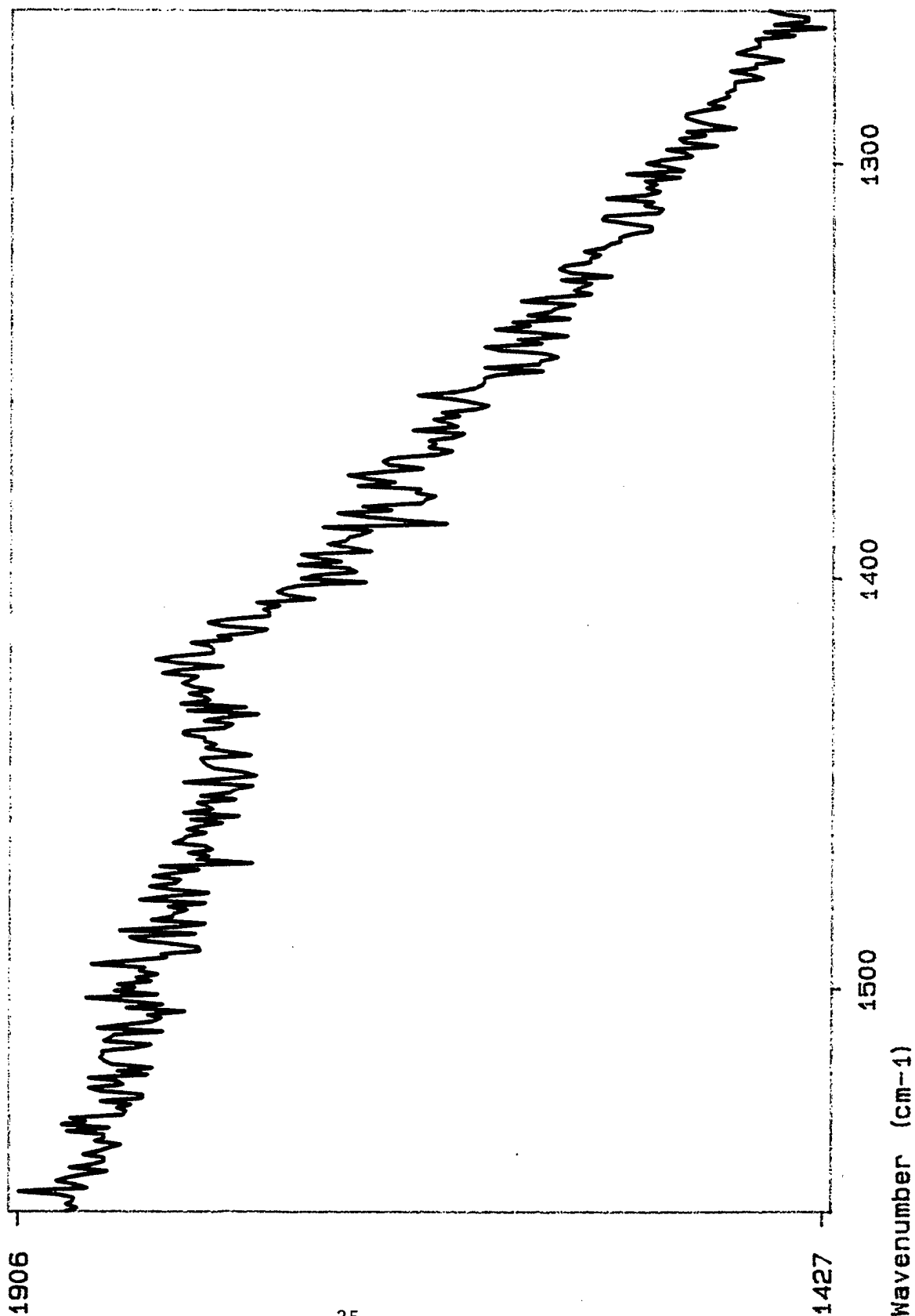
Filename :

c:\yx\JR\KC1191.704

Mode : 1 accu. | CCD Laser : 647.1 (nm) | 150 (mw)

Time (s) : 0060.00

Remark : AP (single crystal) with TET on, 60 minutes



DILOR

XY

Sample :

EDA

Filename :

c:\yx\JF\KC1191.303

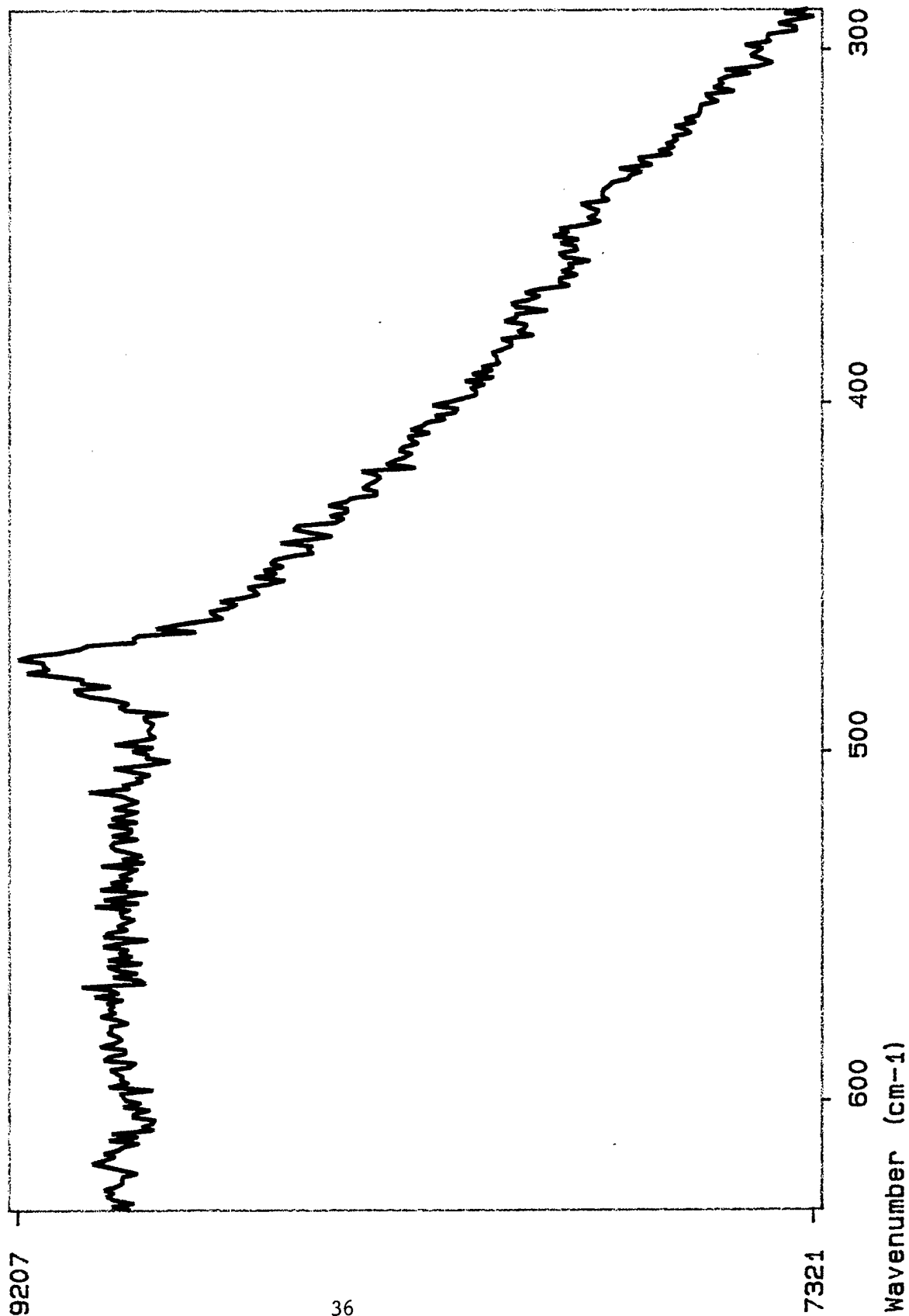
Laser : 647.1 (nm) | 100 (mw)

Mode : 1 accu. | CCD

Time (s) : 0010.00

Remark : Neat

4-75.0



DILOR

XY

Sample :

EDA

Filename :

c: \yx\JR\KC1191.302

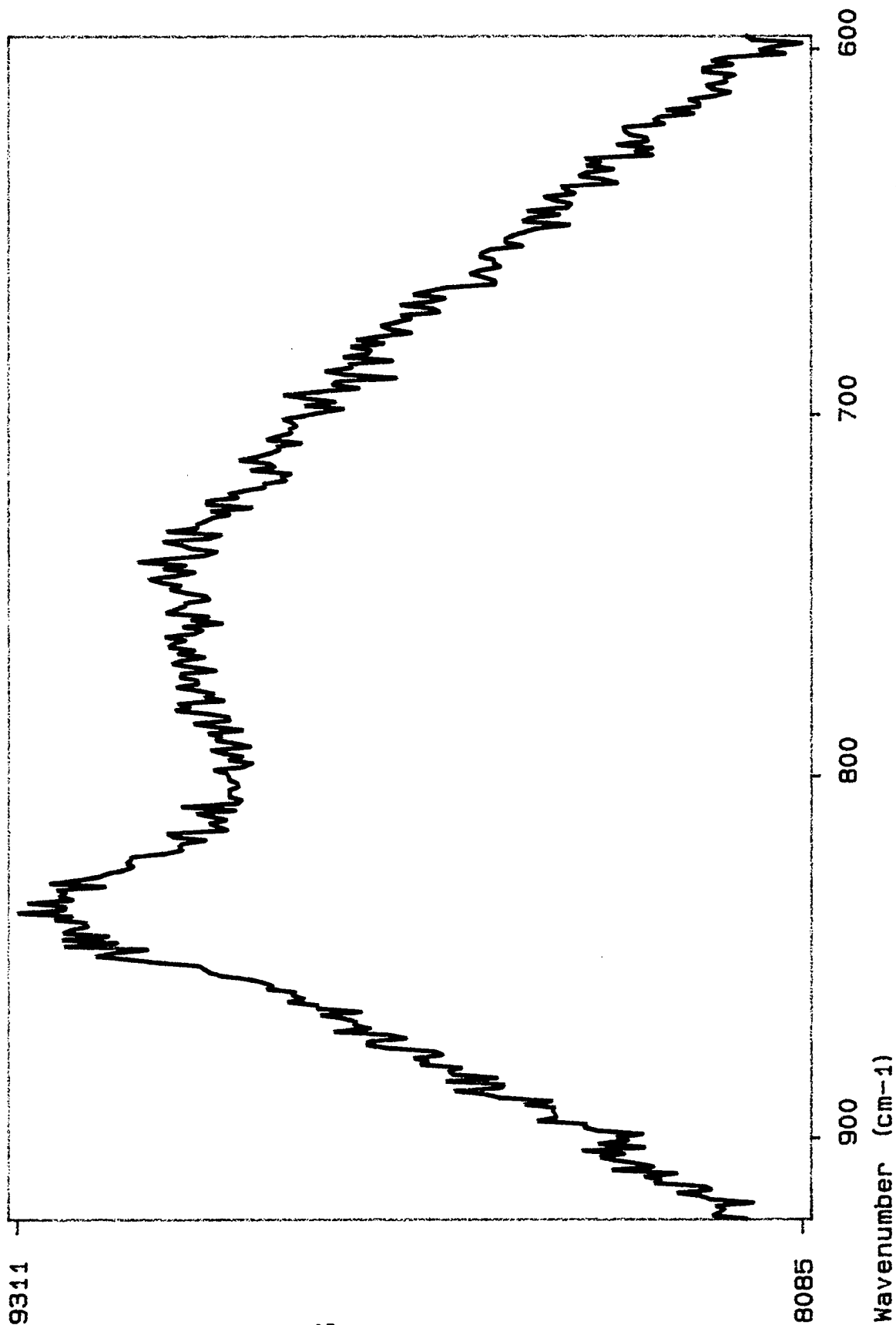
Laser : 647.1 (nm) | 100 (mw)

Mode : 1 accu. | CCD

Time (s) : 0010.00

Remark : Neat

544.3



DILOR

XY

Sample :

EDA

Filename :

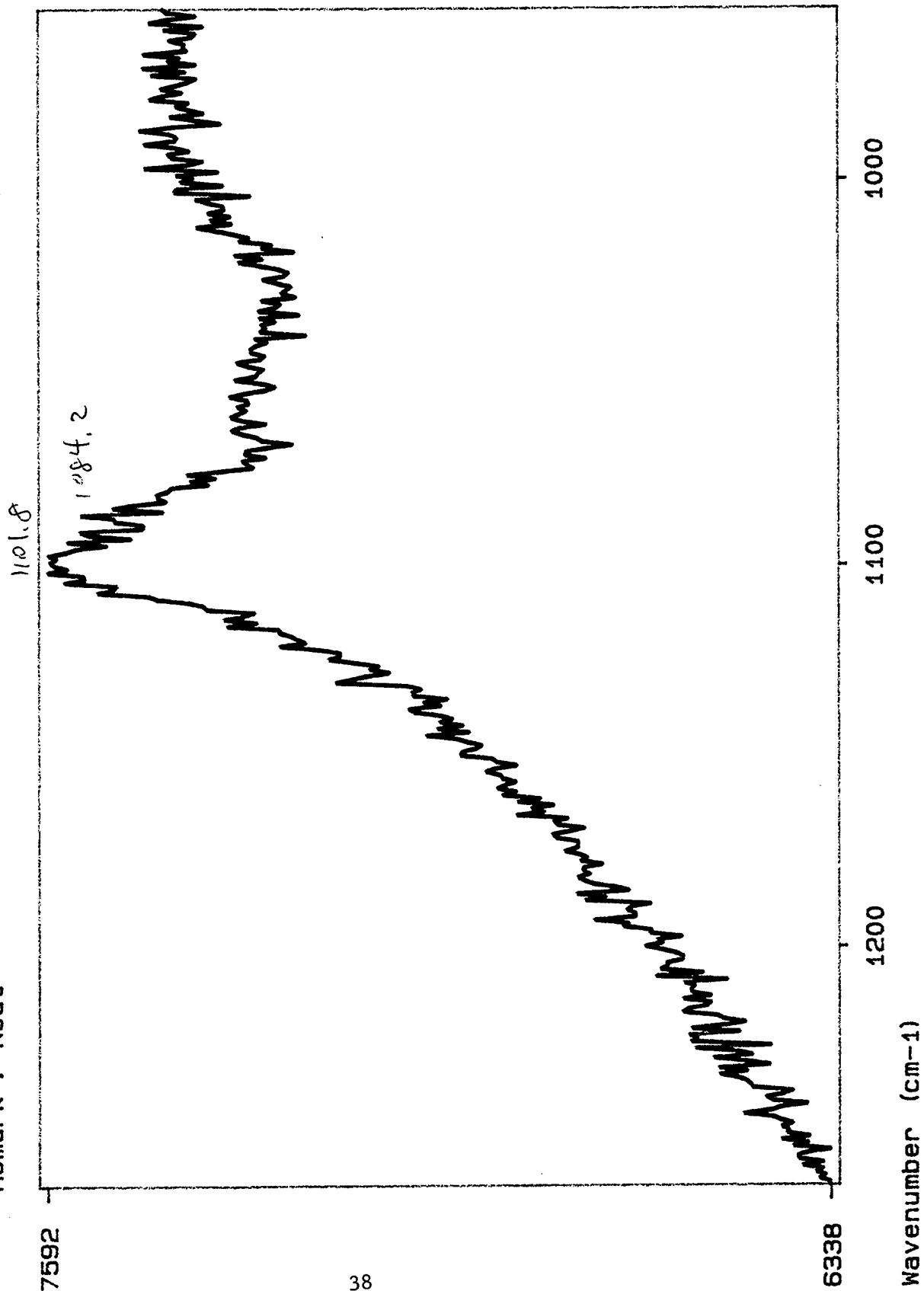
c: \yx\JR\KC1191.301

Laser : 647.1 (nm) | 100 (mw)

Mode : 1 accu. | CCD

Time (s) : 0010.00

Remark : Neat





DILOR

XY

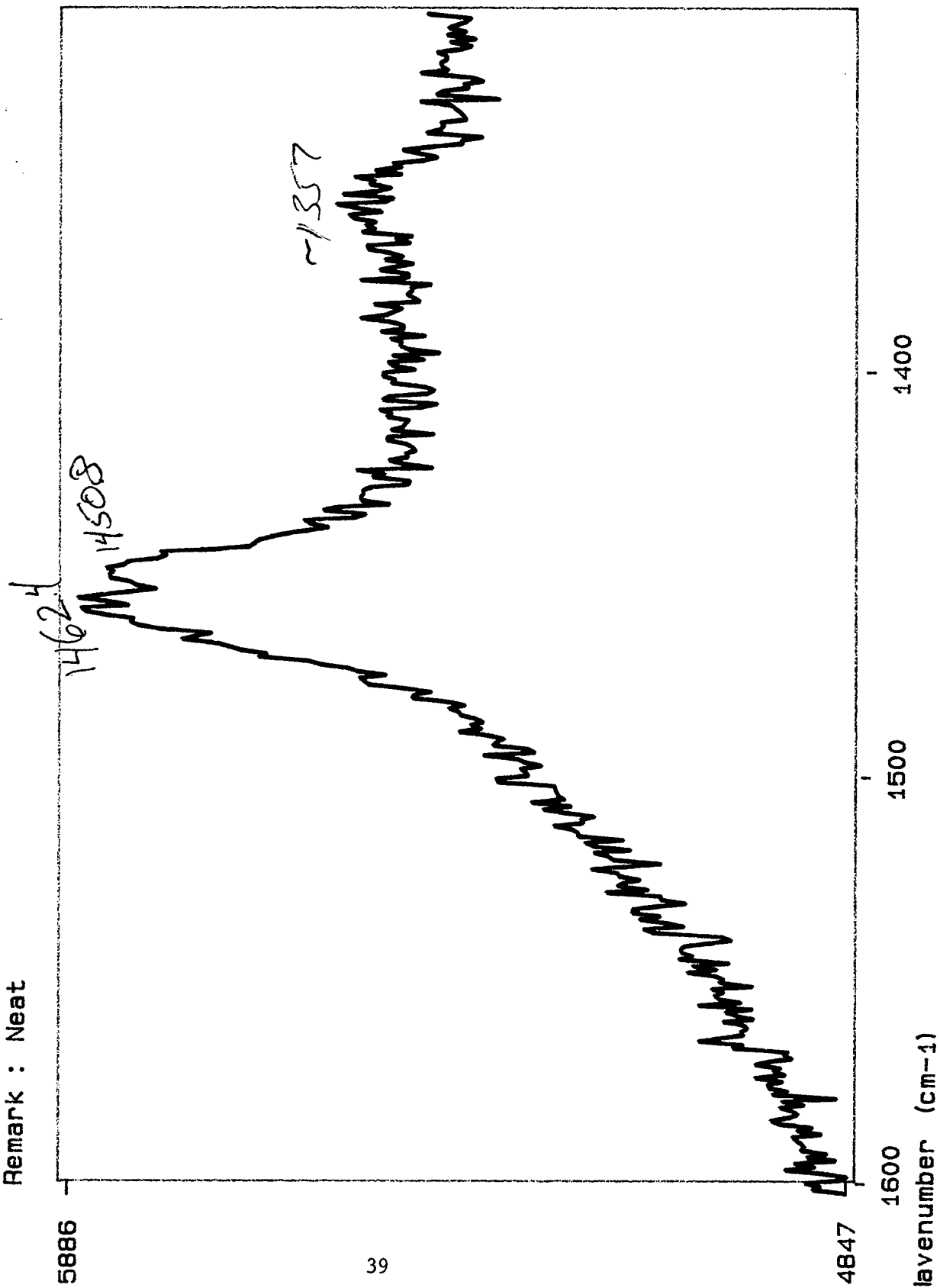
Sample :

EDA

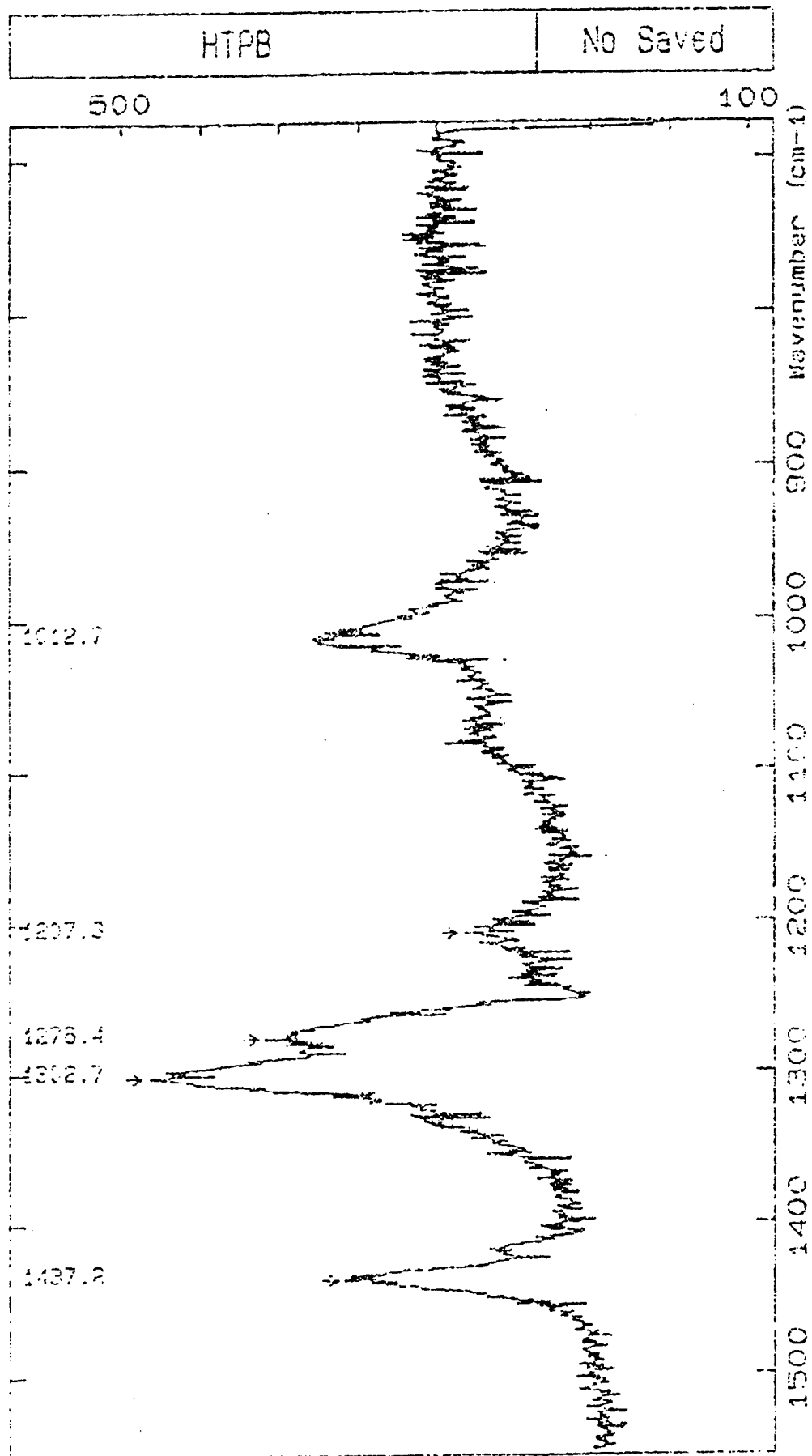
Filename :

c: \yx\JR\KC1191.300

Mode : 1 accu. | CCD  
Time (s) : 0010.00  
Remark : Neat  
Laser : 647.1 (nm) | 100 (mw)



4-pyridyl terminated  
polybutadiene



**APPENDIX B**  
**Dr. Hoffman/CWRU Reports**

**XAFS Analysis of Propellant Materials**  
**RDL Final Report**

by  
Guy A. DeRose  
employee number 398

Summer, 1991

## ABSTRACT

The technique of X-ray Absorption Fine Structure (XAFS) spectroscopy was used to determine local structure and short range order at the Cl K-edge in rocket fuel oxidizers - namely ammonium perchlorate (AP) - , oxidizer/binder systems, and new polymer materials of vital interest to the Air Force. Data was collected at the National Synchrotron Light Source, Brookhaven National Laboratory and analyzed at the Phillips Laboratory, Edwards Air Force Base. This Faculty/Graduate Student Summer research Project also resulted in the acquisition, by the Air Force, of state-of-the-art analysis programs for reducing EXAFS (Extended XAFS) data to a reportable form. Theory of XAFS and a detailed description of the analysis procedure is presented herein, along with limitations of the single-scattering formalism as applied to near-edge structure and suggestions for future work.

## INTRODUCTION

Extended X-ray Absorption Fine Structure (EXAFS) spectroscopy, the modulation of the absorption coefficient above an absorption edge, has found wide ranging application in solving structural problems in recent years. EXAFS spectroscopy is a very useful tool for studying complex or dilute systems whose structures cannot be determined by conventional x-ray diffraction techniques.

Post-absorption edge fine structure was first observed by Kronig<sup>1</sup> on 1931, but it wasn't until the 1970's that the short range order theory was fully worked out.<sup>2,3</sup> These new theoretical developments, coupled with the emergence of dedicated synchrotron radiation sources for x-ray absorption spectroscopies in general, have led to the transformation of EXAFS from a laboratory curiosity available to a very small group of scientists, to a widely available, quantitative tool for structural investigation.

This technique is well suited for studying the structure of rocket fuel oxidizers such as ammonium perchlorate in various local environments and new advanced polymer component materials currently of interest to the Air Force, as a thorough, quantitative understanding of the chlorine-local structure of these complex systems is required for consistent device fabrication.

## THEORY OF EXAFS

The oscillatory structure of the absorption coefficient is attributed to the scattering of the photoelectron emitted due to the absorption of the incident x-ray by the atoms surrounding the absorbing atom. By comparing experimental data with theory and/or model compounds, information about the local ( $\sim 5\text{\AA}$ ) structure of a material can be obtained with a high degree of accuracy ( $\sim 0.01\text{\AA}$ ). By comparing the structures obtained for the various binders in the oxidizer/binder system, a very detailed body of information about the oxidizer's local structure can be constructed.

It has been determined<sup>3,4</sup> that for energies sufficiently high above the absorption edge ( $\geq 50\text{eV}$ ) the single scattering approximation adequately describes the structure. An additional simplification also manifests itself in this region, namely the plane wave approximation. The EXAFS oscillations, following the single-scattering and outgoing plane wave approaches, are given for K-edges as a function of photoelectron wave number  $k$  by<sup>4</sup>

$$\chi(k) = \sum_j \frac{N_j}{kR_j^2} |f_j(k, \pi)| e^{-2\sigma^2 k^2} e^{\frac{-2R_j}{\lambda}} \sin(2kR_j + \delta_j(k)) \quad (1)$$

where  $N_j$  is the number of equivalent scatterers of type  $j$  at a mean distance  $R_j$  from the absorber,  $f_j(k, \pi)$  is the (energy dependent) backscattering function,  $e^{-2\sigma^2 k^2}$  is a Debye-Waller term describing thermal disorder,  $e^{-2R_j/\lambda}$  is a term which accounts for inelastic scattering effects over the photoelectron mean free path  $\lambda$ , and  $\sin(2kR_j + \delta_j(k))$  is the interference term, where  $\delta_j(k)$  is the (energy dependent) phase shift. The photoelectron wave number,  $k$ , is given by

$$k = \left( \frac{2m}{\hbar^2} (E - E_c) \right)^{\frac{1}{2}} \quad (2)$$

where  $m$  is the mass of the electron,  $\hbar$  is Planck's Constant divided by  $2\pi$ ,  $E$  is the incident x-ray energy, and  $E_0$  is the edge energy.

## EXPERIMENTAL PROCEDURE

As the experimental setup, sample preparation, data collection, and associated complexities are described in detail in the report of the faculty half of this faculty/graduate student team, namely Professor R. W. Hoffman, the reader is directed to that work for details. All data for this experiment was collected in the fluorescence mode on beamline X19-A at the National Synchrotron Light Source, Brookhaven National Laboratory between 7 and 13 August, 1991. A pictorial description of a "typical" synchrotron XAFS experimental layout and fluorescence detector is given in Figure 1.

## DATA ANALYSIS

Many complications may hinder one's progress towards quantitative analysis of EXAFS. One must be very careful when stating results to include some particulars about how the analysis was performed. The procedure used here can be divided into two main parts. The first includes the initialization and background removal to obtain normalized EXAFS oscillations. This normalized data can then be analyzed by the theory developed above. The second major step in the analysis extracts the parameters of interest. The analyst has several tools at his disposal for this part of the analysis. These include: Fourier Transform (FT) and Fourier filtering to get radial structure functions, direct comparison of EXAFS spectra, isolation of single shells, and curve fitting or calculation.



## PRELIMINARY ANALYSIS

### INITIALIZATION

The programs used in this study to analyze the data were FORTRAN codes developed over the course of about a decade. They enable one to analyze data from many different synchrotron radiation (SR) beamlines by putting the data into a standard format. After the raw data has been initialized, the analysis proceeds without regard to the origin of the particular data set. A plot of a fluorescence spectrum of AP is shown in Figure 2(A).

### PRE-EDGE SUBTRACTION

Below the absorption edge of interest, the measured background contains contributions from several sources, such as Compton scattering and other (lower energy) absorption edges. It is useful, especially for near-edge studies, to remove this pre-edge background. This is done by fitting the data below the edge to a suitable function and extrapolating to the end of the data set. It is found that a quadratic pre-edge function is a good approximation to this background for transmission, and for fluorescence even a linear function will suffice<sup>5</sup>. Usually this curve is fit between two points in the data set; the first "good" point and the point at which the absorption edge begins to occur. It is possible for the analyst to specify both of these points. This is especially useful when comparing several spectra at the same absorption edge to provide consistency in the analysis. The curve from Figure 2(A) is shown in Figure 2(B) with the pre-edge function overplotted.

### EDGE ENERGY DETERMINATION

Even though the EXAFS technique is relatively insensitive to the absolute

energy calibration of the monochromator it is useful, again to maintain consistency, to define a threshold energy  $E_0$ . This is done by mathematically determining the inflection point in the absorption edge spectrum. When analyzing materials with different chemical or crystallographic compositions it is useful to use the same number for  $E_0$  for the entire group. Therefore, one lets the computer program determine the inflection point of the "pure" or "control" sample, and then manually assigns that number for  $E_0$  to subsequent samples. A plot showing the inflection point for AP X-ray Absorption Near-Edge Structure (XANES) appears in Figure 3(A). Figure 3(B) shows the fluorescence spectrum of AP with the pre-edge function subtracted.

## DEJUMPING

Sometimes one finds that the data contains absorption edges other than that or those of interest. This was the case in this study, due to the closeness of the chlorine k-edge (2823 eV) to that of argon (3205 eV). Since a typical EXAFS scan extends to approximately 1000 eV above the edge, this could cause a problem due to EXAFS arising from the other element(s). Fortunately, Ar is a noble gas and as such there is no fine structure above the edge, so this edge can be carefully "dejumped" or subtracted PRIOR to isolation of the EXAFS oscillations. Since the amplitudes of these features are larger than the EXAFS oscillations themselves at this energy, it is useful to dejump when possible to avoid contaminating the FT performed later. The Ar edge in an AP scan is shown in Figure 4(A) and the dejumping process is illustrated in Figure 4(B).

## BACKGROUND REMOVAL

The background above the edge is more complex than that below it, and must be carefully removed in order to properly normalize the data and later extract structural parameters. There are several methods for determining the

post-edge background function, and in this work the background is obtained as a cubic smoothing-spline approximant to the data<sup>4</sup>. This method, as well as the several others available to the general EXAFS community, depends on the background being slowly varying with respect to the EXAFS oscillations.

Two parameters may be varied by the user- one determines the smoothness of the fit and the other is an inverse weighting parameter. In practice the weighting parameter is held fixed at a small value to force the spline to go through the first data point and the smoothing parameter is varied. The smoothing parameter is varied by an iterative process by which one examines the FT and background derivative. Using a smoothing parameter that is too small will cause non-physical peaks at small radial distance  $R$  in the FT, while if the smoothing parameter is too large the oscillations in the background derivative will too closely follow the EXAFS.

The procedure is to visually compare plots of the FT and background derivative and determine what final value to use for the smoothing parameter. Also important is the  $k$ -range used in the FT. Usually one specifies the  $k$ -range to start at the first zero of  $\chi(k)$  and extend to a  $k$ -value dependent on the quality of the high- $k$  data. Plots showing the effect of varying the smoothing parameter on the FT and background derivative are shown in Figure 5.

## NORMALIZATION

After the background has been subtracted from the data, the next step is to normalize the EXAFS oscillations to enable meaningful comparison of spectra collected from different samples. This is done by choosing a point beyond the near edge structure region, and dividing each data point by the  $\chi$  value of the normalization point. When studying several samples of a given system it is important that the same energy value be used for each to maintain consistency.

Once the data has been normalized it must then be written in a form conducive to detailed Fourier analysis. This procedure writes only the normalized,

isolated EXAFS data into a file that can be read by a program that analyzes and fits the  $\chi$  data. Plots of the normalized  $\chi$  for AP and AP/TET are shown in Figure 6.

## FOURIER ANALYSIS AND EXTRACTION OF STRUCTURAL PARAMETERS

Once a careful preliminary analysis has been completed, detailed Fourier analysis and quantitative comparison may commence. It is well established<sup>2,7</sup> that the Fourier transform can be used to extract information from equation 1 since it is essentially a sum of sines and exponentials. The reason that it is possible to isolate data corresponding to different radial distances is that the sine term in equation 1 contains the strongest  $k$  dependence<sup>8</sup>.

There are several ways to extract information from equation 1, and the method(s) used for a given study will depend on what information is needed. Three well-known techniques are: curve fitting,  $\chi$  calculation and visual comparison. Often, two or more of these methods are used together. The program used in this part of the analysis enables one to overplot several EXAFS ( $\chi$ ) or Fourier transform (RSF) spectra, fit data to a reference material or theoretical information, and calculate EXAFS spectra given a reference material or theoretical information. This also includes Fourier filtering and backtransformation to isolate single shell data.

For a theoretical treatment one may use the calculated phase shifts and backscattering amplitudes of Teo and Lee<sup>9</sup> (plane wave approximation) or McKale *et al*<sup>10</sup> (full curved-wave formalism). This is particularly useful when a suitable reference compound is difficult or impossible to obtain, although one must particularly careful to properly normalize the data in this case. The use of reference materials for fitting or calculation is quite useful for comparing an unknown sample to a well-characterized standard. In addition to providing a reference for phase shifts and backscattering amplitudes, the use of model compounds allows the analyst to visually compare the experimental and

calculated or fitted data to the model.

## DISCUSSION AND CONCLUSIONS

### XANES ANALYSIS

Analysis of the XANES gives information about the density of unoccupied states near the edge. A major complication of XANES analysis is that the full matrix operators must be used and summation over *all* scattering paths is required, unlike EXAFS in which a single scattering process will suffice. It is apparent that most of the information contained in the interaction between AP and various binders is contained in the XANES region. This is a limitation of the present analysis process as well as the general XAFS community and should form an impetus for future work in this rapidly developing field.

### SUMMARY

A powerful experimental technique, that of X-ray Absorption Fine Structure spectroscopy and analysis, was added to the list of in-house capabilities available at Phillips Laboratory OLAC for the investigation of a new set of materials of vital interest to the Air Force. As well as providing computer programs for performing the data analysis chlorine K-edge XAFS was shown, for the first time, in oxidizers and a new class of synthesized polymers. An X-ray fluorescence spectrum for a newly synthesized polymer is shown in Figure 7. As this is part of an ongoing project providing relatively recent data (13 AUG 91), the final analysis is not yet complete. There is additional synchrotron beamtime available this Autumn, and a careful and detailed XANES study should be carried out at that time, as well as a demonstration of the versatile tool of structural determination known as XAFS on other new materials and oxidizer/binder systems at that time.

### ACKNOWLEDGEMENTS

I would like to thank my focal point at the Phillips Laboratory OLAC, Dr. J. Rusek, for giving me the opportunity to work with him this Summer on this exciting project as well as S. Osborn, K. Chaffee and many others at Edwards AFB for being extremely helpful and receptive to new ideas. I would also like to thank my thesis advisor, Prof. R. W. Hoffman of Case Western Reserve University, who also participated in this program with me for all of his help, useful conversations and advice in countless matters over the Summer. This research was funded through the Summer Faculty/Graduate Student Research project of RDL Research and Development Laboratories and the NSLS is supported by the U.S. Department of Energy, Office of Basic Energy Sciences.

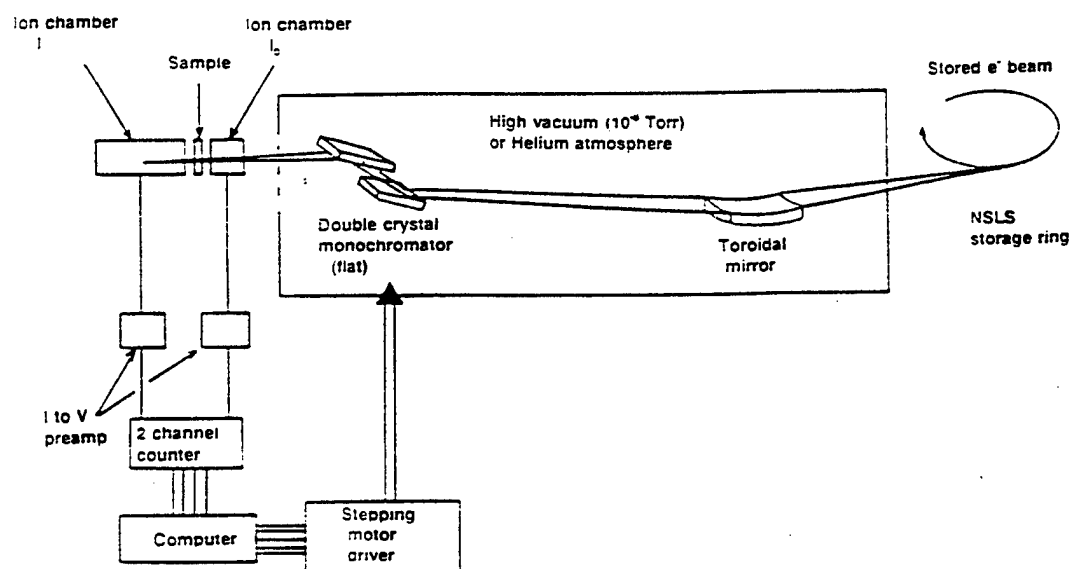
## REFERENCES

- 1) Kronig, R. de L., Z. Phys., **70**, (1931), 317.
- 2) Sayers, D. E., Stern, E. A. and Lytle, F. W., Phys. Rev. Lett., **27**, (1971), 1204.
- 3) Lee, P.A. and Pendry, J. B., Phys. Rev. B, **11**, (1975), 2795.
- 4) Ashley, C. A. and Doniach, S., Phys. Rev. B, **11**, (1975), 1279.
- 5) Sayers, D. E. and Bunker, B. A. in *X-ray Absorption: Principles, Applications, Techniques of EXAFS, SEXAFS and XANES*, Koningsberger, D. C. and Prins, R., eds., (John Wiley, New York, 1988), 216.
- 6) *ibid.*, Sayers and Bunker, 217.
- 7) Stern, E. A., Sayers, D. E., and Lytle, F. W., Phys. Rev. B, **11**, (1975), 4836.
- 8) *ibid.*, Sayers and Bunker, 227.
- 9) Teo, B. K. and Lee, P. A., J. Amer. Chem. Soc., **101**, (1979), 2815.
- 10) Mckale, A. G. et al, J. Amer. Chem. Soc., **110**, (1988), 3763.

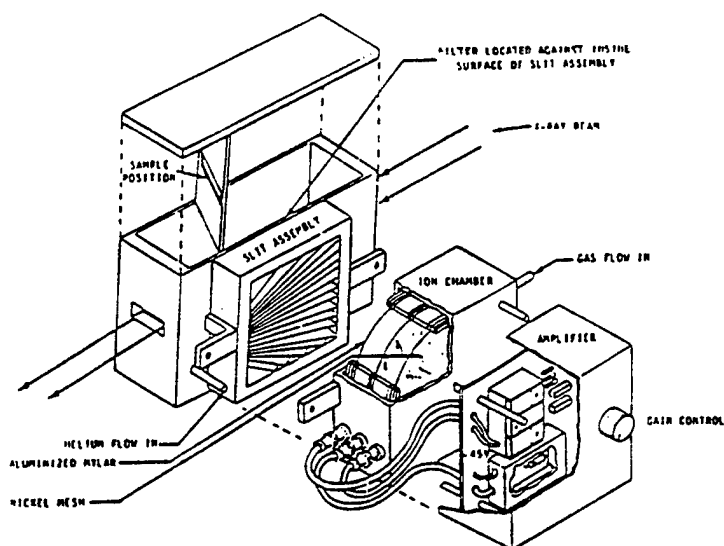
## FIGURE CAPTIONS

- 1) (A) Beamline setup for a typical absorption experiment  
(B) Diagram of a Lytle type fluorescence detector
- 2) (A) X-ray fluorescence vs photon energy in eV of AP  
(B) X-ray fluorescence and quadratic pre-edge vs photon energy in eV of AP
- 3) (A) Cl K-edge XANES of AP  
(B) X-ray fluorescence spectrum minus pre-edge background of AP
- 4) (A) Ar edge appearing in AP data vs photoelectron energy in eV  
(B) Removal of Ar edge by the dejumping process
- 5) (A) Post-edge background derivative and  
(B) Fourier transform magnitude of AP as a function of smoothing parameter
- 6) Normalized EXAFS data of (A) AP and (B) AP with 1 mL of TET diffused
- 7) X-ray fluorescence vs photon energy in eV of "SYN 14"

# SCHEMATIC OF AN X-RAY ABSORPTION EXPERIMENT AT A SYNCHROTRON RADIATION FACILITY

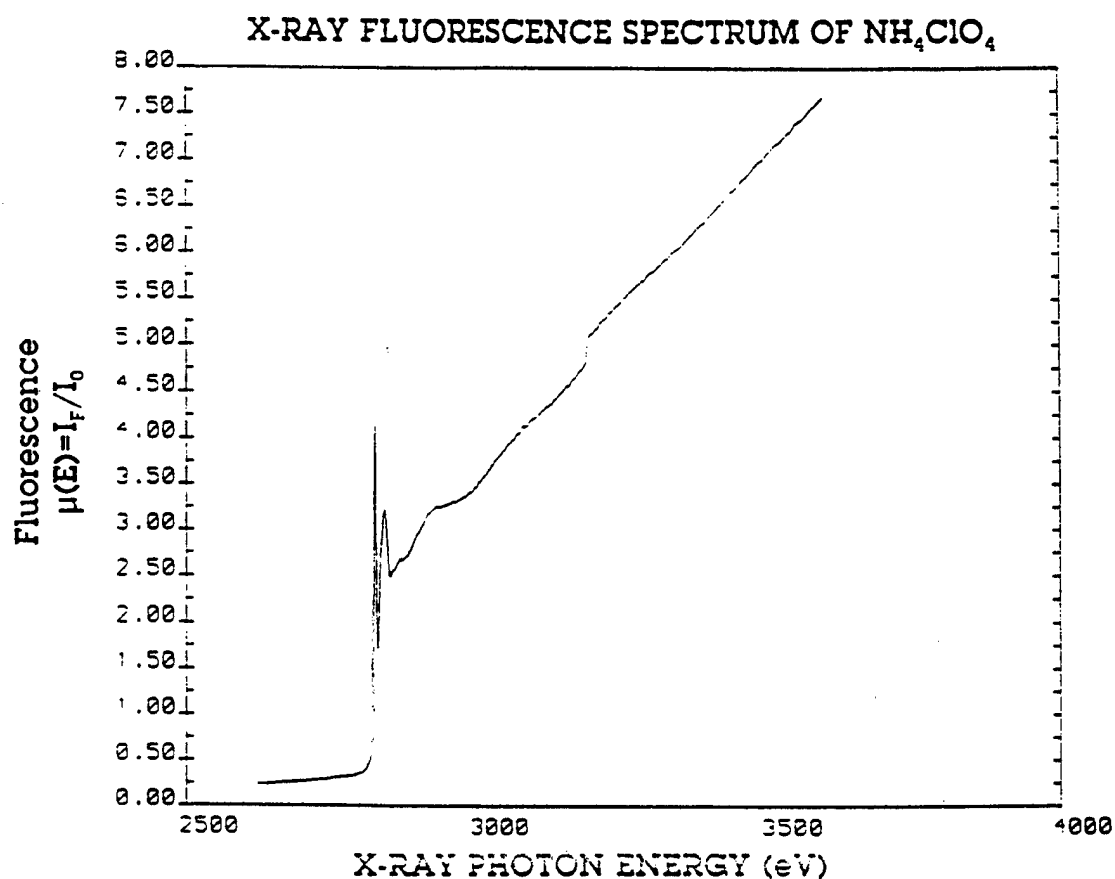


( A )

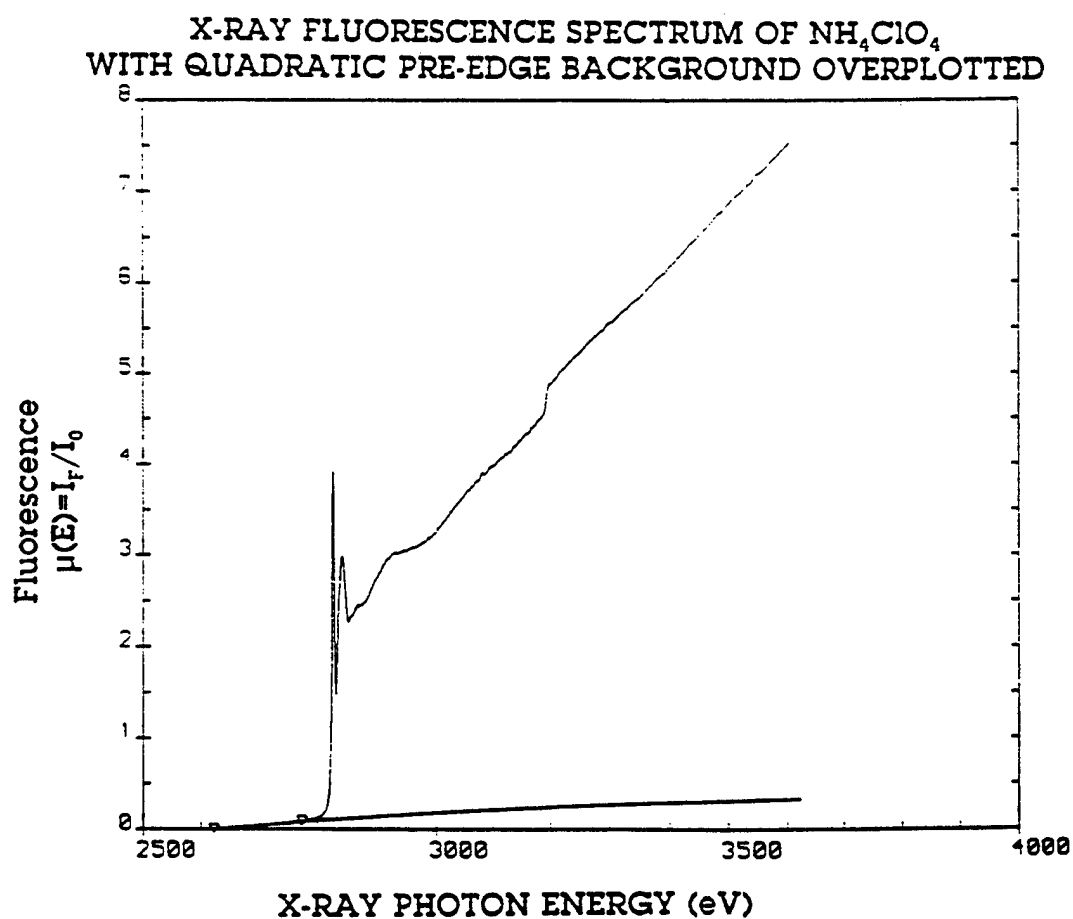


( B )



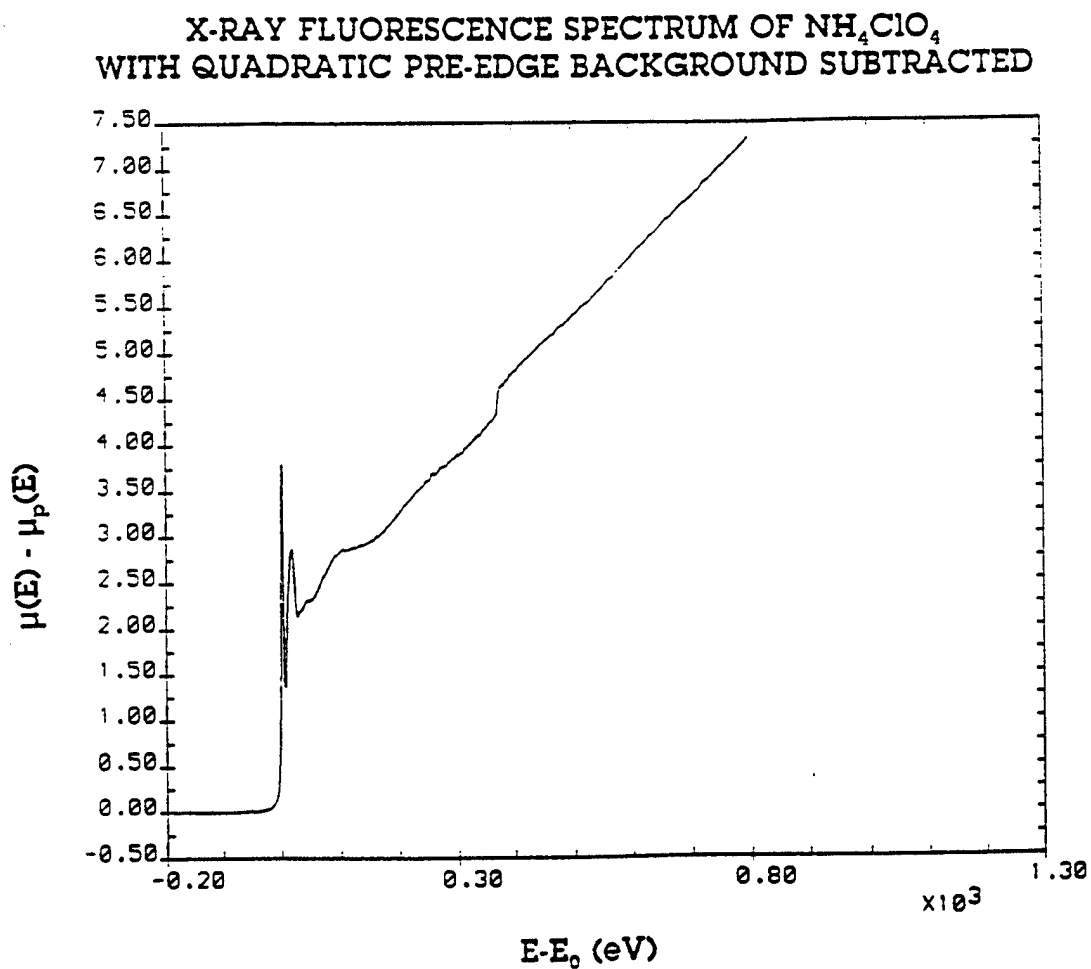
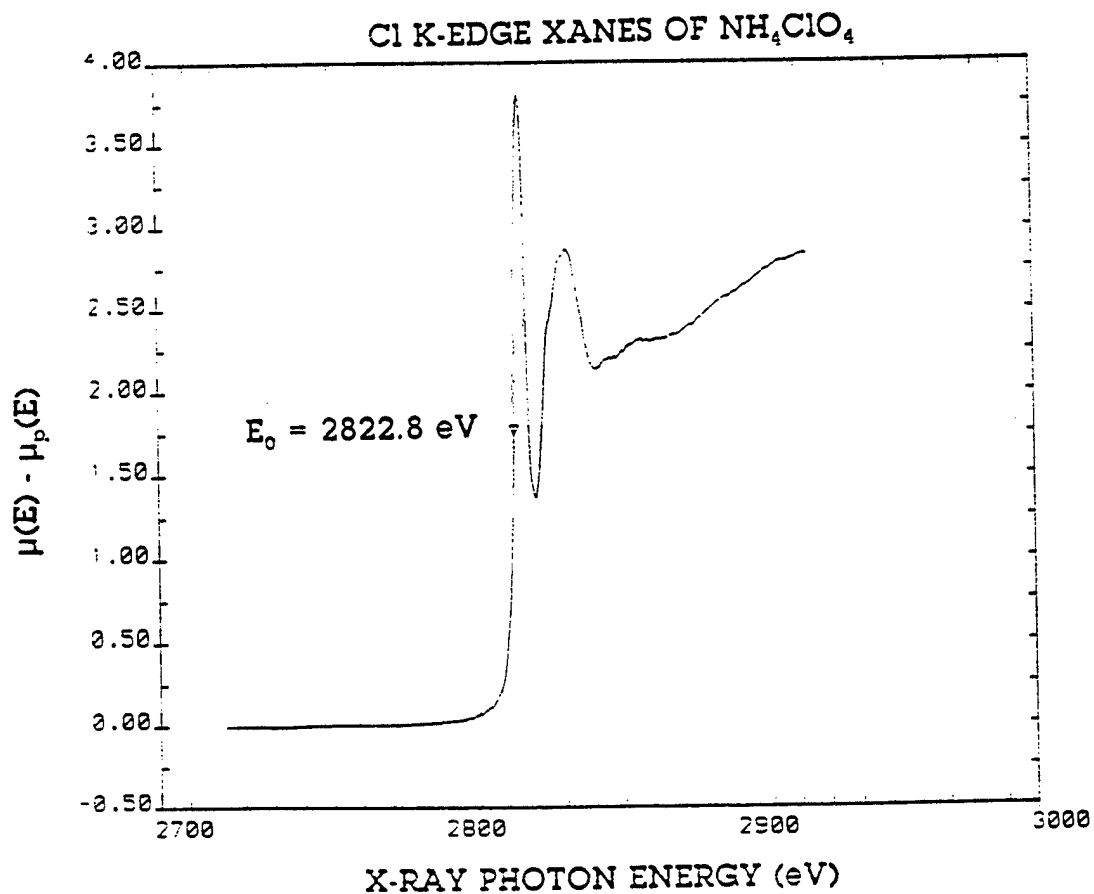


( A )

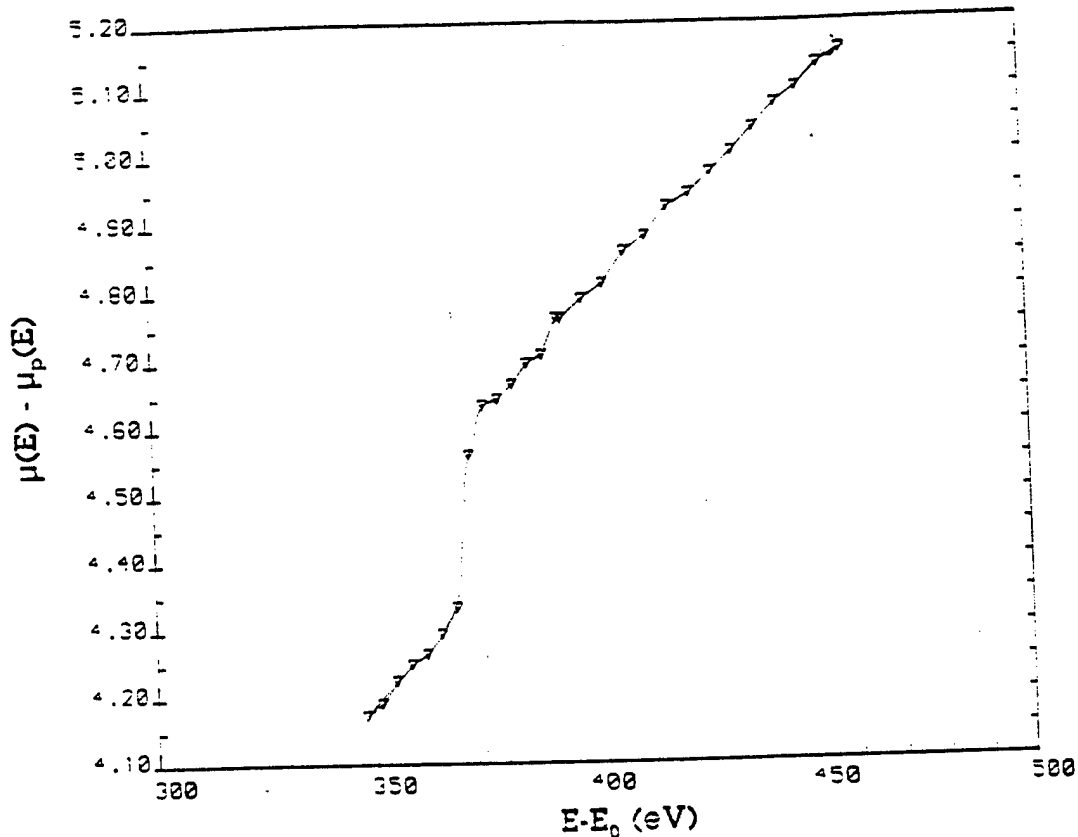


( B ) 55

FIGURE 2

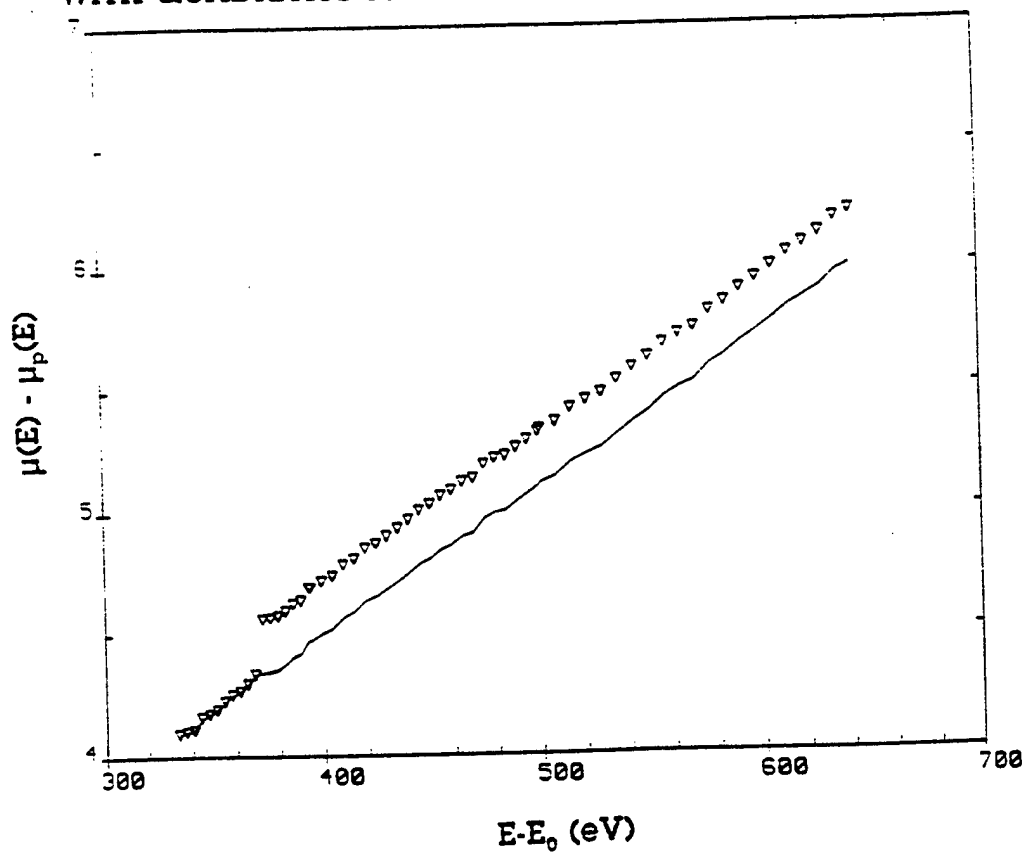


X-RAY FLUORESCENCE SPECTRUM OF  $\text{NH}_4\text{ClO}_4$   
WITH QUADRATIC PRE-EDGE BACKGROUND SUBTRACTED



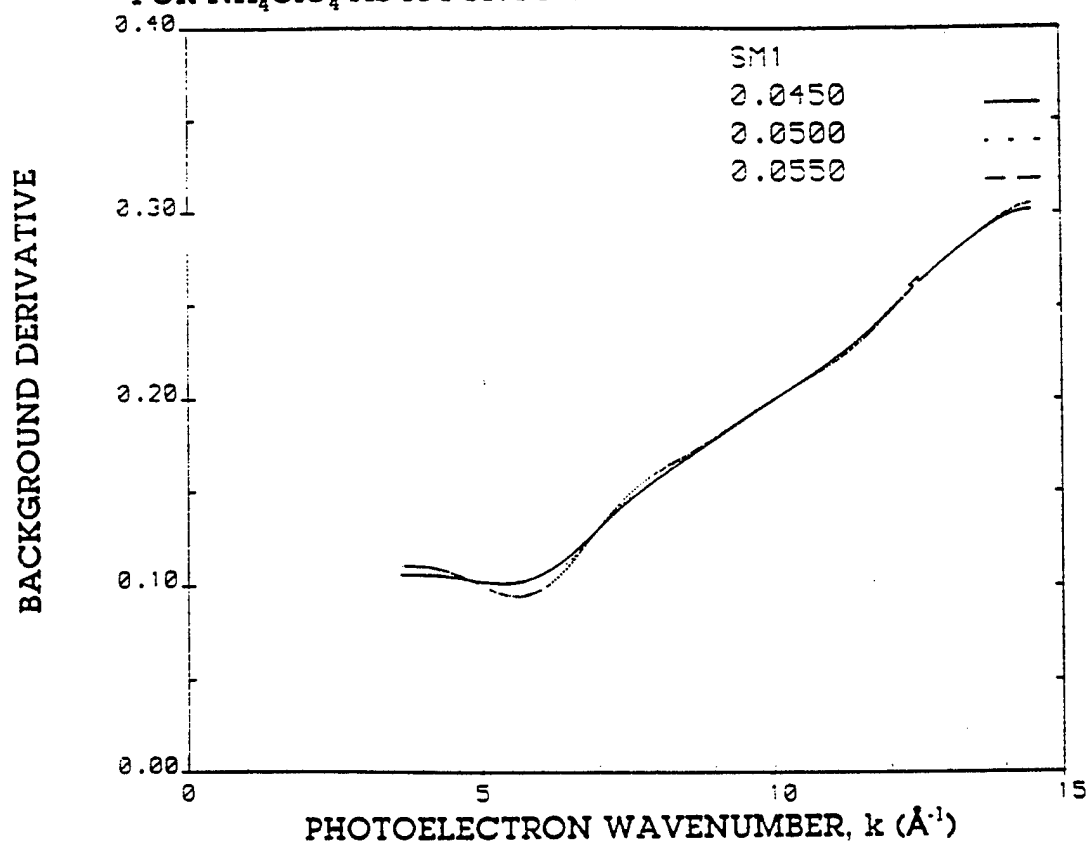
( A )

X-RAY FLUORESCENCE SPECTRUM OF  $\text{NH}_4\text{ClO}_4$   
WITH QUADRATIC PRE-EDGE BACKGROUND SUBTRACTED



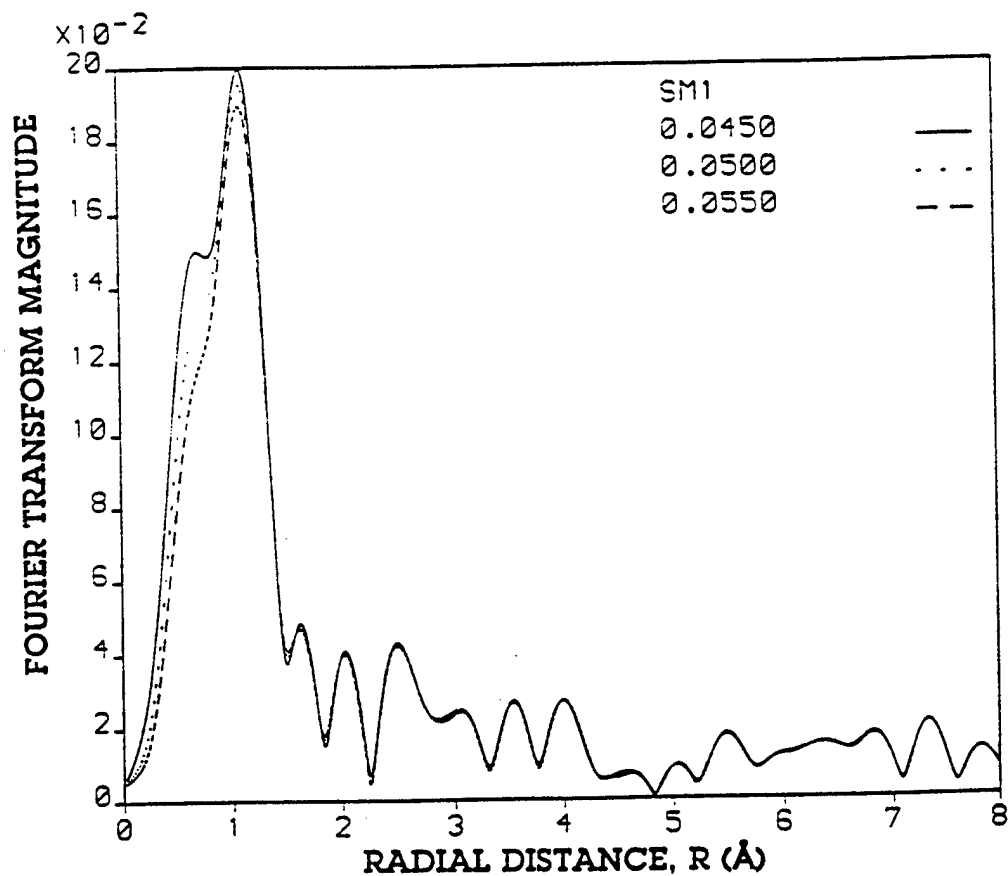
( B ) 57

POST-EDGE BACKGROUND DERIVATIVE vs PHOTOELECTRON WAVE NUMBER  
FOR  $\text{NH}_4\text{ClO}_4$  AS A FUNCTION OF SMOOTHING PARAMETER



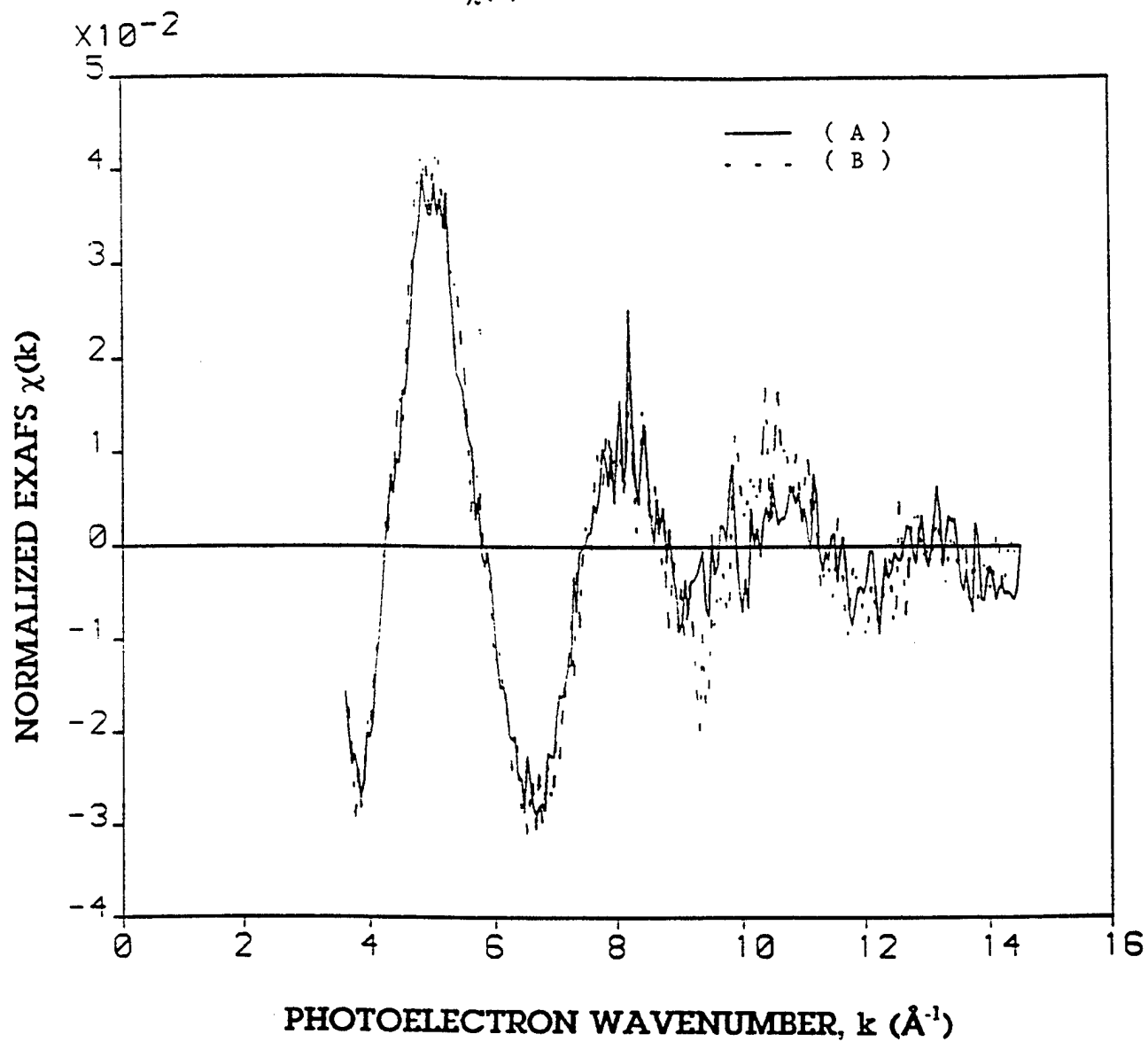
( A )

FOURIER TRANSFORM MAGNITUDE VS RADIAL DISTANCE IN  $\text{\AA}$   
FOR  $\text{NH}_4\text{ClO}_4$  AS A FUNCTION OF SMOOTHING PARAMETER



( B )

NORMALIZED EXAFS DATA  $\chi(k)$  vs PHOTOELECTRON WAVE NUMBER IN  $\text{\AA}^{-1}$



# X-RAY FLUORESCENCE SPECTRUM OF NEWLY SYNTHESIZED POLYMER

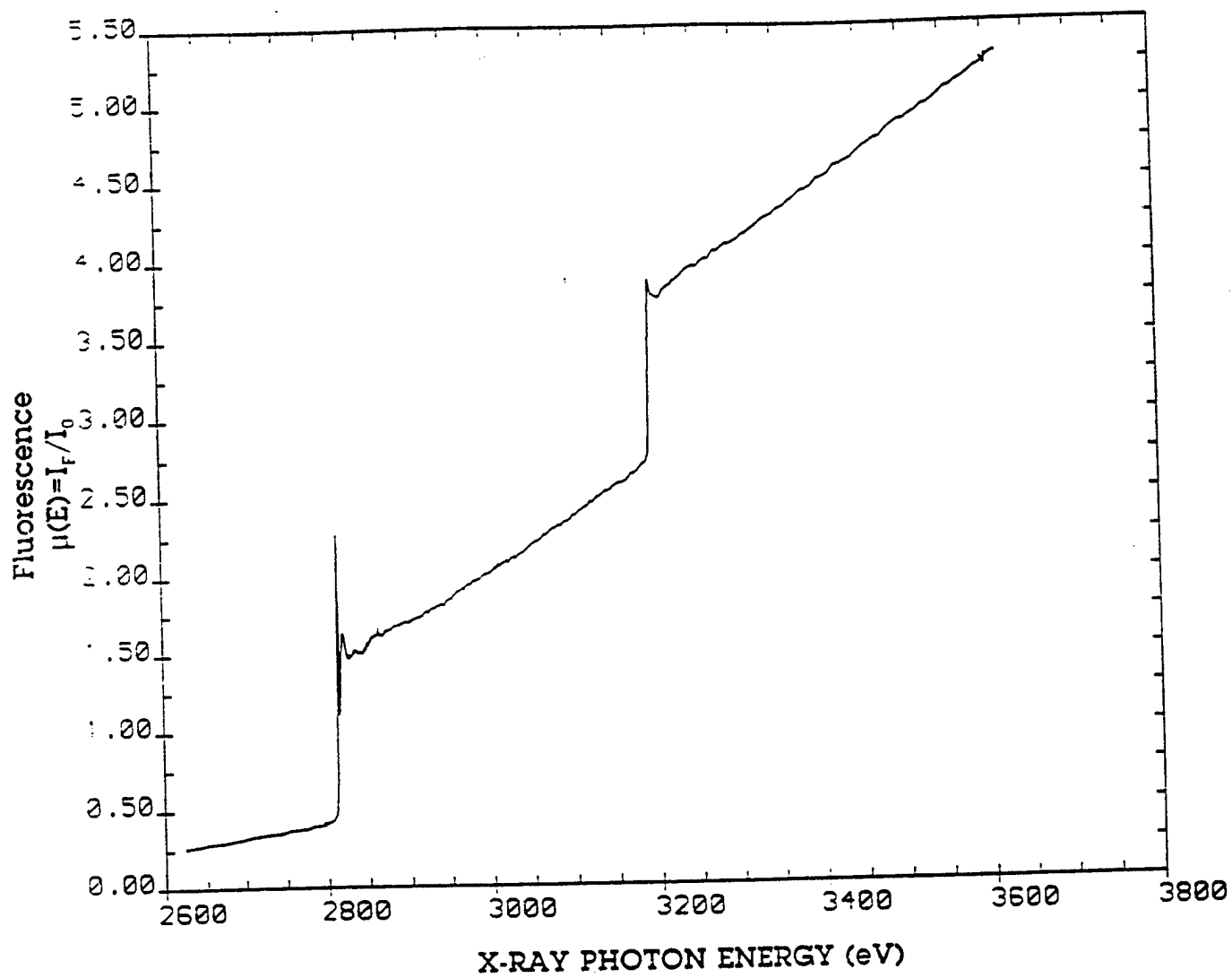


FIGURE 7

RDL AFOSR FINAL REPORT

R. W. Hoffman  
Phillips Laboratory  
Edwards AFB Ca

22 August, 1991

## ABSTRACT

### XAFS of AP and AP/Binder Systems

Techniques of Lytle detection in x-ray fluorescence were applied to 26 distinct chemical samples at the Cl edge, 1 at the K edge, and 7 at the Ti edge. The specimens commonly were pressed from powders, 2.5  $\mu\text{m}$  particle size in the case of AP to thicknesses of about 1/32 in., thus obtaining samples for further experiments of adding binders or remaining uncoated. A special sample holder was designed and constructed to aid in the specimen transfer. The sample thickness necessitated fluorescent detection with an estimated probing depth of 25  $\mu\text{m}$ . The experiments were carried out on beam line X-19A at Brookhaven National Laboratory and are in the process of being quantitatively evaluated. Differences in the XANES spectra between binders are noted, and tentatively related to the steric chemistry and to the local structure and valence of the Cl containing samples. Several new polymeric materials were also examined.



## Introduction

The prime commitment to the RDL/AFOSR Summer Research Program was to make XAFS techniques available to the Phillips Laboratory, Edwards AFB and especially to certain persons who would be trained or updated in many phases of Synchrotron Radiation (SR) research involving absorption fine structure spectroscopy. The persons participating directly in this activity were Dr. John Rusek and Dr. Kevin Chaffee, Phillips Laboratory, and Professor Richard Hoffman and Mr. Guy DeRose, participants in the Summer Research Participation Program. A secondary goal was to explore the conductivity limits for the samples used in Scanning Tunneling Microscopy using the STM existing in the Phillips Laboratory, and will not be discussed in this paper.

The preliminary steps necessary to be able to carry out an XAFS actual sample data acquisition at a synchrotron include

- Synchrotron Selection
- Beam Line selection
- User proposal and approval
- Safety approval
- User financing
- Experimental design, including sample preparation and selection of spectroscopy and apparatus availability.
- Scheduling of experimental time with beam line personnel, including beam line training in safety and operation

For orientation, background information taken from the NSLS literature and relabeled as Figure 1 is reproduced on the following page.

The steps above must be completed prior to actually obtaining data and will not be discussed in detail in this report. In our case 5 days were scheduled from 7-12 August, 1991. AP, various standards, and other runs were completed at Brookhaven National Laboratory at the National Synchrotron Light Source (NSLS), Upton NY during that time. The items to be discussed in this report are concerned with the equipment alignment, data acquisition, and some of the problems arising during the actual run period. Additional details as to the data reduction will be found in the report by Guy A. DeRose to RDL.

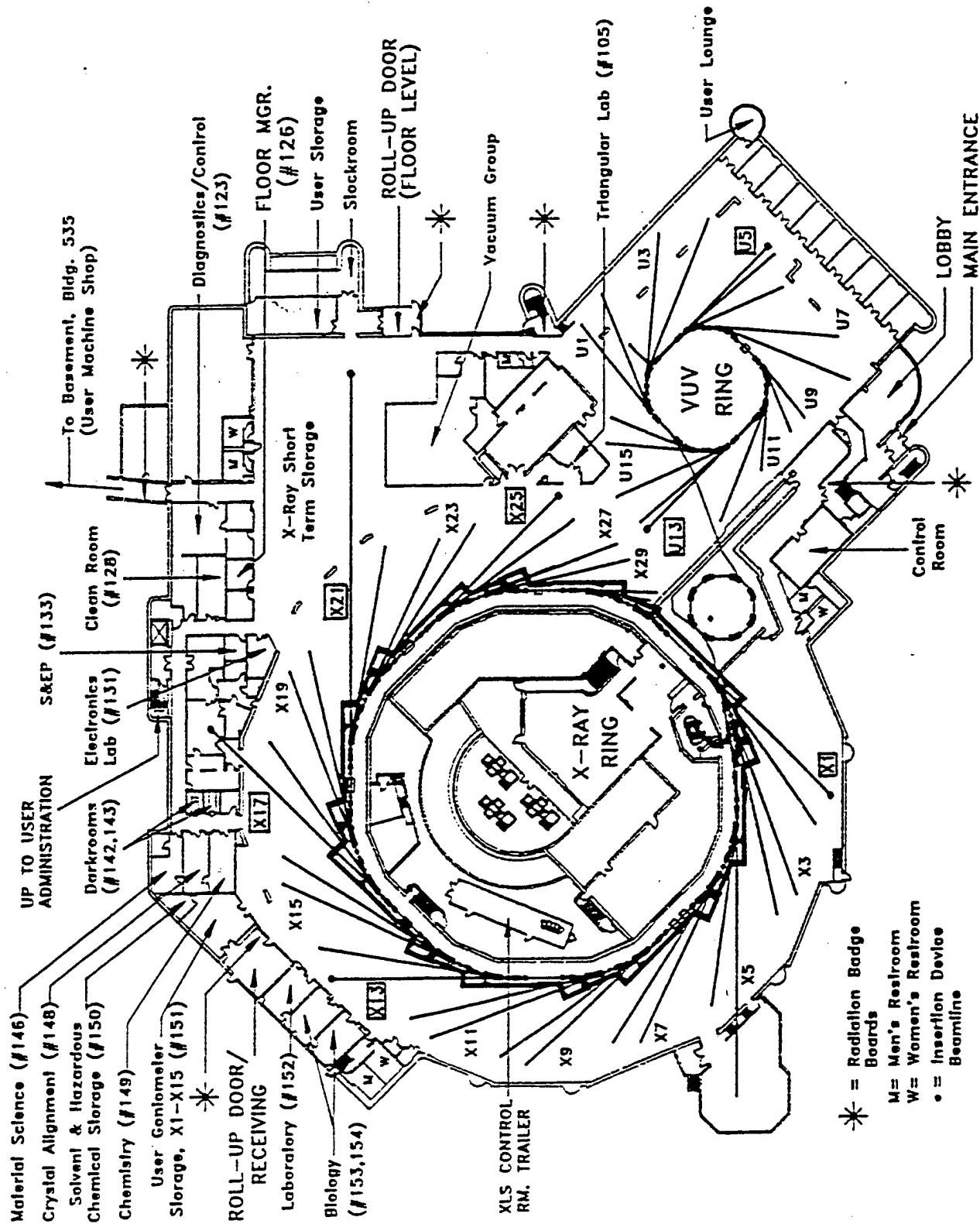


Figure 1 Floor plan of the National Synchrotron Light Source experimental area.

## X-ray Absorption Fine Structure

XAFS is the short hand algorithm for both Extended X-ray Adsorption Fine Structure (EXAFS) and X-ray Absorption Near Edge Structure (XANES) or as is it sometimes called Near Edge X-ray Absorption Fine Structure (NEXAFS). EXAFS as practiced for surfaces is called SEXAFS and uses Auger electron detection. EXAFS, the earlier technique is the generation of outgoing spherical photoelectron waves of varying wavelengths following photoemission and the subsequent backscattering from nearby atoms in coordination shells and the analysis of the resulting raw data to provide elemental coordination distances and numbers in crystalline and modestly disordered samples. All XAFS techniques are commonly practiced using the high intensity SR sources (typically 10 billion photons per second). The Bremsstrahlung radiation arising from bending magnets forms the white radiation of the beam line used (X-19A) for these experiments. The beam line has Si (111) oriented single crystals used as a monochromator to be wavelength tuneable to scan the absorption as a function of energy through and between various edges and is a polarized x-ray source, not used in these first experiments since the samples were powders of all orientations. This beam line was selected for its specialization to low energies and its availability with known personnel. It was well suited to our needs since a feedback system made vertical translation of the sample unnecessary as the energy was scanned. It suffered from having very limited on-line data analysis. Figure 2 on the following page give X-19A beam characteristics and other data.

## XAFS Techniques

The XAFS information may be obtained in transmission, fluorescence emission, photoelectron emission, with X-ray, electron or ion detection using ion chambers or other detectors. One of the most common and versatile is the Lytle detector, a combination of transmission and fluorescence geometries, commonly using ion chambers and optimized for the 3d transition series and using Soller slits and x-ray K beta filtering techniques. For our experiments the Soller slits serve no useful purpose and no simple filters exist and were not used in either the CWRU or UK (X-19A) detectors. In the design of the experiment, proper consideration of the sample and detection geometry must be taken into account to optimize the data for easier analysis. While certain corrections may be made during

the data analysis, it is better to have good data in the beginning. In addition to the noise questions, one important parameter is the depth in the sample to be probed. For the Cl edge in most of the materials studied here, the absorption length is about 17  $\mu\text{m}$  at energies above the Cl edge energy. Since we found in preliminary experiments in preparing samples it was not possible to press sample powders to make proper specimens with thicknesses less than 35  $\mu\text{m}$  for transmission due to the soft radiation (2.623 KeV) used. As the samples were not electrically conducting, and we wished to probe a distance greater than 100  $\text{\AA}$  in order to study buried interfaces, the fluorescent technique was selected and will be emphasized in this report. As stated earlier, we did not take advantage of the polarization of the X-ray beam in this run, but hope to examine oriented samples in the future.

#### SR Experience during August, 1991

Dr. John Rusek, Dr. Kevin Chaffee, Prof. Hoffman, and Mr. Guy DeRose went to the NSLS at BNL to make the measurements. We traveled from EAFB to BNL as a group. Since we had 5 days of beam time and we needed to operate 24 hours per day, we operated in two 12 hr shifts. Except for a major unscheduled beam dump (no X-rays) for a construction mishap and another for natural lightning strikes causing power failures for a total of some 36 hours, we were able to make full use of the NSLS facility and finished most of the samples that were available. Some beam time loss due to beam decay is expected. Taken from our log and end of run report, some statistics follow; more are available upon request.

Table I Beam Statistics 7-12 Aug., 1991

Possible time available (8 hr shifts)	15
No beam for many reasons (8 hr shifts)	6
Beam available (shifts)	9
Initial set up time (shifts)	1.5

## Sample Preparation

Consistent with the necessity of using fluorescent radiation and a Lytle detector we investigated the pressing of AP and other materials into pellets in a die similar to a KBr press. Mr. David Cooke fabricated a very useful die that made samples nominally  $3/8$  in. in diameter. The samples were made  $1/32$  in. thick by filling the die with some 100 mg of AP. These samples were pressed to an oil pressure of about 1000 psig in a Carver press in Cell No 6 at the Chemistry Lab at Phillips Laboratory. We produced about 150 samples which were strong enough to withstand handling and shipment and thus serve as reproducible samples. Mr Tracy Reed assisted with the final pressing.

This die was successful in making samples not only of AP but other standards, perchlorates and polymer samples for XAFS studies. Earlier studies to optimize pressing conditions showed a rather wide range of conditions possible, but a particle size of 2.5  $\mu\text{m}$  was selected for AP. The pellet samples were removed from the die by light pressing. For AP the final pellet density increased slightly with particle size decrease and increased with increasing pressure of pressing. The final density was about 1.7 gm/cm or about 90% of the bulk crystalline density with a volume contraction of about 3 times. Upon extrusion from the die, the first exposed (Upper or Top surface) had a few fine cracks and some surface debris and was noted in the earlier studies. Only  $\text{TiO}_2$ , a standard (calibration) sample was not able to be pressed and required the addition of a binder. It and a  $\text{CuClO}_4$  sample were vise pressed at BNL. The pelletizing technique provided samples of low mass that were easily transported and handled, and is recommended for future use. An appropriate sample holder was designed and fabricated to facilitate the sample insertion into the Lytle detector at the beam line. The geometry is shown in Figure 3 which follows. Reference 1 may be consulted for more details about XAFS experimental design.

## Apparatus and Procedures used at BNL

Most of the operating hardware for the XAFS data acquisition and a Lytle detector was available as part of the X-19A apparatus. We provided the CWRU Lytle detector, samples, and operating experience. Some beam line specifications were reproduced in Fig 2. It is important to contact beam line personnel until the user is familiar with the beam line operation. In our case, Dr. Kumi Panigrahi, a former student,

Beamline:	X19A
Ring:	X-Ray
Operational Status:	Operational

Participating Institutions: NSLS, U. of Kentucky, U. of Michigan, BNL - Department of Applied Science (members of the X19A Stewardship Group)

Local Contact: Fu-Long Lu (516)282-5619, 2338 @ BNL

Spokesperson: Stephen Cramer (BITNET address: CRAMER@BNLCL1)

Research Program: X-ray absorption spectroscopy, EXAFS

Energy Range (keV)	Crystal Type	Resolution $\Delta E$ (eV) @8 keV, Si(111) @12 keV, Si(220)	Flux (photons/sec.)	Spot Size (mm)	Total Horizontal Angular Acceptance (mradians)
2.1 - 7.9	Si(111)	8.1 - 0.7*	$\sim 10^{11}$	40H x 5V unfocused	2.4(unfoc.)
3.4 - 12.9	Si(220)	12 - 0.8	@ 5 keV (100 mA, 2.5 GeV)	$\sim 1$ mm diam focused	1.3(foc.)
7.6 - 13.4	Si(111)	8.1 - 0.7	$\sim 5 \times 10^{11}$	40H x 5V unfocused	2.4(unfoc.)
12.5 - 23.0	Si(220)	12 - 0.8	@ 11 keV (100 mA, 2.5GeV)	$\sim 1$ mm diam focused	1.3(foc.)

\* Largest value corresponds to 2 mm slit. Small value is for 0.1 mm slit.

#### Optical Configuration

##### a) Monochromator

NSLS boomerang-type double flat crystal monochromator; fixed exit geometry; first crystal is water-cooled; operates at UHV; two presertable Bragg angle ranges of  $14.5^\circ - 70^\circ$  and  $8.5^\circ - 15^\circ$ ; located 9.3 meters from the source. Operates primarily in low energy, Si(111), unfocused configuration.

##### b) Mirror

Cylindrical aluminum focusing mirror, electroless nickel plated and overcoated with rhodium, for focusing beam onto sample at 18.5 meters from the source; 3 mradian incidence angle; 23 keV high energy cutoff; mirror may be dropped out of beam path for unfocused mode; located 10.5 meters from the source.

##### c) Windows

Beamline is UHV up to window located inside radiation hut; a 6  $\mu$ m graphite filter is in the beam at all times; the exit window for non-vacuum operation is 10 mil Be.

#### Experimental Apparatus

Positioning table using stepper motor controls, two perpendicular translations and effectively three mutually perpendicular rotations. Germanium array detector available by special arrangement with S.P. Cramer.

#### Computer System Hardware and Software

MicroVAXII computer with CAMAC interface running Micro-VMS operating system; Ethernet link to AMD cluster and major networks.

December 5, 1990

Figure 2 X-19A Beam Line Data

and other beam line people were very helpful. Although many beam lines are similar in their operation, differences exist between PRT groups resulting in differences in data collection and beam line operation. Most beam lines provide documentation and help to new users in order to obtain useful data from the beginning. In our case the CWRU Lytle detector failed near the beginning of our time necessitating the use of the University of Kentucky X-19A ion chamber and electronics being wedged mechanically to the sample chamber of the CWRU instrument. This was successfully accomplished at NSLS. To minimize the absorption of the X-rays of low energy in the air path, we selected a uhv beam line and filled the Lytle detector with helium in the sample region. Helium was also sent to the Io (first) ion chamber after it was repaired. The second (If) ion chamber was filled with nitrogen gas to absorb most of the K beta radiation and maximize the signal. The analog signals from the ion chambers are amplified and sent to a voltage to frequency converted before the signals were recorded by the beam line computers. Background (offset) readings are taken after any X-ray changes. The tuning of the Bremsstrahlung is accomplished by computer control of the monochromator and proper alignment of the X-ray beam. This alignment must be carried out at the beginning and minor realignment done each time a new electron fill is made to the storage ring, approximately once each shift. Part of the alignment procedure is to adjust, by calibration with a known standard sample, the position of the monochromating crystals to the calculated edge energy by following a predetermined (computer) procedure.

The computer for the X-19A operation was able to preload scans for various energies and predetermined integration times to reduce the total time at the expense of a given scan time. This procedure also set the energy resolution of the monochromator. As the data evolved, it was obvious that the XANES region would be more important in showing differences than the EXAFS region so the scans were adjusted to optimize to provide better energy resolution near the edge of interest.

Realignment to find the position of the beam so that the sample may be placed in the proper position, calibration of the energy, and using standard known samples for phase and amplitude information necessary for the data reduction usually takes about half of the total available beam time; thus making use of the 24 hour a day 7 days a week schedule is required. Fortunately, the persons going to NSLS for this run all had prior SR experience.

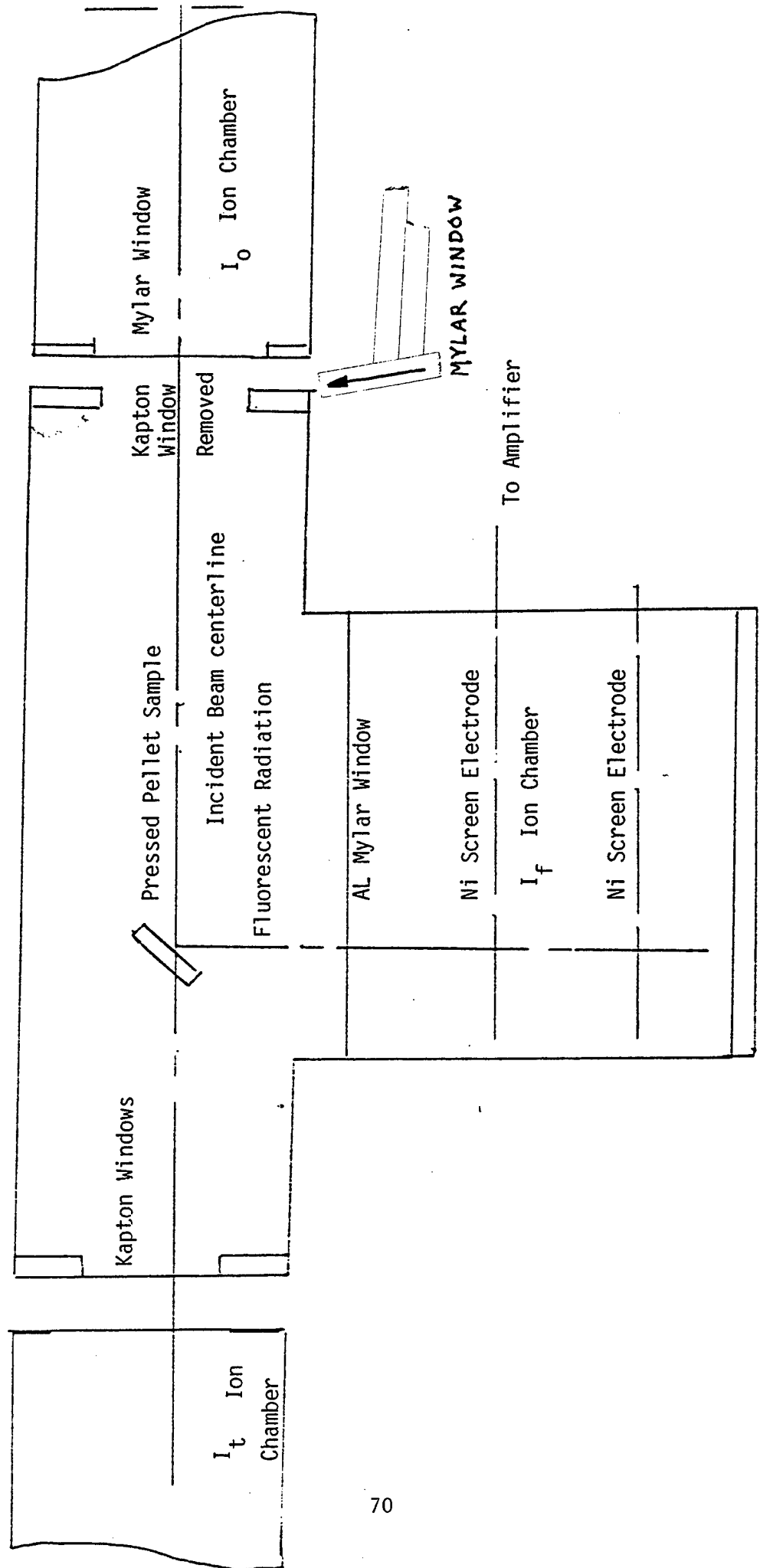


Figure 3 (CWRU) Lytle Detector for Fluorescence Detection of XANES and EXAFS.



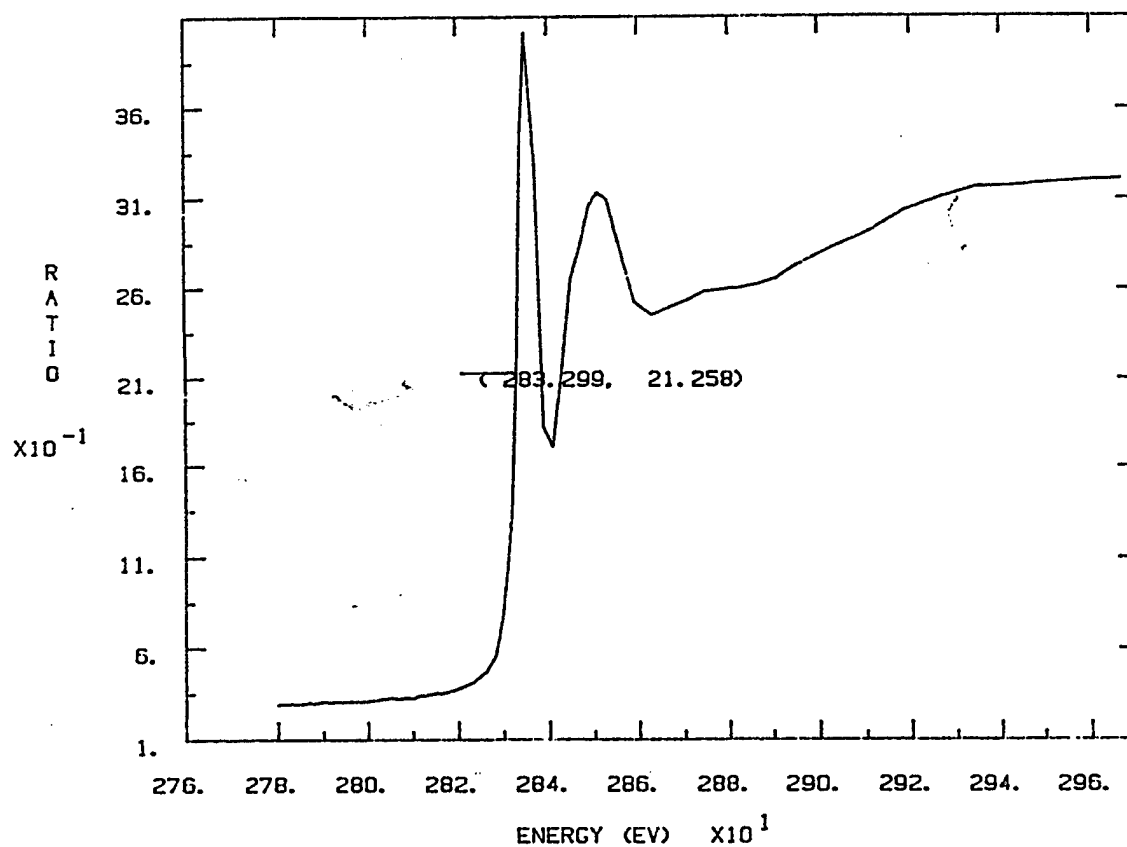
## Analog Results

As stated earlier, no on-line data reduction exists on X-19A so that only data in the form of analog plots were available to bring back. These have been examined with the results reported below. All together some 143 separate scans were carried out. Many of these were for beam alignment purposes and covered only the Cl edge region. Later edge scans were set up to include both the Cl and Ar edges for a reference energy built in to each scan. Finally some full data scans from below the Cl edge to above the K edge were set up to minimize the statistical errors while maximizing the number of specimens that could be examined in a given time. These later scan parameters were used when time was limited during the last two days. In all, the following samples were examined as shown in Table II below:

Table II Sample Summary Scan Data

Sample File	No. of Samples	No. of Scans
AP CLO4NH4	1	30
CLNH4	1	10
CLEDGE	2	22
STD Various		
KCl KCL & CLK	1	8
AP/binders Various	17	37
New Polymers SYN Var.	4	12
TI CVD Various	2	5
TI STD Various	5	12
Various polymer window films	3	3
Totals	36	109

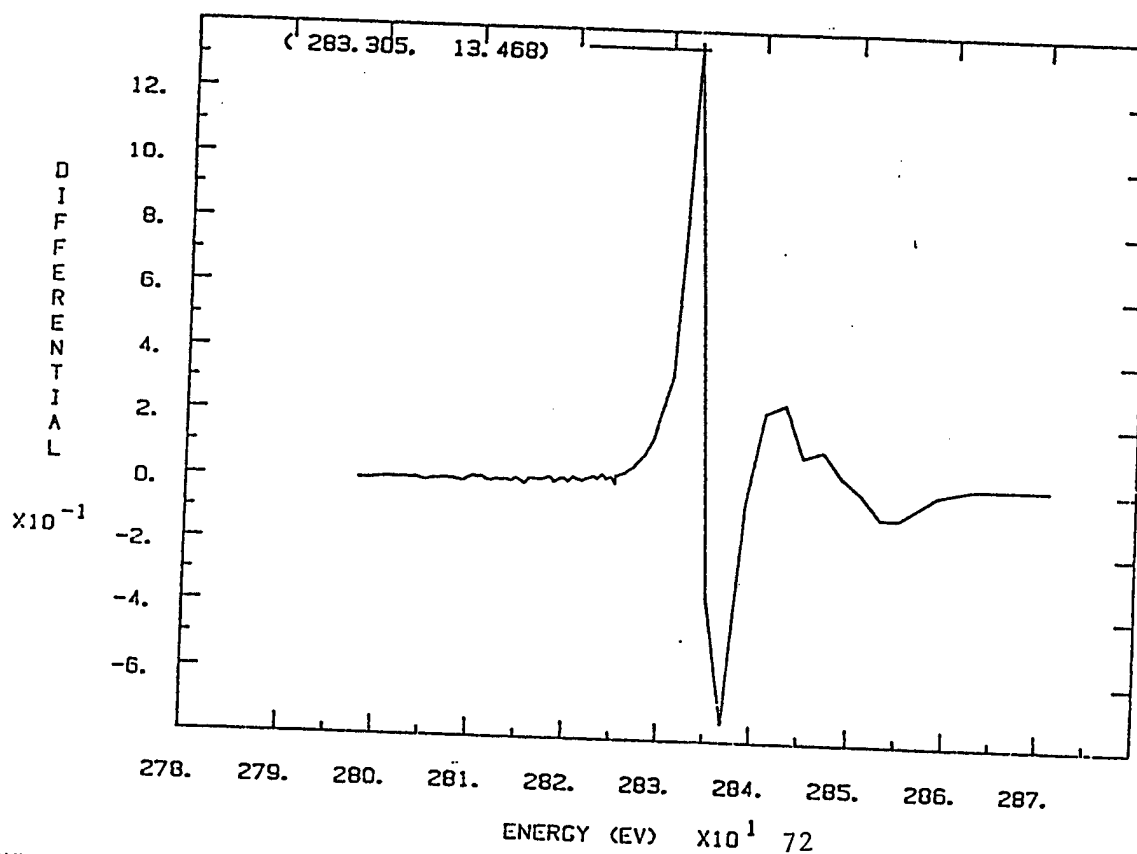
Representative data are shown in Figures 4-8 for both energy calibration, XANES (Multiple scattering), and EXAFS (Single scattering) regions. Details are not given here, but file numbers are on the figures and some details are given in the Figure Caption list.



CLO4NH4.301W 3/1

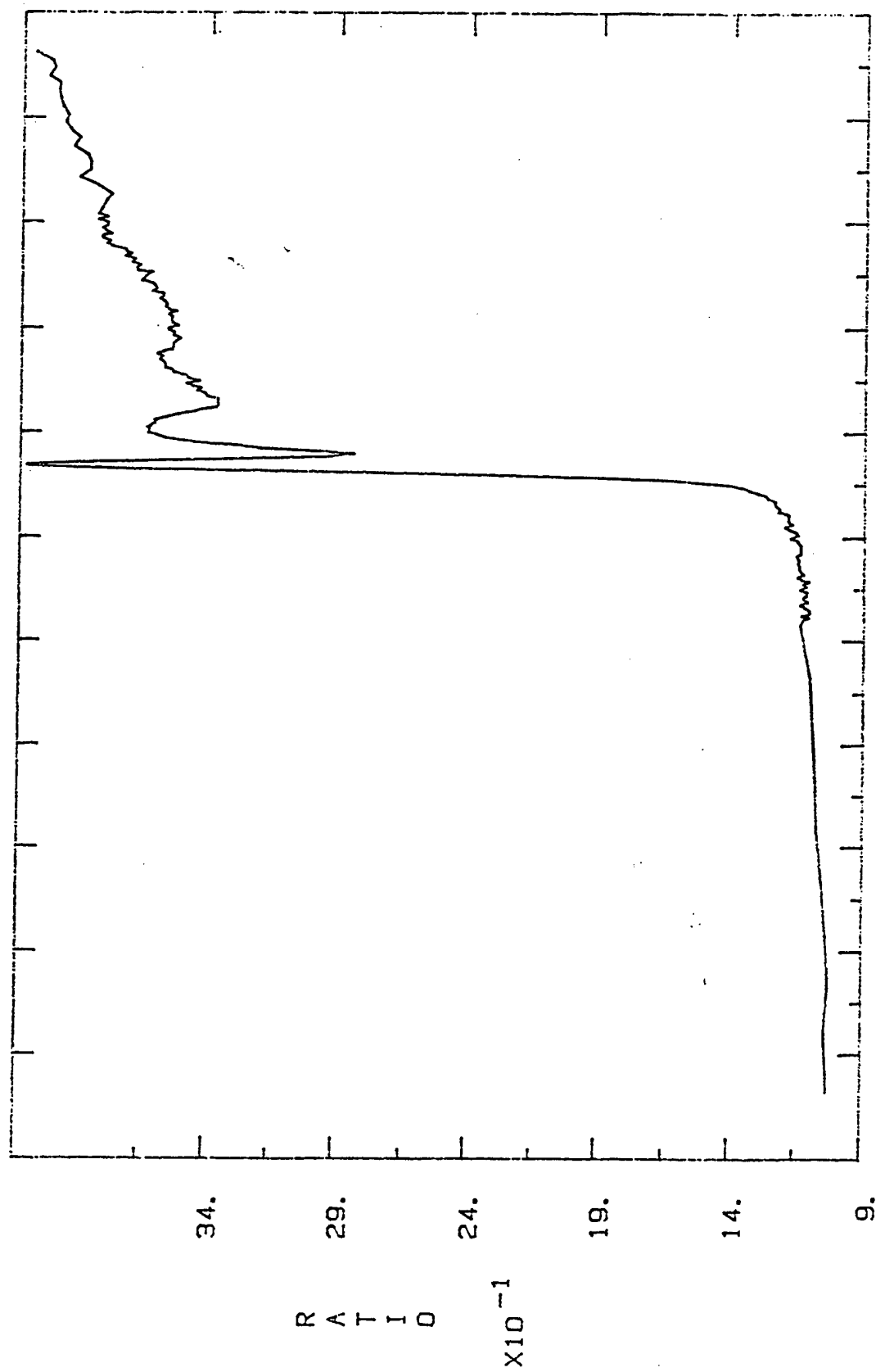
8-AUG-91

Figure 4a Cledge scan for energy calibration



CLO4NH4.301D 3/1

8-AUG-91



269. 271. 273. 275. 277. 279. 281. 283. 285. 287. 289.

ENERGY (eV)  $\times 10^1$

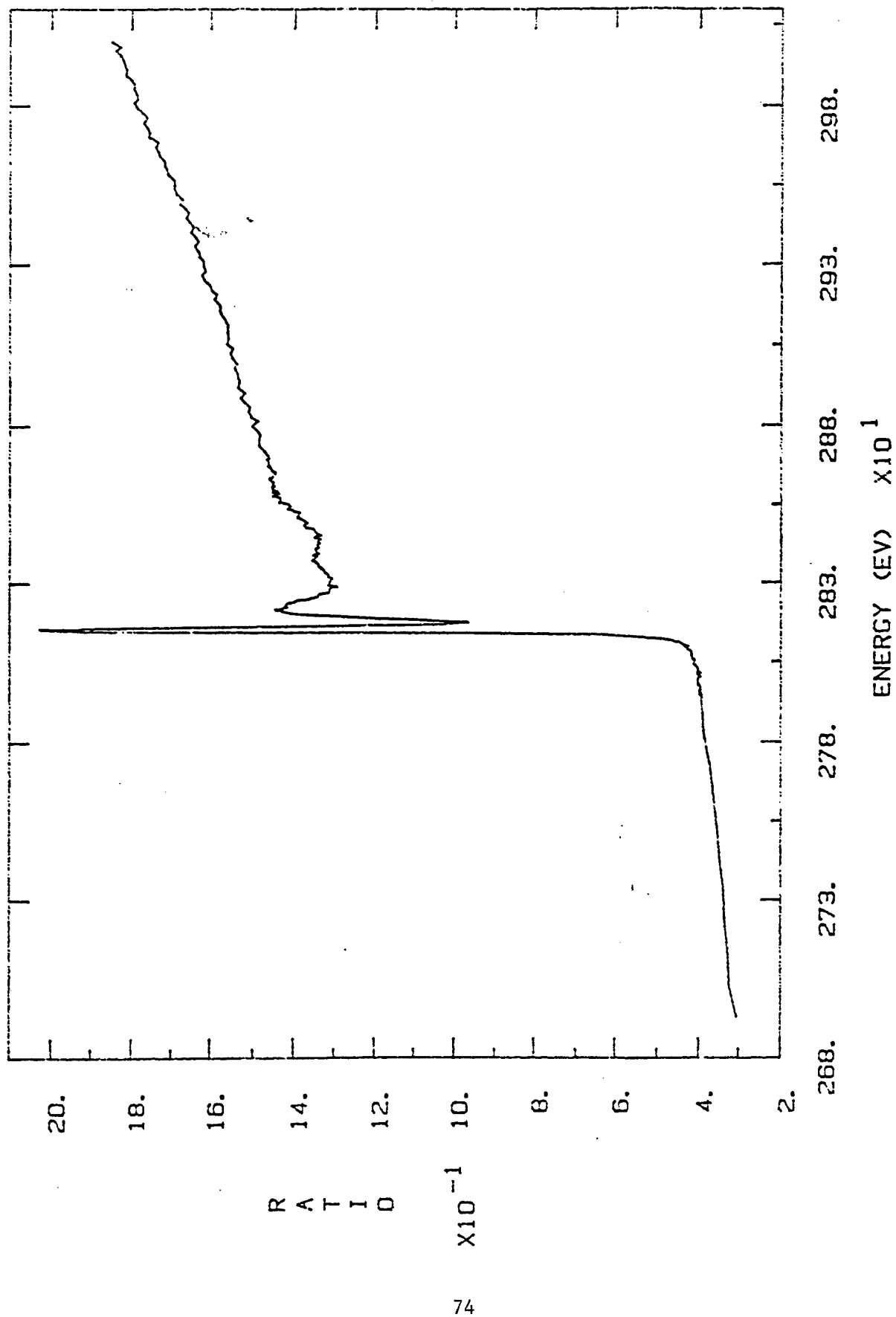
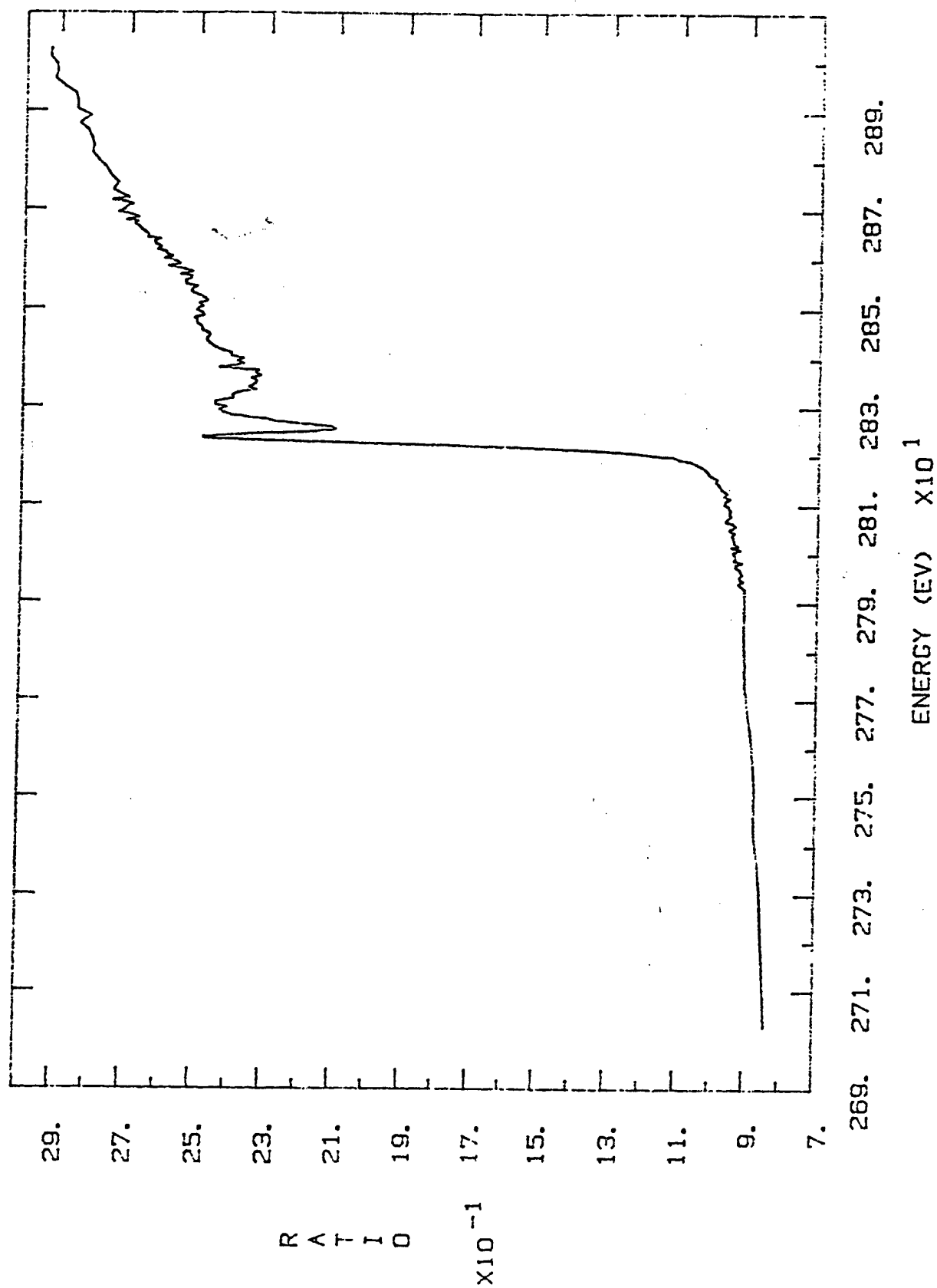
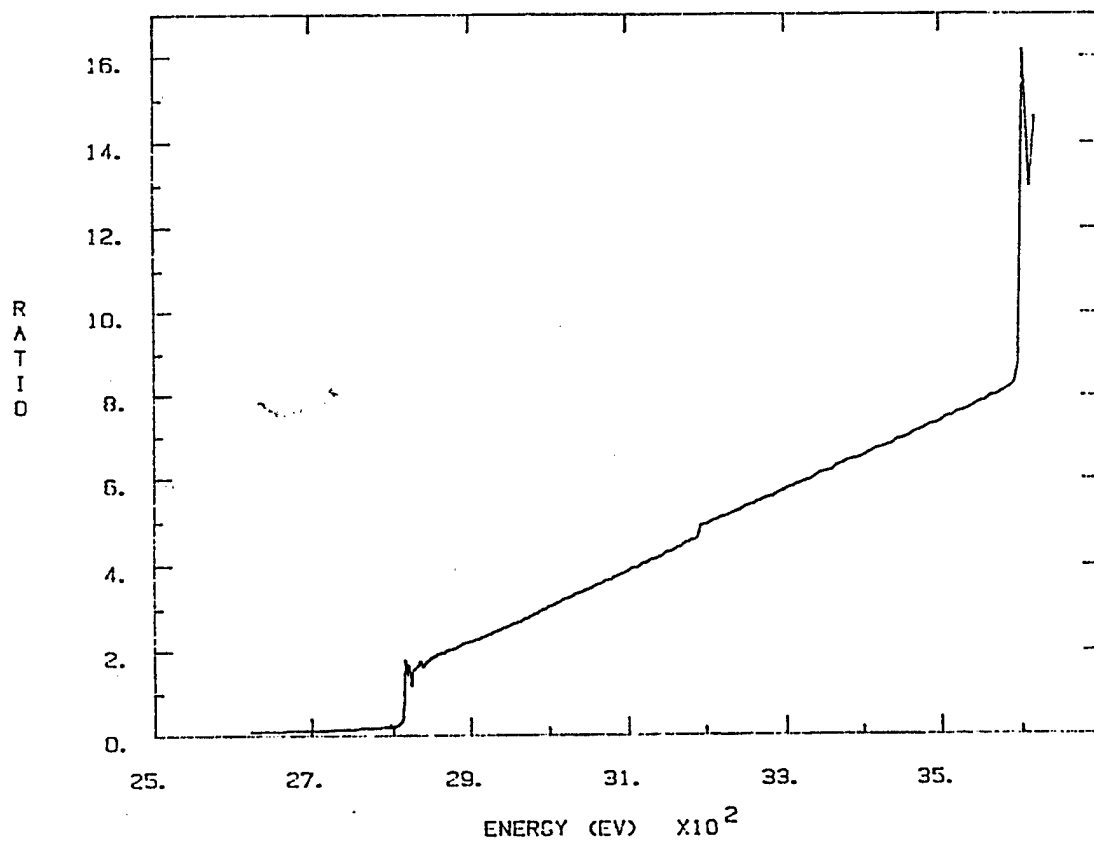


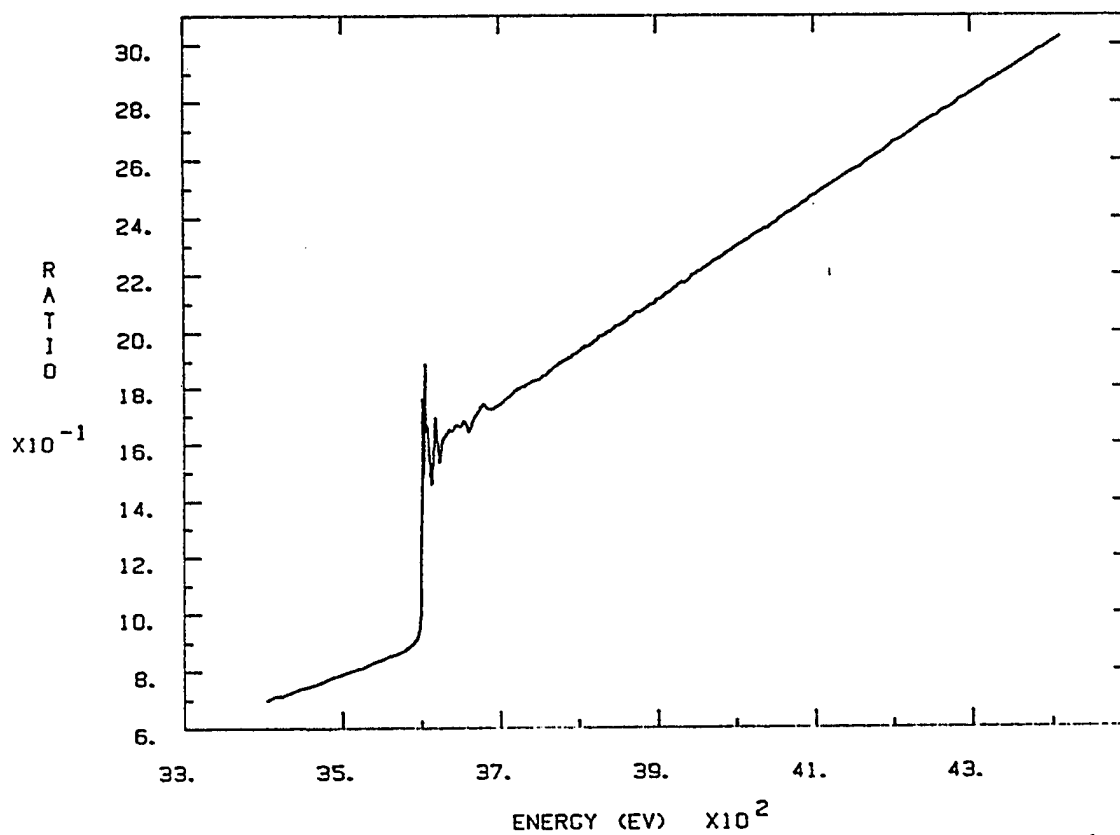
Figure 6 C1 XANES Scan of Newly Synthesized Polymer



CLPACP.001W/3/1 11-AUG-91 Figure 7 Cl XANES Scan Of AP/Binder



CLK.001 3/1 9-AUG-91 Figure 8a KCl Cl edge full scan showing A and K edges and Cl EXAFS



KCL.002 3/1 11-AUG-91 Figure 8b KCl K edge full scan showing K XANES and EXAFS

From the analog data, certain qualitative information may be obtained. For EXAFS, quantitative information may be deduced by carefully fitting the file data by averaging scans to reduce noise, performing background subtraction and energy calibration to obtain the inner potential, then transforming from energy to k space followed by a Fourier transform to obtain the (uncorrected) Radial Structure Function which is similar to a Radial Distribution Function and allows one to select the coordination spheres for proper fitting. This is a long process of interactive data processing involving both standard data from known compounds with a similar coordination and varying degrees of sophistication depending on the program used. It is our purpose to make these programs available to the personnel at Phillips Laboratory as needed for their future work.

It follows for this report that only analog examination is possible at this time. Nevertheless, we have formed the following conclusions based on our first Cl edge experience.

1. It is possible to work at the Cl K-edge with a Lytle detector minus Soller slits and filter. This poses no additional difficulty providing the small adsorption length for the soft radiation is taken into account. Beam line X-19A is an appropriate line for the Cl and Ti edge. The beam must be detuned drastically (70%) to reduce the third harmonic in the incident beam to less than 1/1000 and the contribution from all K emission lines is observed and may need to be corrected in the data analysis.

2. After changing samples, a decreasing intensity Ar edge is found which arises from the impurities in the air that can enter the Lytle detector sample chamber. This edge provides an automatic energy calibration for the Ar edge and, hence, an energy reference for the Cl edge, assuming linearity in the monochromator. We will test this approach since the reference energy for each scan eliminates one additional beam line vagary.

3. The Cl EXAFS region shows rapid damping and will be difficult to quantitatively treat. Good quality data was obtained for the samples. The minimum sample thickness was not determined, but most of our data was obtained from the first adsorption length in the sample. (from a surface layer about 25  $\mu\text{m}$  deep; we estimate a sensitivity limit of about 100  $\text{\AA}$  for this technique at the Cl edge.)

4. The XANES region was extremely rich and worthy of detailed study. It is unfortunate that this energy region is the poorest understood from an analysis point of view, but theoretical progress in curved wave and multiple scattering formulations is being made rapidly. This region shows major differences in structure from one sample to another, especially in the white line region which reflects the multiple scattering in the low energy (above the edge) region. For additional recent

information, see references 1, pg. 573;ref. 2 and 3.

#### Figure Captions

| Fig. No. | Caption   |
|----------|---|
| 1.       | NSLS Site plan.                                       |
| 2.       | X-19A Beam line data.                                 |
| 3.       | Lytle detector geometry, (CWRU).                      |
| 4a.      | Cl edge determination by on line computer windowing.  |
| 4b.      | Cl edge determination by differentiation. (preferred) |
| 5.       | Chlorohydroquinone Cl XANES.                          |
| 6.       | Polymer Cl XANES.                                     |
| 7.       | AP/binder Cl XANES.                                   |
| 8a.      | KCl Cl full scan showing Ar and K edges and Cl EXAFS. |
| 8b.      | KCl K full scan showing K edge XANES and EXAFS.       |



## References

1. X-Ray Absorption, Principles, Applications, Techniques of EXAFS, SEXAFS and XANES, Edited by D. C. Koningsberger and R. Prins, Eindhoven University, John Wiley and Sons, 1988, ISBN 0-471-87547-3 (hardcover).
2. X-Ray Absorption Fine Structure, Proceedings of the sixth International Conference on X-ray Absorption Fine Structures (EXAFS and XANES), York, UK 1991, (Organized by Daresbury Laboratory), Edited by S. Samar Hasnain, Daresbury Laboratory, Ellis Horwood Limited, 1991, ISBN 0-13-973199-7 (hardcover).
3. EXAFS and XANES studies of lead oxides and solutions of Pb(II) and Pb(IV) ions, James McBreen Department of Applied Science Brookhaven National Laboratory Upton, NY 11973 (private communication, submitted for publication 1991).

### Future Work

Little quantitative data reduction has been carried out to date owing to the recent (13 August, 1991) acquisition of the first data. It is also clear that the Xanes data is the most instructive and needs quantitative effort. It is also true that the next scheduled time is 4 days at X-19A during early October, 1991. It is suggested that those runs repeat any required data and concentrate on the determination of buried interfacial differences by fluorescence detection and electron detection or grazing incidence fluorescence be attempted in order to gain sensitivity. Use of the polarized X-ray beam is also recommended for oriented specimens.

## Monthly Report - January 1992

Chris Zorman

### 1. Electron Beam Damage:

Upon review of the data collected during the initial stage of this project, it was determined that some additional analysis could be done. This involved characterizing the damage made by the keV electron beam. By carefully measuring the photographs of the beam damage profile, we were able to show that the resulting damage is gaussian in nature. This is consistent with the beam profile, which is assumed gaussian. Figure 1 shows a typical data set and fit.

### 2. Vacuum System:

The main thrust of this month's work was to secure a UHV chamber in which to dedicate to the project. Such a system was obtained from the Electronics Design Center at CWRU. The system is being transferred to Dr. Hoffman's lab on 30 January and should, barring any major problems, be on line shortly.

### 3. EELS:

To prepare for the first set of experiments, much background work was done on the topic of EELS. Figure 2 shows a representation of previous EELS work done at CWRU.

### 4. EXAFS:

Since Guy DeRose recently defended his thesis, it was determined that I should be made familiar with the EXAFS technique. Under the guidance of Dr. Hoffman and Guy, I was given a "short course" in EXAFS. To get some valuable on-the-job training, I will go to Brookhaven's NSLS on 8 February.

Fig 1

KeV ELECTRON BEAM DAMAGE PROFILE IN SINGLE XTAL AP

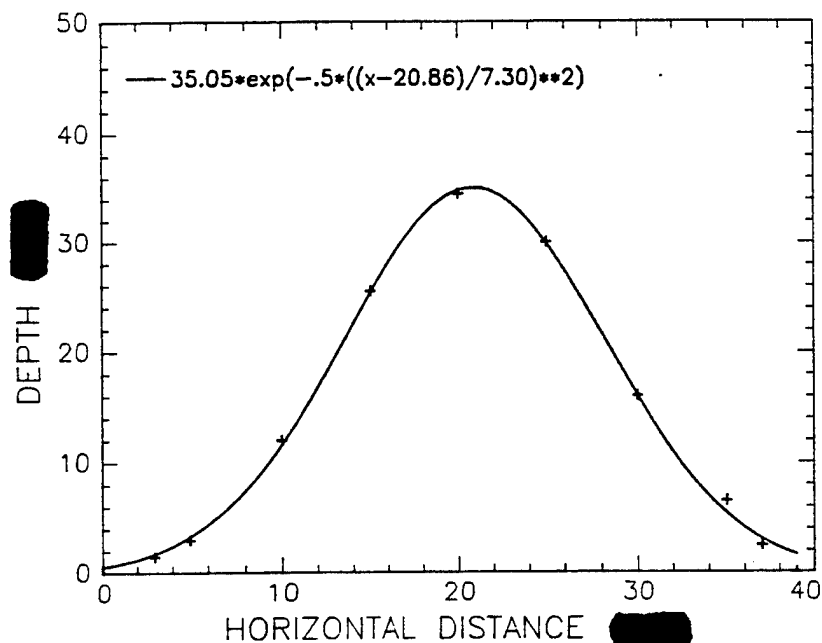
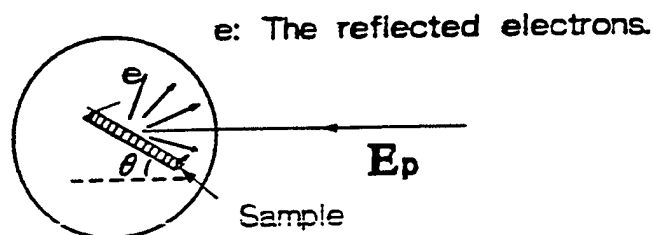


Fig 2

EELS Technique -- Diagram and parameters of CWRU experiment on Carbon Films and Diamond

UHV



$e$ : The reflected electrons.

$E_p$ : Primary electron energy at 1.0 KeV.

$I_e$ : Primary  $e$  beam current about  $-4 \mu A$ .

**CMA** with fixed pass energy at 70 eV.

$\theta$ : Incident angle of electron beam from sample surface at  $30^\circ$ .

**P**: Work pressure about  $1 \times 10^{-10}$  Torr.

## Monthly Report - January 1992

Guy A. DeRose

The feasibility of X-ray Absorption Fine Structure (XAFS) spectroscopy, as applied to materials of vital importance to the Air Force such as ammonium perchlorate (AP) and Cl - containing polymers and salts, was investigated at the National Synchrotron Light Source (NSLS) at Brookhaven National Laboratory. The technique of fluorescence detection with a conventional low-noise current amplifier was used at the Cl K-edge (2823 eV) and the XAFS data for AP,  $\text{NH}_4\text{Cl}$ , NaCl, KCl, 4 newly-synthesized Cl-containing polymers,  $\text{VCl}_3$  at both Cl and V K-edges, RbCl, and chloro- hydro- quinone (CLHQ) were obtained during a 4-day run in October in collaboration with two researchers from the Air Force Phillips Laboratory, Edwards AFB as part of the NEMESIS program. XAFS was also detected for a single crystal AP sample. A reference spectrum of AP, in the form of a pressed powder pellet, is shown in Figure 1 and the XAFS spectrum of a single crystal of AP is shown in Figure 2. An upcoming trip to NSLS is scheduled in which some Ti K-edge samples will be investigated and another student will be trained in all aspects of XAFS data collection and beamline operations.

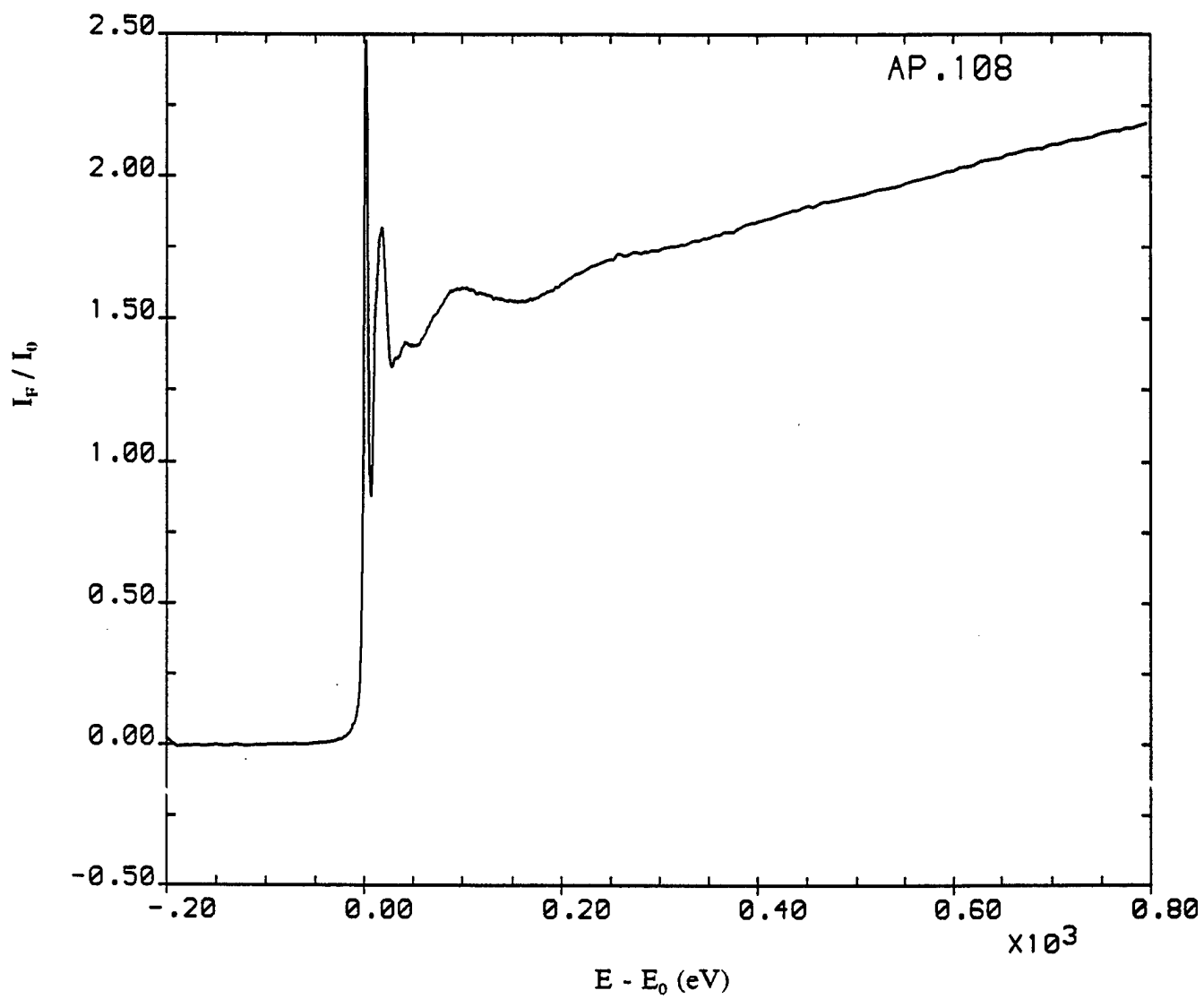


Figure 1: XAFS spectrum of  $\text{NH}_4\text{ClO}_4$  pressed powder pellet with pre-edge removed relative to  $E_0 = 2722.7 \text{ eV}$ .

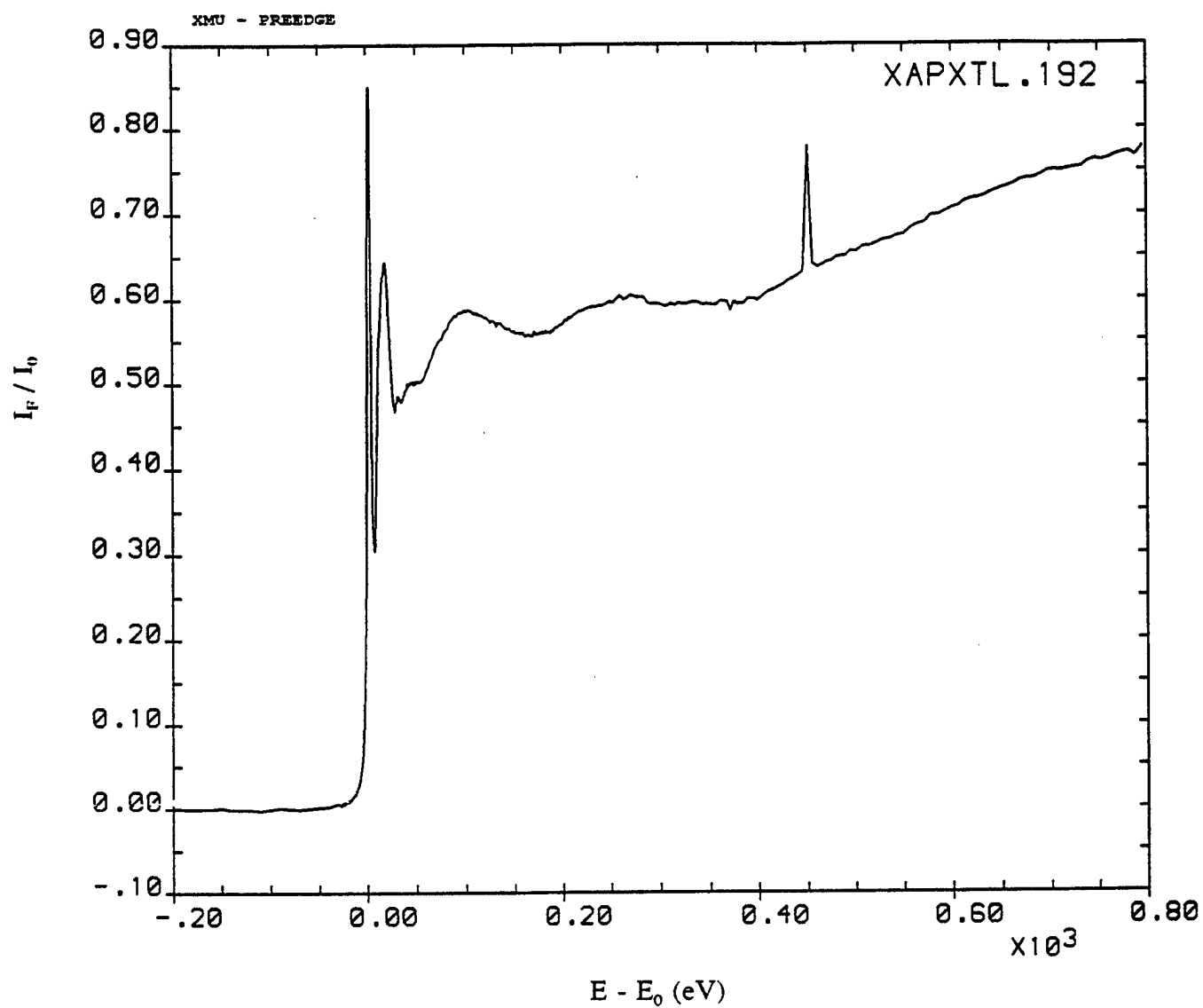


Figure 2: XAFS spectrum of  $\text{NH}_4\text{ClO}_4$  single crystal with pre-edge removed relative to  $E_0 = 2722.7$  eV.



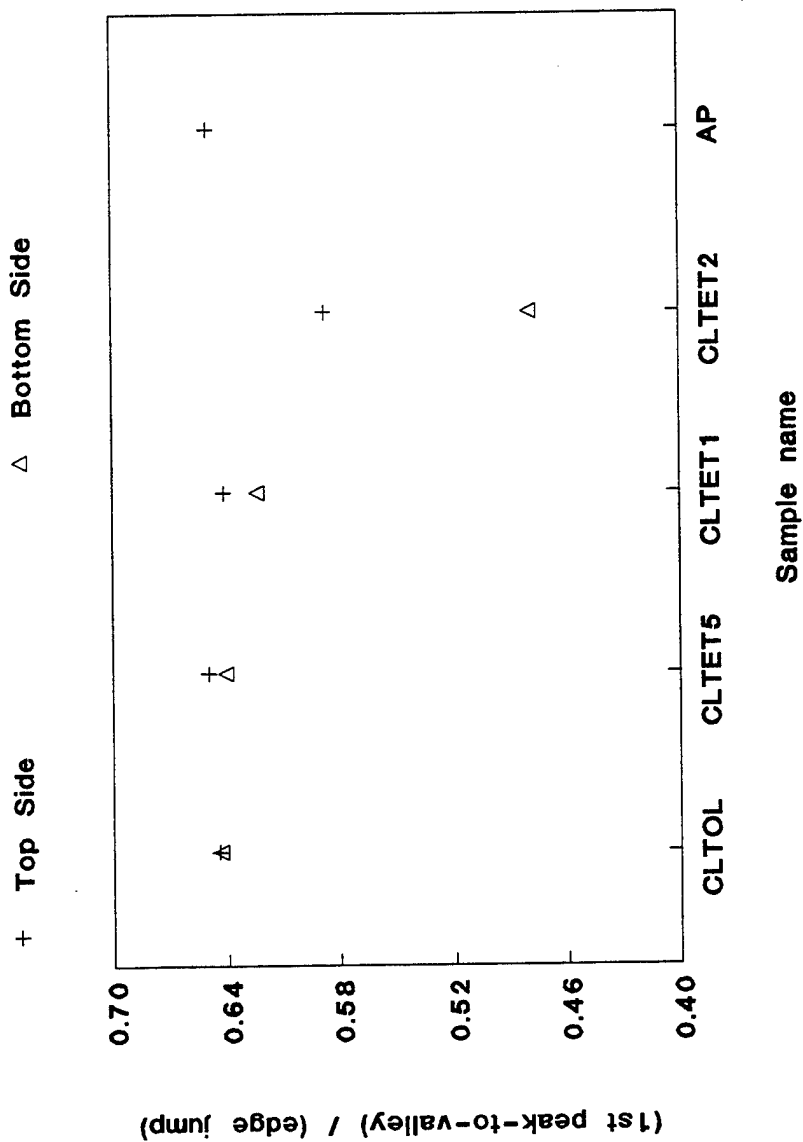
**August, 1991 XANES Results: Sample Side Dependence**

| Sample        | Normalized Jump  |                     |
|---------------|------------------|---------------------|
|               | Top Towards Beam | Bottom Towards Beam |
| AP/Toluene    | 0.645            | 0.644               |
| AP/TET 0.5 ML | 0.650            | 0.641               |
| AP/TET 1.0 ML | 0.642            | 0.624               |
| AP/TET 2.0 ML | 0.588            | 0.480               |
| AP/Blank      | 0.650            |                     |

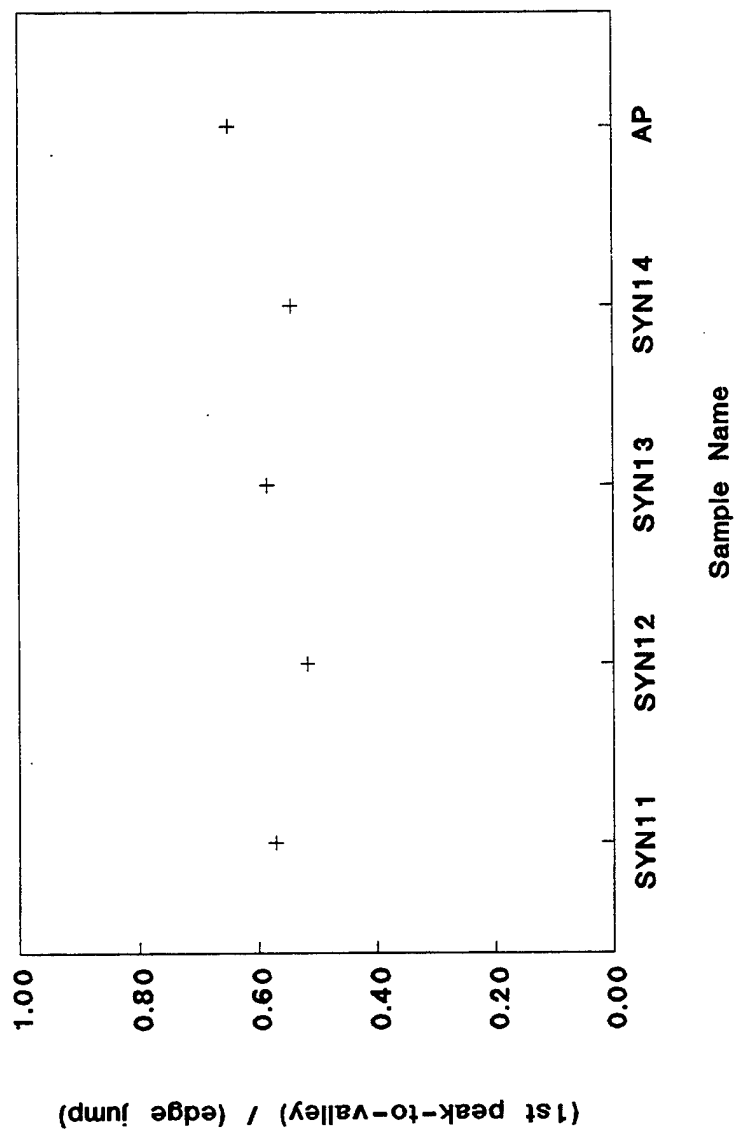
**October, 1991 XANES Results: Cl K-edge samples**

| Sample             | Normalized Jump |
|--------------------|-----------------|
| AP                 | 0.650           |
| AP/CLHQ            | 0.440           |
| AP/PECP            | 0.213           |
| VCl <sub>3</sub> R | 0.131           |
| VCl <sub>3</sub>   | 0.185           |
| KCl                | 0.248           |
| NH <sub>4</sub> Cl | 0.272           |
| NaCl               | 0.408           |
| RbCl               | 0.532           |
| SYN11              | 0.572           |
| SYN12              | 0.516           |
| SYN13              | 0.585           |
| SYN14              | 0.544           |

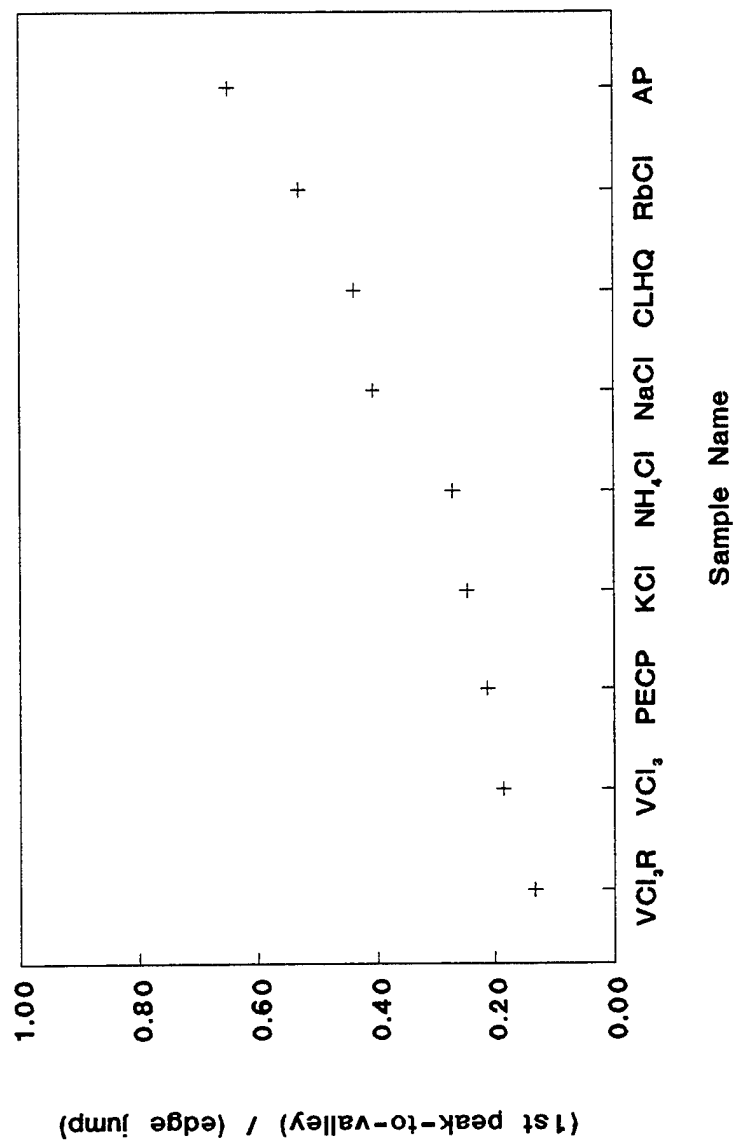
# Normalized 1st Absorption Feature vs sample material - Aug 1991 data



Normalized 1st Absorption Feature  
vs sample material - Oct 1991 data



Normalized 1st Absorption Feature  
vs sample material - Oct 1991 data



## MARS MONTHLY REPORT - FEBRUARY 1992

Thin Film / Surface Science Laboratory

Case Western Reserve University

Analysis of Cl K-edge XANES collected at NSLS Beamline X19-A during August and October, 1991 was ongoing during this reporting period, and some preliminary results are included herein. A "prescription" for fingerprinting XANES spectra was developed and applied to several samples. As shown graphically in Figure 1 for a pure  $\text{NH}_4\text{ClO}_4$  (AP) pressed pellet, we've calculated a normalized jump by dividing the drop in the absorption coefficient  $\mu$ , called  $\Delta\alpha$ , from the absorption peak to the first valley by the edge jump in  $\mu$ ,  $\alpha$ , from the pre-edge background. The pre-edge was obtained by a linear least squares fit. In Figure 2 the results of these calculations are plotted for PECP, PACP, CLHQ, HTPB, pure AP, DER, AND 752 binders. The left-hand ordinate is the difference in edge energy, where the edge position is chosen as the midpoint of the edge rise for this early analysis, between the sample and pure AP. As one might expect, there appear to be no large edge shifts between samples. The right-hand ordinate shows the dependence of the "normalized jump" defined above on sample material.

Another part of the investigation was to look at both sides of the AP pellets doped with toluene and with TET. In Figure 3 we see the difference in normalized jump between the side on which the drop of liquid was placed facing toward the incident beam "TOP SIDE" and placed away from the incident x-rays "BOTTOM SIDE". This normalized jump appears to be consistently smaller in magnitude when looked at for the bottom side than the top. Furthermore, the difference between the top and bottom sides becomes greater as a function of dose in the case

of TET. The sample names in Figure 3 are as follows: CLTET5 - 0.5 monolayer estimated coverage; CLTET1 - 1.0 monolayer coverage, and CLTET2 - 2.0 monolayer coverage. For reference, the normalized jump for AP is also included. Figure 4 shows the normalized jumps for four synthesized polymers from the Cl-edge XANES. Pure AP is also included on that plot as a reference. In Figure 5 the normalized jumps are plotted for several different chlorine-containing samples. Finally, Table 1 presents the numerical results of the calculated jumps as shown in Figures 2-5.

A new student (new to XAFS, not TFSSL) was introduced to synchrotron radiation operations and data collection during a run at the National Synchrotron Light Source (NSLS) on beamline X11-A during the second week of February. This training will allow the transition of XAFS data collection duties to take place once present personnel have completed their part(s) of the project.

This past month one of the main projects was to design the prototype of the proposed x-ray focusing spectrograph. Using a design first proposed by H. H. Johann in 1931 (see Figure 6), we constructed a focussing, wavelength dispersive bent mica spectrometer with a radius of curvature of 5 cm. This apparatus was made out a cardboard cylinder 10 cm in diameter by 7.5 cm high. The radius of the cylinder was the radius of the bent mica. A window was cut into the cylinder and the mica was fit to that window. An entrance window was also cut in the cylinder for passage of the incident x-rays. Upon passing through the entrance window, the incident beam would strike the bent mica at about a 37 degree angle. This angle was determined by considering a first order Bragg diffraction of 4012 eV x-rays from the mica (001) planes.

One shift of synchrotron radiation beam time was devoted to the first prototype, taken to the NSLS on 8 February 1992 for its first test. An x-ray beam of 4012 eV was passed through

the entrance slit and incident on the bent mica. Photographic film was placed opposite the entrance window to collect any Bragg diffracted x-rays. No evidence of Bragg diffraction was found on the Polaroid. It was determined by experiment that x-rays were reaching the bent mica. We are presently analyzing the problem and checking the design to see if there was a flaw, prior to either a  $2\pi$  energy dispersion or electron detection design.

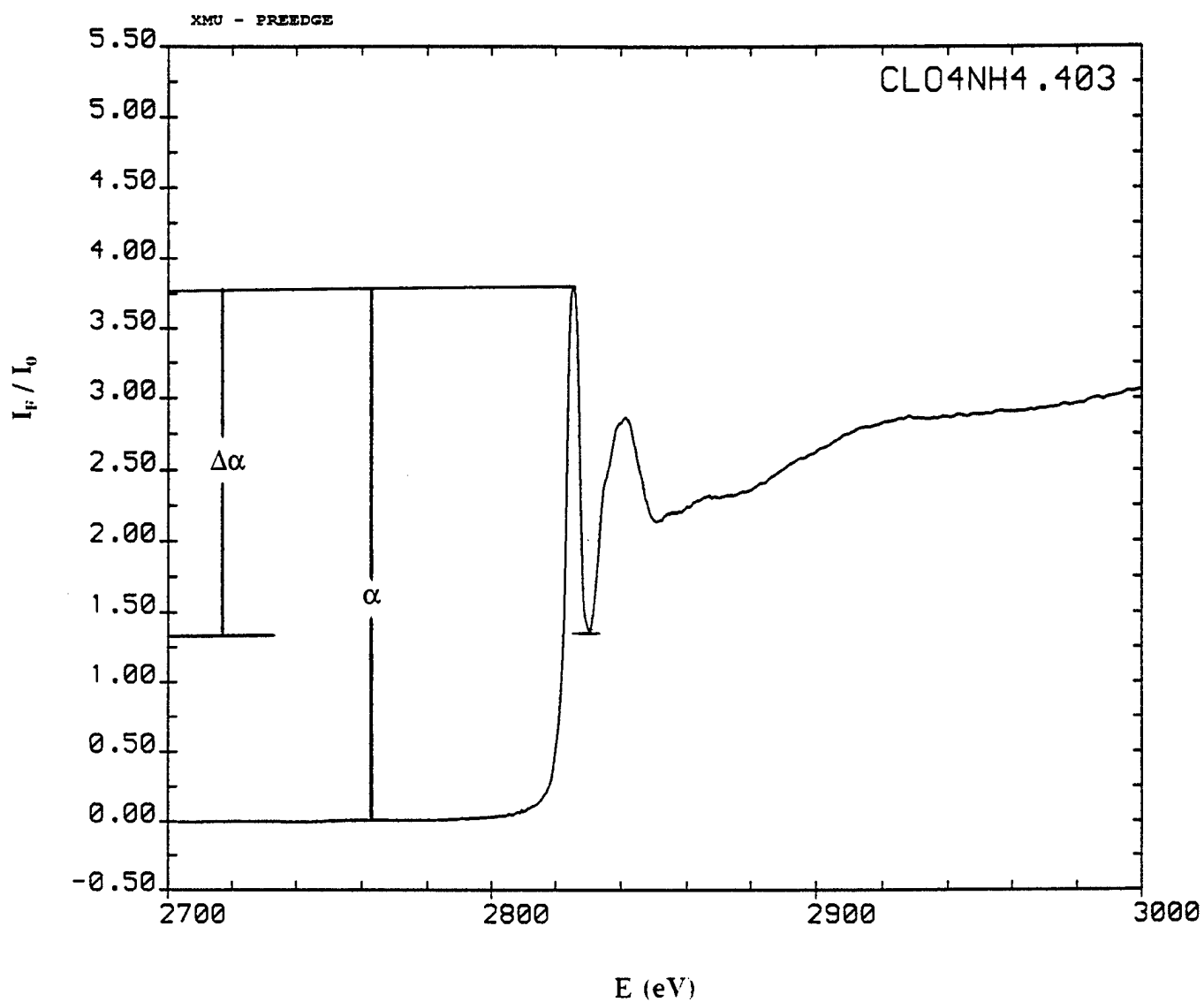


Figure 1: XANES spectrum of  $\text{NH}_4\text{ClO}_4$  pressed powder pellet with linear pre-edge removed.  $\alpha$  is the edge jump in the absorption coefficient and  $\Delta\alpha$  is the drop in absorption for the first post-edge feature. The "normalized jump" described in the text is equal to  $\Delta\alpha/\alpha$ .



AUGUST, 1991 DATA  
 $\text{NH}_4\text{ClO}_4$  Edge Features  
 vs binder material

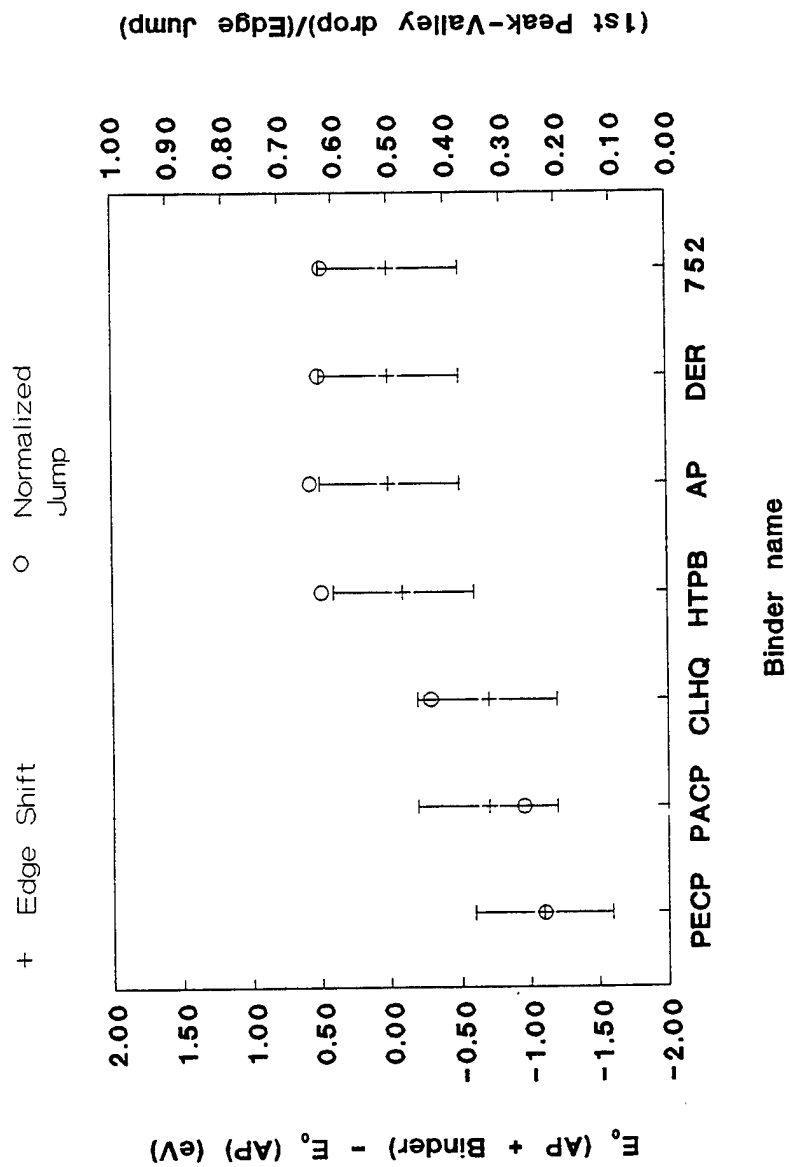


Figure 2

# Normalized 1st Absorption Feature vs sample material - Aug 1991 data

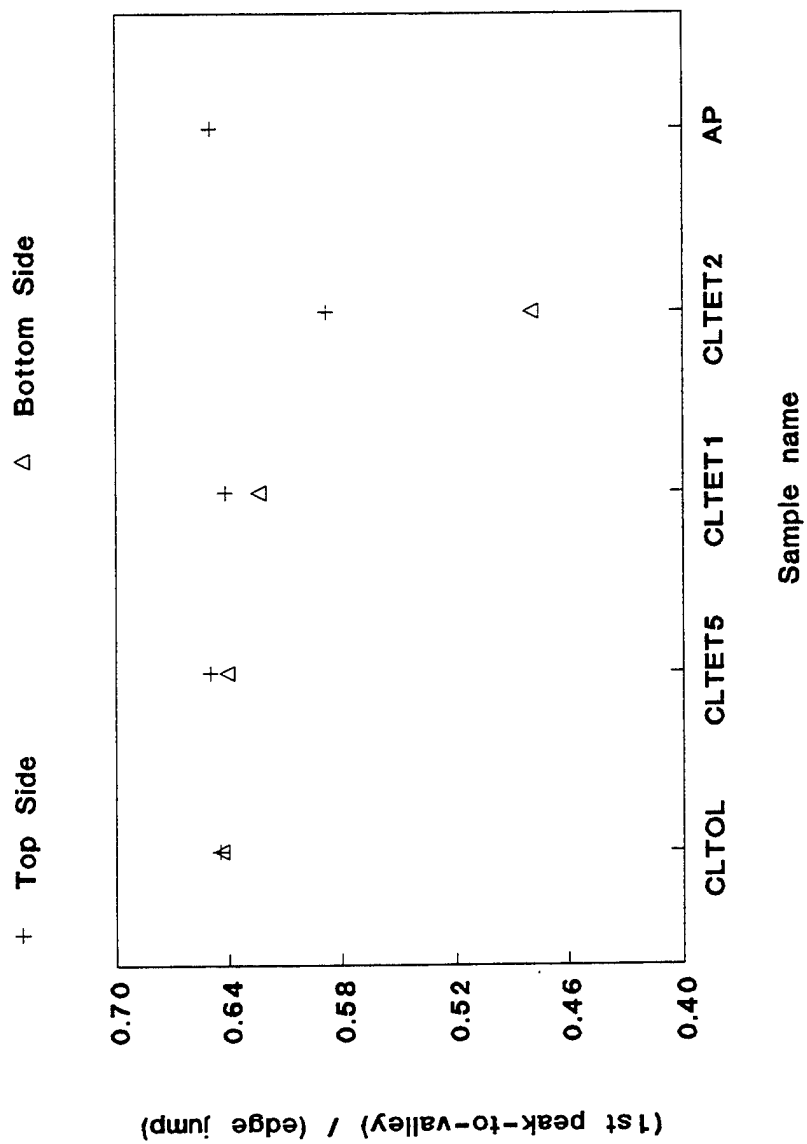


Figure 3

Normalized 1st Absorption Feature  
vs sample material - Oct 1991 data

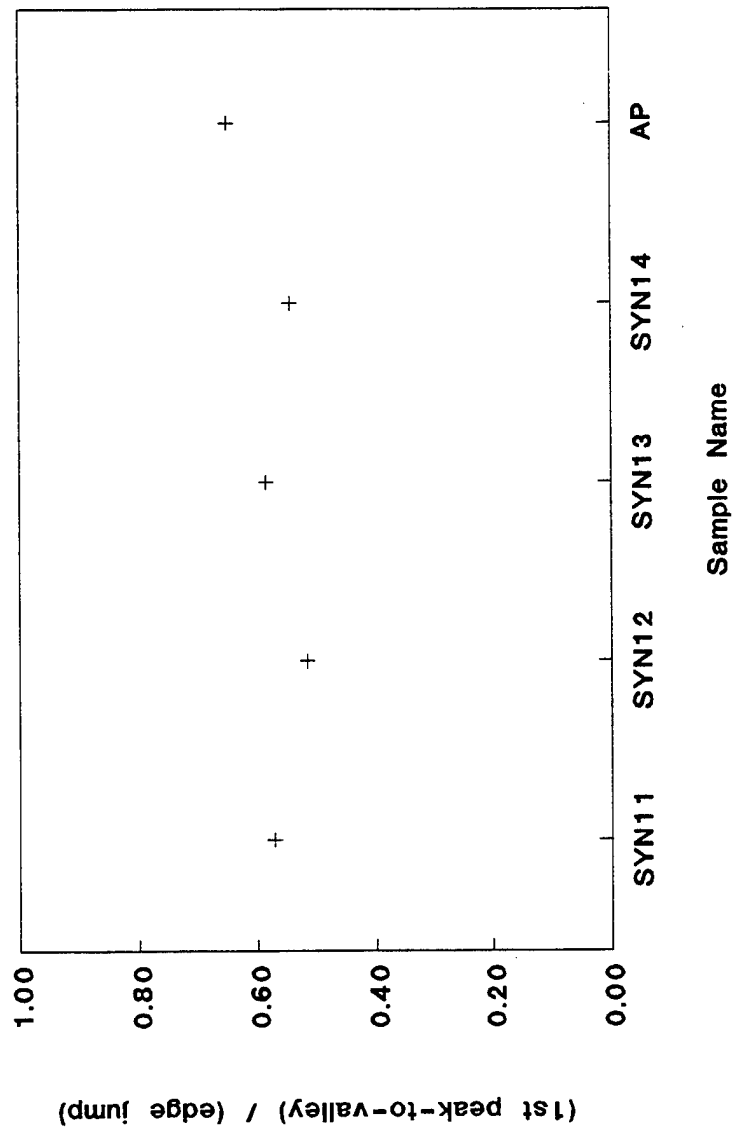


Figure 4

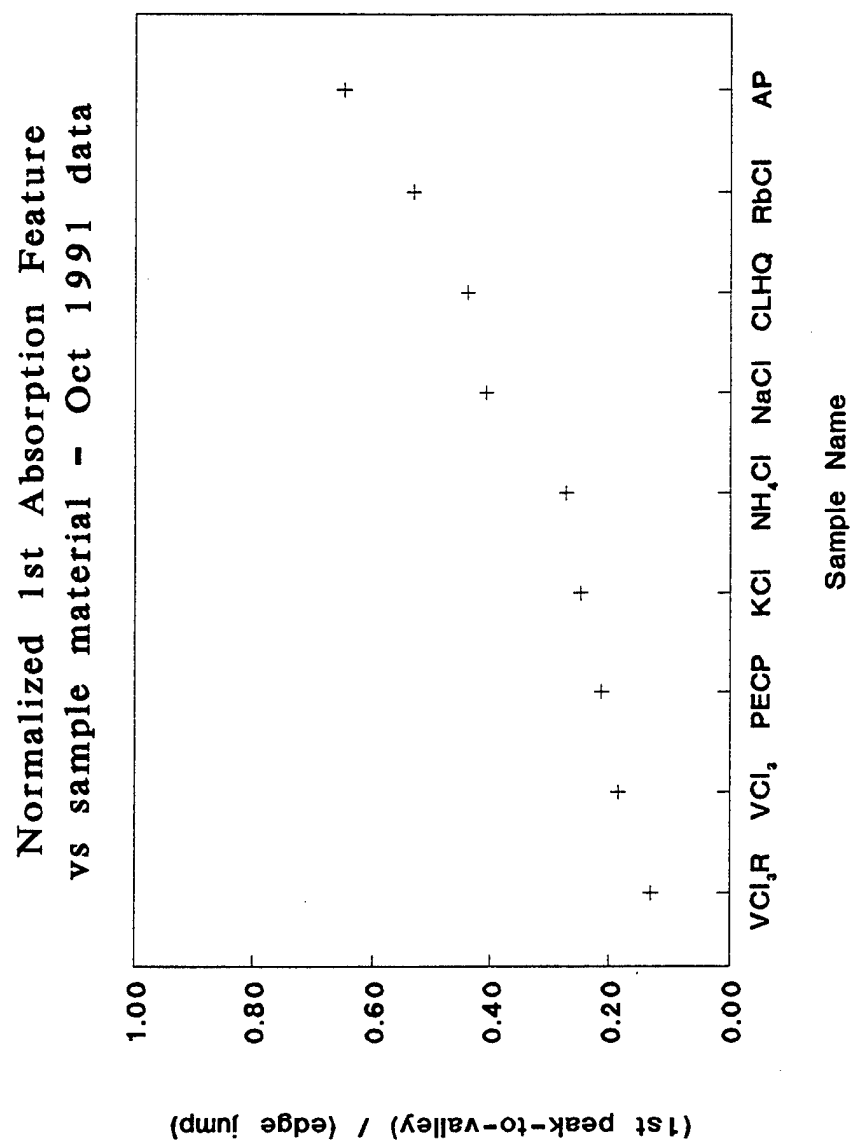


Figure 5

**August, 1991 XANES Results: Sample Side Dependence**

| Sample        | Normalized Jump  |                     |
|---------------|------------------|---------------------|
|               | Top Towards Beam | Bottom Towards Beam |
| AP/Toluene    | 0.645            | 0.644               |
| AP/TET 0.5 ML | 0.650            | 0.641               |
| AP/TET 1.0 ML | 0.642            | 0.624               |
| AP/TET 2.0 ML | 0.588            | 0.480               |
| AP/Blank      | 0.650            |                     |

**October, 1991 XANES Results: Cl K-edge samples**

| Sample             | Normalized Jump |
|--------------------|-----------------|
| AP                 | 0.650           |
| AP/CLHQ            | 0.440           |
| AP/PECP            | 0.213           |
| VCl <sub>3</sub> R | 0.131           |
| VCl <sub>3</sub>   | 0.185           |
| KCl                | 0.248           |
| NH <sub>4</sub> Cl | 0.272           |
| NaCl               | 0.408           |
| RbCl               | 0.532           |
| SYN11              | 0.572           |
| SYN12              | 0.516           |
| SYN13              | 0.585           |
| SYN14              | 0.544           |

Table 1

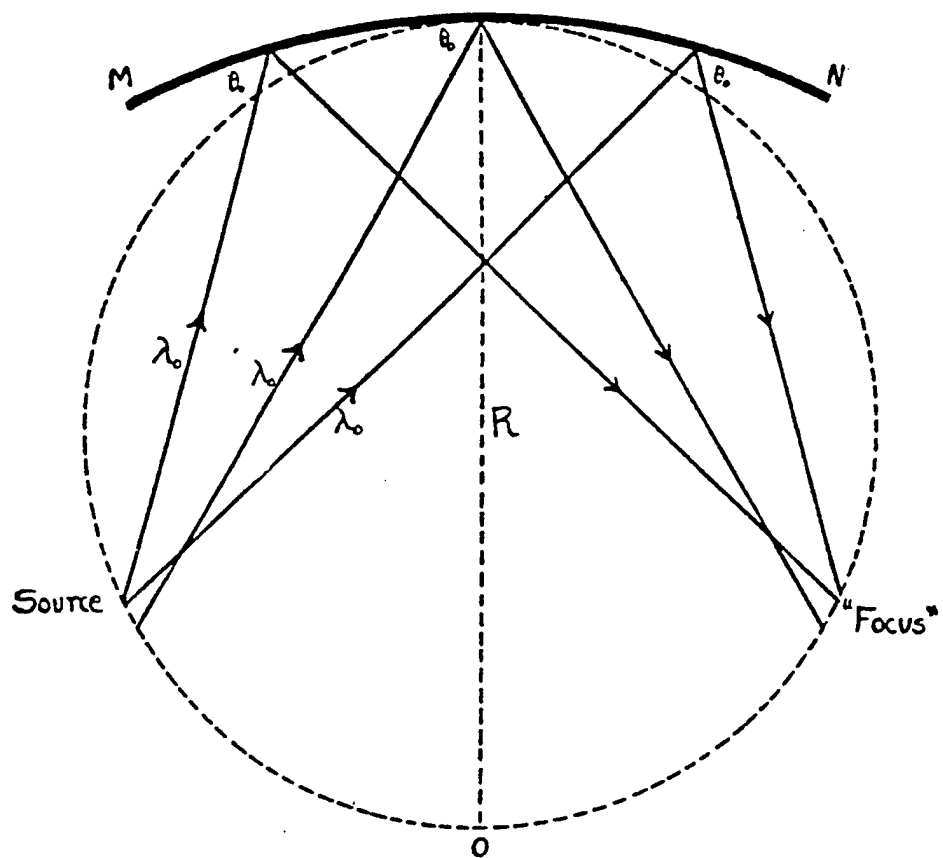


FIG. IX-19. Principle of a bent crystal focussing spectrograph according to Johann.

## MARS MONTHLY REPORT - MARCH 1992

Thin Film / Surface Science Laboratory

Case Western Reserve University

Analysis of Cl K-edge XANES collected at NSLS Beamline X19-A during August and October, 1991 was ongoing during this reporting period, and included much computer programming and testing to calibrate the energy scale as determined by the X19-A monochromator and the Ar absorption edge found in the data sets mentioned above. The procedure was to modify existing code and add a routine to shift the energy axis of the data set to account for the fact that the Ar edge is always fixed and that the edge position is subject to changes from one material to another (i.e., assume XANES may be different in each of the Cl-containing samples and Ar is inert). The procedure discussed above is presently being applied to all of the data obtained during the two XAFS runs of 1991. In Figures 1-3 we see the results of 1) finding the Cl absorption edge as a check on the analysis program, 2) finding the Ar edge in the data set, and 3) subtracting the difference between a) the mathematically determined inflection point ( for the data with positive Ar jump ) or b) the halfway point in the dropping Ar jump and the tabulated Ar edge of 3205.9 eV from the entire data set and re-finding the Cl-edge inflection point in an ammonium perchlorate (AP) sample. Of course, since the Ar edge jump is negative in this case (October, 1991 data) step (3b) was followed in this part of the reduction. Similar plots are shown in Figures 4-6 for ammonium chloride, and from figures 3 and 6 it is apparent that the edges in these two materials differ by about  $6 \pm 0.5$  eV. For reference purposes and cross-checking, the plot labelled "AP1" is the averaged data of the files AP.101, AP.102,

AP.103, AP.104, and AP.105 and "AC" is the average of the files CLNH4.109, CLNH4.110, CLNH4.111, CLNH4.112, CLNH4.113, CLNH4.114, CLNH4.115, and CLNH4.116. Both of those averaged sets are from the October, 1991 XAFS run and show a negative Ar feature. The physical origin of such shifts is being investigated. The procedure described above for the energy calibration is in the process of being applied to all samples from both XAFS runs at BNL and should be completed during the next reporting period.

This March was also spent preparing for the Electron Energy Loss Spectroscopy (EELS) experiments on AP single crystal and pressed pellet samples. This technique was last employed by the TFSSL in 1990 by Dr. Y. X. Wang. He used it to study diamond and diamond-like carbon samples for his PhD dissertation. We used his experience and some of the references he listed as background for the EELS study of AP.

We decided to use the same UHV system as was used by Dr. Wang as a starting point since it has a residual gas analyzer and double pass CMA. This will permit a real time study of electron beam damage on AP for electron energies from 500eV to 1keV. In order to see if the EELS equipment functions properly, we loaded a series of carbon samples (HOPG, diamond and grafoil) in hopes of duplicating Dr. Wang's thesis work. We were successful in repeating his low resolution energy loss and K edge absorption work but are still working on the high resolution low energy loss spectroscopy. A sample data set from HOPG is shown in Figures 7 and 8. We are currently working on using the computerized data analysis programs.

We hope to load the first set of AP samples by April 10. This should enable us to have some good EELS data by our next monthly report. We are also preparing for the June, 1992 BNL X-11 time to further test the background reduction techniques.



E0= 2826.76  
AP1

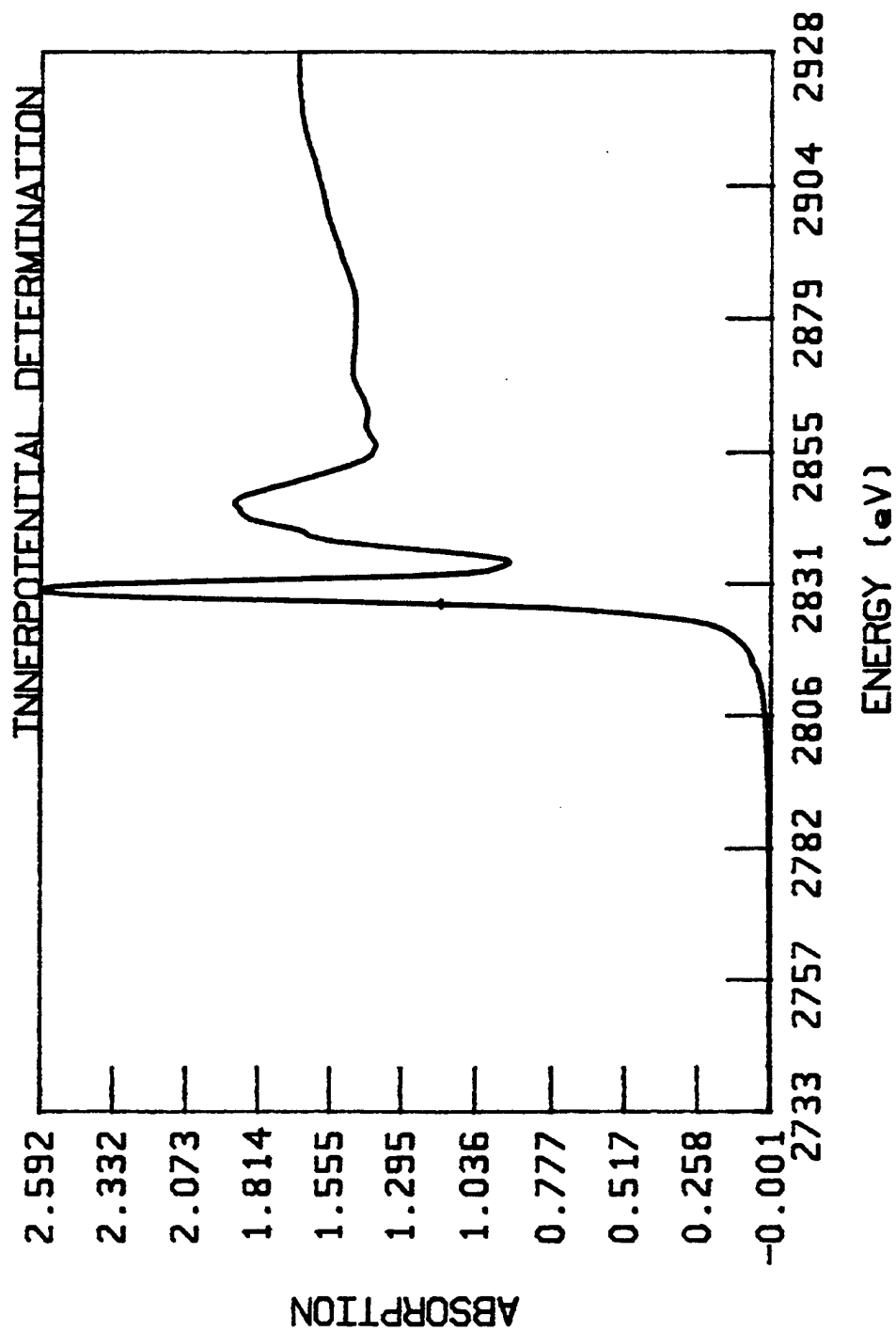


FIGURE 1

E0= 3200.10  
AP1

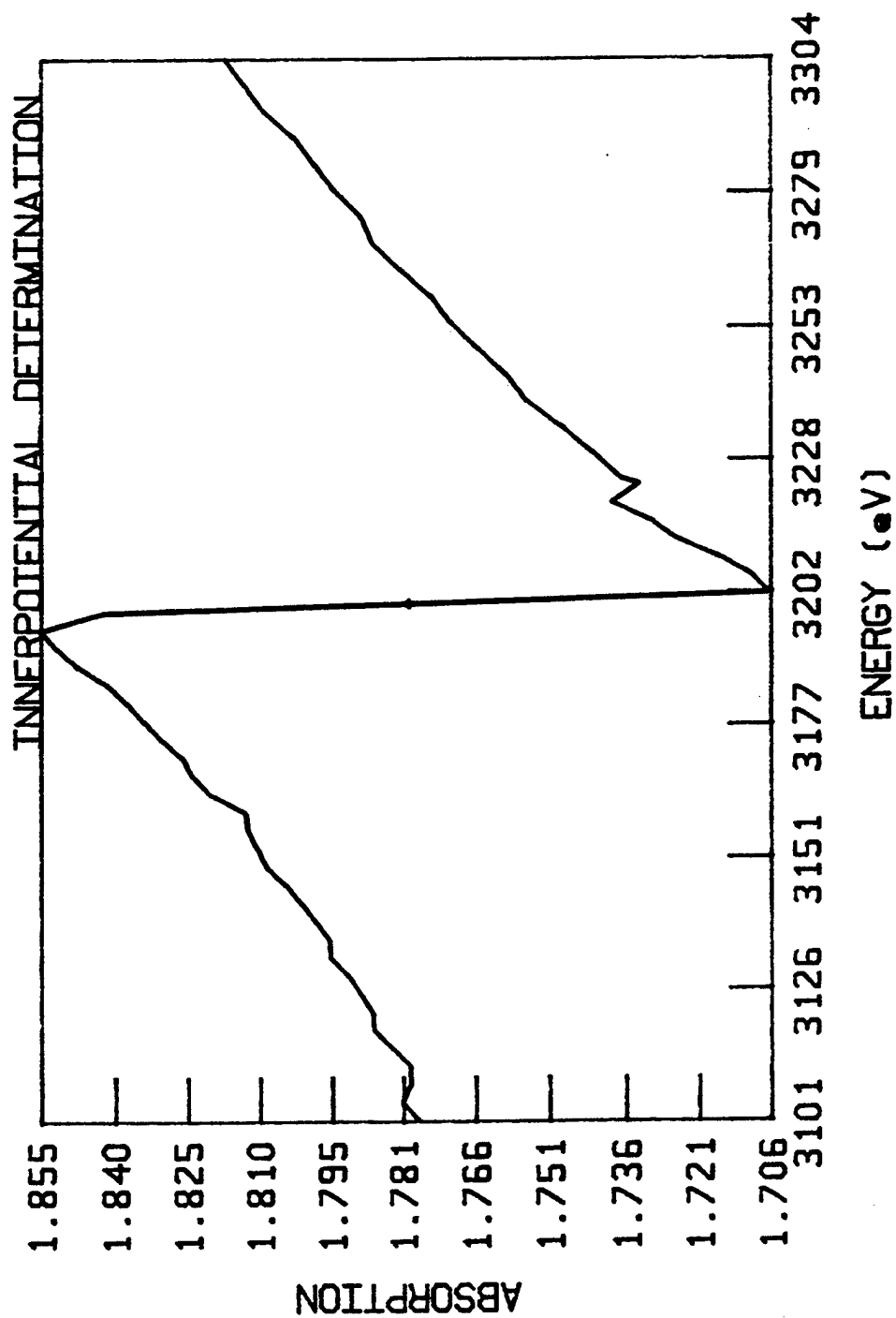


FIGURE 2

E0 = 2832.56  
AP1

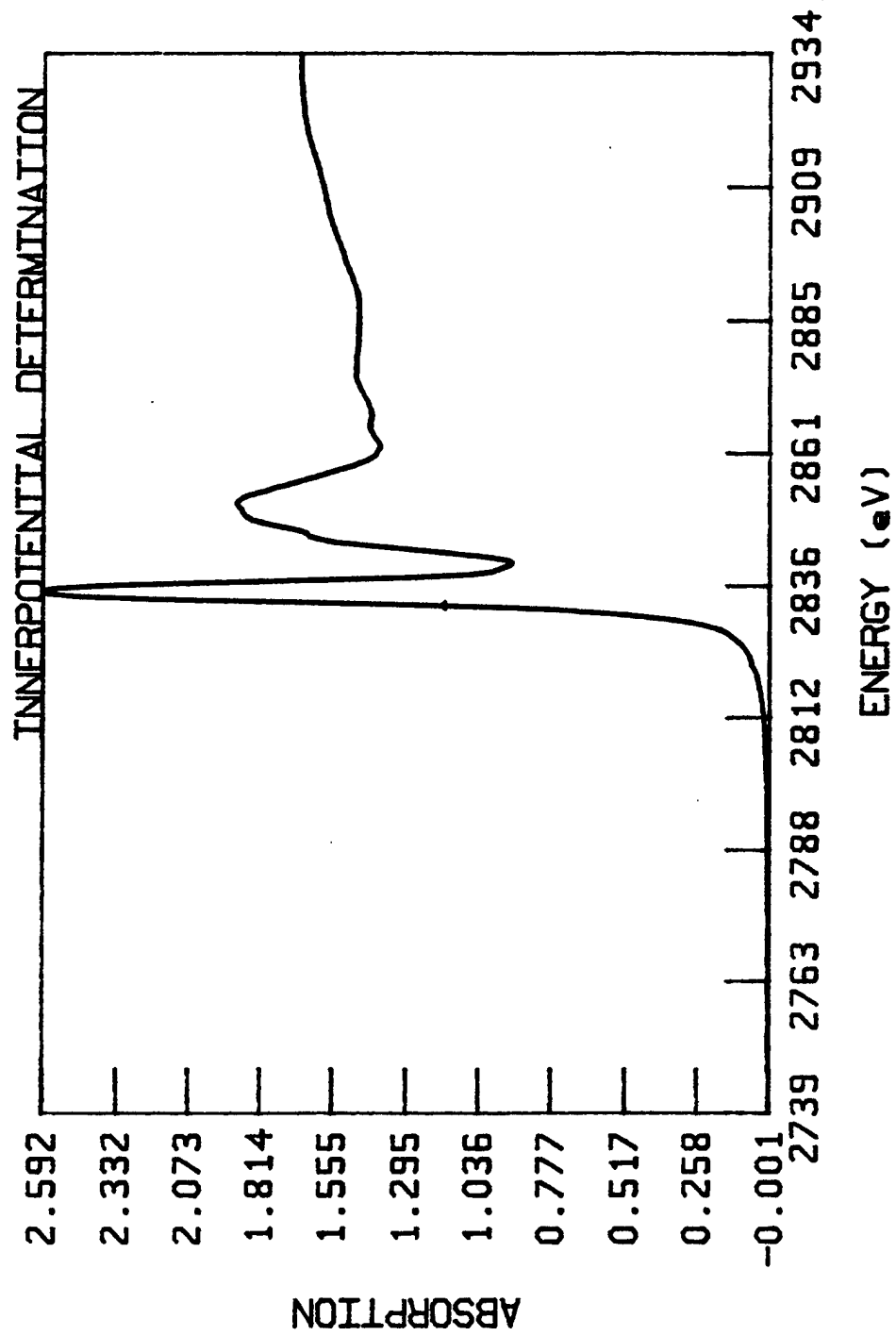


FIGURE 3

E0= 2814.34  
AC

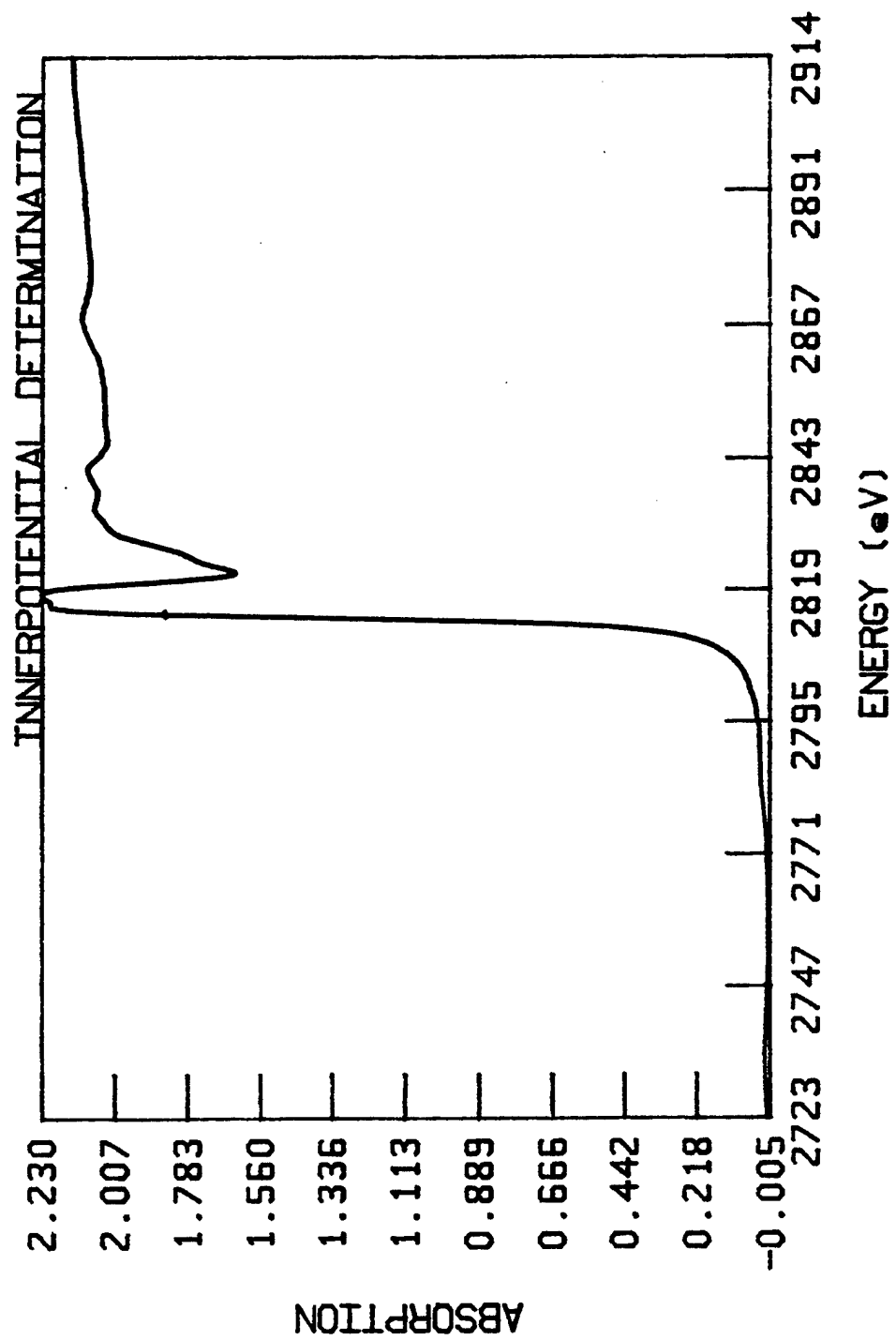


FIGURE 4

E0 = 3193.70  
AC

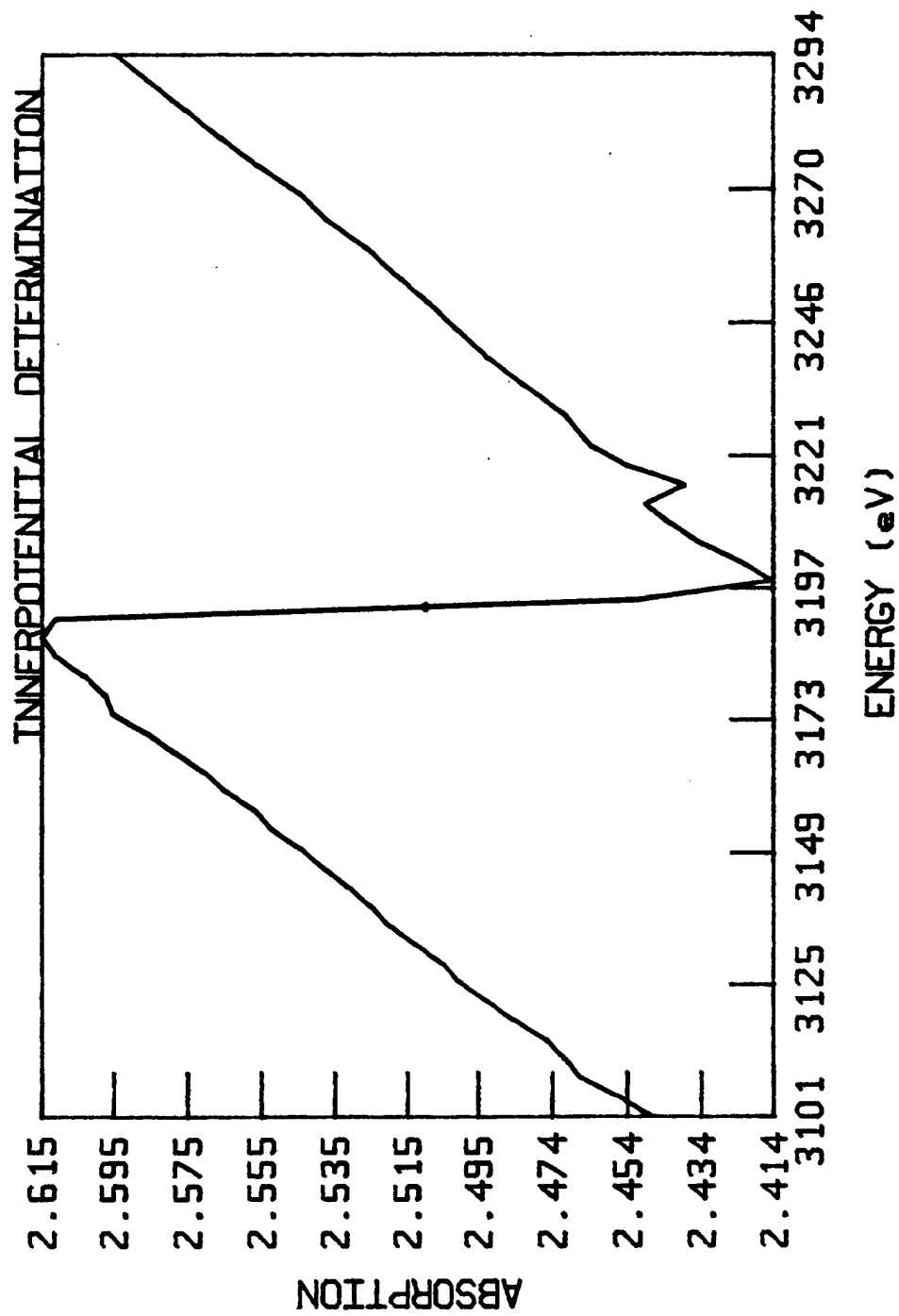


FIGURE 5

E0= 2826.54

AC

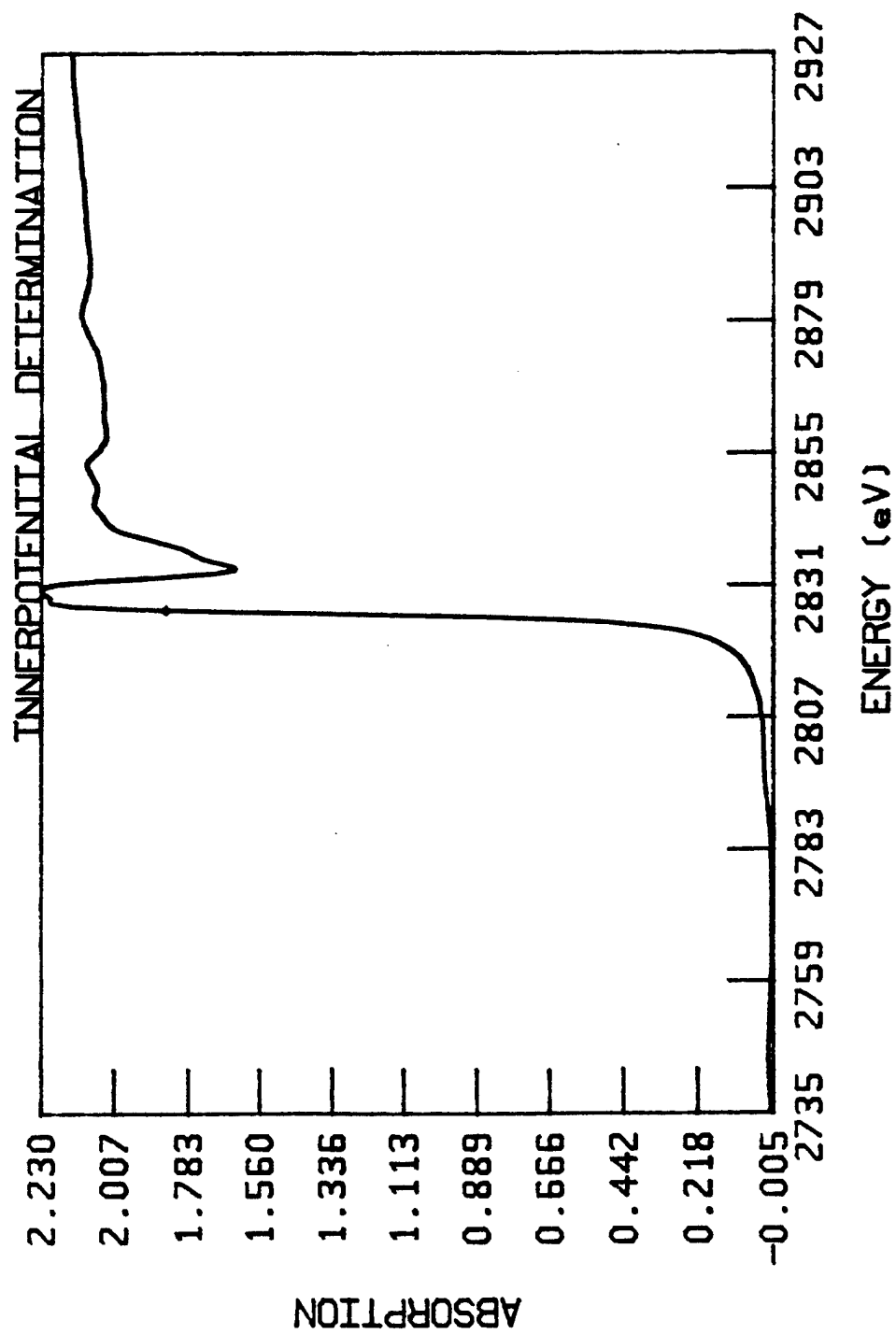


FIGURE 6

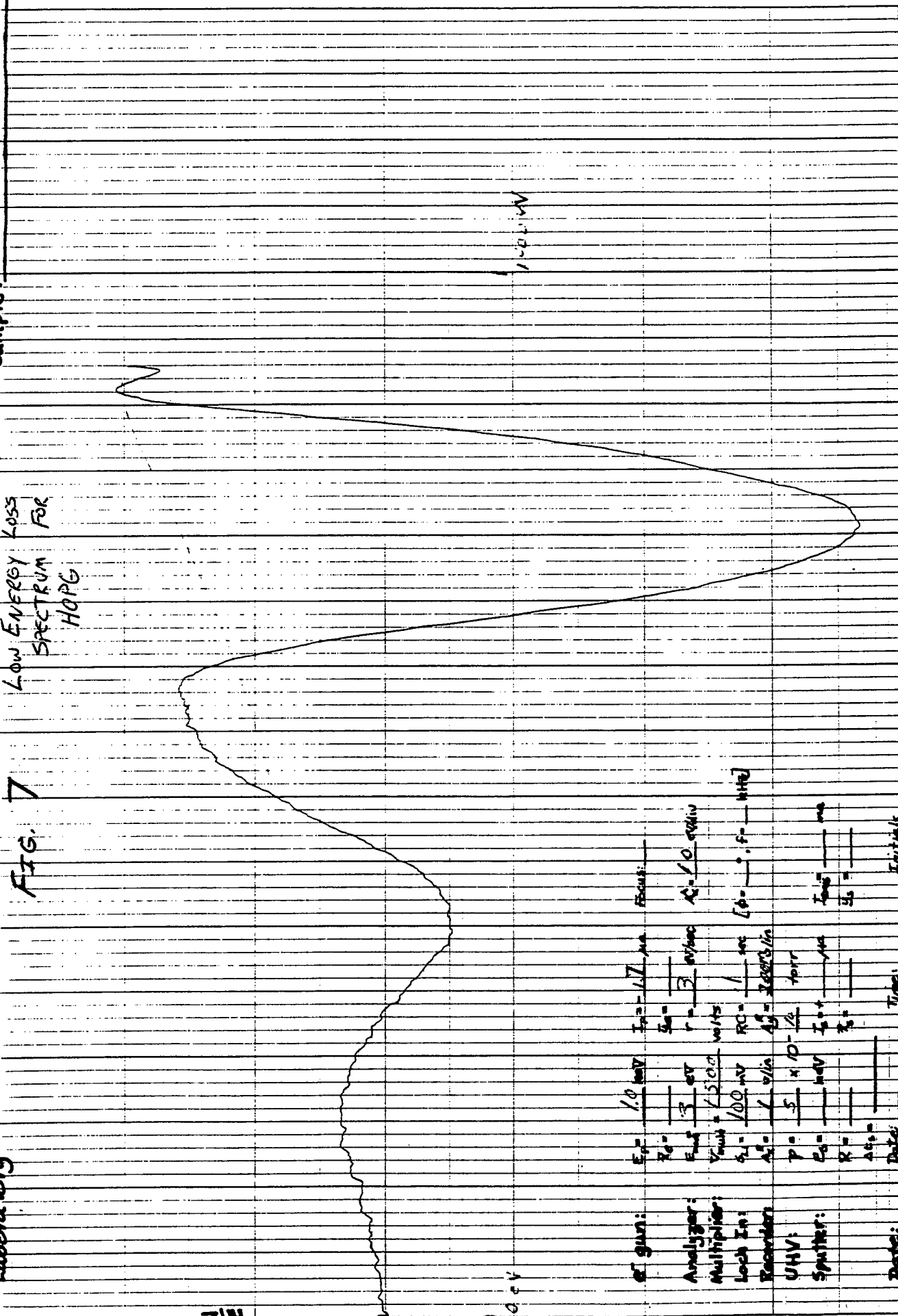
CWRU  
Surface Physics  
Laboratory

# AUGER ELECTRON SPECTRUM

Low Energy Loss  
Spectrum For  
HOPG

FIG. 7

Sample: HOPG



Electron gun:  $E_p = 10 \text{ keV}$   $I_p = 1.7 \text{ mA}$  Focus:  $R = 10 \text{ eV/div}$   
 Analyzer:  $E_a = 3 \text{ eV}$   $r = 3 \text{ mm/sec}$   $R = 10 \text{ eV/div}$   
 Multiplier:  $V_{mult} = 1500 \text{ volts}$   $RC = 1 \text{ sec}$   $f = 1 \text{ MHz}$   
 Lock In:  $A_1 = 100 \text{ mV}$   $A_2 = 100 \text{ mV}$   $A_3 = 100 \text{ mV}$   
 Recorder:  $P = 5 \times 10^{-10} \text{ torr}$   $I_{sp} = 1 \text{ mA}$   
 UHV:  $E_s = 10 \text{ eV}$   $I_s = 1 \text{ mA}$   $I_{sp} = 1 \text{ mA}$   
 Sputter:  $R = 1 \text{ mm}$   $I_s = 1 \text{ mA}$   $I_{sp} = 1 \text{ mA}$   
 Date: \_\_\_\_\_ Time: \_\_\_\_\_ Initials: \_\_\_\_\_

CWRU  
Surface Physics  
Laboratory

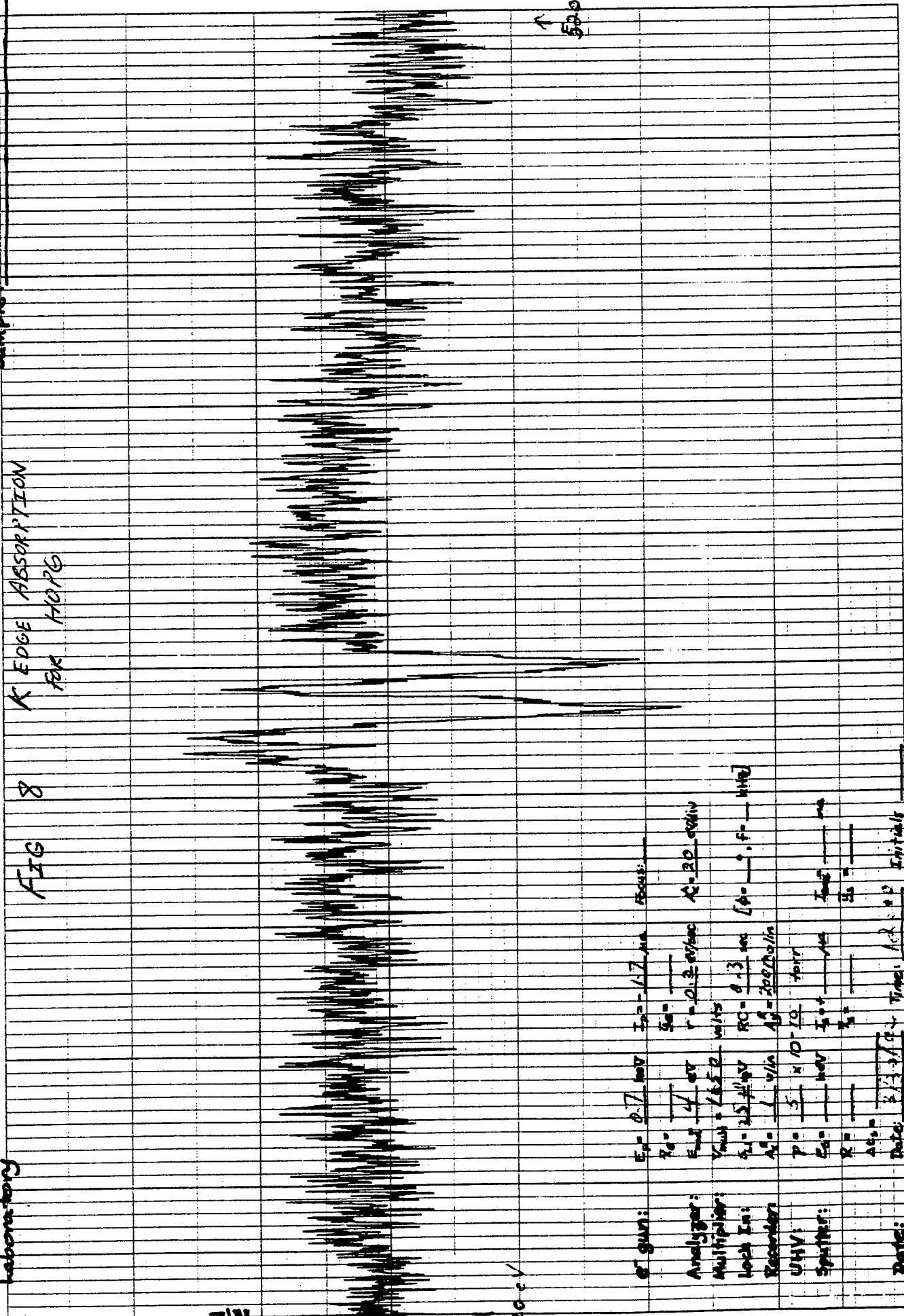
# AUGER ELECTRON SPECTRUM

Sample:

flopG

FIG 8 K EDGE ABSORPTION

FOR HARP



Electron Gun:  $E_p = 0.7$  keV  $I_p = 1.7$  mA Focus:  $A = 3.0$  mm

Analyzer:  $E_a = 4$  eV  $r = 0.3$  mm  $A = 3.0$  mm

Multiplication:  $V_{mult} = 1.5 \times 10^4$  V  $RC = 0.13$  sec  $[A = 0, F = 100]$

Lock In:  $A_0 = 1$  V  $A_1 = 2.5 \times 10^4$  V  $A_2 = 2.0 \times 10^4$  V

Recorder:  $p = 5 \times 10^{-10}$  Torr  $I_{out} = 1$  mA

UHV:  $E_a = 4$  eV  $I_p = 1.7$  mA  $I_{out} = 1$  mA

Splitter:  $R = 1$  V  $I_p = 1.7$  mA  $I_{out} = 1$  mA

Date: 3/3/82 Time: 12:12 Initials: [Signature]



E0= 2838.57  
8781B

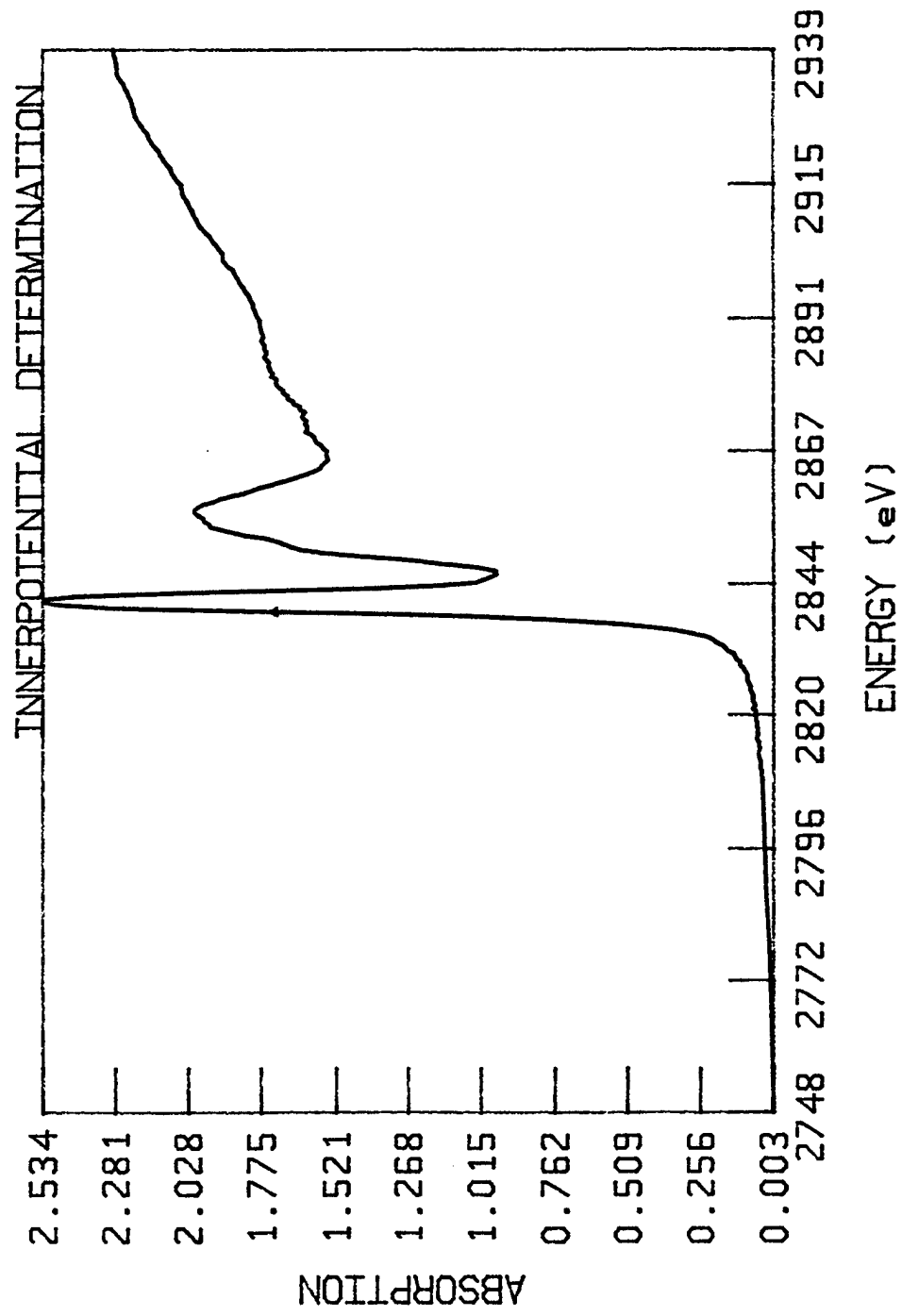


FIGURE 13

E0 = 2836.06  
8791B

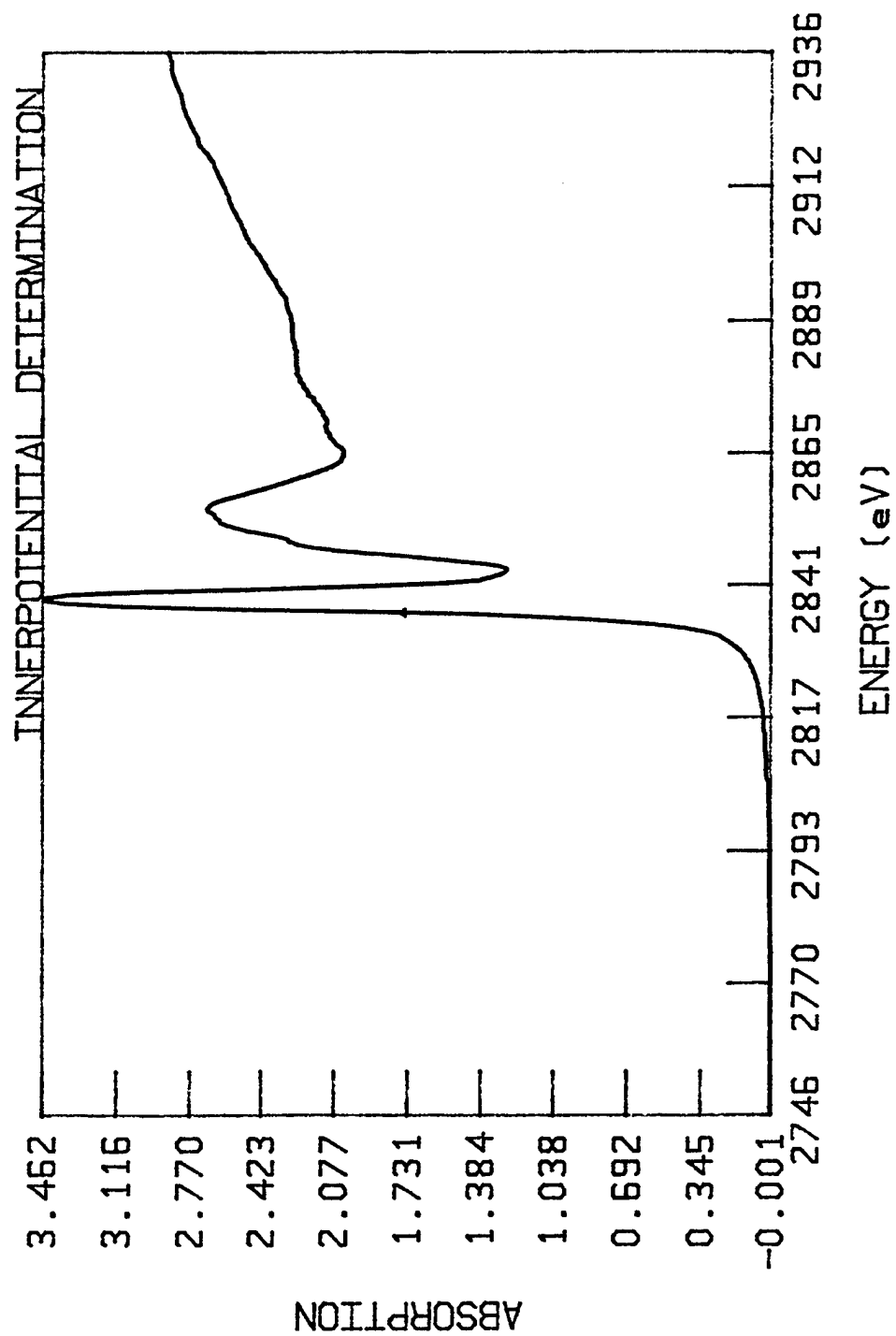


FIGURE 18

## MARS MONTHLY REPORT - APRIL 1992

Thin Film / Surface Science Laboratory

Case Western Reserve University

### **I. X-ray Absorption Near Edge Structure**

The computer code developed during the previous reporting period was refined and applied to the totality of the Cl k-edge X-ray Absorption Fine Structure (XAFS) data collected during August and October 1991. The results of this analysis are tabulated in Tables I and II.

In both tables, all data sets are listed in the order in which they were collected. The first column of the tables lists either the original data file name or the ".JOU" files in the case of averaging. The second column lists the ".JOU" or journal file created for each data set which keeps a record of the analysis operations performed on the data file(s) in the same format as the EXAFS analysis program. The next three columns list the originally determined inflection point for the Cl edge, the Ar inflection point (or picked value as appropriate), and the Ar-corrected Cl edge energy. The amount of shift is obtained by

$$\Delta Ar = E_0^{Ar} (\text{Theoretical}) - E_0^{Ar} (\text{experimental}),$$

where  $E_0^{Ar} (\text{Theoretical}) = 3205.9 \text{ eV}$  and  $E_0^{Ar} (\text{experimental})$  is obtained from column 4, and is added to the Cl edge energy from column 3 to get the results tabulated in column 5. The column labelled " $\Delta Ar$ " is the amount of the shift explained above. The next column, " $\Delta Cl$ ", is the difference between the Cl edge of the sample (column 5) and the theoretical, free Cl energy

(2822.0 eV) from the McMaster tables. Finally, the last column contains the Scan Name - refer to the beamline log book for details. The superscripts are explained at the end of Table II.

Now that the column headings have been defined, a detailed look at the data contained therein is needed. Figures 1, 2, and 3 illustrate the edge determination procedure for a sample of "pure" ammonium perchlorate (AP) powder pellet. Figure 1 graphically shows the determination of  $E_0$  Cl, Figure 2 shows  $E_0$  Ar, and Figure 3  $E_0$  Cl-Corr. for the averaged data set labelled AP4. Figures 4 through 29 show the resultant  $E_0$  Cl-Corr. for TOLT, TOLB, TET1T, TET1B, TET2T, TET2B, TET5B, TET5T1, CLNA2, 8781B, 8782T, 8785B, CLK, AP6 for re-checking purposes, 8791B, SYN141, CLNH420, CLSYN13, CLSYN122, CLSYN11, PACP, PECP, CLHQ, 7521B, DER1B, and CLO4CU, respectively. Similar plots are shown for HTP1B and HTP1B3 in Figures 30 and 31, respectively. In between those scans, an AP "calibration" was done.

Turning to the October data, in which the Ar edge occurred as a drop, the Ar edge position was manually determined as the halfway point in the drop. To illustrate the calibration technique, consider Figures 32, 33, and 34 which show the procedure for AP powder pellet AP1. Figure 35 shows the calibrated Cl edge in AC1 and a comparison with CLNH4O4 from August indicated that a fine step size in the Ar region improves reproducibility.

In Figures 36-49 the corrected Cl edges are plotted for CLNA, CLK, CLHQ, SYN11, SYN1233, AP2, SYN13, SYN1452 and SYN14, CL3V158, CL3VR, CLRB1, PECP, and CLRB2, respectively. It should be noted that for the files which have an  $E_0$  Ar entry of 3205.9 eV (CLRB files) the Ar edge drop was not distinguishable from the data oscillations and as a result the Ar shift for those scans is zero. In addition, the scans which have a noted low inflection

point for  $E_0$  Cl (3rd column) also have a low inflection point in  $E_0$  Cl-Corr. (5th column).

Two points can be concluded from these data at this time. The first is that successive runs for a given sample in the same beam fill without manually reassigning the edge energy online between scans show no monochromator drift and reproducible results. The second conclusion is that using the Ar edge as a point of calibration appears to be useful and we recommend the use of a fine step through the Ar edge.

## **II. Electron Energy Loss Spectroscopy**

This April we began the EELS study of AP. This study was divided into two main parts: An electron beam damage study of AP for incident beams below 2keV and an EELS study of single crystal AP.

### **1. Equipment.**

We loaded single crystal and pressed pellet AP samples into our UHV Auger Analysis chamber. This chamber routinely pumps down to the mid  $10^{-10}$  Torr range, thus allowing us to assess AP's compatibility with a UHV environment. The chamber is equipped with a EAI Quad 250B Residual Gas Analyzer which was used for the electron beam damage study. It has a Phi 15-2256 double pass CMA and all the support electronics which were used for the EELS study. A diagram of the experimental apparatus is shown in Figure 50.

### **2. Electron Beam Damage Study.**

Before doing any EELS work, we wanted to see the extent of electron beam damage on AP for energies in the 500eV to 2keV range. We did such studies for energies up to 3.5keV to

see if we could repeat similar work done previously by this lab. Data for a 500eV beam is shown in Figures 51 - 53. Electron beam currents ranged from .6 to 4 microamps. The electron beam was roughly circular, with a diameter less than .5mm. Scans were taken for mass ranges of 0 - 100amu and 0 - 50amu at various sensitivities. The data for the 500eV beam was typical for this experiment.

The data shows that for all beam energies the AP experienced some beam damage, although the 500eV beam seemed to experience the least amount. A visual inspection of the samples does show beam induced craters. We have high magnification photographs of the craters. We are presently analyzing these photos.

In order to see if the AP affected the components of the vacuum chamber, we aimed a 500eV electron beam at an unoccupied section of the carousel. The mass spec. data from this location resembles that of AP (see Figure 54). The system pressure at this time was in the low  $10^{-9}$  Torr range, suggesting that the AP components readily stick to the stainless steel in the chamber. An interpretation of the mass numbers from the RGA data is shown in Table 17.

### 3. EELS

We decided to try a 500eV electron beam for the EELS study. We used the CMA in the non-retarding (lower resolution) mode since it required no modification of the existing setup. The data along with the experimental conditions are shown in Figures 55 - 58. We have as yet to fully implement the data analysis program for EELS. When fully operational this program will locate the position of the energy loss peaks. Figure 57 shows approximate positions.

TABLE I

| August 1991 Data      |          |                        |                        |                              |          |          |                     |
|-----------------------|----------|------------------------|------------------------|------------------------------|----------|----------|---------------------|
| Data File             | JOU File | E <sub>0</sub> Cl (eV) | E <sub>0</sub> Ar (eV) | E <sub>0</sub> Cl-Corr. (eV) | ΔAr (eV) | ΔCl (eV) | Scan Name           |
| CLO4NH4.201           | AP21     | 2832.26                | 3207.62                | 2830.54                      | -1.7     | 8.5      | CL                  |
| CLO4NH4.301           | AP31     | X                      | X                      | X                            |          |          | CLEDGE <sup>5</sup> |
| CLO4NH4.302           | AP32     | X                      | X                      | X                            |          |          | CLEDGE <sup>5</sup> |
| CLO4NH4.400           | AP40     | 2822.30                | 3192.68                | 2835.52                      | 13.2     | 13.5     | CL                  |
| CLO4NH4.401           | AP41     | 2822.30                | 3192.68                | 2835.52                      | 13.2     | 13.5     | CL                  |
| CLO4NH4.402           | AP42     | 2822.30                | 3192.68                | 2835.52                      | 13.2     | 13.5     | CL                  |
| CLO4NH4.403           | AP43     | 2822.30                | 3192.68                | 2835.52                      | 13.2     | 13.5     | CL                  |
| AP40-3 <sup>A</sup>   | AP4      | 2822.30                | 3192.68                | 2835.52                      | 13.2     | 13.5     |                     |
| CLTOLT.001            | TOLT1    | 2822.30                | 3192.68                | 2835.52                      | 13.2     | 13.5     | CL                  |
| CLTOLT.002            | TOLT2    | 2822.30                | 3192.68                | 2835.52                      | 13.2     | 13.5     | CL                  |
| TOLT1,2 <sup>A</sup>  | TOLT     | 2822.30                | 3192.68                | 2835.52                      | 13.2     | 13.5     |                     |
| CLTOLB.001            | TOLB1    | 2822.30                | 3192.68                | 2835.52                      | 13.2     | 13.5     | CL                  |
| CLTOLB.002            | TOLB2    | 2822.30                | 3192.68                | 2835.52                      | 13.2     | 13.5     | CL                  |
| TOLB1,2 <sup>A</sup>  | TOLB     | 2822.30                | 3192.68                | 2835.52                      | 13.2     | 13.5     |                     |
| CLTET1T.001           | TET1T1   | 2822.30                | 3192.68                | 2835.52                      | 13.2     | 13.5     | CL                  |
| CLTET1T.002           | TET1T2   | 2822.30                | 3192.68                | 2835.52                      | 13.2     | 13.5     | CL                  |
| TET1T1,2 <sup>A</sup> | TET1T    | 2822.30                | 3192.68                | 2835.52                      | 13.2     | 13.5     |                     |
| CLTET1B.001           | TET1B1   | 2822.30                | 3192.68                | 2835.52                      | 13.2     | 13.5     | CL                  |
| CLTET1B.002           | TET1B2   | 2822.30                | 3192.68                | 2835.52                      | 13.2     | 13.5     | CL                  |
| TET1B1,2 <sup>A</sup> | TET1B    | 2822.30                | 3192.68                | 2835.52                      | 13.2     | 13.5     |                     |
| CLTET2T.001           | TET2T1   | X                      | X                      | X                            |          |          | CL <sup>1</sup>     |
| CLTET2T.102           | TET2T2   | 2823.30                | 3193.14                | 2836.06                      | 12.8     | 14.1     | CL                  |
| CLTET2T.103           | TET2T3   | 2823.30                | 3190.64                | 2838.57                      | 15.3     | 16.6     | CL                  |
| CLTET2T.104           | TET2T4   | 2823.30                | 3193.14                | 2836.06                      | 12.8     | 14.1     | CL                  |
| CLTET2T.105           | TET2T5   | 2823.30                | 3190.64                | 2838.57                      | 15.3     | 16.6     | CL                  |
| CLTET2T.106           | TET2T6   | 2823.30                | 3190.64                | 2838.57                      | 15.3     | 16.6     | CL                  |
| CLTET2T.107           | TET2T7   | 2823.30                | 3190.64                | 2838.57                      | 15.3     | 16.6     | CL                  |
| TET2T2-7 <sup>A</sup> | TET2T    | 2823.30                | 3193.14                | 2836.06                      | 12.8     | 14.1     |                     |

| August 1991 Data      |           |                        |                        |                              |          |          |                 |
|-----------------------|-----------|------------------------|------------------------|------------------------------|----------|----------|-----------------|
| Data File             | .JOU File | E <sub>0</sub> Cl (eV) | E <sub>0</sub> Ar (eV) | E <sub>0</sub> Cl-Corr. (eV) | ΔAr (eV) | ΔCl (eV) | Scan Name       |
| CLTET2B.001           | TET2B1    | 2823.30                | 3190.64                | 2838.57                      | 15.3     | 16.6     | CL              |
| CLTET2B.002           | TET2B2    | 2823.30                | 3193.14                | 2836.06                      | 12.8     | 14.1     | CL              |
| TET2B1,2 <sup>A</sup> | TET2B     | 2823.30                | 3190.64                | 2838.57                      | 15.3     | 16.6     |                 |
| CLTET5B.001           | TET5B1    | 2823.30                | 3190.64                | 2838.57                      | 15.3     | 16.6     | CL              |
| CLTET5B.002           | TET5B2    | 2823.30                | 3190.64                | 2838.57                      | 15.3     | 16.6     | CL              |
| TET5B1,2 <sup>A</sup> | TET5B     | 2823.30                | 3190.64                | 2838.57                      | 15.3     | 16.6     |                 |
| CLTET5T.001           | TET5T1    | 2823.30                | 3190.64                | 2838.57                      | 15.3     | 16.6     | CL <sup>2</sup> |
| CLTET5T.002           | TET5T2    | 2821.83                | 3192.44                | 2835.90                      | 14.1     | 13.9     | CL <sup>3</sup> |
| CLNA.001              | CLNA1     | 2814.38                | 3192.44                | 2827.84                      | 13.5     | 5.84     | CL              |
| CLNA.002              | CLNA2     | 2815.79                | 3193.14                | 2828.55                      | 12.8     | 6.55     | CL <sup>3</sup> |
| CL8781B.001           | 8781B1    | 2823.30                | 3190.64                | 2838.57                      | 15.3     | 16.6     | CL              |
| CL8781B.002           | 8781B2    | 2823.30                | 3190.64                | 2838.57                      | 15.3     | 16.6     | CL              |
| 8781B1,2 <sup>A</sup> | 8781B     | 2823.30                | 3190.64                | 2838.57                      | 15.3     | 16.6     |                 |
| CL8782T.001           | 8782T1    | 2823.30                | 3190.64                | 2838.57                      | 15.3     | 16.6     | CL              |
| CL8782T.002           | 8782T2    | 2823.30                | 3190.64                | 2838.57                      | 15.3     | 16.6     | CL              |
| 8782T1,2 <sup>A</sup> | 8782T     | 2823.30                | 3190.64                | 2838.57                      | 15.3     | 16.6     |                 |
| CL8785B.001           | 8785B1    | 2823.30                | 3193.14                | 2836.06                      | 12.8     | 14.1     | CL              |
| CL8785B.002           | 8785B2    | 2823.30                | 3190.64                | 2838.57                      | 15.3     | 16.6     | CL              |
| 8785B1,2 <sup>A</sup> | 8785B     | 2823.30                | 3193.14                | 2836.06                      | 12.8     | 14.1     |                 |
| CLK.001               | CLK1      | 2813.80                | 3191.01                | 2828.69                      | 14.9     | 6.7      | CL              |
| CLK.002               | CLK2      | 2812.89                | 3193.01                | 2825.78                      | 12.9     | 3.8      | CL              |
| CLK.003               | CLK3      | 2812.89                | 3195.44                | 2823.34                      | 10.5     | 1.3      | CL              |
| CLK.004               | CLK4      | 2812.89                | 3197.88                | 2820.91                      | 8.0      | -1.1     | CL              |
| CLK1-4 <sup>A</sup>   | CLK       | 2813.80                | 3193.45                | 2826.25                      | 12.5     | 4.3      |                 |
| CLK.005               | CLK5      | 2812.89                | 3188.44                | 2830.65                      | 17.8     | 8.7      | CL <sup>4</sup> |
| CLK1-5 <sup>A</sup>   | CLK6      | 2813.80                | 3193.45                | 2826.25                      | 12.5     | 4.3      |                 |
| CL04NH4.500           | AP50      | X                      | X                      | X                            |          |          | CL <sup>1</sup> |
| CLO4NH4.501           | AP51      | X                      | X                      | X                            |          |          | CL <sup>1</sup> |
| CLO4NH4.503           | AP53      | X                      | X                      | X                            |          |          | CL <sup>5</sup> |
| CLO4NH4.600           | AP60      | 2823.60                | 3193.14                | 2836.06                      | 12.5     | 14.1     | CL              |



| August 1991 Data        |          |                        |                        |                              |          |          |                     |
|-------------------------|----------|------------------------|------------------------|------------------------------|----------|----------|---------------------|
| Data File               | JOU File | E <sub>0</sub> Cl (eV) | E <sub>0</sub> Ar (eV) | E <sub>0</sub> Cl-Corr. (eV) | ΔAr (eV) | ΔCl (eV) | Scan Name           |
| CLO4NH4.601             | AP61     | 2823.30                | 3193.14                | 2836.06                      | 12.8     | 14.1     | CL                  |
| AP60-61 <sup>A</sup>    | AP6      | 2823.30                | 3193.14                | 2836.06                      | 12.8     | 14.1     |                     |
| CL8791B.001             | 8791B1   | 2823.30                | 3193.14                | 2836.06                      | 12.8     | 14.1     | CL                  |
| CL8791B.002             | 8791B2   | 2823.30                | 3193.14                | 2836.06                      | 12.8     | 14.1     | CL                  |
| 8791B1-2 <sup>A</sup>   | 8791B    | 2823.30                | 3193.14                | 2836.06                      | 12.8     | 14.1     |                     |
| CLSYN14.001             | CLSYN141 | 2813.29                | 3193.14                | 2826.05                      | 12.8     | 4.1      | CL                  |
| CLSYN14.002             | CLSYN142 | 2813.29                | 3193.14                | 2826.05                      | 12.8     | 4.1      | CL                  |
| SYN141-142 <sup>A</sup> | SYN141   | 2813.29                | 3193.14                | 2826.05                      | 12.8     | 4.1      |                     |
| CLNH4.001               | CLNH401  | 2823.16                | X                      | X                            |          |          | CLAR <sup>1,2</sup> |
| CLNH4.002               | CLNH402  | X                      | X                      | X                            |          |          | CLAR <sup>1</sup>   |
| CLNH4.003               | CLNH403  | X                      | X                      | X                            |          |          | CLAR <sup>1</sup>   |
| CLNH4.004               | CLNH404  | 2809.37                | 3189.0                 | 2826.27                      | 16.9     | 8.3      | CLAR <sup>1,6</sup> |
| CLNH4.100               | CLNH410  | X                      | X                      | X                            |          |          | CLAR <sup>1</sup>   |
| CLNH4.200               | CLNH420  | 2821.79                | 3204.87                | 2822.83                      | 1.0      | 0.8      | CL2                 |
| CLSYN13.001             | CLSYN131 | 2821.79 <sup>P</sup>   | 3204.87 <sup>P</sup>   | 2822.83 <sup>P</sup>         | 1.0      | 0.8      | CL2 <sup>1</sup>    |
| CLSYN13.002             | CLSYN132 | X                      | X                      | X                            |          |          | CL2 <sup>1,7</sup>  |
| CLNH4.300               | CLNH430  | X                      | X                      | X                            |          |          | CLAR <sup>2</sup>   |
| CLNH4.301               | CLNH431  | X                      | X                      | X                            |          |          | CLAR                |
| CLNH4.302               | CLNH432  | X                      | X                      | X                            |          |          | CLAR                |
| CLSYN13.003             | CLSYN133 | 2821.79 <sup>P</sup>   | 3204.87 <sup>P</sup>   | 2822.83 <sup>P</sup>         | 1.0      | 0.8      | CL2                 |
| CLSYN131,3 <sup>A</sup> | CLSYN13  | 2821.79 <sup>P</sup>   | 3204.87 <sup>P</sup>   | 2822.83 <sup>P</sup>         | 1.0      | 0.8      |                     |
| CLSYN12.001             | CLSYN121 | X                      | X                      | X                            |          |          | CL2 <sup>1</sup>    |
| CLSYN12.002             | CLSYN122 | 2821.79                | 3204.87                | 2822.83                      | 1.0      | 0.8      | CL2 <sup>3</sup>    |
| CLSYN11.001             | CLSYN111 | 2821.79                | 3204.87                | 2822.83                      | 1.0      | 0.8      | CL2                 |
| CLSYN11.002             | CLSYN112 | 2821.79                | 3207.35                | 2820.34                      | -1.5     | -1.7     | CL2                 |
| CLSYN111-2 <sup>A</sup> | CLSYN11  | 2821.79                | 3204.87                | 2822.83                      | 1.0      | 0.8      |                     |
| CLPACP.001              | PACP1    | 2821.79                | 3204.87                | 2822.83                      | 1.0      | 0.8      | CL2                 |
| CLPACP.002              | PACP2    | 2821.79                | 3204.87                | 2822.83                      | 1.0      | 0.8      | CL2                 |
| CLPACP1,2 <sup>A</sup>  | PACP     | 2821.79                | 3204.87                | 2822.83                      | 1.0      | 0.8      |                     |
| CLPECP.001              | PECP1    | 2821.79                | 3202.38                | 2825.31                      | 3.5      | 3.3      | CL2                 |

| August 1991 Data        |           |                        |                        |                              |          |          |           |
|-------------------------|-----------|------------------------|------------------------|------------------------------|----------|----------|-----------|
| Data File               | .JOU File | E <sub>0</sub> Cl (eV) | E <sub>0</sub> Ar (eV) | E <sub>0</sub> Cl-Corr. (eV) | ΔAr (eV) | ΔCl (eV) | Scan Name |
| CLPECP.002              | PECP2     | 2821.79                | 3202.38 <sup>P</sup>   | 2825.31                      | 3.5      | 3.3      | CL2       |
| CLPECP1,2 <sup>A</sup>  | PECP      | 2821.79                | 3202.38                | 2825.31                      | 3.5      | 3.3      |           |
| CLCLHQ.001              | CLHQ1     | 2821.79                | 3204.87                | 2822.83                      | 1.0      | 0.8      | CL2       |
| CLCLHQ.002              | CLHQ2     | 2821.79                | 3204.87                | 2822.83                      | 1.0      | 0.8      | CL2       |
| CLHQ1,2 <sup>A</sup>    | CLHQ      | 2821.79                | 3204.87                | 2822.83                      | 1.0      | 0.8      |           |
| CLO4NH4.602             | AP62      | 2831.73                | 3204.87                | 2832.77                      | 1.0      | 10.8     | CL2       |
| CL7521B.001             | 7521B     | 2831.73                | 3204.87                | 2832.77                      | 1.0      | 10.8     | CL2       |
| CLDER1B.001             | DER1B     | 2831.73                | 3204.87                | 2832.77                      | 1.0      | 10.8     | CL2       |
| CLHTP1B.001             | HTP1B1    | 2831.73                | 3204.87                | 2832.77                      | 1.0      | 10.8     | CL2       |
| CLHTP1B.002             | HTP1B2    | 2831.73                | 3204.87                | 2832.77                      | 1.0      | 10.8     | CL2       |
| HTP1B1,2 <sup>A</sup>   | HTP1B     | 2831.73                | 3204.87                | 2832.77                      | 1.0      | 10.8     |           |
| CLO4NH4.603             | AP63      | X                      | X                      | X                            |          |          | CLAR      |
| CLO4NH4.604             | AP64      | X                      | X                      | X                            |          |          | CLAR      |
| CLHTP1B.003             | HTP1B3    | 2821.79                | 3192.94                | 2835.25                      | 13.0     | 13.3     | CL2       |
| CLO4CU.001              | CLO4CU    | 2821.79                | 3192.44                | 2835.25                      | 13.5     | 13.3     | CL2       |
| CLSYN14.003             | CLSYN143  | X                      | 3192.44                | 2825.31 <sup>P</sup>         | 13.5     | 3.3      | CL2       |
| CLSYN14.004             | CLSYN144  | 2811.85                | 3192.44                | 2825.31                      | 13.5     | 3.3      | CL2       |
| CLSYN14.005             | CLSYN145  | 2811.85                | 3192.44                | 2825.31                      | 13.5     | 3.3      | CL2       |
| CLSYN143-5 <sup>A</sup> | SYN142    | 2811.85                | 3192.44                | 2825.31                      | 13.5     | 3.3      |           |
| CLSYN144,5 <sup>A</sup> | SYN143    | 2811.85                | 3192.44                | 2825.31                      | 13.5     | 3.3      |           |

TABLE II

| October 1991 Data       |          |                        |                                     |                              |          |          |                  |
|-------------------------|----------|------------------------|-------------------------------------|------------------------------|----------|----------|------------------|
| Data File               | JOU File | E <sub>0</sub> Cl (eV) | E <sub>0</sub> Ar (eV) <sup>P</sup> | E <sub>0</sub> Cl-Corr. (eV) | ΔAr (eV) | ΔCl (eV) | Scan Name        |
| AP.100                  | AP100    | 2826.76                | 3200.0                              | 2832.66                      | 5.9      | 10.7     | CL2 <sup>2</sup> |
| AP.101                  | AP101    | 2826.76                | 3200.1                              | 2832.56                      | 5.8      | 10.6     | CL2              |
| AP.102                  | AP102    | 2826.76                | 3200.1                              | 2832.56                      | 5.8      | 10.6     | CL2              |
| AP.103                  | AP103    | 2826.76                | 3200.1                              | 2832.56                      | 5.8      | 10.6     | CL2              |
| AP.104                  | AP104    | 2826.76                | 3200.1                              | 2832.56                      | 5.8      | 10.6     | CL2              |
| AP.105                  | AP105    | 2826.76                | 3200.1                              | 2832.56                      | 5.8      | 10.6     | CL2              |
| AP101-5 <sup>A</sup>    | AP1      | 2826.76                | 3200.1                              | 2832.56                      | 5.8      | 10.6     |                  |
| AP.108                  | AP108    | 2821.79                | 3194.0                              | 2833.69                      | 11.9     | 11.7     | CL2              |
| CLAR.100                | CLAR100  | 2823.16                | X                                   | X                            |          |          | CLAR             |
| CLNH4.109               | AC109    | 2814.34                | 3193.2                              | 2827.04                      | 12.7     | 5.0      | CL2              |
| CLNH4.110               | AC110    | 2814.34                | 3193.7                              | 2826.54                      | 12.2     | 4.5      | CL2              |
| CLNH4.111               | AC111    | 2811.85 <sup>d</sup>   | 3193.7                              | 2824.05                      | 12.2     | 2.1      | CL2              |
| CLNH4.112               | AC112    | 2814.34                | 3193.7                              | 2826.54                      | 12.2     | 4.5      | CL2              |
| CLNH4.113               | AC113    | 2811.85 <sup>d</sup>   | 3193.7                              | 2824.05                      | 12.2     | 2.1      | CL2              |
| CLNH4.114               | AC114    | 2811.85 <sup>d</sup>   | 3193.5                              | 2824.25                      | 12.4     | 2.3      | CL2              |
| CLNH4.115               | AC115    | 2814.34                | 3193.7                              | 2826.54                      | 12.2     | 4.5      | CL2              |
| CLNH4.116               | AC116    | 2814.34                | 3193.7                              | 2826.54                      | 12.2     | 4.5      | CL2              |
| AC109-16 <sup>A</sup>   | AC1      | 2814.34                | 3193.7                              | 2826.54                      | 12.2     | 4.5      |                  |
| CLNA.117                | CLNA117  | 2814.34                | 3193.6                              | 2826.64                      | 12.3     | 4.6      | CL2              |
| CLNA.118                | CLNA118  | 2814.34                | 3193.2                              | 2827.04                      | 12.7     | 5.0      | CL2              |
| CLNA.119                | CLNA119  | 2814.34                | 3193.2                              | 2827.04                      | 12.7     | 5.0      | CL2              |
| CLNA.120                | CLNA120  | 2814.34                | 3193.6                              | 2826.64                      | 12.3     | 4.6      | CL2              |
| CLNA117-20 <sup>A</sup> | CLNA     | 2814.34                | 3193.2                              | 2827.04                      | 12.7     | 5.0      |                  |
| CLK.121                 | CLK121   | 2814.34                | 3193.9                              | 2826.34                      | 12.0     | 4.3      | CL2              |
| CLK.122                 | CLK122   | 2814.34                | 3193.7                              | 2826.54                      | 12.2     | 4.5      | CL2              |
| CLK.123                 | CLK123   | 2811.85 <sup>d</sup>   | 3193.8                              | 2823.95                      | 12.1     | 2.0      | CL2              |
| CLK.124                 | CLK124   | 2811.85 <sup>d</sup>   | 3193.8                              | 2823.95                      | 12.1     | 2.0      | CL2              |
| CLK121-4 <sup>A</sup>   | CLK      | 2814.34                | 3193.8                              | 2826.44                      | 12.1     | 4.4      |                  |

| October 1991 Data       |           |                        |                                     |                              |          |          |                       |
|-------------------------|-----------|------------------------|-------------------------------------|------------------------------|----------|----------|-----------------------|
| Data File               | .JOU File | E <sub>0</sub> Cl (eV) | E <sub>0</sub> Ar (eV) <sup>P</sup> | E <sub>0</sub> Cl-Corr. (eV) | ΔAr (eV) | ΔCl (eV) | Scan Name             |
| CLHQ.125                | CLHQ125   | 2811.85                | 3193.0                              | 2824.75                      | 12.9     | 2.8      | CL2                   |
| CLHQ.126                | CLHQ126   | 2811.85                | 3194.0                              | 2823.75                      | 11.9     | 1.8      | CL2                   |
| CLHQ.127                | CLHQ127   | 2811.85                | 3193.0                              | 2824.75                      | 12.9     | 2.8      | CL2                   |
| CLHQ.128                | CLHQ128   | 2811.85                | 3193.0                              | 2824.75                      | 12.9     | 2.8      | CL2                   |
| CLHQ125-8 <sup>A</sup>  | CLHQ      | 2811.85                | 3193.0                              | 2824.75                      | 12.9     | 2.8      |                       |
| SYN11.129               | SYN1129   | 2811.85 <sup>B</sup>   | 3193.0                              | 2824.75                      | 12.9     | 2.8      | CL2 <sup>A</sup>      |
| SYN11.130               | SYN1130   | 2811.85 <sup>B</sup>   | 3193.2                              | 2824.55                      | 12.7     | 2.6      | CL2 <sup>A</sup>      |
| SYN11.131               | SYN1131   | 2811.85 <sup>B</sup>   | 3193.2                              | 2824.55                      | 12.7     | 2.6      | CL2 <sup>A</sup>      |
| SYN11.132               | SYN1132   | 2811.85 <sup>B</sup>   | 3193.2                              | 2824.55                      | 12.7     | 2.6      | CL2 <sup>A</sup>      |
| SYN1129-32 <sup>A</sup> | SYN11     | 2811.85 <sup>B</sup>   | 3193.2                              | 2824.55                      | 12.7     | 2.6      |                       |
| SYN12.133               | SYN1233   | 2813.01                | 3193.2                              | 2825.71                      | 12.7     | 3.7      | CL2 <sup>A</sup>      |
| SYN12.134               | SYN1234   | 2811.85 <sup>B</sup>   | 3193.2                              | 2824.55                      | 12.7     | 2.6      | CL2 <sup>A</sup>      |
| SYN12.135               | SYN1235   | 2811.85 <sup>B</sup>   | 3193.2                              | 2824.55                      | 12.7     | 2.6      | CL2 <sup>A</sup>      |
| SYN12.136 <sup>3</sup>  | SYN1236   | 2811.85 <sup>B</sup>   | 3193.2                              | 2824.55                      | 12.7     | 2.6      | CL2 <sup>A</sup>      |
| AP.137                  | AP137     | 2821.79                | 3193.1                              | 2834.59                      | 12.8     | 12.6     | CL2                   |
| AP.138                  | AP138     | 2821.79                | 3193.5                              | 2834.19                      | 12.4     | 12.2     | CL2                   |
| AP.139                  | AP139     | 2821.79                | 3193.1                              | 2834.59                      | 12.8     | 12.6     | CL2                   |
| AP.140                  | AP140     | 2821.79                | 3193.2                              | 2834.49                      | 12.7     | 12.5     | CL2                   |
| AP137-40 <sup>A</sup>   | AP2       | 2821.79                | 3193.1                              | 2834.59                      | 12.8     | 12.6     |                       |
| CLNH4.141               | AC141     | 2811.85 <sup>B</sup>   | 3193.3                              | 2824.45                      | 12.6     | 2.5      | CL2                   |
| CLNH4.142               | AC142     | 2811.85 <sup>B</sup>   | 3193.3                              | 2824.45                      | 12.6     | 2.5      | CL2                   |
| CLNH4.143               | AC143     | 2814.34                | 3193.3                              | 2826.94                      | 12.6     | 4.9      | CL2                   |
| CLNH4.144               | AC144     | 2814.34                | 3193.3                              | 2826.94                      | 12.6     | 4.9      | CL2                   |
| AC141-4 <sup>A</sup>    | AC2       | 2814.34                | 3193.2                              | 2827.04                      | 12.7     | 5.0      |                       |
| SYN13.145               | SYN1345   | 2813.5                 | X                                   | X                            |          |          | CLEDGE <sup>2.5</sup> |
| SYN13.146               | SYN1346   | 2821.63 <sup>B</sup>   | 3207.3                              | 2820.23                      | -1.4     | -1.8     | CL2                   |
| SYN13.147               | SYN1347   | 2821.79 <sup>B</sup>   | 3207.3                              | 2820.39                      | -1.4     | -1.6     | CL2                   |
| SYN13.148               | SYN1348   | 2821.79 <sup>B</sup>   | 3207.3                              | 2820.39                      | -1.4     | -1.6     | CL2                   |
| SYN13.149               | SYN1349   | 2821.79 <sup>B</sup>   | 3207.3                              | 2820.39                      | -1.4     | -1.6     | CL2                   |
| SYN1346-9 <sup>A</sup>  | SYN13     | 2821.79 <sup>B</sup>   | 3207.3                              | 2820.39                      | -1.4     | -1.6     |                       |

| October 1991 Data       |           |                        |                                     |                              |          |          |                    |
|-------------------------|-----------|------------------------|-------------------------------------|------------------------------|----------|----------|--------------------|
| Data File               | .JOU File | E <sub>0</sub> Cl (eV) | E <sub>0</sub> Ar (eV) <sup>P</sup> | E <sub>0</sub> Cl-Corr. (eV) | ΔAr (eV) | ΔCl (eV) | Scan Name          |
| SYN14.150               | SYN1450   | 2821.79 <sup>s</sup>   | 3207.3                              | 2820.39                      | -1.4     | -1.6     | CL2                |
| SYN14.151               | SYN1451   | 2821.79 <sup>s</sup>   | 3207.3                              | 2820.39                      | -1.4     | -1.6     | CL2                |
| SYN14.152               | SYN1452   | 2824.28                | 3207.3                              | 2822.88                      | -1.4     | -0.9     | CL2                |
| SYN14.153               | SYN1453   | 2821.79 <sup>s</sup>   | 3208.0                              | 2819.69                      | -2.1     | -2.3     | CL2                |
| SYN1450-3 <sup>A</sup>  | SYN14     | 2821.79 <sup>s</sup>   | 3207.3                              | 2820.39                      | -1.4     | -1.6     |                    |
| CL3V.154                | CL3V154   | X                      | X                                   | X                            |          |          | CL2 <sup>1</sup>   |
| CL3V.155                | CL3V155   | X                      | X                                   | X                            |          |          | CL2 <sup>1</sup>   |
| CL3V.156                | CL3V156   | 2821.79                | 3207.0                              | 2820.69                      | -1.1     | -1.6     | CL2 <sup>4</sup>   |
| CL3V.157                | CL3V157   | 2819.31 <sup>s</sup>   | 3207.0                              | 2818.21                      | -1.1     | -3.8     | CL2 <sup>4</sup>   |
| CL3V.158                | CL3V158   | 2819.31 <sup>s</sup>   | 3207.0                              | 2818.21                      | -1.1     | -3.8     | CL2 <sup>4</sup>   |
| CL3V.159                | CL3V159   | 2819.31 <sup>s</sup>   | 3207.0                              | 2818.21                      | -1.1     | -3.8     | CL2 <sup>4</sup>   |
| CL3V.160                | CL3V160   | 2822.87                | 3207.0                              | 2821.77                      | -1.1     | -0.2     | CL2 <sup>4</sup>   |
| CL3V.161                | CL3V161   | 2819.31 <sup>s</sup>   | 3207.0                              | 2818.21                      | -1.1     | -3.8     | CL2 <sup>3,4</sup> |
| CL3VR.162               | CL3VR162  | 2819.31 <sup>s</sup>   | 3207.0                              | 2818.21                      | -1.1     | -3.8     | CL2                |
| CL3VR.163               | CL3VR163  | 2819.31 <sup>s</sup>   | 3207.0                              | 2818.21                      | -1.1     | -3.8     | CL2                |
| CL3VR.164               | CL3VR164  | 2819.31 <sup>s</sup>   | 3207.0                              | 2818.21                      | -1.1     | -3.8     | CL2                |
| CL3VR.165               | CL3VR165  | 2819.31 <sup>s</sup>   | 3207.0                              | 2818.21                      | -1.1     | -3.8     | CL2                |
| CL3VR162-5 <sup>A</sup> | CL3VR     | 2819.31 <sup>s</sup>   | 3207.0                              | 2818.21                      | -1.1     | -3.8     |                    |
| CLRB.166                | CLRB166   | 2821.79 <sup>s</sup>   | 3205.9                              | 2821.79                      | 0.0      | -0.2     | CL2 <sup>4,6</sup> |
| CLRB.167                | CLRB167   | 2821.79 <sup>s</sup>   | 3205.9                              | 2821.79                      | 0.0      | -0.2     | CL2 <sup>4,6</sup> |
| CLRB.168                | CLRB168   | 2826.76                | 3205.9                              | 2826.76                      | 0.0      | 4.8      | CL2 <sup>4,6</sup> |
| CLRB.169                | CLRB169   | 2824.28                | 3205.9                              | 2824.28                      | 0.0      | 2.3      | CL2 <sup>4,6</sup> |
| CLRB.170                | CLRB170   | 2821.79 <sup>s</sup>   | 3205.9                              | 2821.79                      | 0.0      | -0.2     | CL2 <sup>4,6</sup> |
| CLRB.171                | CLRB171   | 2826.76                | 3205.9                              | 2826.76                      | 0.0      | 4.8      | CL2 <sup>4,6</sup> |
| CLRB.172                | CLRB172   | 2824.28                | 3205.9                              | 2824.28                      | 0.0      | 2.3      | CL2 <sup>4,6</sup> |
| CLRB.173                | CLRB173   | 2821.79 <sup>s</sup>   | 3205.9                              | 2821.79                      | 0.0      | -0.2     | CL2 <sup>4,6</sup> |
| CLRB.174                | CLRB174   | 2821.79 <sup>s</sup>   | 3205.9                              | 2821.79                      | 0.0      | -0.2     | CL2 <sup>4,6</sup> |
| CLRB.175                | CLRB175   | 2821.79 <sup>s</sup>   | 3205.9                              | 2821.79                      | 0.0      | -0.2     | CL2 <sup>4,6</sup> |
| CLRB166-75 <sup>A</sup> | CLRB1     | 2821.79 <sup>s</sup>   | 3205.9                              | 2821.79                      | 0.0      | -0.2     |                    |
| PECP.176                | PECP76    | 2821.79                | 3207.3                              | 2820.39                      | -1.4     | -1.6     | CL2                |

| October 1991 Data      |           |                      |                            |                     |                  |                  |                      |
|------------------------|-----------|----------------------|----------------------------|---------------------|------------------|------------------|----------------------|
| Data File              | .JOU File | $E_0$ Cl (eV)        | $E_0$ Ar (eV) <sup>P</sup> | $E_0$ Cl-Corr. (eV) | $\Delta$ Ar (eV) | $\Delta$ Cl (eV) | Scan Name            |
| PECP.177               | PECP77    | 2821.79              | 3207.3                     | 2820.39             | -1.4             | -1.6             | CL2 <sup>A</sup>     |
| PECP.178               | PECP78    | 2821.79              | 3207.3                     | 2820.39             | -1.4             | -1.6             | CL2 <sup>A</sup>     |
| PECP.179               | PECP79    | 2821.79              | 3207.3                     | 2820.39             | -1.4             | -1.6             | CL2 <sup>A</sup>     |
| PECP76-9 <sup>A</sup>  | PECP      | 2821.79              | 3207.3                     | 2820.39             | -1.4             | -1.6             |                      |
| CLRB.180               | CLRB180   | 2821.79 <sup>8</sup> | 3205.9                     | 2821.79             | 0.0              | -1.2             | CL2 <sup>3,4,6</sup> |
| CLRB.181               | CLRB181   | 2821.79 <sup>8</sup> | 3205.9                     | 2821.79             | 0.0              | -0.2             | CL2 <sup>4,6</sup>   |
| CLRB.182               | CLRB182   | 2821.79 <sup>8</sup> | 3205.9                     | 2821.79             | 0.0              | -0.2             | CL2 <sup>4,6</sup>   |
| CLRB181-2 <sup>A</sup> | CLRB2     | 2821.79 <sup>8</sup> | 3205.9                     | 2821.79             | 0.0              | -0.2             |                      |

#### Table Notes

1. Bad Scan. Not able to reliably determine edge.
  2. First scan with new beam.
  3. Could not average scans of this group.
  4. Ar not well-defined.
  5. Edge scan.
  6. Noisy data.
  7. Lost beam during scan.
  8. Inflection point located low on edge.
- P. Energy point picked manually.
- A. Averaged data.

TABLE III

| Mass # | Component   |
|--------|---|
| 1      | H <sup>+</sup>  |
| 2      | H <sub>2</sub> <sup>+</sup>                           |
| 4      | He <sup>+</sup>                                       |
| 12     | C <sup>+</sup>  |
| 14     | CH <sup>+</sup> , N <sup>+</sup>                      |
| 16     | O <sup>+</sup>  |
| 17     | OH <sup>+</sup>                                       |
| 18     | H <sub>2</sub> O <sup>+</sup>                         |
| 20     | Ar <sup>++</sup>                                      |
| 22     | CO <sub>2</sub> <sup>+</sup>                          |
| 28     | N <sub>2</sub> <sup>+</sup>                           |
| 30     | NO <sup>+</sup>                                       |
| 32     | O <sub>2</sub> <sup>+</sup>                           |
| 35     | <sup>35</sup> Cl <sup>+</sup>                         |
| 36     | HCl <sup>+</sup>                                      |
| 37     | <sup>37</sup> Cl <sup>+</sup>                         |
| 38     | HCl <sup>+</sup>                                      |
| 44     | CO <sub>2</sub> <sup>+</sup>                          |
| 46     | NO <sub>2</sub> <sup>+</sup>                          |
| 51     | ClO <sup>+</sup>                                      |
| 52     | HClO <sup>+</sup>                                     |
| 53     | (H <sub>2</sub> ClO <sup>+</sup> + ClO <sup>+</sup> ) |
| 54     | HClO <sup>+</sup>                                     |

| Mass # | Component                 |
|--------|---------------------------|
| 67     | $\text{ClO}_2^+$          |
| 69     | $^{37}\text{ClO}_2^+$     |
| 70     | $\text{Cl}_2^+$           |
| 72     | $\text{H}_2\text{Cl}_2^+$ |
| 74     | $^{37}\text{Cl}_2^+$      |



E0= 2822.30  
AP4

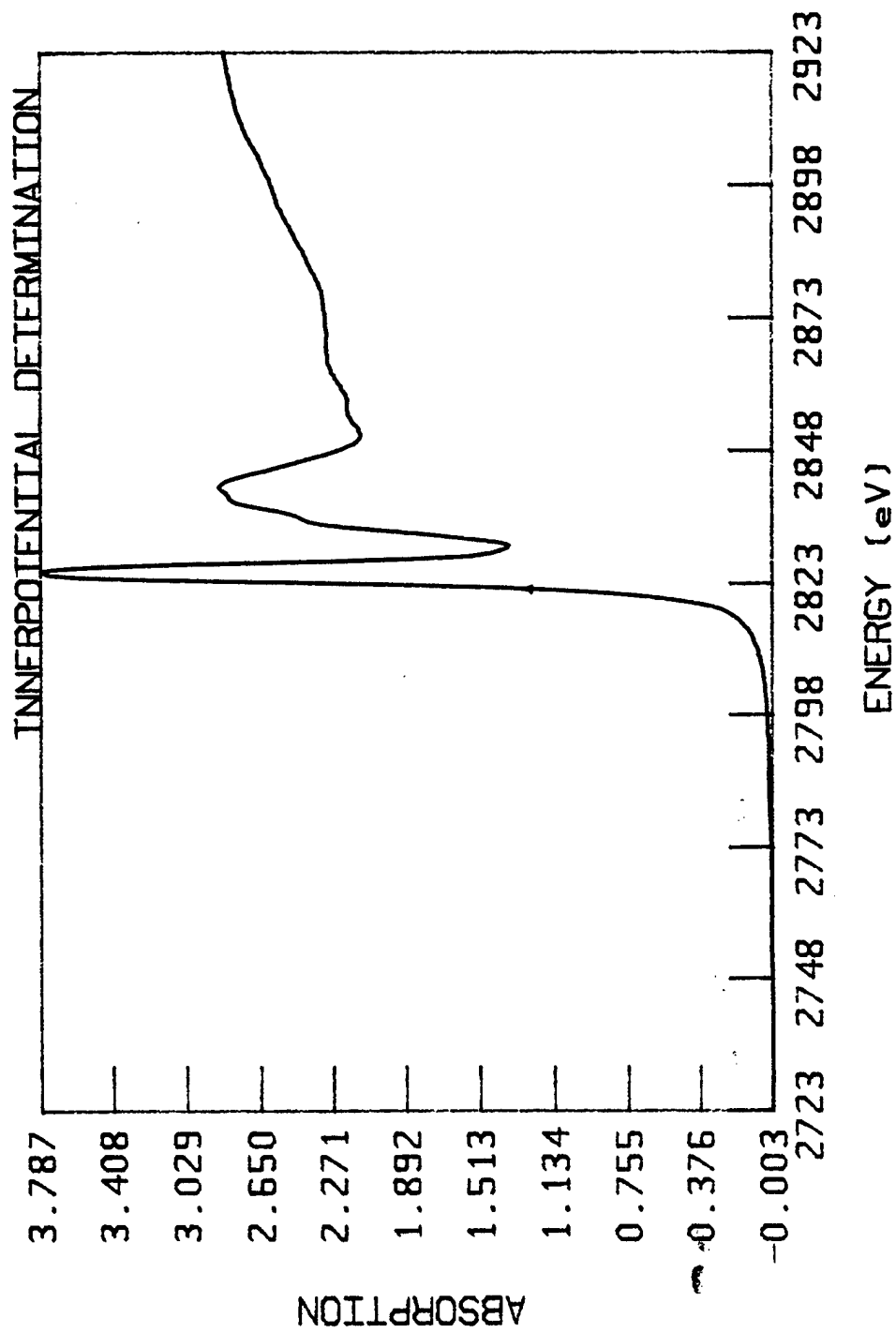


FIGURE 1

E0 = 3192.68  
AP4

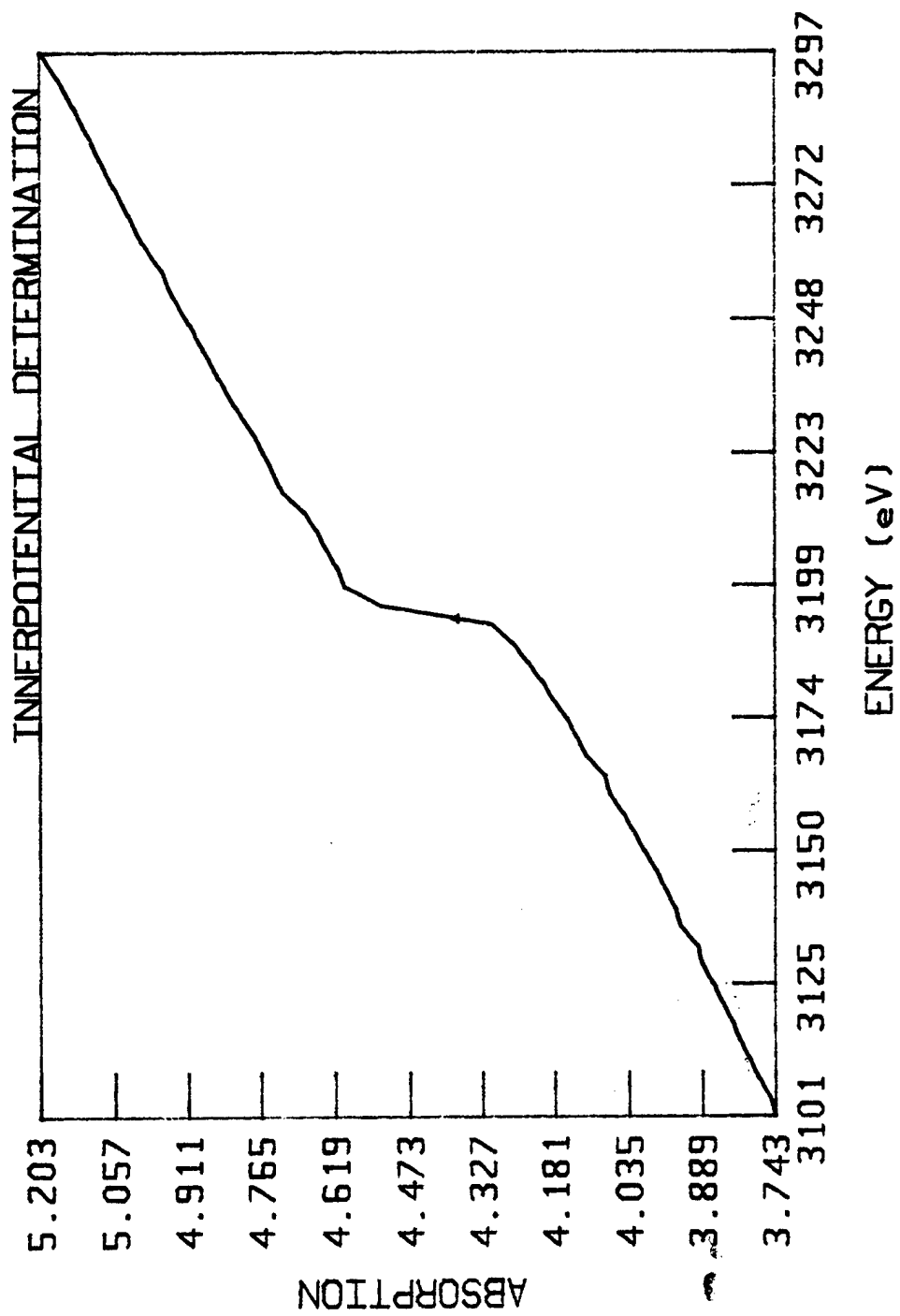


FIGURE 2

E0 = 2835.52  
AP4

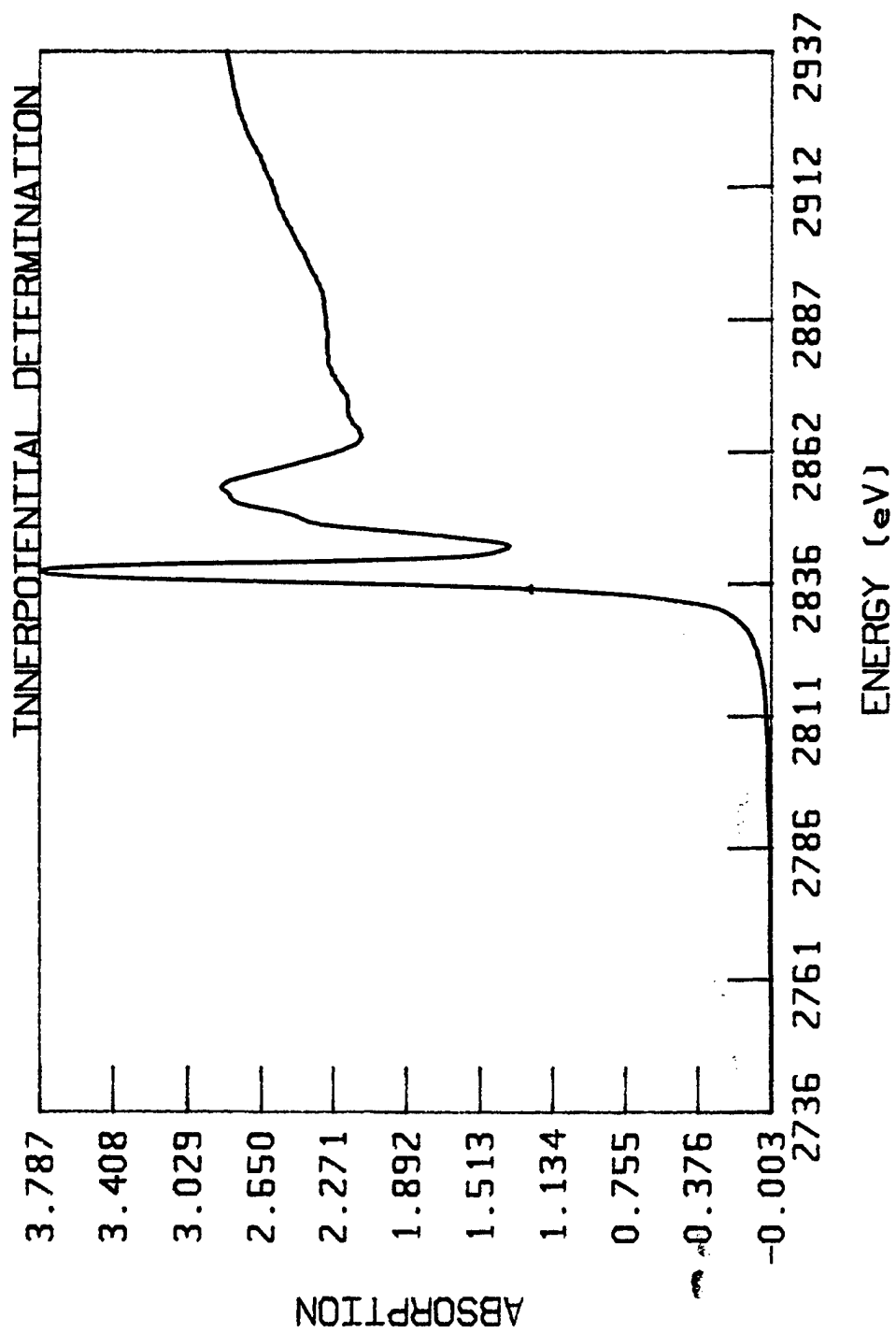


FIGURE 3

E0= 2835.52

TOLT

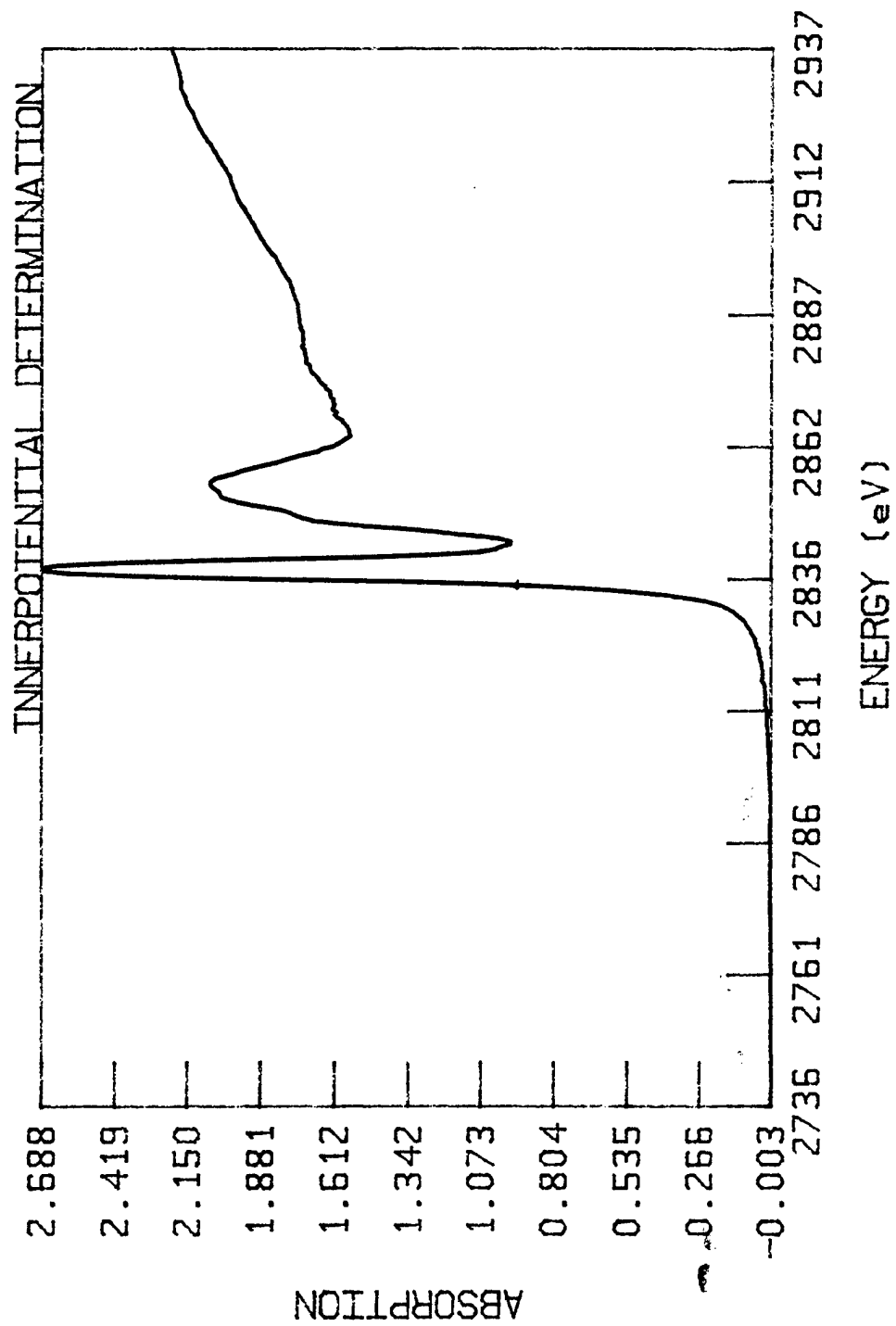


FIGURE 4

E0= 2835.52

TOLB

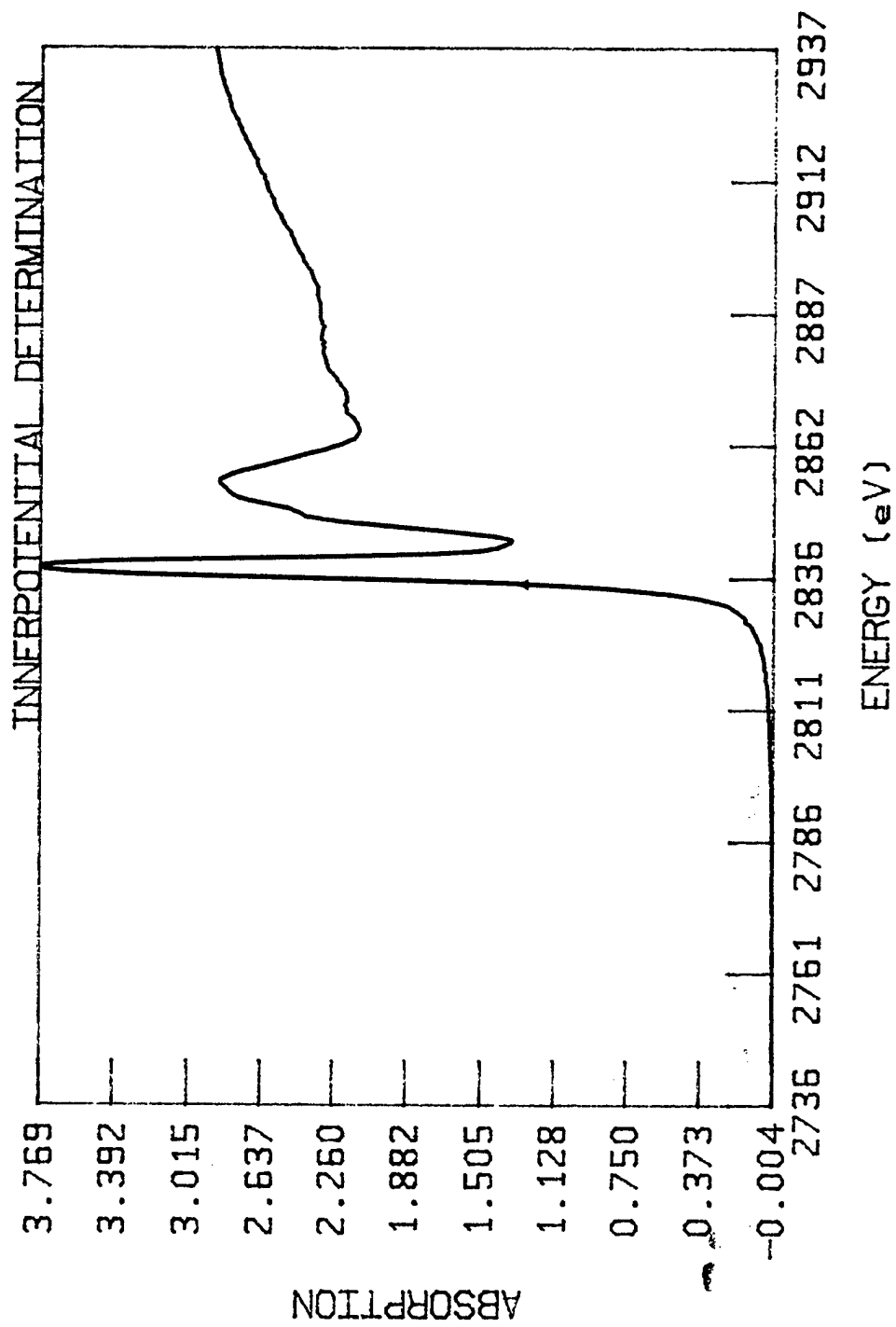


FIGURE 5

E0 = 2835.52  
TET1T

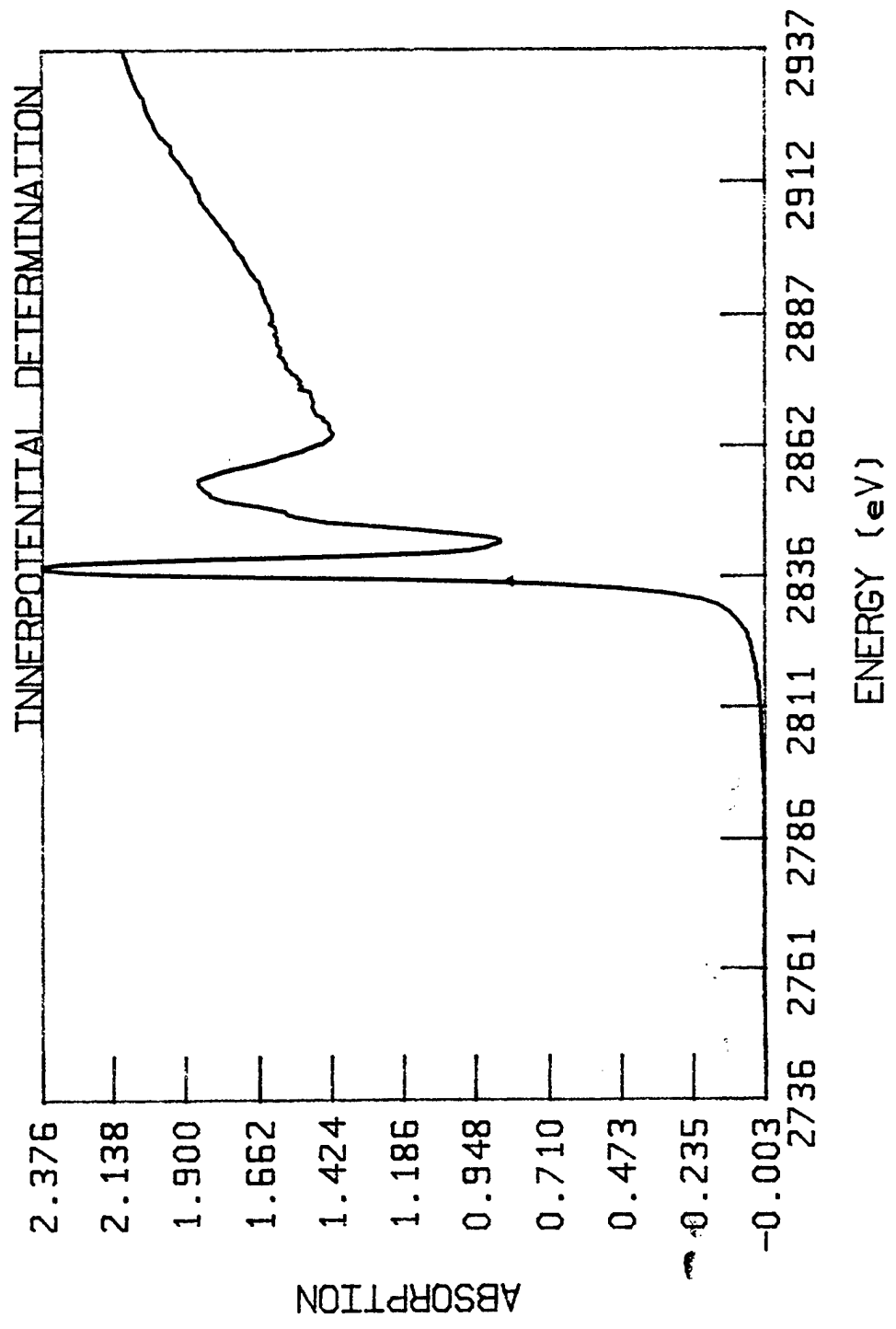


FIGURE 6

E0 = 2835.52  
TET1B

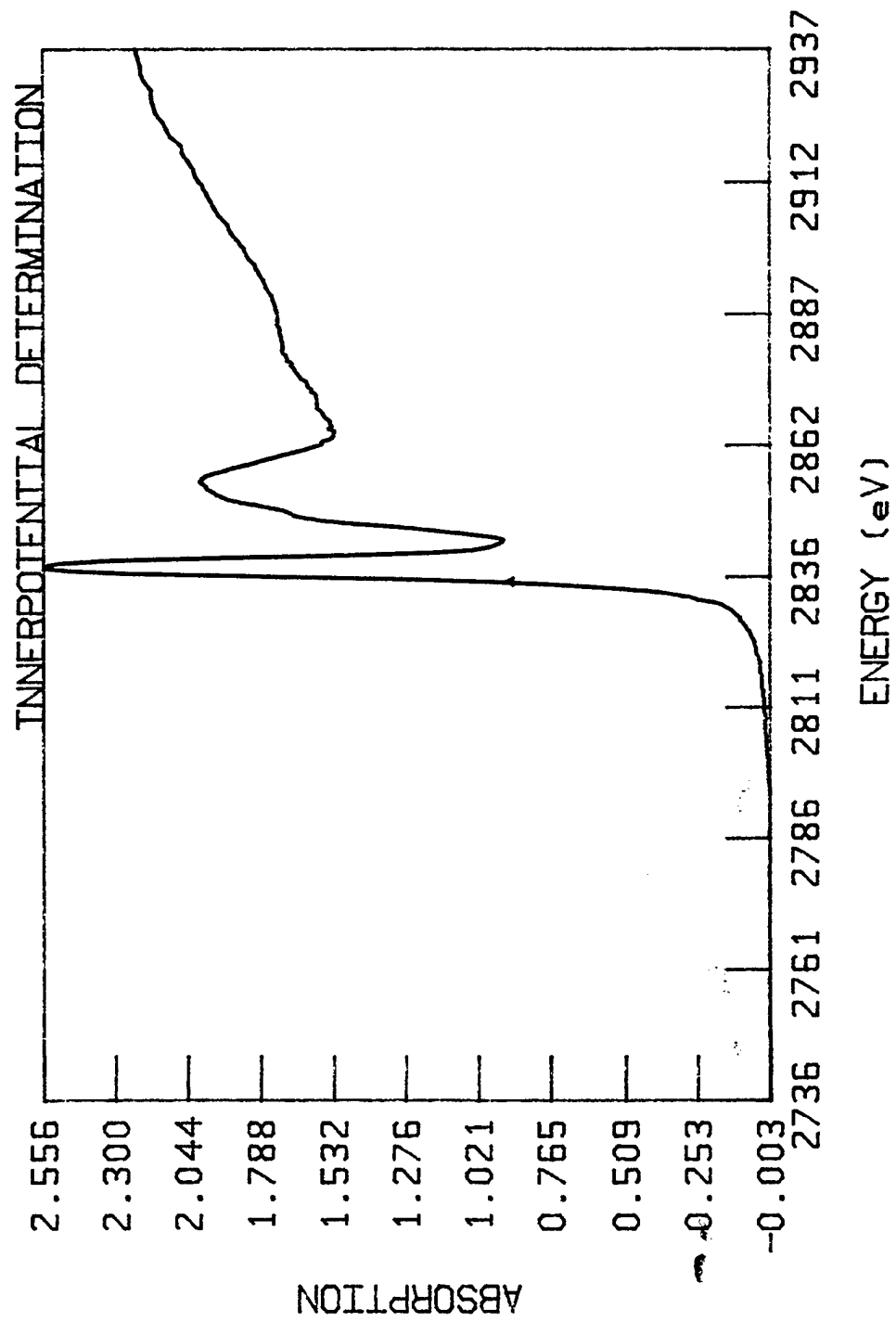


FIGURE 7

E0= 2836.06  
TET2T

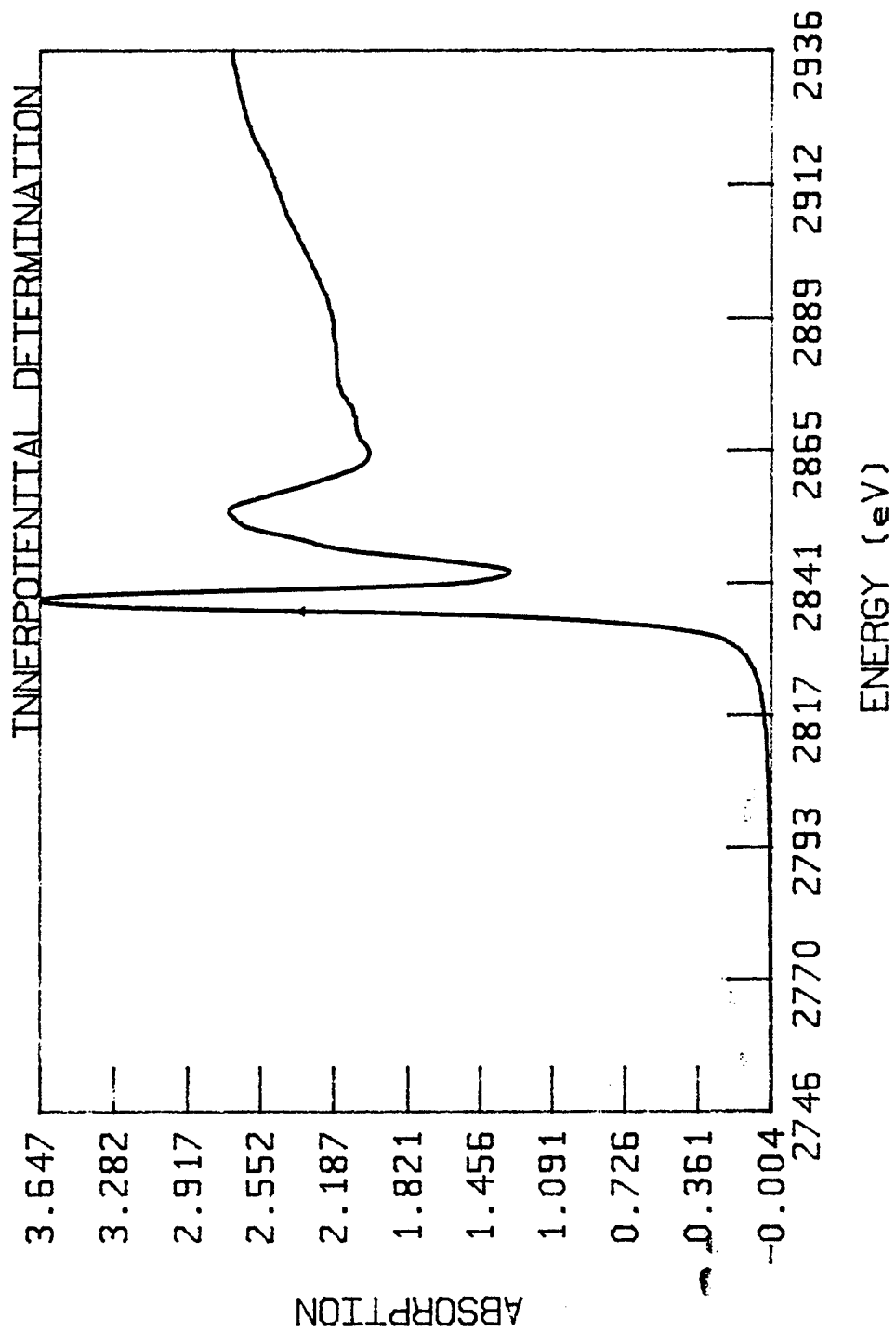


FIGURE 8



E0 = 2838.57  
TET2B

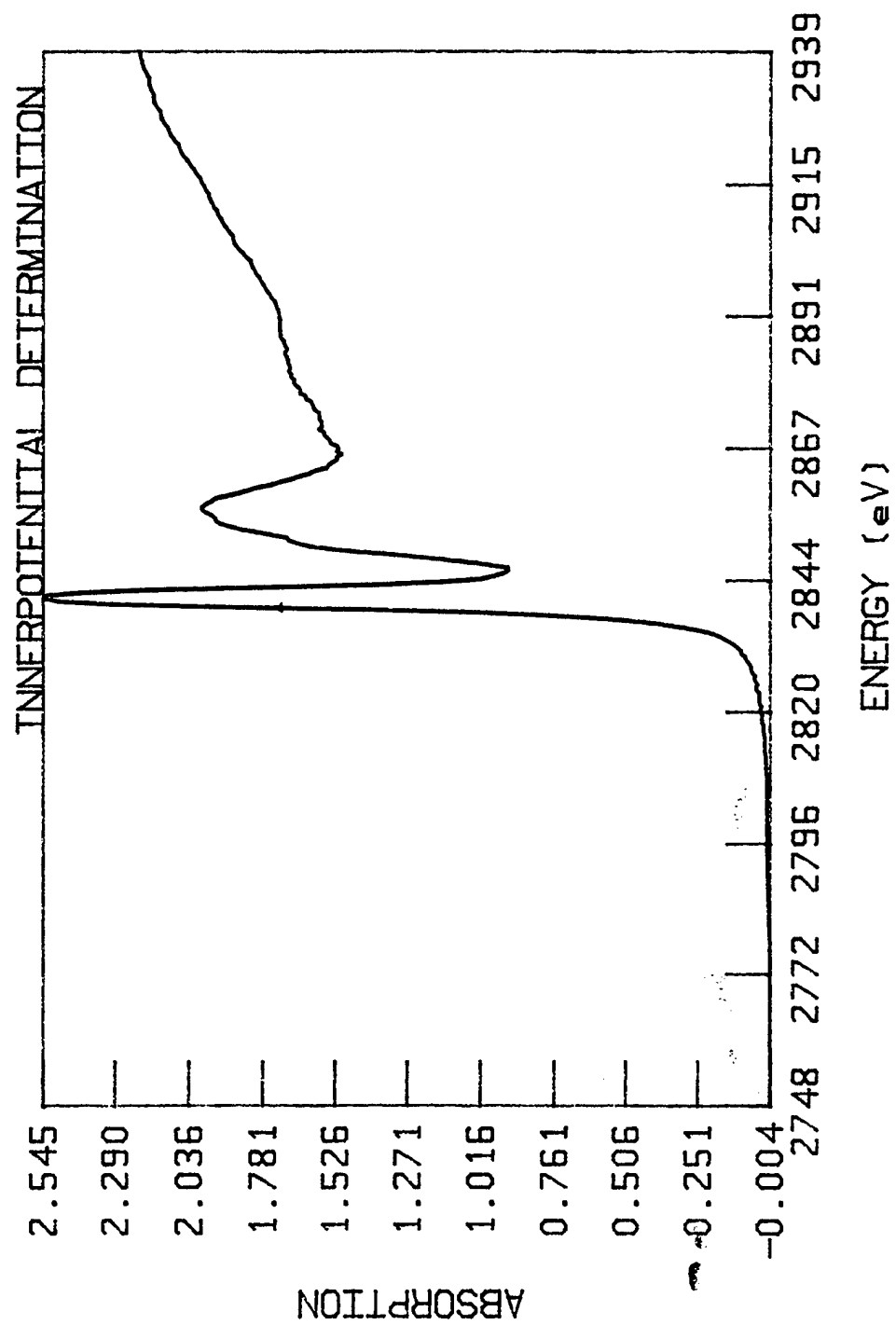


FIGURE 9

E0 = 2838.57

TET5B

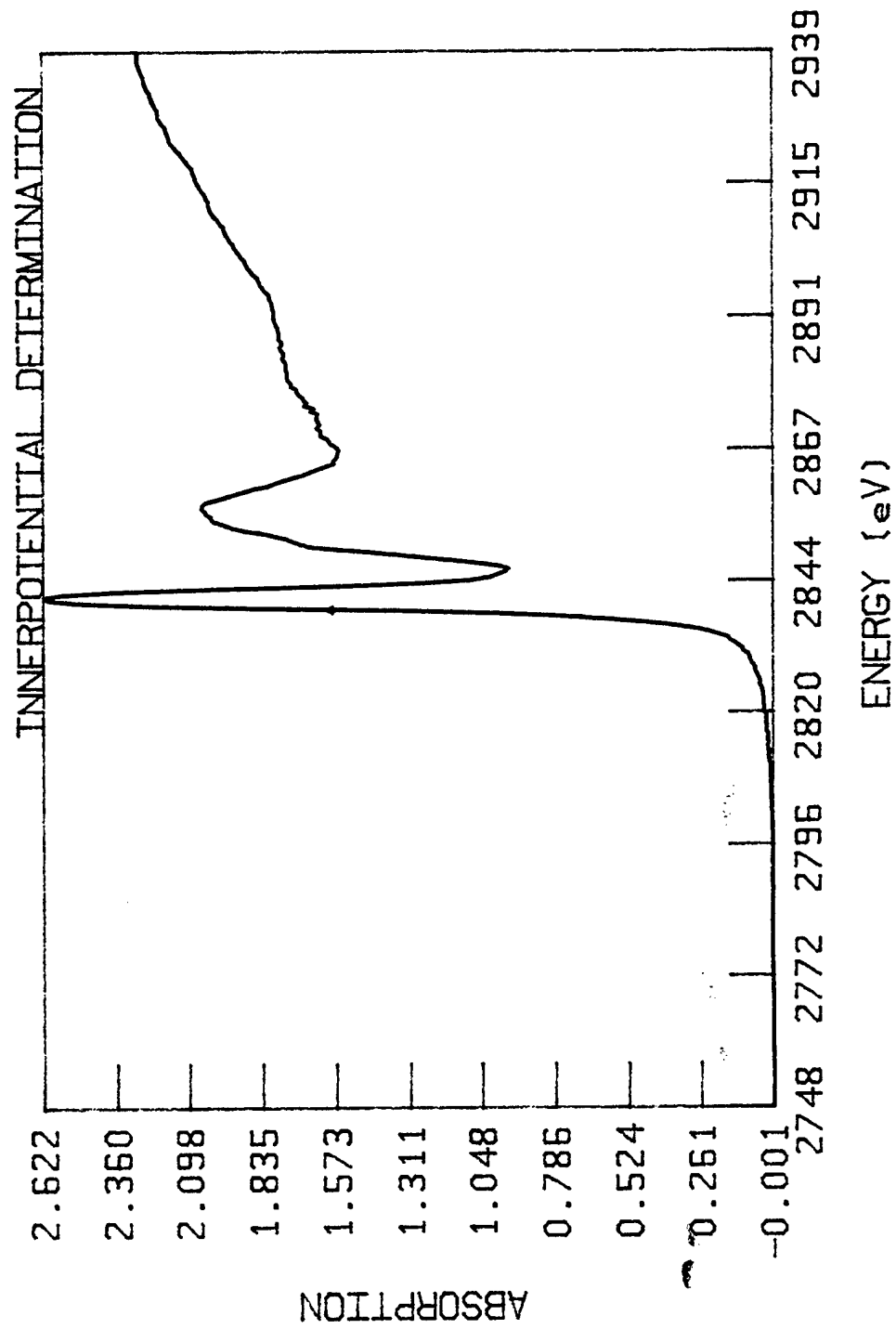


FIGURE 10

E0 = 2838.57  
CLTET5T.001

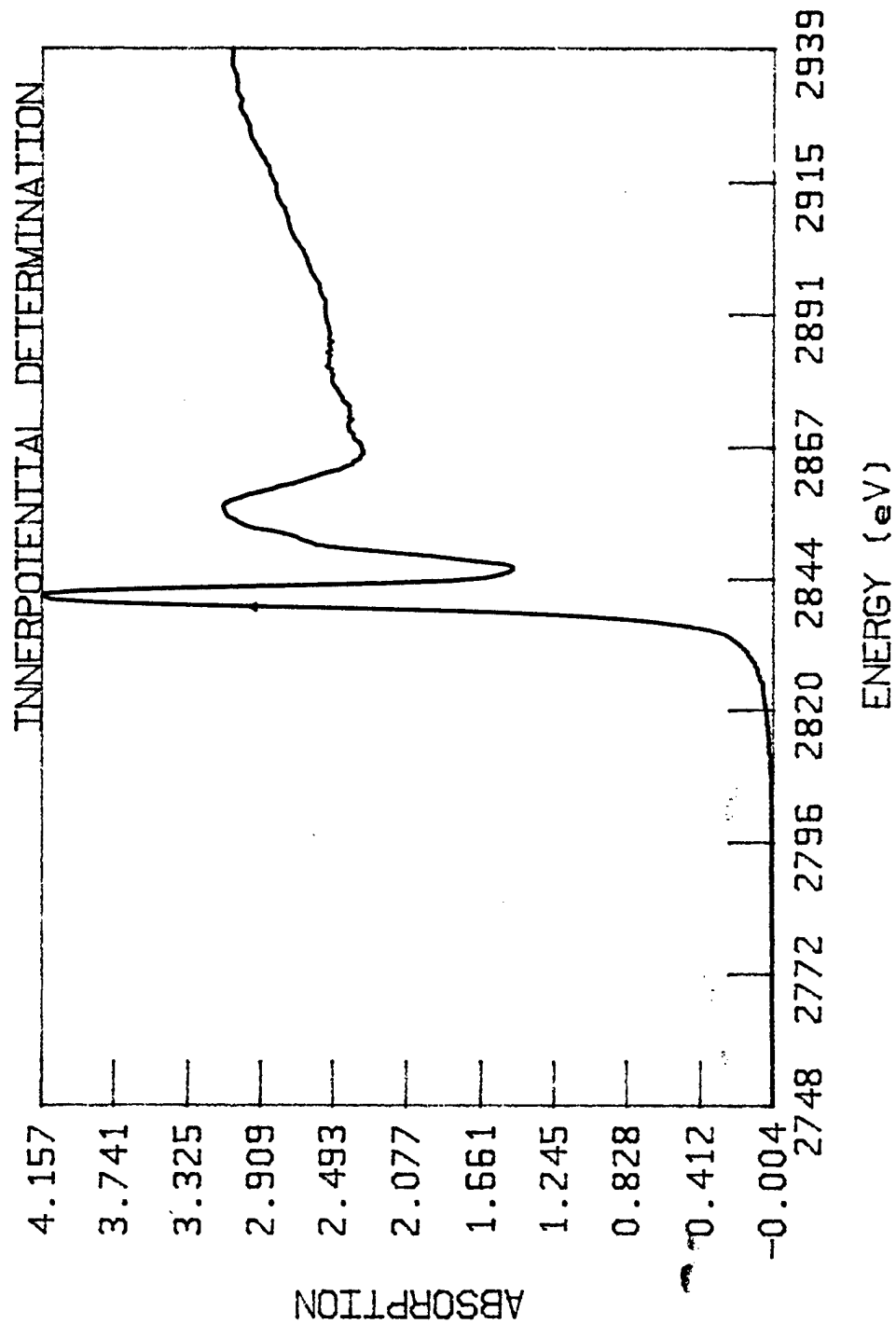


FIGURE 11

E0= 2828.55  
CLNA.002

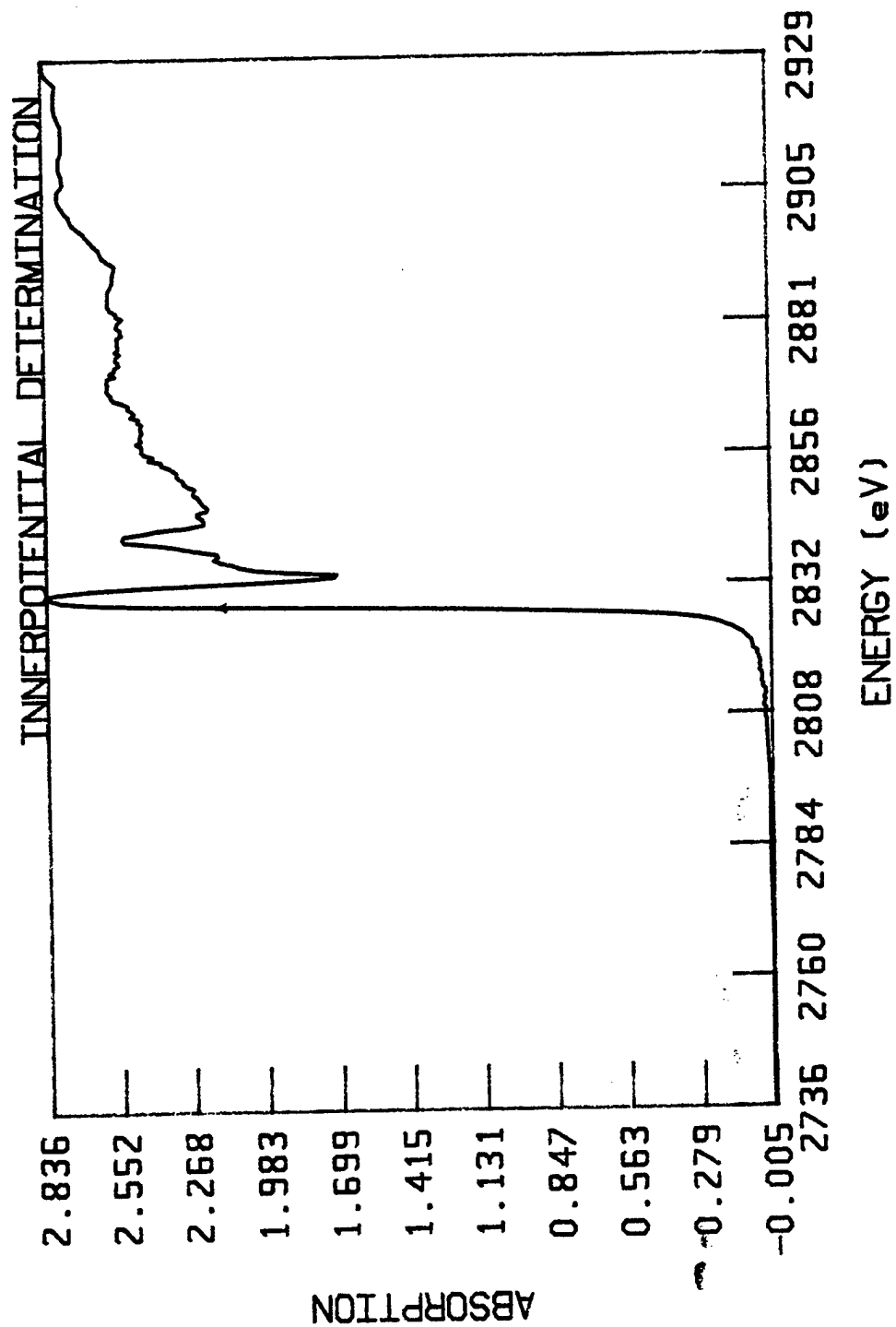


FIGURE 12

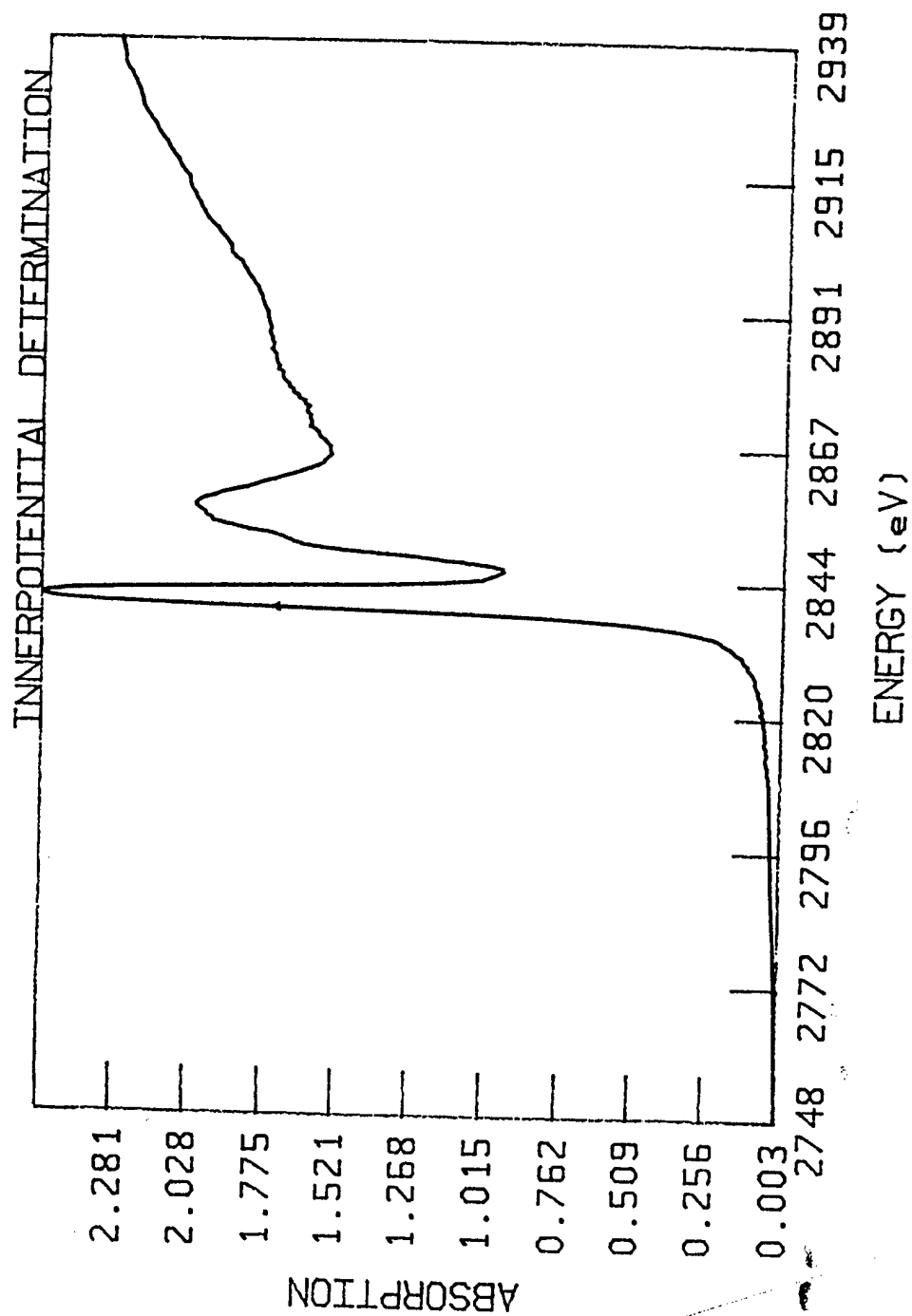


FIGURE 13

E0 = 2838.57  
8782T

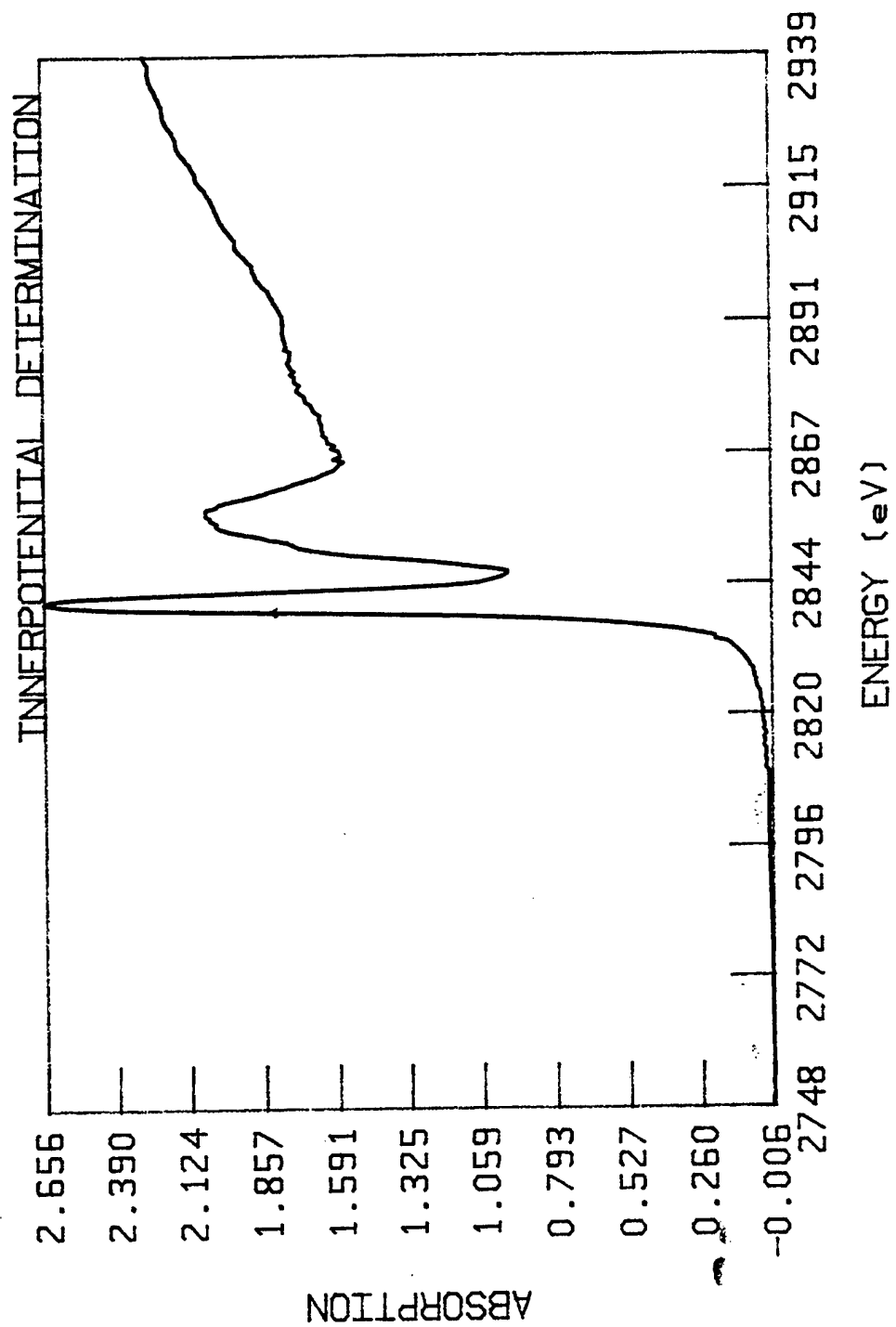


FIGURE 14

E0= 2836.06  
8785B

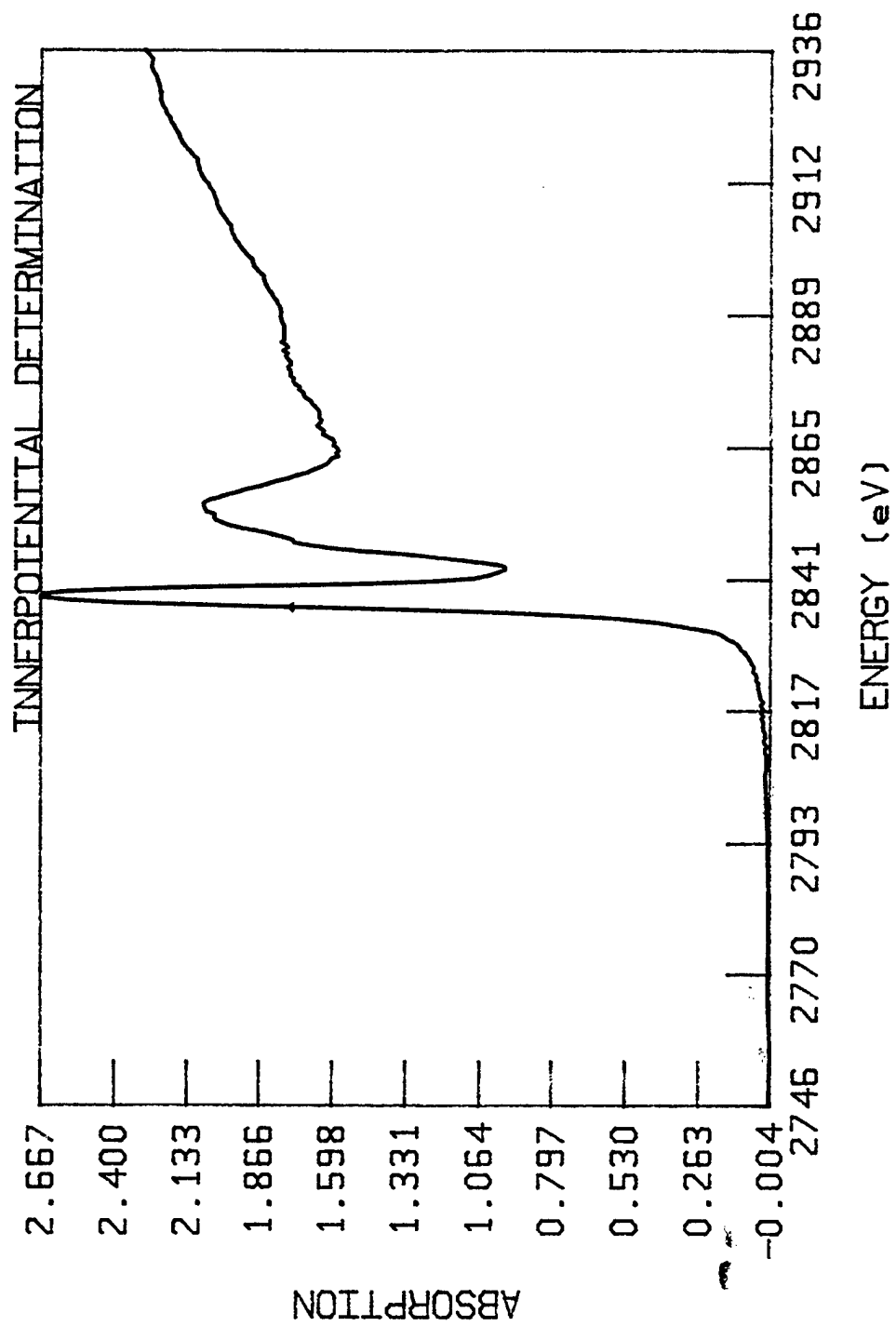


FIGURE 15

E0= 2826.25  
CLK

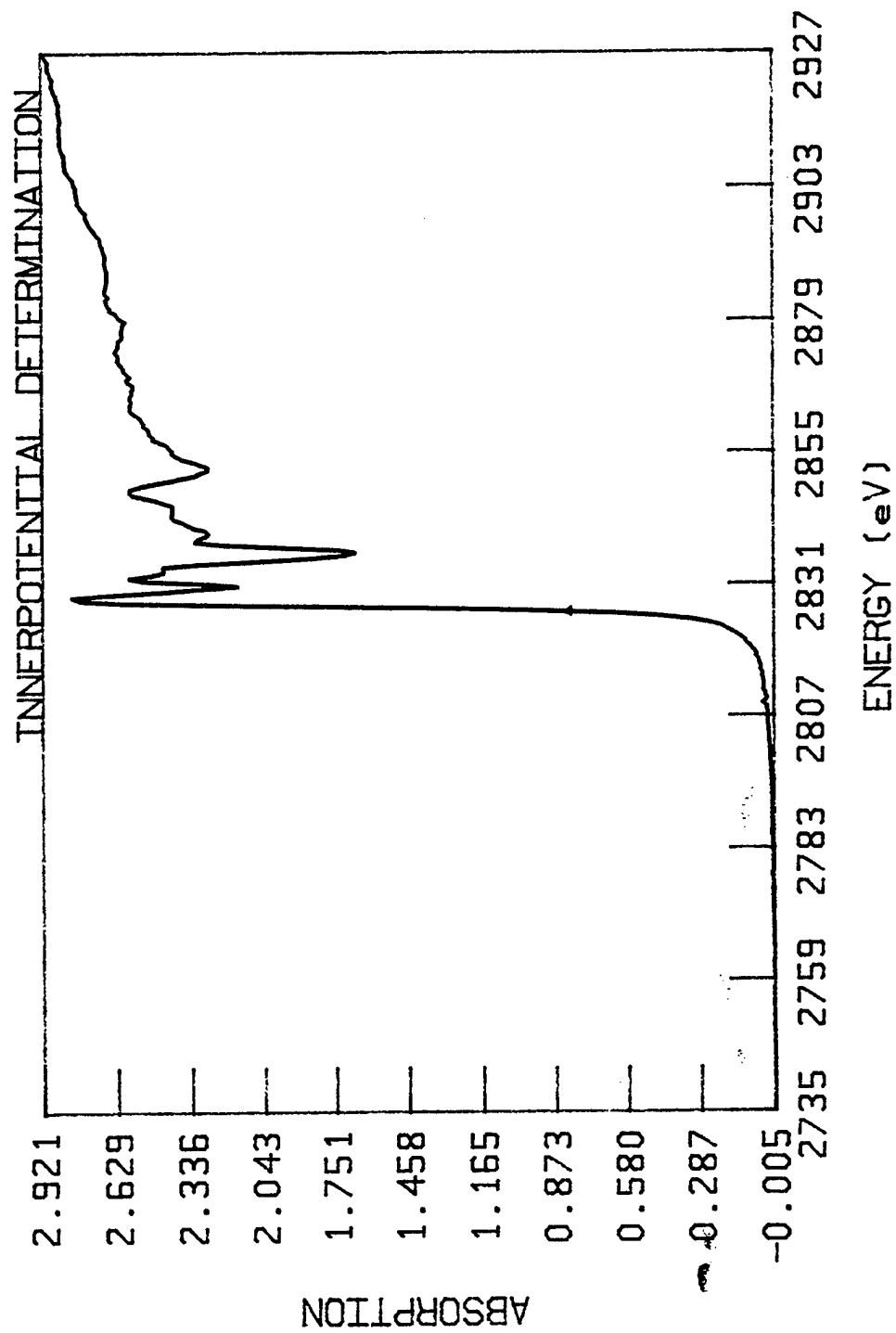


FIGURE 16



E0= 2836.06

AP6

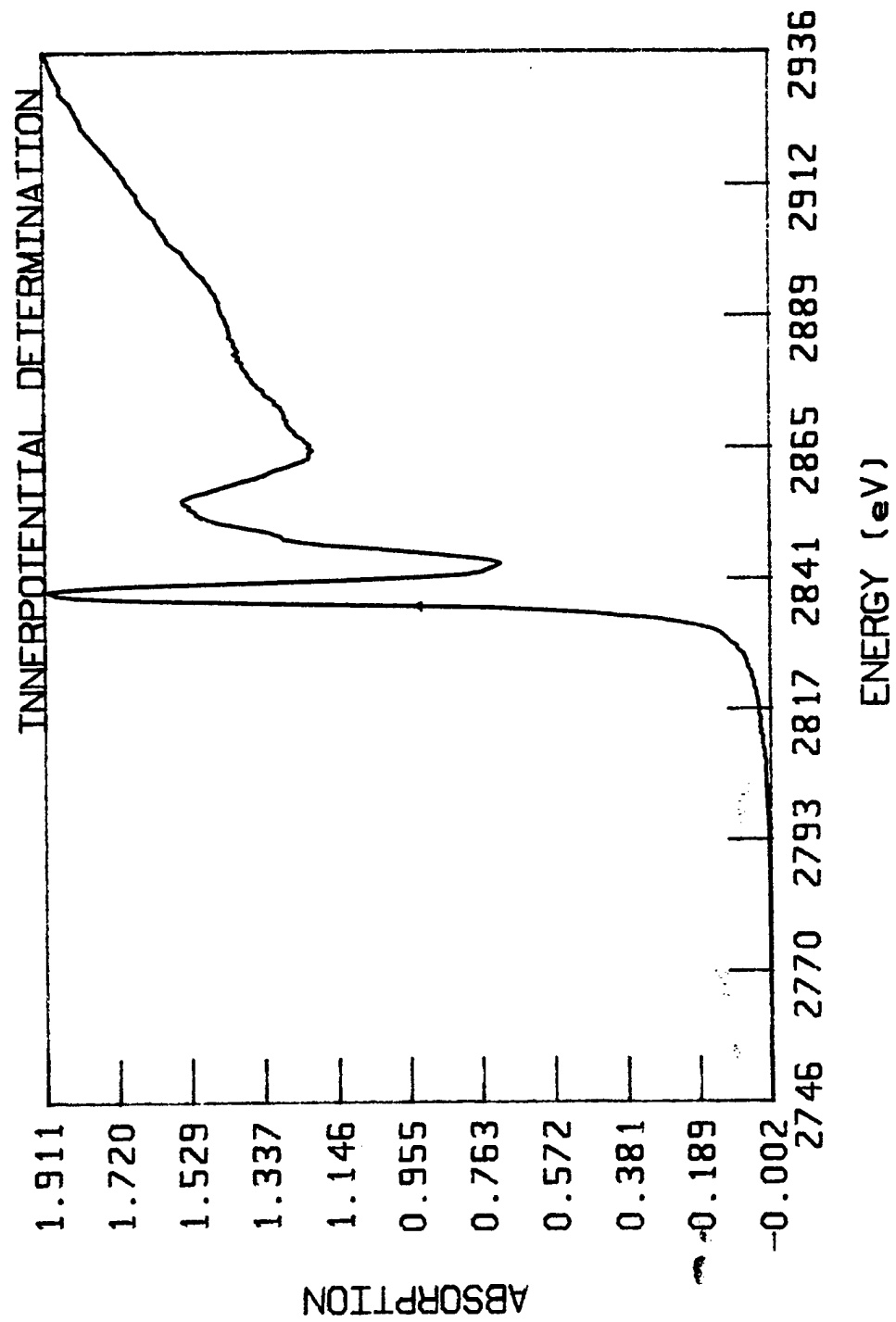


FIGURE 17

E0= 2836.06  
8791B

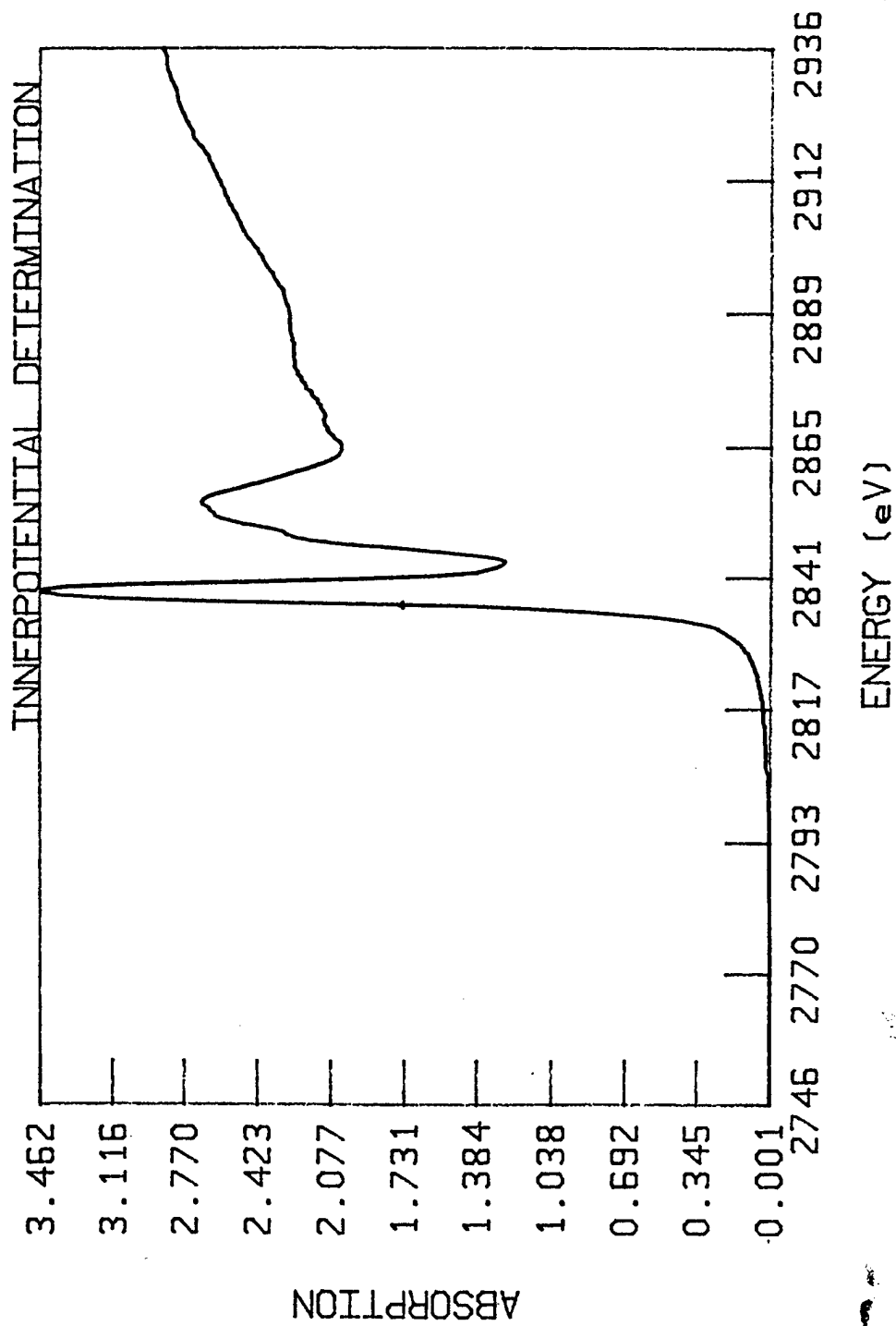


FIGURE 18

E0 = 2826.05

SYN141

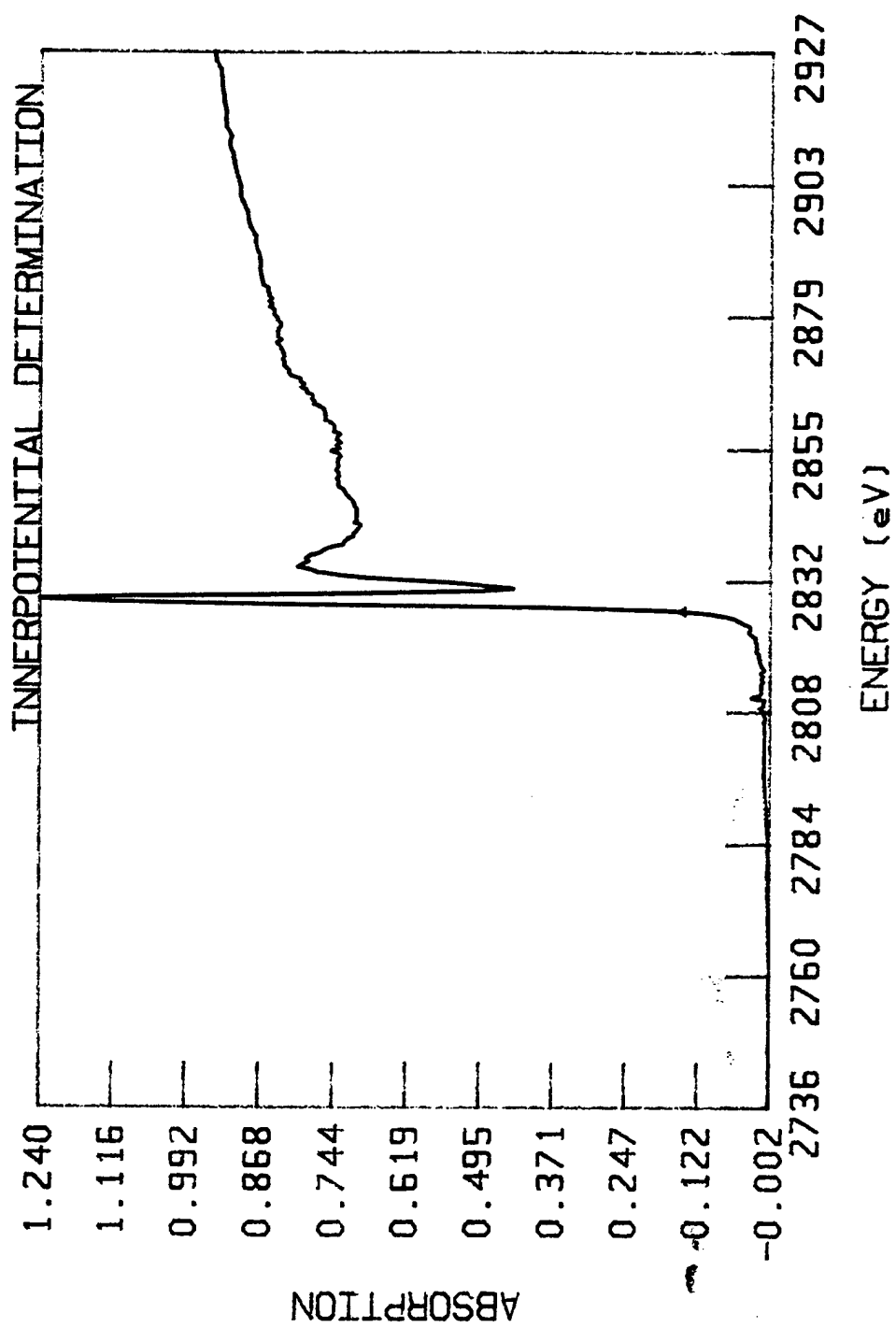


FIGURE 19

E0= 2822.83

CLNH4.200

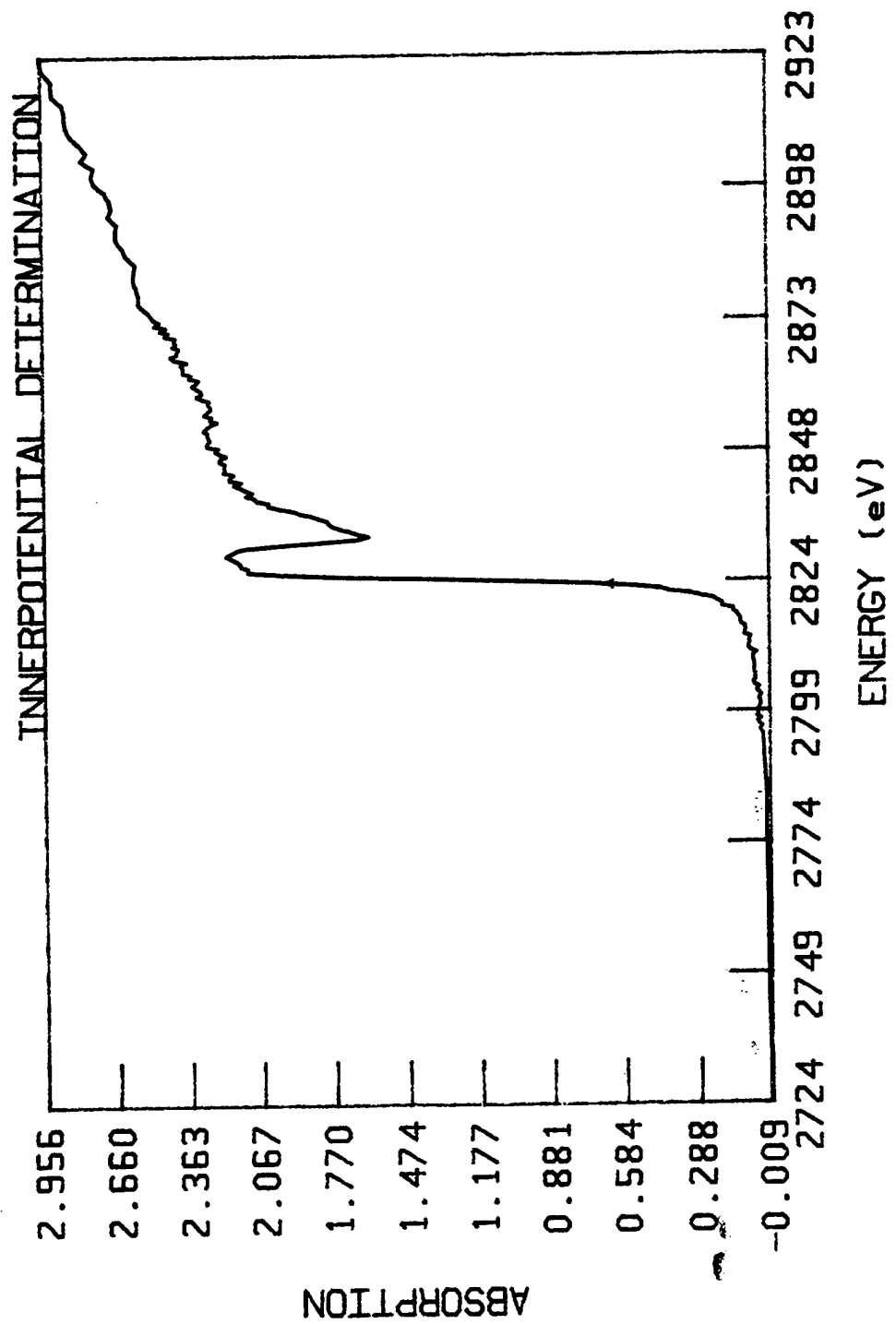
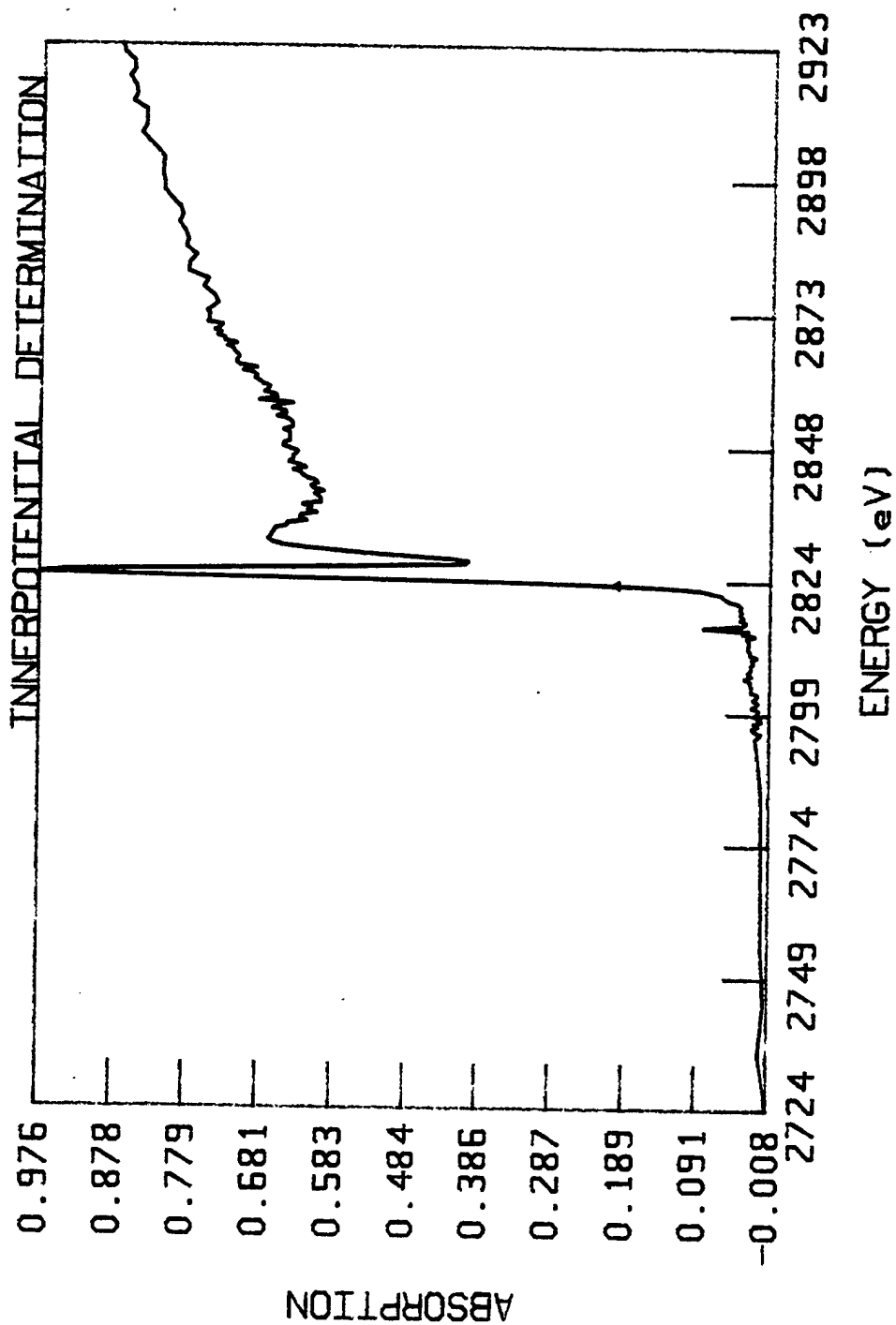


FIGURE 20

E0= 2822.83

CLSYN13



E0= 2822.83  
CLSYN12.002

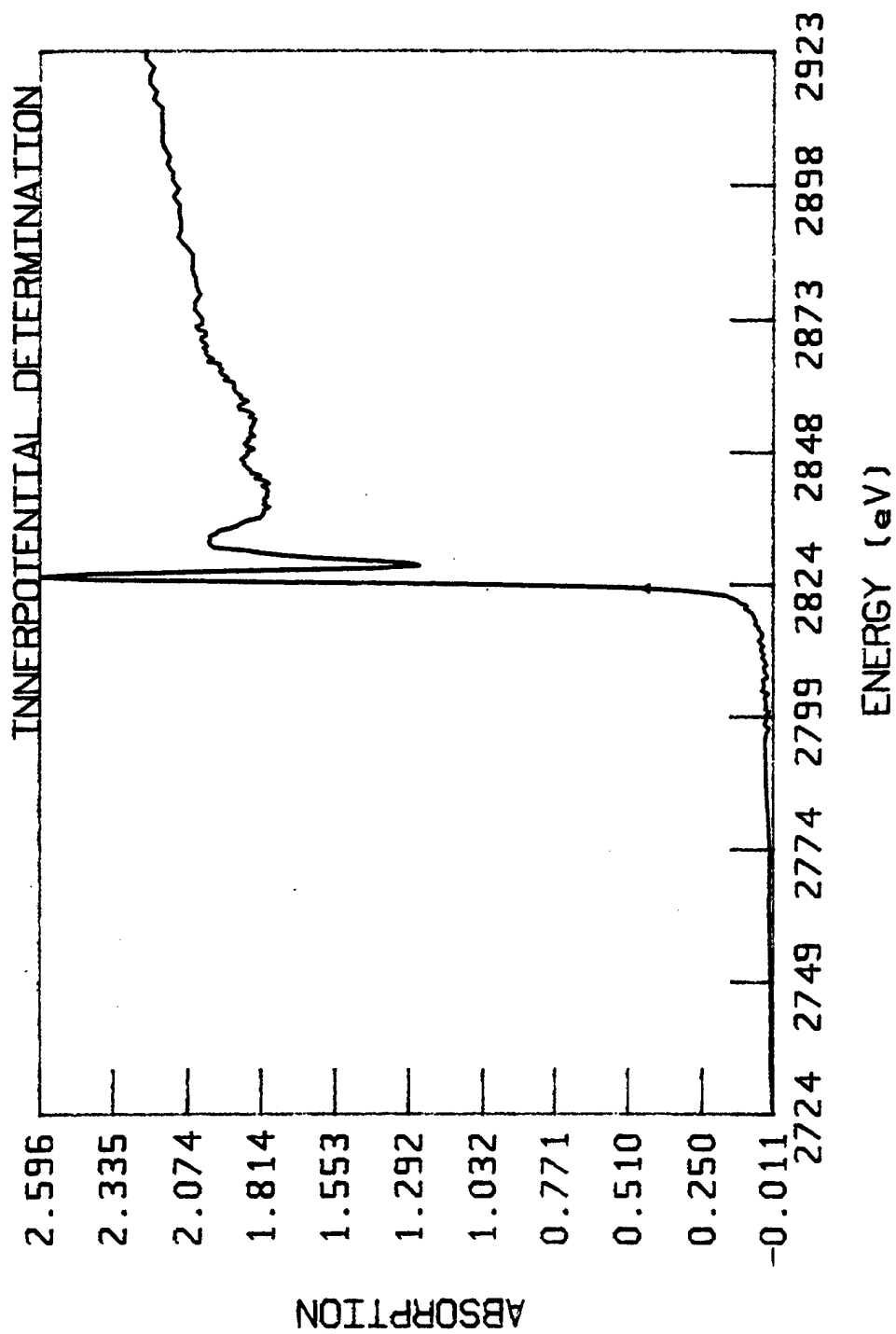


FIGURE 22

E0 = 2822.83

CLSYN11

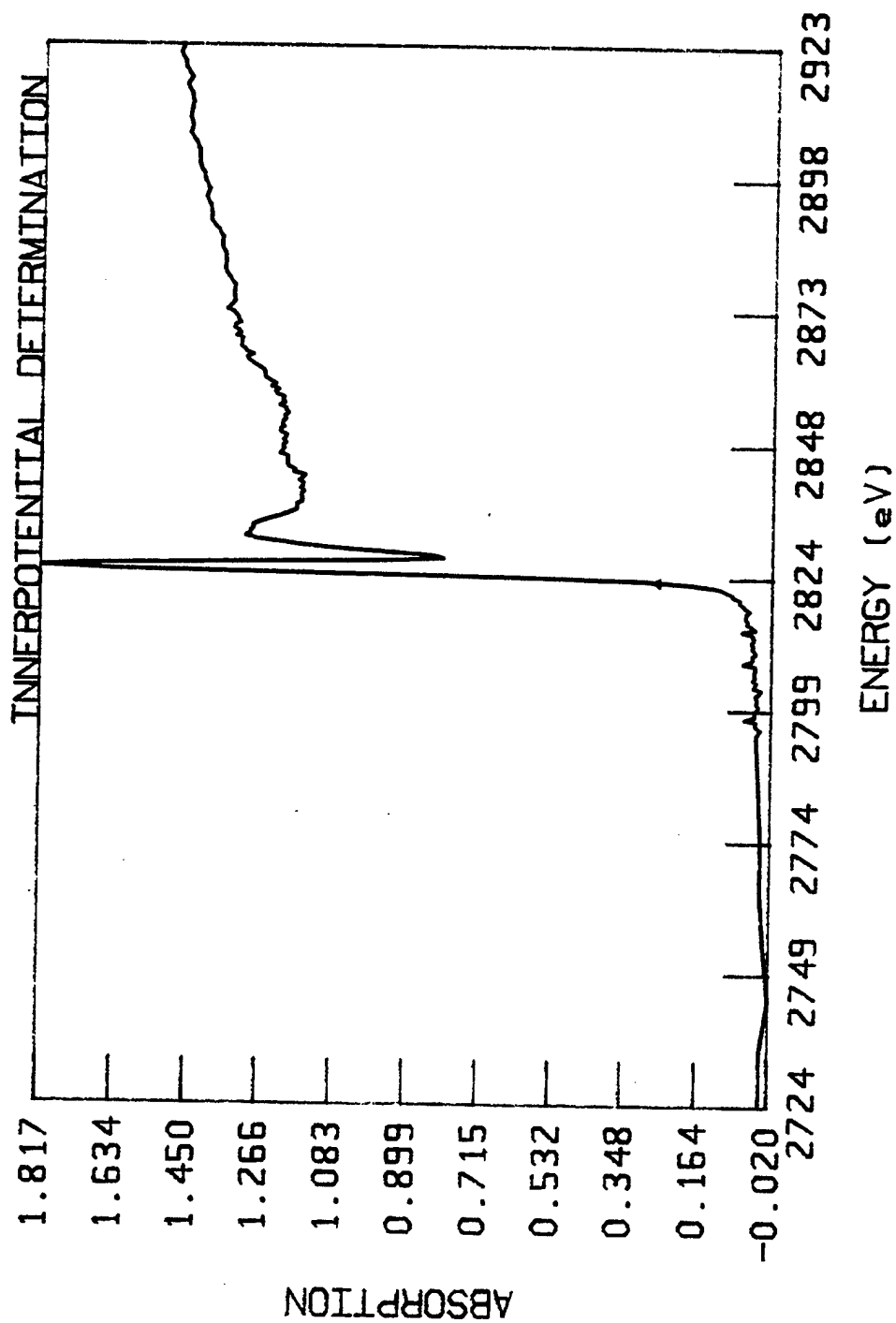


FIGURE 23

E0= 2822.83

PACP

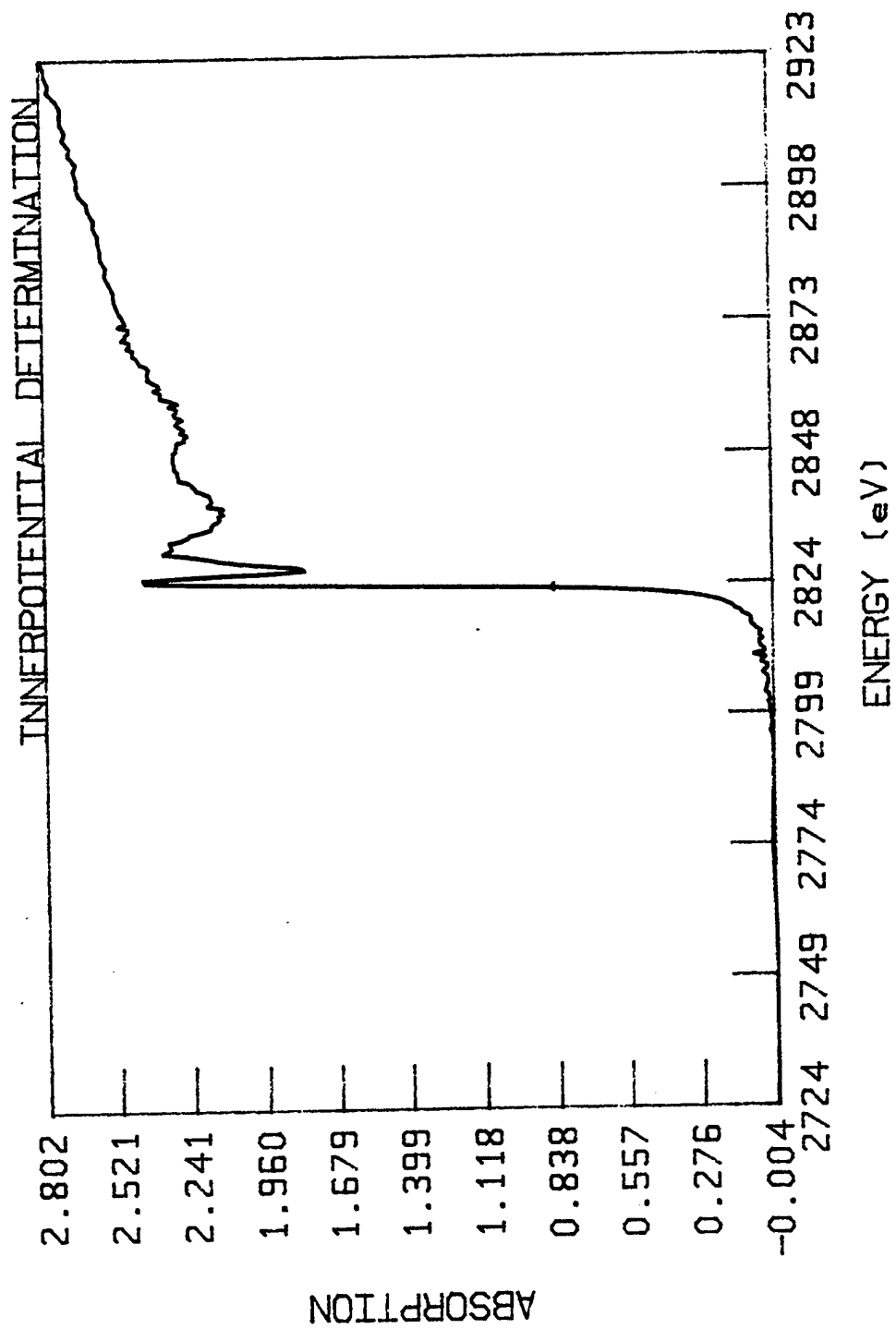


FIGURE 24



E0= 2825.31  
PECP

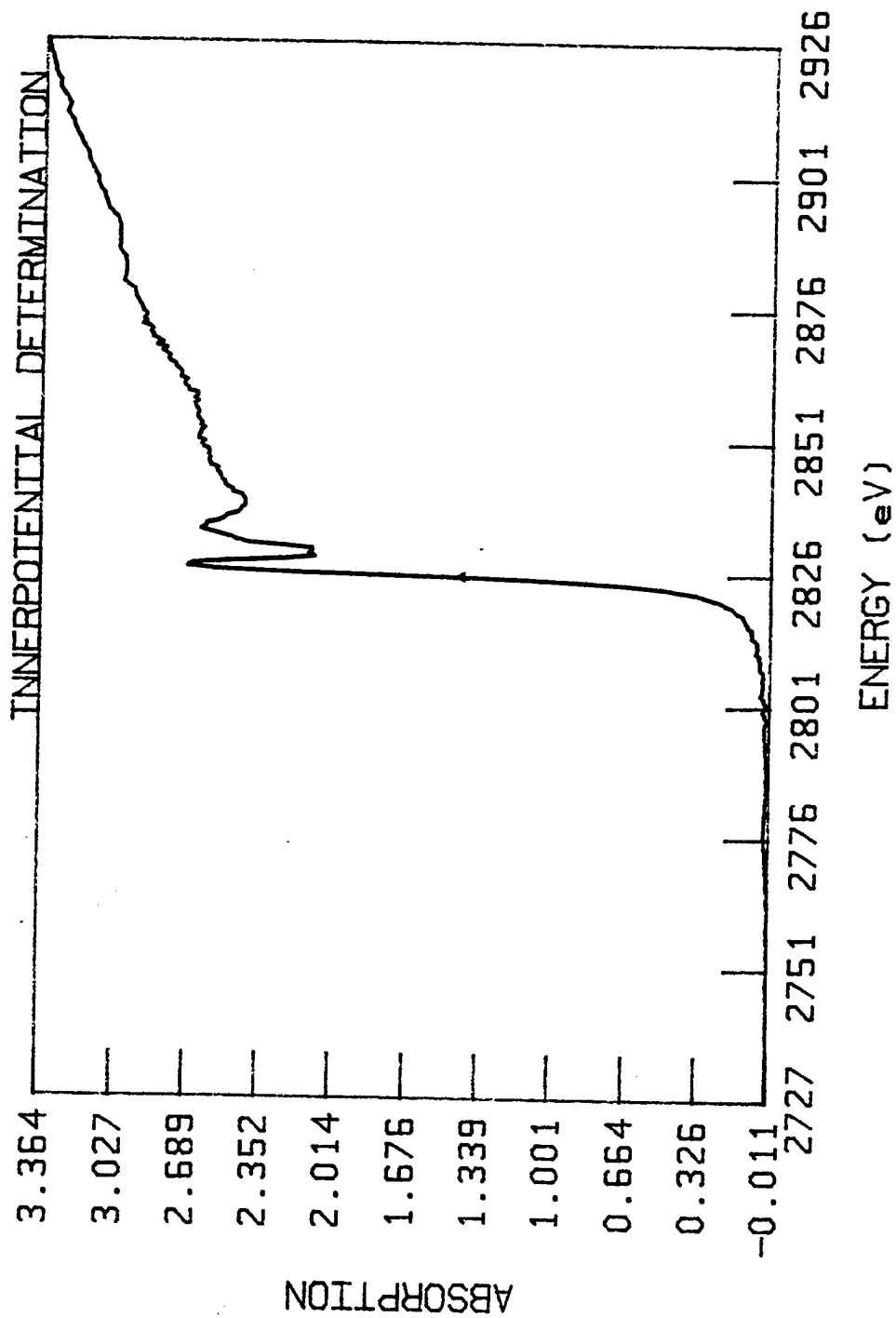


FIGURE 25

E0 = 2822.83

CLHO

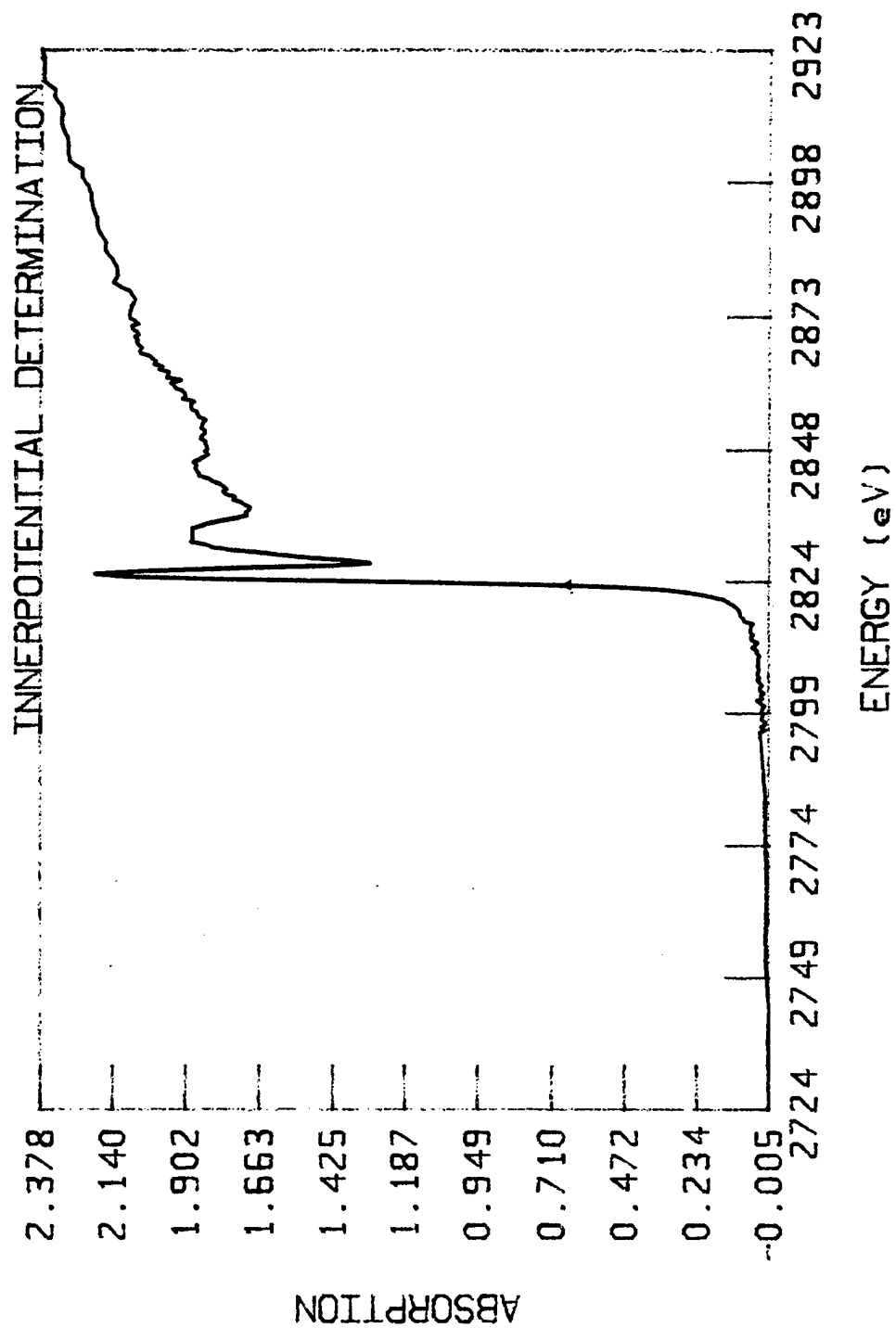


FIGURE 26

E0= 2832.77  
CL7521B.001

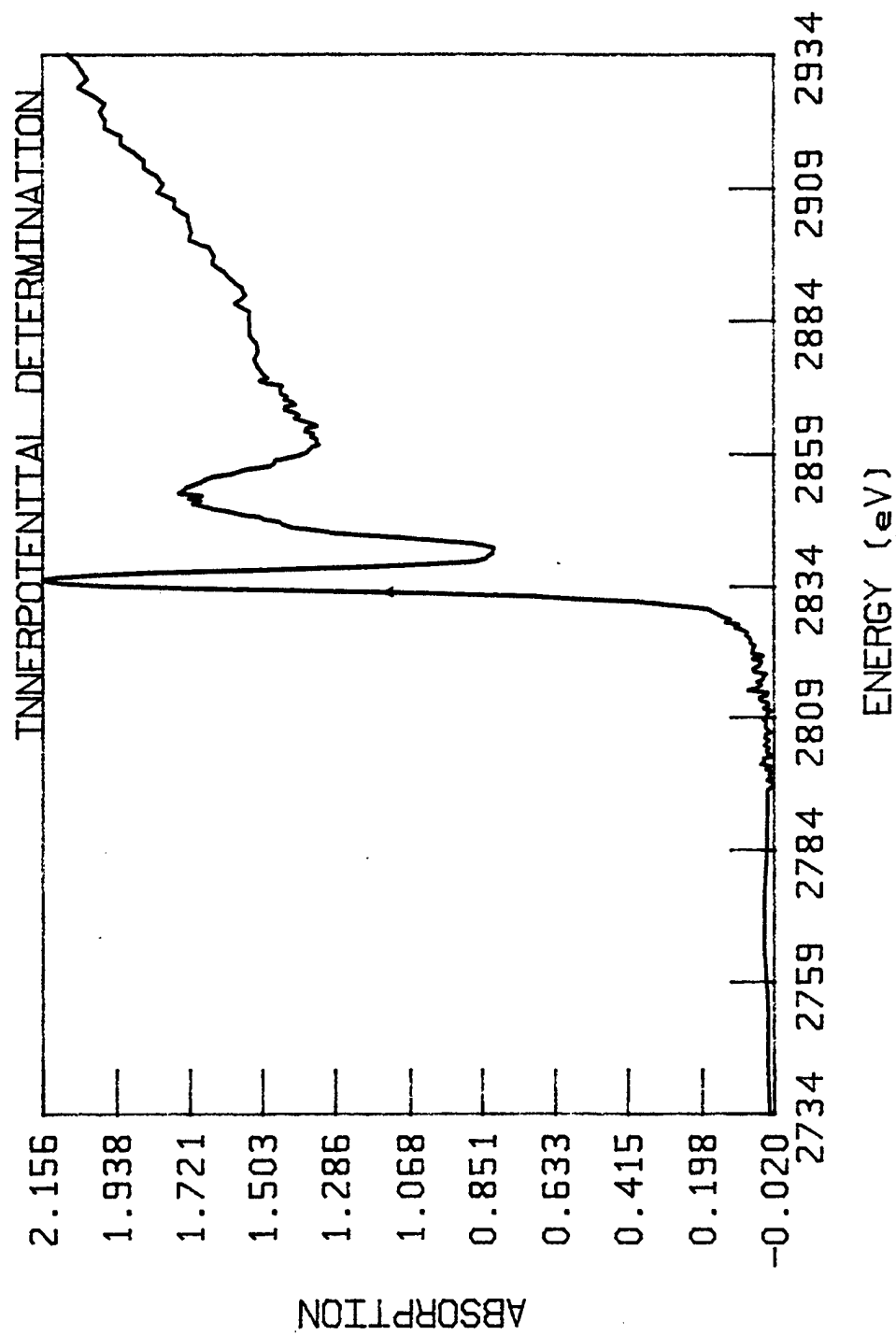


FIGURE 27

E0= 2832.77  
CLDER1B.001

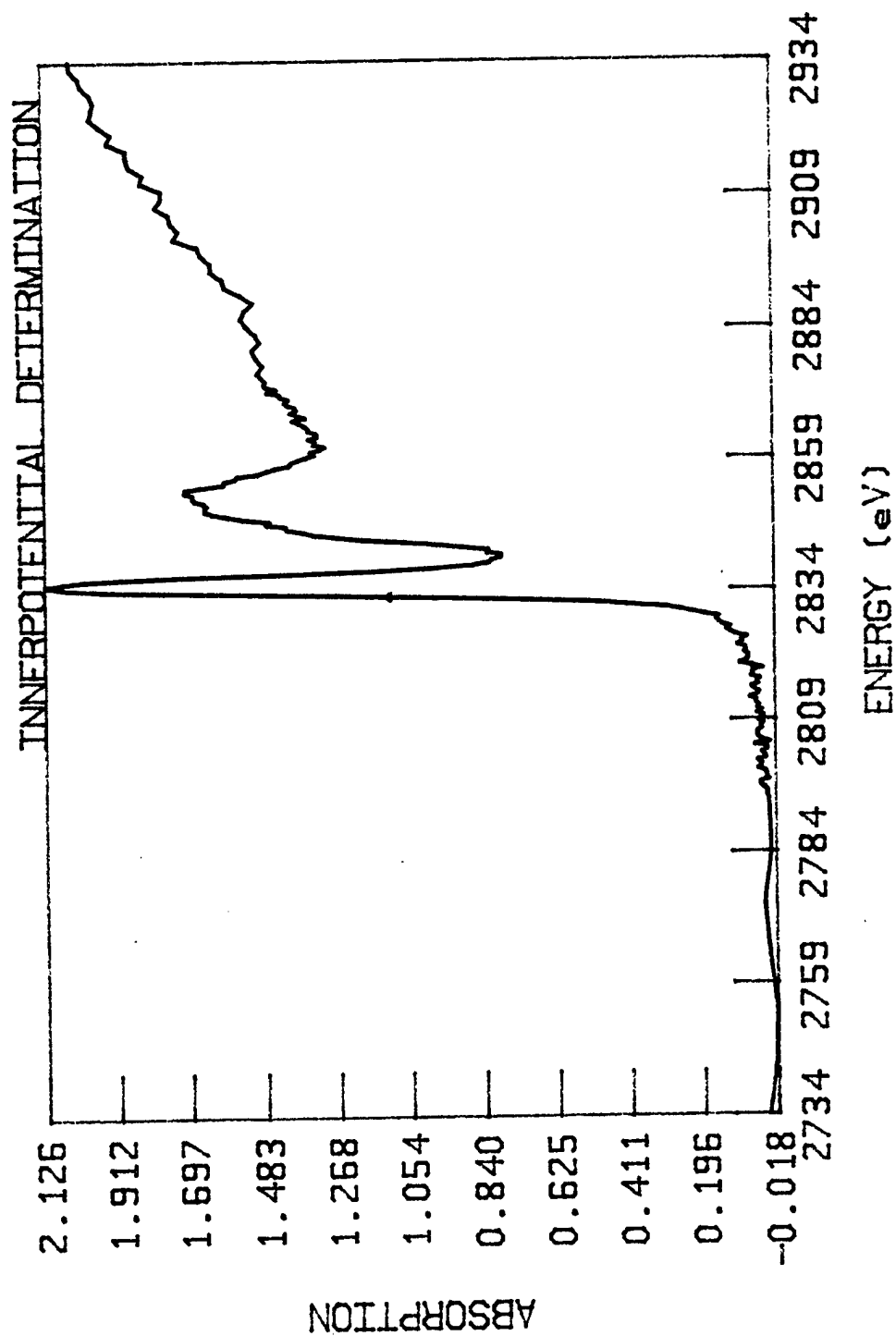


FIGURE 28

E0 = 2835.25  
CL04CU.001

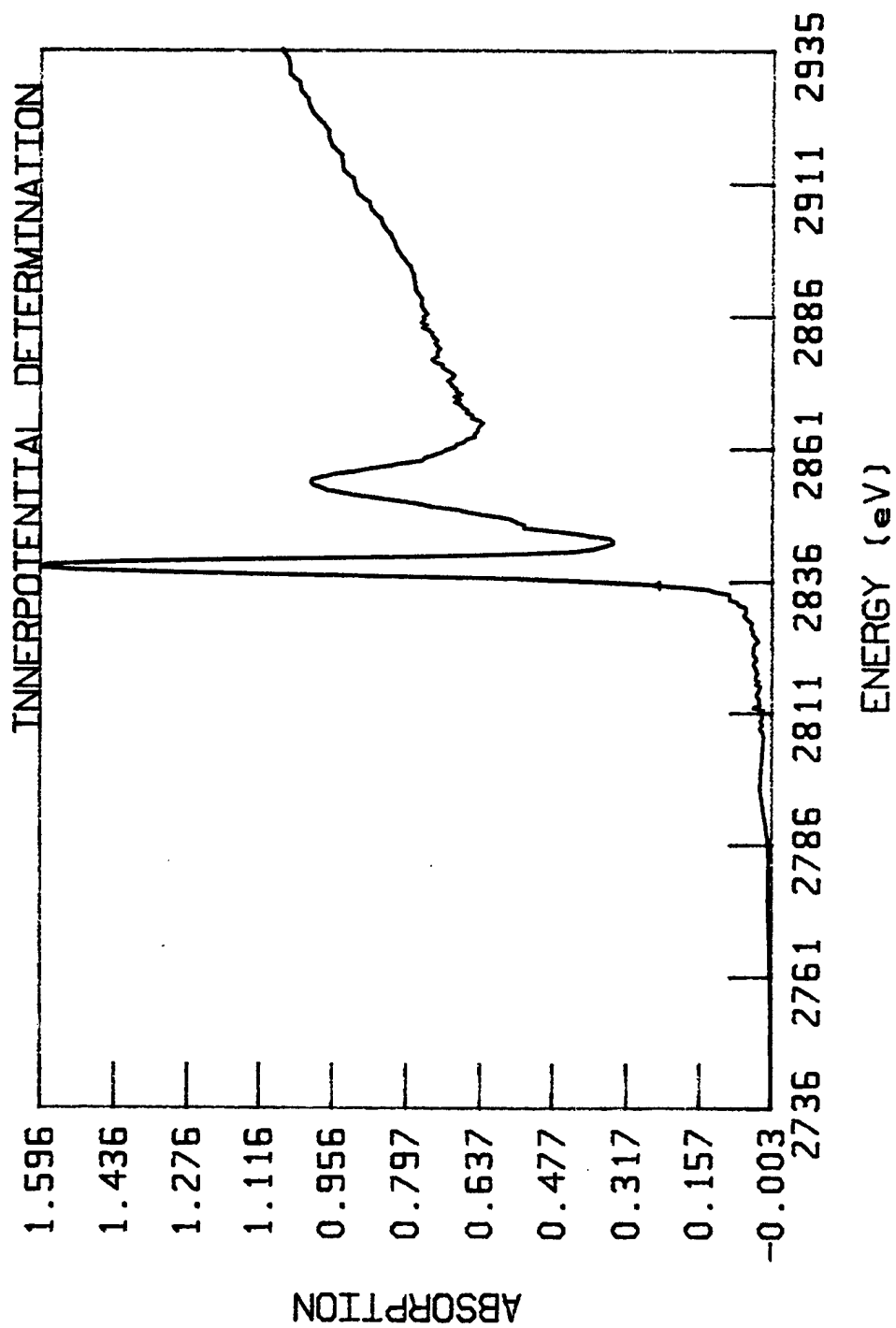


FIGURE 29

E0= 2832.77  
HTP1B

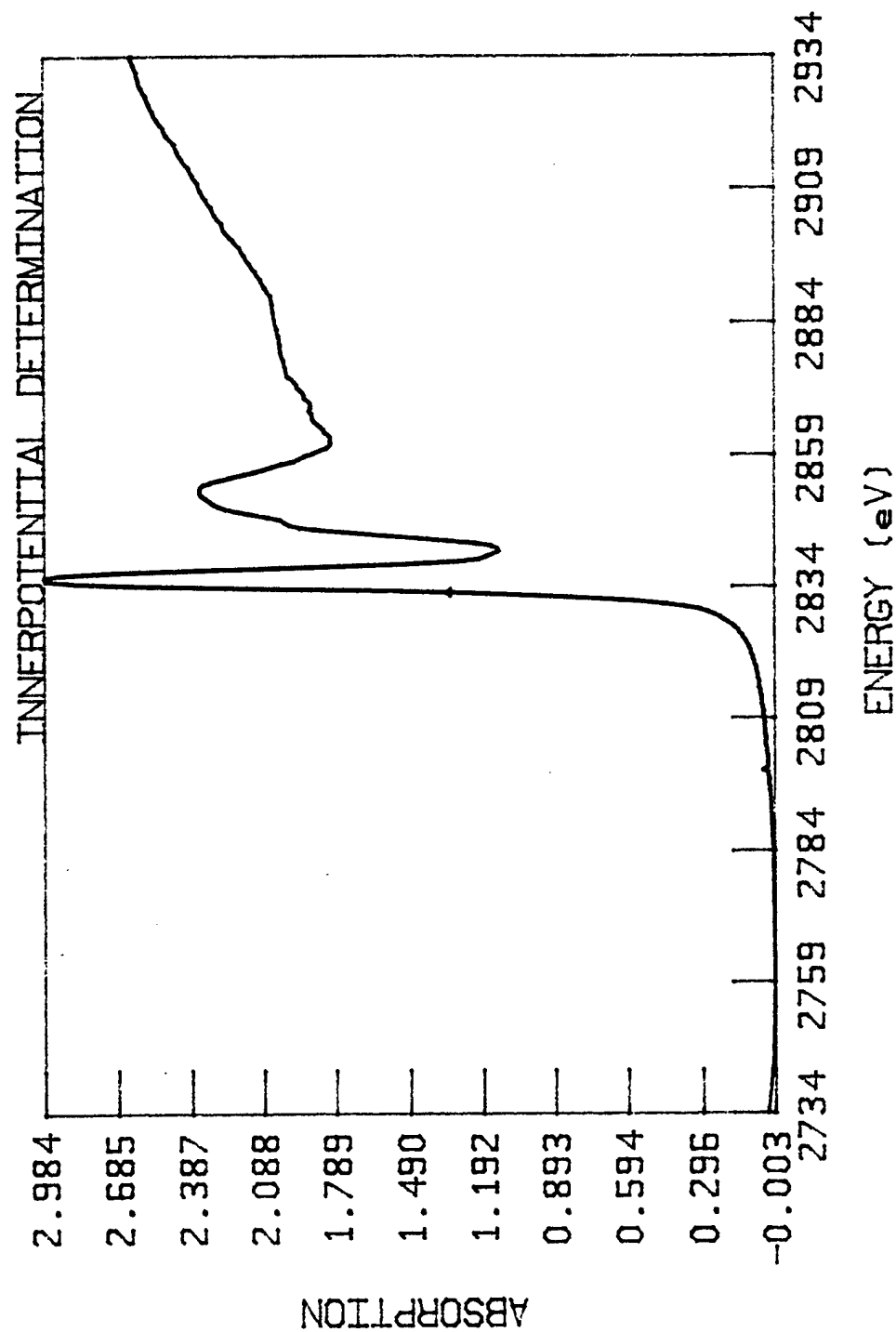


FIGURE 30

E0= 2835.25  
CLHTP1B.003

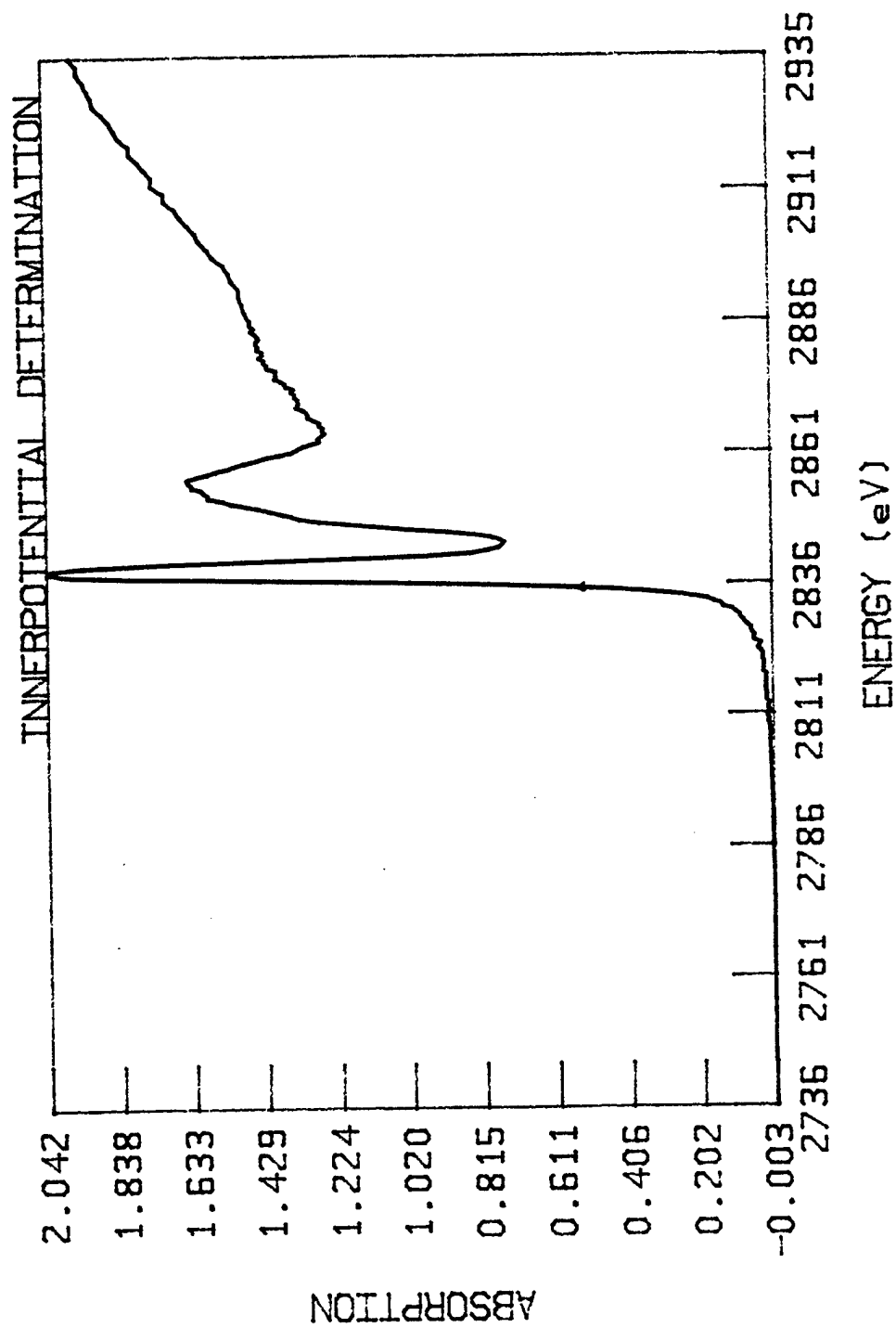


FIGURE 31

E0 = 2826.76

AP1

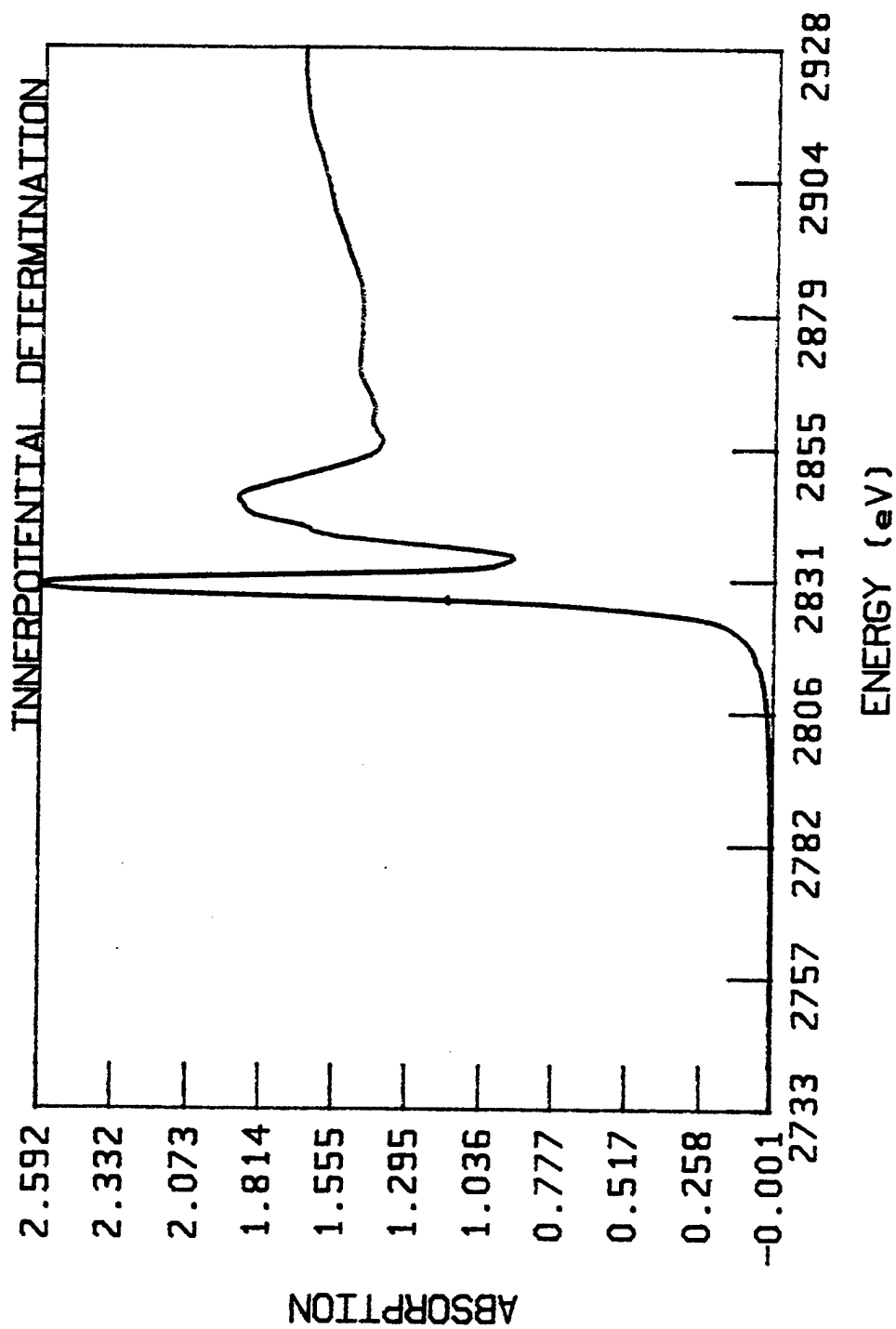


FIGURE 32



E0= 3200.10

AP1

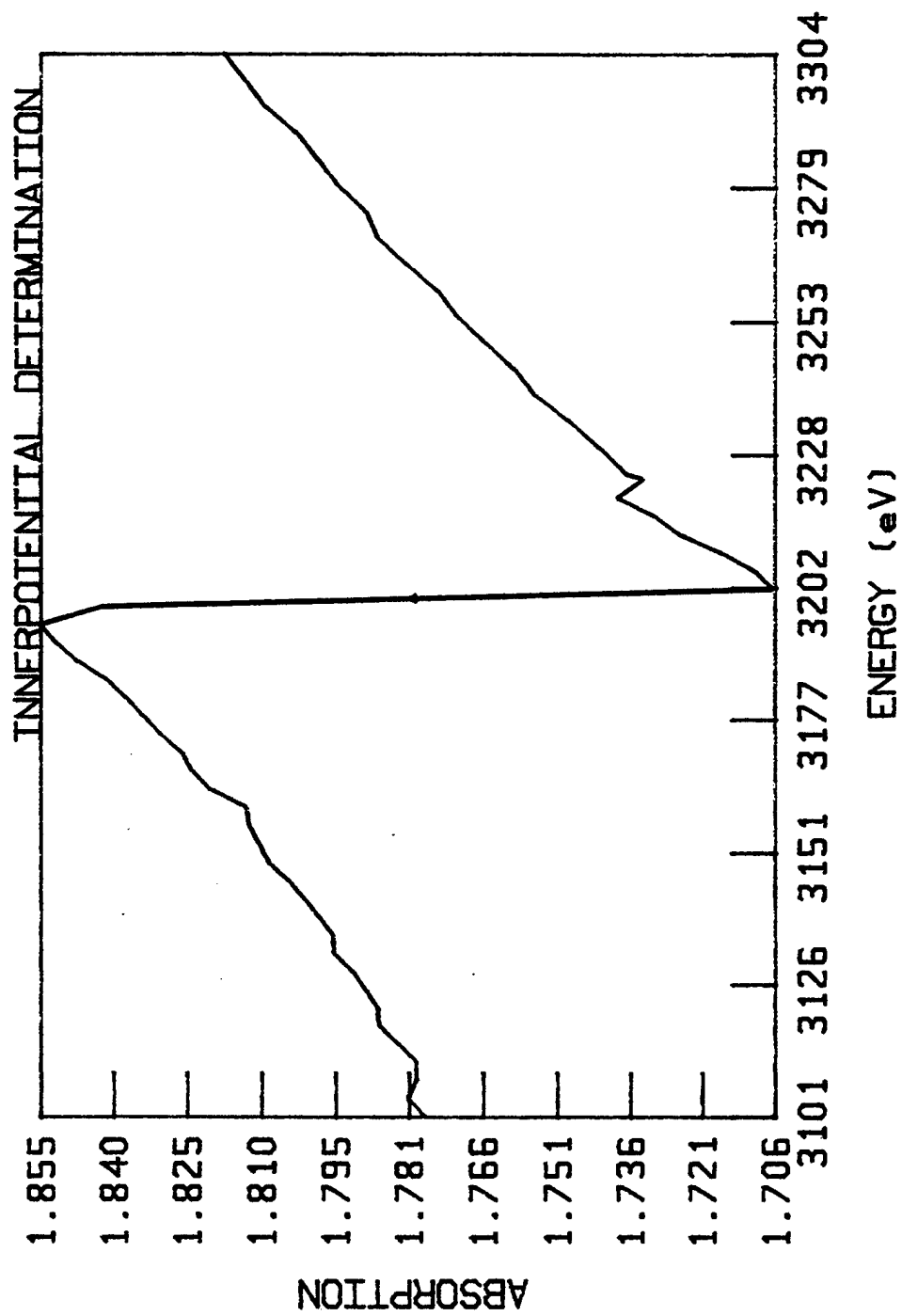


FIGURE 33

E0= 2832.56

AP1

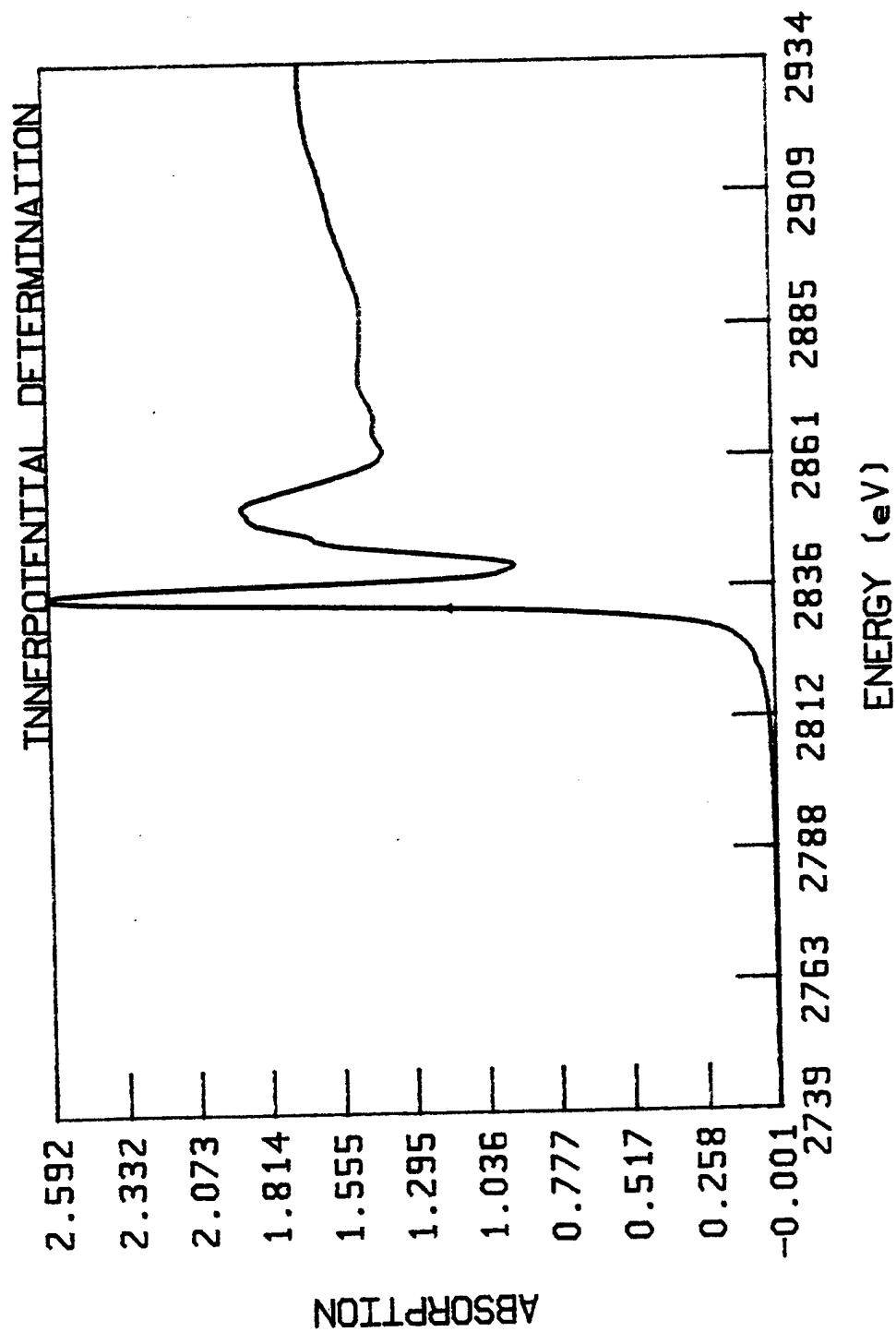


FIGURE 34

E0= 2826.54

AC1

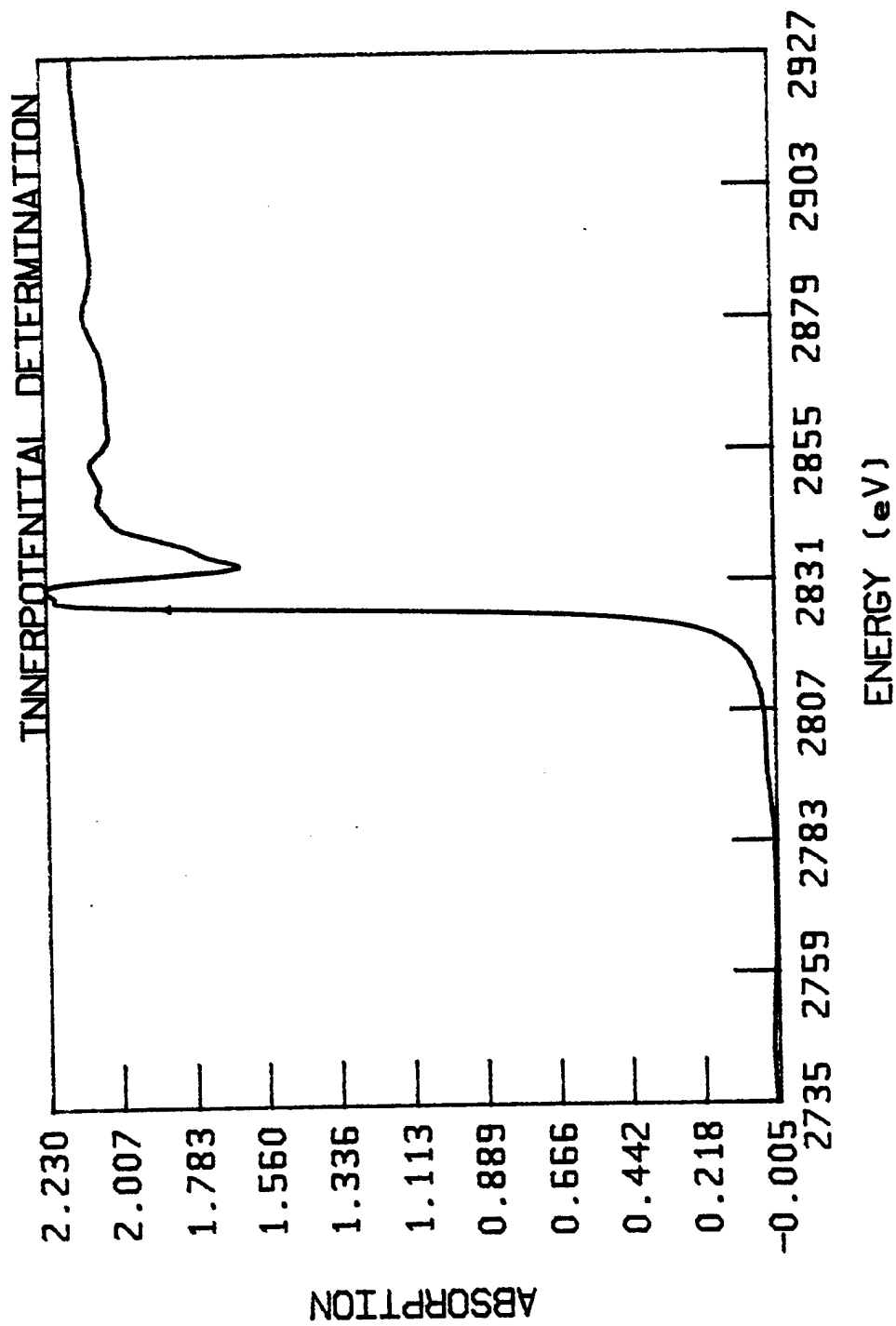


FIGURE 35

E0= 2827.04  
CLNA

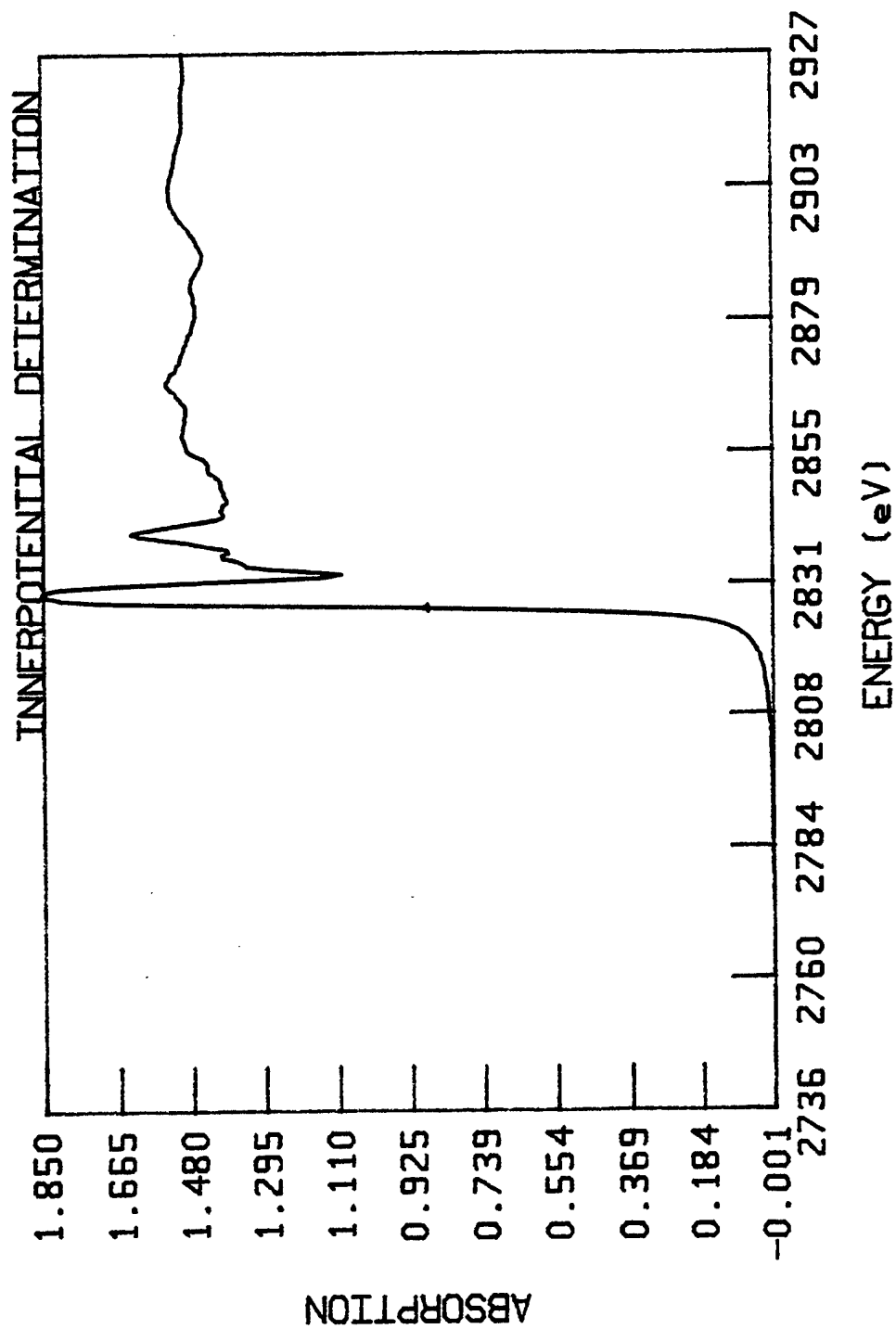


FIGURE 36

E0= 2826.44  
CLK

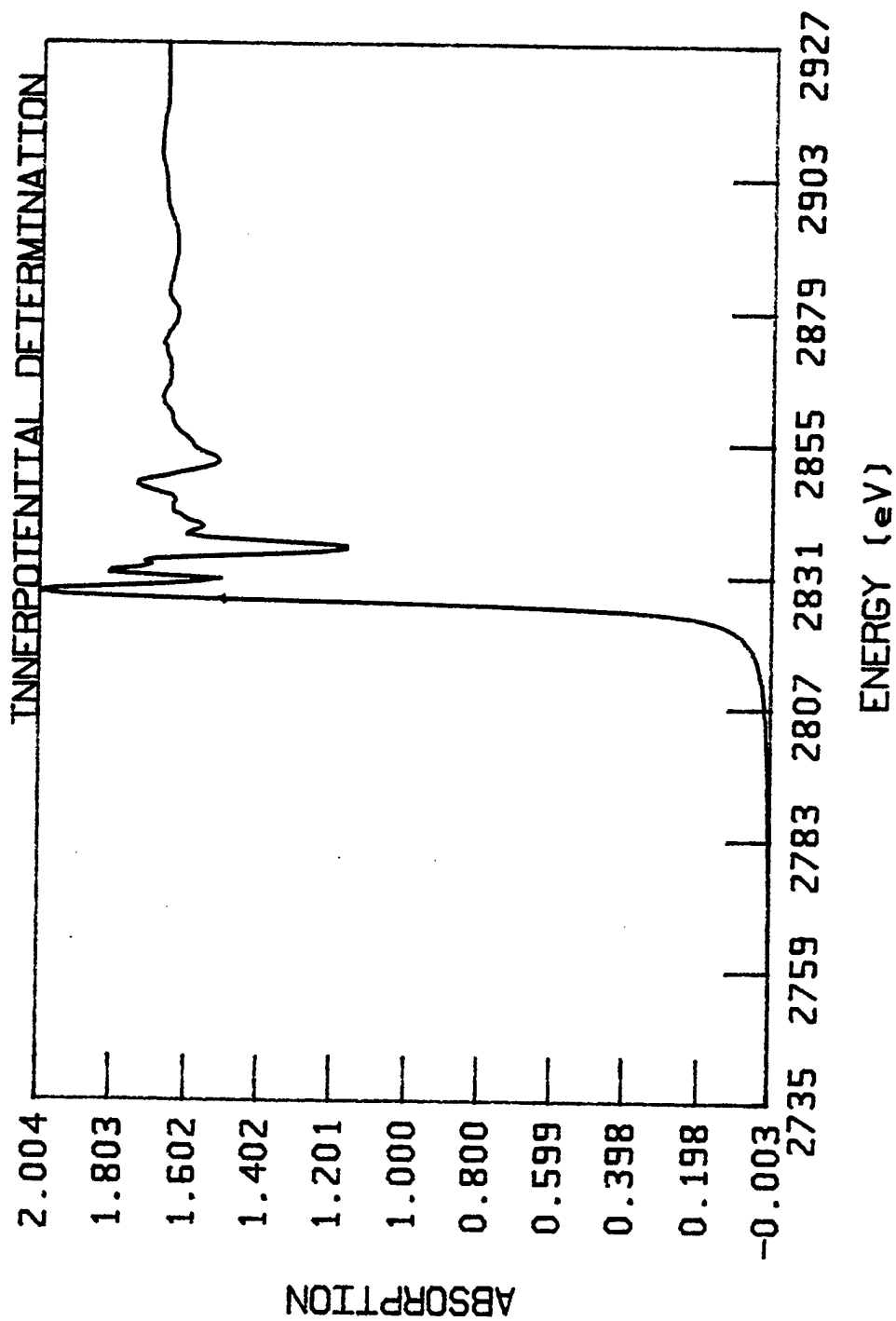


FIGURE 37

E0 = 2824.75

CLHQ

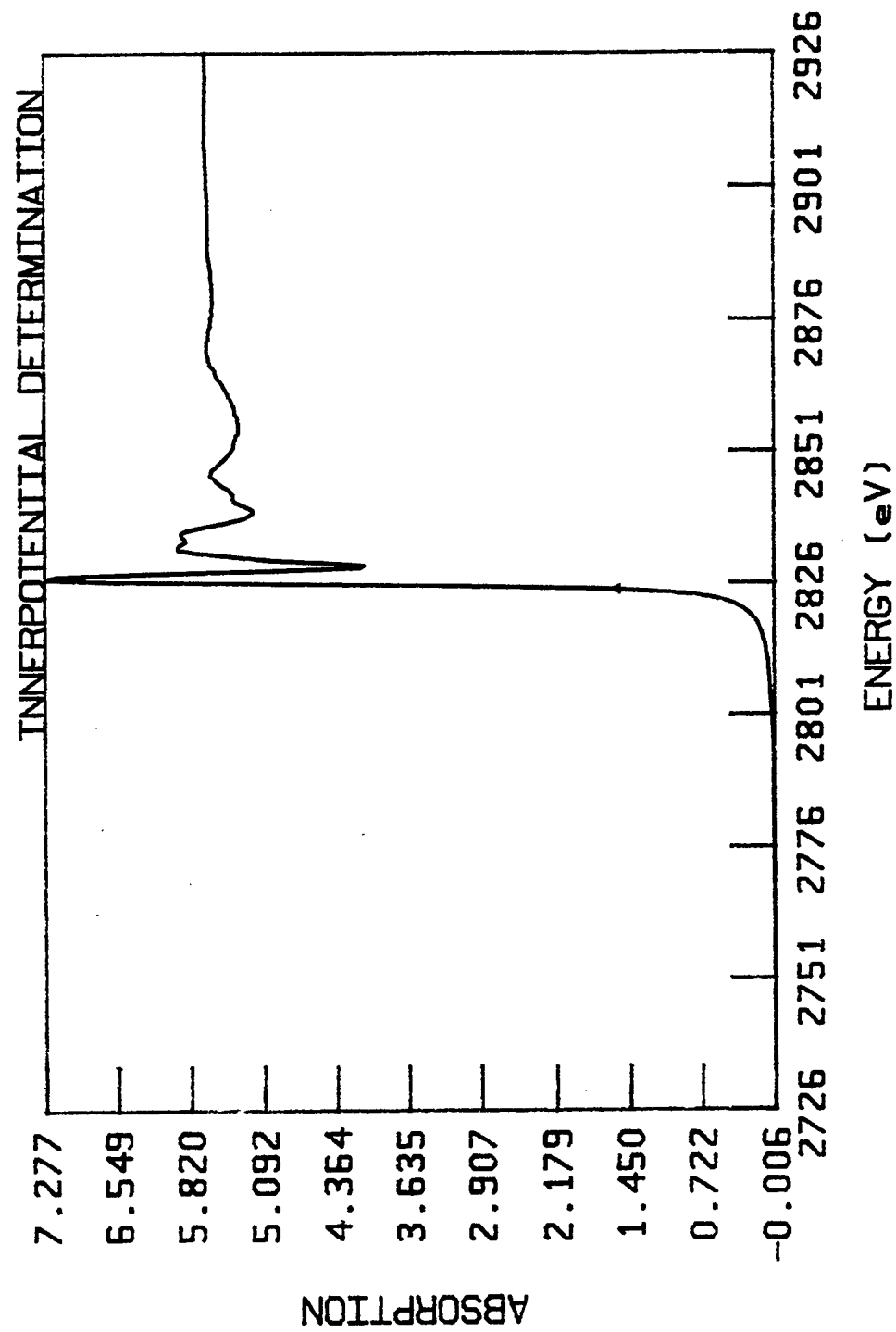


FIGURE 38

E0= 2824.55  
SYN11

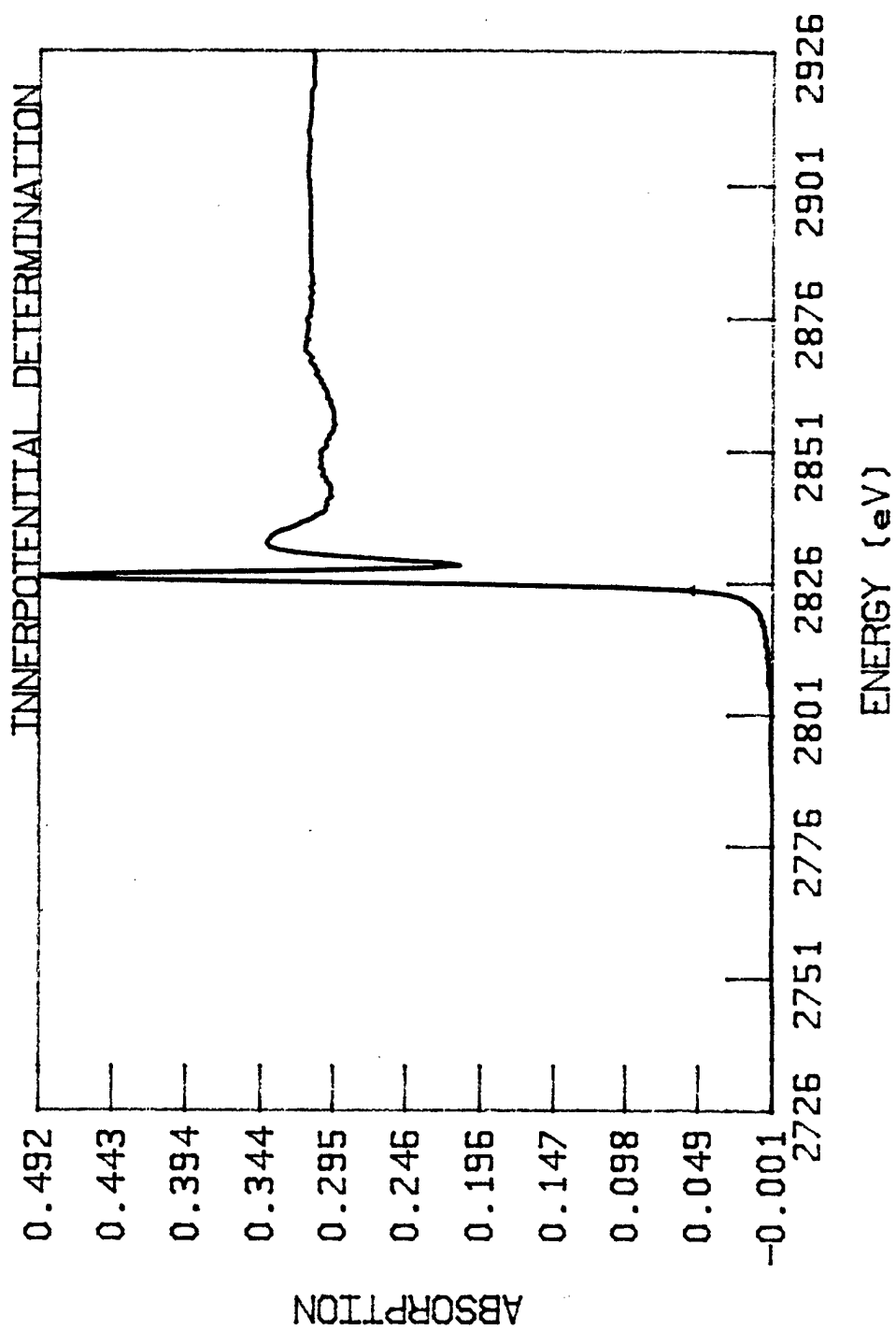


FIGURE 39

E0= 2825.71  
SYN12.133

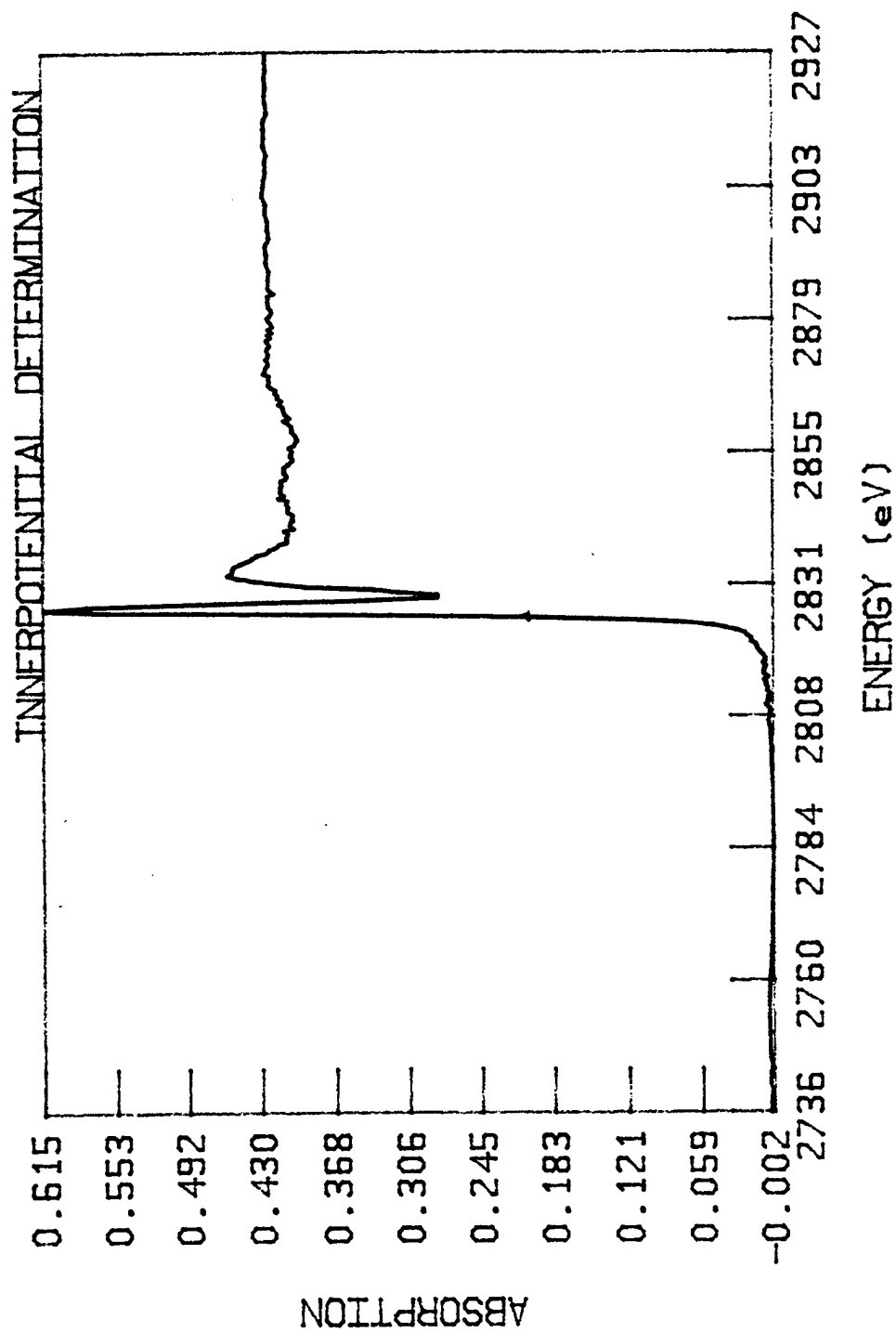


FIGURE 40



E0= 2834.59

AP2

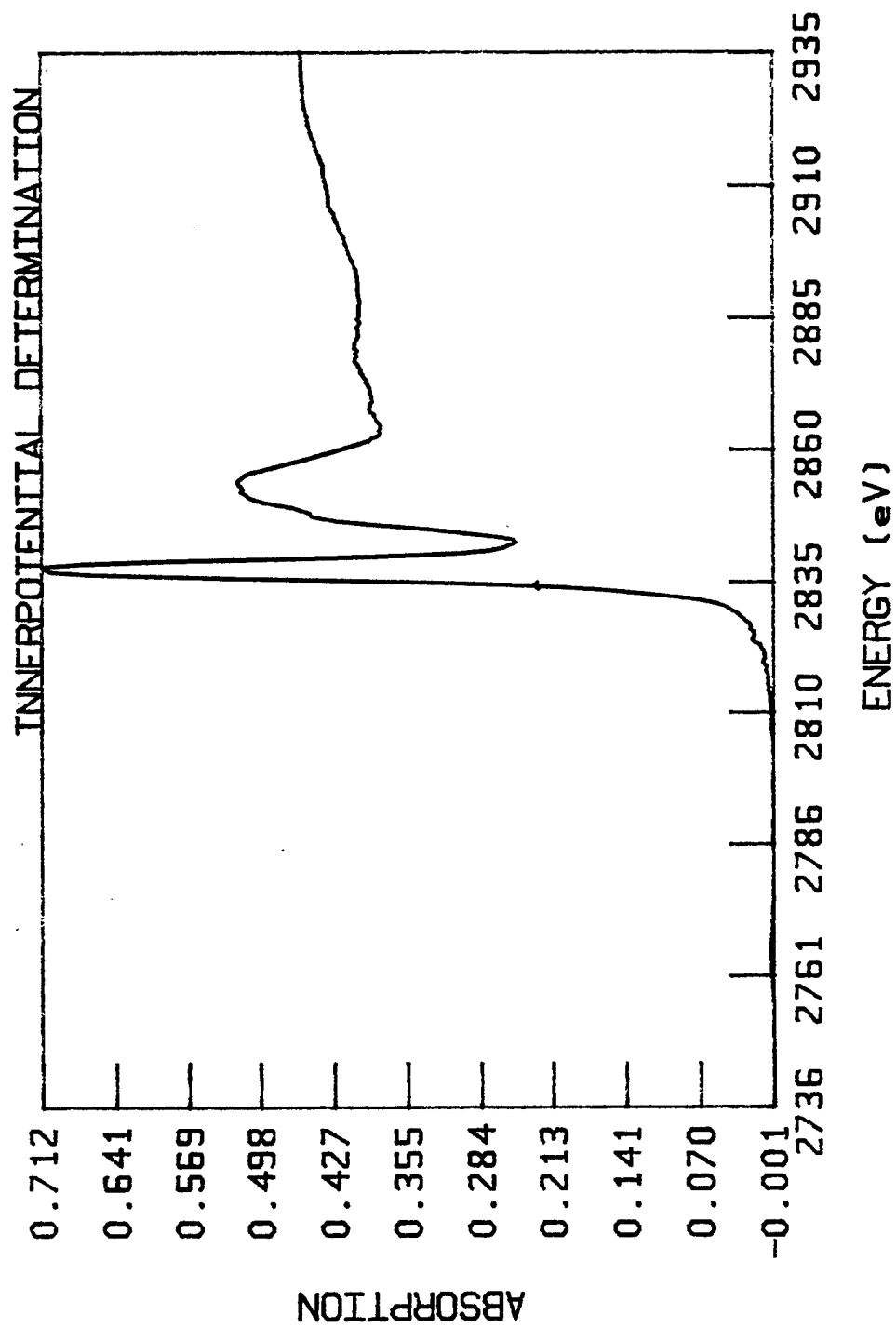


FIGURE 41

E0= 2820.39  
SYN13

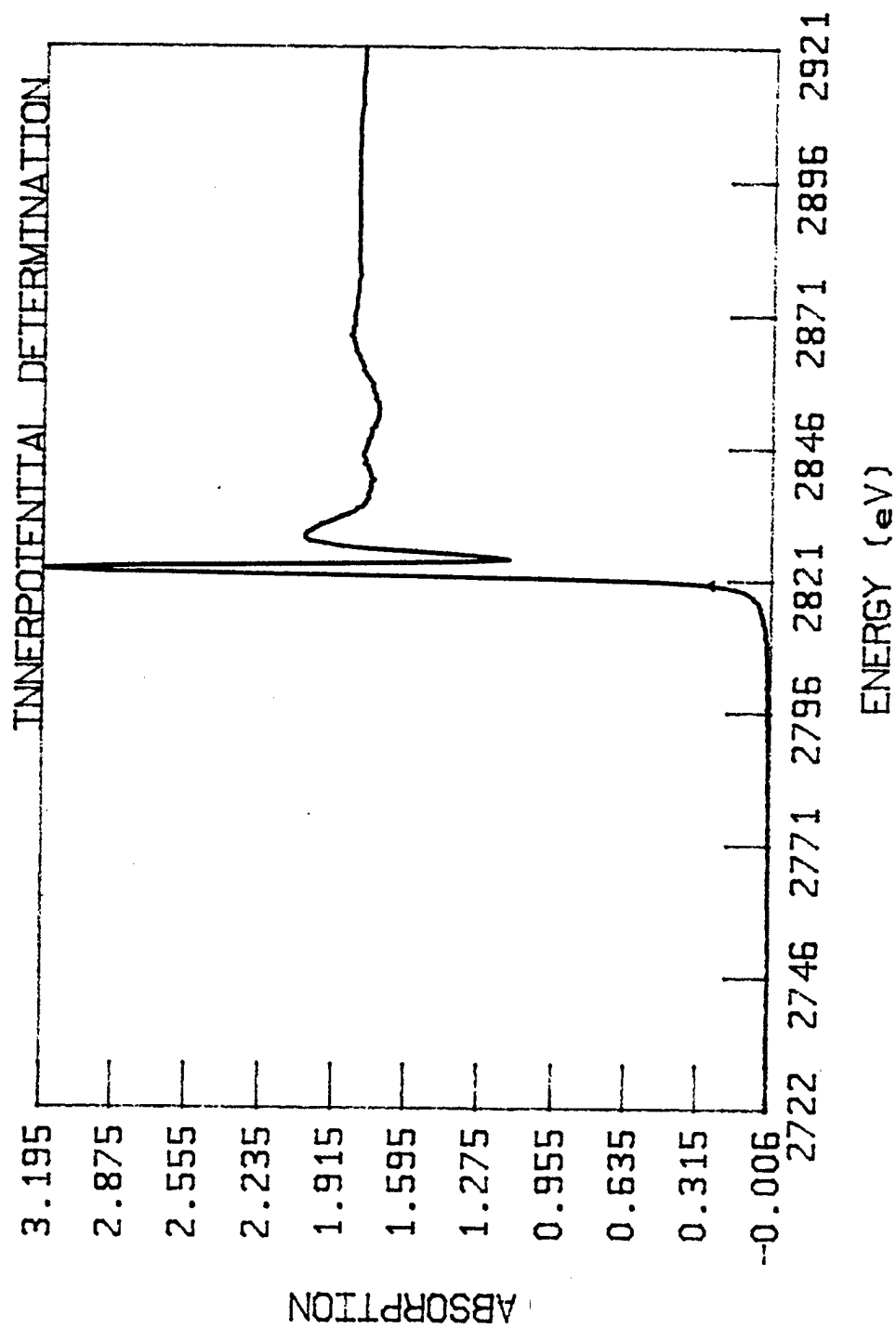


FIGURE 42  
168

E0= 2822.88

SYN14.152

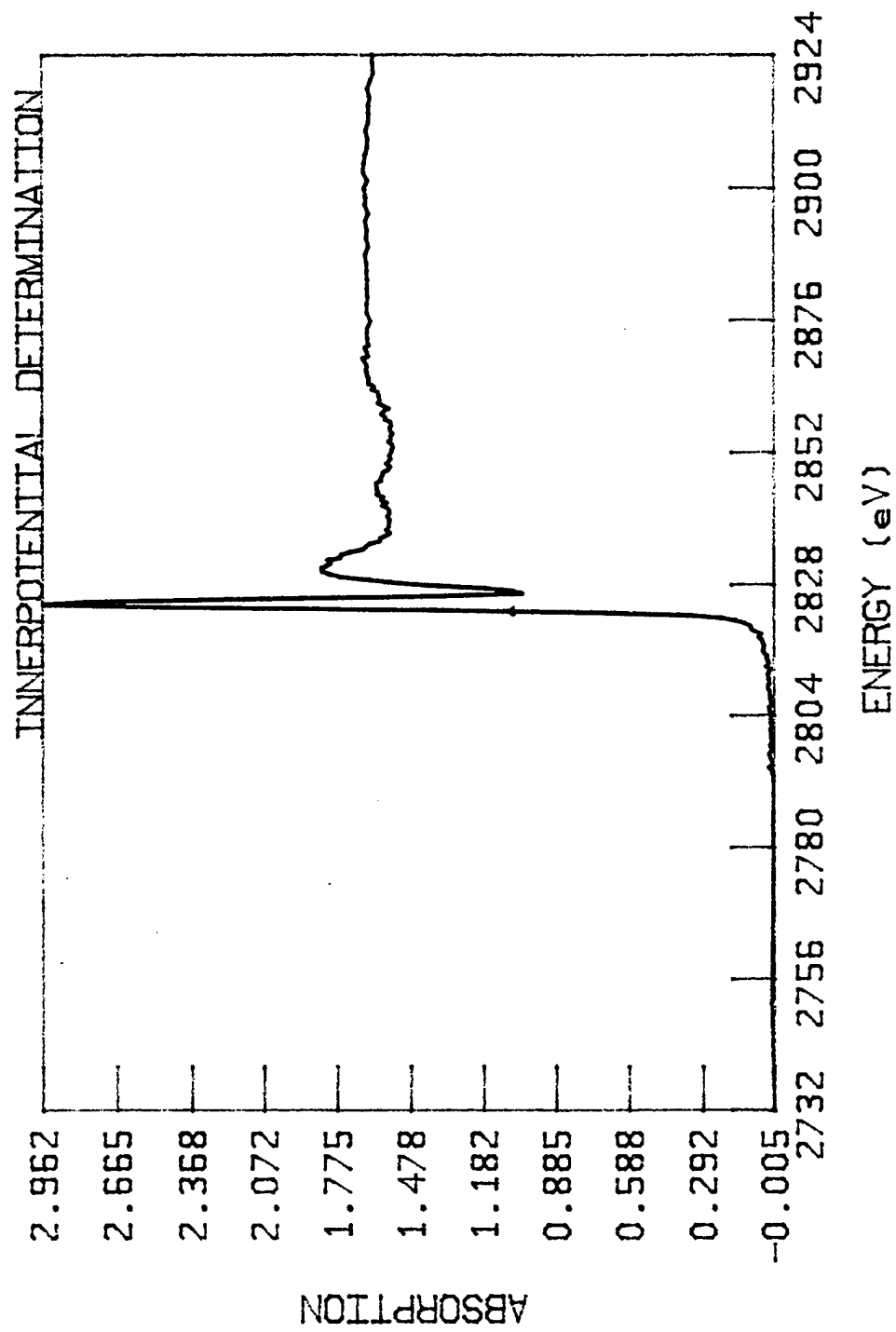


FIGURE 43

E0= 2820.39

SYN14

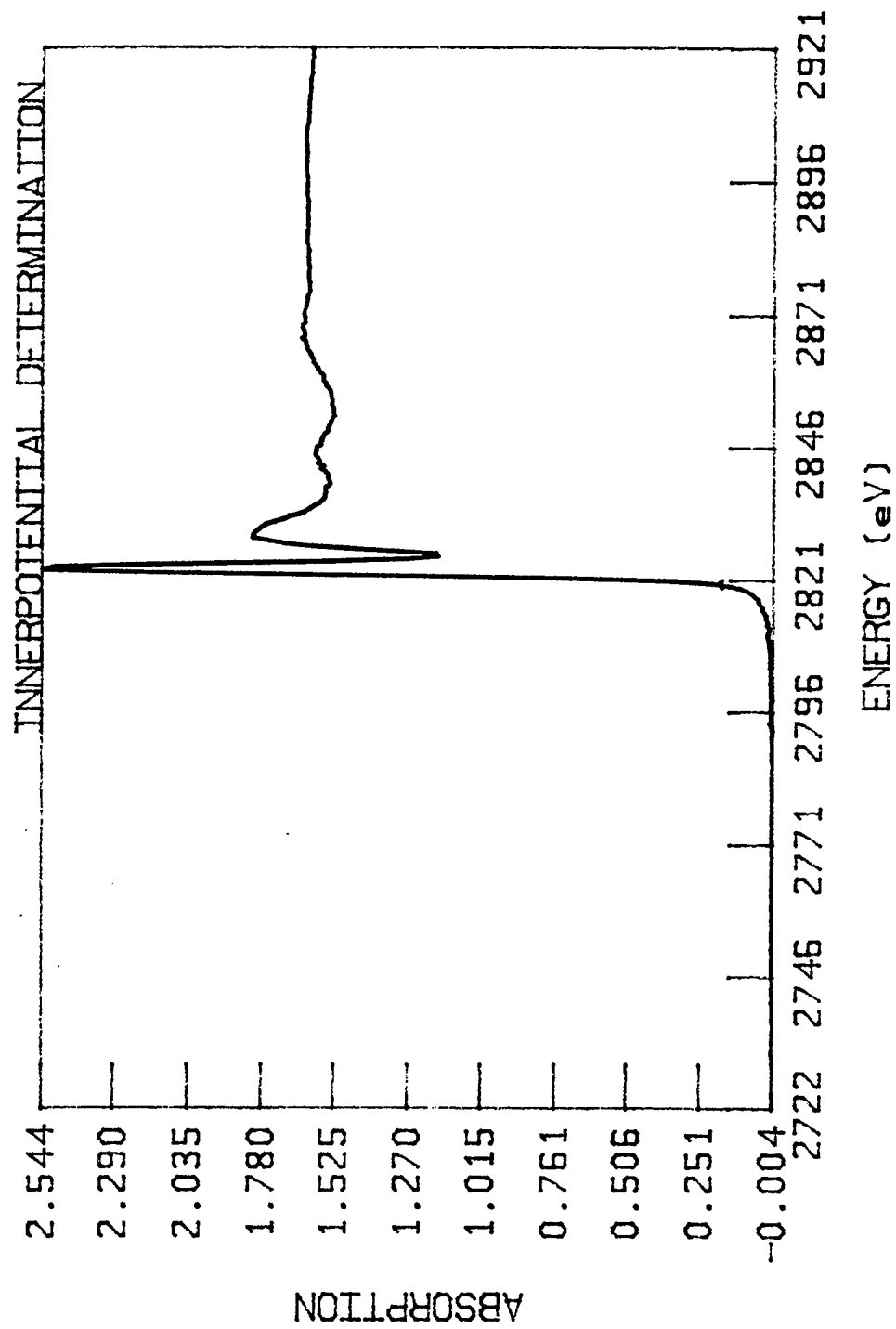


FIGURE 44  
170

E0= 2818.21  
CL3V.158

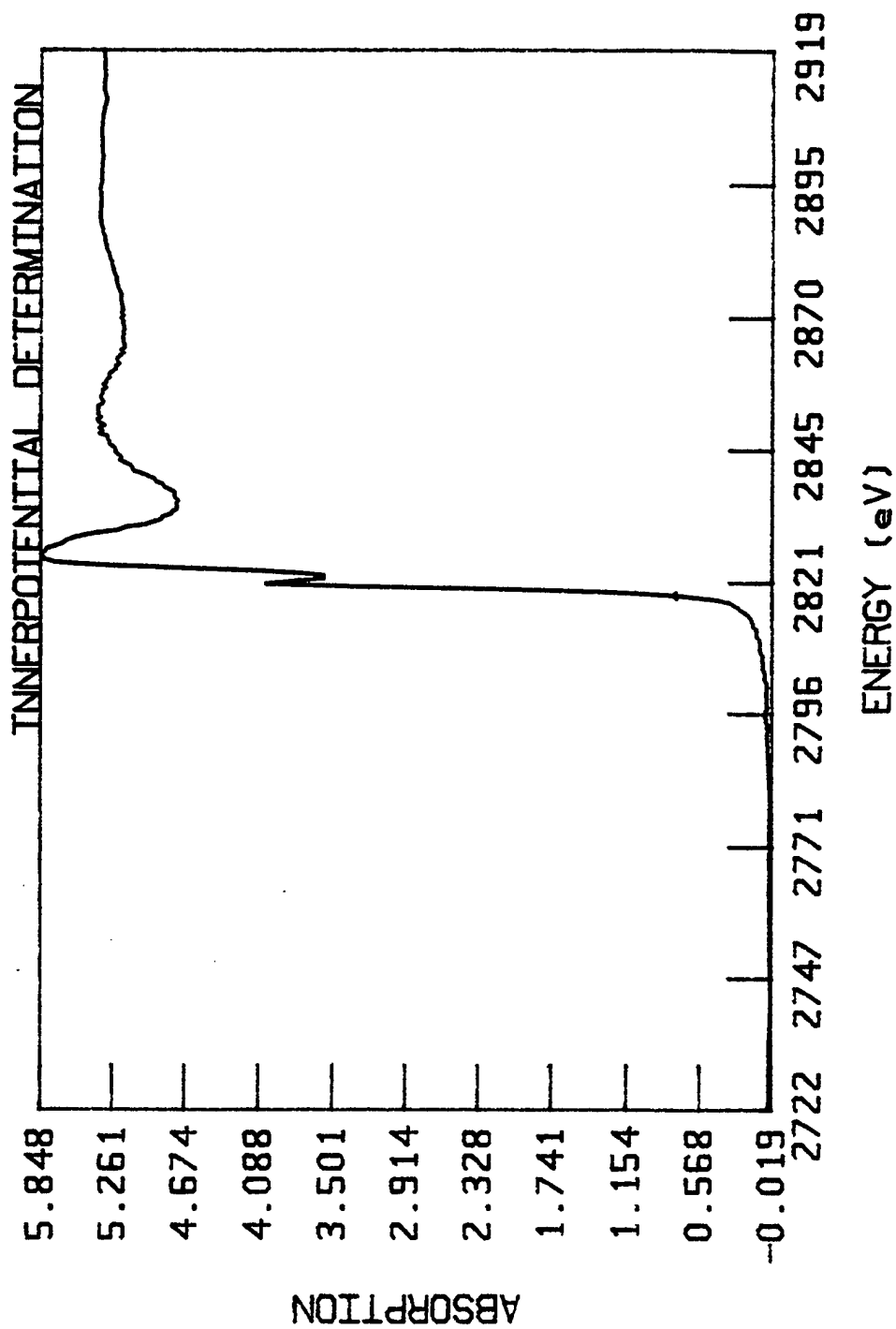


FIGURE 45

E0= 2818.21

CL3VR

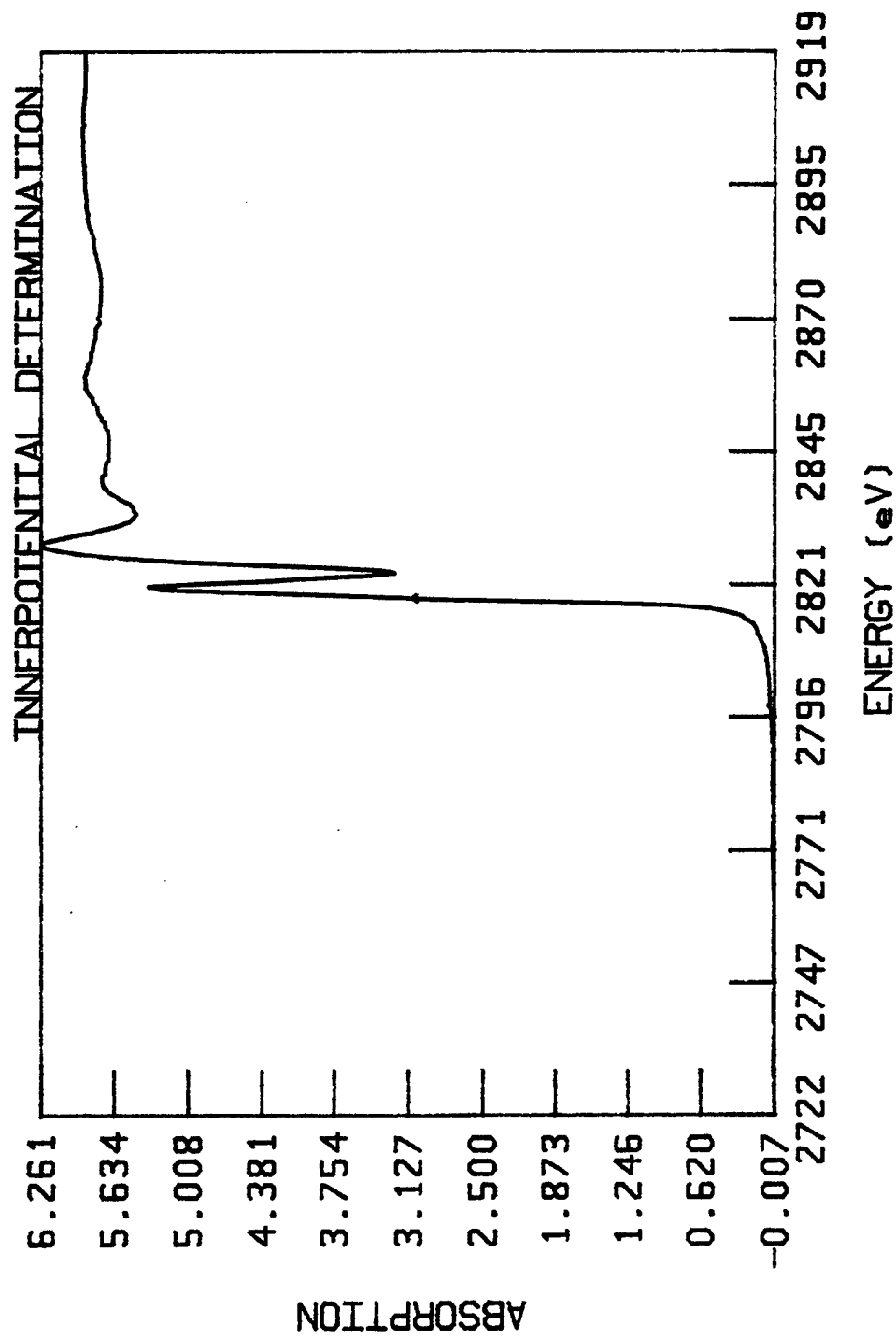


FIGURE 46

E0= 2821.79  
CLRB1

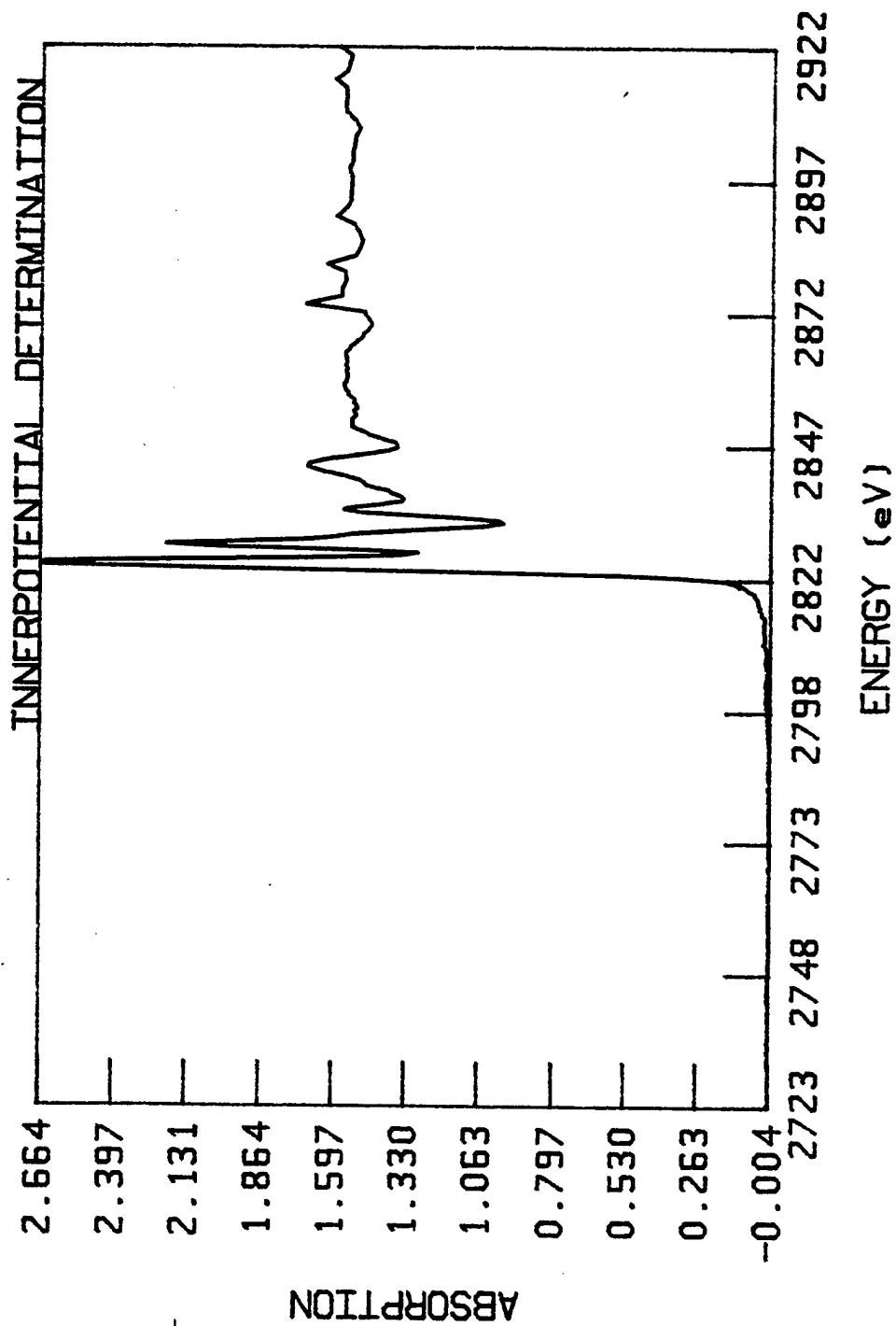


FIGURE 47

E0= 2820.39

PECP

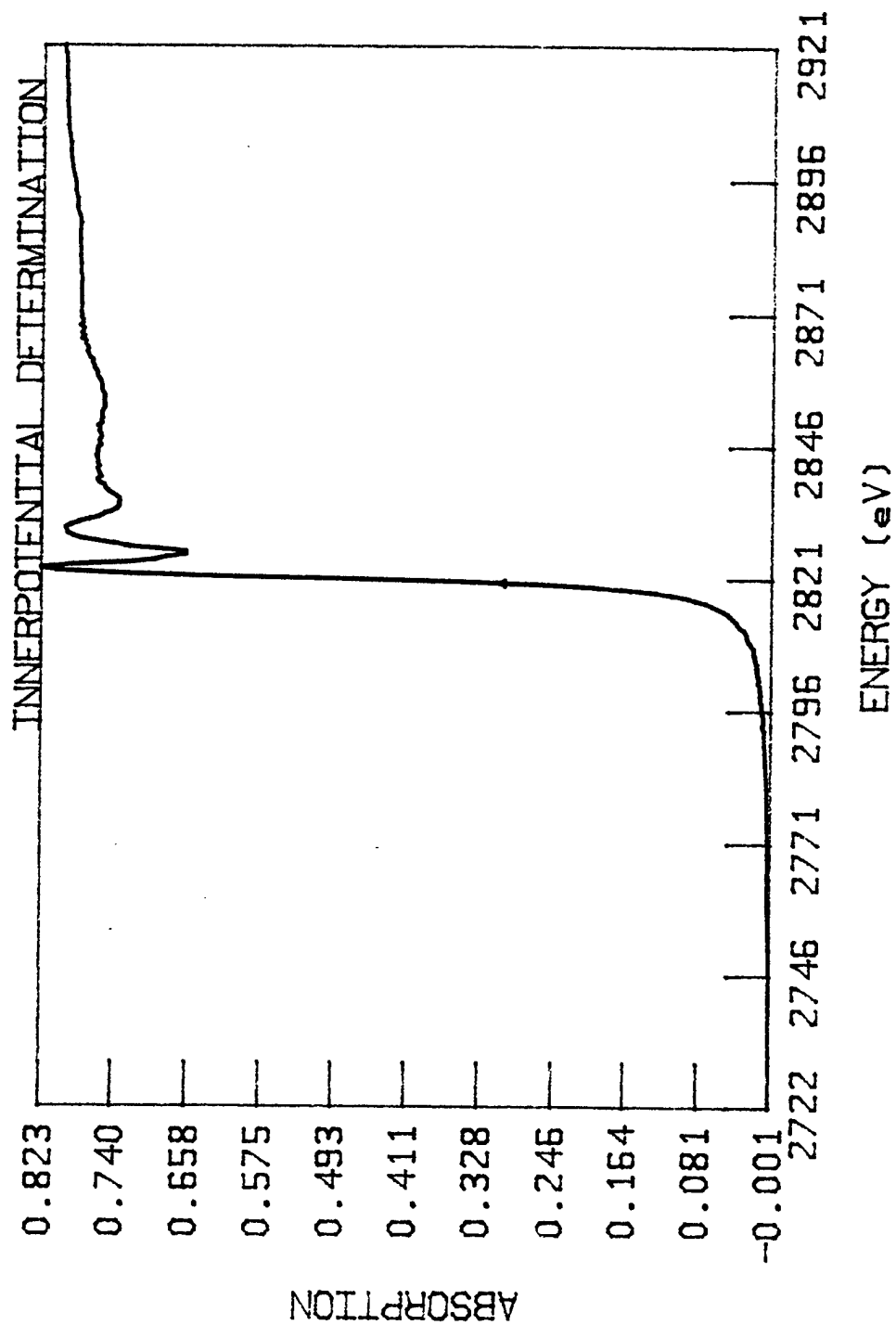


FIGURE 48



E0= 2821.79  
CLRB2

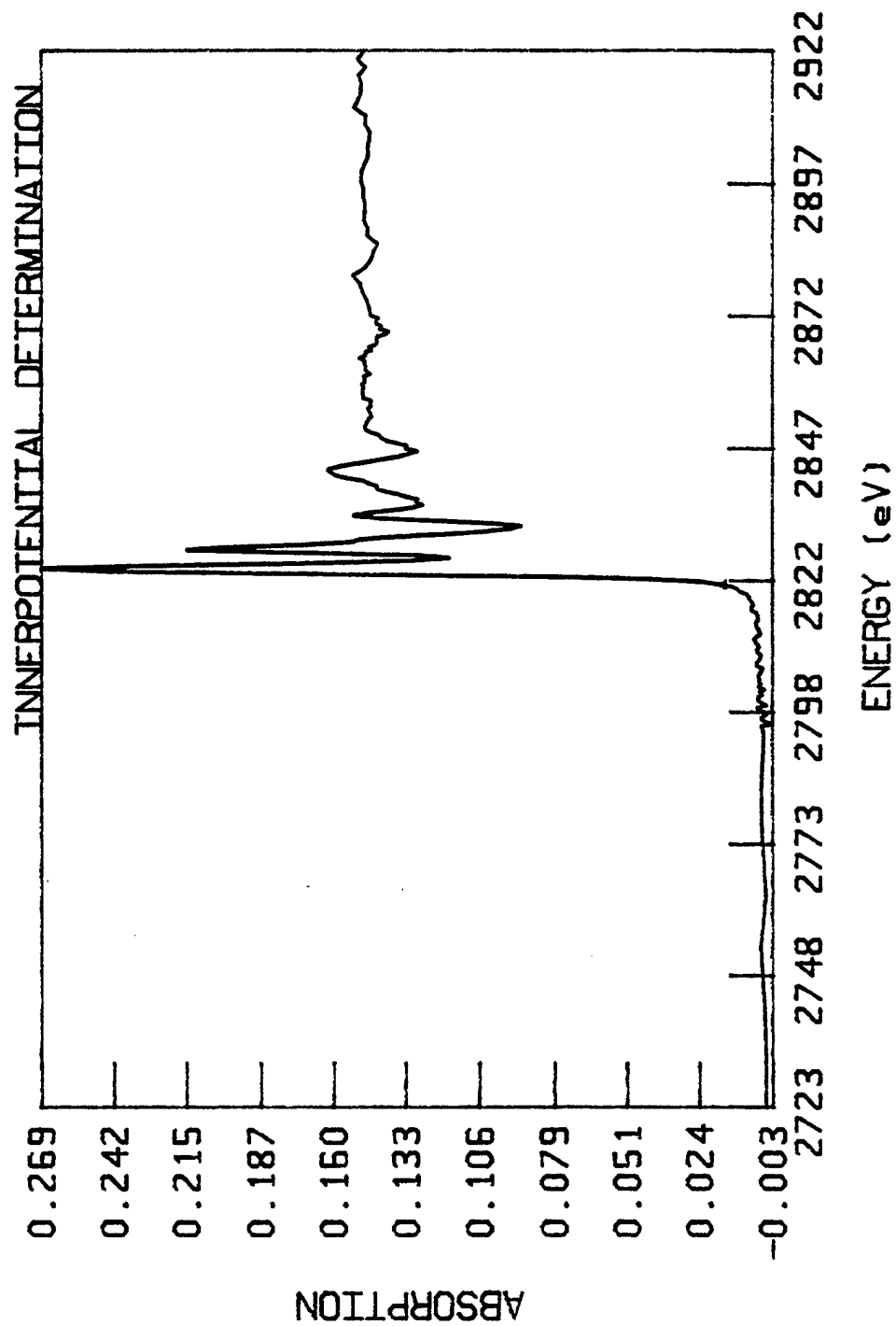


FIGURE 49

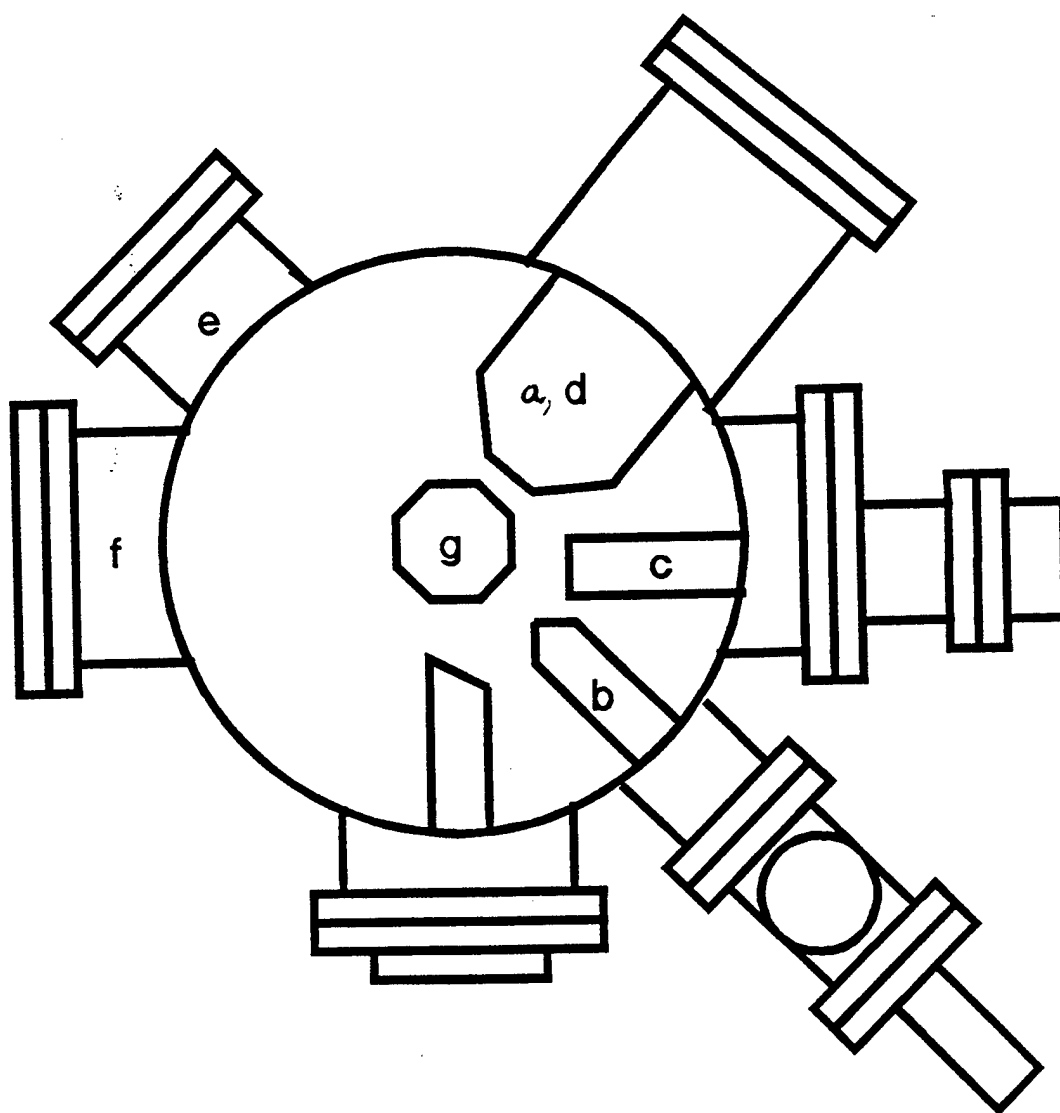


Figure 50 Schematic view of the experimental apparatus. a) electron source, b) ion gun, c) mass spectrometer, d) cylindrical mirror analyzer, e,f) windows, g) sample carousel.

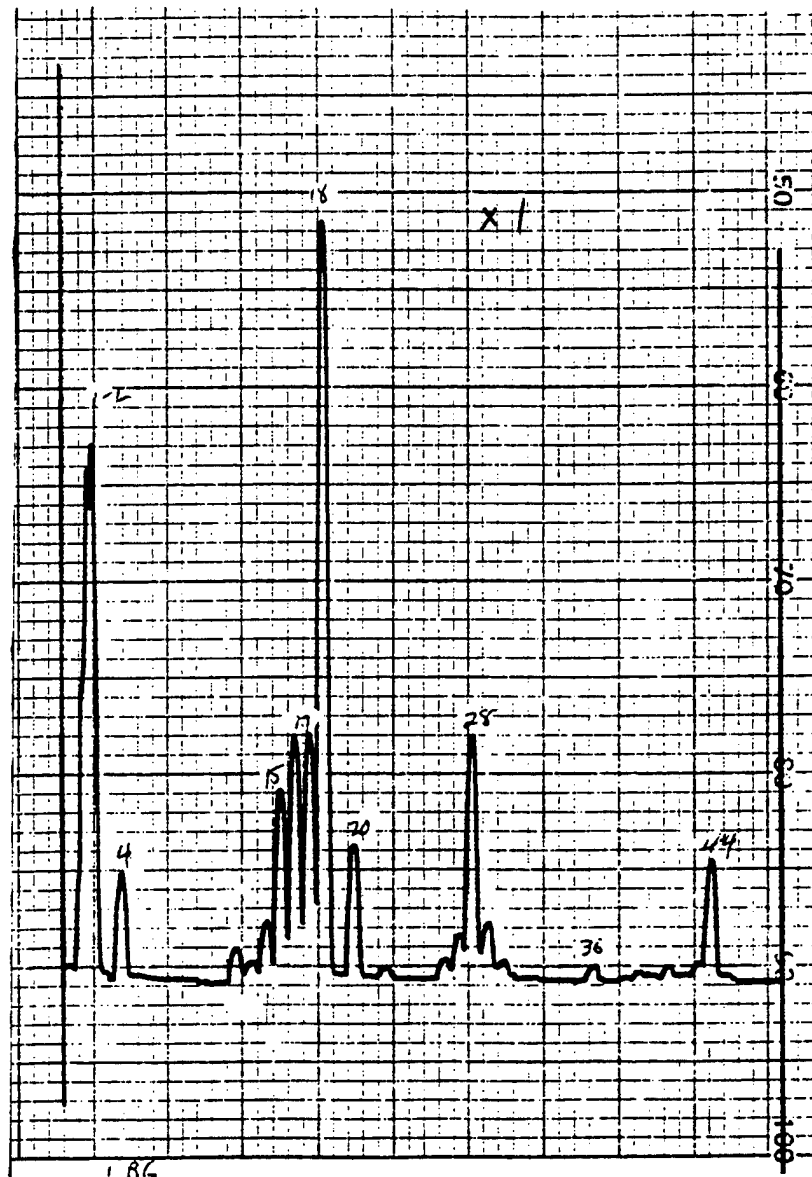


FIGURE 51 BACKGROUND ELECTRON GUN: ON  
BEAM ENERGY: 0.0keV

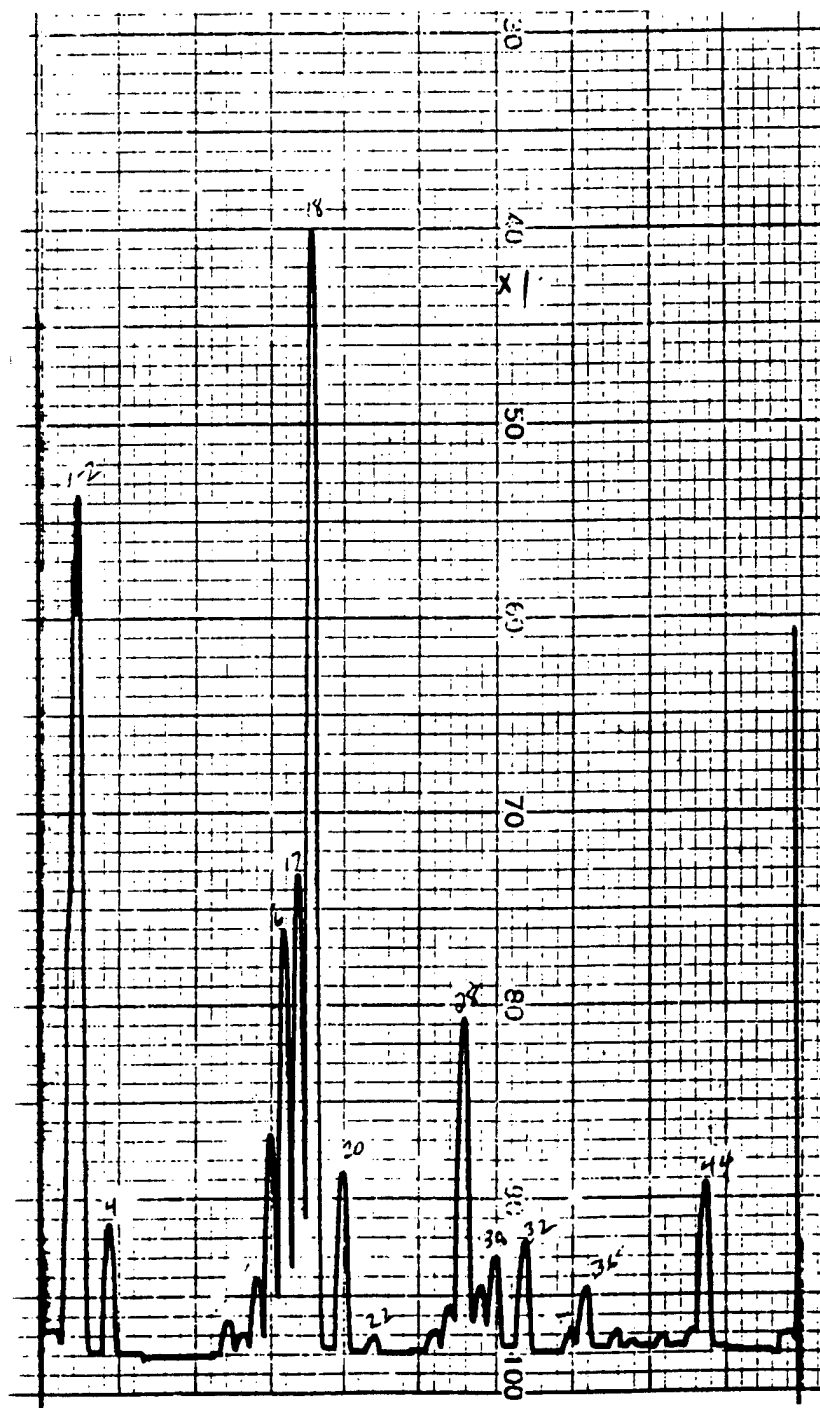


FIGURE 52

ELECTRON GUN: ON  
 BEAM ENERGY: 500eV  
 BEAM CURRENT: 4 microamps

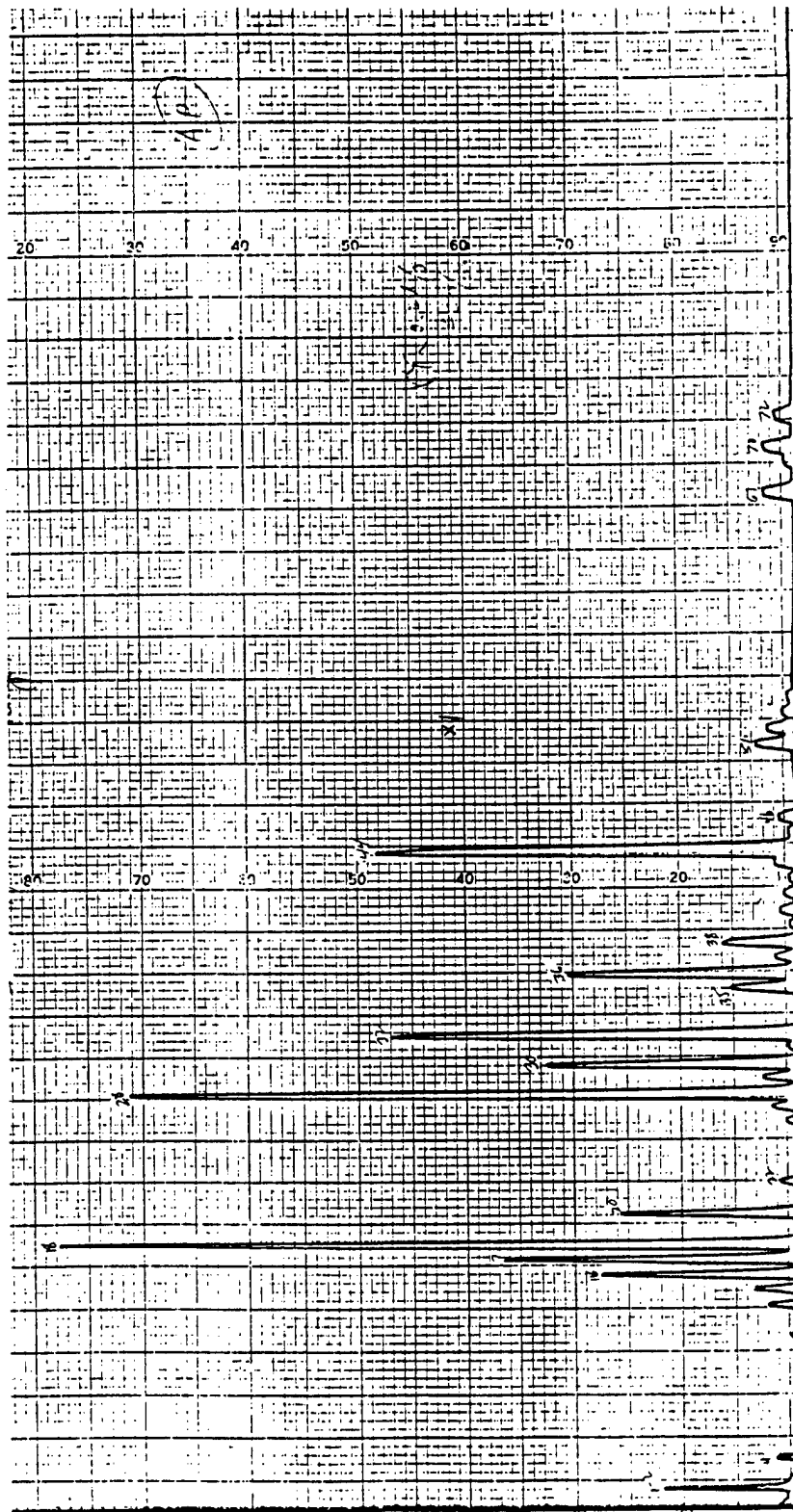


FIGURE 53

ELECTRON GUN: ON  
BEAM ENERGY: 500eV  
BEAM CURRENT: 3.9 microamps

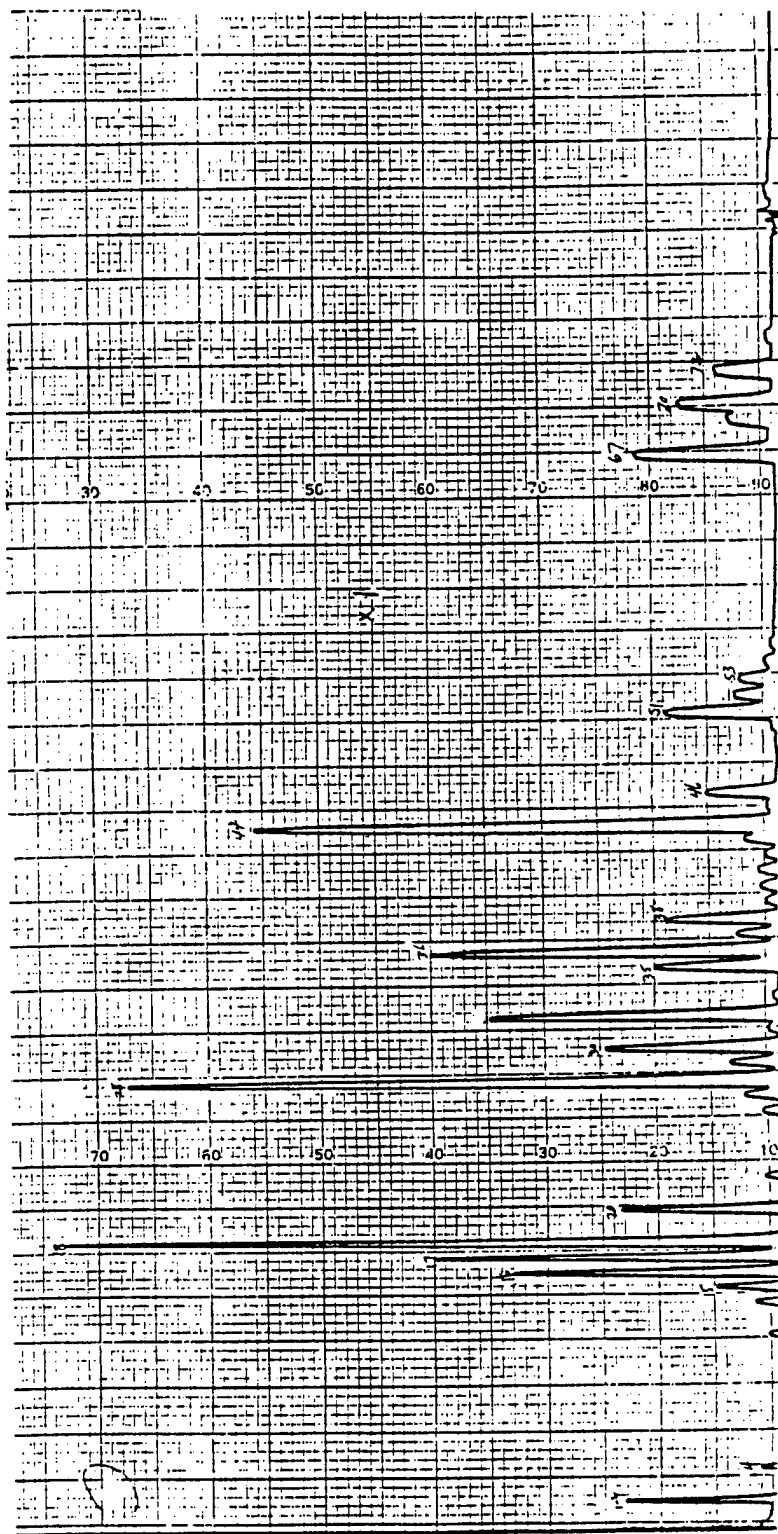


FIGURE 54

ELECTRON BEAM: ON  
BEAM ENERGY: 500eV  
BEAM CURRENT: 3.9 microamps

TARGET: STAINLESS STEEL CAROUSEL

### Conditions

$$E_p = 500 \text{ eV} \quad I_p = 4.2 \mu\text{A}$$

$$E_{\text{mod}} = 2 \text{ eV} \quad r = 3 \text{ eV/sec}$$

$$V_{\text{MULT}} = 1650 \text{ V}$$

$$\text{Sens. } I_{\text{LOSS}} = 10 \text{ mV} \quad RC = .1 \text{ sec}$$

$$\text{Pressure} = 4 \times 10^{-9} \text{ torr}$$

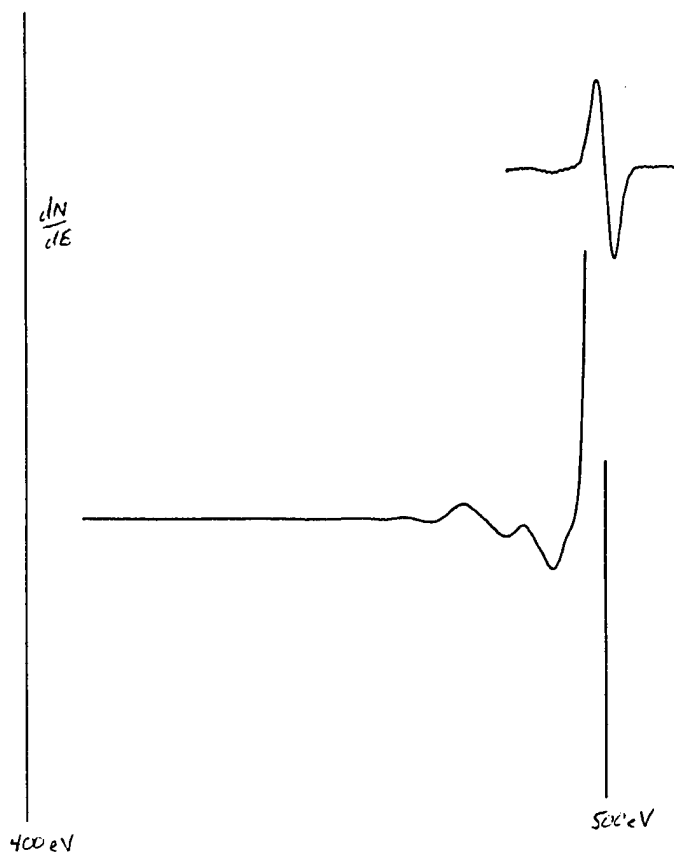


FIGURE 55 EELS DATA SINGLE XTAL AP

Conditions

$E_p = 500 \text{ eV}$      $I_p = 4.2 \mu\text{A}$   
 $E_{mod} = 2 \text{ eV}$      $r = 3 \text{ eV/sec}$   
 $V_{mod-T} = 1650 \text{ V}$      $i$   
 $Sens_{\omega I} = 2.5 \text{ mV}$      $RC = .1 \text{ sec}$

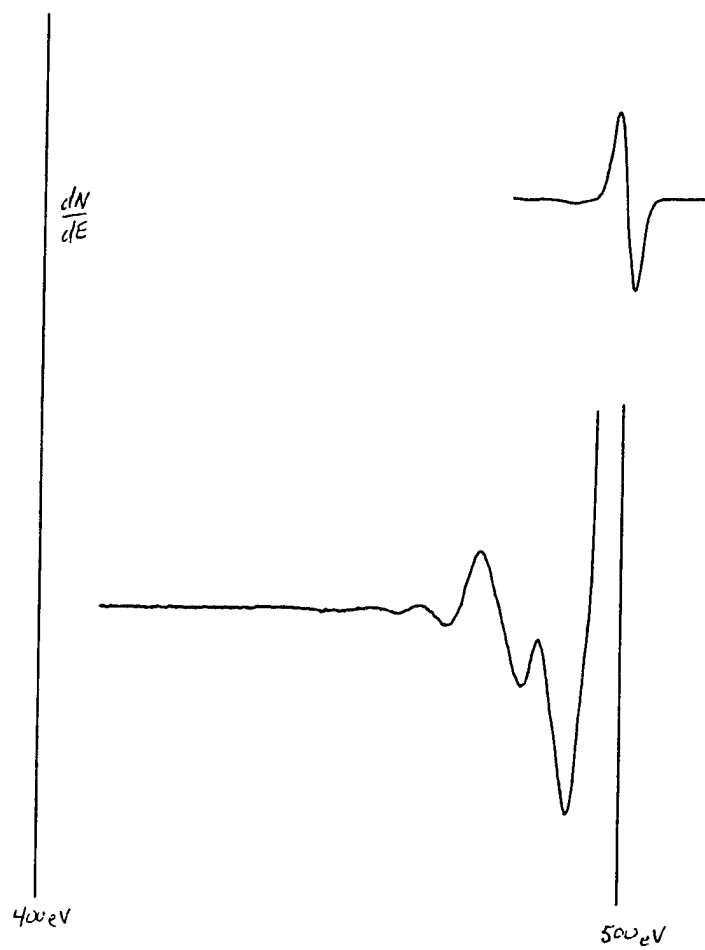


FIGURE 56 EELS DATA: SINGLE XTAL AP



### Conditions

$$E_p = 500 \text{ eV}$$

$$E_{\text{mod}} = 2 \text{ eV}$$

$$U_{\text{mod}} = 1650 \text{ V}$$

$$\text{Sens}_{\text{LX}} = 1 \text{ mV}$$

$$I_p = 4.2 \mu\text{A}$$

$$r = 3 \text{ eV/sec}$$

$$RC = 1 \text{ sec}$$

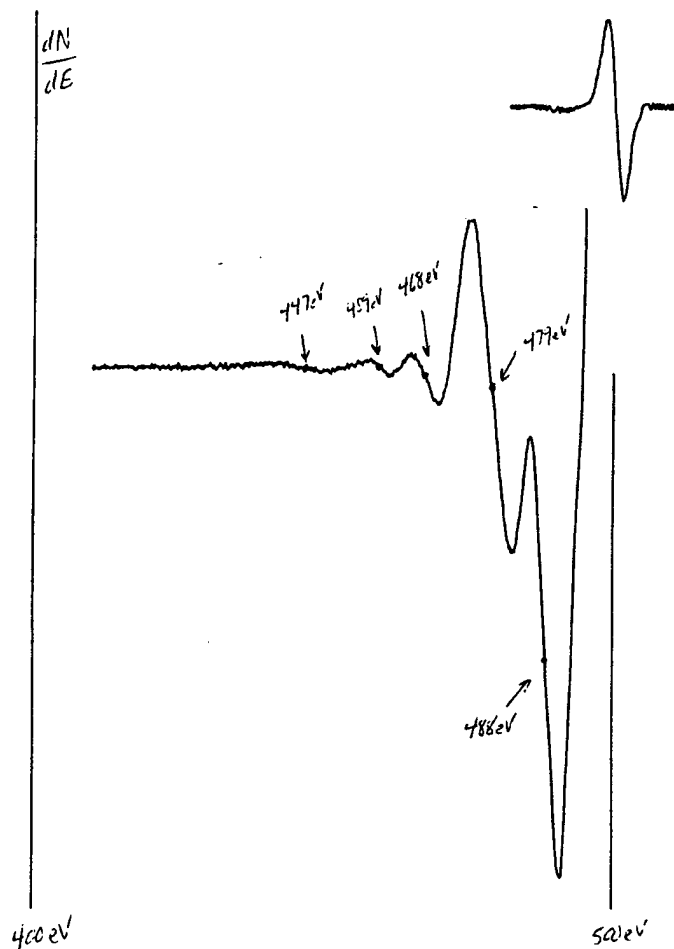


FIGURE 57 EELS DATA: SINGLE XTAL AP

Conditions

$$E_p = 500 \text{ eV} \quad I_p = 4.2 \text{ } \mu\text{A}$$

$$E_{\text{mod}} = 2 \text{ eV} \quad r = 3 \text{ eV/sec}$$

$$V_{\text{MULT}} = 1650 \text{ V}$$

$$\text{Sens}_{\text{LI}} = 250 \text{ } \mu\text{V} \quad RC = .1 \text{ sec}$$

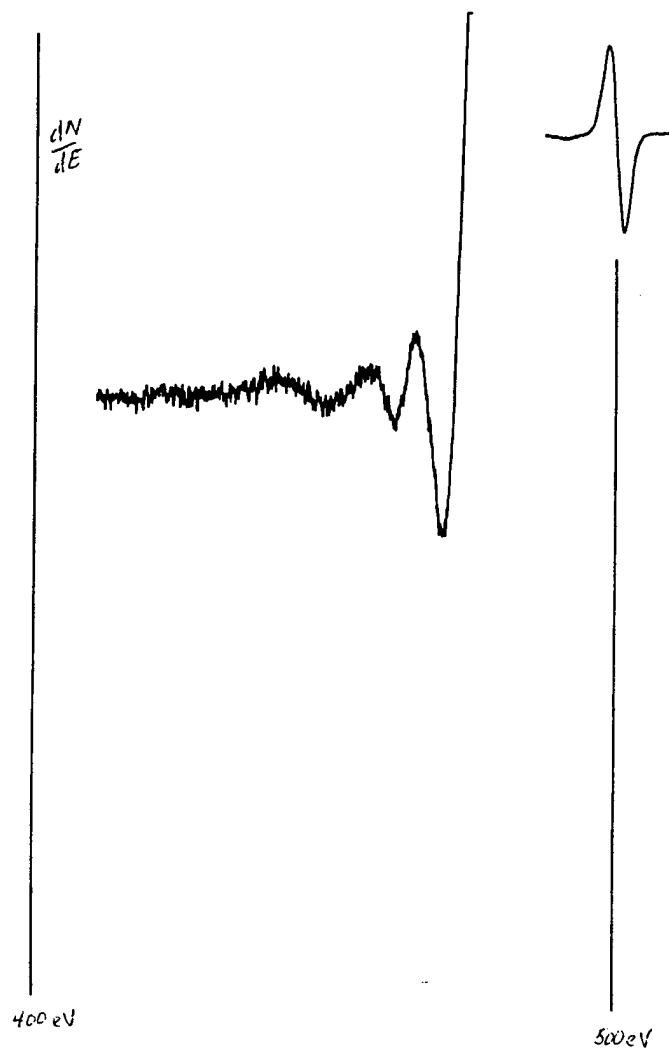


FIGURE 58 EELS DATA: SINGLE XTAL AP

## MARS MONTHLY REPORT - MAY 1992

Thin Film / Surface Science Laboratory

Case Western Reserve University

### **I. X-ray Absorption Fine Structure**

Analysis of the data from last month's Tables was continued to the isolation of the EXAFS for some of those data, but the majority of the effort was spent in preparation for the upcoming synchrotron run on Beamline X11-A, at the National Synchrotron Light Source (NSLS) early next month. It was determined that an experiment analogous to that conducted earlier at the Cl edge be performed on samples containing Br and using the Kr k-edge as a noble gas calibration source. In the same manner as before, fluorescence detection will be used to determine the XAFS of four Br-containing samples. These are pressed pellets of KBr, CuBr, CsBr, and RbBr which will be "thinned" with BN to allow simultaneous collection of fluorescence and transmission data. For a 1/2 inch diameter pellet, the masses of each material to optimize the edge jump in the sample are tabulated in Table I of this report. It is necessary that the particle size be smaller than the material's absorption length, and this will be accomplished by grinding the powders in a mortar and pestle and sifting them through a nylon screen of appropriate opening size. The absorption lengths are also shown in Table I. The *ab initio* code FEFF was used to calculate chi functions for the first shell of each of these and plots appear in Figures 1-4.

## **II. EELS**

After finishing the initial stage of the low resolution EELS project, we conducted a study of the effects of electron bombardment of AP on the UHV chamber. We found that the vacuum system pumps down to its typical operating range (minus 10 torr) at its usual rate, but residual Cl remains in the chamber. The amounts were not extremely large but were detectable with our residual gas analyzer. The sample carousel definitely had Cl on its surface. When an electron beam was incident on the carousel, the Cl signal on the RGA increased. Cleaning the carousel appears to help the situation very little. We are presently considering our options.

## **III. RHEED**

We began the initial stage of the RHEED project. The system is being set up and will be tested on known samples. The RHEED system is not in the same UHV chamber as the EELS system. We must, therefore, resolve the residual Cl problem in some way before doing RHEED on AP.

## **IV. TPD**

We also began the setup stage of the TPD project. This method will not necessarily require an extensive UHV system so we will probably proceed on this project next month. The setup is relatively straightforward and we have lab personnel experienced in this technique.

## **V. X-RAY FOCUSING SPECTROGRAPH**

We continued work on the proposed x-ray focusing spectrograph. Because the first design yielded a null result (as reported in Feb. 1992), we decided to use an in-house x-ray unit to determine the proper geometry for the second design. This work is continuing in preparation for a scheduled trip to the National Synchrotron Light Source at Brookhaven National Laboratory on June 5 and 6.

TABLE I

| Material | Density<br>(gm/cm <sup>3</sup> ) | Abs. length<br>at 13.469 keV<br>(microns) | Abs. Length at<br>13.481 keV<br>(microns) | mass for<br>$\Delta\mu x \leq 1.5$<br>(mg) | mass for<br>$\mu_a \approx 2.6$<br>(mg) |
|----------|----------------------------------|---|---|--|---|
| CuBr     | 4.98                             | 35.64                                     | 16.29                                     | 28.39                                      | 26.76 <sup>†</sup>                      |
| CsBr     | 4.44                             | 38.22                                     | 21.66                                     | 42.07                                      | 31.71 <sup>†</sup>                      |
| KBr      | 2.75                             | 140.74                                    | 34.12                                     | 23.57 <sup>†</sup>                         | 30.95                                   |
| RbBr     | 3.35                             | 126.57                                    | 36.55                                     | 32.45 <sup>†</sup>                         | 40.39                                   |

Compilation of materials, densities in gm/cm<sup>3</sup>, absorption lengths above and below the Br K-edge ( $E_0 = 13.474$  keV) in microns, and calculated masses in milligrams for a 1/2" diameter pellet of the given material to satisfy the requirements of ideal edge jump or post-edge absorption coefficient. <sup>†</sup> indicates the mass which satisfies both conditions and thus that which will be used. In order to make a self-supporting sample, a certain amount of BN powder must be added to bring the total mass of the pellet to approximately 100-150 mg for pressing. BN is used because it contains light elements which make a very small contribution to the total absorption of the sample at these energies.

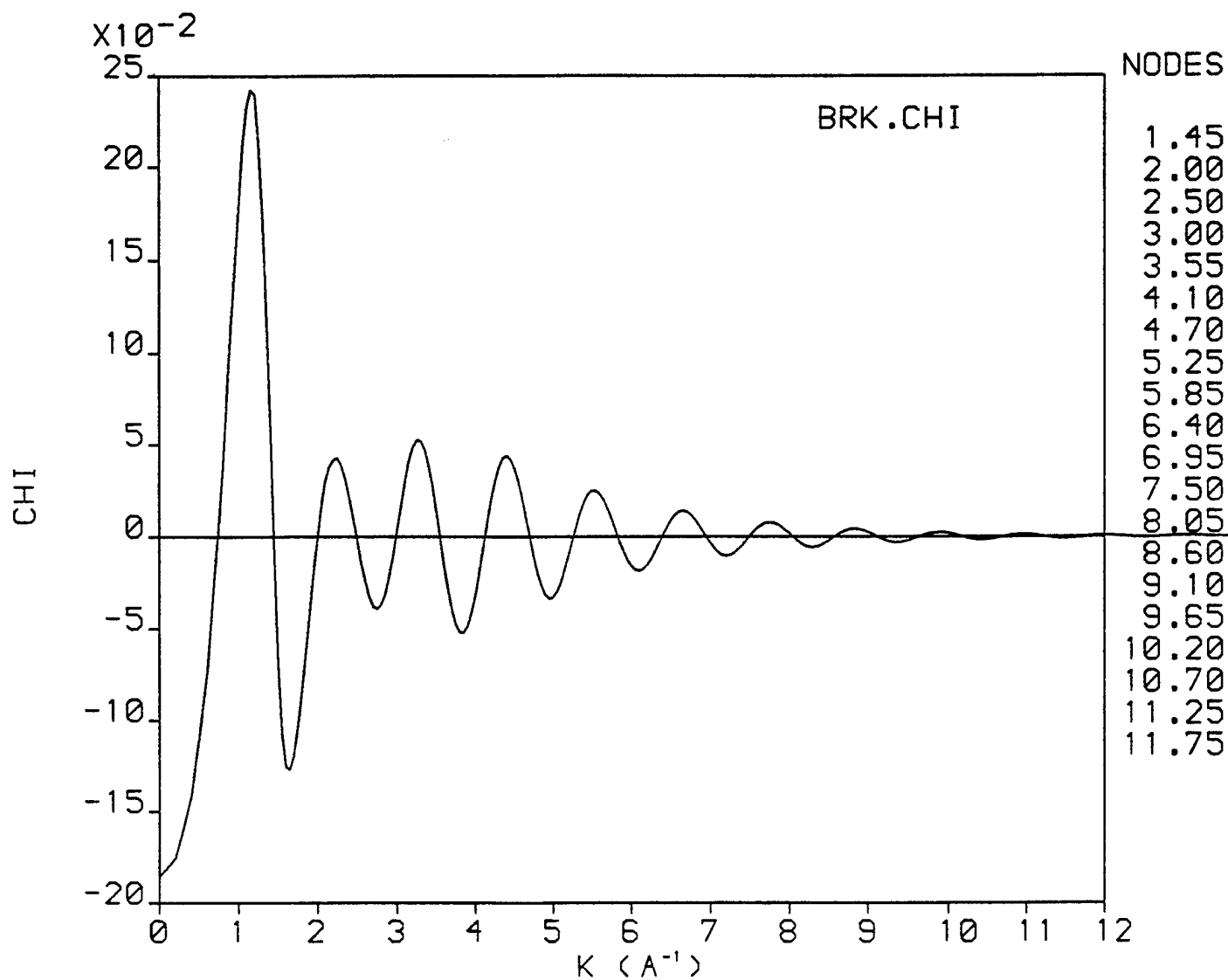


Figure 1. FEFF-Calculated  $\chi(k)$  for KBr nearest neighbors (first shell) using the NaCl structure.

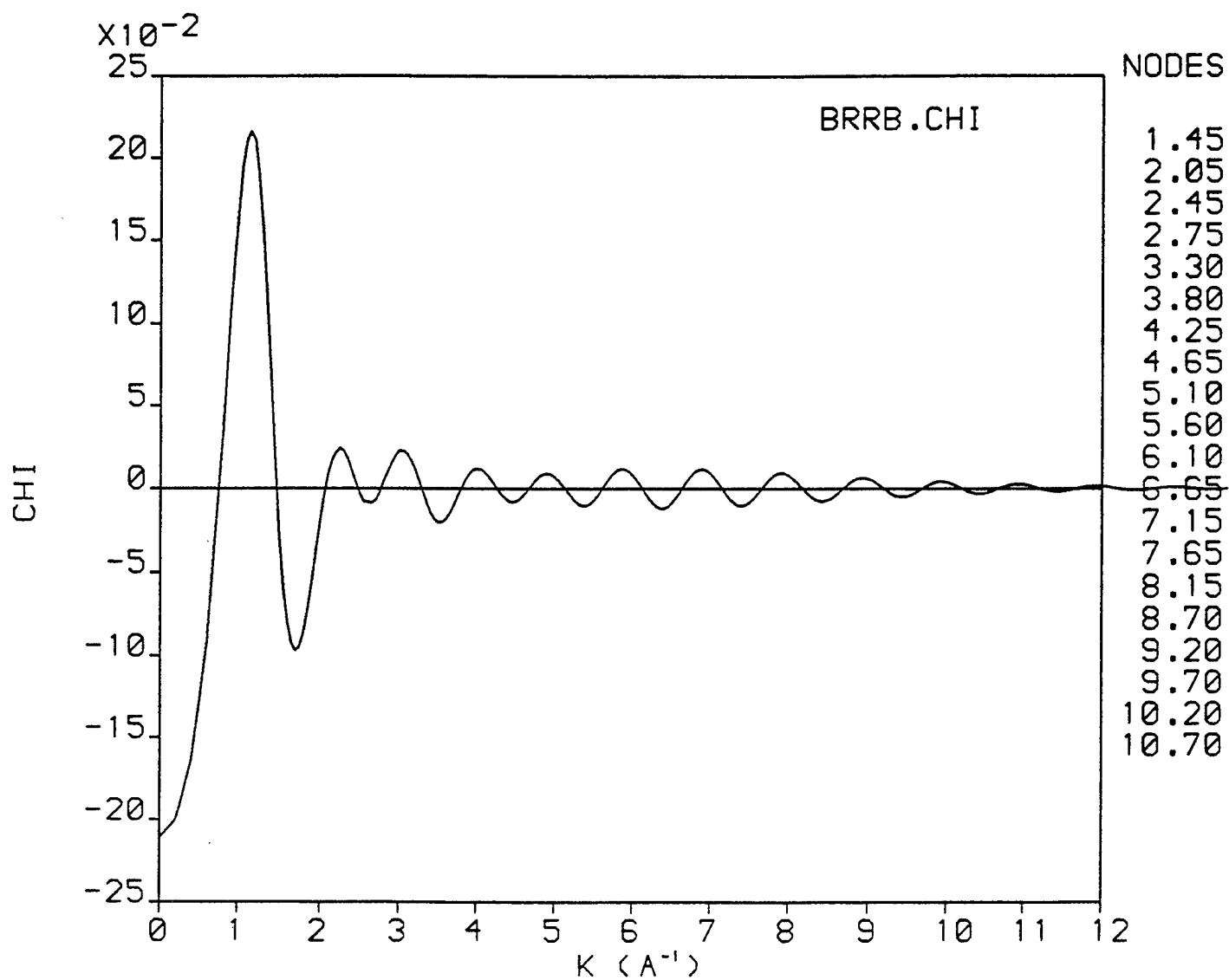


Figure 2. FEFF-Calculated  $\chi(k)$  for RbBr nearest neighbors (first shell) using the NaCl structure.



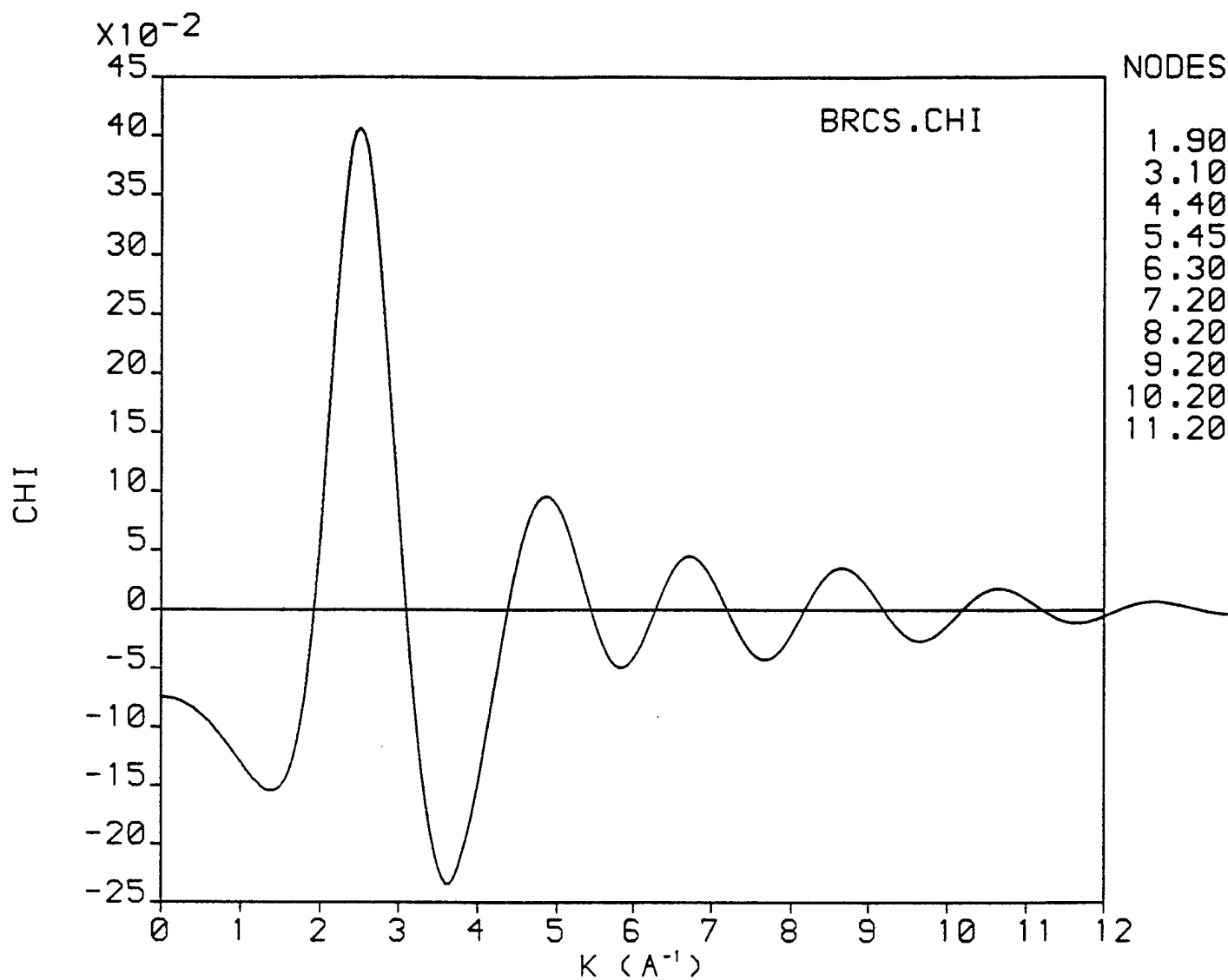


Figure 3. FEFF-Calculated  $\chi(k)$  for CsBr nearest neighbors (first shell) using the CsCl structure.

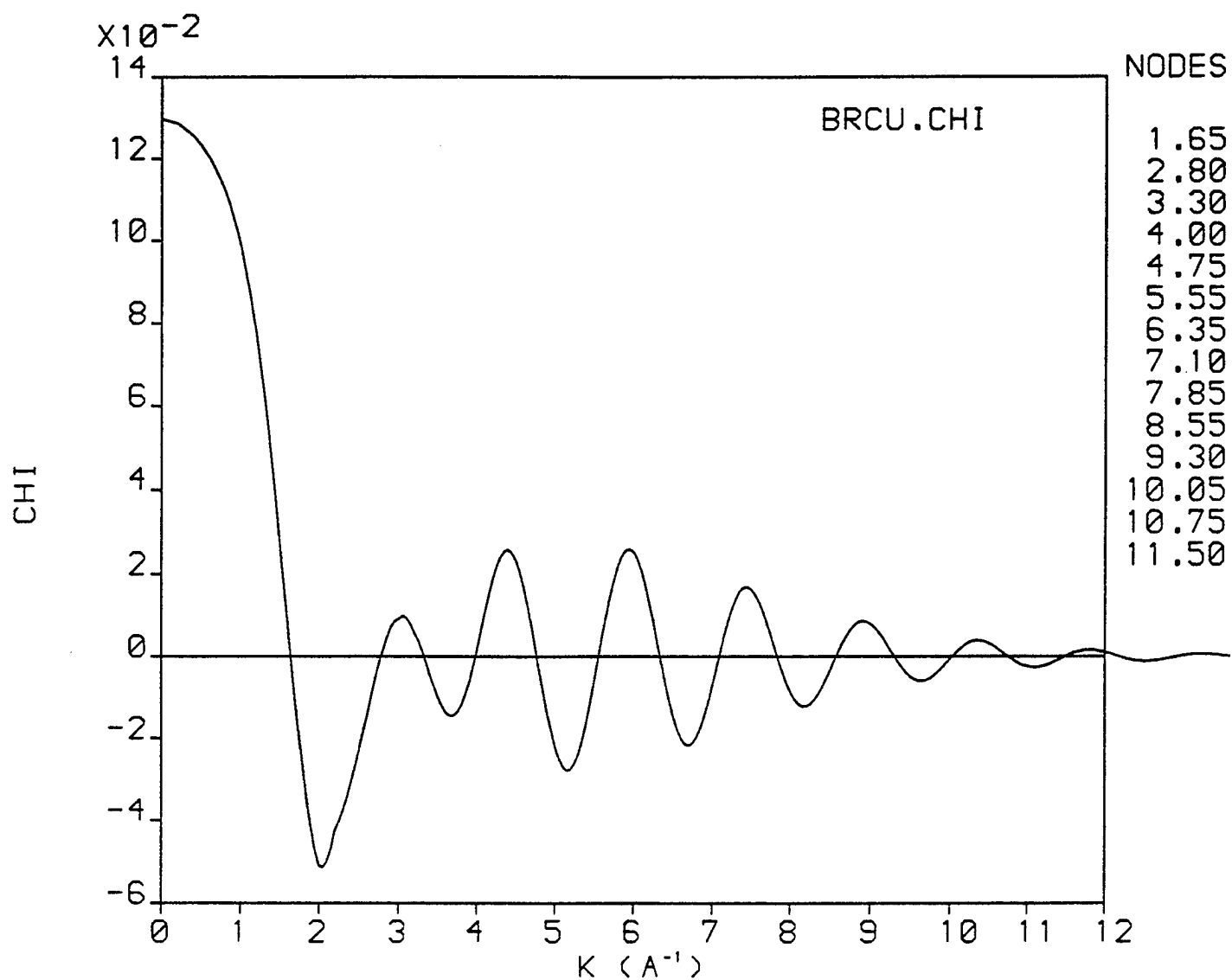


Figure 4. FEFF-Calculated  $\chi(k)$  for CuBr nearest neighbors (first shell) using the Zincblende structure.

## MARS MONTHLY REPORT - JUNE 1992

Thin Film / Surface Science Laboratory

Case Western Reserve University

### **I. X-ray Absorption Fine Structure**

#### **A. New Data - Br compounds test of edge calibration procedure**

The plans for new data at the Br K-edge put forth in last month's report were laid to waste by a faulty safety shutter system at beamline X11-A. Upon arrival at X11-A on Wednesday 3 June, 1992, GAD found that a glance at the beamline control panel next to the computer indicated that the SAFETY shutter (upstream) was both opened and closed simultaneously (red/green lights both flashing). In other words, the "Phase 1 Safety Interlock System" on X11-A failed, causing the beam in the X-ray ring to dump. This occurred the day before GAD's arrival. Some people from safety and/or the PRT came by to attempt repairs on the safety shutters and their attempts were met with failure. At that point the line was locked out and another "emergency access" was scheduled for Thursday morning from 0600-0900. This would also require dumping the beam in the X-ray ring to allow access to the beamline vacuum systems so far upstream. At this point some hope still remained for the CWRU contingent to get data on X11-A during the run and since both GAD and CAZ's plane tickets were nonrefundable/nonchangeable it was decided that at minimum CAZ could use the time to be

trained by GAD on the X11 computer systems.

On Thursday morning the ring was dumped and the repair team once again attempted to repair the safety systems. Gerry Lamble, of the X11 PRT, informed GAD that once again the repair team had not with failure and that they could not even isolate the cause of the problem, but that standardized NSLS troubleshooting procedures would be followed at the next access. A meeting of NSLS safety/administration people decided that a new policy would be enacted in response to this situation: After 2 "emergency access" attempts to repair a safety system, they must wait until the next scheduled studies period to open up again. The X-ray ring was next scheduled for studies on Monday 8 June, 1992, after the CWRU run on X11-A. GAD was told by Gerry that this decision was made because every time the beam suddenly dumped the control room had 30 beamlines calling them wondering what was going on and 10 hours of beam had already been lost on the entire X-ray ring due to this problem. This information was conveyed to GAD at approximately 1600 hrs on Thursday.

Fortunately, Johnny Kirkland, of Sachs-Freeman Associates, is now working on developing some systems on X11-B and Azzam Mansour of the Naval Surface Warfare Center talked to him about the situation, as he was scheduled on X11-A when the failure took place. As it turned out, nobody was scheduled on X23-B until after the studies period, so in exchange for the use of GAD's strong back and weak mind to help move the Huber goniometer out of the X23-B hutch and moving the XAFS table back into that hutch, we got to use X23-B for the entire weekend. The energy range of that line did not allow us to look at the Br K-edge (13474 eV) but Ti (4966 eV) was fine and the energy dispersive detector should operate at any energy. At that point our base of operations got moved to X23-B for the duration of our time. The

EXAFS data on Ti thin films deposited on polymers is rather noisy, as X23-B does not have the energy resolution of X11-A but we figured it was worth a try. Those data are not worth reporting yet. Most of the allocated time was spent on the energy dispersive spectrometer as reported below.

## **B. Analysis of AP/binders**

The edge-corrected (as per April, 1992 report) data from the AP/binder systems was further refined to determine the existence of spectral shifts in  $\chi$  as a function of binder. The Ar features (all positive steps in the August data) were removed by a manual dejumping procedure contained in the program EXAFS . EXE on the VAXstation and then the background was removed by the iterative fitting procedure also contained in that program. To determine whether or not the resulting  $\chi$  functions were reasonable, a Cl-O  $\chi$  function was calculated by the program EXAFSANA . EXE using the tables of Teo and Lee, and overplotted with a filtered first shell  $\chi$  from AP (experimentally measured). It appears, from Figure 1, that based on that calculation the oscillations resulting from the background subtraction are real. One must, however, keep in mind the limitations of Teo and Lee's tables at the low end of the K range. It may be possible to calculate and compare  $\chi$  from the program FEFF with experimental data, and this is presently being investigated.

For reasons of consistency, all of the experimental .CHI files were "normalized" at EVNORM=110 eV above the edge for each data set. That is, the x-axis of the  $\chi$  spectrum was forced to go through the data at EVNORM and then extrapolated back to the edge by the

equation:

$$\chi(E) = \frac{\mu(E) - \mu(EVNORM)}{\mu(EVNORM)}$$

Fourier transforms of these data were made and the Cl-O first shell filtered by using a pure AP spectrum as a phase reference. The resulting first shell spectra were fit using this reference file with both 4 (N, R,  $\Delta\sigma^2$ , and  $\Delta E_0$ ) and 3 (R,  $\Delta\sigma^2$ , and  $\Delta E_0$ ) free parameters. In the 3 parameter fits,  $N \equiv 4$ . The results of these fits appear in Tables I and II, respectively. To decode the column labelled File refer to the April 1992 report for the .JOU filenames. For technical reference, the files in Table I are all .INF files. In Tables I and II the remaining columns are: N - coordination number (see above for 3-parameter fits), R - Cl-O first shell distance in Å,  $\Delta\sigma^2$  - relative disorder squared in Å<sup>2</sup> between the sample and the reference (pure AP) including thermal and static terms,  $\Delta E_0$  - the difference in energy origin "phase shift" between the sample and the reference, and  $\Sigma(\text{res})^2$  - sum of the squares of the residuals or goodness of fit parameter. For a perfect fit,  $\Sigma(\text{res})^2$  approaches 0. Some of these results, particularly the coordination numbers, are hard to understand and will require further investigation and interpretation.

The next phase of the analysis is to visually compare difference spectra of AP/binder-AP for each binder. As the reader can see from Tables I and II the "binder on the bottom" series is most complete and so those comparisons are shown in Figures 2 - 13.

## II. Bent Mica X-ray Focussing Spectrograph

During the first week in June, we were able to test the second prototype of our x-ray focussing spectrograph at Brookhaven National Laboratory's National Synchrotron Light Source. Originally scheduled for beamline X-11A, we were transferred to X-23B due to a malfunction at X-11A. This did not affect this experiment in any way. A schematic diagram of the second prototype is shown in Figure 14.

Prior to the Brookhaven trip, we did extensive work at CWRU with the mica crystals. We used an in-house Picker x-ray diffractometer as an x-ray source for a series of x-ray diffraction experiments. The machine was equipped with a copper target, producing x-rays with a wavelength of  $1.54 \text{ \AA}$ . From these experiments we were able to confirm that the spacing between planes normal to the surface is  $19.96 \text{ \AA}$ . These planes are intended to be the scattering planes for the spectrograph.

Upon our arrival at X-23B, we wanted to confirm the preliminary work done at CWRU and check the alignment of the mica holder. A diagram of this apparatus is shown in Figure 15. Not only did we use this setup for calibration and alignment, but also for a study of the angular tolerance of the Bragg condition. We found that the intensity of the diffracted beam falls off dramatically at angles more than 0.5 degrees from the Bragg angle. Picture #1 shows transmitted and diffracted beam spots from the flat mica crystal. For this photo,  $E = 7183 \text{ eV}$ ,  $d = 19.96 \text{ \AA}$ ,  $n = 8$  and the calculated Bragg angle is 20.2 degrees. This photo shows a diffraction angle of 19.5 deg, which is within our measurement and alignment error.

After we were convinced that the flat mica was behaving properly, we tested the

prototype. Picture #2 shows a typical result. The sharp line circled in the photograph is what we believe to be the focussed x-rays emitted from the iron target. To see if this line is a results from bending the mica, we replaced the bent mica with a flat crystal. This yielded no lines. We then replaced the flat crystal with the bent mica and the sharp line reappeared. This sharp line is located where we would expect to see any focussing effect. We believe that bending the mica focusses the x-rays.

---



TABLE I

## 4-PARAMETER FIT RESULTS: AUG, 1991 DATA

| File   | N               | R (Å)            | $\Delta\sigma^2$ (Å <sup>2</sup> ) | $\Delta E_0$ (eV) | $\Sigma(\text{res})^2$ |
|--------|-----------------|------------------|------------------------------------|-------------------|------------------------|
| AP4    | 4               | 1.455            | 0                                  | 0                 | $1.58 \times 10^{-9}$  |
| TOLT   | $4.50 \pm .15$  | $1.451 \pm .002$ | $(1.36 \pm .04) \times 10^{-3}$    | $2.37 \pm .92$    | 38.69                  |
| TOLB   | $5.06 \pm .07$  | $1.449 \pm .001$ | $(3.75 \pm .09) \times 10^{-3}$    | $2.67 \pm .37$    | 5.39                   |
| TET1T  | $8.42 \pm 1.32$ | $1.439 \pm .012$ | $(1.34 \pm .15) \times 10^{-2}$    | $7.41 \pm 3.66$   | 280.07                 |
| TET1B  | $5.11 \pm .20$  | $1.447 \pm .002$ | $(2.95 \pm .24) \times 10^{-3}$    | $4.78 \pm 1.02$   | 43.39                  |
| TET2T  | $5.85 \pm .12$  | $1.450 \pm .001$ | $(5.35 \pm .15) \times 10^{-3}$    | $2.63 \pm .55$    | 12.68                  |
| TET2B  | $5.48 \pm .20$  | $1.456 \pm .002$ | $(4.25 \pm .26) \times 10^{-3}$    | $2.32 \pm .97$    | 40.94                  |
| TET5B  | $6.03 \pm .28$  | $1.447 \pm .003$ | $(5.24 \pm .33) \times 10^{-3}$    | $5.87 \pm 1.23$   | 59.97                  |
| TET5T2 | $5.08 \pm .10$  | $1.435 \pm .001$ | $(4.88 \pm .14) \times 10^{-3}$    | $4.99 \pm .53$    | 8.55                   |
| 8781B  | $5.23 \pm .20$  | $1.458 \pm .002$ | $(3.66 \pm .26) \times 10^{-3}$    | $2.10 \pm 1.00$   | 43.71                  |
| 8782T  | $5.29 \pm .19$  | $1.446 \pm .002$ | $(3.66 \pm .25) \times 10^{-3}$    | $3.94 \pm 1.01$   | 42.26                  |
| 8785B  | $5.93 \pm .19$  | $1.442 \pm .002$ | $(5.48 \pm .23) \times 10^{-3}$    | $6.58 \pm .86$    | 26.68                  |
| AP6    | $5.55 \pm .32$  | $1.439 \pm .004$ | $(4.19 \pm .40) \times 10^{-3}$    | $8.85 \pm 1.62$   | 95.11                  |
| 8791B  | $5.37 \pm .15$  | $1.446 \pm .002$ | $(4.47 \pm .19) \times 10^{-3}$    | $3.34 \pm .74$    | 21.43                  |
| 7521B  | $4.52 \pm .22$  | $1.485 \pm .003$ | $(5.46 \pm .41) \times 10^{-3}$    | $-3.62 \pm 1.05$  | 31.77                  |
| DER1B  | $4.08 \pm .32$  | $1.459 \pm .005$ | $(0.46 \pm .48) \times 10^{-3}$    | $4.45 \pm 2.23$   | 200.62                 |
| HTP1B  | $4.71 \pm .11$  | $1.447 \pm .002$ | $(3.59 \pm .16) \times 10^{-3}$    | $2.88 \pm .63$    | 13.83                  |

TABLE II  
3-PARAMETER FIT RESULTS: AUG, 1991 DATA

| File   | R (Å)            | $\Delta\sigma^2$ (Å <sup>2</sup> ) | $\Delta E_0$ (eV) | $\Sigma(\text{res})^2$ |
|--------|------------------|------------------------------------|-------------------|------------------------|
| AP4    | $1.454 \pm .001$ | $(3.8 \pm .4) \times 10^{-4}$      | $-.22 \pm .54$    | 13.55                  |
| TOLT   | $1.451 \pm .002$ | $(6.6 \pm .8) \times 10^{-4}$      | $2.33 \pm 1.04$   | 43.59                  |
| TOLB   | $1.451 \pm .002$ | $(2.30 \pm .07) \times 10^{-3}$    | $2.00 \pm .79$    | 20.13                  |
| TET1T  | $1.448 \pm .015$ | $(8.41 \pm .80) \times 10^{-3}$    | $2.95 \pm 5.16$   | 353.31                 |
| TET1B  | $1.448 \pm .003$ | $(1.49 \pm .11) \times 10^{-3}$    | $4.31 \pm 1.37$   | 62.60                  |
| TET2T  | $1.452 \pm .003$ | $(2.96 \pm .12) \times 10^{-3}$    | $1.40 \pm 1.29$   | 50.15                  |
| TET2B  | $1.458 \pm .004$ | $(2.32 \pm .13) \times 10^{-3}$    | $1.29 \pm 1.45$   | 69.76                  |
| TET5B  | $1.449 \pm .005$ | $(2.72 \pm .17) \times 10^{-3}$    | $4.64 \pm 1.95$   | 104.72                 |
| TET5T2 | $1.437 \pm .002$ | $(3.37 \pm .08) \times 10^{-3}$    | $4.25 \pm .91$    | 20.94                  |
| 8781B  | $1.460 \pm .003$ | $(2.03 \pm .12) \times 10^{-3}$    | $1.30 \pm 1.38$   | 65.57                  |
| 8782T  | $1.445 \pm .003$ | $(1.94 \pm .12) \times 10^{-3}$    | $3.79 \pm 1.43$   | 64.82                  |
| 8785B  | $1.444 \pm .004$ | $(3.02 \pm .14) \times 10^{-3}$    | $5.51 \pm 1.57$   | 63.03                  |
| AP6    | $1.439 \pm .005$ | $(2.22 \pm .17) \times 10^{-3}$    | $8.31 \pm 2.17$   | 124.32                 |
| 8791B  | $1.448 \pm .003$ | $(2.65 \pm .11) \times 10^{-3}$    | $2.49 \pm 1.22$   | 44.47                  |
| 7521B  | $1.486 \pm .003$ | $(4.56 \pm .17) \times 10^{-3}$    | $-4.16 \pm 1.12$  | 34.07                  |
| DER1B  | $1.459 \pm .005$ | $(3.4 \pm 1.6) \times 10^{-4}$     | $4.30 \pm 2.23$   | 200.77                 |
| HTP1B  | $1.448 \pm .002$ | $(2.58 \pm .07) \times 10^{-3}$    | $2.36 \pm .82$    | 20.67                  |

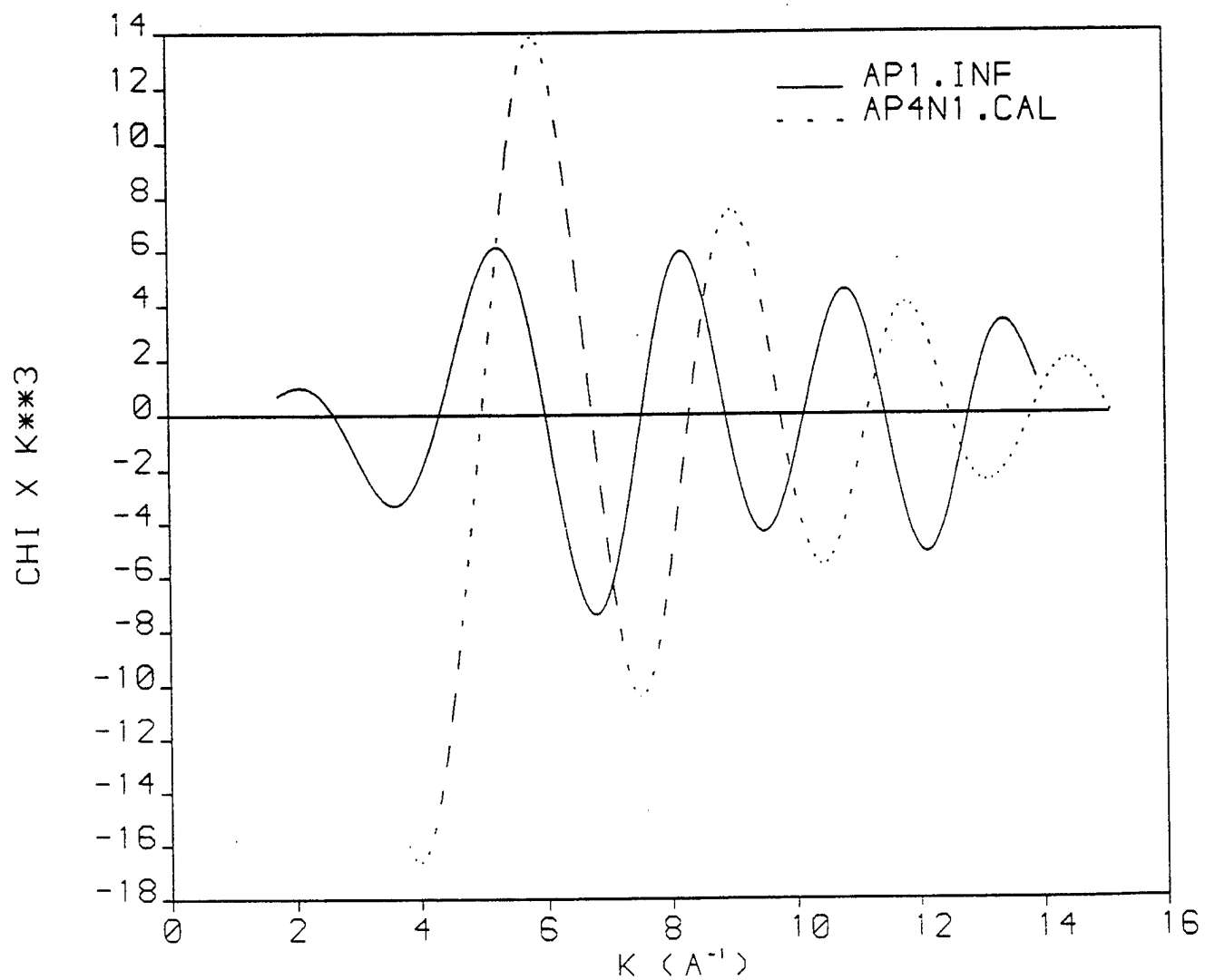


FIG 1: Overplot of experimental and calculated 1st C1-O shell X for AP.

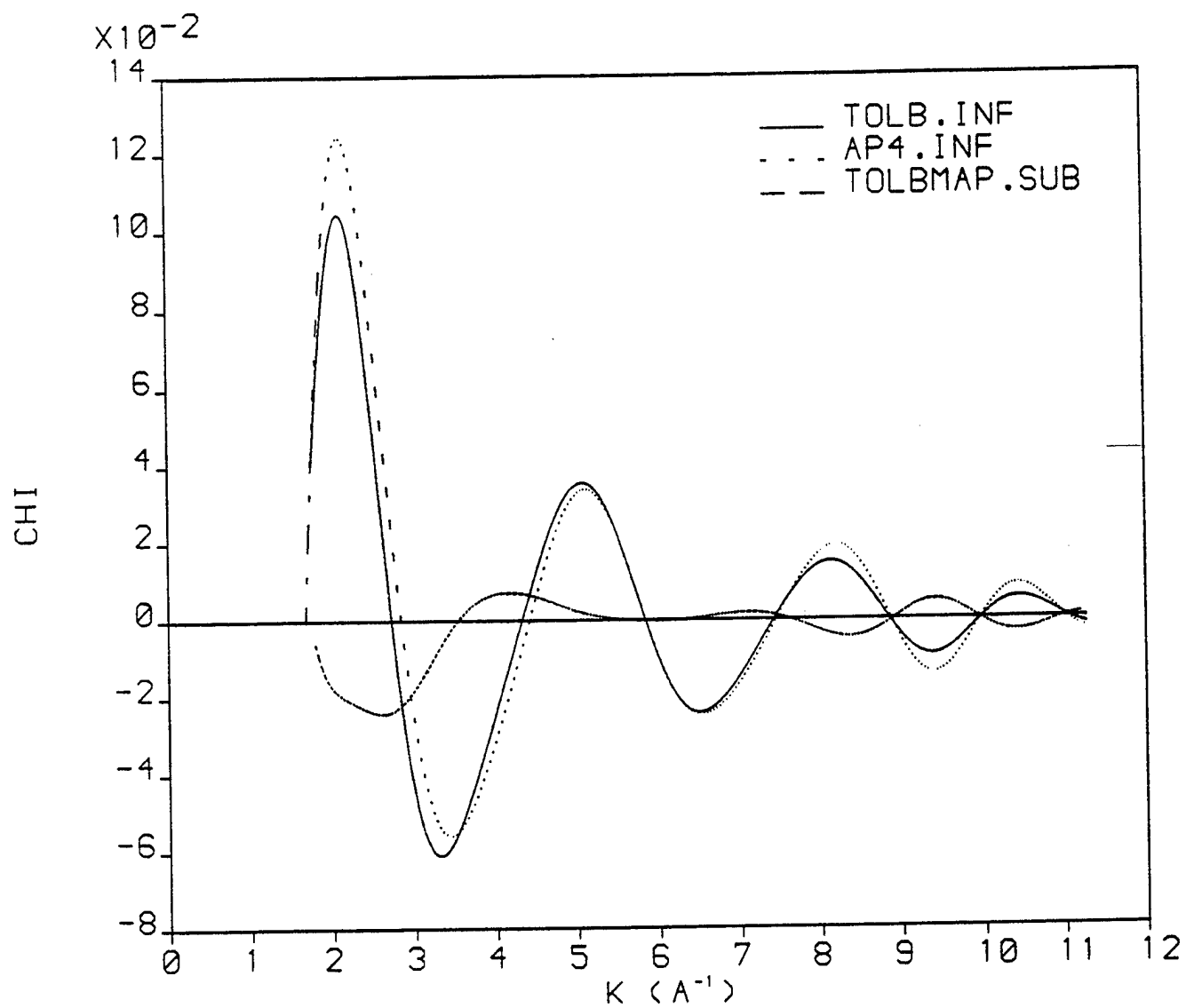


FIG 2: Overplot of first shell chi of TOLB, AP4 and the difference of the two.

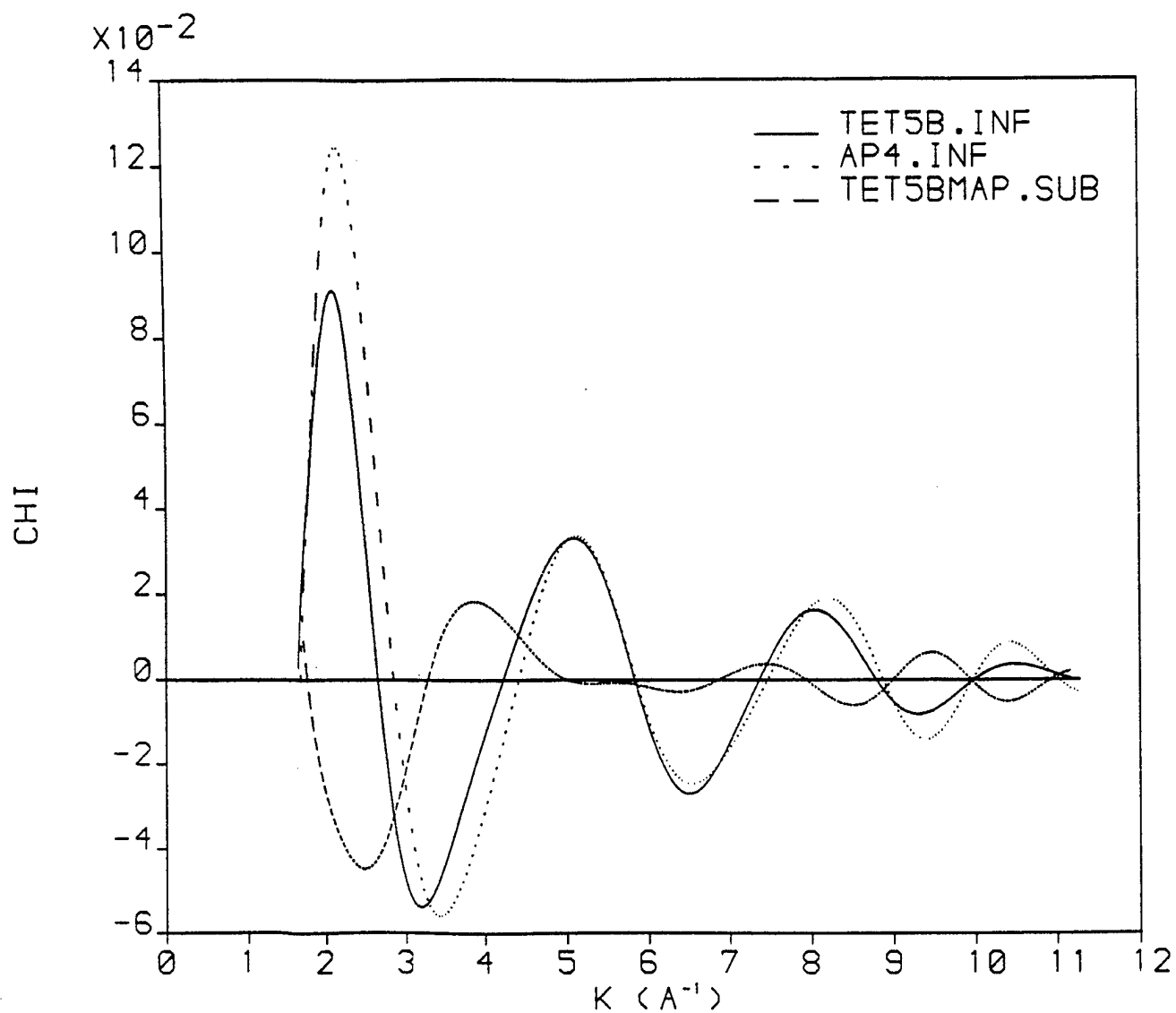


FIG 3: Overplot of the first shell chi of TET5B, AP4 and the difference of the two.

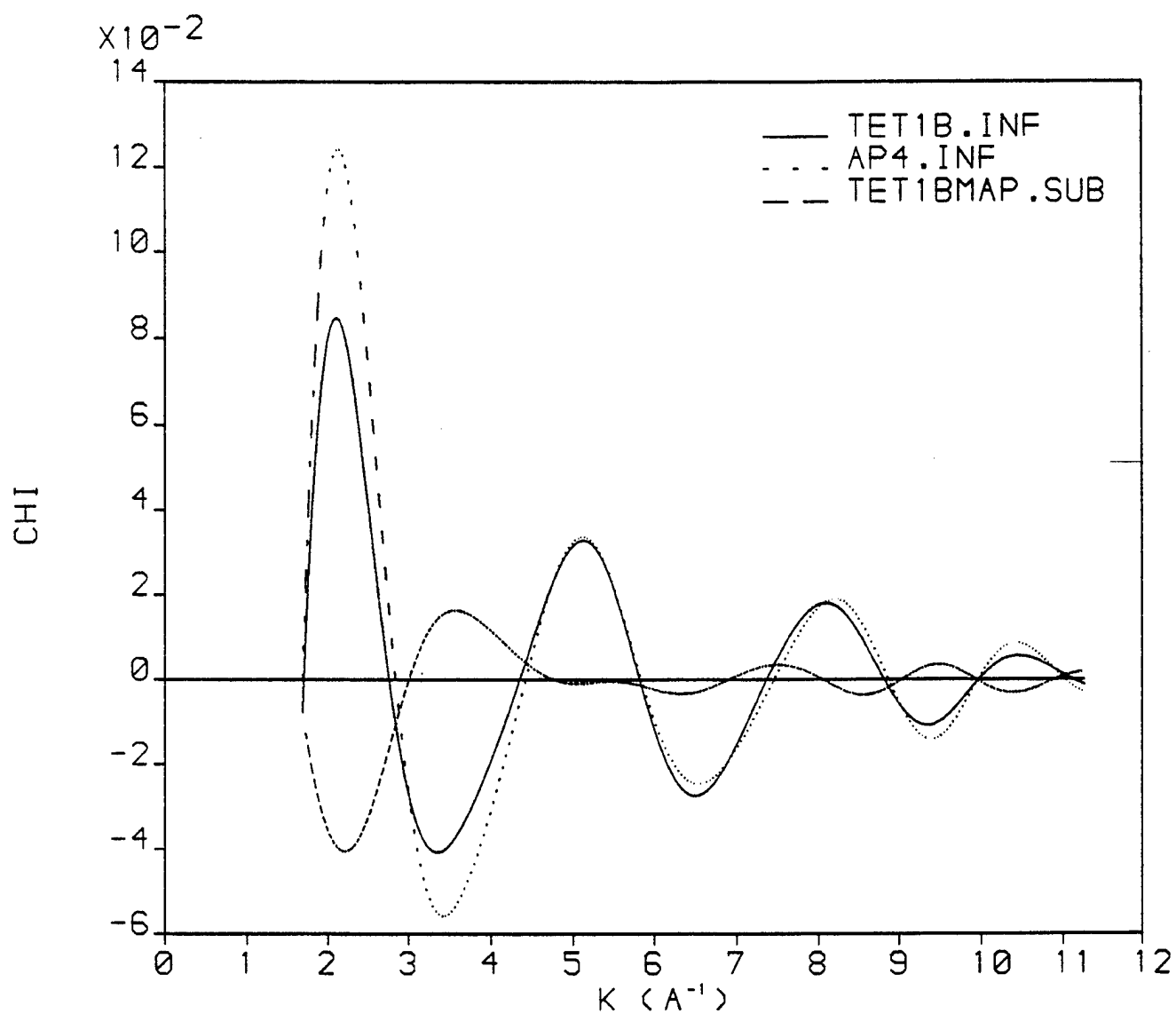


FIG 4: Overplot of the first shell chi of TET1B, AP4 and the difference of the two.

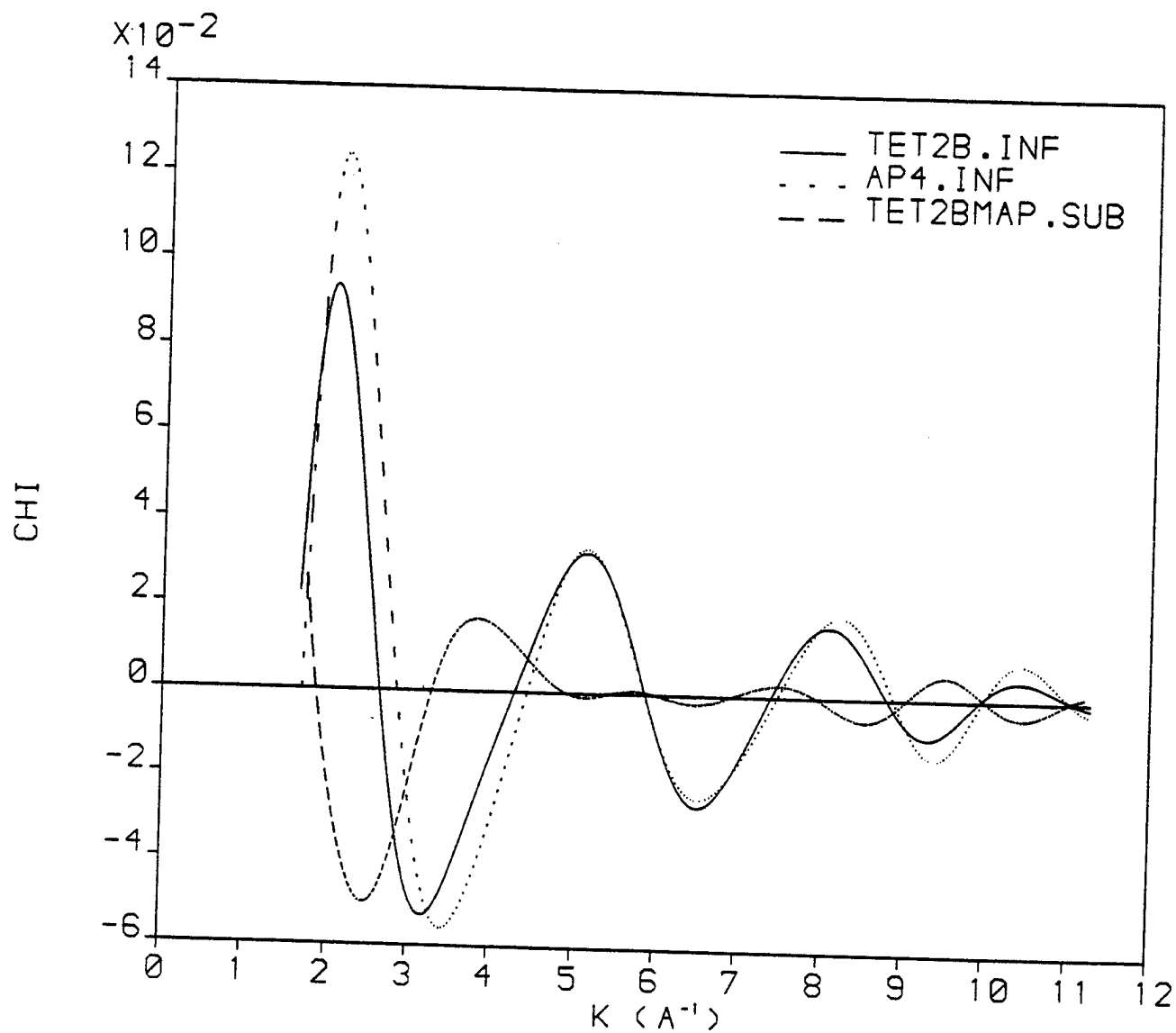


FIG 5: Overplot of the first shell chi of TET2B, AP4 and the difference of the two.

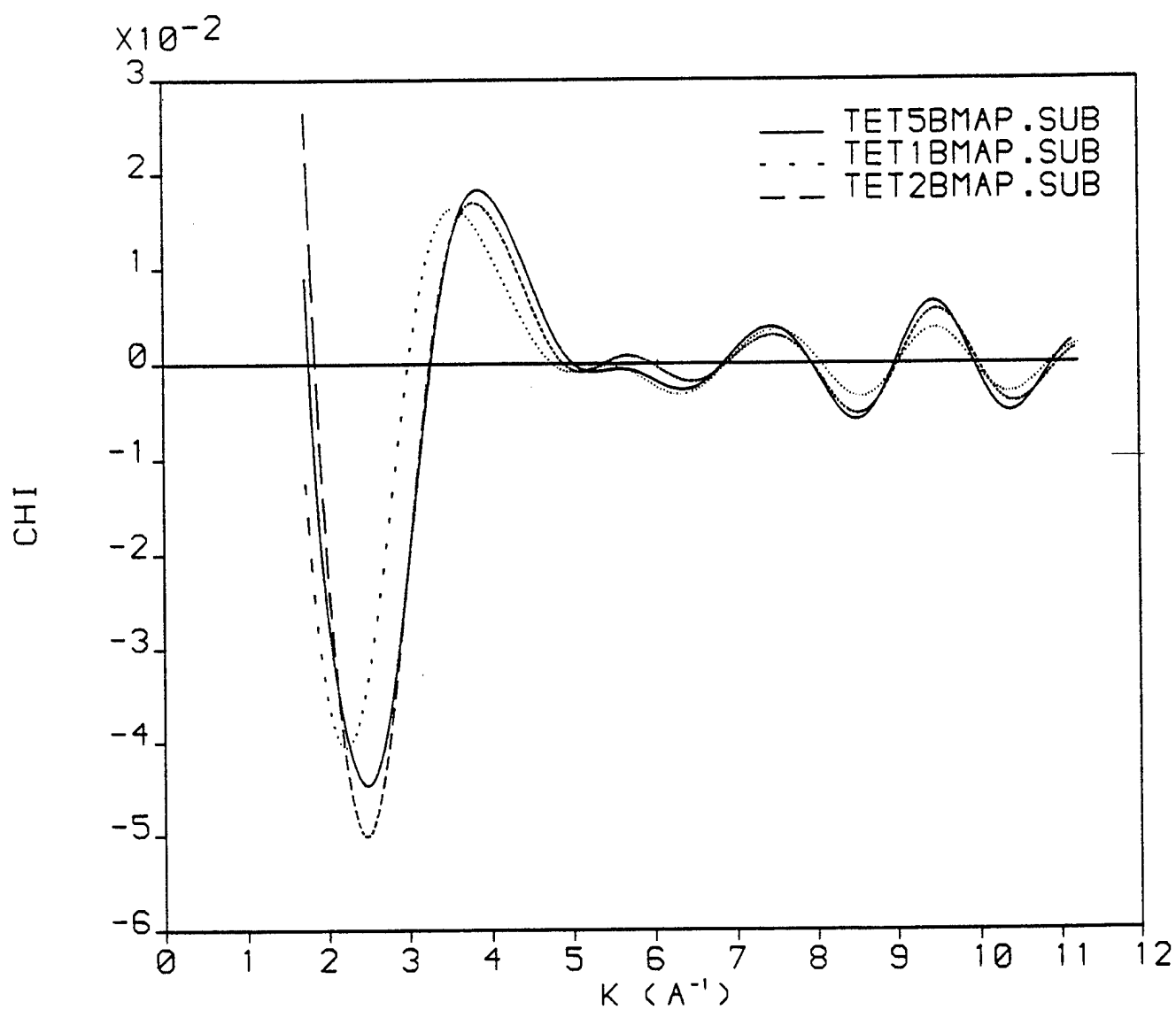


FIG 6: Overplot of the differences between TET5B, TET1B and TET2B with AP4.



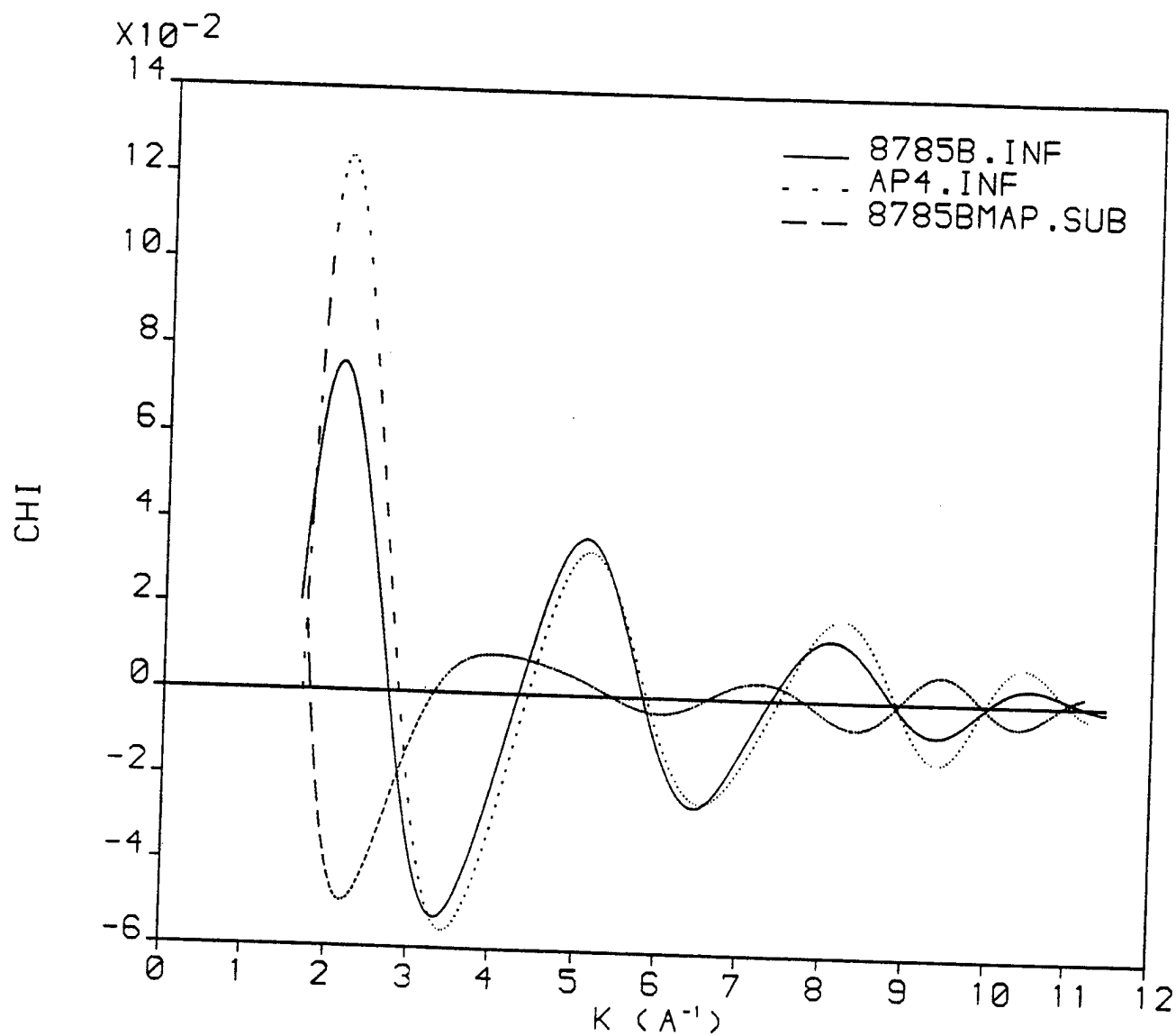


FIG 7: Overplot of the first shell chi of 8785B, AP4 and the difference of the two.

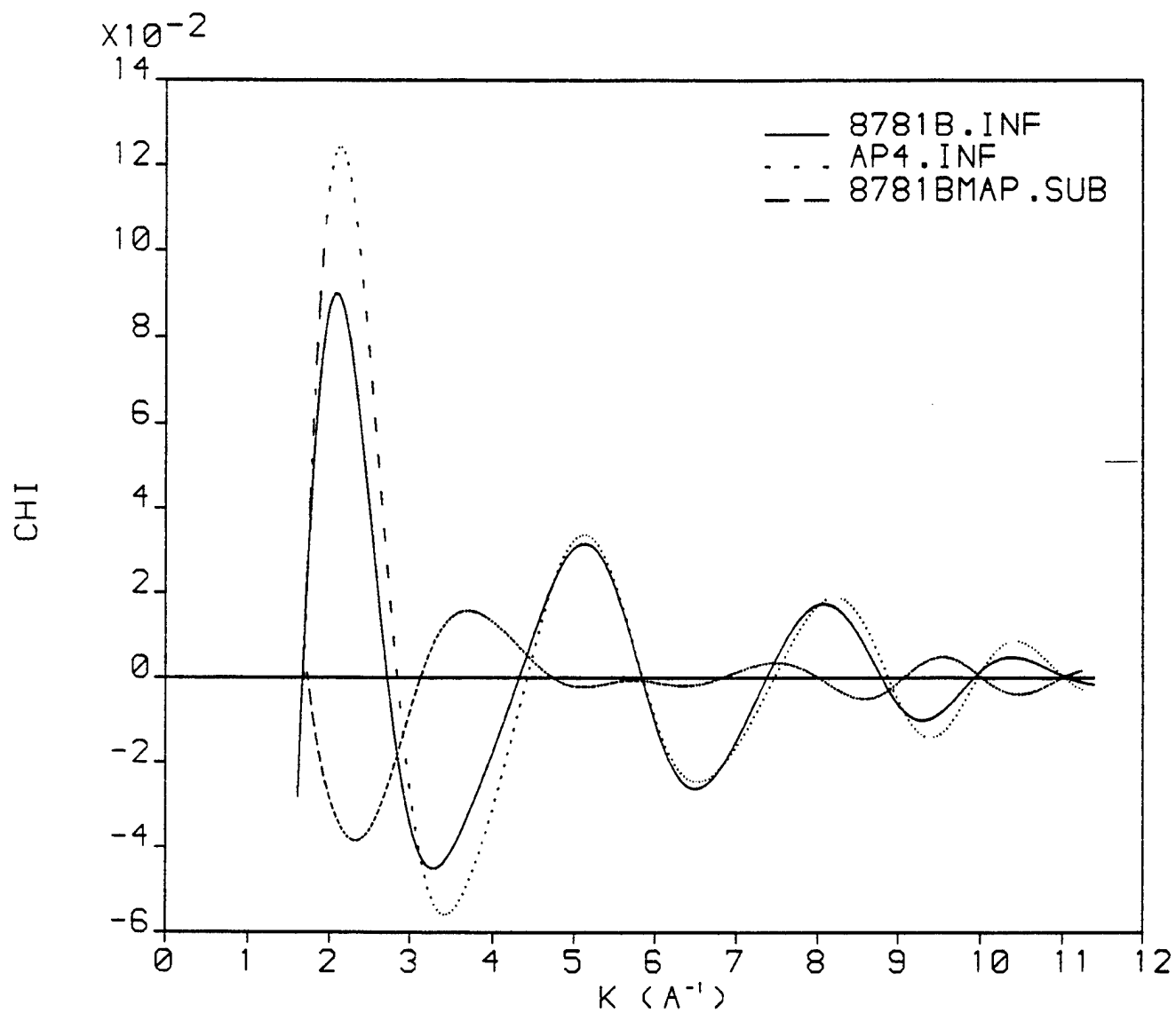


FIG 8: Overplot of the first shell chi of 8781B, AP4 and the difference of the two.

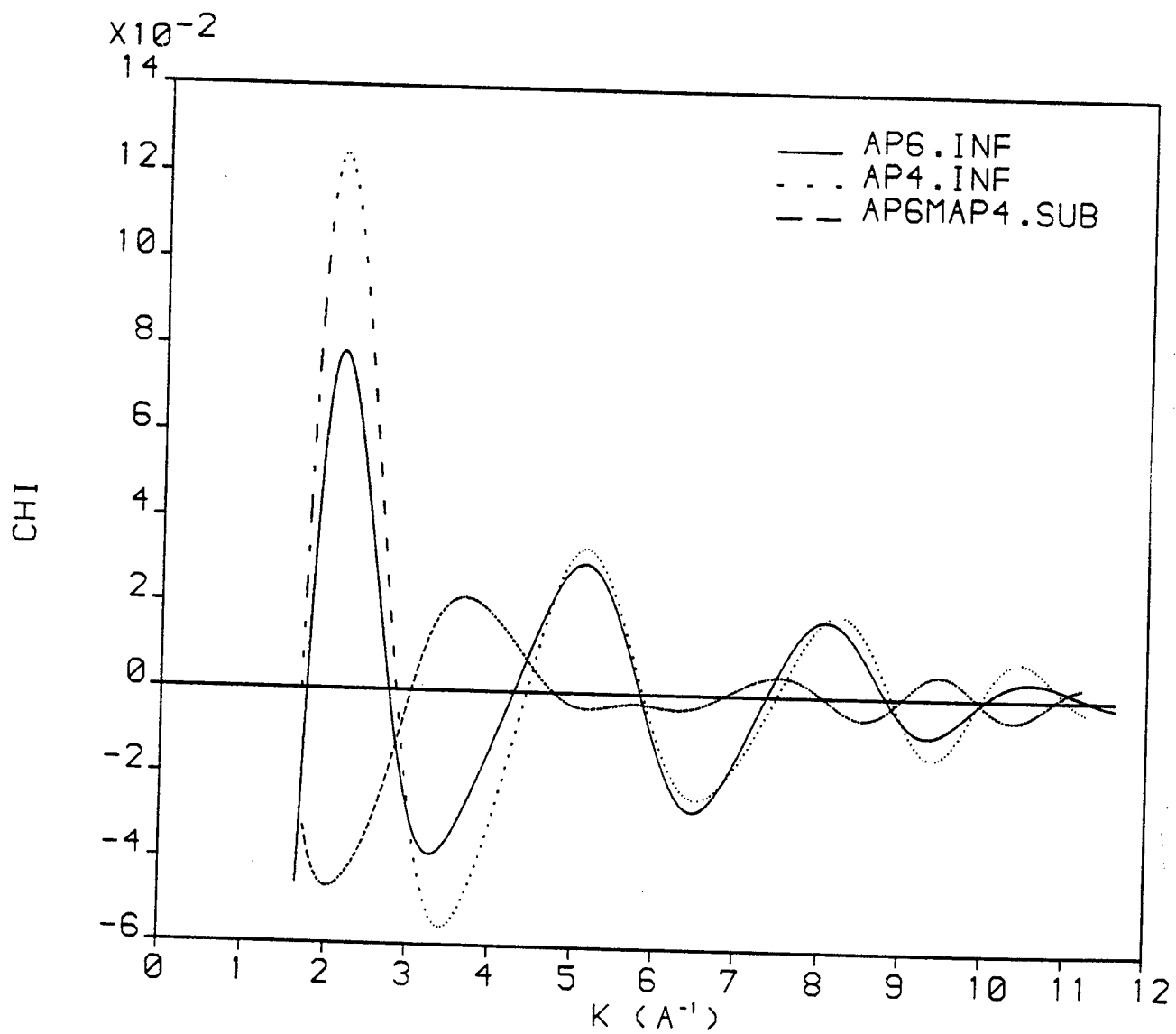


FIG 9: Overplot of the first shell chi of AP6, AP4 and the difference of the two.

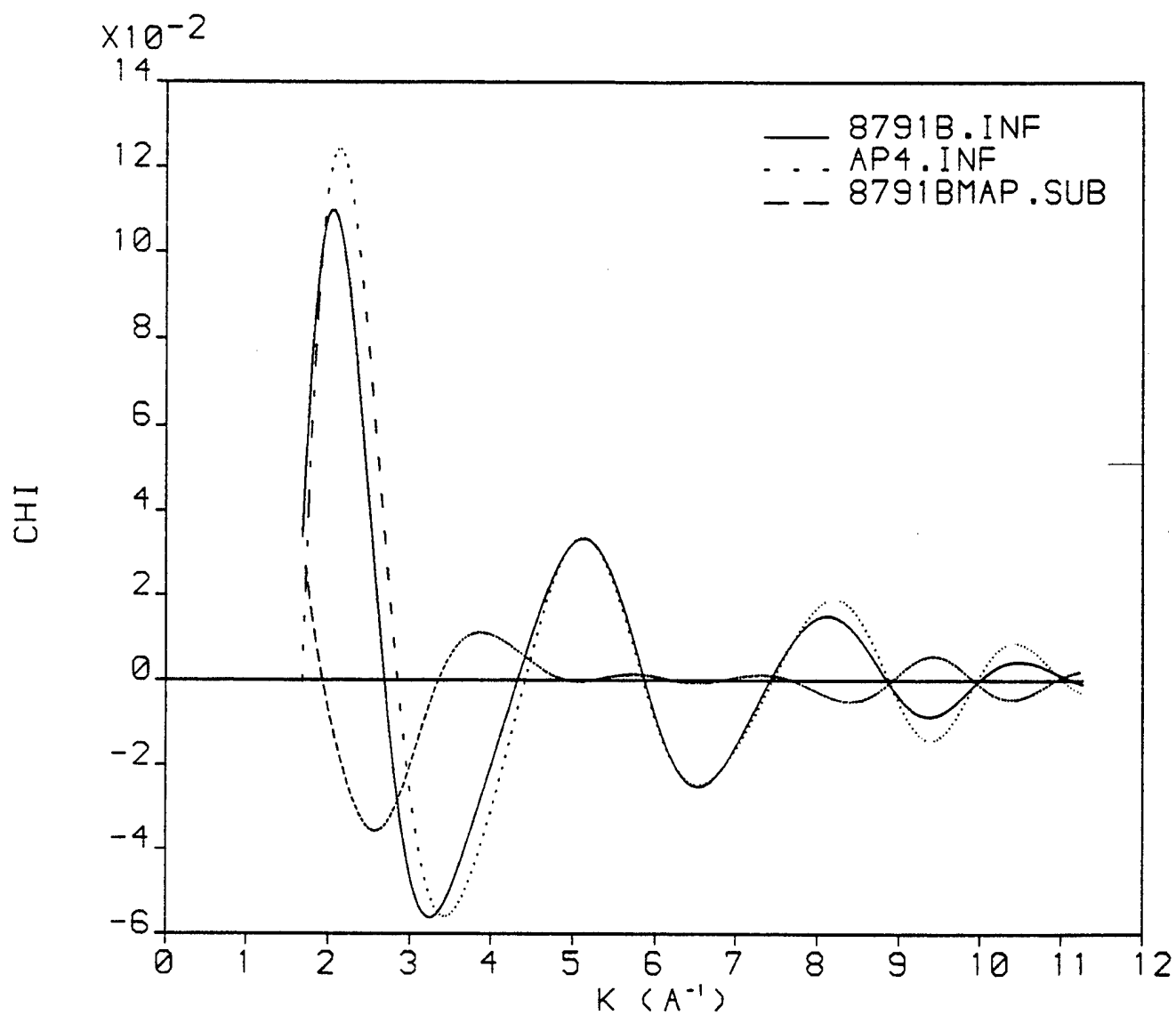


FIG 10: Overplot of the first shell chi of 8791B, AP4 and the difference fo the two.

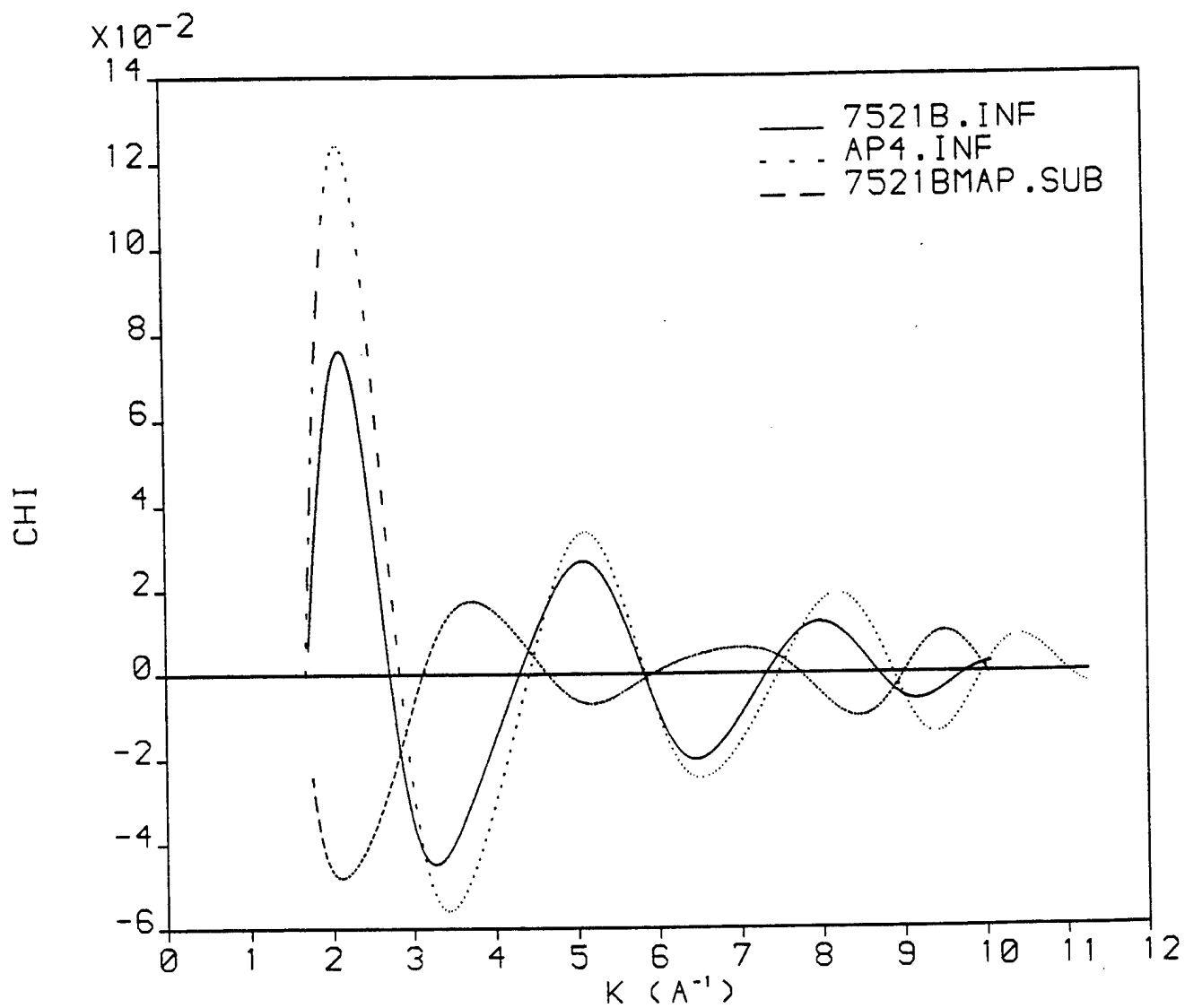


FIG 11: Overplot of the first chell chi of 7521B, AP4 and the difference of the two.

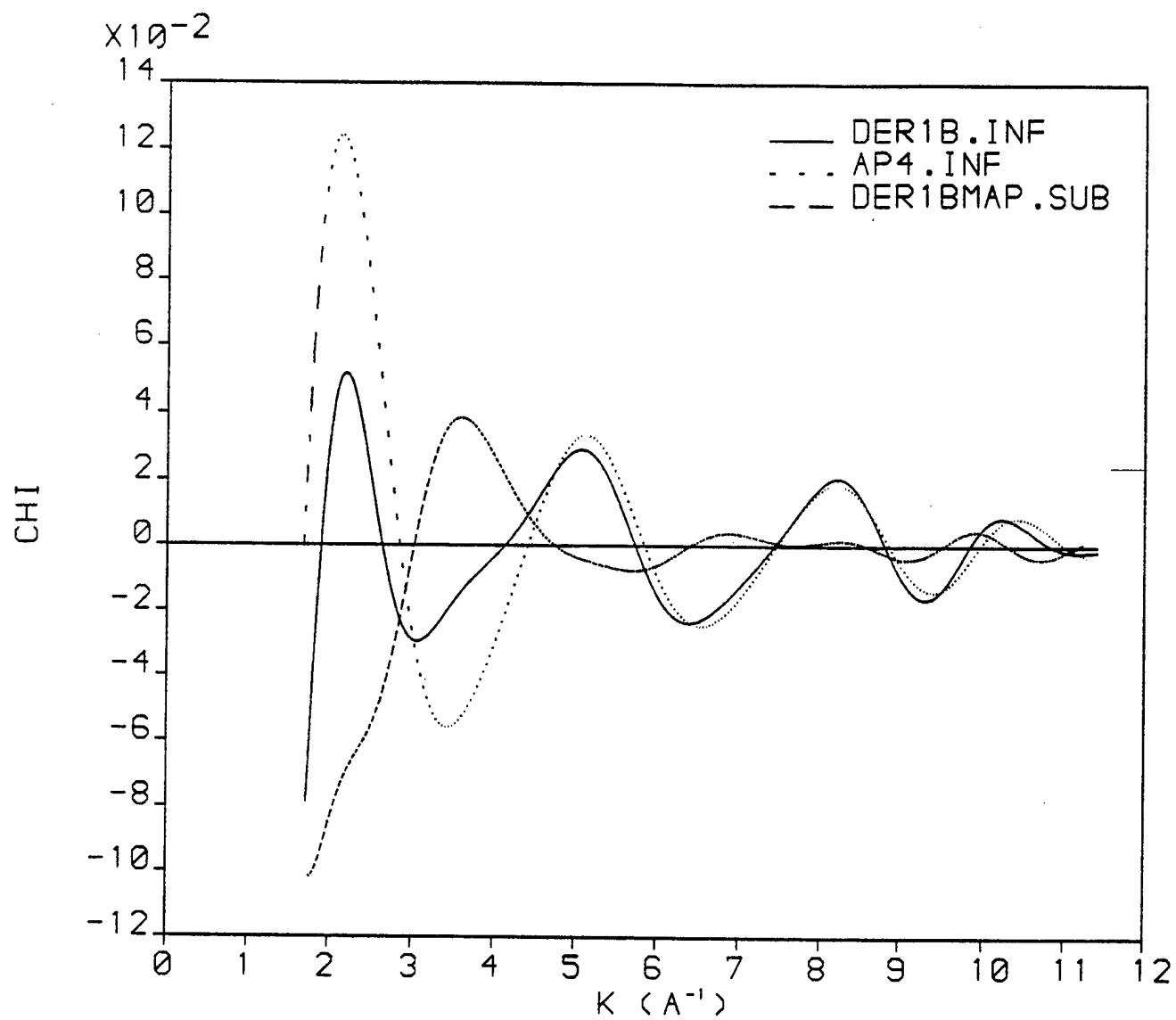


FIG 12: Overplot of the first shell chi of DER1B, AP4 and the difference of the two.

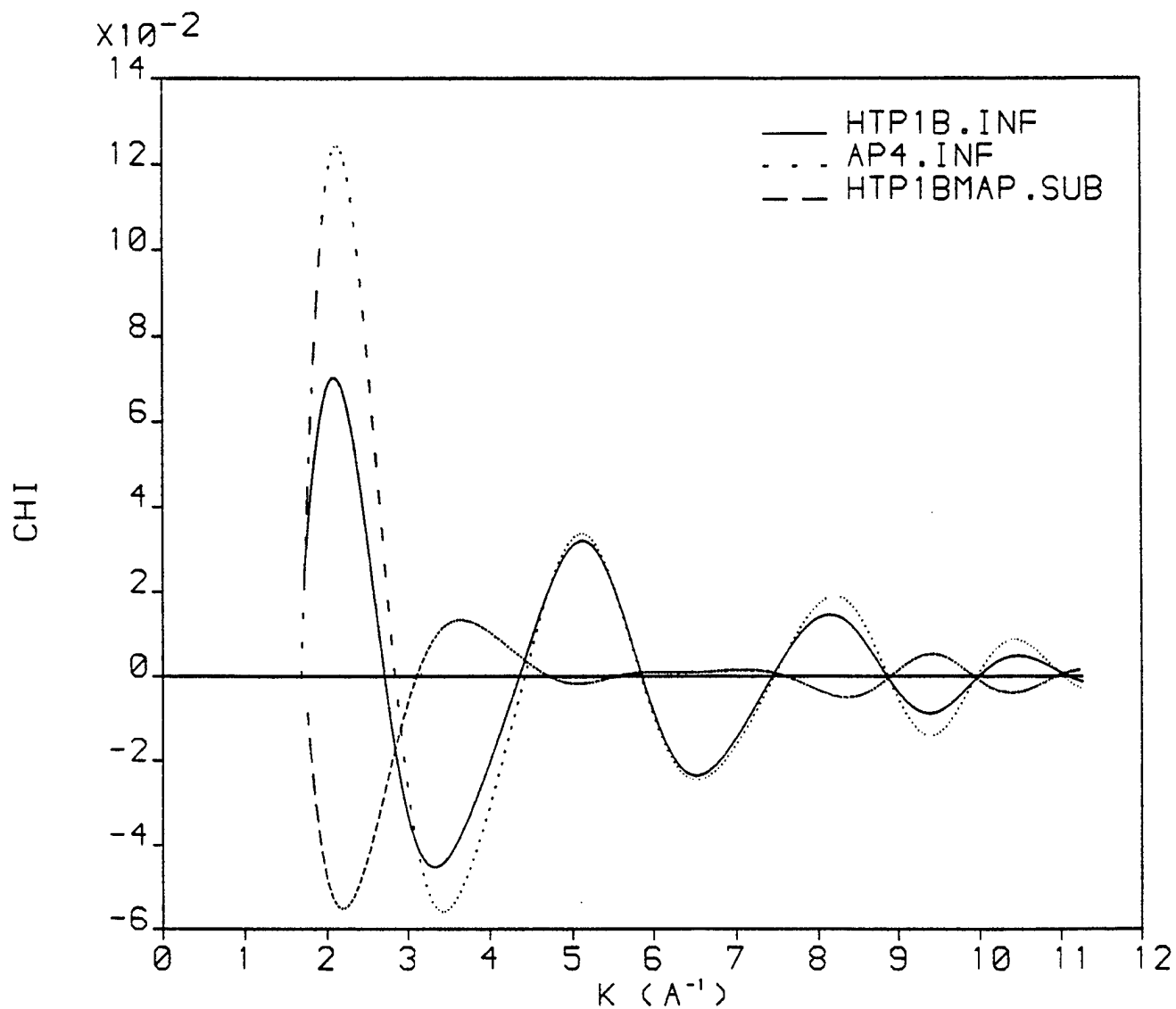


FIG 13: Overplot of the first chell chi of HTP1B, AP4 and the difference of the two.

FIGURE 14

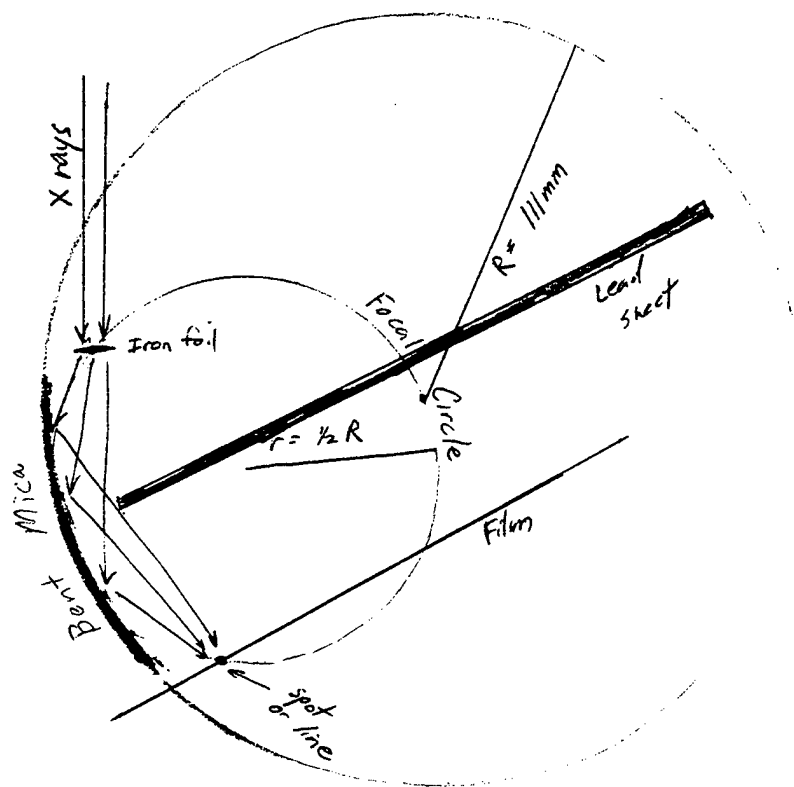
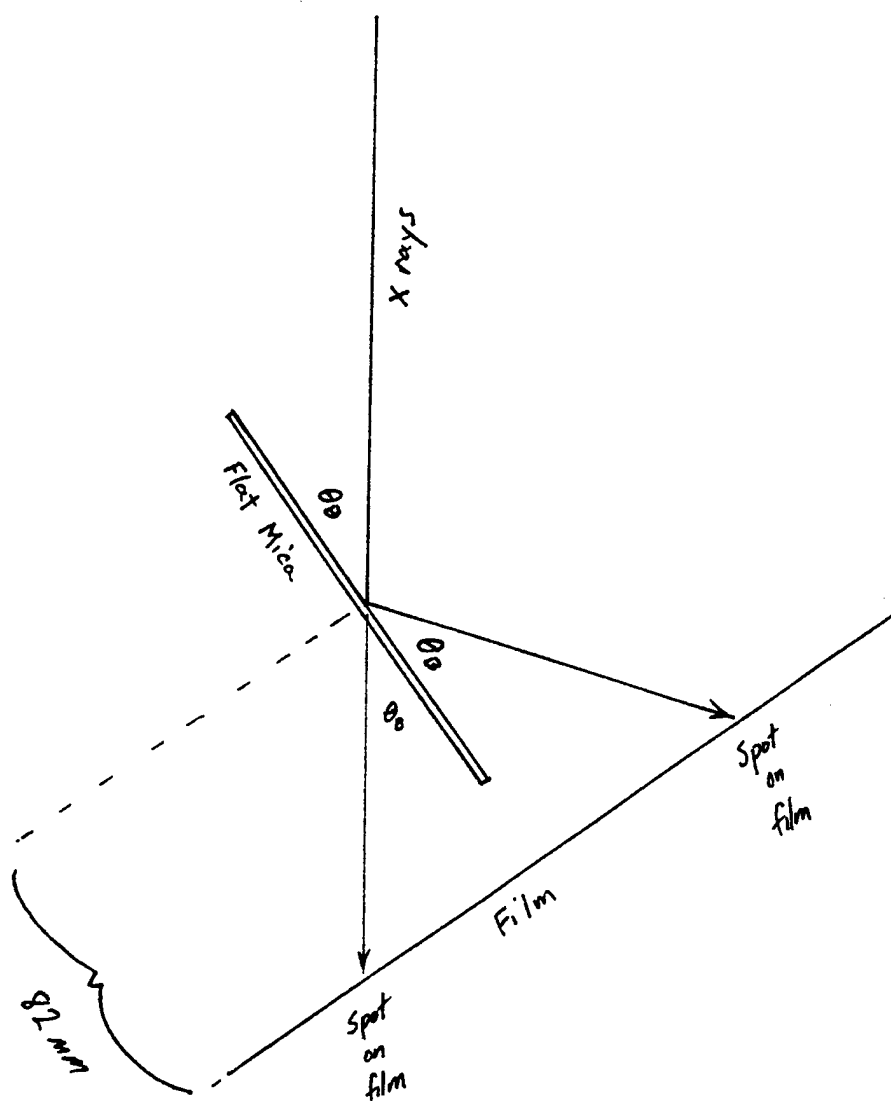
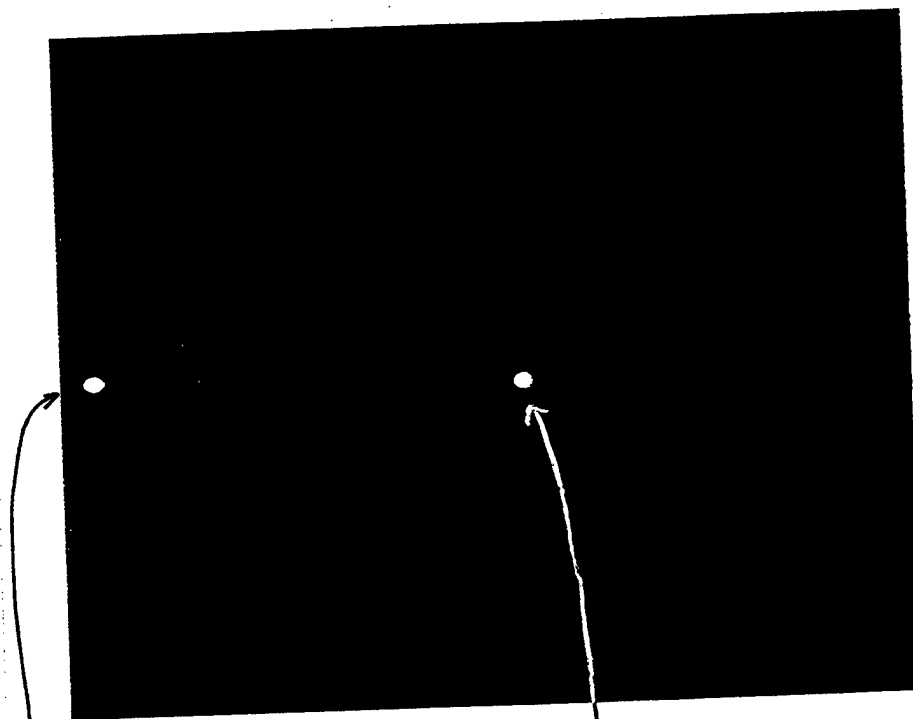




FIGURE 15



Picture # 1



$E = 7183 \text{ eV}$   
 $\alpha = 0^\circ$

Exposure # 13  
Exposure time 6 min

Transmitted Spot

Diffracted Spot

Picture # 2



Exposure # 29  
Exposure Time = 2 min

## MARS MONTHLY REPORT - JULY 1992

Thin Film / Surface Science Laboratory

Case Western Reserve University

### **I. X-ray Absorption Fine Structure**

#### **DATA ANALYSIS**

As discussed in last month's report, we were able to calculate a Cl-O  $\chi$  function using the program FEF3 .25 and overplot the calculated spectrum with experimental data from pure Ammonium Perchlorate (AP). A direct comparison of the two spectra is shown in Figure 1. To optimize overlap and determine that the calculation and experiment agree to within a phase factor, we applied a  $V_0$  correction to the experimental  $\chi$  and graphically compared the resulting  $\chi$  to the calculated  $\chi$  for several  $\Delta V_0$  values. In Figure 2 the  $V_0$ -shifted  $\chi$  for 10, 15 and 20 eV are shown with the calculated  $\chi$ . Table I lists the first 6 node locations for each of these data sets and  $\Delta V_0=15.5$  eV is the closest to the calculated spectrum. The reader should note that this  $\Delta V_0$  is not the same quantity that resulted from the EDGE program, but rather a "phase correction" term to determine whether or not the experimental  $\chi$  functions were reasonable .

It was reported last month that we would next investigate the difference spectra of AP with AP/binder. In a fashion similar to Table I, Table II shows the node, as well as the peak positions for each of the .INF files and the experimental standard AP4 .INF.

## COMPUTER RESOURCE MANAGEMENT

A "portable" University of Washington EXAFS analysis package was received at CWRU from a PRT contact via ftp. Due to problems with the file transfer program at Brookhaven this task was difficult but was finally accomplished. Shortly after installation and preliminary testing of the programs at CWRU, the package was then ported to the VAX cluster at Edwards AFB. The standard method to use is to transfer the entire VMS SAVE\_SET as a unit via ftp (File Transfer Protocol) over the INTERNET. After several failed attempts due to network interruption between CWRU and EAFB, an attempt to SEND individual files was made. Since the network response time between CWRU and EAFB is quite slow, with ~ 27% data loss enroute, this tool a couple of days to complete. Again accessing the EAFB VAX via remote TELNET, GAD set up the directory structure and modified the command procedures on PL-EDWARDS.AF.MIL to allow execution of the programs.

The directory structure for the UWEXAFS package is as follows. The "root" directory is USER\$DISK33:[OSBORNS.UWPROGS]. GAD has modified the LOGIN.COM and related procedures to setup the UWEXAFS package for execution. The logical assignments are:

```
XAS          USER$DISK33:[OSBORNS.UWPROGS]
XASPROC      USER$DISK33:[OSBORNS.UWPROGS.PROC]
XASPROG      USER$DISK33:[OSBORNS.UWPROGS.PROG]
XASLIB       USER$DISK33:[OSBORNS.UWPROGS.LIB]
XASUTIL      USER$DISK33:[OSBORNS.UWPROGS.UTIL]
```

There are a number of useful utility programs, such as MAT (McMaster lookup), MUGAS (calculate ionization chamber fill gasses), STRUC (calculate crystal structures) and a host of

others. Online help is available by typing \$EXA[FS]. In most directories there exists a file called AAAREAD.ME. To access it, type \$AA. The online help is quite useful. See the topic INTRO for more help. Note: In the preceding description, words in COURIER 12pt are actual computer inputs.

## **II. RHEED/TPD Project**

During the month of July, we continued to work on the RHEED/TPD system. In order to simplify the sample preparation and eliminate any unnecessary handling of the AP, we decided to put the two techniques in one vacuum chamber. Since the vacuum system in Room 116 has RHEED capabilities, we opted for this system. We tested the RHEED equipment on a silicon sample and were able to get a rough image. This was probably due to contaminants on the surface of the sample. Thus we are considering in-situ ways to clean sample surfaces. This may or may not be so easy with AP. Currently, the sample manipulator has been removed from the system in order to modify it for TPD. Once these are completed, we can proceed. We are also working on some problems with the system's Auger electronics. AP contamination may force the use of other UHV systems. Initial TPD experiments will be done in a separate UHV turbo pumped 6-way cross.

## **III. X-ray Spectrograph**

We are currently evaluating possible detector designs to maximize efficiency for use with the x-ray spectrograph.

| $\Delta V_0$<br>(eV) | Node 1<br>( $\text{\AA}^{-1}$ ) | Node 2<br>( $\text{\AA}^{-1}$ ) | Node 3<br>( $\text{\AA}^{-1}$ ) | Node 4<br>( $\text{\AA}^{-1}$ ) | Node 5<br>( $\text{\AA}^{-1}$ ) | Node 6<br>( $\text{\AA}^{-1}$ ) |
|----------------------|---------------------------------|---------------------------------|---------------------------------|---------------------------------|---------------------------------|---------------------------------|
| Calc.                | 2.00                            | 4.00                            | 5.50                            | 7.05                            | 8.50                            | 9.85                            |
| 0                    | 2.83                            | 4.41                            | 5.82                            | 7.44                            | 8.85                            | 9.97                            |
| 5                    | 2.59                            | 4.25                            | 5.71                            | 7.35                            | 8.78                            | 9.90                            |
| 10                   | 2.33                            | 4.10                            | 5.59                            | 7.26                            | 8.70                            | 9.83                            |
| 14                   | 2.09                            | 3.97                            | 5.50                            | 7.18                            | 8.64                            | 9.78                            |
| 14.5                 | 2.06                            | 3.95                            | 5.49                            | 7.17                            | 8.64                            | 9.77                            |
| 15                   | 2.02                            | 3.93                            | 5.48                            | 7.17                            | 8.63                            | 9.77                            |
| 15.5                 | 1.99                            | 3.92                            | 5.46                            | 7.16                            | 8.62                            | 9.76                            |
| 16                   | 1.96                            | 3.90                            | 5.45                            | 7.15                            | 8.61                            | 9.75                            |
| 20                   | 1.67                            | 3.76                            | 5.36                            | 7.07                            | 8.55                            | 9.70                            |

Table 1. Node locations in  $\text{\AA}^{-1}$  for several  $V_0$  shifts of experimental  $\chi$  from AP4.INF to compare phase shifting to calculated data marked "Calc.".

| File  | $n_1$<br>( $\text{\AA}^{-1}$ ) | $p_1$<br>( $\text{\AA}^{-1}$ ) | $n_2$<br>( $\text{\AA}^{-1}$ ) | $p_2$<br>( $\text{\AA}^{-1}$ ) | $n_3$<br>( $\text{\AA}^{-1}$ ) | $p_3$<br>( $\text{\AA}^{-1}$ ) | $n_4$<br>( $\text{\AA}^{-1}$ ) | $p_4$<br>( $\text{\AA}^{-1}$ ) | $n_5$<br>( $\text{\AA}^{-1}$ ) | $p_5$<br>( $\text{\AA}^{-1}$ ) |
|-------|--------------------------------|--------------------------------|--------------------------------|--------------------------------|--------------------------------|--------------------------------|--------------------------------|--------------------------------|--------------------------------|--------------------------------|
| AP4   | 1.68                           | 2.15                           | 2.83                           | 3.41                           | 4.41                           | 5.10                           | 5.82                           | 6.52                           | 7.44                           | 8.21                           |
| TOLB  | DNE                            | 2.11                           | 2.72                           | 3.30                           | 4.33                           | 5.10                           | 5.82                           | 6.52                           | 7.44                           | 8.13                           |
| TET5B | DNE                            | 2.07                           | 2.64                           | 3.18                           | 4.21                           | 5.10                           | 5.82                           | 6.48                           | 7.36                           | 8.05                           |
| TET1B | 1.68                           | 2.11                           | 2.76                           | 3.34                           | 4.33                           | 5.14                           | 5.82                           | 6.48                           | 7.36                           | 8.09                           |
| TET2B | DNE                            | 2.03                           | 2.60                           | 3.18                           | 4.25                           | 5.14                           | 5.86                           | 6.52                           | 7.40                           | 8.09                           |
| 8785B | DNE                            | 2.07                           | 2.72                           | 3.34                           | 4.29                           | 5.06                           | 5.79                           | 6.44                           | 7.36                           | 8.09                           |
| 8781B | 1.68                           | 2.07                           | 2.72                           | 3.30                           | 4.33                           | 5.14                           | 5.82                           | 6.52                           | 7.36                           | 8.09                           |
| 8791B | DNE                            | 2.03                           | 2.68                           | 3.26                           | 4.33                           | 5.14                           | 5.86                           | 6.52                           | 7.44                           | 8.13                           |
| 7521B | DNE                            | 2.15                           | 2.72                           | 3.26                           | 4.29                           | 5.10                           | 5.82                           | 6.48                           | 7.32                           | 7.98                           |
| DER1B | 1.91                           | 2.19                           | 2.64                           | 3.07                           | 4.14                           | 5.06                           | 5.71                           | 6.37                           | 7.44                           | 8.21                           |
| HTP1B | DNE                            | 2.11                           | 2.72                           | 3.34                           | 4.37                           | 5.14                           | 5.86                           | 6.52                           | 7.44                           | 8.13                           |

Table 2. Node and peak positions in  $\text{\AA}^{-1}$  for experimental  $\chi$  spectra of filtered shells. All files are .INF files. The symbol DNE means "Does Not Exist" and occurs when the low end of the data set did not contain a node due to truncation resulting from the inverse FT calculation.

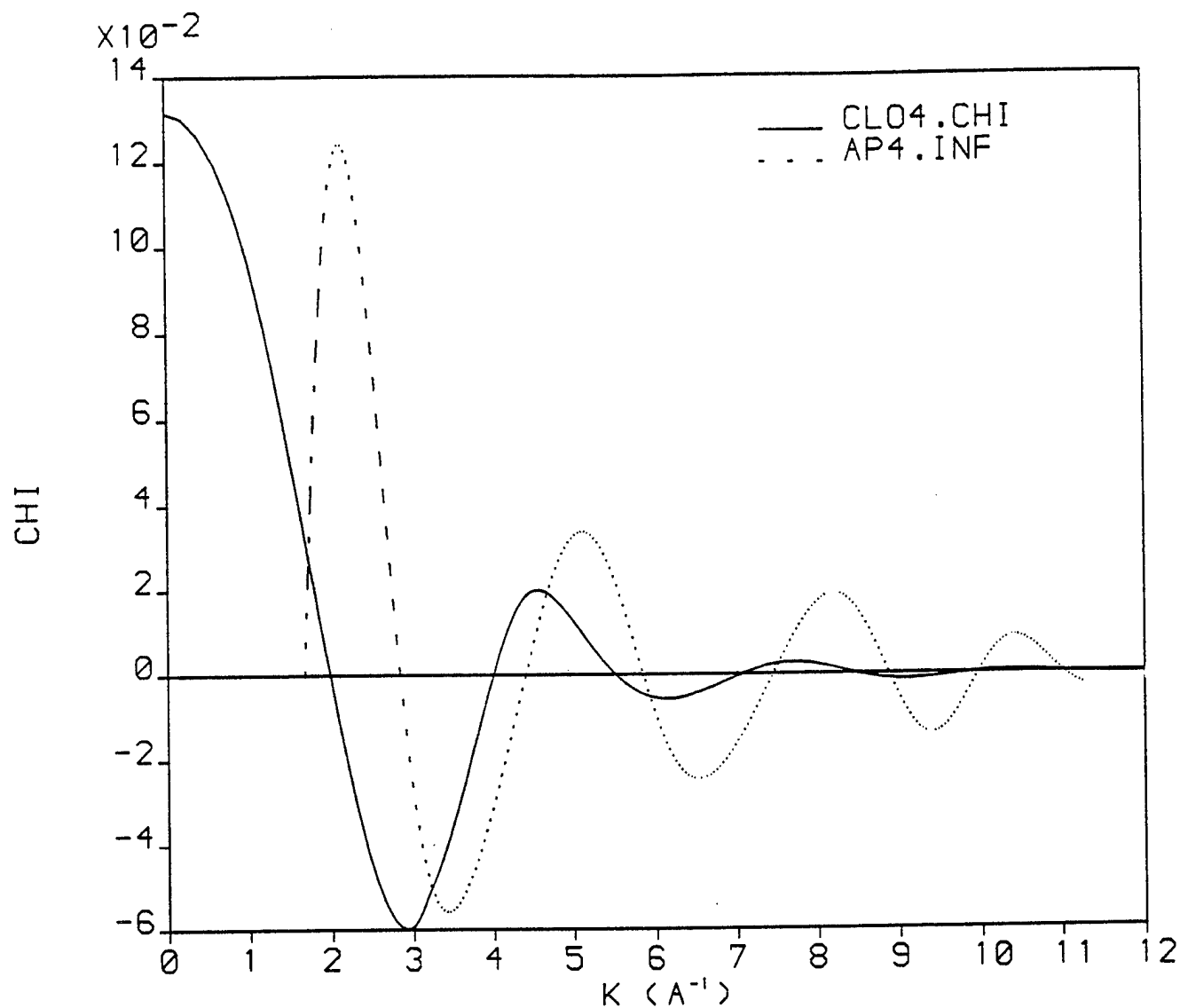


FIGURE 1. Direct comparison of inverse Fourier Transformed chi functions for FEFF-calculated (solid line) and experimentally measured (dashed line) data. The calculation is for a 1st shell around Cl containing 4 oxygen atoms.



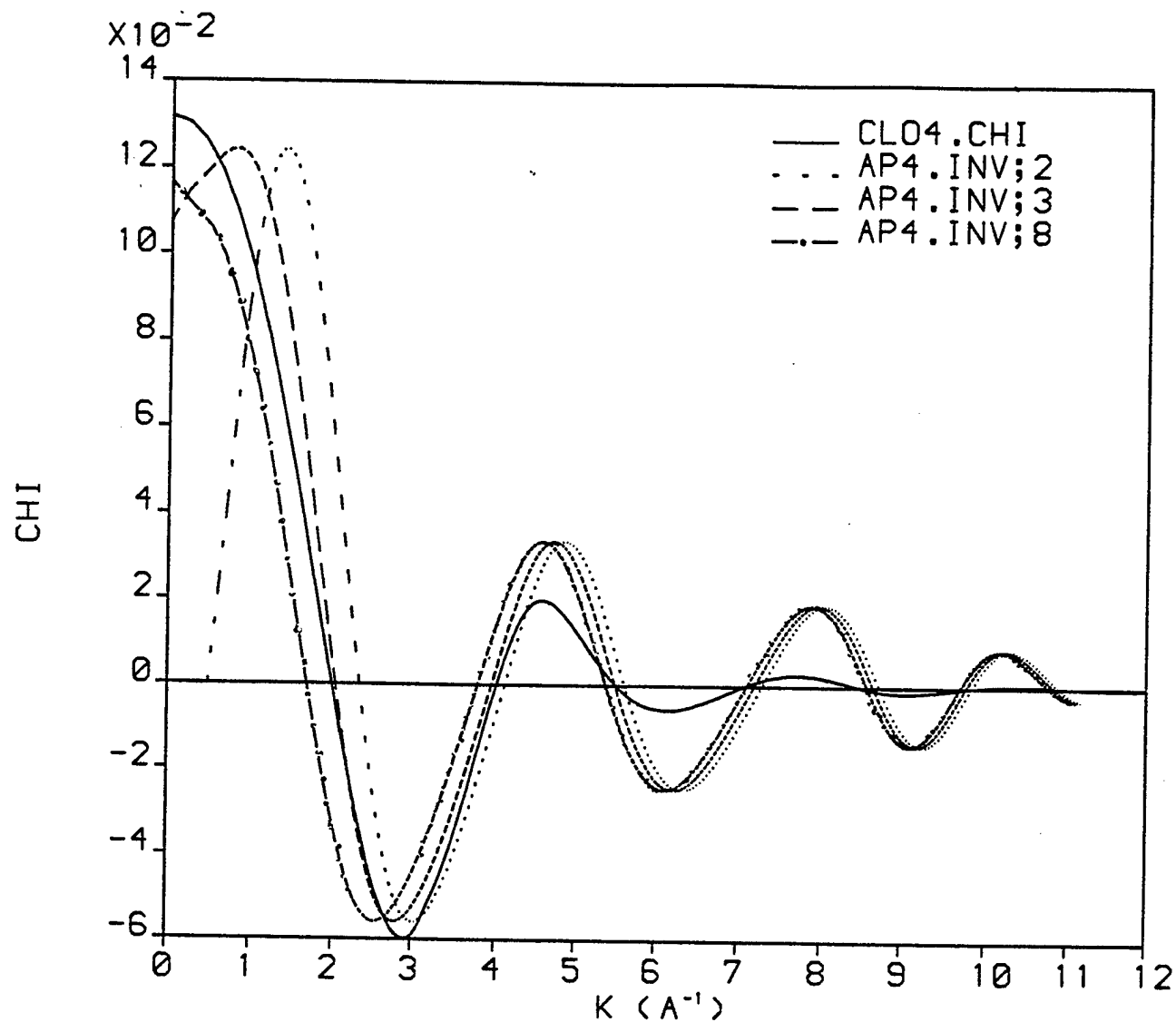


Figure 2. Overplot of calculated 1st shell chi from FEFF V3.25 with experimental data given a  $V_0$  shift of 10 (.....), 15 (-----), and 20 eV (-.-.-.-).

## MARS MONTHLY REPORT - AUGUST 1992

Thin Film / Surface Science Laboratory

Case Western Reserve University

### **I. X-ray Absorption Fine Structure**

Continuing the investigation of the differences between EXAFS spectra from various binders on AP, we now turn our attention to the nodes and peaks in the inverse (filtered) Fourier Transforms for the first (presumably Cl-O) shell. It is hoped that the k-space analysis will tell the story of any effects, if they exist, on the Cl-local structure of AP caused by any of the binders. In the case of TET, XAFS data are available for coverages of 0.5, 1.0 and 2.0 monolayers with beam impinging on both the "top" and the "bottom" of the sample with respect to which side the drop of TET was placed. Any differences between these two cases were investigated as a function of coverage and general trends between binders were also analyzed. It is indeed unfortunate that the TFSSL's primary MS-DOS platform suffered a (non-recoverable) system crash during the 22-23 August weekend. As a result, the plots in this report are not as refined as one would like, and new ones will not be available until the new machine arrives (~14 September) and the old hard disk becomes accessible. Fortunately some hard copies were made prior to the system crash and (hopefully) represent the data satisfactorily.

The data in Table 1 is the supplement to last month's Table 2 except that this one is for binder on top. Figure 1 shows the plot of feature location in  $\text{\AA}^{-1}$  vs binder type for binder on the top. The data for binders on the bottom is shown in Figure 2. In all of the plots the ordinate is wavenumber in  $\text{\AA}^{-1}$  (could not get Slidewrite to print  $\text{\AA}$  before crash) and the labels in the

header refer to node and peak column headings in the two tables mentioned above where B and T stand for bottom and top, respectively. The peak/node positions with a  $\pm 1$  data point error bar on the feature position are shown in Figures 3 and 4. The horizontal lines in those figures mark the feature position  $\pm 1$  data point (error bar) for AP. The AP values are experimental ones, as are all the others, in order to look for deviations from pure AP. An examination of those two figures supports the conclusion that the differences in the local structure caused by the binder are more prevalent at low  $k$  and thus most of the spectral information is from the near edge region. The most obvious exception to this conclusion is DER1 which warrants further investigation into the interactions involved. Plots out to  $n_5$  and  $p_5$  will be made once the computer with the data comes back online.

Figures 5, 6, 7(a) and 7(b) show feature positions vs TET coverage in monolayers. In Figures 5 and 7(a) the feature position vs coverage was fit using linear least squares techniques and 6 and 7(b) are qualitative plots with error bars as before. The least squares fit parameters for Figures 5 and 7(a) are shown in Table 2. The fit results may indicate that very little difference is seen between top and bottom and if any differences do exist, they are most predominant at low  $k$  (Figure 7(a)). Computer modelling programs have recently become available which could be used to calculate the effect of each binder on the local structure of AP as an aid in the interpretation of these data, and will be pursued.

## II. X-Ray Spectrograph

This month we investigated different types of X-ray film for use in the detector. We

would like to decrease the exposure time and increase image sensitivity. We spoke with radiologists at University Hospitals to get their insights on this problem, since they have similar concerns. We also investigated some references on position sensitive detectors. One such reference is Annual Review of Nuclear and Particle Science 1984, pps 334 - 346.

### III. TPD

We continued work on the TPD apparatus and investigated references in this area. Some are listed below:

1. *Physical Basis of Ultrahigh Vacuum*. R. A. Redhead.  
pp. 203 - 211.
2. LANGMUIR 1987, 3, 973 - 975.
3. SURFACE SCIENCE 223 (1990) pp. 355 - 365.
4. SURFACE SCIENCE 199 (1988) pp. 43 - 53.
5. APPLICATIONS OF SURFACE SCIENCE 1 (1978) p. 360 - 376.

# Peak / Node positions in k-space vs binder on top

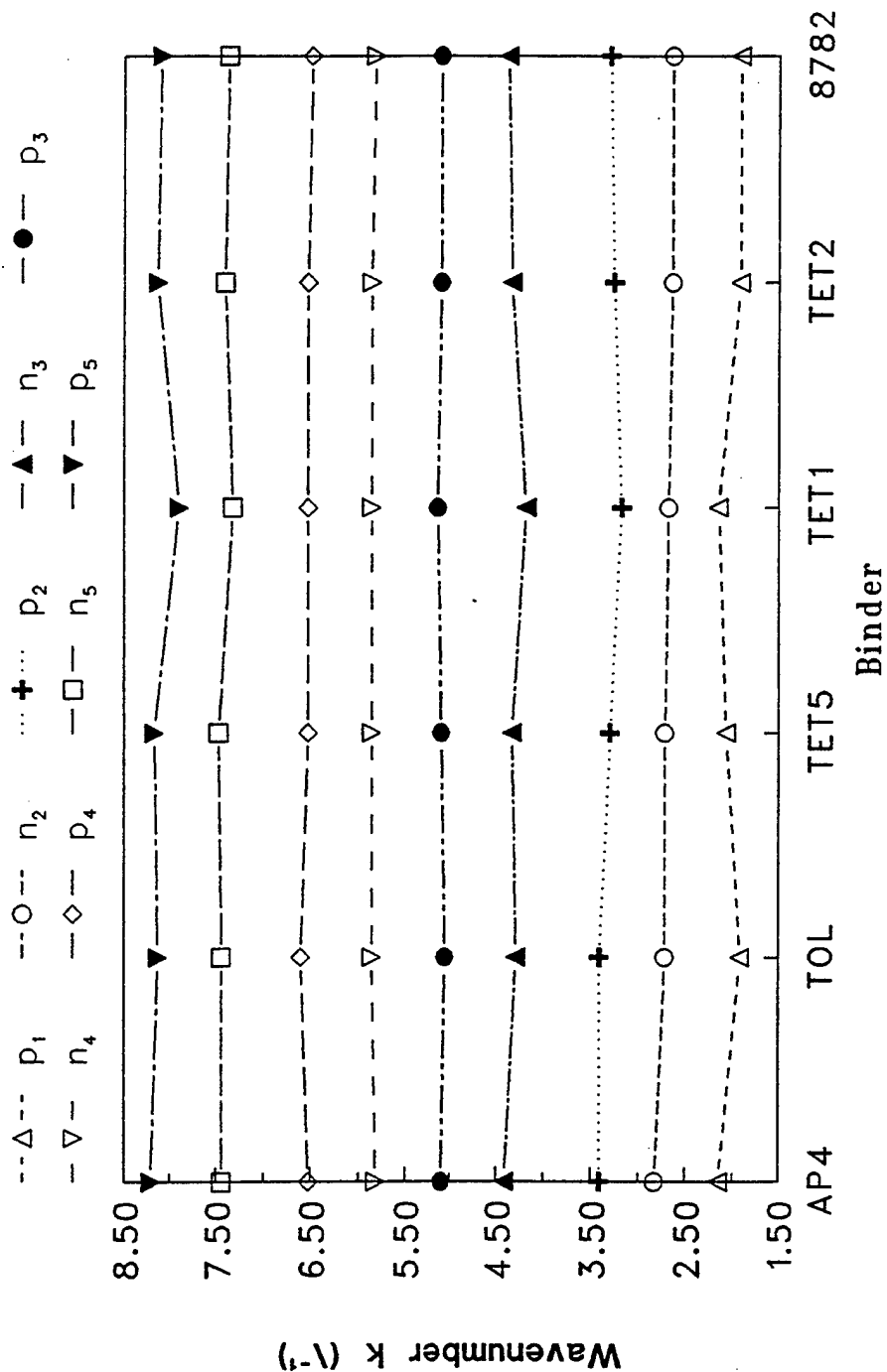


FIGURE 1

# Peak/Node positions in k-space vs binder on bottom

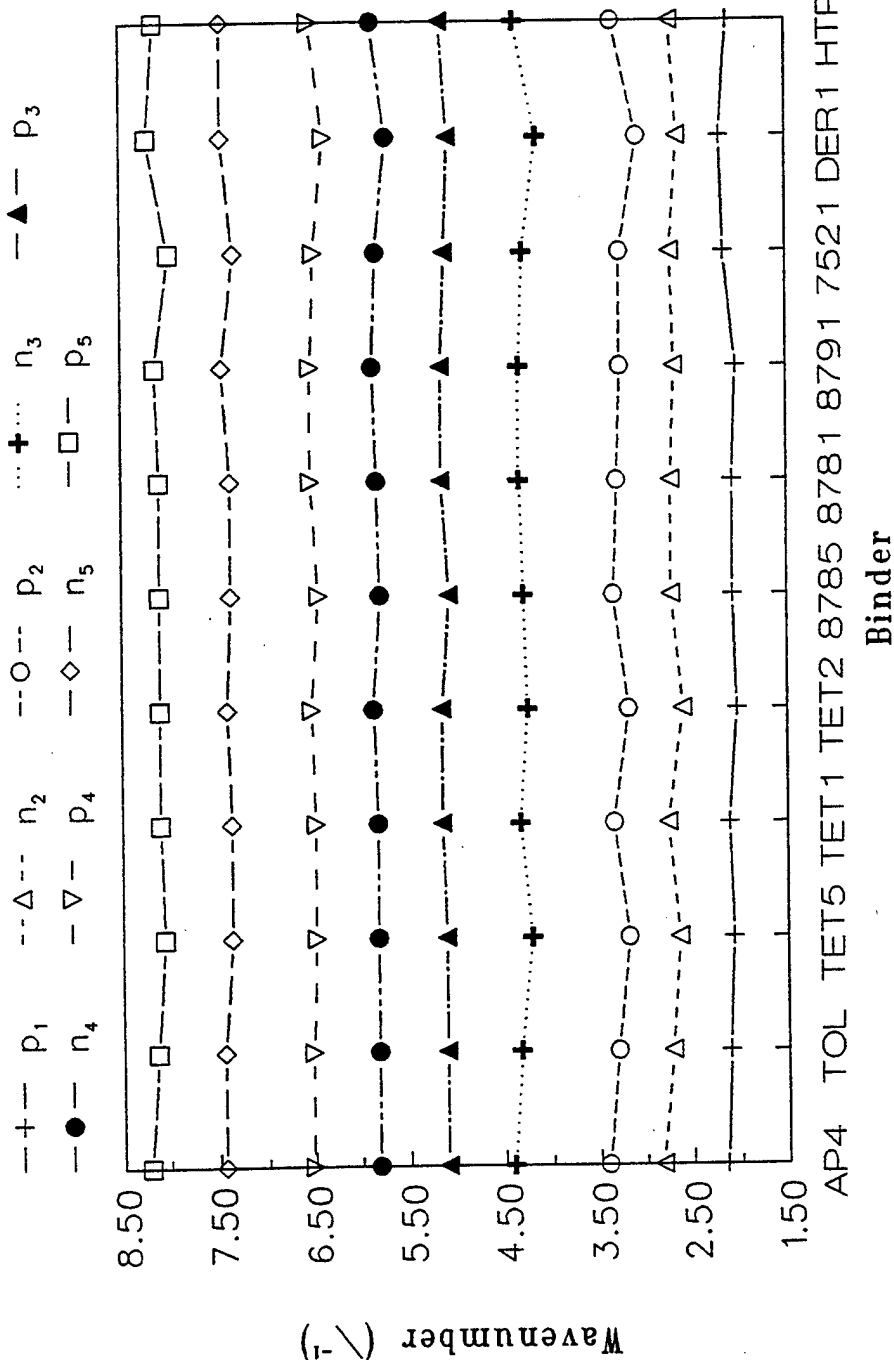


FIGURE 2

# Node positions in k-space vs binder

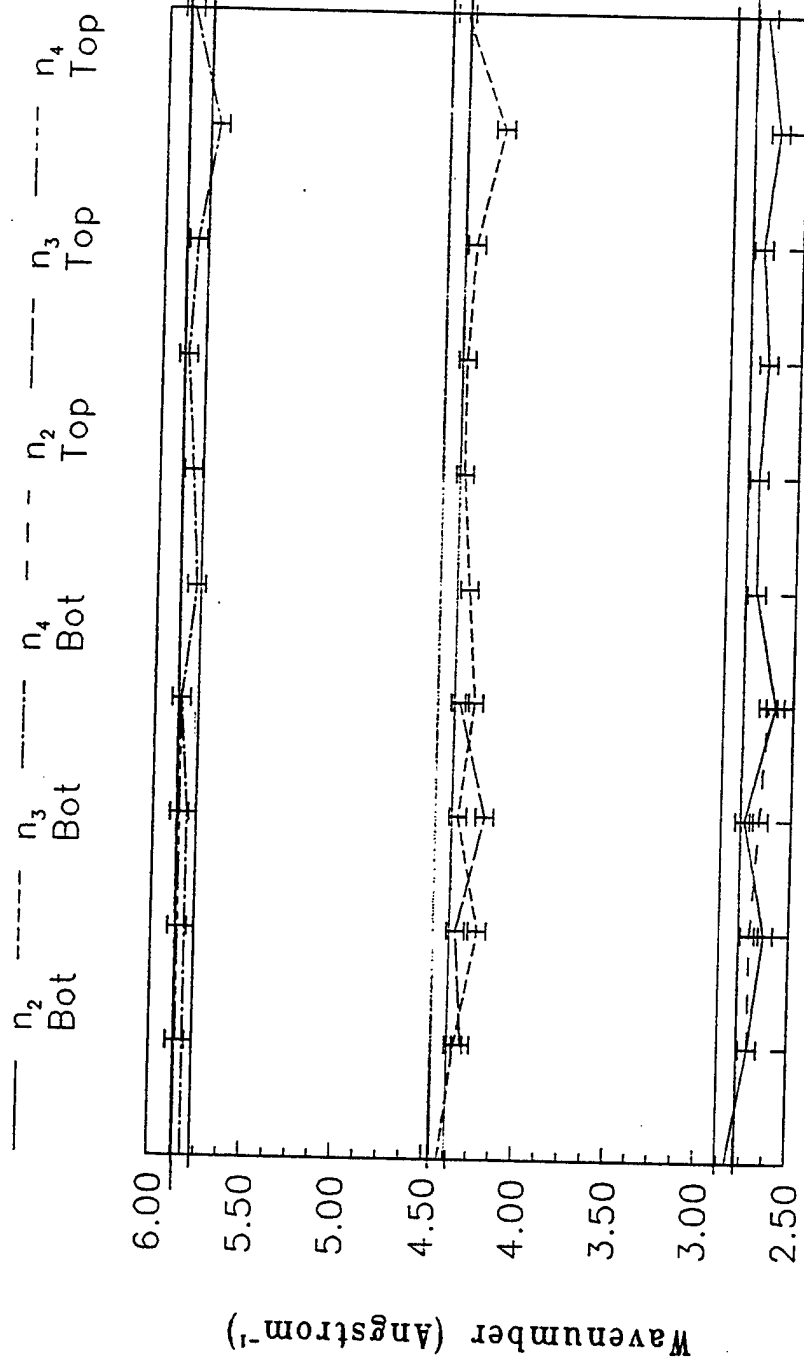


FIGURE 2

# Peak positions in k-space vs binder

$\rho_1$   $\rho_2$   $\rho_3$   $\rho_1$   $\rho_2$   $\rho_3$   
 B T B T B T

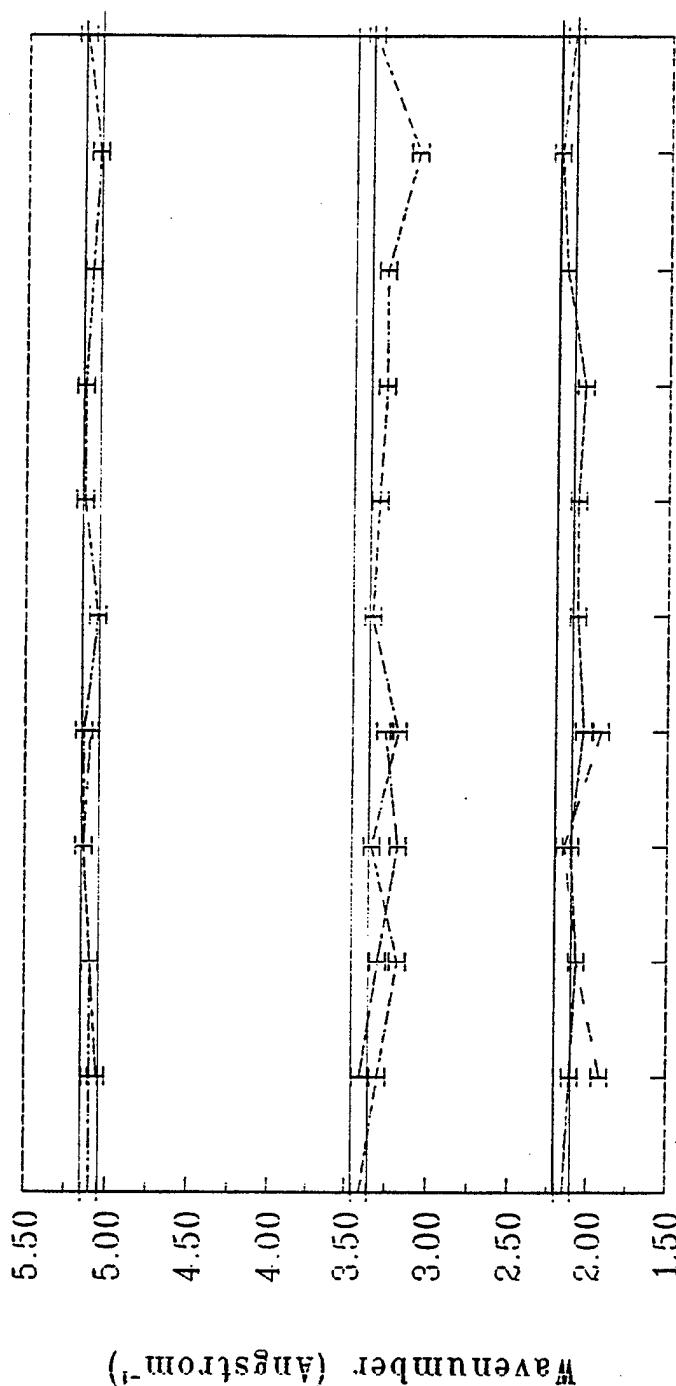


FIGURE 4



# Node positions in k-space vs TET coverage

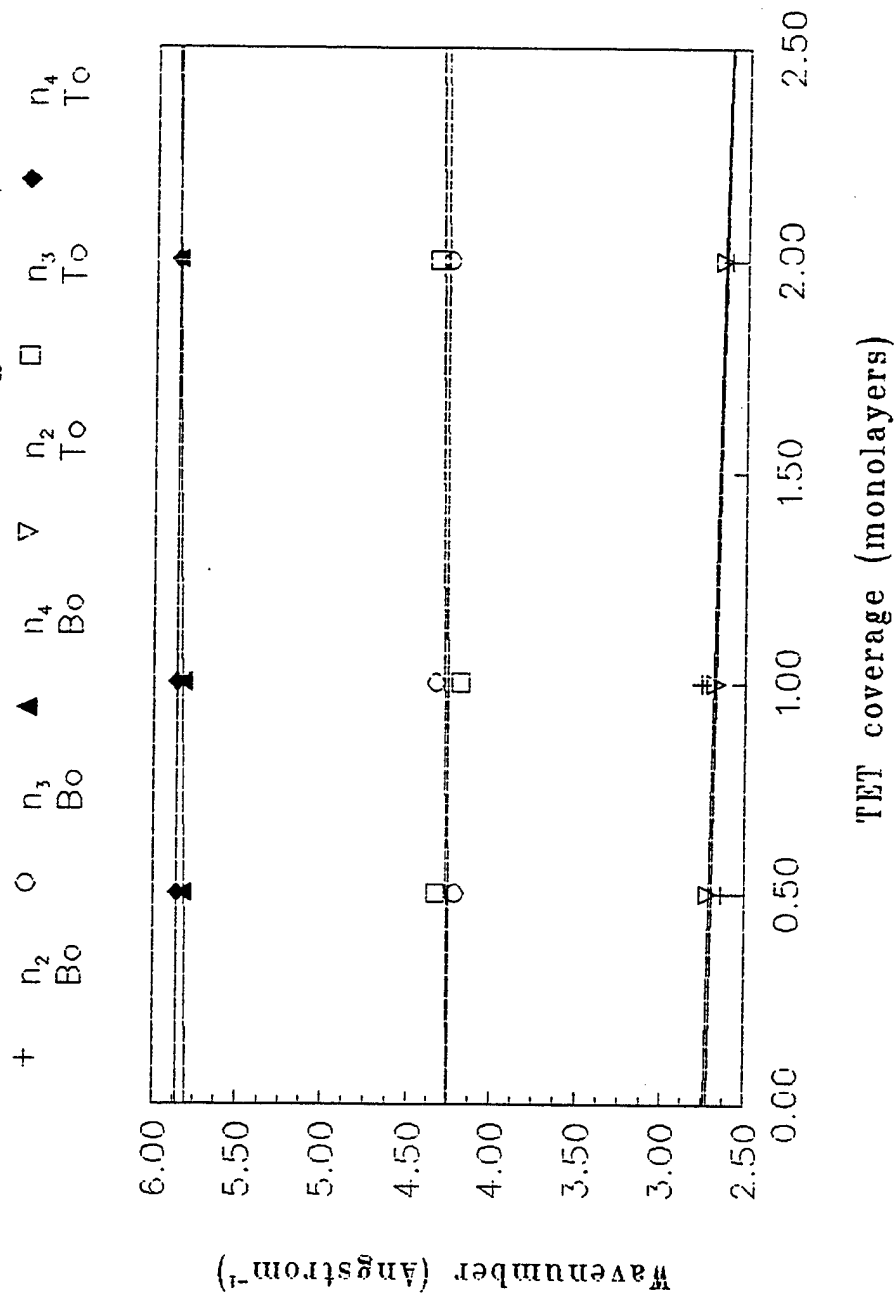


FIGURE 5

# Node positions in k-space vs TET coverage

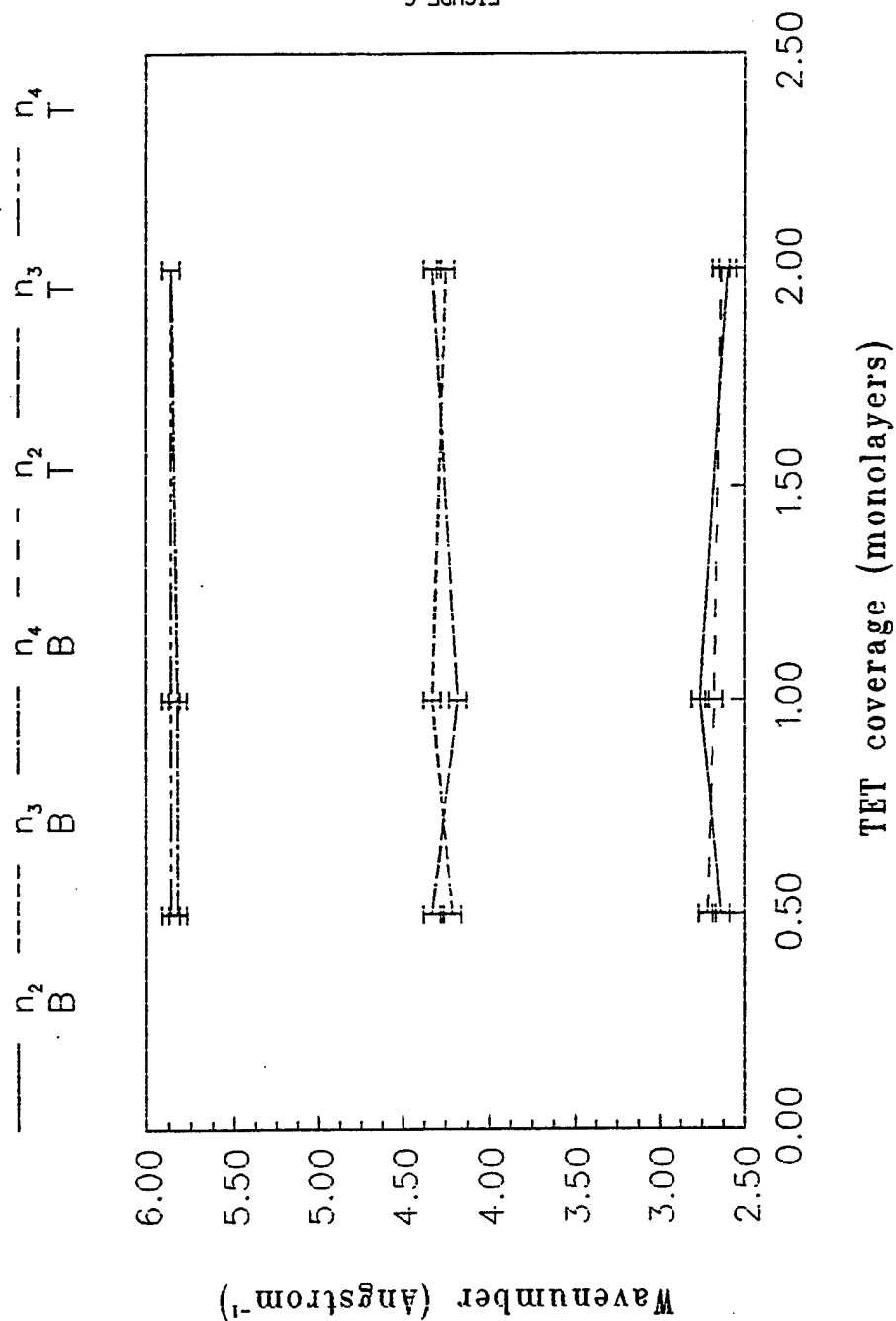


FIGURE 6

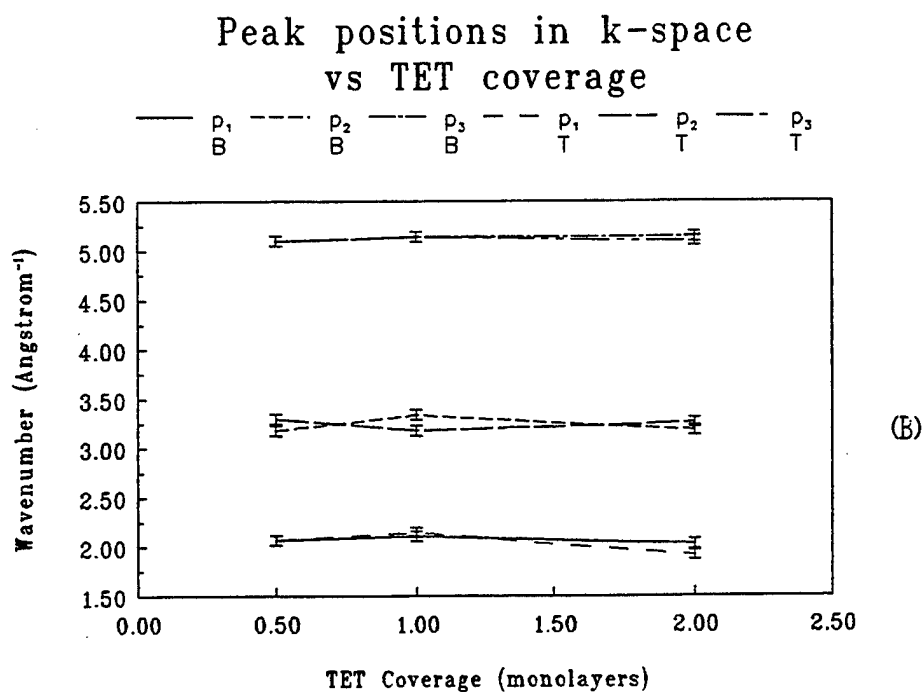
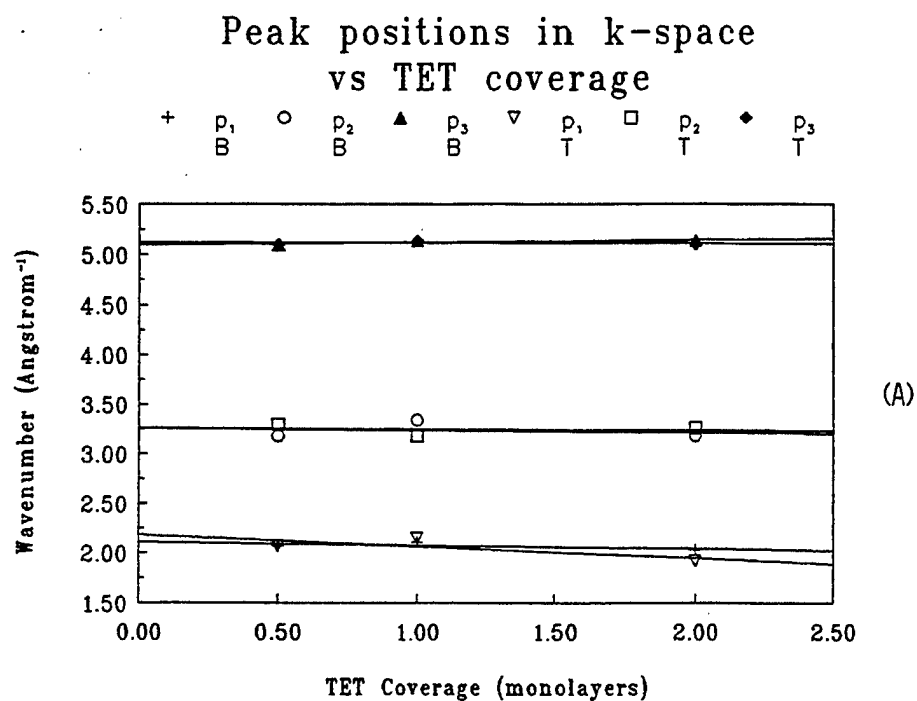


FIGURE 7

| File   | $n_1$<br>( $\text{\AA}^{-1}$ ) | $p_1$<br>( $\text{\AA}^{-1}$ ) | $n_2$<br>( $\text{\AA}^{-1}$ ) | $p_2$<br>( $\text{\AA}^{-1}$ ) | $n_3$<br>( $\text{\AA}^{-1}$ ) | $p_3$<br>( $\text{\AA}^{-1}$ ) | $n_4$<br>( $\text{\AA}^{-1}$ ) | $p_4$<br>( $\text{\AA}^{-1}$ ) | $n_5$<br>( $\text{\AA}^{-1}$ ) | $p_5$<br>( $\text{\AA}^{-1}$ ) |
|--------|--------------------------------|--------------------------------|--------------------------------|--------------------------------|--------------------------------|--------------------------------|--------------------------------|--------------------------------|--------------------------------|--------------------------------|
| AP4    | 1.68                           | 2.15                           | 2.83                           | 3.41                           | 4.41                           | 5.10                           | 5.82                           | 6.52                           | 7.44                           | 8.21                           |
| TOLT   | DNE                            | 1.92                           | 2.72                           | 3.41                           | 4.29                           | 5.06                           | 5.86                           | 6.60                           | 7.44                           | 8.13                           |
| TET5T2 | DNE                            | 2.07                           | 2.72                           | 3.30                           | 4.33                           | 5.10                           | 5.86                           | 6.52                           | 7.47                           | 8.17                           |
| TET1T  | DNE                            | 2.15                           | 2.68                           | 3.18                           | 4.18                           | 5.14                           | 5.86                           | 6.52                           | 7.32                           | 7.90                           |
| TET2T  | DNE                            | 1.92                           | 2.64                           | 3.26                           | 4.33                           | 5.10                           | 5.86                           | 6.52                           | 7.40                           | 8.13                           |
| 8782T  | DNE                            | 1.92                           | 2.64                           | 3.30                           | 4.37                           | 5.10                           | 5.82                           | 6.48                           | 7.36                           | 8.09                           |

TABLE 1

Node and peak positions in  $\text{\AA}^{-1}$  for experimental  $\chi$  spectra of filtered shells for binder on top. All files are .INF files. The symbol DNE means "Does Not Exist" and occurs when the low end of the data set did not contain a node due to truncation resulting from the inverse FT calculation.

|                     | p <sub>1</sub> | n <sub>2</sub> | p <sub>2</sub> | n <sub>3</sub> | p <sub>3</sub> | n <sub>4</sub> | p <sub>4</sub> | n <sub>5</sub> | p <sub>5</sub> |
|---------------------|----------------|----------------|----------------|----------------|----------------|----------------|----------------|----------------|----------------|
| a <sub>0 top</sub>  | 2.185          | 2.74           | 3.26           | 4.255          | 5.12           | 5.86           | 6.52           | 7.43           | 8.055          |
| a <sub>1 top</sub>  | -0.119         | -0.051         | -0.011         | 0.021          | -0.006         | 0              | 0              | -0.029         | 0.01           |
| Rval <sub>top</sub> | .7756          | .9820          | .1429          | .1890          | .1890          | 0              | 1              | .2907          | .0524          |
| a <sub>0 bot</sub>  | 2.11           | 2.72           | 3.26           | 4.25           | 5.1            | 5.8            | 6.46           | 7.34           | 8.05           |
| a <sub>1 bot</sub>  | -0.034         | -0.046         | -0.023         | 0.011          | 0.023          | 0.029          | 0.029          | 0.029          | 0.023          |
| Rval <sub>bot</sub> | .6547          | .4193          | .1890          | .1429          | .7559          | .9449          | .9449          | .9449          | .7559          |

Table 2. Linear least squares fit parameters for TET on AP Peak/node positions vs coverage in monolayers. If X is coverage and Y is feature position, the equation is  $Y = a_1X + a_0$ . Rval is the goodness of fit parameter.

## MARS MONTHLY REPORT - SEPTEMBER 1992

Thin Film / Surface Science Laboratory

Case Western Reserve University

### **I. Synchrotron Radiation Studies**

Contrary to prior understanding between this Laboratory and Brookhaven National Laboratory, we were notified in late August that we were scheduled to run on beamline X19-A 16-19 September. Since no experiment was planned due to not expecting beamtime, we deferred to the Winter and submitted a continuation proposal to the National Synchrotron Light Source User Administration, a copy of which is enclosed. Also, no beam time was requested for X11-A in the Fall. As such we anticipate scheduling on that line in the Winter period.

### **II. Computer Developments**

During this past month, the Thin Films / Surface Science Laboratory obtained a new TOPSS 486DX/33 MHz computer to be used for calculations and modelling of molecular structure. As a result there are a small number of new items and procedures to learn, as well as getting the machine running optimally. A new software package was installed on the machine called ALCHEMY II, by Tripos Associates, Inc.. This program can calculate molecular structures by a free-energy minimization procedure based on user-furnished constraints. It is presently in the learning and evaluation stages in this Laboratory.

### **III. Publication**

Two of us (GAD, RWH) submitted a paper to *Journal of Vacuum Science and Technology* in which this AFOSR funding is acknowledged. A copy of the manuscript (as submitted) is enclosed with this report.

## MARS MONTHLY REPORT - OCTOBER 1992

Thin Film / Surface Science Laboratory

Case Western Reserve University

### AP/Binders Modelling

In order to interpret the XAFS data for the Cl-edge in AP, it is necessary to understand 1) the chemical nature of the additives (binders or bonding agents) and 2) proposed reactions of those agents with AP. The first of these approaches was pursued this month, along with one possible reaction discussed earlier<sup>1</sup>.

During the past month, the Laboratory obtained a copy, for official use only, of *Principles of Solid Propellant Development*, by Adolph E. Oberth (Chemical Propulsion Information Agency, 1987) during an informal visit by GAD to OLAC PL, Edwards AFB. That volume, along with the several library references listed below, was used to collect chemical information on each of the materials under consideration. The translation of the codes (from earlier data files and reports) for each oxidizer/binder/bonding agent are:

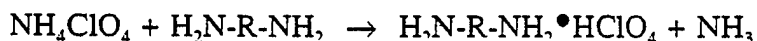
|               |   |
|---------------|---|
| AP:           | Ammonium Perchlorate  |
| TET: TETA.    | Triethylene Tetramine <sup>2</sup> or 1,2-ethanediamine, N, N'-bis(2-aminoethyl)-<br>[112-24-3] <sup>3</sup>  |
| DER: DER-332. | Bisphenyl A diglycidyl ether <sup>2</sup> or Oxirane, 2,2'-[(methylethylidene) bis(4,1-phenyleneoxymethylene)]bis-, homopolymer [25085-99-8] <sup>3</sup> |
| TOL:          | Toluene or benzene, methyl- [108-88-3] <sup>3</sup>   |
| HTP: HTPB.    | HydroxyTerminated PolyButadiene <sup>2</sup>  |



- 752: HX-752. Isophthaloyl bis(2-methylethylemeimide)<sup>2</sup> or Aziridine, 1,1'-(1,3-phenylenedicarbonyl) bis[2-methyl- [7652-64-4]<sup>3</sup>
- 879: HX-879. TEPAN<sup>2</sup>. Chemical name unknown. "The product of the partial reaction of tetraethylenepentamine with acrylonitrile."<sup>2</sup>
- 878: HX-878. TEPANOL<sup>2</sup>. Chemical name unknown. "The product of the partial reaction of TEPAN with glycidol. This reaction places a dihydroxypropyl group on the polyamine<sup>2</sup>.

Aziridine is also known as ethyleneimine and oxirane as ethylene oxide. Structural diagrams of each of these molecules are shown below for those molecules whose structures have been found.

A possible surface reaction linking AP to the polymer is given below as<sup>1</sup>



#### REFERENCES

- 1) J. J. Rusek, MARS program presentation viewgraph. 1991
- 2) A. E. Oberth, *Principles of Solid Propellant Development* (Chemical Propulsion Information Agency, 1987).
- 3) Chemical Abstracts Index.

#### Additional Bibliography

R. F. Gould, ed., *Propellants Manufacture, Hazards, and Testing* (ACS Publications, 1967).

G. P. Sutton, *Rocket Propulsion Elements: An Introduction to the Engineering of Rockets*, 6th edition (Wiley-Interscience, 1992).

## MARS MONTHLY REPORT - NOVEMBER 1992

Thin Film / Surface Science Laboratory

Case Western Reserve University

### **AP/Binders Modelling**

As an aide to the interpretation of the XAFS data for the Cl-edge in AP, we plotted the first shell fit results reported in tabular form earlier<sup>1</sup> as shell radius vs binder. These results are shown in Figures 1 and 2. The horizontal line in each of these figures corresponds to the model distance of 1.455 Å for untreated AP. The error bars on these plots are the  $\pm$  values from the nonlinear least squares fit.

In the case of toluene (TOLx) it is found that the Cl-O distance is contracted wrt pure AP and does not seem to depend on which side of the pellet faced the incident beam, from Figure 1. For TET, there does seem to be an increase of the Cl-O distance as a function of TET coverage when the TET is on top from 0.5 to 2 monolayers coverage. A possible increase in Cl-O distance for TET on the bottom is seen in Figure 1, and in each of these cases other than TET2B the shell distance is less than the reference.

In Figures 3 and 4, first Cl-O shell radius was plotted vs coverage for TETnT and TETnB, respectively, for the data reported in Figure 1. Over the range studied, the following numerical relationships were determined by a least squares fit. However, the small number of data points on the graph should encourage using caution in their interpretation. The linear least squares fit (LSF) results are:

---

<sup>1</sup>TFSSL (CWRU), MARS Monthly Report, June, 1992, Tables I and II.

TETnT: 3 param:  $R(\text{\AA}) = 1.435 + 0.00914\theta$ ; Rval = 0.899

4 param:  $R(\text{\AA}) = 1.430 + 0.01014\theta$ ; Rval = 0.997

TETnB: 3 param:  $R(\text{\AA}) = 1.444 + 0.00657\theta$ ; Rval = 0.911

4 param:  $R(\text{\AA}) = 1.443 + 0.00643\theta$ ; Rval = 0.945

where R is the first shell radius in  $\text{\AA}$  and  $\theta$  is the binder coverage in monolayers.

Turning our attention to Figure 2, the first shell radius data for 878nT seems to peak at 1 ML coverage and then return to the value that it had for 0.5 ML. In Figure 5 the linear LSF for those data are plotted as in Figures 3 and 4. The fit results for HX-878nT are:

878nT: 3 param:  $R(\text{\AA}) = 1.452 - 0.00157\theta$ ; Rval = 0.134

4 param:  $R(\text{\AA}) = 1.448 + 0.000571\theta$ ; Rval = 0.0524 .

The first CL-O shell radius for 7521B shows the greatest difference wrt AP of the entire range of additives studied. It is hoped that acquisition of proposed chemical reactions from researchers at the Phillips Laboratory, EAFB, will help in the final, physical interpretation of these results.

# First Shell Cl-O distance Binders on AP

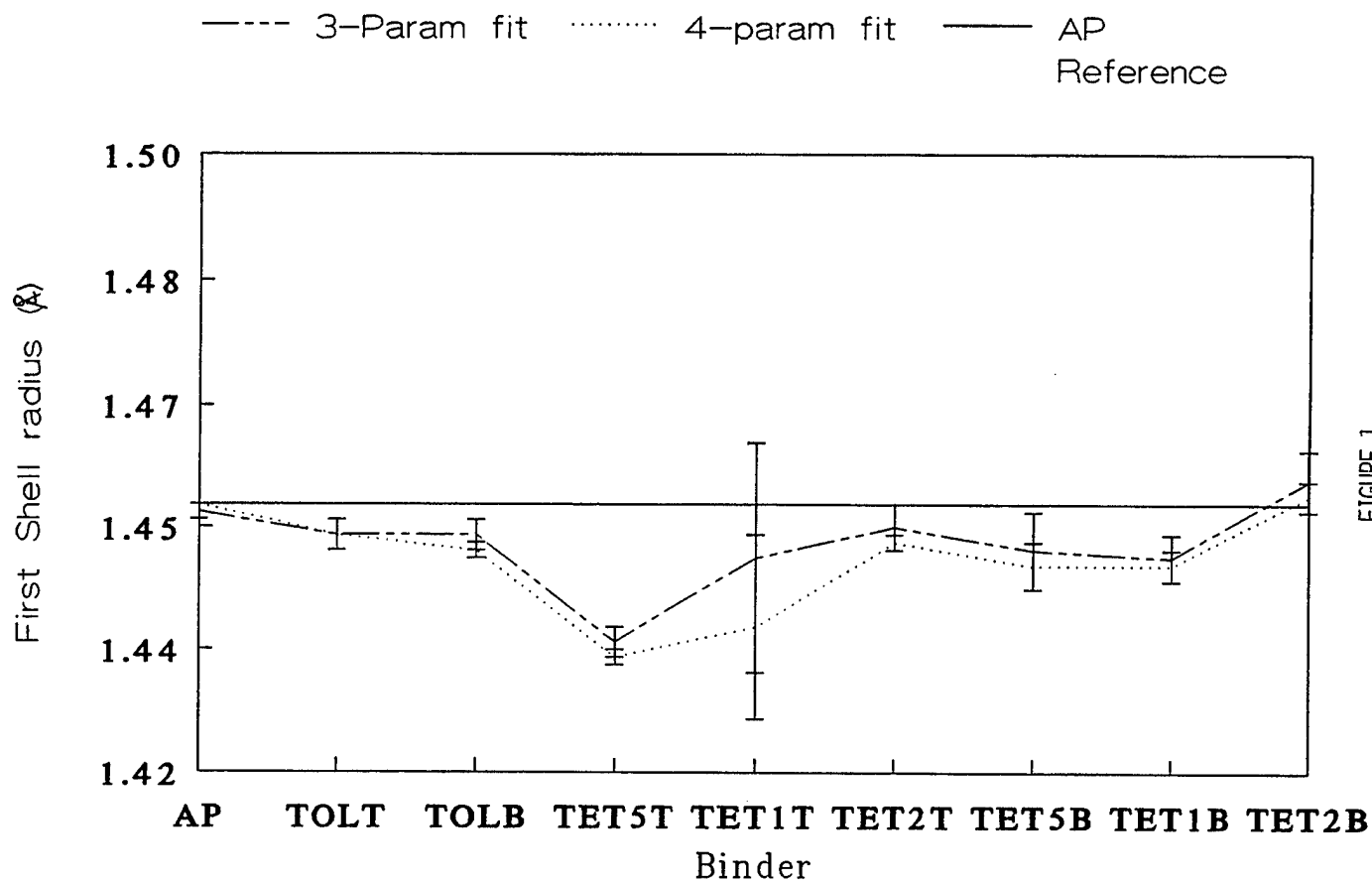


FIGURE 1

# First Shell Cl-O distance Binders on AP

----- 3-Param fit      ..... 4-param fit      — AP      Reference

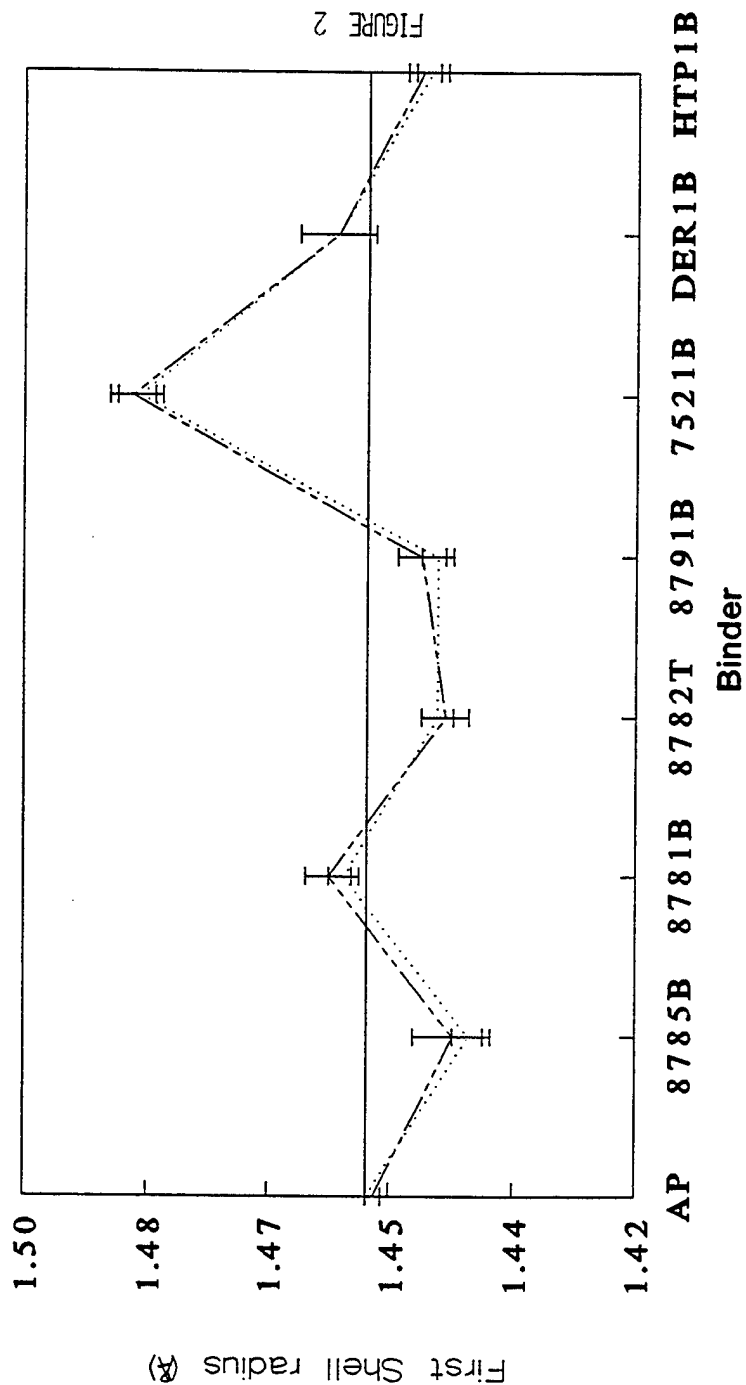


FIGURE 2

# First Shell Cl-O distance vs TET coverage + 3-Param fit TETnT ○ 4-param fit TETnT

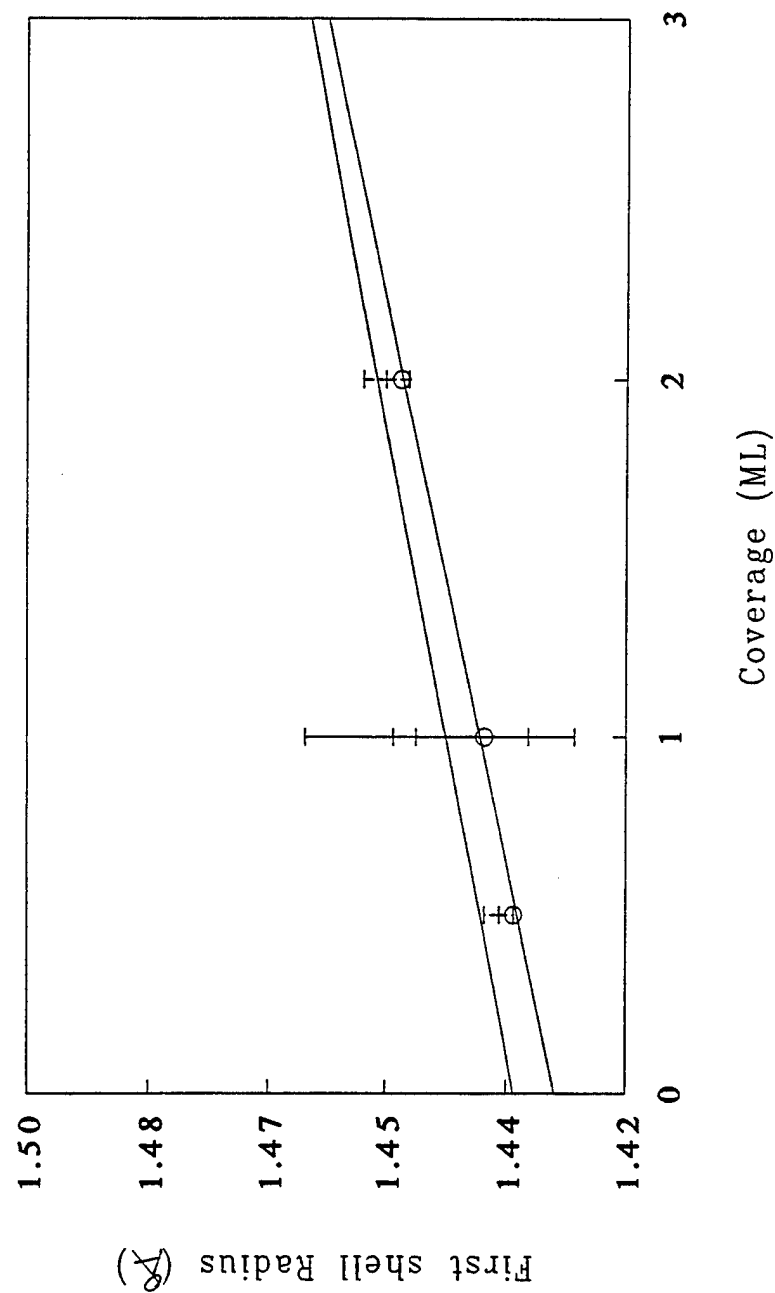


FIGURE 3

# First Shell Cl-0 distance vs TET coverage ▲ 3-param fit TETnB      ▽ 4-param fit TETnB

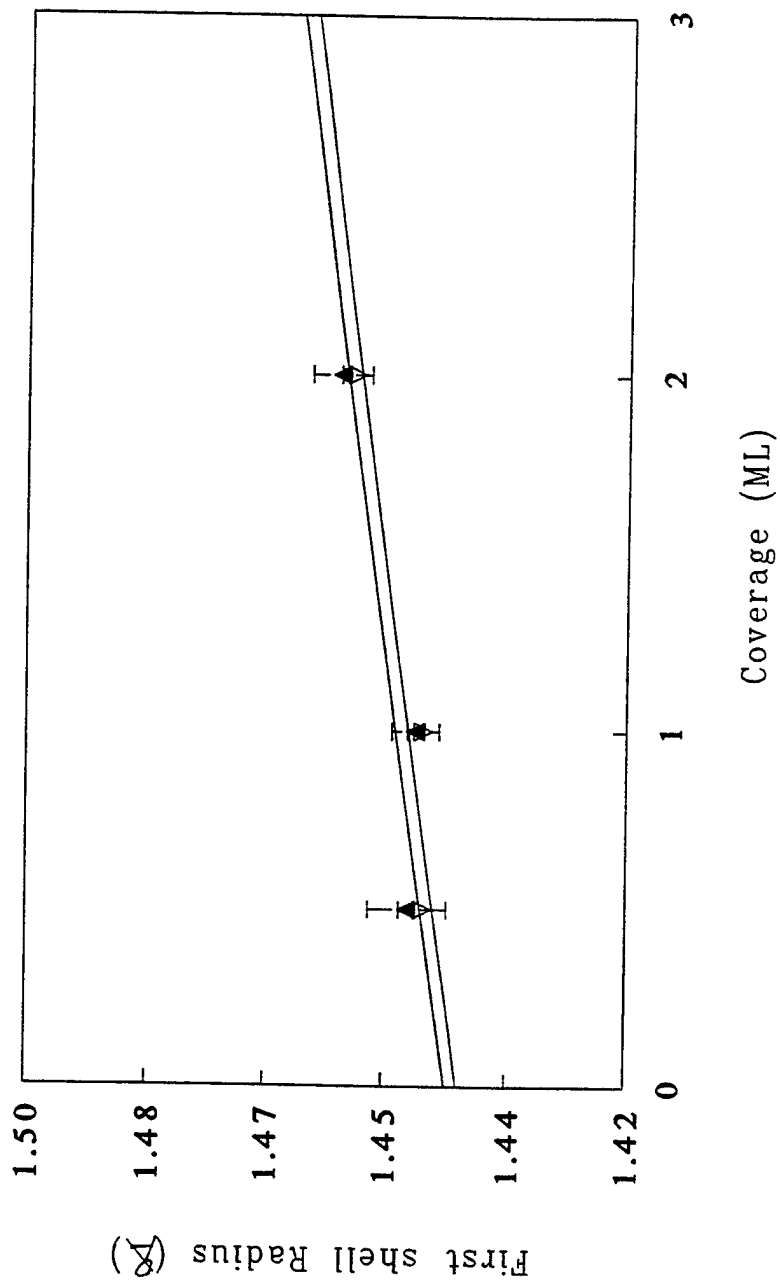


FIGURE 4

# First Shell Cl-0 distance vs coverage HX-878 on bottom

+ 3-Param fit      ○ 4-param fit

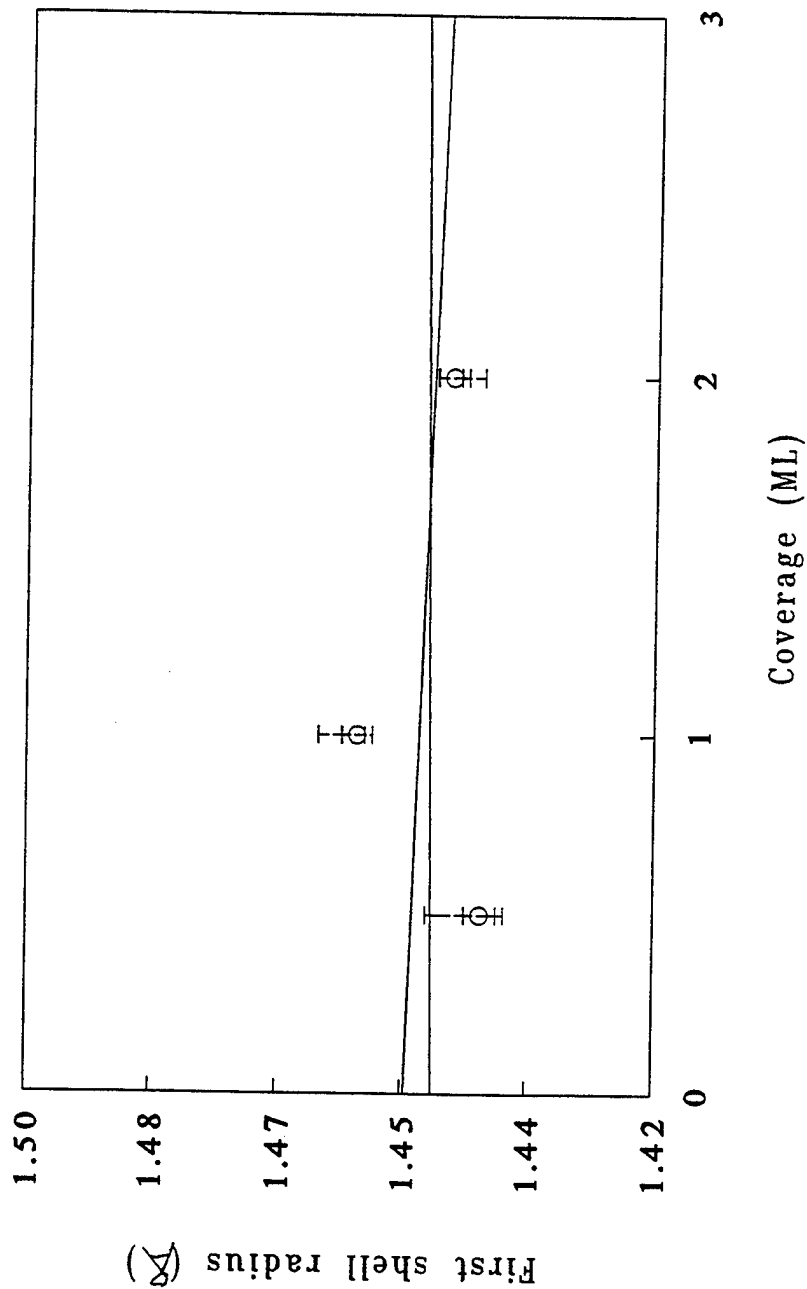


FIGURE 5



MARS MONTHLY REPORT - DECEMBER 1992

Thin Films / Surface Science Laboratory  
Case Western reserve University

X-ray Absorption Spectroscopy

This month, further refinements of the XAFS data from the binders on AP were considered from the viewpoint of modelling the surface reactions. Consultations with Phillips Lab personnel were undertaken in the latter part of the month to determine the direction of next approach in the solutions to these problems.

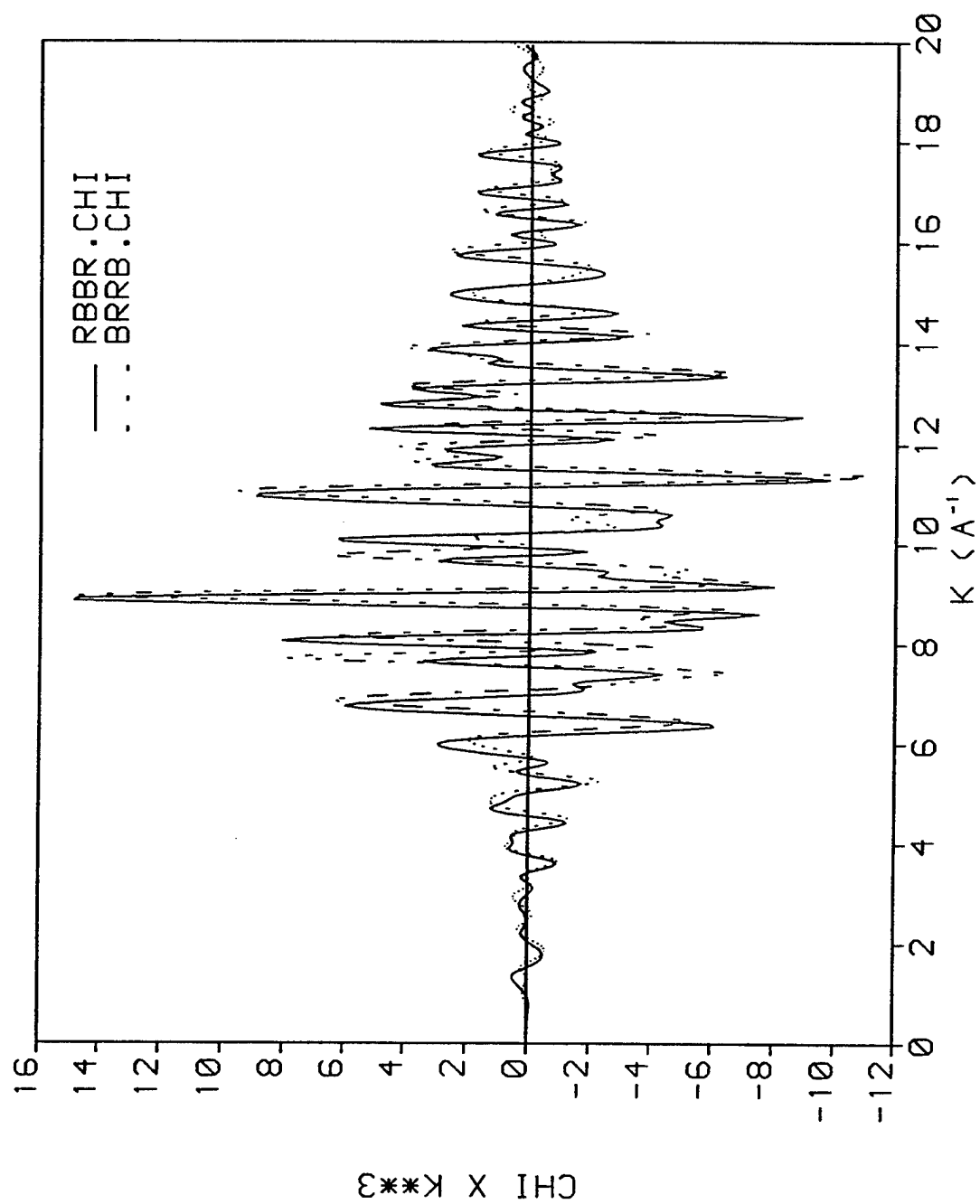
As it was anticipated that Guy DeRose would be taking a position at Wright Laboratory, much of the month was spent training Chris Zorman in the tasks that Guy performed on this project. This included preparing all the experimental gear for future EXAFS runs at BNL and training Chris as a system manager on the VAX 3100.

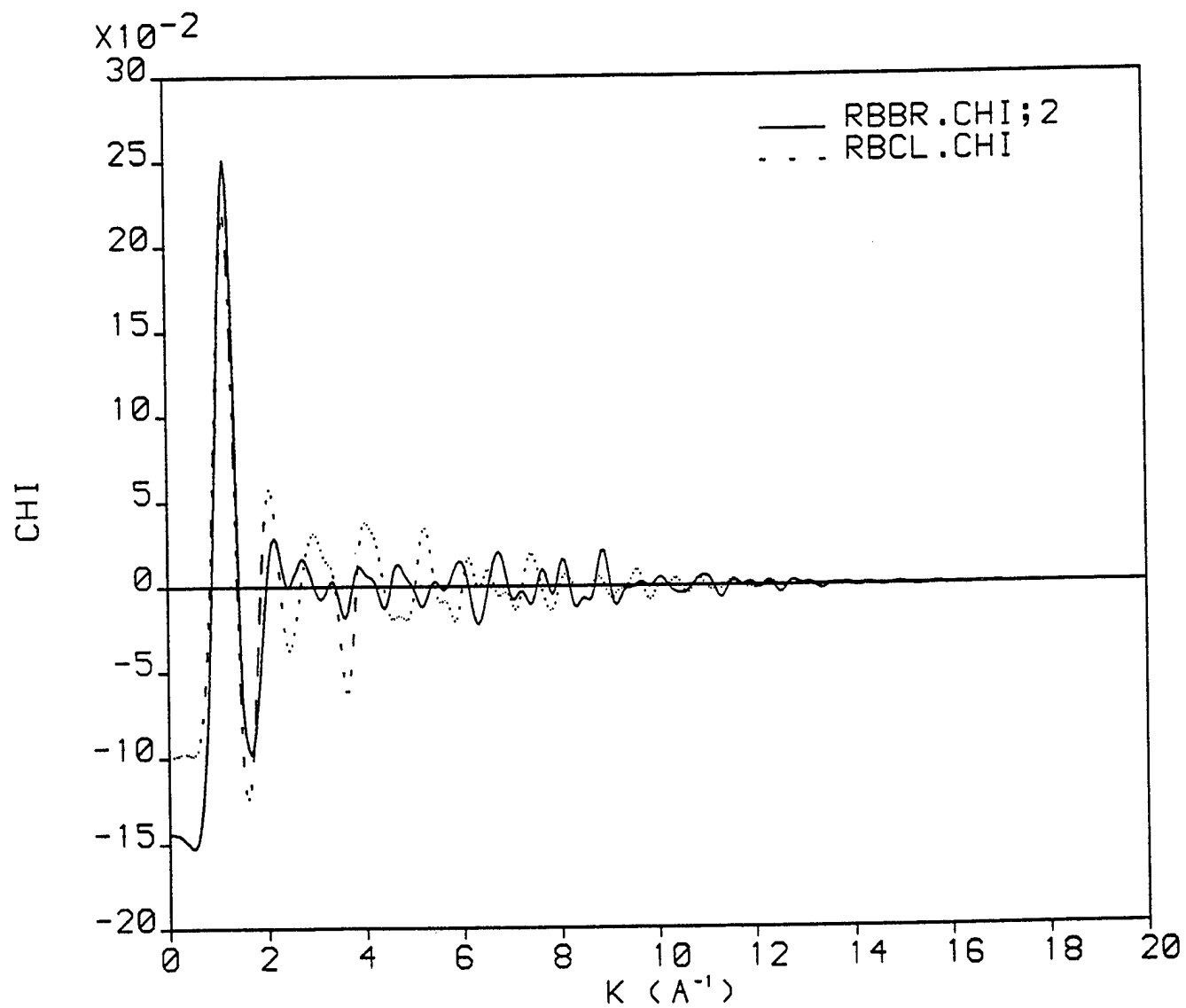
## MARS MONTHLY REPORT - January 1993

Thin Films / Surface Science Laboratory  
Case Western reserve University

### X-ray Absorption Spectroscopy

This month was spent in preparation for two upcoming runs in February at the NSLS. The first run will be on beamline X-11A from 1-4 February and the second from 19-22 February on beamline X-19A. The CWRU TFSSL will collaborate with Phillips Laboratory personnel and Wright Laboratory contract personnel on the synchrotron data collection. The trip to beamline X-11A will concentrate on Br and Rb edge work as it relates to the AP project. Cl edge work will be undertaken at beamline X19A. For both trips EAFB personnel will prepare the samples while TFSSL personnel will provide the experimental equipment and computational facilities. The TFSSL will serve as the contact point between the project and Brookhaven. At the request of the Phillips Laboratory contract manager FEEF calculations of EXAFS for RbBr at both the Rb and Br K-edges were done on the TFSSL VAXstation by TFSSL personnel. Plots of those chi spectra are shown in Figures 1 and 2.





## INTERIM REPORT

### 1) STM/AFM

This research was divided roughly equally in terms of scanning tunneling, microscopy, (STM) and atomic force microscopy, (AFM) and synchrotron radiation work for the development of a new detector. We describe our progress for the two projects in that order.

Based on the preliminary work carried out while at Edwards Air Force Base during the summer of 1990, and based in part on the mechanical property measurements made at CWRU, we have proposed that the thin film mechanics of diamond like carbon films is highly dependent on the stress and the development of cracks in the film. Some cracks were observable optically, and it was decided to investigate the structure using an STM. Tunneling microscopy (STM) was chosen not because it is necessarily the best technique, but that it was available and promising with the new apparatus then available at EAFB. The continuation of work initiated in this way formed the basis for the present effort. Fortunately for this problem, atomic resolution is not required as the cracks are expected to range in width up to about 1 micron.

The progress on this portion of the work has been "spotty". Initial commitments for the update of an existing STM were withdrawn on the CWRU campus, and as a result, that portion was not finished. In September, 1992 it became obvious that there was a possibility of getting a combined research quality STM/AFM instrument and electronics from Park Instrument Corporation with the major

instrumental funding coming from NSF as part of the diamond and diamond like films project. This funding although following a successful May, 1992 review, still has not reached the CWRU campus. In October, 1992 Professor J.A. Mann, chairman of the department of Chemical Engineering and Professor R.W. Hoffman, in Physics made a trip to Purdue University to see the new Park instrument in operation. It's purchase was recommended after the visit. The addition of the AFM would allow the examination of surfaces routinely Several insulating DLC films were taken with us which showed a well resolved structure. With the samples chosen and the areas examined, no cracks were observed.

In order to provide hard copy from the electronic information, the purchase of a Mitsubishi hard copier was approved. The initial discussions called for immediate delivery upon receipt of the PO with both sufficient time and emphasis to allow the completion of the RDL effort on schedule.

Unfortunately the NSF equipment funding was further delayed thus not received; hence the PO could not be issued on time and this state is still being resolved by re-examining the entire bidding process with updated information.

Both Professors Hoffman and Mann are committed to finishing the project and we expect completion approximately three months after the delivery of the instrument. The samples must be redone, but AFM will now be available.

## **2) SYNCHROTRON RADIATION EXPERIMENTS**

### **A. X-RAY FOCUSING SPECTROGRAPH AT BEAMLINE X-11A**

#### **1. Introduction**

Development and testing of a mica crystal x-ray focussing spectrograph continued during a trip to Brookhaven's Nation Synchrotron Light Source from 30 January to 4 February 1993. The testing was done on beamline X-11A at energies around the florescence edge of iron. The objectives of the trip were twofold. First we wanted to determine the alignability of the mica crystal. Secondly we wanted to test the apparatus in an actual EXAFS experiment. Figures 1 and 2 show the geometry of the prototype system used.

## 2. Alignment Study

Figure 1 shows the setup for the crystal alignment study. The x-ray beam was directed at the mica crystal, incident at the Bragg angle, and photographic film was placed in the path of the diffracted beam. In order to determine the angular tolerance of the Bragg condition, the crystal was rotated through the Bragg rotation. It was determined that the alignment tolerance is about plus or minus 20 minutes of an arc.

## 3. EXAFS Data

Figure 2 shows the setup for collecting EXAFS data. The photographic film was replaced by an ionization chamber and the x-ray energy was ramped from 6883eV in order to scan across the iron florescence energy (7112eV). Figure 3 shows data collected to check the alignment of the crystal and detector. The x-rays were

incident directly on the mica. The Bragg angle was set at 20.24 deg. which corresponds to an energy of 7183eV. Clearly there is a prominent peak at about 7183eV. The background signal is an iron florescence signal, probably from a stainless steel screw used to hold the mica in place. Because of space and time limitations, we were not able to completely eliminate this background. We were not able to eliminate the line of sight between the screw and the detector face.

Figures 4 and 5 are EXAFS data collected from an Fe foil. The foil was placed in the beam path before the mica crystal. Again there is a peak at 7183eV, as one would expect. This time the background is primarily from the sample itself. We were unable to eliminate the line of sight. The smaller peak in figure 5 is probably due to another Bragg diffraction event.

#### 4. Future Work

Further attempts to perfect this device are in order.

On this trial, we also collected over 130 other unrelated scans. For the spectrograph, we demonstrated that radiation from a fluorescing sample can be diffracted into an ionization chamber. Alignment is tedious at the present time, but with assistance from a laser it may be easier. In order to eliminate background problems, the line of sight problem must be eliminated. This is best done by collimating the ionization detector face.

#### B. X-RAY FOCUSING SPECTROGRAPH AT BEAMLINE X-19A



## 1. Introduction

Testing of the mica crystal x-ray focussing spectrograph progressed during a trip to BNL's NSLS from 18 February to 23 February 1993. The beamline used was X-19A and the energies under study were the fluorescence edges of Ti and Cl. The objective was to see if the mica spectrograph would function in proper capacity in the soft x-ray region of the Cl fluorescence edge. The mica crystal spectrograph has the most potential in this energy regime, since good filters for low energy x-rays are lacking.

## 2. Setup

The experimental geometry was similar to that of the X-11A run. However, the Cl. edge work required that the entire apparatus be enclosed in a He flushed plexiglass box. The box was necessary because the absorption length of Cl fluorescence edge x-rays in air is much shorter than our prototype setup. By enclosing the spectrograph in a He environment, we were able to use the apparatus without noticing a significant attenuation of the x-ray beam. The box was equipped with the necessary feedthroughs to operate an ionization chamber as the main detector for Bragg scattered operators to change setup parameters without opening the lid. Typical He flush times were about 15 minutes.

## 3. Data Collection

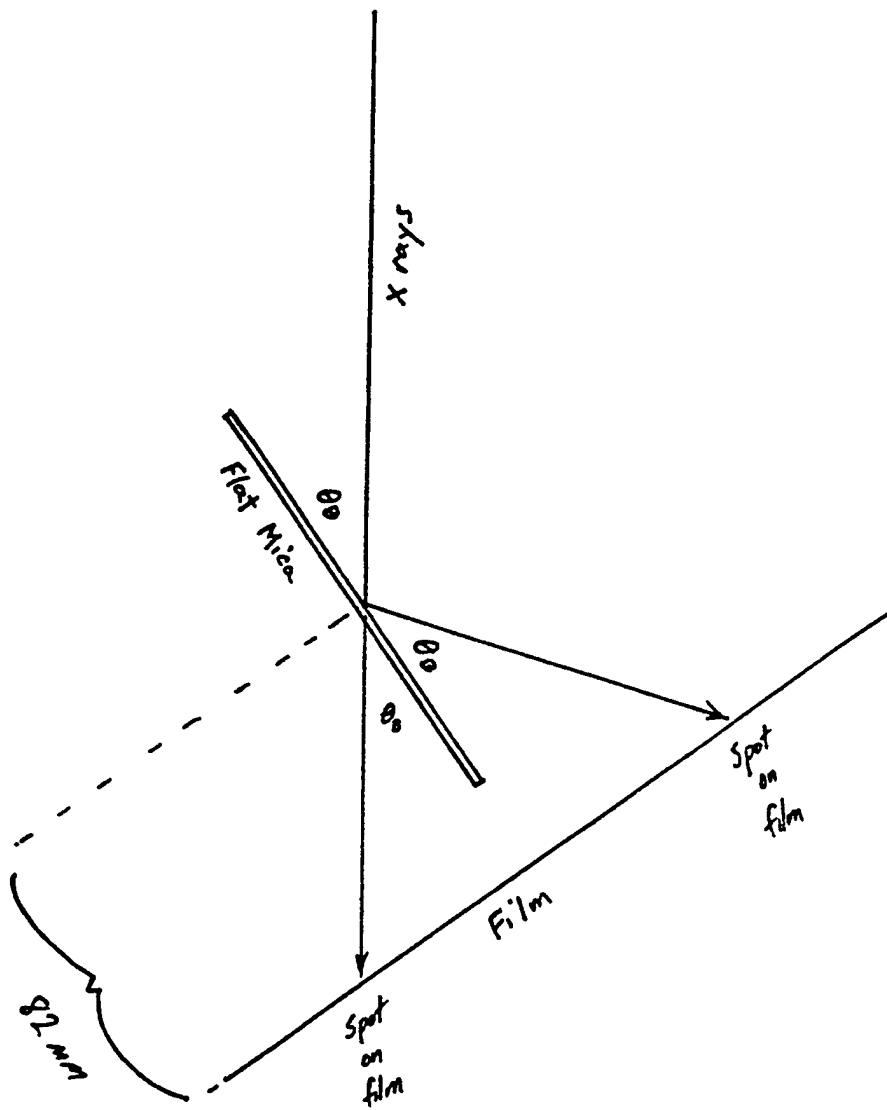
Figure 6 shows a typical energy scan at the Cl edge. The data shows that once a Bragg condition is met, a significant signal is detected by the ionization chamber. The background is quite low, as one would expect. The incident x-rays were not quite striking the mica at the Bragg angle for Cl fluorescence radiation, as seen in the energy shift of the Bragg peak. The second peak (at slightly lower energy) is not understood at this time.

Figure 7 shows data collected over a broad energy range. the diffraction peaks are clearly seen, as is an EXAFS spectrum. This spectrum is the fluorescence spectrum from potassium in the mica crystal.

#### 4. Future Work

The next step in developing the mica spectrograph for use with low energy x-rays is to reduce the overall size of the apparatus. This must be done in order to make the device useful with existing fluorescence detector rigs. Also the geometry must be adjusted in order to Bragg diffract fluorescence radiation from the incident beam side of the sample. This eliminates any sample thickness problems. Sensitivity issues ( Ion chamber vs electron yield) must also be explored. We expect these to be solved by the next X-11 Beam time in June.

FIGURE 1



MICA CRYSTAL ALIGNMENT GEOMETRY

FIGURE 2

DETECTOR/MICA CRYSTAL ALIGNMENT GEOMETRY

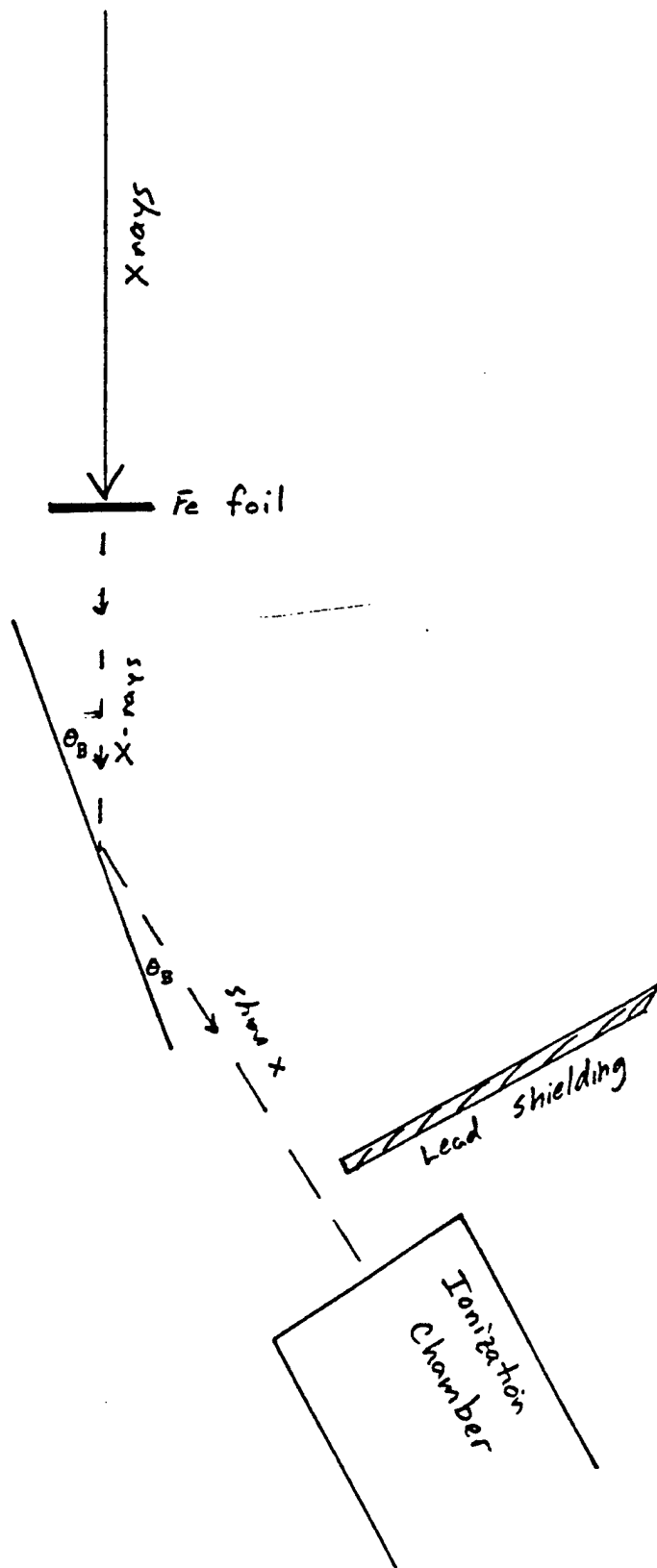


FIGURE 3

DATA COLLECTED TO CHECK ALINGMENT OF CRYSTAL AND DETECTOR

MICFLT.004

04-Feb-93 09:53:48

FLAT MICA CRYSTAL TEST WITH LYTLE DET. TO TUNE PEAK PB SHIEL

E0= 7183.0

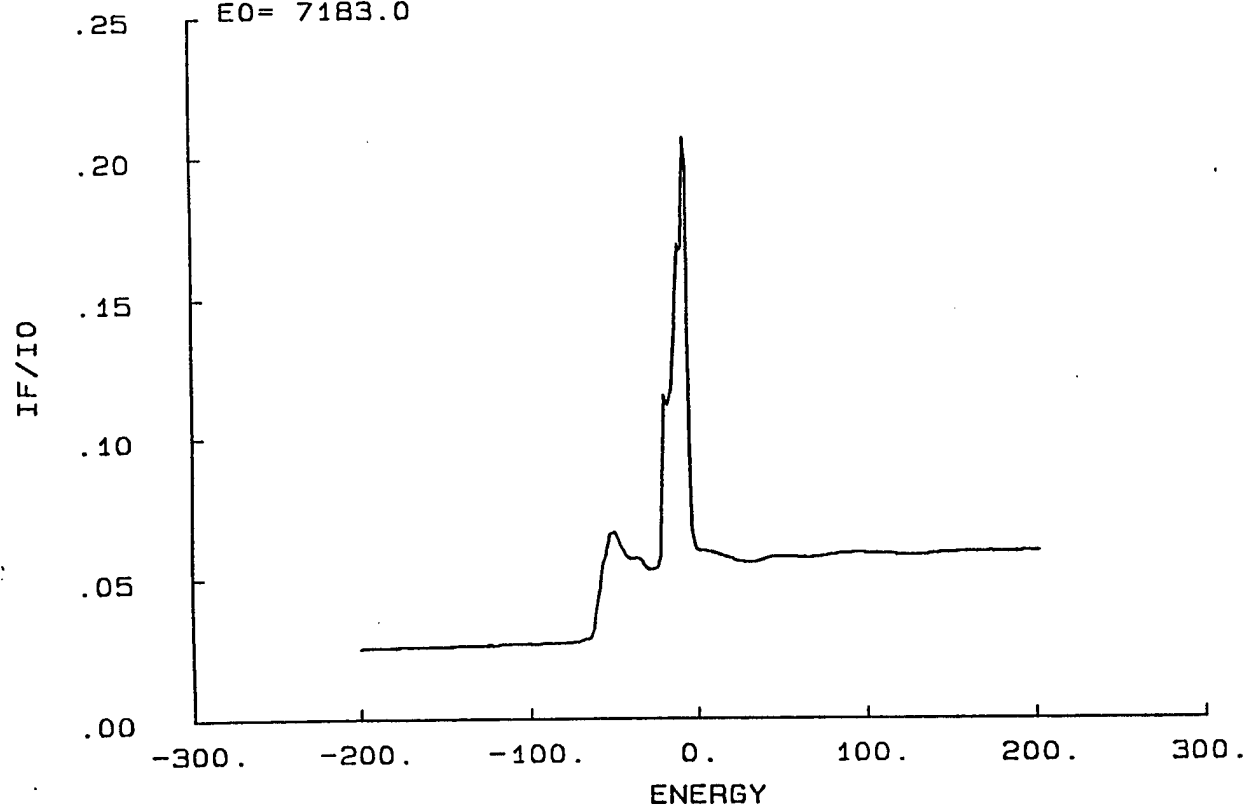


FIGURE 4

EXAFS DATA COLLECTED FROM AN Fe FOIL USING THE MICA CRYSTAL

FEMIC.002

04-Feb-93 10:52:45

FE FOIL WITH FLAT MICA DISPERSION TEST

E0 = 7112.0

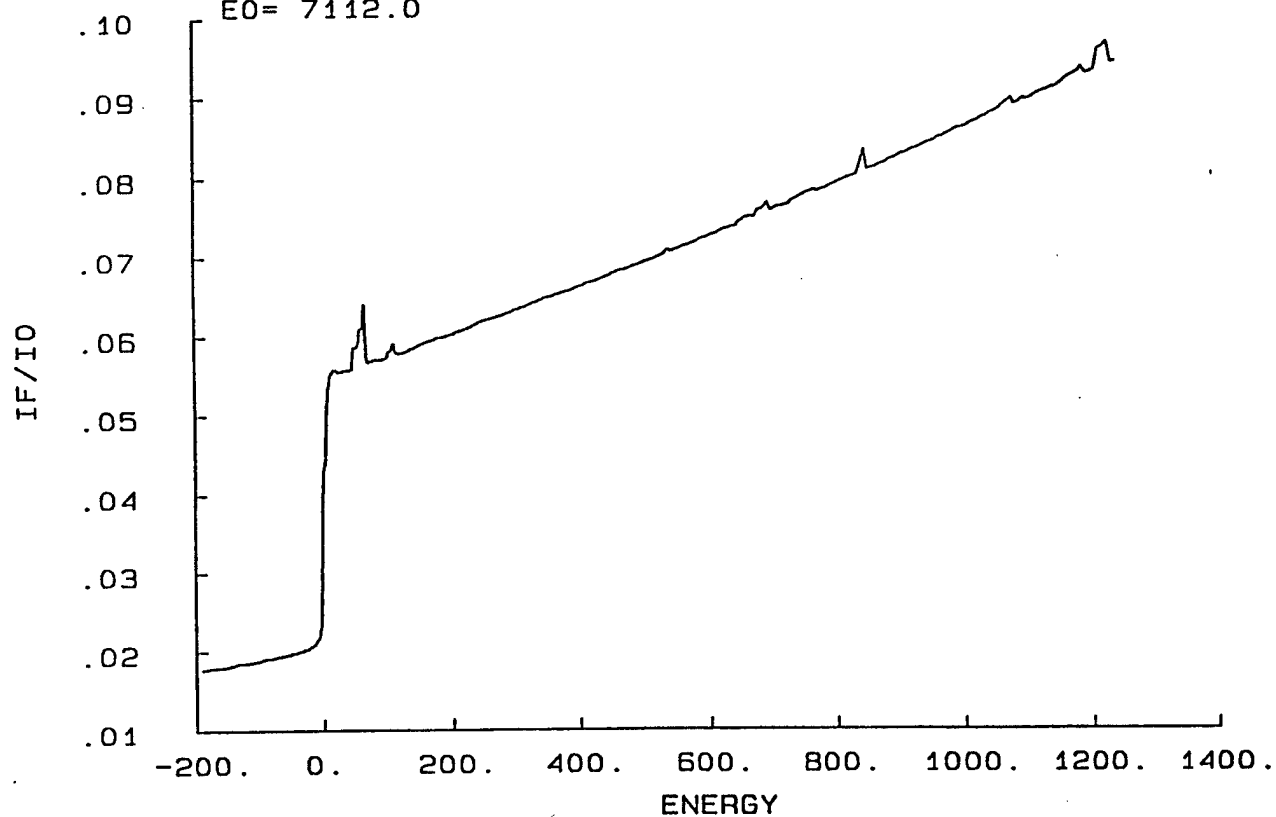


FIGURE 5

BLOWUP OF FIGURE 4 ABOUT THE DIFFRACTION PEAKS

FEMIC.002

04-Feb-93 10:52:45

FE FOIL WITH FLAT MICA DISPERSION TEST

E0= 7112.0

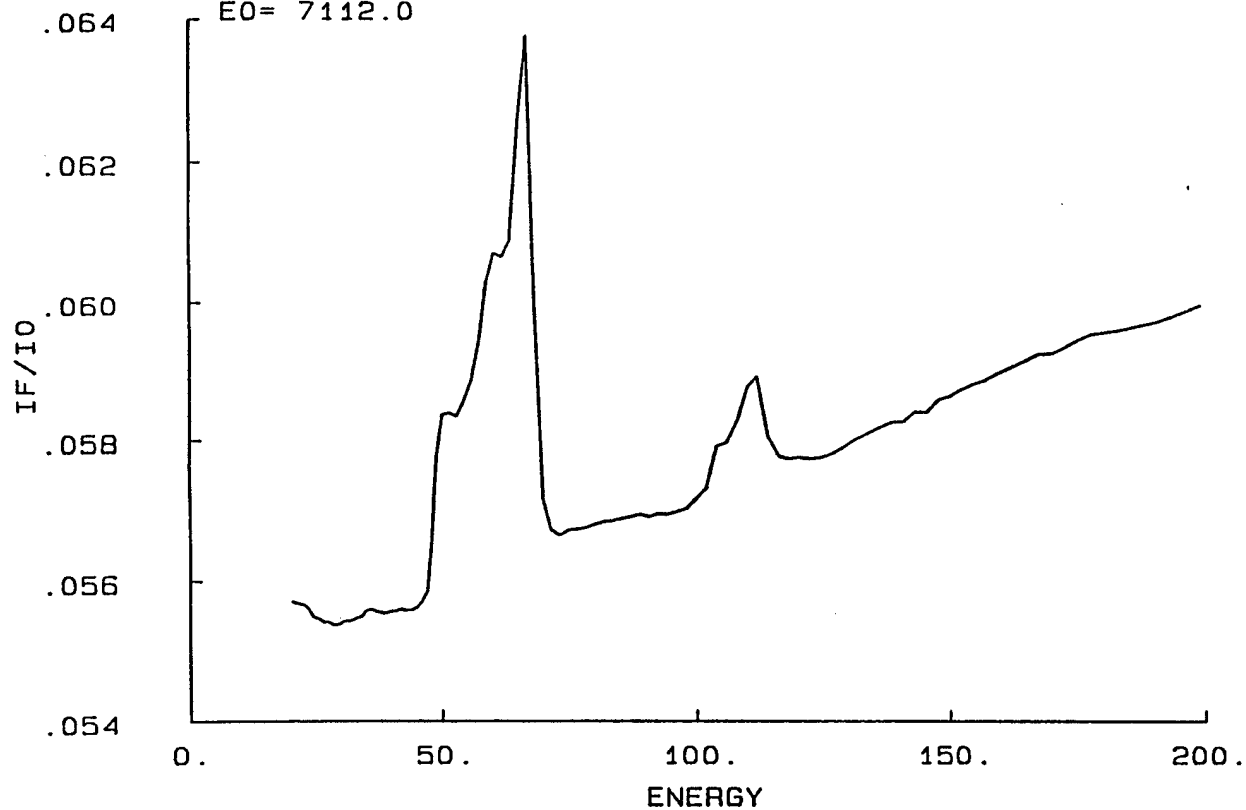


FIGURE 6

DIFFRACTION PEAK FROM THE MICA AT THE Cl K ALPHA 1 ENERGY

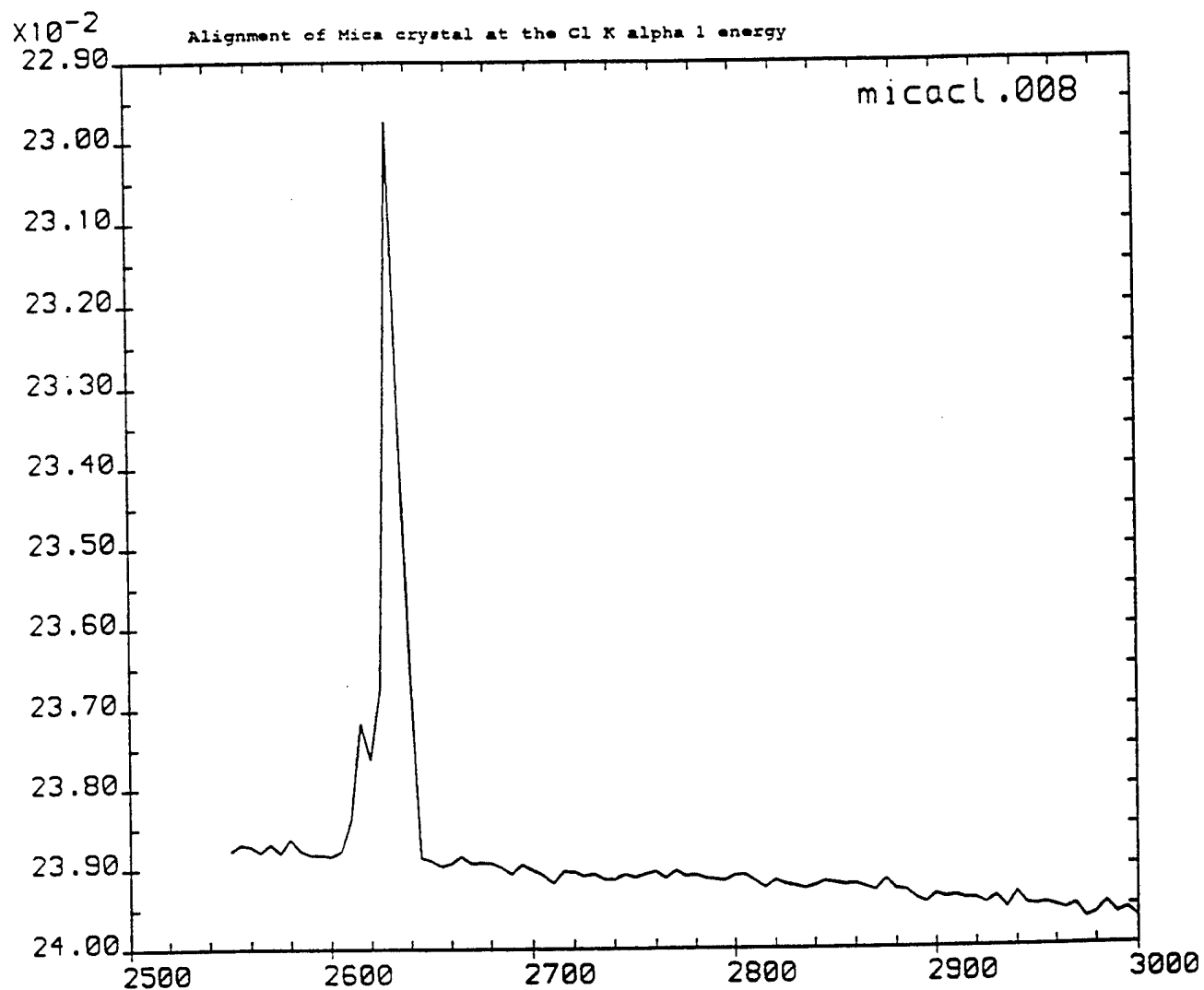
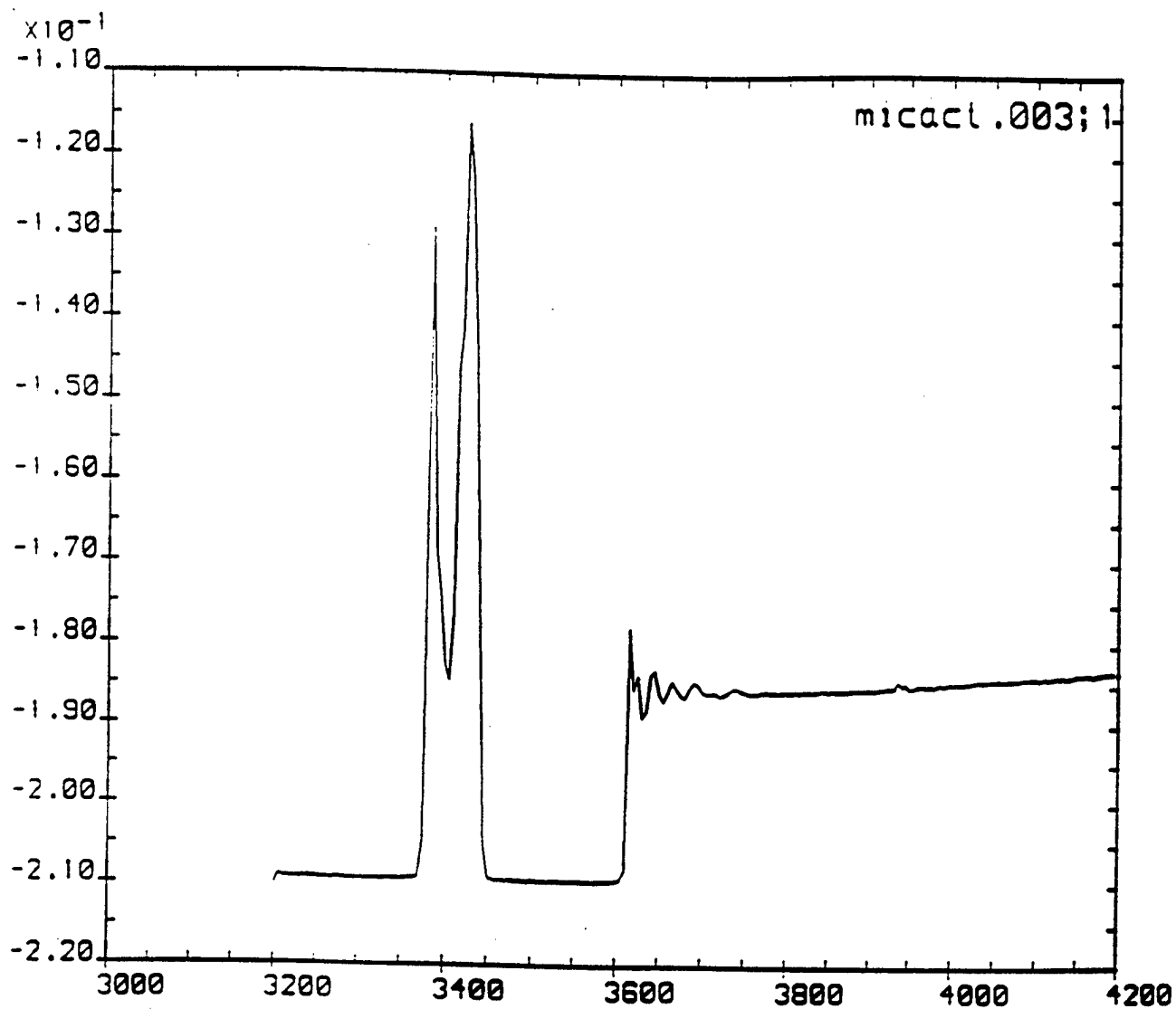




FIGURE 7

DIFFRACTION PEAKS NEAR THE C1 EDGE AND POTASSIUM EXAFS FROM THE MICA



MARS Monthly Report - April/May 1993

Thin Films / Surface Science Laboratory  
Case Western Reserve University

### X-Ray Focussing Spectrograph

The past two months were spent primarily preparing the bent mica x-ray focussing spectrograph for the next series of tests at NSLS. Much of the time was spent doing an extensive literature search on the subject. While no-one has used this apparatus to do fluorescence EXAFS at low energy, some have used a similar device to focus x-rays onto a sample at higher energies. The main difference between the bulk of the work and ours is that we are trying to focus x-rays emanating from a sample while they are focussing x-rays from an intense source onto a sample. We believe that our burden is much tougher because of the intensity differences.

Another big difference is the type of crystal used. Our crystal is a "run of the mill" sheet of mica. Most others use an oriented Si or other type crystal. The big difference is in the bending radius. The Si type focusser requires an elaborate bending mechanism. Also the Si crystal cannot be bent very much, thus leaving the focal point prohibitively far from the sample. Mica, on the other hand, is easy to bend and not very expensive. The sample to focal point distance is about 15 cm which easily fits on the average beamline hutch table.

In preparation for the next NSLS run, we are going to do some

preliminary testing at CWRU, using the Physics Department's X-ray source. It functions best at higher energies than we would like to use but it allows us to check the geometry and test new ideas before we get to Brookhaven.

**APPENDIX C**  
**Dr. Lieb's Reports**

## Abstract

Title: Mechanism of Adhesion in Solid Propellents

The essential ingredients for a solid rocket booster are an oxidizer and a fuel. In order to mix these two, intermediating material(s) is needed (the binder). The fuel is a nonpolar material (such as aluminium) and the oxidizer is a very polar ammonium perchlorate. One of the functions of the binder is to produce an interface which will disperse the oxidizer uniformly within the fuel. When the binder does not produce proper adhesion with the oxidizer, there results either poor propulsion or detonation. There have been some failures in this area in the recent past and therefore a more in depth understanding of the mechanism of adhesion of the binder to the ammonium perchlorate surface is becoming a more pressing issue. The goal of this proposal is to theoretically model the surface interactions between binder and oxidizer for the purposes of understanding conditions necessary for good adhesion and suggesting alterations in the binder to make it more effective. There are experimental aspects to this project that are in direct support of uncovering the intermolecular forces needed to develop the theoretical modeling and serve as references by which the theory can be compared.

## Introduction

An overview of the technical and practical aspects of solid propellant development is given by Adolf E. Oberth<sup>1</sup>. Among the many technical difficulties encountered in the development of solid rocket propellants is that of void formation about the ammonium perchlorate grains. Void formation or tearing is brought about by hoop stresses which develop around solid inclusions in the elastomer phase. The geometry of the inclusion dictates the hoop stress (which is greater than the applied stress). Spherical particles are associated with the lowest hoop stresses and needle-like particles are associated with the highest. In the case of spherical particles the stress is greatest in the surrounding binder phase where void formation initially occurs. As stress continues to be applied, the voids reach the surface of the particle and eventually debonding occurs. Once debonding has occurred the load is no longer supported by the particle which places a higher load on nearby particles which increases their propensity to debond as well. The voids create an increase in the burning surface around ammonium perchlorate crystals which in turn produces a larger quantity of gas. The gas can not escape out the exhaust nozzle which means a larger internal pressure. This increased internal pressure enhances the burning rate which translates into a self enhancing feed-back loop (i.e., detonation). One way to avoid the formation of voids around ammonium perchlorate (AP) is to understand the mechanism of adhesion between binder and the AP and thereby avoid debonding even in the face of tearing in the elastomer or binder phase.

In order to effect an analysis of this problem which will lead to better ways of preparing the propellant mixture, a detailed molecular interpretation of adhesion seems to be the appropriate approach to this problem. In the past decade, there has been the development of more reliably accurate ab initio calculations to deal with inter and intramolecular potential parameters. This type of calculation can be used to develop necessary potential parameters by investigating small, model systems. Along with this development at the ab initio level, there has been a development of the application of Newtonian mechanics to the macromolecular problem. This approach is based on the Quantum Mechanical potentials found within and between molecules, but does not involve the proper quantization of

---

<sup>1</sup>Adolf E. Oberth, Principles of Solid Propellant Development, Chemical Propulsion Information Agency Publication 469, John Hopkins University (Sept. 1987).

states found in "real" molecular systems. This approach allows the solution of energy minimum searches or time evolution of a large molecular system via classical mechanics which could not be even contemplated in a complete Quantum Mechanical framework. The description of this approach for biological systems is described in volume 71 of *Advances in Chemical Physics*<sup>2</sup>

## Theory

The theoretical development will proceed along two paths; a quantum mechanical investigation and a statistical thermodynamical perspective. The first path is that of studying model systems in order to get the internal rotational energies as well as other vibrational force constants. These can be computed from small model systems such as methanol and allyl alcohol. There already have been some calculations of partial charges and harmonic force constants for perchlorate anion that were obtained by the use of the CADPAC program at the Kirtland Air Force Base supercomputer. Table I presents a summary of some of these results.

Table I

Summary of CADPAC SCF geometry optimization calculation of  $\text{ClO}_4^-$  using 631G\* basis plus an f orbital basis<sup>(a)</sup> on Cl

| Atomic Populations             |  | charge  |
|--------------------------------|--|---|
| Cl                             | 15.41143                                     | +1.58857  |
| O                              | 8.64714                                      | -0.64714  |
| O                              | 8.64714                                      | -0.64714  |
| O                              | 8.64714                                      | -0.64714  |
| O                              | 8.64714                                      | -0.64714  |
| Molecular Geometry (Angstroms) |  |   |
| atom pair                      | calculated                                   | experimental <sup>(b)</sup>                                   |
| Cl--O                          | 1.439  | 1.445   |
| O--O                           | 2.350  | 2.360   |
| Harmonic Frequencies           |  |   |
| mode                           | calculated<br>frequency ( $\text{cm}^{-1}$ ) | experimental <sup>(c)</sup><br>frequency ( $\text{cm}^{-1}$ ) |
| A <sub>1</sub>                 | 1033   | 935   |
| E                              | 494  | 462   |
| T <sub>2</sub>                 | 1247   | 1102  |
| T <sub>2</sub>                 | 692  | 628   |

<sup>2</sup>C. L. Brooks III, M. Karplus and B. M. Pettitt, Proteins: A Theoretical Perspective of Dynamics, Structure and Thermodynamics, Adv. Chem. Phys., Vol LXXI, John Wiley and Sons, New York (1988).

(a) E. D. Simandiras, J. E. Rice, T. J. Lee, R. D. Amos and N. C. Handy, "On the necessity of f Basis Functions for Bending Frequencies", *J. Chem. Phys.* **88**, 3187-95 (1988).

(b) the averaged Cl--O and O--O bond distances from H. G. Smith and H. A. Levy, "Neutron Diffraction Study of Ammonium Perchlorate", *Acta Cryst.* **15**, 1201-4 (1962).

(c) T. Chakraborty, S. S. Khatri and A. L. Verma, "Temperature- Dependent Raman Study of Ammonium Perchlorate Single Crystals: The Orientational Dynamics of the  $\text{NH}_4^+$  Ions and Phase Transitions", *J. Chem. Phys.* **84**, 7018-27 (1986).

In addition to the individual molecular species calculations, one can simulate the interaction of a molecular species with an ionic surface through the use of the LATTICE directive found in the CADPAC package. It would be useful to get an estimate of the relative interaction energy differences between the polar and nonpolar portions of the binder with the ionic surface of ammonium perchlorate. A semiempirical package referred to as MOPAC is also available at the Kirtland supercomputer which will allow somewhat larger problems to be addressed. This package also includes a directive referred to as "sparkles" which mimics an ionic lattice with which one can have a polymer interact as well. The parametrization of the matrix elements for different atoms and their interactions considerably reduces the computational effort necessary for ab initio calculations (i.e., CADPAC) allowing the attack of larger molecular systems. In order to visualize the binding configurations that are being sought, figure 1 below gives a rough pictorialization of an example of one polymer adhering to the surface of the ammonium perchlorate and then another picture with several polymers near one another.

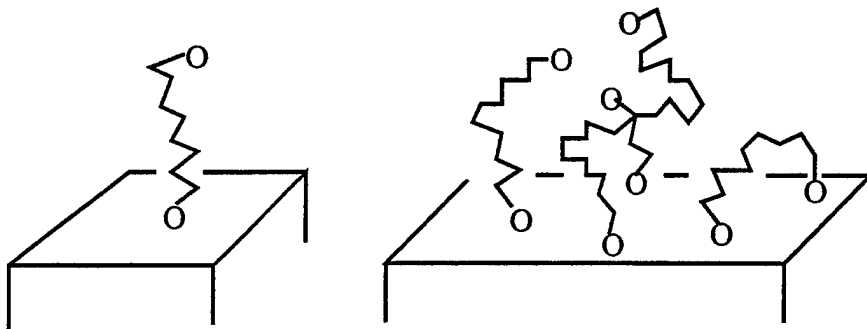


Figure 1. A characterization of one and several polymers adhering to a surface

Beyond the ab initio calculation it is essential to use the above results to investigate the large scale interactions. That is, one can use the small system results as input into molecular mechanics programs



such as CHARMM<sup>3</sup> or Polymer Dynamics<sup>4</sup>. These types of programs are based on classical mechanics and therefore requires considerably less intensive computational schemes than a quantum mechanical calculation. The use of the classical dynamics approach in the investigation of macromolecular systems by finding molecular configurational energy minima of a given large molecule, and developing a time evolving picture of an ensemble of interacting molecular species has been well established in biopolymer systems. Its use here is obvious. Using the graphics capability found in workstations which support CHARMM, one can generate movies of the molecular motions of a system as it develops. This type of representation produces a quicker understanding of processes which are going on within the Newtonian mechanics framework.

Later investigations will include statistical-thermodynamic approaches such as found in the research of A. Balazs, et. al.<sup>5</sup>, or I. Szleifer, A. Ben-Shaul and W. M. Gelbart<sup>6</sup> or H. Takeuchi<sup>7</sup>. These approaches deal with polymers attaching to surfaces and interacting with one another, as well as, how they distribute themselves along the surface to which they are attaching. For instance, if the polymer has two "sticky" ends it can attach one or both ends to the surface. In addition, the remaining portion of the polymer may stand away from the surface or form loops that touch the surface. The analysis of the configurations available to the surfactant (binder) and an idea of how those configurations distribute themselves over the surface will better our understanding of adhesion of the binder to the ammonium perchlorate surface. The Takeuchi reference (5) deals more with small molecule diffusion through polymers and how chain length affects the diffusion process. There is a question of humidity and its effect on binding, so it would seem natural to determine the

---

<sup>3</sup> B. R. Brooks, R. E. Bruccoleri, B.D. Olafson, D.J. States, S. Swaminathan and M. Karplus, "CHARMM: A Program for Macromolecular Energy, Minimization and Dynamics Calculations", J. Comp. Chem. **4**, 187-217 (1983).

<sup>4</sup> Comparable dynamics program to CHARMM supplied by Polygen Corporation.

<sup>5</sup>(a) A. C. Balazs and J. Y. Hu, "Effects of Surfactant Concentration on Polymer-Surfactant Interactions in Dilute Solutions: A Computer Model", Langmuir **5**, 1230-34 (1989).

(b) A. C. Balazs, C. Anderson and M. Muthukumar, "A Computer Simulation for the Aggregation of Associating Polymers", Macro. **20**, 1999-2003 (1987).

<sup>6</sup> I. Szleifer, A. Ben-Shaul and W. M. Gelbart, "Chain Packing Statistics and Thermodynamics of Amphiphile Monolayers", J. Chem. Phys. **94**, 5081-89 (1990).

<sup>7</sup> H. Takeuchi, "Molecular Dynamics Simulations of Diffusion of Small Molecules in Polymers: Effect of Chain Length" J. Chem. Phys. **93**, 4490-91 (1990).

rate of diffusion of the water molecules through the binder and determine its relative ability to displace the binder from the ionic surface causing a loss in adhesion. Based on these considerations, one could modify the structure of the binder to enhance its properties with the configurational considerations and humidity conditions in mind.

## Experimental

Along with a theoretical development, there needs to be some experimental backup work. Although experimental work is not the major thrust of this proposal, there is spectroscopic equipment available to this end. In our department there is a dispersive infrared spectrometer (Perkin Elmer 283B) with a computer interface which makes analysis of band shape and relative band areas rather routine. Also, there is a BioRad FTIR (Fourier Transform Infra-Red) which is also computer interfaced and because of the time resolved technique involved, is extremely sensitive. There is as part of its software package a band deconvoluting routine which can be used to resolve overlapped peaks and thereby attain relative amounts of a functional group which are in several different chemical environments. The infrared studies can be carried out to get an idea of the effect of binding on the O-H stretch of the binder. One technique that could be tried with the dispersive IR, is to use the polybutadiene binder as a nujol mull agent because of its high viscosity and prepare different amounts of ammonium perchlorate ground up in the binder. There are temperature controlled Infrasil cells in which solutions of the alcohols can be prepared to ascertain the amount of hydrogen bonding that occurs between alcohol molecules as a function of mole fraction of alcohol and as a function of temperature. The temperature study will allow the evaluation of the enthalpy of hydrogen-bond formation for dimer, trimer and tetramer formation. Alternatively, a ZnSe rod which is used with the FTIR can be coated with ammonium perchlorate and then solutions of varying percentages of the binder in a nonpolar solvent can be introduced into the "boat" that holds the ZnSe rod. The rod is transparent to the infrared and has the infrared radiation enter into the rod on the one end and then the light is internally reflected to give a spectrum of the material(s) at the surface of the rod. Obviously there are many technical details to attend to in order to get the results desired. These types of experiments are excellent for an undergraduate researcher to become involved because they are capable of understanding the scope of the general problem and the

details of these specific experimental problems by the time they are juniors and seniors in college (the typical maturity of our undergraduates involved in our research program). In fact, it has been my experience that the undergraduate best develops with an experimental problem of this kind and is most useful to me in this role.

In addition to infrared spectroscopy, there are two nuclear magnetic resonance (NMR) instruments both of which operate at 90 Megahertz and have variable temperature controls. One of them is an older research grade Perkin-Elmer (model R32). The other is an FTNMR made by JOEL (model FX90Q). The JOEL spectrometer is also computer interfaced and makes analysis of proton and carbon-13 isotopic spectra more routine. The NMR spectra of varied mole fractions of ammonium perchlorate and binder in carbon tetrachloride should show the amount of binding going on in a nonpolar solution. Since hydrogen bonding may also be involved in this problem, the study of the degree of association of the binder with itself as a function of concentration can be studied by watching the change in field shift of the hydroxyl proton. This field shift with degree of hydrogen bonding has been observed for many alcohols. Since the relative concentration effect for hydrogen bonding can be ascertained, there will be a different field shift due to binding on the ionic surface. More detailed information of chemical environment will be revealed by studying the C-13 spectra of these solutions.

## Summary

The hypothesis upon which this proposal is based is that the types and strengths of surface/polymer binding can be uncovered through a theoretical and experimental set of approaches. The tools of the theoretical side of this project have been programs with which I have had some experience in the past. The CADPAC and MOPAC packages are available to me through the Kirtland supercomputer and recently MOPAC has been installed on the Butler University VAX. Also the purchase of a Silicon Graphics Personal Iris and the dynamics programs have just been made and will soon be installed in the chemistry department here at Butler. The Infrasil cells (needed for the temperature controlled infrared studies) have been purchased and the experimental details have been initially investigated this past summer. The materials are at hand for theoretical and experimental research into this problem

**First Quarter Report**

**Mechanism of Adhesion in Solid Propellents**

**(PIN) F04611-92-M-0002**

**Submitted by Dr. Shannon G. Lieb  
Butler University  
Indianapolis, IN 46208  
(317) 283-9410**

**Submitted to:**

- (1) David J. Wyner ONR Resident Representative  
Department of the Navy  
Office of Naval Research  
Federal Building, Room 286  
536 South Clark Street  
Chicago, IL 60605-1588**
- (2) Monique Sullivan  
AFFTC/PKRE  
Department of the Air Force  
Edwards Air Force Base, CA 93523-5000**
- (3) Dr. John J. Rusek, P.E.  
OLAC PL/RKCP  
Edwards AFB, CA 93523-5000**

This quarter was been spent on acquiring and learning to use the Silicon Graphics - Personal IRIS. There is facility to create solid surfaces and look at the interaction of molecules approaching that surface, so I am working on the development of the computation of the electrostatic charges found on ionic surfaces relative to the crystallographic cleavage plane that is chosen. The electrostatics work will be addressed further in the theoretical section. I am also learning the rudiments of polymer chemistry<sup>1</sup> to familiarize myself with the jargon and types of information found most useful to other polymer chemists. The experimental work that I have in mind will be carried out in large part by a student who worked with me last summer to develop a method of determining some important characteristics of the binder, hydroxy-terminated polybutadiene. She will work this summer (May to August) and is planning to complete her Master's degree in chemistry from Butler using this work of two summers as the thesis portion of that work. The following report will be broken into two parts which represent work contemplated and under way presently.

## Experimental

The experimental work that is envisioned will be divided into three approaches: (1) FTIR (Fourier Transform InfraRed) spectroscopy, (2) NMR (Nuclear Magnetic Resonance) and (3) viscometry.

The FTIR work will be a continuation of last summer's work in which the amount of monomer, dimer, trimer and tetramer formation of the binder, HTPB, will be studied as a function of concentration in a non-polar solvent such as carbon tetrachloride. This will allow for the determination of the equilibrium constants between the various hydrogen-bonded forms of HTPB. A temperature study will further allow the determination of the relative strengths of the different hydrogen-bonded forms through the van't Hoff equation. At the other end of the concentration scale (i.e., pure HTPB), one can evaluate the same parameters using a horizontal attenuated internal reflectance accessory to the FTIR. A thin wafer of ammonium perchlorate (AP) can be made in a pellet press and the FTIR spectrum can be cataloged to compare with the spectrum with pure HTPB applied to the surface. This will allow the investigation of the binding capabilities of HTPB to AP. Likewise, an

---

<sup>1</sup> Malcolm P. Stevens, Polymer Chemistry an Introduction, 2nd Ed., Oxford Press, New York, 1990, ISBN 0-19-505759-7

aziridine solution<sup>2</sup> can be applied to the AP pellet and the treated surface can be characterized relative to the chemical interactions that occur on the treated surface. The purpose is to determine the relative binding strength of HTPB to the use of an aziridine pre-coating.

The second experimental technique is to look at the NMR spectrum of the diol. The different types of protons are shown in figure 1 along with their tau scale positions.

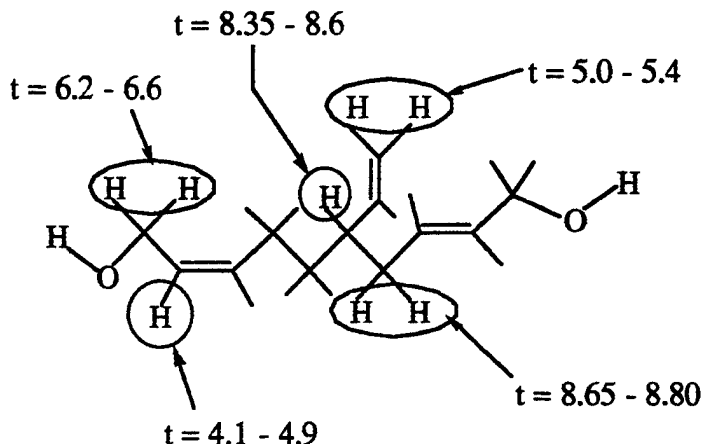


Figure 1. The "t" values are the tau values typically found for these types of protons. On the tau scale TMS has a value of 10.0

Using these protons along with the O-H protons, the integrated intensities will give the DP and also identify the % of vinyl, cis and trans bonds in the average molecule.

The viscosity of the polymer will add one more distribution parameter to the overall molecular weight or degree of polymerization. The intrinsic viscosity,  $[\eta]$ , is related to the viscosity average molecular weight,  $M_v$ , by the Mark-Houwink-Sakurada equation:

$$[\eta] = K(M_v)^a$$

The viscosity average molecular weight is defined as:

$$M_v = \frac{\sum_{i=1}^{\infty} n_i M_i^{1+a}}{\sum_{i=1}^{\infty} n_i M_i}$$

<sup>2</sup> Adolf E. Oberth, Principle of Solid Propellant Development, CPIA Publication 469, September 1987.

The number average molecular weight,  $M_n$ , is the value directly related to the FTIR and NMR experiments suggested above. The number average molecular weight is defined as:

$$M_n = \frac{\sum_{i=1}^{\infty} n_i M_i}{\sum_{i=1}^{\infty} n_i}$$

If one multiplies  $M_n$  by  $M_v$ , the result is an average of the molecular weight to the  $1+a$  power; that is:

$$M_n M_v = \frac{\sum_{i=1}^{\infty} n_i (M_i)^{1+a}}{\sum_{i=1}^{\infty} n_i}$$

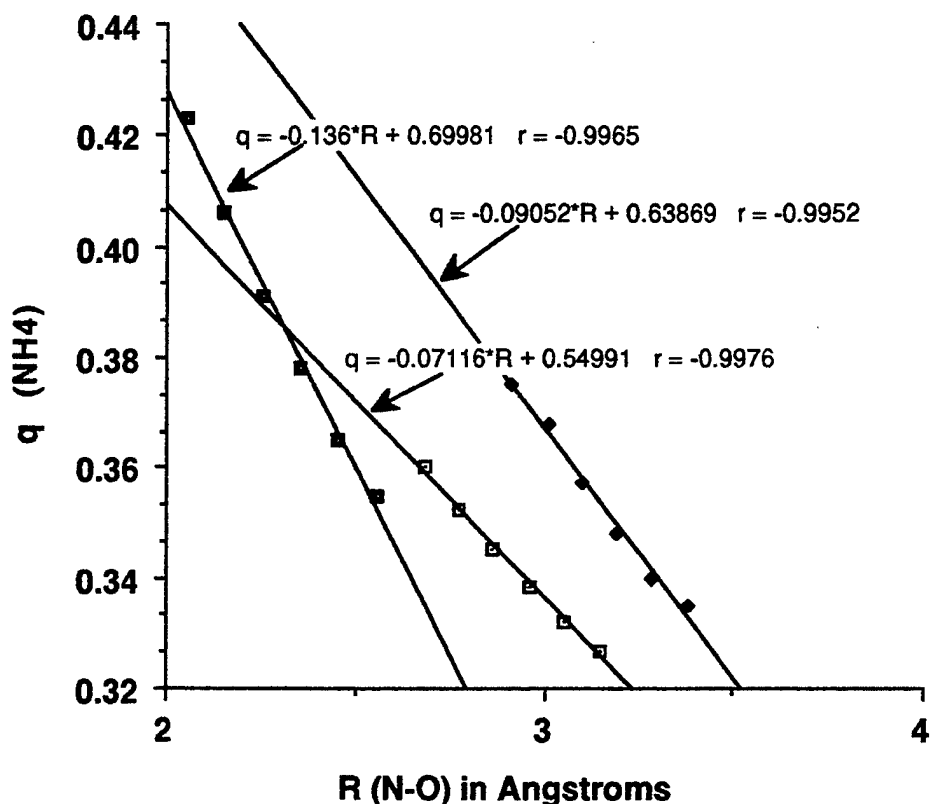
For a rod-like, extended polymer, "a" can be as large as 1. More typically, "a" is between 0.5 to 0.8. If "a" were as large as 1, then the product of the number and viscosity average molecular weights would be the average of the square of the molecular weight,  $\langle M_n^2 \rangle$ . The difference between the average of the square and the square of the average of a quantity is the variance of that quantity. Once the distribution function which describes the distribution of the fraction of oligomers having "n" monomers versus "n" is known (in the case of radical additions like this reaction, that distribution function looks like a Poisson distribution), the two parameters - average molecular weight and the variance of the molecular weight - should be able to define the distribution of molecular weights in the material. Since "a" is not expected to be unity, a different spread of molecular weights will be deduced rather than the variance, but none the less, a distribution function can be fit to the two parameters.

### Theoretical

Currently in this area I have been trying to compute the extended atom description of the ammonium ion found in ammonium perchlorate. The ammonium ion charge has been computed with many orientations relative to the perchlorate ion oriented with 3 oxygens symmetrically displaced above the ammonium ion, with 2 oxygens astride the ammonium ion and finally with 1 oxygen pointing directly toward the ammonium ion. These three perchlorate orientations are the three straight lines shown on the graph on the next page. The data points on each line are comprized of an average of five ammonium ion orientations. The line with the largest slope in magnitude has the 1 oxygen closest the ammonium ion; the next largest slope in magnitude has 3 oxygens as nearest neighbors to the ammonium ion and finally the line with the least slope belong to the

orientation having 2 oxygens of the perchlorate astride the ammonium ion. Each of the six points per straight line are calculated at the same ammonium nitrogen to perchlorate chlorine separation. These points bracket the experimental nitrogen - chlorine separation found in ammonium perchlorate.

Data from "ave'd NH4 charge"



What is presently being investigated is the calculation of the parameters which define the ammonium ion as an atom in the Charge Equilibration formalism. Those parameters are the electronegativity, the self coulomb interaction and the Slater exponent in the wavefunction of the ammonium group. The object is to reproduce the above lines as nearly the same as possible.



**Interm-Technical Report**

**Second Quarter Report**

**Mechanism of Adhesion in Solid Propellents**

**(PIN) F04611-92-M-0002**

Submitted by Dr. Shannon G. Lieb  
Butler University  
Indianapolis, IN 46208  
(317) 283-9410

Submitted to:

- (1) David J. Wyner ONR Resident Representative  
Department of the Navy  
Office of Naval Research  
Federal Building, Room 286  
536 South Clark Street  
Chicago, IL 60605-1588
- (2) Monique Sullivan  
AFFTC/PKRE  
Department of the Air Force  
Edwards Air Force Base, CA 93523-5000
- (3) Dr. John J. Rusek, P.E.  
OLAC PL/RKCP  
Edwards AFB, CA 93523-5000

## *Mechanism of Adhesion in Solid Propellents*

### **Introduction**

This summer brings the return of Michele Shultz to the experimental portion of this work. We are currently setting up an experiment to discern the type and strength of hydrogen-bonding occurring between the hydroxy-terminated polybutadiene (HTPB) and ammonium perchlorate (AP). Along with the experimental work, there is a theoretical development of the interactions among and between HTPB and AP.

### **Experimental**

Michele's work on the Fourier Transform Infrared (FTIR) spectrometer will be useful in determining the way in which the HTPB bonds to the AP surface. The primary technical problem is to determine changes in hydrogen-bonding within the HTPB itself relative to bonding with an ionic surface. One of the procedures is to make a pure  $\text{NH}_4\text{ClO}_4$  pellet and place it in the infrared beam. Following "standard" procedures of grinding about 10% by mass of the material to be studied in with KBr was quite successful for obtaining a good dispersive IR spectrum. However, the KBr is also an ionic material which would compete with the AP for surface binding of the HTPB. Pressing very thin wafers of 100% AP has not produced a sample which does not cause the peaks to be clipped by their overly intense absorption. Preliminary studies of other materials in the diffuse reflectance (DRIFT) cell used in the FTIR indicate that pure materials of low molecular weight (100 to 200 grams/mole) do not produce any different spectra than those mixed with KBr. The amount of absorbance is significantly different, but so little light is reflected to the detector that it has become apparent that the detector is receiving sufficient light relative to the amount of light that is completely transmitted that peak clipping is not observed. This approach is promising for the study of both the pure HTPB and AP. A mixture of HTPB and AP can be studied as a function of concentration to see the effects of binding. The pure HTPB and/or AP spectrum can be subtracted from the mixture to help isolate the spectral features identifiable as the "bound" HTPB.

A side project to be investigated is the NMR of HTPB. This could be used to confirm the freezing point depression estimate of ten monomer units in the average polymer of HTPB. As noted in the

previous report it could also give insight into the average number of vinyl, cis and trans units in the chain. This type of information will be useful in theoretical modeling of HTPB properties, such as, radius of gyration and excluded volume.

## Theory

In the theoretical development of this project, one simplifying step is the creation of an "extended atom" description of the ammonium ion of AP. The extended atom concept was originally designed to model the CH<sub>3</sub>, CH<sub>2</sub> and CH groups in protein structures. The terminal hydrogens tend to do little more than provide a larger van der Waals radius to the carbon to which they are attached. Therefore, in large protein structure problems the computational time is significantly reduced without sacrificing accuracy by eliminating explicit reference to the hydrogens attached to aliphatic carbons. In a similar vein, if one removes the explicit reference to the hydrogens in the ammonium ion of ammonium perchlorate there is a significant reduction in expenditures computational resources. This not only reduces the number of atoms in the formula unit from 10 to 6, but it also gives a more accurate description of the ammonium ion in the AP crystal above 100-110 Kelvins<sup>1</sup>. Neutron diffraction studies indicate that the ammonium ion is a free rotor above this temperature, so that a more accurate description of the ion would be a spherically averaged "super atom". The calculations for which I intend to use this super atom description start with the electrostatics calculations based on the Charge Equilibration<sup>2</sup>. The details of the averaging were included in the First Quarter report, but the averaging of the ammonium ion with respect to three orientations of the perchlorate anion is reproduced here (top of the next page). The steepest line represents the averaged ammonium ion with an orientation of one of the perchlorate oxygens pointing directly toward the ammonium nitrogen (i.e., along the C<sub>3</sub> axis of the perchlorate anion). The next steepest line has the averaged ion located on the C<sub>2</sub> axis of the perchlorate ion (i.e., there are two perchlorate oxygens straddling the ammonium ion). The line with the smallest slope is associated with the averaged ion along the C<sub>3</sub>

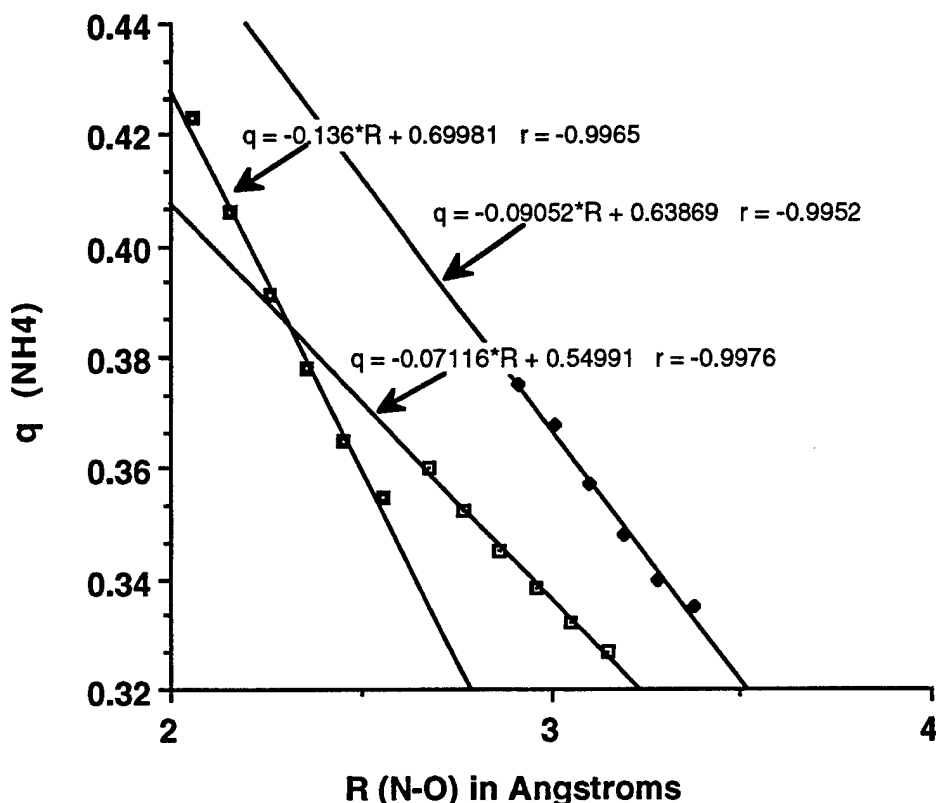
---

<sup>1</sup>C.S. Choi, H.J. Prask and E. Prince "Crystal Structure of NH<sub>4</sub>ClO<sub>4</sub> at 298, 78, and 10 K by Neutron Diffraction", J. Chem. Phys., **61**, 3523-29 (1974).

<sup>2</sup>A.K. Rappe and W.A. Goddard III, "Charge Equilibration for Molecular Dynamics Simulations", J. Phys. Chem., **95**, 3358-63 (1991).

axis again, but with three oxygens close and equidistant from the ammonium nitrogen. With this condensation of ammonium ion

#### Data from "ave'd NH4 charge"



charge behavior with distance and orientation with respect to the perchlorate anion, one is left with assessing a method for producing the appropriate parameters in the charge equilibration scheme to create an equivalent super atom. The primary parameters in this computational scheme are the electronegativity,  $\chi_o$ , of the atom, the self coulomb energy of the atom,  $J_o$ , and the Slater-type orbital exponent,  $\zeta_o$ . This last parameter is related to the average covalent radius,  $r_o$  (in Angstroms), by the following equation:

$$\zeta_o = \frac{\lambda a_o (2n + 1)}{2 r_o} = 0.1299899 \frac{(2n + 1)}{r_o}$$

where  $\lambda$  is a parameter which least squares fit by Rappe and Goddard and determined to be 0.4913,  $a_o$  is the Bohr radius (i.e., the conversion between atomic units and Angstroms - 0.529167 Angstroms/au) and  $n$  is the principle quantum number for the given atom. The Slater orbital exponent is essential in the evaluation of the two-center, two-electron coulomb integral. Since the definition of  $\chi_o$ ,

$J_0$  and  $\zeta_0$  ( $r_0$ ) are not unambiguous for this super atom, it was decided that the initial guess for these parameters would be the weighted average of their values for the hydrogen and nitrogen atomic parameters (i.e., multiply the hydrogen value by 4, add the nitrogen value and divide that sum by 5). It was further decided to fix  $\chi_0$  and vary  $J_0$  and  $r_0$  until a best fit of the average charge for the cases graphed above was obtained. This produced the final values of  $\chi_0 = 5.002$  eV,  $J_0 = 13.760$  eV and  $r_0 = 0.710$  Angstroms compared with the initial values of  $J_0 = 13.464$  eV and  $r_0 = 0.376$  Angstroms. In addition to these variations, the separation distance from the center of the super atom to the oxygen or chlorine (for which a coulomb integral needed to be evaluated) was decreased by the nitrogen - hydrogen bond length. The overall standard deviation for the fit of the super atom charge relative to the averaged charge is 0.0046. For one comparison, the estimated charge on the perchlorate anion (and hence the charge with opposite sign on the ammonium ion) is -0.34. This value is an averaged value from several perchlorate salts and inferred from lattice energy calculations<sup>3</sup>. This value fits in with the ten or so estimates which Donald, Jenkins and Pratt list within their paper. Based on the crystal structure of AP the nitrogen - chlorine distance is roughly 3.6 Angstroms and the ammonium ion lies along the  $C_2$  axis of the perchlorate ion. This produces an ammonium ion charge of +0.37 which is in excellent agreement with the lattice energy estimate. With these parameters in hand not only is the number of atoms reduced to allow larger clusters of AP formula units to be computed, but there is a further reduction in calculation because the hydrogens in the charge equilibration scheme have a charge dependence on the evaluation of  $J_0$  and  $\zeta_0$  which leads to a self-consistent charge evaluation of 10 to 20 iterations, typically, for each internuclear separation evaluated. This super atom has the charge dependence averaged into a range of orientations and separations which translates into one calculation per orientation and internuclear separation leading to at least an overall time savings of 17 fold; not to mention that the spherically averaged super atom is a more accurate representation of the actual crystalline structure above 110 Kelvins.

The other theoretical front is the modeling of the HTPB with itself and with the AP surface. At present we are creating a torsion angle profile of cis and trans 3-hexene, as well as, cis and trans 4-octene. The potential energy surface of the various torsional angles

---

<sup>3</sup>H. Donald, B. Jenkins and K.F. Pratt, "Single Ion Properties by Lattice Energy Minimization", *J. Chem. Soc. Faraday II*, **73**, 968-81 (1977).

locates the energy minima and helps determine an averaged overall shape of the HTPB. From this type of data we want to correlate the amount of hydrogen-bonding that occurs in HTPB. The surface of the AP will have many more available sites for hydrogen-bonding between it and the HTPB depending on how well the HTPB "packs" itself at the AP surface. That is the current direction the CHARMM calculations are now proceeding.

**Third Quarter Report**

**Reporting Period June 1, 1992 to August 31, 1992**

**Mechanism of Adhesion in Solid Propellents**

**(PIN) F04611-92-M-0002**

**Submitted by Dr. Shannon G. Lieb  
Butler University  
Indianapolis, IN 46208  
(317) 283-9410**

**Submitted to:**

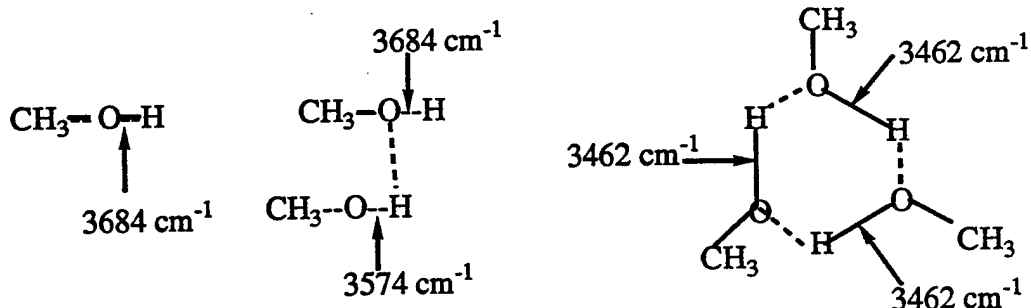
- (1) David J. Wyner ONR Resident Representative  
Department of the Navy  
Office of Naval Research  
Federal Building, Room 286  
536 South Clark Street  
Chicago, IL 60605-1588**
- (2) Monique Sullivan  
AFFTC/PKRE  
Department of the Air Force  
Edwards Air Force Base, CA 93523-5000**
- (3) Dr. John J. Rusek, P.E.  
OLAC PL/RKCP  
Edwards AFB, CA 93523-5000**

## Introduction

This report will consist of two parts. The first part deals with the spectroscopic evidence of hydrogen bonding in allyl alcohol and a characterization of the effect on concentration of the alcohol on the amount of monomer versus polymer formed. The second part will look at molecular mechanics generated potential surfaces in the understanding of the polymer chain equilibrium conformations.

## Spectroscopy

Fourier Transform Infrared (FTIR) spectroscopy of allyl alcohol in the nonpolar solvent carbon tetrachloride was performed this past summer to identify the different hydrogen bonded species and their relative amounts as a function of concentration. The C-H stretching bands are immediately adjacent to the O-H stretching polymer bands. The band assignments are made with the help of molecular beam studies of methanol clusters<sup>1</sup>. Three bands were assigned: (1) monomer at  $3684\text{ cm}^{-1}$ , (2) dimer at  $3574\text{ cm}^{-1}$  and (3) trimer at  $3462\text{ cm}^{-1}$ . The dimer peak has two different O-H stretching frequencies associated with it as pictured below.



The observed O-H stretching frequencies in carbon tetrachloride are solvent shifted to the red as indicated at the bottom of Table 1 (next page). The peaks for the dimer and trimer are not well resolved, but are evident in the spectra. The spectra were not deconvoluted because the peaks seemed evident enough without that particular enhancement. Gaussian peaks were placed under the monomer and polymer bands and allowed to be adjusted in width, height and position until the simulated spectrum was minimized with respect to

<sup>1</sup>F. Huiskens, A. Kulcke, C. Laush and J.M. Lisy, "Dissociation of small methanol clusters after excitation of the O-H stretch vibration at  $2.7\text{ }\mu\text{m}$ ", *J. Chem. Phys.* **95**, 3924-3929 (1991).



its deviation with the experimentally determined bands. At one point more Gaussian peaks than two were placed under the polymer band, to see if a tetramer peak might become evident. The result was that there was not a significant improvement in the overall match between simulated and experimental bands and the "tetramer" band had no significant area contribution either. At the present concentrations the appearance of tetramer bands is not inferred from the band fitting procedure.

Table 1 Allyl Alcohol room temperature FTIR study of monomer, dimer and trimer peaks of the O-H stretch

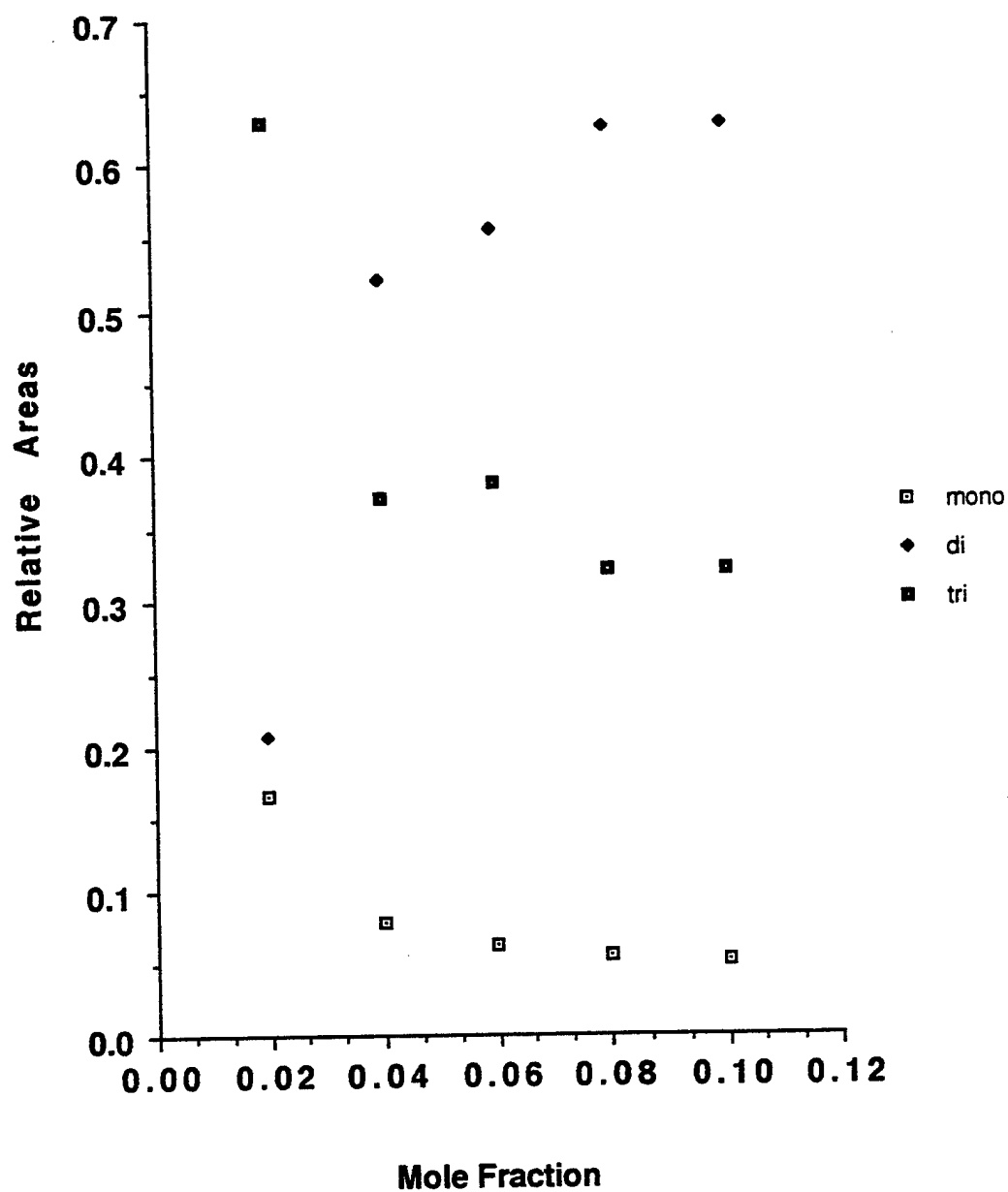
| $\chi_{OH}$                  | <u>monomer</u>            |                   | <u>dimer</u>              |                   | <u>trimer</u>             |                   |
|------------------------------|---------------------------|-------------------|---------------------------|-------------------|---------------------------|-------------------|
|                              | $\nu$ (cm <sup>-1</sup> ) | area              | $\nu$ (cm <sup>-1</sup> ) | area              | $\nu$ (cm <sup>-1</sup> ) | area              |
| 0.02                         | 3622                      | 25.15<br>(0.165)* | 3495                      | 31.71<br>(0.207)* | 3354                      | 96.02<br>(0.628)* |
| 0.04                         | 3623                      | 29.43<br>(.0780)* | 3443                      | 208.0<br>(0.552)* | 3284                      | 139.7<br>(0.370)* |
| 0.06                         | 3621                      | 42.85<br>(.0626)* | 3441                      | 380.4<br>(0.556)* | 3274                      | 261.3<br>(0.382)* |
| 0.08                         | 3621                      | 41.20<br>(.0549)* | 3452                      | 469.7<br>(0.625)* | 3251                      | 240.1<br>(0.320)* |
| 0.10                         | 3621                      | 36.33<br>(.0515)* | 3478                      | 442.6<br>(0.627)* | 3255                      | 226.5<br>(0.321)* |
| <u>ave. <math>\nu</math></u> | 3622                      |                   | 3462(23)**                |                   | 3284(42)**                |                   |
| <u>gas phase</u>             | 3684                      |                   | 3574                      |                   | 3462                      |                   |
| <u>solvent shift</u>         | -62 cm <sup>-1</sup>      |                   | -112 cm <sup>-1</sup>     |                   | -178 cm <sup>-1</sup>     |                   |

\* numbers in parenthesis are the fractional areas

\*\* numbers in parenthesis are the standard deviation

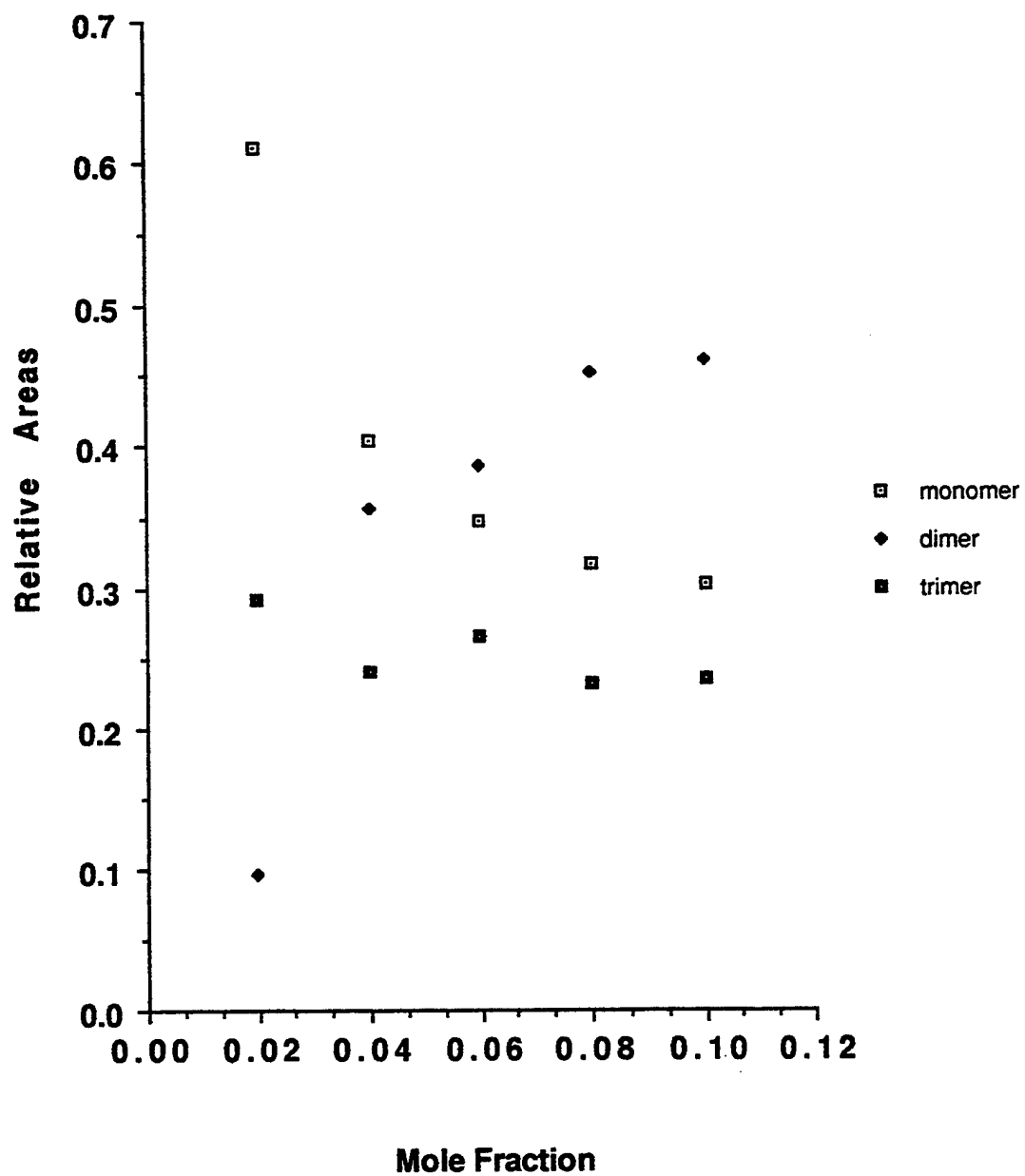
# Relative Areas of Monomer, Dimer and Trimer Peaks of Allyl Alcohol

at Room Temperature

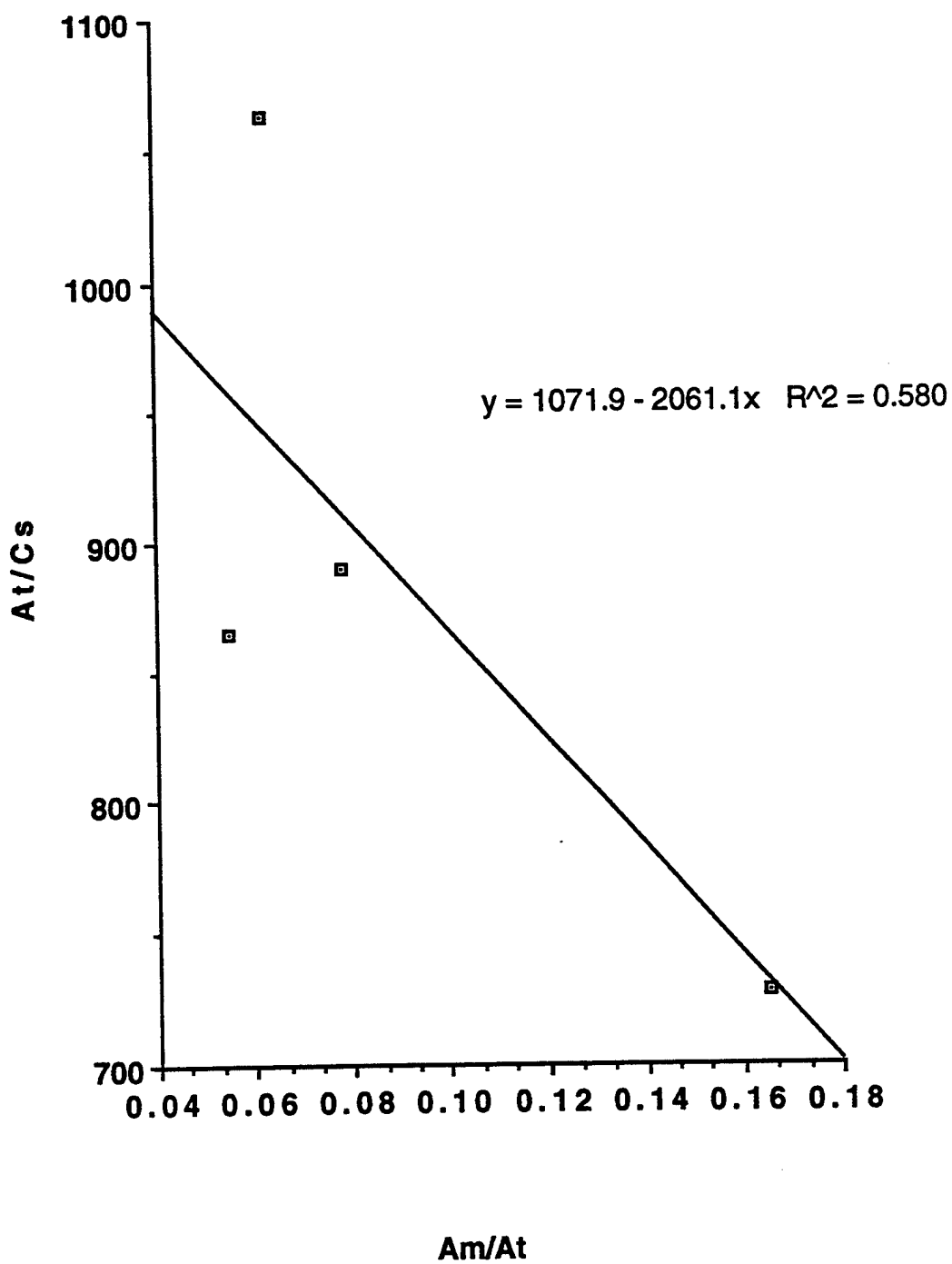


# Relative Areas of Monomer, Dimer and Trimer of Allyl Alcohol

Room Temperature with Peak Intensities Adjusted



**Room Temperature Determination of the Relative  
Intensities of Monomer vs. Polymer OH Bands of Allyl Alcohol**

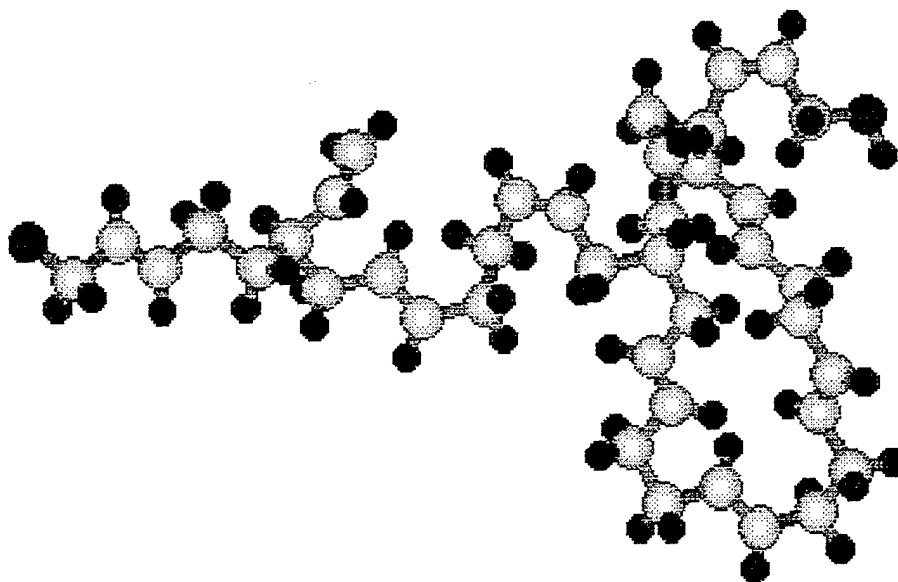


From the data in Table 1. a determination of a reasonable concentration of alcohol which has a fair amount of monomer remaining in solution was sought. Assumedly, to enhance the binding of the hydroxy-terminated polybutadiene (HTPB) to an ionic surface one would minimize the amount of hydrogen bonding among the HTPB's. The fractional areas for each of the species was then plotted versus mole fraction to look for an optimal region. Looking at the first plot (next page), it can be seen that the monomer fractional concentration levels off in the region between 0.06 to 0.1 mole fraction. A mole fraction of 0.1 of HTPB is roughly 50% by weight in carbon tetrachloride. Pure HTPB was recorded using a horizontal ATR on the FTIR and no monomer band could be found.

Another piece of information gained from reference 1, is that the relative intensity of dimer to monomer band is roughly 8:1. This correction to the first plot is incorporated in the second plot. The result is that there is no qualitative difference in the leveling out region, but there is a marked increase in the fraction of monomer present at each mole fraction. Since the frequencies are red shifted by the solvent, is it not reasonable to assume that the intensities may be affected as well by the solvent? To resolve that question, the relationships between the concentration of the solution, the absorbances and the intensities (i.e., the molar absorptivities) is presented in Appendix A. If the ratio of the total area under the bands to the solution concentration ( $A_t/C_s$ ) is plotted against the monomer area to total area ( $A_m/A_t$ ) a straight line should result whose slope equals  $(1-x^2)/\epsilon_m$  and intercept is  $x \epsilon_m$ ; where  $x$  is the multiplicative enhancement of the monomer molar absorptivity,  $\epsilon_m$ . This is the third plot. The ratio of the slope to intercept is  $(1-x^2)/x$ . Using this ratio for the data plotted in the third graph results in an enhancement of 2.3 for the polymer peaks. The correlation of the fit is not good, suggesting further refinement of the experimental procedure. Dropping a data point to improve the overall correlation produces results of the enhancement factor in the range of 2 to 3 (average about 2.5).

### **Molecular Mechanics Potential Surface of 3-hexenes**

The HTPB structure is composed of three substructures. Sixty percent of the double bonds are in the backbone in the trans configuration. Twenty percent are in the cis configuration and the remaining twenty percent are pendant vinyl groups. A picture of an example of this for an average length polymer is shown below.



color key: Hydrogen = blue, Oxygen = red, Carbon = grey

To model part of the backbone, trans-3-hexene and cis-3-hexene were studied. The two torsional angles that were allowed to vary were around the single bonds adjacent to the double bond. The methyl groups at the ends of the hexene were not allowed to rotate. The resulting topographical maps of the energies associated with each conformation follow in the pages after this one. The energy key to the topographic lines is to the upper right corner of the picture. These energies are in kcal/mole. The bottom of that key has the name of the file associated with the topographical map. The first map has "3thexene.csr" which stands for trans-3-hexene. What is so striking about this picture is the very high degree of symmetry of the design. The high energy points on the map are marked with x's. The lowest energy spots are found in the open circles located at torsion angles  $120^\circ$  for both torsions,  $120^\circ$  and  $240^\circ$  for each and  $240^\circ$  for both. Along the borders there are also energy minima which are nearly as deep as those displaced about the center of the map. Those along the border are located at  $0^\circ$  (and continued at  $360^\circ$ ) for one of the torsions and at  $120^\circ$  and  $240^\circ$  for the other torsion. What this indicates is that the most stable positions have one hydrogen of the methylene group just beyond the double bond pointing  $180^\circ$  away from the hydrogen on the double bond as you look end on at the first single bond connected to the double bond. The best way to visualize this is to use a hand-held model, keeping in mind that the torsional angles are defined in terms of the backbone carbons.

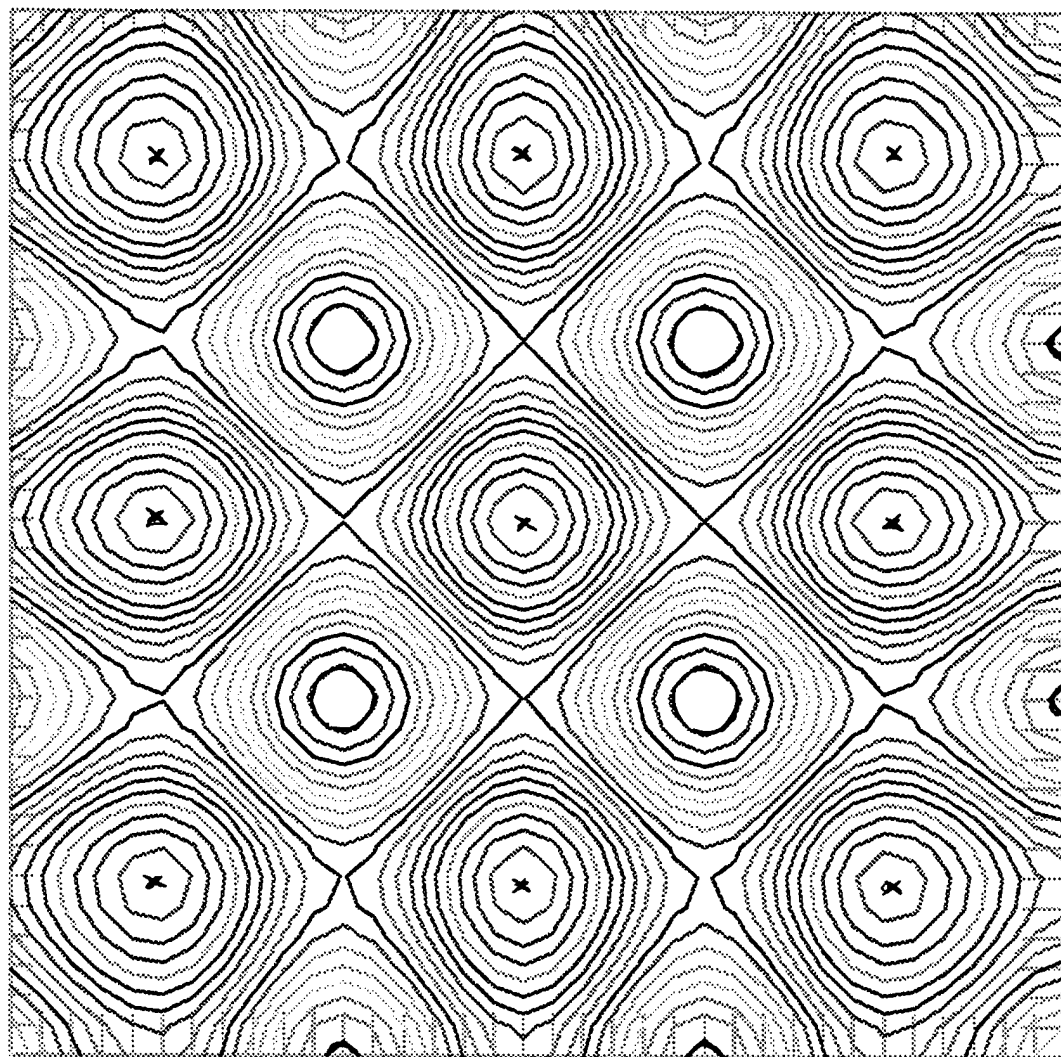
# Contour Levels

3.1 **3.7**  
 4.3 **4.9**  
 5.6 6.2  
 6.8 7.4  
 8.1 8.7  
 9.3 9.9  
 10.6 11.2  
 11.8 12.4  
 13.1 13.7  
 14.3 14.9

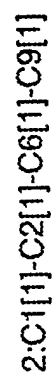
Non-X,Y-Axes Torsions  
 Adjusted to give  
 Lowest quantity value

Input Search File Name:  
 3thexene.csr

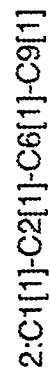
Contour Plot



340.0  
 330.0  
 320.0  
 310.0  
 300.0  
 290.0  
 280.0  
 270.0  
 260.0  
 250.0  
 240.0  
 230.0  
 220.0  
 210.0  
 200.0  
 190.0  
 180.0  
 170.0  
 160.0  
 150.0  
 140.0  
 130.0  
 120.0  
 110.0  
 100.0  
 90.0  
 80.0  
 70.0  
 60.0  
 50.0  
 40.0  
 30.0  
 20.0  
 10.0  
 0.0







The next topographical map is of the cis arrangement of the carbon backbone. The striking feature here is that the middle portion of the torsional contour plot is qualitatively the same as the trans isomer. To further emphasize this similarity, a transparency of the same range of torsional angles of the trans isomer is laid over top of the cis topographical map. The range of the torsional angles had to be reduced to the range of  $60^\circ$  to  $300^\circ$ , otherwise the rather enormous repulsive energies swamp out the much smaller peaks and valleys found in the center of the topographical map. Once the two end methyl groups get within  $120^\circ$  of one another on the same side of the cis double bond, a great deal of steric repulsion takes over the majority of the total energy. The final result is that the equilibrium positions cause the backbone to twist at  $120^\circ$  intervals (except across double bonds) in a rather random fashion regardless of whether the double bond adds a cis or trans kink to the backbone. With this information one can compute the average end to end length of the polymer and an excluded volume about the polymer.

## Appendix A Derivation of the relationship between the absorbances of monomer and polymer peaks and the increased intensity of the polymer peaks.

The absorbances (areas) of the peaks associated with monomer,  $A_m$ , and polymer,  $A_p$ , are separated and assigned different molar absorptivities,  $\epsilon_m$  and  $\epsilon_p$ , respectively. Using Beer's Law, one can write:

$$A_m + A_p = \epsilon_m C_m + x \epsilon_m C_p$$

where  $C_m$  is the concentration of the monomer and "x" is the multiplicative factor by which the polymer absorptivity differs from the monomer absorptivity. If one introduces  $C_s = C_m + C_p$ , where  $C_s$  is the concentration of the alcohol (as written on the label of the bottle), then:

$$\begin{aligned} A_m + A_p &= \epsilon_m C_m + x \epsilon_m (C_s - C_m) \\ &= (1-x) \epsilon_m C_m + x \epsilon_m C_s \end{aligned}$$

or

$$\frac{A_m + A_p}{C_s} = (1-x) \epsilon_m f_m + x \epsilon_m$$

$$\text{where } f_m = \frac{C_m}{C_s} = \frac{A_m / \epsilon_m}{A_T / \epsilon_m (1+x)} = (1+x) \frac{A_m}{A_T}$$

where  $A_T$  is the total area of both monomer and polymer. Substituting  $f_m$  back into the previous equation yields:

$$\frac{A_m + A_p}{C_s} = \frac{A_T}{C_s} = (1-x)(1+x) \epsilon_m \frac{A_m}{A_T} + x \epsilon_m$$

As indicated in the above equation, if  $A_T/C_s$  is plotted versus  $A_m/A_T$ , the slope will equal  $(1-x^2)\epsilon_m$  and the intercept will equal  $x\epsilon_m$ . The ratio of the slope to the intercept will yield the following expression which is the ratio of the polymer intensity over the monomer intensity:

$$\frac{\text{slope}}{\text{intercept}} = \frac{(1-x^2)}{x}$$

## **Fourth Quarter Report**

**Reporting Period September 1, 1992 to November 30, 1992**

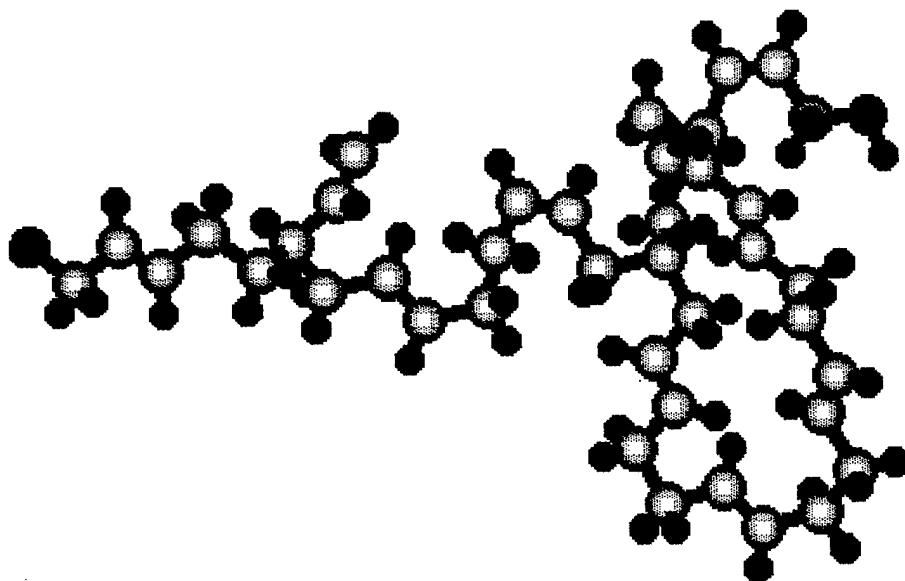
### **Mechanism of Adhesion in Solid Propellents**

**(PIN) F04611-92-M-0002**

Submitted by Dr. Shannon G. Lieb  
Butler University  
Indianapolis, IN 46208  
(317) 283-9410

Submitted to:

- (1) David J. Wyner ONR Resident Representative  
Department of the Navy  
Office of Naval Research  
Federal Building, Room 286  
536 South Clark Street  
Chicago, IL 60605-1588
- (2) Sandra Jenkins  
AFFTC/PKRE  
Building #2800  
Department of the Air Force  
Edwards Air Force Base, CA 93523-5000  
phone: (805) 277-9818
- (3) Dr. John J. Rusek, P.E.  
OLAC PL/RKCP  
Edwards AFB, CA 93523-5000  
phone: (805) 275-5407



## Introduction

This report is a further extension of the last quarter's report. The data for allyl alcohol was reexamined with the desire to extract more information from the data than just the monomer parameters (molar absorptivity, peak position, etc.). Using an algebraic manipulation of the equations generated by Beer's Law and using the area under the curve rather than the absorption at the peak maximum, provided the essential ingredients to dissecting the data into monomer, dimer and trimer parameters. The area under the curve was deemed the appropriate measure of the concentration rather than the peak height, because the peak height is generally used in Beer's Law with the assumption that the peak is Gaussian and therefore its area is directly proportional to the peak height - making both the area and peak height proportional to the concentration of the species in solution.

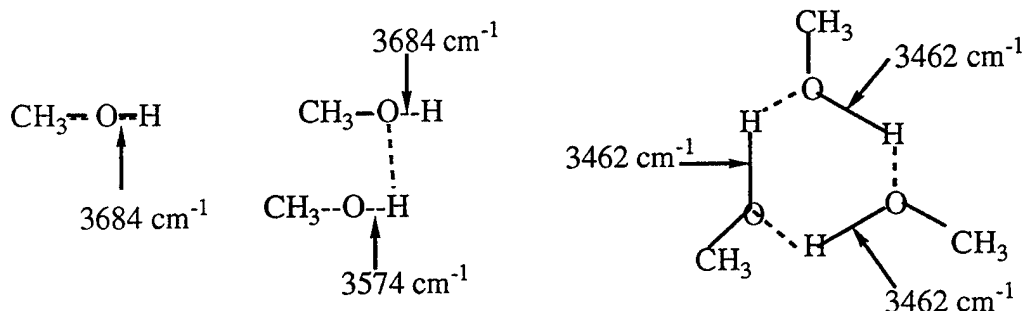
## Spectroscopy

Fourier Transform Infrared (FTIR) spectroscopy of allyl alcohol in the nonpolar solvent carbon tetrachloride was performed this past summer to identify the different hydrogen bonded species and their relative amounts as a function of concentration. The C-H stretching bands are immediately adjacent to the O-H stretching polymer bands. The band assignments are made with the help of molecular beam studies of methanol clusters<sup>1</sup>. Three bands were assigned: (1) monomer at  $3684\text{ cm}^{-1}$ , (2) dimer at  $3574\text{ cm}^{-1}$  and (3)

---

<sup>1</sup>F. Huisken, A. Kulcke, C. Laush and J.M. Lisy, "Dissociation of small methanol clusters after excitation of the O-H stretch vibration at  $2.7\text{ }\mu$ ", *J. Chem. Phys.* **95**, 3924-3929 (1991).

trimer at  $3462\text{ cm}^{-1}$ . The dimer peak has two different O-H stretching frequencies associated with it as pictured below.



The observed O-H stretching frequencies in carbon tetrachloride are solvent shifted to the red as indicated at the bottom of Table 1 (next page). The peaks for the dimer and trimer are not well resolved, but are evident in the spectra. The spectra were not deconvoluted because the peaks seemed evident enough without that particular enhancement. Gaussian peaks were placed under the monomer and polymer bands and allowed to be adjusted in width, height and position until the simulated spectrum was minimized with respect to its deviation with the experimentally determined bands. At one point more Gaussian peaks than two were placed under the polymer band, to see if a tetramer peak might become evident. The result was that there was not a significant improvement in the overall match between simulated and experimental bands and the "tetramer" band had no significant area contribution either. At the present concentrations the appearance of tetramer bands is not inferred from the band fitting procedure.

Table 1 Allyl Alcohol room temperature FTIR study of monomer, dimer and trimer peaks of the O-H stretch

|                              | <u>monomer</u>                |       | <u>dimer</u>                  |       | <u>trimer</u>                 |       |
|------------------------------|-------------------------------|-------|-------------------------------|-------|-------------------------------|-------|
| Molarity                     | $\nu\text{ (cm}^{-1}\text{)}$ | area  | $\nu\text{ (cm}^{-1}\text{)}$ | area  | $\nu\text{ (cm}^{-1}\text{)}$ | area  |
| 0.210                        | 3622                          | 25.15 | 3495                          | 31.71 | 3354                          | 96.02 |
| 0.424                        | 3623                          | 29.43 | 3443                          | 208.0 | 3284                          | 139.7 |
| 0.644                        | 3621                          | 42.85 | 3441                          | 380.4 | 3274                          | 261.3 |
| 0.869                        | 3621                          | 41.20 | 3452                          | 469.7 | 3251                          | 240.1 |
| 1.10                         | 3621                          | 36.33 | 3478                          | 442.6 | 3255                          | 226.5 |
| <u>ave. <math>\nu</math></u> | 3622                          |       | 3462(23)**                    |       | 3284(42)**                    |       |
| gas                          |                               |       |                               |       |                               |       |
| <u>phase*</u>                | 3684                          |       | 3574                          |       | 3462                          |       |
| solvent                      |                               |       |                               |       |                               |       |
| <u>shift</u>                 | -62 $\text{cm}^{-1}$          |       | -112 $\text{cm}^{-1}$         |       | -178 $\text{cm}^{-1}$         |       |

\* gas phase refers to methanol in the gas phase

\*\* numbers in parenthesis are the standard deviation

Table 2 Allyl alcohol room temperature FTIR study of O-H stretching frequency dependency on polymerization. The symbol "A" refers to area under a peak, the subscript "T" refers to total, "m" monomer, "d" dimer and "s" to solution, and the symbol "c" refers to concentration.

| <u>Molarity</u> | <u>A<sub>T</sub>/c<sub>s</sub></u> | <u>A<sub>m</sub>/c<sub>s</sub></u> | <u>A<sub>d</sub>/c<sub>s</sub></u> |
|-----------------|------------------------------------|------------------------------------|------------------------------------|
| 0.210           | 728.0                              | 119.8                              | 151.0                              |
| 0.424           | 889.5                              | 69.41                              | 490.6                              |
| 0.644           | 1063                               | 66.44                              | 590.7                              |
| 0.869           | 864.2                              | 47.41                              | 540.5                              |
| 1.10            | 641.3                              | 33.03                              | 402.4                              |

From the data in Table 1. a determination of a reasonable concentration of alcohol which has a fair amount of monomer remaining in solution was sought. Assumedly, to enhance the binding of the hydroxy-terminated polybutadiene (HTPB) to an ionic surface, one would minimize the amount of hydrogen bonding among the HTPB's.

Another piece of information gained from reference 1, is that the relative intensity of dimer to monomer band is roughly 8:1. To get at this intensity a multilinear regression analysis was devised to extract the enhancement factors of the dimer and trimer above the monomer extinction coefficient. The following derivation shows the relationship between the measured areas to the sought after parameters.

$$\begin{aligned}
 A_T &= A_m + A_d + A_t \\
 &= \epsilon_m c_m + \epsilon_d c_d + \epsilon_t c_t \\
 &= \epsilon_m c_m + x \epsilon_m c_d + y \epsilon_m c_t
 \end{aligned}$$

where A is the area under the curve, "m" subscript refers to monomer, "d" subscript refers to dimer, "t" subscript refers to trimer, "s" subscript refers to the solution (as a whole), "c" refers to concentration (moles/liter), "x" is the enhancement factor of the dimer over monomer and "y" is the enhancement factor of the trimer over monomer. Noting that the concentration of the solution, c<sub>s</sub>, is equal to the monomer concentration, c<sub>m</sub>, plus twice the dimer concentration, c<sub>d</sub>, plus three times the trimer concentration, c<sub>t</sub>, modifies the last equation to the form:

$$\begin{aligned}
 A_T &= \epsilon_m c_m + x \epsilon_m c_d + y \epsilon_m \frac{1}{3} (c_s - c_m - 2c_d) \\
 &= \epsilon_m \left(1 - \frac{y}{3}\right) c_m + \epsilon_m \left(x - \frac{2y}{3}\right) c_d + \frac{y \epsilon_m}{3} c_s
 \end{aligned}$$

dividing through by  $c_s$

$$\frac{A_T}{c_s} = \epsilon_m \left(1 - \frac{y}{3}\right) \frac{c_m}{c_s} + \epsilon_m \left(x - \frac{2y}{3}\right) \frac{c_d}{c_s} + \frac{y \epsilon_m}{3}$$

using the substitutions:

$$\frac{c_m}{c_s} = \frac{A_m / \epsilon_m}{c_s} \quad \text{and} \quad \frac{c_d}{c_s} = \frac{A_d / x \epsilon_m}{c_s}$$

leads to the final form of the equation which is:

$$\frac{A_T}{c_s} = \left(1 - \frac{y}{3}\right) \frac{A_m}{c_s} + \frac{\left(x - \frac{2}{3}y\right)}{x} \frac{A_d}{c_s} + \frac{y \epsilon_m}{3}$$

Solving this equation with the data in Table 2, results in the value of  $(1 - y/3) = 4.816$  (variance = 0.452),  $(x - 2/3 y)/x = 1.288$  (variance = 0.016) and  $y \epsilon_m / 3 = -47.08$ . This makes  $x = 26.6$  (quite a bit higher than 8),  $y = -11.4$  (wrong sign for physical significance) and  $\epsilon_m = 12.3$  (it should be noted that the measurements were carried out in a cell with a 1 mm pathlength).

The mathematical analysis seems appropriate for this problem, but the apparent failure to produce physically reasonable results seem to come from two possible sources. First, it could be that the analysis is outside the Beer's Law procedure and the linear dependence on the area of the peak with respect to concentration is not correct. We will be investigating lower concentrations of these solutions to ascertain the validity of Beer's Law. Secondly, the overlap of the C-H stretching region with the O-H polymer band region could be distorting the results and causing some loss of accuracy. To this end we have recently produced spectra of  $\text{CD}_3\text{OH}$  which have only a small amount of a C-H stretching band which can be readily corrected for. The initial analysis in band fitting indicates that there are some distinct differences in peak positions and concentration dependences of hydrogen bonding between methanol and allyl alcohol. The same concentration region of allyl alcohol which seems to give reasonable looking spectra (1.0 M to 0.2 M) produce polymer bands whose absorption bands exceed 1 absorbance unit for methanol. Since there are no thinner cells than 1 mm made of Infrasil, the methanol spectra will be obtained at lower concentrations.



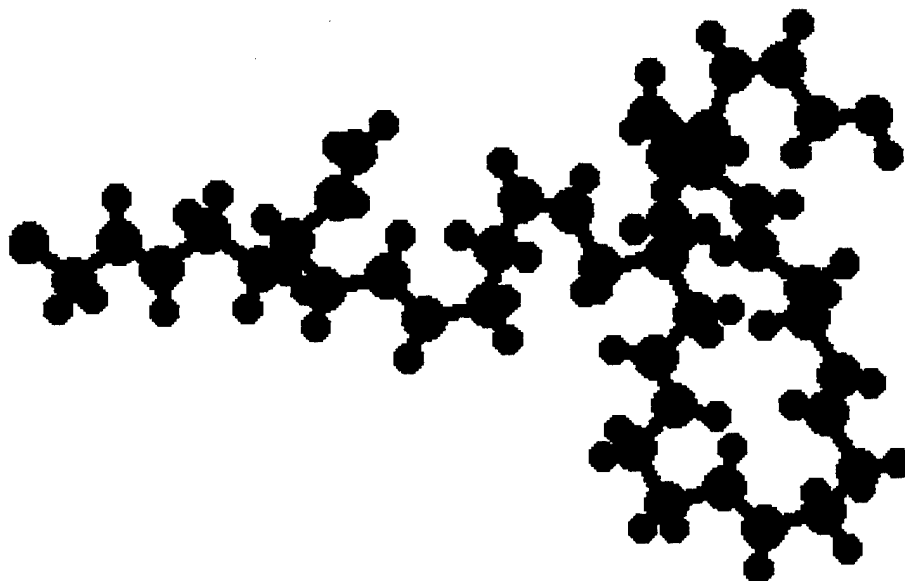
**Final Report**  
**Mechanism of Adhesion in Solid Propellents**

**(PIN) F04611-92-M-0002**

Submitted by Dr. Shannon G. Lieb  
Butler University  
Indianapolis, IN 46208  
(317) 283-9410

Submitted to:

- (1) David J. Wyner ONR Resident Representative  
Department of the Navy  
Office of Naval Research  
Federal Building, Room 286  
536 South Clark Street  
Chicago, IL 60605-1588
- (2) Sandra Jenkins  
AFFTC/PKRE  
Building #2800  
Department of the Air Force  
Edwards Air Force Base, CA 93523-5000  
phone: (805) 277-9818
- (3) Dr. John J. Rusek, P.E.  
OLAC PL/RKCP  
Edwards AFB, CA 93523-5000  
phone: (805) 275-5407



## Introduction

This report is a further extension of the last quarter's report. The data for allyl alcohol was reexamined with the desire to extract more information from the data than just the monomer parameters (molar absorptivity, peak position, etc.). Using an algebraic manipulation of the equations generated by Beer's Law and using the area under the curve rather than the absorption at the peak maximum, provided the essential ingredients to dissecting the data into monomer, dimer and trimer parameters. The area under the curve was deemed the appropriate measure of the concentration rather than the peak height, because the peak height is generally used in Beer's Law with the assumption that the peak is Gaussian and therefore its area is directly proportional to the peak height - making both the area and peak height proportional to the concentration of the species in solution.

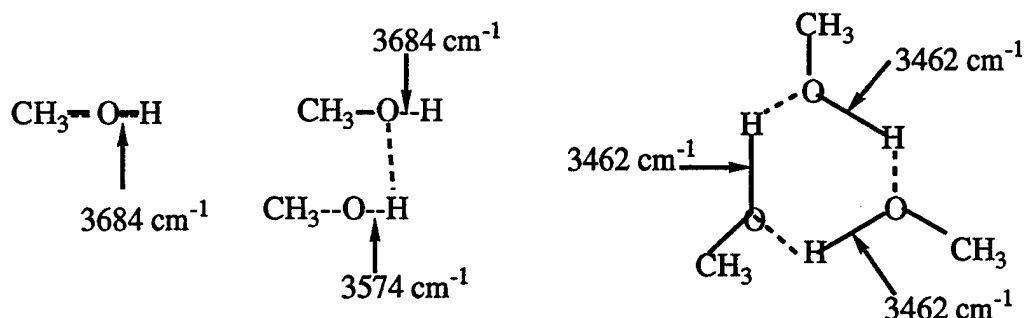
## Spectroscopy

Fourier Transform Infrared (FTIR) spectroscopy of allyl alcohol in the nonpolar solvent carbon tetrachloride was performed this past summer to identify the different hydrogen bonded species and their relative amounts as a function of concentration. The C-H stretching bands are immediately adjacent to the O-H stretching polymer bands. The band assignments are made with the help of molecular beam studies of methanol clusters<sup>1</sup>. Three bands were assigned: (1) monomer at  $3684\text{ cm}^{-1}$ , (2) dimer at  $3574\text{ cm}^{-1}$  and (3)

---

<sup>1</sup>F. Huisken, A. Kulcke, C. Laush and J.M. Lisy, "Dissociation of small methanol clusters after excitation of the O-H stretch vibration at  $2.7\text{ }\mu$ ", J. Chem. Phys **95**, 3924-3929 (1991).

trimer at  $3462\text{ cm}^{-1}$ . The dimer peak has two different O-H stretching frequencies associated with it as pictured below.



The observed O-H stretching frequencies in carbon tetrachloride are solvent shifted to the red as indicated at the bottom of Table 1 (next page). The peaks for the dimer and trimer are not well resolved, but are evident in the spectra. The spectra were not deconvoluted because the peaks seemed evident enough without that particular enhancement. Gaussian peaks were placed under the monomer and polymer bands and allowed to be adjusted in width, height and position until the simulated spectrum was minimized with respect to its deviation with the experimentally determined bands. At one point more Gaussian peaks than two were placed under the polymer band, to see if a tetramer peak might become evident. The result was that there was not a significant improvement in the overall match between simulated and experimental bands and the "tetramer" band had no significant area contribution either. At the present concentrations the appearance of tetramer bands is not inferred from the band fitting procedure.

**Table 1** Allyl Alcohol room temperature FTIR study of monomer, dimer and trimer peaks of the O-H stretch

|                              | <u>monomer</u>                |       | <u>dimer</u>                  |       | <u>trimer</u>                 |       |
|------------------------------|-------------------------------|-------|-------------------------------|-------|-------------------------------|-------|
| Molarity                     | $\nu\text{ (cm}^{-1}\text{)}$ | area  | $\nu\text{ (cm}^{-1}\text{)}$ | area  | $\nu\text{ (cm}^{-1}\text{)}$ | area  |
| 0.210                        | 3622                          | 25.15 | 3495                          | 31.71 | 3354                          | 96.02 |
| 0.424                        | 3623                          | 29.43 | 3443                          | 208.0 | 3284                          | 139.7 |
| 0.644                        | 3621                          | 42.85 | 3441                          | 380.4 | 3274                          | 261.3 |
| 0.869                        | 3621                          | 41.20 | 3452                          | 469.7 | 3251                          | 240.1 |
| 1.10                         | 3621                          | 36.33 | 3478                          | 442.6 | 3255                          | 226.5 |
| <u>ave. <math>\nu</math></u> | 3622                          |       | 3462(23)**                    |       | 3284(42)**                    |       |
| <u>gas</u>                   |                               |       |                               |       |                               |       |
| <u>phase*</u>                | 3684                          |       | 3574                          |       | 3462                          |       |
| <u>solvent</u>               |                               |       |                               |       |                               |       |
| <u>shift</u>                 | -62 $\text{cm}^{-1}$          |       | -112 $\text{cm}^{-1}$         |       | -178 $\text{cm}^{-1}$         |       |

\* gas phase refers to methanol in the gas phase

\*\* numbers in parenthesis are the standard deviation

**Table 2** Allyl alcohol room temperature FTIR study of O-H stretching frequency dependency on polymerization. The symbol "A" refers to area under a peak, the subscript "T" refers to total, "m" monomer, "d" dimer and "s" to solution, and the symbol "c" refers to concentration.

| <u>Molarity</u> | <u>A<sub>T</sub>/c<sub>s</sub></u> | <u>A<sub>m</sub>/c<sub>s</sub></u> | <u>A<sub>d</sub>/c<sub>s</sub></u> |
|-----------------|------------------------------------|------------------------------------|------------------------------------|
| 0.210           | 728.0                              | 119.8                              | 151.0                              |
| 0.424           | 889.5                              | 69.41                              | 490.6                              |
| 0.644           | 1063                               | 66.44                              | 590.7                              |
| 0.869           | 864.2                              | 47.41                              | 540.5                              |
| 1.10            | 641.3                              | 33.03                              | 402.4                              |

From the data in Table 1. a determination of a reasonable concentration of alcohol which has a fair amount of monomer remaining in solution was sought. Assumedly, to enhance the binding of the hydroxy-terminated polybutadiene (HTPB) to an ionic surface, one would minimize the amount of hydrogen bonding among the HTPB's.

Another piece of information gained from reference 1, is that the relative intensity of dimer to monomer band is roughly 8:1. To get at this intensity a multilinear regression analysis was devised to extract the enhancement factors of the dimer and trimer above the monomer extinction coefficient. The following derivation shows the relationship between the measured areas to the sought after parameters.

$$\begin{aligned}
 A_T &= A_m + A_d + A_t \\
 &= \epsilon_m c_m + \epsilon_d c_d + \epsilon_t c_t \\
 &= \epsilon_m c_m + x \epsilon_m c_d + y \epsilon_m c_t
 \end{aligned}$$

where A is the area under the curve, "m" subscript refers to monomer, "d" subscript refers to dimer, "t" subscript refers to trimer, "s" subscript refers to the solution (as a whole), "c" refers to concentration (moles/liter), "x" is the enhancement factor of the dimer over monomer and "y" is the enhancement factor of the trimer over monomer. Noting that the concentration of the solution, c<sub>s</sub>, is equal to the monomer concentration, c<sub>m</sub>, plus twice the dimer concentration, c<sub>d</sub>, plus three times the trimer concentration, c<sub>t</sub>, modifies the last equation to the form:

$$A_T = \epsilon_m c_m + x \epsilon_m c_d + y \epsilon_m \frac{1}{3} (c_s - c_m - 2c_d)$$

$$= \epsilon_m \left(1 - \frac{y}{3}\right) c_m + \epsilon_m \left(x - \frac{2y}{3}\right) c_d + \frac{y \epsilon_m}{3} c_s$$

dividing through by  $c_s$

$$\frac{A_T}{c_s} = \epsilon_m \left(1 - \frac{y}{3}\right) \frac{c_m}{c_s} + \epsilon_m \left(x - \frac{2y}{3}\right) \frac{c_d}{c_s} + \frac{y \epsilon_m}{3}$$

using the substitutions:

$$\frac{c_m}{c_s} = \frac{A_m / \epsilon_m}{c_s} \quad \text{and} \quad \frac{c_d}{c_s} = \frac{A_d / x \epsilon_m}{c_s}$$

leads to the final form of the equation which is:

$$\frac{A_T}{c_s} = \left(1 - \frac{y}{3}\right) \frac{A_m}{c_s} + \frac{\left(x - \frac{2y}{3}\right)}{x} \frac{A_d}{c_s} + \frac{y \epsilon_m}{3}$$

Solving this equation with the data in Table 2, results in the value of  $(1 - y/3) = 4.816$  (variance = 0.452),  $(x - 2/3 y)/x = 1.288$  (variance = 0.016) and  $y \epsilon_m / 3 = -47.08$ . This makes  $x = 26.6$  (quite a bit higher than 8),  $y = -11.4$  (wrong sign for physical significance) and  $\epsilon_m = 12.3$  (it should be noted that the measurements were carried out in a cell with a 1 mm pathlength).

The mathematical analysis seems appropriate for this problem, but the apparent failure to produce physically reasonable results seem to come from two possible sources. First, it could be that the analysis is outside the Beer's Law procedure and the linear dependence on the area of the peak with respect to concentration is not correct. We will be investigating lower concentrations of these solutions to ascertain the validity of Beer's Law. Secondly, the overlap of the C-H stretching region with the O-H polymer band region could be distorting the results and causing some loss of accuracy. To this end we have recently produced spectra of  $CD_3OH$  which have only a small amount of a C-H stretching band which can be readily corrected for. The initial analysis in band fitting indicates that there are some distinct differences in peak positions and concentration dependences of hydrogen bonding between methanol and allyl alcohol. The same concentration region of allyl alcohol which seems to give reasonable looking spectra (1.0 M to 0.2 M) produce polymer bands whose absorption bands exceed 1 absorbance unit for methanol. Since there are no thinner cells than 1 mm made of Infrasil, the methanol spectra will be obtained at lower concentrations.